

# **Climate change induced shifts in polar microalgae nutritional content: species, community and trophic implications**

by **Rebecca Julianne Duncan**

Thesis submitted in fulfilment of the requirements for  
the degree of

**Doctor of Philosophy**

under the supervision of Associate Professor Katherina  
Petrou, Professor Janne Søreide, Professor Øystein Varpe  
& Dr Mark Tobin.

University of Technology Sydney  
Faculty of Science

April 2024

## **CERTIFICATE OF ORIGINAL AUTHORSHIP**

I, Rebecca Julianne Duncan, declare that this thesis is submitted in fulfilment of the requirements for the award of Doctor of Philosophy, in the School of Life Sciences, Faculty of Science, at the University of Technology Sydney.

This thesis is wholly my own work unless otherwise referenced or acknowledged. In addition, I certify that all information sources and literature used are indicated in the thesis.

This document has not been submitted for qualifications at any other academic institution.

This research is supported by the Australian Government Research Training Program and an AINSE Ltd. Postgraduate Research Award (PGRA).

Signature:

Production Note:  
Signature removed prior to publication.

Date: 22.04.24

## ACKNOWLEDGMENTS

An enormous thank you to Katherina Petrou. I am so grateful for your unwavering support throughout my PhD. I have always felt that you were on my team, particularly through challenging years during the pandemic, and that has been incredibly meaningful. It has been an absolute pleasure to work with you and I am so appreciative of the time and effort you have invested in me as a researcher - your assistance has been invaluable. You have taught me so much and fostered in me a curiosity to want to keep learning more. You have been patient and kind whilst always pushing me to do my best, and I feel lucky to have you as a mentor. I have really enjoyed these past years, and I am finishing my candidature passionate about research and excited for the future.

Thank you to Daniel Nielsen for your assistance in many different areas of my PhD research. It has been a great reassurance to know I can come to you with almost any problem and you will help me find a solution. Thank you particularly for your patience with my messy R scripts and encouraging me with coding, it would have been difficult to develop those skills without you. I have enjoyed our long days on the beamline at the Synchrotron and I have learnt a lot under your guidance during these past years.

To the Petrou Lab group, in particular Billy and Alyson, it has been great fun to work alongside you all. Thank you for all the PhD life chats over coffee breaks, Chinese food, and around the fire in the mountains.

A huge thank you to Janne Søreide for all of your support in Svalbard and facilitating such rewarding and exciting field work and projects. You always make the seemingly impossible, possible. I have really enjoyed our long days in the field and time spent in cabins all over Svalbard. I have learnt so much from you, and you are a hardworking, passionate mentor who I admire. You have provided me with a wealth of opportunities over the years for which I am very grateful.

Thank you to Øystein Varpe for all of your support, assistance and kindness. You have added many fresh perspectives to my research over the years and I greatly appreciate you always encouraging me to ask questions, think big and produce the best quality work I can. I am very grateful for all of your scientific input, advice and our discussions, through which you have taught me a lot.

Thank you to Józef Wiktor for sharing your incredible taxonomic knowledge with me. Your passion for protists is infectious and I feel very lucky to have gained the important skill of taxonomic identification through your guidance.

To Mark Tobin, Pimm Vongsvivut and Annaleise Klein, thank you for your ongoing support at the Australian Synchrotron. From the moment I arrived at the Synchrotron, wide-eyed and full of imposter syndrome, you have made me feel welcome on the IR Beamline. I am very appreciative of the time you have spent training me on the instrument and supporting our work. Thank you also to the wonderful team at AINSE, particularly Michael Rose and Michelle Durant, for your constant support of me and my research.

A special thank you to Vanessa Pitusi, my PhD partner in crime. I simply could not have done this PhD without you. Our field seasons were long and arduous, but they were the absolute time of my life, thanks to our partnership. I am so grateful for everything you have done for me (and it is a lot!), from your extremely hard work in the field, to keeping me laughing through the longest of days in the seawater lab. Thank you for being the best research partner and friend I could ever ask for.

Thank you to UNIS Svalbard, where I was a guest PhD student and spent many happy years – my home away from home! To the staff and students, particularly the UNIS Arctic Biology department, you have always made me feel so welcome and for that I will always be grateful. I have loved chatting about science, life, and sharing the Arctic with you all over the years. You are wonderful scientists and great friends – thank you for everything.

Thank you to Stuart Thomson, you have been an invaluable help during field work and in the lab throughout my time at UNIS. Your support, often out of hours, has been instrumental to me obtaining and analysing my samples. I have really enjoyed our time in the field, complete with candy and chocolate milk, and I am so appreciative of your assistance in getting my samples collected against the odds.

Thank you to Leni Runge, our field season in 2021 was a long and wild ride and it would not have been so wonderful without you. It took a huge effort to make that season happen and your involvement was critical to its success. Even on the long, cold days of sampling, snowmobiling and water filtering, you were enthusiastic and positive, and for that I will be forever grateful.

Thank you to all the amazing people that helped with my field work, particularly Stina Skånhoff, Sam Huset-Dwinnell, Einar Bergland, Audun Tholfsen and Elina Vadze. Each one of you has made a crucial contribution to my PhD research and we always had great fun in the field. I have learnt so much from all of you. Thank you also to Craig Hammock for your valuable assistance with qGIS to create figures using satellite imagery.

To my Svalbard family, particularly Vanessa, Stina, Sam, Kirsa, Markus, Kristin, Will, Veerle, Craig, Karlotta, Maria, Eivind, Margot, Cheshtaa, Victor, Robynne and Sheila. You are the unexpected friends who have turned into family. I deeply cherish all of the crazy times that we have spent together, and the relentless support you have provided me over the years. I have never laughed so hard, or been on such incredible adventures as I have with you all. You are amazing people and scientists, and it is a privilege to call you my friends. Our times together are certainly amongst the best days of my life.

A huge thank you to my parents, Julie and Garry. You have relentlessly supported my pursuit of my dreams, whatever they may be, and for that I will always be grateful beyond measure. Words cannot express how much you have done for me and how pivotal your support has been to my completion of my PhD. Thank you for instilling in me a love of nature and adventure, and nurturing in me a curiosity about the world. I am so glad you managed to visit me in Svalbard and witness the beauty of the Arctic for yourselves. A special thank you to my brother, Alex, your spirit of adventure and love of exploration has driven and inspired me more than you will ever know.

Finally, to my husband, Duncan. I couldn't have done this without you. Thank you for wholeheartedly supporting my long absences in the field and being so genuinely excited for me during this journey. Your positivity and enthusiasm for me following my dreams has been invaluable. I deeply appreciate all the scientific discussions we have had - you have listened to me talk about my research so often that sometimes I feel you might know more about it than I do. Your unconditional patience, support and love has made even the hardest days feel okay. Thank you for everything you do, and everything you are.

### **Funding Contributed to This Thesis:**

R.J. Duncan was supported by an Australian Government Research Training Program Scholarship and an AINSE Ltd. Postgraduate Research Award (PGRA) throughout the duration of her candidature. R.J. Duncan was a recipient of two AINSE Ltd. International Conference Scholarships (2021 and 2022), and an Antarctic Science Foundation (ASF) Traversing the COVID Gap grant (2022).

Sample collection in Svalbard during 2021 was supported by the Research Council of Norway through Arctic Field Grants awarded to R.J. Duncan (310664) and E. Runge (310692). Sample collection in Svalbard during 2022 was again supported by the Research Council of Norway through Arctic Field Grants, awarded to R.J. Duncan (33156) and V. Pitusi (350579). The samples obtained in Svalbard in 2021 and 2022 were imported to Australia under permit no. 0005032399.

Southern Ocean sample collection was conducted as part of Australian Antarctic Science Project (4026), awarded to A.T. Davidson. These samples were imported to Australia under permit no. IP13019928.

Analysis performed on the Infrared Microscopy (IRM) beamline at the Australian Synchrotron (ANSTO) was funded by the Australian Synchrotron through merit-based beamtime in 2015 (AS153/IRM/10005), 2021 (AS213/IRM/17447) and 2022 (AS222/IRM/18486).

Additional funding was supplied by the Australian Research Council (DP210101360), awarded to K. Petrou. Funding was also supplied by the Research Council of Norway through the ACCES (De-icing of Arctic Coasts: Critical or new opportunities for marine biodiversity and Ecosystem Services?) Project 296836, awarded to J. E. Søreide and through the 2017-2018 Belmont Forum and BiodivERsA joint call for research proposals, under the BiodivScen ERA-Net COFUND programme (296836), awarded to J. E. Søreide. Further funding was provided by the National Science Centre Poland (UMO-2015/17/B/NZ8/02473), awarded to J. E. Søreide.

## THESIS OVERVIEW

This thesis is presented as ‘thesis by compilation’ format, comprising of five data chapters. These data chapters are all in the form of a journal manuscript. At the time of final thesis submission, these chapters are all published (Chapters 2, 3, 4, 5, and 6).

### **Chapter 2:**

**Duncan, R. J., & Petrou, K. (2022).** Biomolecular composition of sea ice microalgae and its influence on marine biogeochemical cycling and carbon transfer through polar marine food webs. *Geosciences*, *12*(1), 38.

### **Chapter 3:**

**Duncan, R. J., Søreide, J. E., Varpe, Ø., Wiktor, J., Pitusi, V., Runge, E., & Petrou, K. (2024).** Spatio-temporal dynamics in microalgal communities in Arctic land-fast sea ice. *Progress in Oceanography*. *224*, 103248

### **Chapter 4:**

**Duncan, R. J., Nielsen, D., Søreide, J. E., Varpe, Ø., Tobin, M. J., Pitusi, V., Heraud, P., & Petrou, K. (2024).** Biomolecular profiles of Arctic Sea-ice diatoms highlight the role of under-ice light in cellular energy allocation. *ISME Communications*, *10*(4), 1.

### **Chapter 5:**

**Duncan, R. J., Søreide, J. E., Nielsen, D., Varpe, Ø., Wiktor, J., Tobin, M. J., Pitusi, V. & Petrou, K. (2024).** Seasonal environmental transitions and metabolic plasticity in a sea-ice alga from an individual cell perspective. *Scientific Reports*, *14*, 14984.

### **Chapter 6:**

**Duncan, R. J., Nielsen, D. A., Sheehan, C. E., Deppeler, S., Hancock, A. M., Schulz, K. G., Davidson, A. T., & Petrou, K. (2022).** Ocean acidification alters the nutritional value of Antarctic diatoms. *New Phytologist*, *233*(4), 1813-1827.

### **Other Publications During PhD Candidature:**

**Duncan, R.J.**, Andrew, M.E., Forchhammer, M.C., 2021, Snow mediates climatic impacts on Arctic herbivore populations, *Polar Biology* 44(7), 1251-1271.

Dance, M., **Duncan, R.J.**, Gevers, M., Honan, E.M., Runge, E., Schalamon, F.R., Walch, D.M.R\*, (2024), Coming in from the cold: addressing the challenges experienced by women conducting remote polar fieldwork, *PLOS Climate*, 3(6), e0000393. \*all authors contributed equally.

Fitzgerald-Lowry, B., Thompson, G., **Duncan, R. J.**, Nielsen, D., Theseira, A. & Petrou, K. (*in review*), Ocean shoaling under high pCO<sub>2</sub> in two diatoms reveals interaction between light and CO<sub>2</sub>, mediated by silicification, *Limnology & Oceanography*.

**Duncan, R. J.**, Søreide, J. E., Nielsen, D., Wiktor, J., Tobin, M. J., & Petrou, K. *in preparation*, Species-specific biomolecular adaptation in seven dominant sea ice algae taxa.

**Duncan, R. J.**, Søreide, J. E., Nielsen, D., Wiktor, J., Campbell, K., Varpe, Ø., Klein, A., & Petrou, K. *in preparation*, Predicting the nutritional value of sea ice microalgae in a 'new Arctic' regime with reduced land-fast ice cover and thinning drift ice.



*The Arctic does not yield its secrets for the price of a ship's ticket. You must live through the long night, the storms. You must have gazed on the deadness of all things to grasp their livingness. In the return of light, in the magic of the ice, in the life-rhythm of the animals observed in the wilderness, in the natural laws of all beings, revealed here in their completeness, lies the secret of the Arctic and the overpowering beauty of its lands"*

- Christiane Ritter (A Woman in the Polar Night)

*I am among those who think that science has great beauty.*

- Marie Curie

## TABLE OF CONTENTS

<b>CERTIFICATE OF ORIGINAL AUTHORSHIP .....</b>	<b>I</b>
<b>ACKNOWLEDGMENTS.....</b>	<b>II</b>
<b>THESIS OVERVIEW.....</b>	<b>VI</b>
<b>LIST OF TABLES .....</b>	<b>XII</b>
<b>LIST OF FIGURES .....</b>	<b>XVI</b>
<b>ABBREVIATIONS .....</b>	<b>XXIV</b>
<b>ABSTRACT .....</b>	<b>XXV</b>
<b>CHAPTER 1.....</b>	<b>1</b>
<b>GENERAL INTRODUCTION</b>	
1.1 THE POLAR OCEANS .....	1
1.2 ROLE OF MICROALGAE IN POLAR OCEANS.....	3
1.3 SEA ICE AS A HABITAT FOR MICROALGAE .....	5
1.4 THE SEASONAL CYCLE OF POLAR MICROALGAE IN ICE AND WATER.....	8
1.5 BIOMOLECULAR COMPOSITION OF MICROALGAE AND THE INFLUENCE ON FOOD WEBS .....	10
1.6. CLIMATE CHANGE DRIVEN ENVIRONMENTAL PERTURBATIONS AND POTENTIAL IMPLICATIONS FOR POLAR MICROALGAE .....	12
1.6.1 <i>Sea Ice</i> .....	13
1.6.2 <i>Snow Fall and Under-Ice Light</i> .....	15
1.6.3 <i>Warming Temperatures</i> .....	16
1.6.4 <i>Ocean Freshening</i> .....	17
1.6.5 <i>Ocean Acidification</i> .....	18
1.7 KNOWLEDGE GAPS.....	19
1.8 THESIS AIMS, OBJECTIVES AND OUTLINE .....	21
<b>CHAPTER 2.....</b>	<b>24</b>
<b>BIOMOLECULAR COMPOSITION OF SEA ICE MICROALGAE AND ITS INFLUENCE ON MARINE BIOGEOCHEMICAL CYCLING AND CARBON TRANSFER THROUGH POLAR MARINE FOOD WEBS</b>	
ABSTRACT .....	25
2.1 INTRODUCTION.....	25
2.2 BIOMOLECULAR COMPOSITION OF SEA-ICE ALGAE FROM POLAR REGIONS .....	30
2.3 MEASURING BIOCHEMICAL COMPOSITION IN MICROALGAE .....	35
2.4 ENVIRONMENTAL FACTORS THAT INFLUENCE BIOMOLECULAR COMPOSITION .....	40
2.4.1 <i>Temperature</i> .....	41
2.4.2 <i>Salinity</i> .....	41
2.4.3 <i>Light</i> .....	42
2.4.5 <i>Nutrient limitation</i> .....	43
2.4.6 <i>pH</i> .....	44
2.5 SEA-ICE MICROALGAE BIOCHEMISTRY AND CARBON TRANSFER THROUGH THE POLAR MARINE FOOD WEB WITH CLIMATE CHANGE .....	46
2.6 CONCLUSIONS .....	48
<b>CHAPTER 3.....</b>	<b>50</b>
<b>SPATIO-TEMPORAL DYNAMICS IN MICROALGAL COMMUNITIES IN ARCTIC LAND-FAST SEA ICE</b>	
ABSTRACT .....	51
INTRODUCTION .....	52
<i>Study Area</i> .....	54
MATERIALS & METHODS.....	55
<i>Sample Collection</i> .....	55
<i>Physical Parameters</i> .....	56
<i>Light Measurements and Modelling</i> .....	57

<i>Biological Parameters</i> .....	58
<i>Data Analyses</i> .....	59
RESULTS .....	60
<i>Physical Characteristics</i> .....	60
<i>Chlorophyll a, Carbon and Nitrogen</i> .....	61
<i>Under-ice Light Transmissivity</i> .....	64
<i>Species Composition</i> .....	65
<i>Influence of Light Transmissivity on Protist Community Composition</i> .....	67
<i>Relationships between Light Transmissivity and Community Diversity</i> .....	69
DISCUSSION .....	71
SUPPLEMENTARY INFORMATION .....	78
<b>CHAPTER 4.....</b>	<b>84</b>
<b>BIOMOLECULAR PROFILES OF ARCTIC SEA-ICE DIATOMS HIGHLIGHT THE ROLE OF UNDER-ICE LIGHT IN CELLULAR ENERGY ALLOCATION</b>	
ABSTRACT .....	85
INTRODUCTION .....	86
MATERIALS & METHODS .....	89
<i>Study Area</i> .....	89
<i>Sample Collection</i> .....	90
<i>Environmental Parameters</i> .....	91
<i>Species-specific Biomolecular Composition by FTIR</i> .....	92
<i>Data Analyses</i> .....	94
RESULTS .....	96
<i>Physical Parameters</i> .....	96
<i>Species-specific Biomolecular Composition</i> .....	98
DISCUSSION .....	102
SUPPLEMENTARY INFORMATION .....	109
<b>CHAPTER 5.....</b>	<b>116</b>
<b>SEASONAL ENVIRONMENTAL TRANSITIONS AND METABOLIC PLASTICITY IN A SEA-ICE ALGA FROM AN INDIVIDUAL CELL PERSPECTIVE</b>	
ABSTRACT .....	117
INTRODUCTION: .....	118
MATERIALS & METHODS .....	120
<i>Study Area</i> .....	120
<i>Sample Collection</i> .....	120
<i>Biological variables</i> .....	121
<i>Environmental Variables</i> .....	122
<i>Data analyses</i> .....	124
RESULTS .....	126
<i>Physical and Chemical Environment</i> .....	126
<i>Protist Community Composition</i> .....	130
<i>Biomolecular Composition</i> .....	130
<i>Fatty Acid Composition</i> .....	134
<i><math>\delta^{13}</math> and <math>\delta^{15}</math>N Stable Isotopes</i> .....	136
DISCUSSION .....	138
SUPPLEMENTARY INFORMATION: .....	144
<b>CHAPTER 6.....</b>	<b>145</b>
<b>OCEAN ACIDIFICATION ALTERS THE NUTRITIONAL VALUE OF ANTARCTIC DIATOMS</b>	
ABSTRACT .....	146
INTRODUCTION .....	147
MATERIALS AND METHODS .....	150
<i>Experimental Design and Mesocosm Set Up</i> .....	150
<i>Macronutrient Analyses</i> .....	151
<i>Diatom Community Structure</i> .....	151
<i>Cell Volume and Photophysiological Status</i> .....	152

<i>Species-specific Macromolecular Content by FTIR</i> .....	152
<i>Data Analyses</i> .....	153
RESULTS.....	155
<i>Chemistry, Cell Density and Photophysiology</i> .....	155
<i>Cell Specific Macromolecular Partitioning</i> .....	155
<i>Lipid vs. Protein Content</i> .....	159
<i>Cell Volume vs. Lipid and Protein Content</i> .....	162
DISCUSSION.....	163
SUPPLEMENTARY INFORMATION.....	172
<b>CHAPTER 7: .....</b>	<b>179</b>
<b>SYNTHESIS OF RESULTS, FUTURE DIRECTIONS AND CONCLUSIONS</b>	
UNDER-ICE LIGHT STRONGLY INFLUENCES SEA-ICE MICROALGAL COMMUNITY COMPOSITION: .....	181
ENVIRONMENTAL CONDITIONS DETERMINE BIOMOLECULAR CONTENT OF SEA-ICE MICROALGAE	
EXPOSING SPECIES SPECIFIC METABOLIC PLASTICITY.....	185
FUTURE DIRECTIONS.....	190
<i>Cellular Level Changes</i> .....	190
<i>Trophic-level Changes and Alterations to Food Web Dynamics</i> .....	191
<i>Broad Temporal and Spatial Scales, and Effects of Multi-Drivers</i> .....	194
CONCLUDING REMARKS.....	195
<b>REFERENCES: .....</b>	<b>196</b>
<b>APPENDIX: .....</b>	<b>232</b>

## LIST OF TABLES

**Table 2.1:** Compilation of studies that have measured biomolecules in sea-ice microalgae in the Arctic and Antarctic. N/A: Sampling date not available.

**Table 2.2:** Summary of the various analytical techniques that have been used to measure biomolecules (proteins and amino acids, lipids and fatty acids, carbohydrates and polysaccharides) in sea-ice microalgae, their advantages, and disadvantages.

**Table 3.1:** Parameters measured associated with sea-ice core extraction; snow depth ( $\pm$  SD,  $n = 18$ ), ice thickness ( $\pm$  SD,  $n = 6$ ), and within the bottom 3 cm of sea-ice core; salinity (ppt), brine salinity (ppt), brine volume (% of ice volume), chlorophyll *a* concentration ( $\text{mg m}^{-2}$ ) ( $n = 3$ ), daylight hours at time of sampling, carbon:nitrogen (C:N) molar ratio, carbon isotope ratio ( $\delta^{13}\text{CVPDB}$  (‰)) and nitrogen isotope ratio ( $\delta^{15}\text{NAir}$  (‰)). ND represents measurement not taken.

**Supplementary Table S3.1:** Sampling locations including fjord, site name, location coordinates (latitude, longitude) and dates sampled.

**Supplementary Table S3.2:** Comparison of irradiance measurements ( $\mu\text{mol photons m}^{-2}\text{s}^{-1}$ ) taken in situ using Li-COR under and above the ice and modelled irradiance measurements, including conversion to percent (%) incoming PAR values.

**Supplementary Table S3.3:** Physical, chemical, and biological variables measured in under-ice water (0.5 m below ice) at each sampling site and date including ammonium, silicic acid, nitrate and phosphate concentrations ( $\mu\text{M}$ ), chlorophyll *a* concentration ( $\text{mg m}^{-3}$ ), water temperature  $^{\circ}\text{C}$ , water salinity (ppt), C:N molar ratios and bottom depth (m) of the sampling site. NA represents data not available.

**Supplementary Table S3.4:** Relative percentage (%) contribution of species to the bottom ice algae community at each sampling site and date.

**Supplementary Table S3.5:** Counts per mL per species present in the bottom ice algae community at each sampling site and date.

**Supplementary Table S3.6:** Statistical output of the regression models of taxa group and Log10 percent (%) incoming PAR. Multiple  $R^2$ , adjusted  $R^2$  Log10,  $F$  statistic, associated degrees of freedom (DF) p-value model. Statistically significant p-values ( $< 0.05$ ) are marked in bold.

**Table 4.1:** Infrared (IR) band assignments for s-FTIR microspectroscopy used in this study.

**Table 4.2:** Parameters measured associated with sea-ice core extraction; snow depth ( $\pm$  SD,  $n = 18$ ), ice thickness ( $\pm$  SD,  $n = 6$ ), % incoming PAR and under ice light ( $\mu\text{mol m}^{-2}\text{s}^{-1}$ ). Measurements from within the bottom 3 cm of sea-ice core; temperature ( $^{\circ}\text{C}$ ), salinity (ppt), brine salinity (ppt), brine volume (% of ice volume), chlorophyll *a* concentration ( $\text{mg m}^{-2}$ ) ( $n = 3$ ), particulate organic carbon (POC) to particulate organic nitrogen (PON) molar ratio (C:N). Parameters measured in under-ice water at each sampling site; ammonium ( $\text{NH}_4$ ), silicic acid ( $\text{Si}(\text{OH})_4$ ), nitrate ( $\text{NO}_3$ ) and phosphate ( $\text{PO}_4$ ) concentrations ( $\mu\text{M}$ ) and temperature ( $^{\circ}\text{C}$ ), where N.D. denotes not measured.

**Supplementary Table S4.1:** Location and dates of sampling events, with longitude and latitude provided in decimal degrees.

**Supplementary Table S4.2:** Approximate cell length and width of the five taxa analysed.

**Supplementary Table S4.3:** Number of cells measured via synchrotron-based Fourier transform infrared microspectroscopy (s-FTIR) per site, per taxa.

**Supplementary Table S4.4:** Output of Spearman's rank correlation coefficient ( $\rho$  (rho) and associated p-values) between environmental variables (% incoming photosynthetically active radiation (PAR), nitrite + nitrate ( $\text{NO}_3^- + \text{NO}_2^-$ ) ( $\text{NO}_x$ ) concentration in the water at ice-water interface, silicic acid ( $\text{Si}(\text{OH})_4$ ) concentration in the water at ice-water interface, ice temperature ( $^{\circ}\text{C}$ ), under ice water temperature ( $^{\circ}\text{C}$ ) and bulk ice salinity ( $^{\circ}\text{C}$ ) and biomolecular content (based on mean of each of the five taxa, per each set of pooled cores (total  $n = 86$ )). Statistically significant p-values ( $< 0.05$ ) and  $R^2$  exceeding 0.5 or -0.5 are marked in bold. Mean ( $\bar{x}$ )  $\pm$  standard deviation ( $\sigma$ ) for each environmental variable is provided in brackets.

**Supplementary Table S4.5:** Statistical output of the species-specific regression models for each biomolecular compound vs. under-ice light. Multiple  $R^2$ , adjusted  $R^2$ , F statistic, associated degrees of freedom (DF) and p-value, Spearman's rank correlation coefficient and associated p-value. Statistically significant p-values ( $< 0.05$ ) are marked in bold.

**Supplementary Table S4.6:** Statistical output of the biomolecular regression models. Multiple  $R^2$ , adjusted  $R^2$ , F statistic, associated degrees of freedom (DF) and p-value. Statistically significant p-values ( $< 0.05$ ) are marked in bold. The low light transmissivity sites include VM-1, VM-2 and VM-3 and the high light transmissivity sites include VM-4, VM-5 and TF-2.

**Table 5.1:** Infrared (IR) band assignments for s-FTIR microspectroscopy used in this study.

**Table 5.2:** Parameters measured associated with sea-ice core extraction (white) and under-ice water (grey); snow depth ( $\pm$  SD,  $n = 18$ ), albedo (%) ice thickness ( $\pm$  SD,  $n = 6$ ), temperature ( $^{\circ}\text{C}$ ), bulk ice salinity (ppt), brine salinity (ppt), brine volume (% of ice volume), chlorophyll *a* concentration (ice:  $\text{mg m}^{-2}$ ,  $n = 3$  and water:  $\text{mg/m}^3$ ), particulate organic carbon (POC) to particulate organic nitrogen (PON) molar ratio (C:N), stable isotope of carbon  $\delta^{13}\text{C}_{\text{VPDB}}$  (‰), stable isotope of nitrogen  $\delta^{15}\text{N}_{\text{VPDB}}$  (‰), silicic acid ( $\text{Si}(\text{OH})_4$ ), nitrate + nitrite ( $\text{NO}_x$ ) and phosphate ( $\text{PO}_4$ ) concentrations ( $\mu\text{M}$ ) and average water temperature at the ice-water interface ( $^{\circ}\text{C}$ ).

**Table 5.3:** Fatty acid (FA) composition of the entire sea-ice algae community at the inner and outer site of Van Mijenfjorden, Svalbard on the 12<sup>th</sup> May and 13<sup>th</sup> May 2022, respectively, as % total FA displayed (with SUM % total lipid dry matter (DM) displayed in brackets), for 6 ice cores pooled. FAs accounting for  $<0.1\%$  of total in both sites are not displayed. FA: Fatty acids, PUFA: polyunsaturated fatty acids; MUFA: monounsaturated fatty acids; SAFA: saturated fatty acids, EPA: eicosapentaenoic acid and DHA: docosahexaenoic acid.

**Supplementary Table S5.1:** Number of *Nitzschia frigida* cells measured per site, per date.

**Supplementary Table S5.2:** Statistical output from regression models of *Nitzschia frigida* biomolecular content with time. Multiple  $R^2$ , adjusted  $R^2$ , F statistic, associated degrees of freedom (DF) and p-value. Statistically significant p-values ( $< 0.05$ ) are marked in bold.

**Table 6.1:** Infrared (IR) band assignments for s-FTIR microspectroscopy used in this study.

**Supplementary Table S6.1:** Summary of initial seawater (T0) conditions (italicised) and mesocosm conditions on day 18. Fugacity of carbon dioxide ( $f\text{CO}_2$ ), nitrogen ( $\text{NH}_4$  and  $\text{NO}_x$ ), soluble reactive phosphorous (SRP) silica, dissolved inorganic carbon (DIC), total pH (pHT), practical alkalinity (PA), salinity and temperature, across the six mesocosms. Where measurements were below detection limits, it is marked as not detected (ND). Full physiochemical parameters can be found in Deppeler et al., (2018).

**Supplementary Table S6.2:** Summary of number of cells, per taxa, per mesocosm, measured for species-specific macromolecular content using FTIR-microspectroscopy. For each, the total number of cells measured ( $n$ ) and the mean number of cells measured across all taxa per mesocosm is supplied. For Mesocosm 5 (M5), *Fragilariopsis cylindrus* was not analysed.

**Supplementary Table S6.3:** Cell density and community photosynthetic efficiency on day 18. Cell density of selected diatoms (cells/L-1), total cell density of whole phytoplankton community and % diatoms of whole phytoplankton community, across the 6 mesocosms. Maximum quantum yield of PSII (FV/FM)  $\pm$  the standard deviation (SD) of three pseudo-triplicated measurements taken from each of the six mesocosms on day 18.

**Supplementary Table S6.4:** Mean cell volume ( $\mu\text{m}^3$ ) on day 18 for taxa from Mesocosms 1 (M1) and Mesocosm 6 (M6). For each taxa, per mesocosm, the mean cell volume, standard deviation (SD), number of cells analysed (n) and difference between mean in M1 and M6  $\pm$  standard deviation (SD) is supplied.

**Supplementary Table S6.5:** Statistical output of the species-specific regression models (Figures 6.1-6.5). Multiple  $R^2$ , adjusted  $R^2$ , F statistic, associated degrees of freedom (DF) p-value and equation of regression model. Statistically significant p-values ( $< 0.05$ ) are marked in bold.

**Supplementary Table S6.6:** Statistical output of the lipid (ester carbonyl) to protein (amide II) ratios models (Figure 6.6). Multiple  $R^2$ , adjusted  $R^2$ , F statistic, associated degrees of freedom (DF), p-value and equation of regression model. Statistically significant p-values ( $< 0.05$ ) are marked in bold.

**Supplementary Table S6.7:** Data corresponding to cell volume ( $\mu\text{m}^3$ ) and protein (amide II) or lipid (ester carbonyl) content; for diatoms in the low  $f\text{CO}_2$  treatment (288  $\mu\text{atm}$ ) in Mesocosm 1 (M1) and high  $f\text{CO}_2$  treatment (1263  $\mu\text{atm}$ ) in Mesocosm 6 (M6). For all taxa investigated, the mean, standard deviation (SD), total number of cells analysed (n) and standard error (SE) are supplied.

**Supplementary Table S6.8:** Statistical output of the cell volume ( $\mu\text{m}^3$ ) and protein (amide II) or lipid (ester carbonyl) content models (Figure 6.7). Multiple  $R^2$ , adjusted  $R^2$ , F statistic, associated degrees of freedom (DF), p-value and equation of regression model. Statistically significant p-values ( $< 0.05$ ) are marked in bold.



## LIST OF FIGURES

**Figure 1.1:** Surface chlorophyll *a* concentration ( $\text{mg m}^{-3}$ ) in the Arctic (left) and Antarctic (right) during summer (July and January, respectively) of 2023. Maps were generated using QGIS, and include monthly binned AQUA MODIS level 3 mapped chlorophyll data, obtained from NASA (2024).

**Figure 1.2:** Conceptual diagram demonstrating the annual cycles within the seasonal sea-ice environment, of sea-ice cover (grey) and open water (blue), sympagic (sea-ice associated) productivity (light brown) and pelagic (open-water associated) productivity (green), demonstrating that the peaks of sympagic and pelagic productivity occur asynchronously. Daylight hours are indicated in the background with dark blue representing constant night and light blue representing constant daylight. The seasons are denoted within the grey stipple line boxes, with the relevant months given for the Arctic (top) and Antarctic (bottom).

**Figure 1.3:** Illustration of the frozen matrix at the ice-water interface from a side view (top left) demonstrating the penetration of brine channels from the interface into the columnar ice, and from a close-up view (bottom left) illustrating how microalgae inhabit the channels. EPS: Exopolysaccharides. A schematic of the seasonal progression of sympagic and pelagic microalgae is provided (right) in which there is limited productivity in the dark winter, followed by sympagic blooms supporting zooplankton reproduction in the spring before being released to the pelagic and benthic zones, followed by pelagic blooms supporting zooplankton juvenile feeding once the ice has melted in the summer.

**Figure 1.4:** Overview of the key climate change driven environmental changes affecting polar microalgae. Some of the main drivers are provided in roman text and the major environmental changes are given in bold text.

**Figure 1.5:** The Arctic (left) and Southern (right) Oceans, including ocean floor depth, indicated through colour gradient. Approximate minimum sea-ice extent (SIE) is given for 1979 (light pink) and 2023 (dark pink). Maps generated in R Studio (v. 2023.09.0463) using ggOceanMaps (v.2.1.1). Sea ice extents are adapted from National Snow and Ice Data Center sea ice extent data (NSIDC, 2023).

**Figure 1.6:** Conceptual figure of albedo (the fraction of incoming light that is reflected) of different surfaces. Incoming light is denoted in yellow, with the approximate percentage of reflected light denoted in red, and approximate percentage of light transmitted to the ocean denoted in blue. The grey arrows (bottom) denote that albedo is

highest for fresh snow and lowest for open water, and that the amount of incoming light transmitted to the water increases, as albedo decreases.

**Figure 2.1:** Sea-ice zones in both polar regions. Stippled lines indicate the maximum (SI-Max) and minimum (SI-Min) extent of sea ice in the Arctic (top left) and Southern Ocean (top right). Black open circles indicate the poles. Schematic of the spatial and temporal evolution and decay of sea ice in polar marine ecosystems. Arrows indicate seasonal changes in salinity from brine extrusion and freshwater melt, as well as light attenuation, solar angle, and mixing depth. The entrainment of microalgae into the sea ice as it forms, its proliferation and re-release into the water column during melt is also shown.  $I_0$  = percent incident irradiance.

**Figure 2.2:** Schematic showing the direction of change (increase or decrease) in biomolecules in sea-ice microalgae exposed to variations in (A) temperature, (B) salinity, (C) irradiance, (D) nitrogen concentration, (E)  $p\text{CO}_2$ . Changes are not indicative of magnitude. The different biomolecules are coded by colour and line type as described in the legend. Shaded areas indicate where results from studies have revealed both a change and no change with environmental perturbation. Data were obtained from the studies listed in Table 2.1.

**Figure 3.1:** Land-fast sea ice sampling locations visited between April–May 2021, within various fjords of Svalbard, Norway.

**Figure 3.2:** Bottom ice microalgal community composition from low light transmissivity (left) and high light transmissivity (right) sites sampled during April 2021, in Svalbard, Norway. Snow depth (grey), ice thickness (blue), and chlorophyll *a* concentration ( $\text{mg m}^{-2}$ ) (green circles) are displayed in the upper panels  $\pm$  SD ( $n = 18$ ,  $n = 6$  and  $n = 3$ , respectively), relative abundance (%) of taxonomic groups are shown in the lower panels.

**Figure 3.3:** Bottom ice microalgal community composition from low light transmissivity (left) and high light transmissivity (right) sites sampled during May 2021, in Svalbard, Norway. Snow depth (grey), ice thickness (blue), and chlorophyll *a* concentration ( $\text{mg m}^{-2}$ ) (green circles) are displayed in the upper panels  $\pm$  SD ( $n = 18$ ,  $n = 6$  and  $n = 3$ , respectively), relative abundance (%) of taxonomic groups are shown in the lower panels.

**Figure 3.4:** Non-metric multidimensional scaling (nMDS) of microalgal communities for (A) April and (B) May, based on resemblance using Bray-Curtis similarity. Sample sites are shown by colour and dates by shape. The 2D stress is shown in the lower left.

**Figure 3.5:** Significant relationships for species-specific relative contribution to community composition vs. Log<sub>10</sub> percent (%) incoming PAR during April and May,

(A) *Nitzschia frigida*, (B) *Gymnodinium* spp., (C) Colony forming *Navicula* spp., (D) Dinophyceae and (E) *Thalassiosira* spp. Data are fitted using linear regression with 95% confidence intervals (shading).

**Figure 3.6:** (A) Correlation matrix of the relative abundance of main taxonomic groups found throughout April and May 2021, in Svalbard, Norway. The strength of the positive (blue) and negative (red) correlations is displayed according to dot size. (B) Redundancy analysis (RDA) biplot of the relative abundance of taxonomic groups with environmental variables. Only significant vectors are shown.

**Figure 3.7:** Spatial and temporal microalgal diversity dynamics (A) in relation to Log10 percent (%) incoming PAR for all data and (B) as a function of time for the outermost (VM-5) (light blue) and innermost (VM-1) (dark blue) sites within Van Mijenfjorden. Data are fitted using linear regression with 95% confidence intervals (shading). The outlier on 27<sup>th</sup> April has been excluded from the regression within the VM-1 site data.

**Figure 4.1:** Conceptual model of the synchrotron infrared light source measuring and the biomolecules within an individual cell, and the corresponding wavelengths on the infrared (IR) spectrum (second derivative transformed) (bottom), in which the coloured sections represent the peak area of the biomolecules studied. A simplified overview of the transfer of these biomolecules up the polar marine food chain is displayed (right).

**Figure 4.2:** Location of Svalbard, Norway, within the Arctic (left), sampling locations visited between April-May 2021 in Svalbard (middle), overview of the snow depth, sea-ice thickness, and under-ice light at each of the sampling stations (right).

**Figure 4.3:** Smoothed and normalised spectra of each of the five taxa, (A) *Entomoneis* spp., (B) *Haslea* spp., (C) *Navicula* spp., (D) *N. frigida*, (E) *Pleurosigma* spp., with each site denoted in colour. Images of example cells of each taxa (right) with blue dots denoting the S-FTIR measurement points (where the aperture (actual measuring area) for each point was larger than the point indicated), demonstrating the entire cell contents were measured.

**Figure 4.4:** Mean cell-specific biomolecular content (based on normalised peak areas – see Table 4.1) for photosynthetically derived (energy-rich, storage) biomolecules (unsaturated fatty acids, saturated fatty acids, saturated lipid, lipid (ester carbonyl), lipid (CH-stretch II) and carbohydrate) (A) *Entomoneis* spp., (B) *Haslea* spp., (C) *Navicula* spp., (D) *N. frigida*, (E) *Pleurosigma* spp., and functional (structural and cell function) biomolecules (protein (amide II), carboxylated molecules, phosphorylated molecules), (F) *Entomoneis* spp., (G) *Haslea* spp., (H) *Navicula* spp., (I) *N. frigida*, (J) *Pleurosigma*

spp. as a function of the proportion of light reaching the ice-water interface. Coloured shading indicates 95% confidence intervals, applied to log-transformed data.

**Figure 4.5:** (A) Correlation plot based on Spearman's rank correlation coefficient for biomolecular content across all taxa and sampling sites where dark blue represents a strong positive correlation and dark red represents a strong negative correlation. (B) Principal component analysis (PCA) of biomolecular content at each under-ice light level for all taxa combined (*Entomoneis* spp., *Haslea* spp., *Navicula* spp., *N. frigida*, and *Pleurosigma* spp.). Direction and strength of individual biomolecules are displayed with an ordination bi-plot overlay.

**Figure 4.6:** (A) Lipid (ester carbonyl) vs. Carbohydrate content, (B) Lipid (ester carbonyl) vs. Protein (amide II) content and (C) Carbohydrate vs Protein content, based on normalised peak areas, for all taxa combined and data are divided into HLT sites (VM-4, VM-5, TF-2) and LLT sites (VM-1, VM-2, VM-3), with light levels indicated with colour fill and taxa are denoted by shape. The data are fitted with linear regressions, with 95% confidence intervals (coloured shading), applied to log-transformed data. Only statistically significant regressions are shown.

**Figure 4.7:** Silica content (based on normalised peak areas) with increasing % photosynthetically active radiation (PAR) reaching the ice-water interface, per taxa. Each data point represents one measured cell. The data are fitted with linear regressions, with 95% confidence intervals (coloured shading), applied to log-transformed data. Only statistically significant regressions are shown.

**Supplementary Figure S4.1:** Lipid (ester carbonyl) to protein (amide II) ratios (top) and carbohydrate to protein (amide II) ratios (bottom) for (A, F) *Entomoneis* spp., (B, G) *Haslea* spp., (C, H) *Navicula* spp., (D, I) *Nitzschia frigida* and (E, J) *Pleurosigma* spp. All data are log(10) transformed and each data point represents a cell. % incoming PAR levels are represented by colour.

**Figure 5.1:** Location of sampling sites (A) visited between April-May 2022; inner site – blue dot and outer site – green dot, in Van Mijenfjorden, within Svalbard, Norway (inset box). Photographs of bottom ice cores collected from the inner and outer sites on the 12.5.22 and 13.5.22 respectively, demonstrate more heterogeneity and lumping of biomass at the outer site (B). Snow depth (cm)  $\pm$  SD (grey bars), sea-ice thickness (cm)  $\pm$  SD (blue bars) and photosynthetically active radiation (PAR) ( $\mu\text{mol photons m}^{-2}\text{s}^{-1}$ ), measured by the light sensor (LI-193 Spherical Quantum Sensor; Li-COR) deployed under the ice throughout the season (yellow line). (C) Under-ice water temperature (black

line) as measured by the temperature sensor (RBR $_{solo}^3$  T) deployed alongside the light sensor, solid line indicates average temperature (blue). **(D)** Nutrients and chlorophyll *a* concentration are displayed (bottom panel), including nitrate (light pink), phosphate (medium pink), silicic acid (dark pink) and chlorophyll *a* concentration (green) in the sea ice (solid line) and under-ice water (dashed line), on all sampling dates at the outer site (left) and inner site (right).

**Figure 5.2:** Bottom ice microalgal community composition from outer site (left) and inner site (right) sampled during April–May 2022, in Van Mijenfjorden, Svalbard, Norway. Raw counts of *Nitzschia frigida* cells per mL are displayed in the top panels, and the relative abundance (%) of taxonomic groups are shown in the lower panels. *Nitzschia* spp. includes all *Nitzschia* species identified with the exception of *Nitzschia frigida*. Rare Taxa includes: *Hantzchia* spp., *Diploneis littoralis*, *Stenoneis inconspicua*, *Pinnularia quadratarea*, *Plagiotropis* spp. *Manguinea rigida*, *Tropidoneis* spp.

**Figure 5.3:** Smoothed and normalised 2<sup>nd</sup> derivative spectra for *Nitzschia frigida* at the **(A)** outer and **(B)** inner site with each sampling week denoted by colour gradient. Dashed vertical lines indicate respective wavenumber for peaks of interest. Principal component analysis (PCA) of biomolecular content at the **(C)** outer and **(D)** inner site with sampling week denoted by colour, in which each dot represents the measurements of one cell. Direction and strength of individual biomolecules are displayed with an ordination bi-plot overlay.

**Figure 5.4:** Biomolecular content based on normalised peak areas of specific biomolecules, for *Nitzschia frigida* per sampling week for the outer **(A-D)** and inner site **(E-H)**; specifically **(A, E)** Carbohydrate **(B, F)** Lipid (ester carbonyl), **(C, G)** Protein (amide II) and **(D, H)** Silica content. Data are presented as violin plots where coloured shading indicates SE and yellow triangle represents the mean, individual cells are shown by transparent dots. Site location is represented with colour; outer site (green; top panels) and inner site (blue; bottom panels). Redundancy analysis (RDA) biplot (I) of the mean biomolecular content (divided into functional biomolecules and photosynthetically derived biomolecules, denoted by colour) from each sampling site and date with environmental variables displayed with ordination bi-plot overlay. Only significant vectors are shown and RDA model is significant ( $p < 0.05$ ).

**Figure 5.5:** Fatty acid (FA) content as % total lipid content of the whole bottom ice community at the outer and inner site **(A)**, during week 6. The different FA types, monounsaturated fatty acid (MUFA), polyunsaturated fatty acid (PUFA) and saturated

fatty acid (SAFA) per site, are denoted by colour. Site-specific FA content as a proportion of total FA are presented in pie charts (right). Cell-specific SAFA vs. unsaturated fatty acid (USFA) content of *Nitzschia frigida*, as determined by s-FTIR (**B**), with site denoted by colour. The ratio of SAFA:USFA content per cell is displayed (inset), as a boxplot with yellow triangles representing the mean.

**Figure 5.6:**  $\delta^{15}\text{N}$  (light grey square),  $\delta^{13}\text{C}$  (dark grey square) and chlorophyll *a* concentration (green star) from the bottom-ice (solid line) and water directly below the ice (stippled line) at the (**A**) outer site and (**B**) inner site, across all sampling weeks. Redundancy analysis (RDA) biplot (**C**) of the mean biomolecular content of *Nitzschia frigida* cells from each sampling site and time point with  $\delta^{13}\text{C}$  and  $\delta^{15}\text{N}$  stable isotope values from the sea ice and water below displayed with ordination bi-plot overlay, only significant vectors are shown and RDA model is significant ( $p < 0.05$ ). (**D**) Content of lipid (ester carbonyl; top panel) and protein (amide II) (bottom panel) vs.  $\delta^{13}\text{C}$  values, at the outer site (green) and inner site (blue). The data (both locations combined) are fitted with linear regressions, with 95% confidence intervals (coloured shading).

**Figure 6.1:** Cell specific macromolecular content (based on normalised peak areas) and growth rates for *Chaetoceros* spp. (**A-F**) Relative content of selected macromolecules along an  $f\text{CO}_2$  gradient. Data are visualised using box plots with overlain grey dots showing the macromolecular content of individual cells from within  $f\text{CO}_2$  treatment mesocosm. Data are fitted with a second order polynomial regression, with 95% confidence intervals (dark blue shading), applied to log transformed data (\*  $p < 0.05$ , \*\*\*  $p < 0.0005$ ). The y-axis is free and units are arbitrary. Data means are displayed as blue triangles. (**F**) Growth rate ( $\text{d}^{-1}$ ) is displayed as diamonds, fitted with a second order polynomial regression (grey line).

**Figure 6.2:** Cell specific macromolecular content (based on normalised peak areas) and growth rates for *Fragilariopsis cylindrus* (**A-F**). Relative content of selected macromolecules along an  $f\text{CO}_2$  gradient. Data are visualised using box plots with overlain grey dots showing the macromolecular content of individual cells from within  $f\text{CO}_2$  treatment mesocosm. Data are fitted with a second order polynomial regression, with 95% confidence intervals (dark blue shading), applied to log transformed data (\*\*  $p < 0.005$ , \*\*\*  $p < 0.0005$ ). The y-axis is free and units are arbitrary. Data means are displayed as blue triangles. (f) Growth rate ( $\text{d}^{-1}$ ) is displayed as diamonds, fitted with a second order polynomial regression (grey line).

**Figure 6.3:** Cell specific macromolecular content (based on normalised peak areas) and growth rates for *Proboscia truncata* (A-F). Relative content of selected macromolecules along an  $f\text{CO}_2$  gradient. Data are visualised using box plots with overlain grey dots showing the macromolecular content of individual cells from within  $f\text{CO}_2$  treatment mesocosm. Data are fitted with a linear or a second order polynomial regression, with 95% confidence intervals (dark blue shading), applied to log transformed data (\*  $p < 0.05$ , \*\*  $p < 0.005$ , \*\*\*  $p < 0.0005$ ). The y-axis is free and units are arbitrary. Data means are displayed as blue triangles. (F) Growth rate ( $\text{d}^{-1}$ ) is displayed as diamonds, fitted with linear regression (grey line).

**Figure 6.4:** Cell specific macromolecular content (based on normalised peak areas) and growth rates for *Stellarima microtrias* (A-F). Relative content of selected macromolecules along an  $f\text{CO}_2$  gradient. Data are visualised using box plots with overlain grey dots showing the macromolecular content of individual cells from within  $f\text{CO}_2$  treatment mesocosm. Data are fitted with linear regression, with 95% confidence intervals (dark blue shading), applied to log transformed data (\*  $p < 0.05$ , \*\*  $p < 0.005$ , \*\*\*  $p < 0.0005$ ). The y-axis is free and units are arbitrary. Data means are displayed as blue triangles. (F) Growth rate ( $\text{d}^{-1}$ ) is displayed as diamonds, fitted with linear regression (grey line).

**Figure 6.5:** Cell specific macromolecular content (based on normalised peak areas) and growth rates for Discoid centric diatoms  $>20 \mu\text{M}$ . Relative content of selected macromolecules along an  $f\text{CO}_2$  gradient. Data are visualised using box plots with overlain grey dots showing the macromolecular content of individual cells from within  $f\text{CO}_2$  treatment mesocosm. Data are fitted with linear or second order polynomial regression, with 95% confidence intervals (dark blue shading), applied to log transformed data (\*  $p < 0.05$ , \*\*\*  $p < 0.0005$ ). The y-axis is free and units are arbitrary. Data means are displayed as blue triangles. (F) Growth rate ( $\text{d}^{-1}$ ) is displayed as diamonds, fitted with linear regression (grey line).

**Figure 6.6:** Lipid (ester carbonyl) to protein (amide II) ratios for (A) *Chaetoceros* spp., (B) *Fragilariopsis cylindrus*, (C) *Proboscia truncata*, (D) *Stellarima microtrias* and (E) Discoid centric diatoms  $>20 \mu\text{M}$ . All data are  $\log(10)$  transformed.  $f\text{CO}_2$  ( $\mu\text{atm}$ ) levels are represented by colour. Data are fitted with linear regression, with 95% confidence intervals (blue shading).

**Figure 6.7:** Cell volume ( $\mu\text{m}^3$ ) and protein (amide II) or lipid (ester carbonyl) content;

(A) – (B) for diatoms in the low  $f\text{CO}_2$  treatment (288  $\mu\text{atm}$ ) and (C) – (D) high  $f\text{CO}_2$  treatment (1263  $\mu\text{atm}$ ). Data have been  $\log(10)$  transformed and fitted with linear or a second order polynomial regression with 95% confidence intervals (shading). The data represent mean  $\pm$  SD ( $n > 19$ ), with all regressions applied to the mean.

**Figure 6.8:** Summary of measured changes to diatoms under high  $f\text{CO}_2$  and expected ecological implications. (A) Projected increase in  $\text{CO}_2$  by the end of next century (2200) results in a shift in dominance towards smaller diatom species with increased lipid and protein content, but reduced silicification, while larger diatoms become scarce with lower lipid content and reduced silica content. (B) These changes alter food quality and availability for large zooplankton species such as krill and large copepods, affecting zooplankton growth and fecundity. A reduction in large diatoms and large zooplankton grazing would likely reduce carbon and silica export efficiency and alter energy transfer through to higher trophic organisms. Lowered silica production may alleviate some of this loss by increasing grazing on the abundant lipid and protein rich small diatoms by smaller zooplankton. Smaller cells and high grazing rates by smaller zooplankton would likely increase microbial loop activity and nutrient recycling in surface waters. Solid lines represent measured changes to relative protein (P) and lipid (L) content, while stippled lines represent the measured decline in silicification (Si) in the same diatoms from a parallel study (Petrou et al., 2019).



## **ABBREVIATIONS**

**AA** – Amino Acids  
**AO** – Arctic Ocean  
**DHA** – Docosaehaenoic acid  
**EPA** – Eicosapentaenoic acid  
**EPS** – Exopolysaccharides  
**DIC** – Dissolved Inorganic Carbon  
**FA** – Fatty Acid  
**FSW** – Filtered Sea Water  
**FTIR** – Fourier Transform InfraRed  
**FYI** – First Year Ice  
**IRM** – InfraRed Microscope  
**HLT** – High Light Transmissivity  
**LLT** – Low Light Transmissivity  
**MUFA** – Monounsaturated Fatty Acid  
**nMDS** – non-Metric Multidimensional Scaling  
**OA** – Ocean Acidification  
**PA** – Practical Alkalinity  
**PAR** – Photosynthetically Available Radiation  
**PCA** – Principal Component Analysis  
**PUFA** – Polyunsaturated Fatty Acid  
**POC:PON** – Particulate Organic Carbon:Particulate Organic Nitrogen  
**RCP** – Representative Concentration Pathway  
**RDA** – Redundancy Analysis  
**RPM** – Rotations Per Minute  
**SAFA** – Saturated Fatty Acid  
**SNV** – Standard Normal Variate  
**SO** – Southern Ocean  
**SRP** – Soluble Reactive Phosphorus  
**SST** – Sea Surface Temperature  
**WSC** – West Spitsbergen Current

## ABSTRACT

The Arctic and Southern oceans are some of the most rapidly changing environments on the planet. At the base of the productive polar marine food webs are phytoplankton and sea-ice algae. Together, the pulsed production of spring bottom-ice blooms and summer open-water blooms are responsible for structuring ocean biogeochemical dynamics and supplying energy to marine biota. The nutritional value of microalgae depends on the community composition, and individual cellular biomolecular content (i.e. storage of proteins, lipids, fatty acids, carbohydrates). However, climate change driven environmental perturbations, including decreasing sea-ice extent and ocean acidification, are expected to alter microalgal carbon allocation and community structure, inevitably having cascading effects on the entire marine ecosystem.

Detecting the ecological consequences of environmental change on species' nutritional quality requires disentangling community responses from taxon-specific effects. Such high-resolution insight can best be achieved by investigating marine microalgae metabolisms, one cell at a time. Using synchrotron-based Fourier transform microspectroscopy (s-FTIR) on natural microalgal communities from Arctic sea ice and Southern Ocean waters, this thesis explores the metabolic plasticity of polar microalgae at a single-cell level, elucidating how key taxa are likely to alter their biomolecular content under environmental perturbations. These cell-specific analyses provide a resolution rarely seen, but critically needed, in ecological studies.

Our findings show that the nutritional content of sea-ice diatoms are taxon-specific and closely linked to environmental changes. Key findings from this work revealed that light transmittance to bottom-ice determined microalgal community composition and regulated lipid and fatty acid content in dominant sea-ice taxa, where increasing irradiance resulted in greater lipid content, until a threshold (~15% incoming irradiance). In tracing one taxon over time, it was revealed that environmental triggers indicating the end of primary productivity in the ice and onset of ice melt, including nitrogen limitation and increased water temperature, drove an increase in lipid and fatty acid content, with a concomitant decline in protein and carbohydrate stores. We may anticipate future assemblages with higher lipid, fatty acid and carbohydrate content, as light transmitted to

the bottom-ice and ocean temperatures increase, but only until certain thresholds. Finally, projected ocean acidification for 2100 was shown to drive a community shift toward smaller taxa whilst increasing lipid and protein stores in key pelagic Southern Ocean diatoms, revealing that end of century conditions may alter food quality and availability for secondary production.

These results provide new knowledge on the nutritional diversity of polar sea-ice algae and phytoplankton and deliver key insights into how a range of anticipated environmental changes may impact polar microalgal community composition and species cellular carbon allocation. This thesis delivers unprecedented insight into individual species' phenotypic plasticity, exposing the adaptation potential of polar microalgae, and enabling projections of how energy supply to the polar marine ecosystem may be affected under expected climate change driven scenarios.

# Chapter 1

## General Introduction

### 1.1 The Polar Oceans

The polar oceans are dynamic environments of ice and water at the extreme end of Earth's environmental gradients. Characterised by sea-ice cover, frigid temperatures and strong seasonality of light, these environments are both harsh places for life to thrive and particularly vulnerable to climate change. And yet, the polar oceans are home to productive and diverse ecosystems.

Whilst the Arctic and Antarctic have similar climates and seasonality due to their high latitudes, each have unique geography and features which shapes their characteristics. The Arctic is characterised by shallow shelf seas surrounding a primarily land-locked Arctic Ocean (AO) (14.1 million km<sup>2</sup>). On the other hand, Antarctica is a land mass approximately the same size as the AO, surrounded by deep continental shelf and the open Southern Ocean (SO) (20.3 million km<sup>2</sup>) (Comiso, 2010). Being three times greater in area, and substantially deeper, the SO has approximately eight times the volume of the AO (Comiso, 2010).

Common to both poles, is the seasonal formation and decay of sea ice. These ice-covered waters account for approximately 10% of the global ocean surface area ( $34 \times 10^6$  km<sup>2</sup>) (see Section 1.6). During the maximum extent in winter, Arctic sea ice can extend as far south as 40 °N (Comiso, 2010) and Antarctic sea ice can extend to 60 °S (NSIDC, 2024). Sea ice can persist over the summer (perennial ice) or form in winter and melt in summer (seasonal ice). Perennial ice is typically not connected to land (drift ice), whereas seasonal ice can be either drift ice or connected to land (land-fast ice), and this thesis primarily investigates seasonal land-fast ice ecosystems.

Polar waters experience extreme light seasonality, with prolonged periods of darkness in winter, and continuous daylight in summer. For example, at 78 °N where much of the sampling in this thesis was conducted, 24 h hour daylight persists for ~129 days, 24 h

darkness persists for ~112 days and the transition between constant darkness and daylight occurs inside 42 days (Cohen et al., 2020). Associated with this polar night and day, are strong seasonal fluctuations in surface air temperatures, sea-ice cover, salinity and consequently, ocean productivity and biochemical changes. Sea ice forms during the dark, cold winter months (December-February in the AO and June-August in the SO) when air temperatures are persistently below zero. The sea ice then melts during the summer months when the daylight is constant, providing prolonged solar heat input, and warmer air temperatures. The waters are cold enough to sustain sea ice growth, as the AO is characterised by a ~100 m thick halocline, which is a stratified layer at the ocean surface of cold (-1 °C), low-density water (Aagaard, 1981; Comiso, 2010). The SO waters, on the other hand, are not so strongly stratified, however the upper 200 m are persistently cold (Auger et al., 2021). As the ocean freezes during frigid winter air temperatures, salty brine is ejected from the newly formed ice (see Section 1.3), thereby increasing ocean salinity. Following the sea-ice melt during the summer, the surface waters experience a drop in salinity as the sea ice melts and freshwater runoff from glaciers and rivers is discharged into the ocean (particularly in the AO), and so the cycle continues. Nutrients in the water column vary seasonally and are typically replenished during winter, due to water column mixing and low uptake by organisms. In the AO, the waters become depleted during the productive summer months (Cota et al., 1996; Rysgaard et al., 1999), with nitrogen as the primary element limiting primary production. The waters of the SO, on the other hand, are generally iron-limited but typically remain replete in other macronutrients (Moore et al., 2001).

Despite the extreme environmental gradients and strong seasonal changes, productivity in the polar regions is similar to that of lower latitudes (Sakshaug et al., 2004). Net primary production estimates vary across studies, however they generally range between 350 – 600 Tg C yr<sup>-1</sup> in the AO (Arrigo & van Dijken, 2015; Codispoti et al., 2013; Pabi et al., 2008) and 1300 – 2000 Tg C yr<sup>-1</sup> in the SO (Arrigo et al., 1998, 2008) (Fig. 1.1), with primary production thought to be increasing over recent years in the polar regions (Arrigo & van Dijken, 2011, 2015; Lewis et al., 2020) (see Section 1.6). The primary production occurring in the polar oceans (Figure 1.1) is a result of proliferation within the water and sea ice of polar-adapted microalgae, which are the base of the highly productive polar food webs.

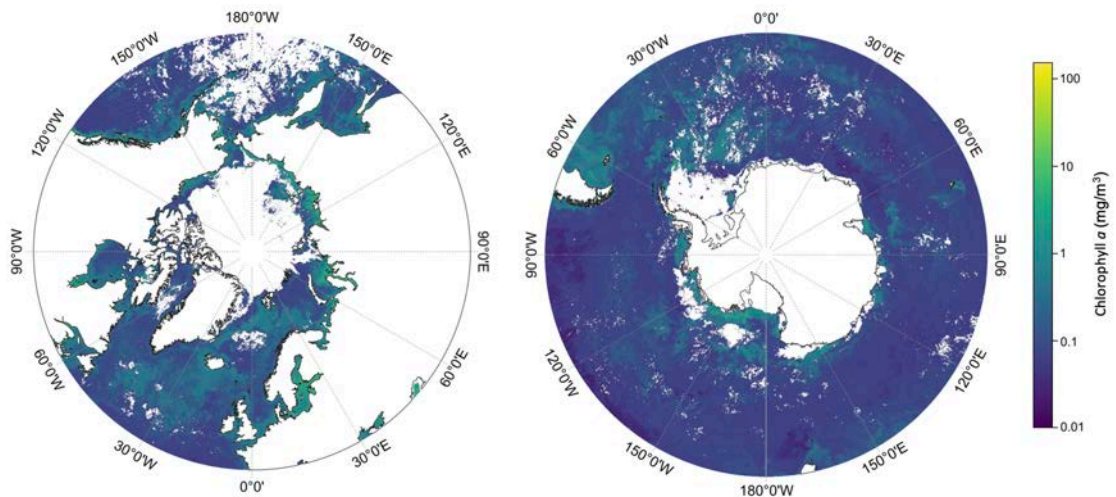


**Figure 1.1:** Surface chlorophyll *a* concentration ( $\text{mg m}^{-3}$ ) in the Arctic (left) and Antarctic (right) during summer (July and January, respectively) of 2023. Maps were generated using QGIS, and include monthly binned AQUA MODIS level 3 mapped chlorophyll data, obtained from NASA (2024).

## **1.2 Role of Microalgae in Polar Oceans**

At the base of the highly productive polar marine food webs are photosynthetic microalgae. These are microscopic, unicellular autotrophs responsible for supplying energy and nutrients to marine biota, and for structuring ocean biogeochemical dynamics. Both sympagic (sea-ice associated) and pelagic (open-water associated) polar microalgal communities are typically dominated by diatoms (Bacillariophyceae), which thrive in cold, seasonally mixed waters (Medlin & Priddle, 1990). In addition, Prymnesiophyceae and Haptophyceae (e.g. Coccolithales and Phaeocystales), Cryptophyceae, chloroplast-containing protists such as ciliates, and cyanobacteria are also present in these microbial communities (Horner, 1985; Medlin & Priddle, 1990). Whilst the diversity of the communities can vary from fewer than 20 taxa to over 150 taxa (Arrigo, 2014; Campbell et al., 2018; Hop et al., 2020), depending on environmental conditions (see Chapter 2), sea-ice communities are typically dominated by pennate diatoms whilst centric diatoms tend to be the most abundant in pelagic communities (Arrigo, 2014; Garrison et al., 1987; Hop et al., 2020; Horner & Schrader, 1982). These microalgae are key players in the biogeochemical cycling in the polar oceans. Diatoms are the major carbon producer in polar oceans, and control biogenic silica cycling through their siliceous cell wall (Armbrust, 2009). Dinoflagellates influence the phosphorus (P) cycle, through the high P

demands of heterotrophy. Dinoflagellates and the prymnesiophyte, *Phaeocystis* spp., influence the sulphur (S) cycle through synthesising substantial quantities of dimethylsulfoniopropionate (DMSP), whilst cyanobacteria play a key role in the nitrogen (N) cycle through creating bioavailable N through N-fixation (Gruber, 2008; Arrigo et al. 2024). Hence, environmentally-driven shifts in community composition have cascading effects on the marine food webs, through their influence on nutrient and biogeochemical cycling and carbon export.

Together, the contributions of pelagic and sympagic microalgae make up primary production in polar waters, with majority of the production generally occurring during the pelagic phytoplankton blooms. Whilst pelagic blooms typically occur in open water during the summer months in the absence of sea-ice cover, recent advances have highlighted the significant additional contribution of pelagic blooms occurring under the sea ice (Ardyna et al., 2020; Arrigo et al., 2012, 2014b; Clement Kinney et al., 2020; Tremblay et al., 2012). These under-ice pelagic blooms differ from sympagic blooms, which occur within the ice matrix. The contribution of sympagic blooms varies substantially across time and space. Whilst estimates of the contribution to total annual primary production are typically up to 25% in seasonally ice-covered Arctic waters (Legendre et al., 1992) and up to 57% in perennially ice-covered Arctic waters (Fernández-Méndez et al., 2015; Gosselin et al., 1997; Gradinger, 2009), sympagic contributions have been recorded to be as little as 1% (Rysgaard et al., 2001) and as high as 74% (Lee et al., 2008b). In the SO, primary production in sea ice is typically estimated to contribute approximately 5% of total primary production per year (Arrigo et al., 1997; Legendre et al., 1992; Thomas & Dieckmann, 2002a). However, what appears a minor contribution by sympagic microalgae is actually significant, in that sea-ice algae bloom asynchronously with pelagic algae and are the primary source of organic carbon for pelagic consumers during the ice-covered winter and spring (Michel et al., 1996; Riedel et al., 2008) (Fig. 1.2). In this way, sea-ice algae can extend biological production in polar waters by up to three months (Cota et al., 1991; Ji et al., 2013) and play a vital role in the success of zooplankton reproduction (see Section 1.4).

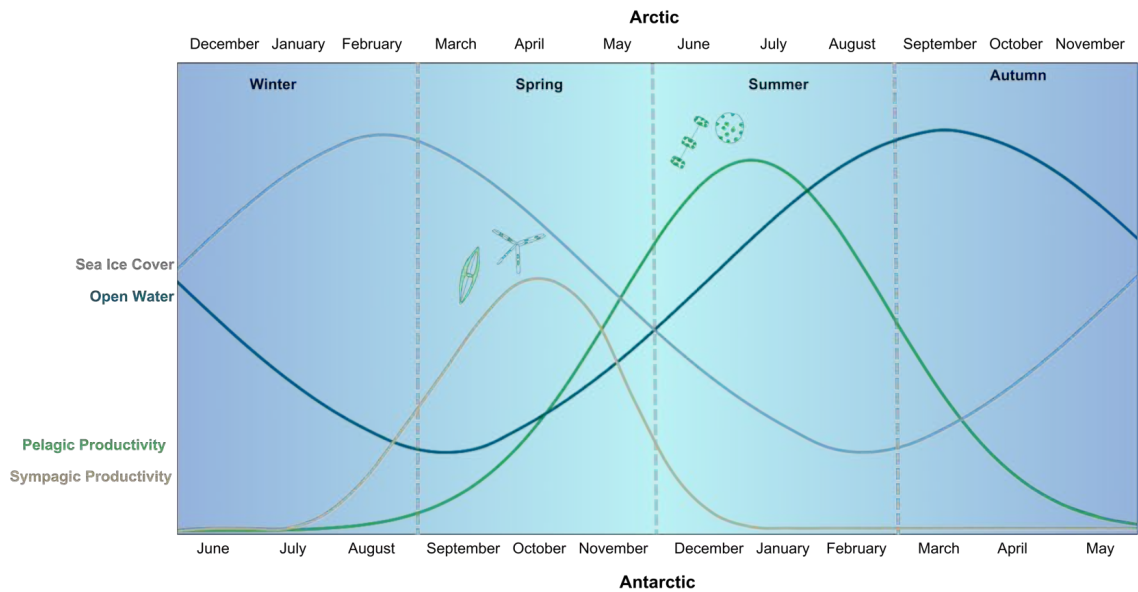


**Figure 1.2:** Conceptual diagram showing the annual cycles within the seasonal sea-ice environment, of sea-ice cover (grey) and open water (blue), sympagic (sea-ice associated) productivity (light brown) and pelagic (open-water associated) productivity (green), demonstrating that the peaks of sympagic and pelagic productivity occur asynchronously. Daylight hours are indicated in the background with dark blue representing constant night and light blue representing constant daylight. The seasons are denoted within the grey stipple line boxes, with the relevant months given for the Arctic (top) and Antarctic (bottom).

### **1.3 Sea Ice as a Habitat for Microalgae**

Sympagic algae inhabit the ice at the ice-water interface, in a labyrinth-style habitat which allows microalgae to proliferate with access to light, space, nutrients and protection from extensive grazing (Fig. 1.3). During sea-ice formation, salty brine is rejected from the ice and into the water below (Eicken, 2003), resulting in brine channels within the skeletal layer of the actively growing bottom ice, ranging from several micrometres to millimetres wide (Mundy et al., 2007). Providing the brine volume of these channels remains above 5% (corresponding to a temperature of  $-5\text{ }^{\circ}\text{C}$  and bulk ice salinity of 5 ‰), channels remain connected to one another in a matrix (Golden et al., 2007). These channels are consequently flooded with sea water, trapping microalgae and the dissolved nutrients (nitrogen, phosphorus, silicate and iron), necessary for algae growth and survival (Arrigo, 2014). These nutrients are resupplied from ocean water through convection currents



resulting from the interplay of ice accretion and salty brine rejection (Arrigo, 2014), and from downward flushing of surface deposited nutrients (Granskog et al., 2003). However, due to the semi-closed system within the ice and the high photosynthetic activity, inorganic nutrients are consumed by the proliferating community. Dissolved inorganic carbon is readily depleted, which raises the pH of the brine and can make the channels hyperoxic (Gleitz et al., 1995; Thomas & Dieckmann, 2002a). Thus, despite the generally hospitable labyrinth, the microalgae have to be adaptable to oxidative, osmotic and nutrient stress in these environments (Mundy & Meiners, 2021; Thomas & Dieckmann, 2002a).

Much of the microalgal community in the ice, and in particular pennate diatoms, assist in creating a more hospitable environment through the production of exopolysaccharides (EPSs) (Meiners et al., 2003) (Fig. 1.3). EPSs create a viscous biofilm within the channels, which slows brine drainage, increases channel complexity and assists the algae to ameliorate chemical stresses (Krembs et al., 2011; Thomas & Dieckmann, 2002a), whilst also regenerating nutrients within the ice through harbouring metabolically active bacteria (Meiners et al., 2008). Facing gradients of light, salinity, temperature, space and nutrients (Lyon & Mock, 2014) and often rapid physical and chemical changes (Thomas & Dieckmann, 2002a), sea-ice algae have many adaptations, in addition to EPS production, which allow them to thrive in the extreme environments they inhabit. Whilst comprehensive discussion of the cellular adaptations to the polar environments is beyond the scope of this thesis and has been previously reviewed (Kirst & Wiencke, 1995; Lyon & Mock, 2014; Thomas & Dieckmann, 2002a), some of these adaptations include; an ability to synthesise and accumulate polyunsaturated fatty acids (PUFAs) to retain membrane fluidity at cold temperatures, cryoprotectant proteins to combat cold-shock, and extracellular compounds such as ice-binding proteins to prevent external ice-growth and salt-shock. Importantly, sea-ice algae also have a broad photosynthetic range, as taxa are able to photosynthesise with as little as 0.01% incoming irradiance ( $< 0.5 \mu\text{mol photons m}^{-2} \text{s}^{-1}$ ) (Cota, 1985; Hancke et al., 2018; Mock & Gradinger, 1999) whilst still being capable of acclimating to high light ( $>200 \mu\text{mol photons m}^{-2} \text{s}^{-1}$ ) (Petrou et al., 2010; Petrou et al., 2011). This large range allows the maintenance of photosynthetic performance despite the highly variable light environment.

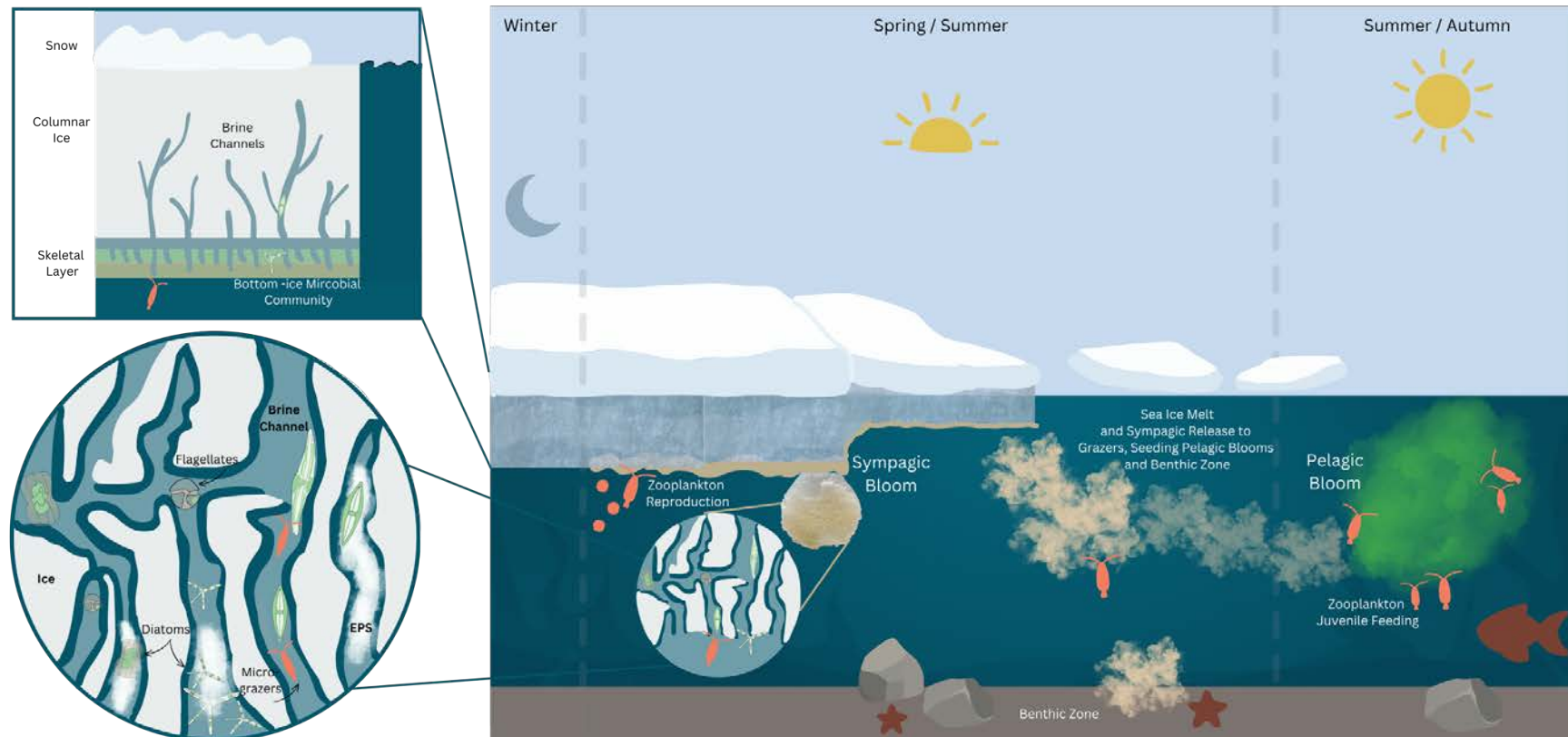


**Figure 1.3:** Illustration of the frozen matrix at the ice-water interface from a side view (top left) demonstrating the penetration of brine channels from the ocean interface into the columnar ice, and from a close-up view (bottom left) illustrating how microalgae inhabit the channels. EPS: Exopolysaccharides. A schematic of the seasonal progression of sympagic and pelagic microalgae is provided (right) in which there is limited productivity in the dark winter, followed by sympagic blooms supporting zooplankton reproduction in the spring before being released to the pelagic and benthic zones, followed by pelagic blooms supporting zooplankton juvenile feeding once the ice has melted in the summer.

#### **1.4 The Seasonal Cycle of Polar Microalgae in Ice and Water**

The microbial community are typically captured in the brine pockets of the sea ice during ice formation and growth in the winter months when darkness persists for 24 h. At this time, the microalgae are typically in vegetative and dormant states and rely on a range of overwintering strategies such as cyst or spore formation, heterotrophy and consumption of stored energy products (Bunt & Lee, 1972; Palmisano & Sullivan, 1983; Reeves et al., 2011; Riedel et al., 2008; Zhang et al., 1998). However, the traditional view of a pause in biological activity during the darkness has been recently challenged as evidence of a diverse community with mechanisms for dark-survival and continued biological activity emerges (Berge et al., 2015; Kennedy et al., 2019). Evidence of photosynthesis occurring in sea ice at extremely low light levels has been observed ( $< 0.2 \mu\text{mol photons m}^{-2} \text{ s}^{-1}$ ) (Barlow et al., 1988; Hancke et al., 2018) and new insights into the photosynthetic plasticity and photoadaptive strategies of polar microalgae are coming to light. For example, some taxa have been shown to simply down-regulate a fully functional photosynthetic apparatus, to ensure they are ready to take rapid advantage of re-illumination (Kvernvik et al., 2018), and other taxa have been shown regulate their lipidome to maintain growth in low quality light, by increasing the inclusion of polar lipids and primary light-harvesting pigments (Svenning et al., 2024).

With the early spring period typically characterised by sufficient inorganic nutrients supplied from the water below (Cota et al., 1991), the initial limiting factor for ice algae proliferation is daylight. Once daylight returns, photosynthesis by the entire microbial community gets into full swing and the community can flourish and bloom (Gosselin et al., 1986; Leu et al., 2015; Meiners et al., 2012) (Fig. 1.3). Whilst the intensity of sea-ice algal blooms varies substantially across space and time, the biomass within the bottom-ice can be up to ten times higher than for the adjacent seawater (Comeau et al., 2013; Michel et al., 1996). These blooms form a key source of energy for the polar marine food web, with ice algal carbon shown to support a range of top polar predators, including seals and polar bears (Brown et al., 2018; Goutte et al., 2014; Kohlbach et al., 2016; Kunisch et al., 2021). The particular importance of ice algae blooms, however, is in providing a nutrient source at a critical time in zooplankton reproductive cycles (Durbin & Casas, 2014; Renaud et al., 2007; Søreide et al., 2010), with ice algal grazing shown to promote zooplankton oogenesis and oocyte maturation (Tourangeau & Runge, 1991). Through the

provision of a food source prior to the pelagic phytoplankton blooms (Leu et al., 2015; Selz et al., 2018), the ice algae bloom allows certain key zooplankton species access to a high quality food source after the dark winter, and prior to egg release (Fig. 1.3). This means that by the time the open-water blooms occur in summer, the juvenile zooplankton are of a stage where they can feed and take advantage of the pelagic bloom (Hirche & Kosobokova, 2003; Runge & Ingram, 1991; Søreide et al., 2010).

As the season progresses toward summer, the persistent daylight and often reducing snow cover means that under-ice irradiance transitions from being a limiting factor, to reaching potentially harmful levels (Leu et al., 2016; Mock & Thomas, 2005) (albeit less so in the Antarctic where under-ice irradiance levels in spring typically remain lower (Arndt et al., 2017)). Nutrient concentrations within the ice decline following prolific use by the microbial community (Cota et al., 1987; Cota et al., 1990) and water temperatures below the ice increase, leading to ice melting from below and rapid brine drainage (Campbell et al., 2014; Mundy et al., 2005). These conditions typically lead to energy (lipid) accumulation in the microalgae cells as they prepare for overwintering outside of the ice and with limited photosynthetically active radiation (Duncan et al., 2024a; Lee et al., 2008a). Ultimately, the sea ice melts substantially (drift ice) or completely (seasonal ice), releasing a lipid-rich microbial community to the pelagic and benthic zones below (Koch et al., 2023; Renaud et al., 2007). These cells are either consumed or deposited to depths in a dormant or vegetative state. In shallow areas and the littoral zone, these cells are generally resuspended the following winter and spring (Vonnahme, 2021), whereas in deeper areas, they are largely deposited on the ocean floor and remineralised (Boetius et al., 2013). Whilst debated in the literature (Riebesell et al., 1991; Selz et al., 2018), it is likely that the ecological function of sea-ice algae extends to seeding phytoplankton blooms, with some taxa able to survive in both the sympagic and pelagic environment. In this way, it is thought that ice algae may both shape the initial community composition and influence the timing of pelagic blooms (Benkort et al., 2020; Garrison et al., 1987; Haecky et al., 1998; Jin et al., 2007; Michel et al., 1993; Szymanski & Gradinger, 2016; Tedesco et al., 2012).

As the incoming solar irradiance increases, the snow depth declines, melt ponds form, and sea ice retreats, resulting in a growing expanse of open water and increased light transmitted to the surface waters (Mundy et al., 2014). Phytoplankton quickly exploit the

rapidly increasing irradiance and become the dominant primary producers (Gosselin et al., 1997; Lewis et al., 2019), relying on availability of nitrogen, iron and other nutrients (Arteaga et al., 2020; Tremblay & Gagnon, 2009). These pelagic blooms are extensive, with pelagic microbial biovolume increasing ~40-fold from winter to summer (Eriksen et al., 2018; Sherr et al., 2003). As such, they are the predominant source of energy for marine food webs (Søreide et al., 2006) with most zooplankton timing their life cycle to ensure juveniles can take full advantage of this plentiful food supply (Bernard et al., 2019; Søreide et al., 2010) (Fig. 1.3). Initially, the pelagic bloom communities are characterised by pennate and centric diatoms, with community succession typically resulting in flagellate dominance toward the end of the blooms, as nutrients becoming limiting (Ardyna et al., 2011; Eriksen et al., 2018; Sherr et al., 2003). In the AO, the surface waters become increasingly nitrate depleted as bloom termination is approached, as nitrate is assimilated by the phytoplankton into N-containing biomolecules (Danielson et al., 2017; Varela et al., 2013). The SO, on the other hand, has residually high nitrate concentrations so typically remains nitrate replete, whilst primary production eventually becomes limited by insufficient iron supply (Boyd, 2002; Petrou et al., 2016). Ultimately, these blooms export carbon to the deeper ocean through phytoplankton sinking and zooplankton migration (Boyd et al., 2019; Jónasdóttir et al., 2015; Moreau et al., 2020).

Following the cessation of the summer blooms, a period characterised by minimal incoming solar irradiance, nutrient depletion and low production ensues (Lewis et al., 2019), as the cycle continues with winter returning and sea-ice forming again. Evidently, in the highly seasonal polar environments which have severely restricted productivity for substantial portions of the year, the provision of energy through sympagic and pelagic microalgae is critical to the polar marine ecosystem (Arteaga et al., 2020; Campbell et al., 2022).

### **1.5 Biomolecular Composition of Microalgae and the Influence on Food Webs**

Microalgae are the cornerstone of energy and nutrient supply to marine food webs through the transfer of their biomolecular (e.g. proteins, lipids and carbohydrates) stores. The allocation of photosynthetically derived carbon to biomolecular content determines the nutritional value of microalgae, and determines the supply of these essential compounds to higher trophic levels. Lipid is responsible for most of the energy transfer through the

food web, as it is the most energy-rich biomolecule with a caloric value approximately twice that of carbohydrate and protein (Hagen & Auel, 2001; Kim et al., 2015). These high energy reservoirs play a crucial role in the overwinter survival of these polar marine ecosystems, with some zooplankton (e.g. calanoid copepods and Antarctic krill) having up to 50% of their dry weight as lipid, and metabolising much of this in the deeper waters during winter (Hagen et al., 1996; Jónasdóttir et al., 2015; Kattner & Hagen, 2009; Tarling et al., 2022). It is the production and storage of lipids by microalgae, and the acquisition and storage of these lipids by zooplankton, which allows these cornerstone organisms to cope with extended periods of no sunlight and very limited food availability.

Carbohydrate supply is also important in terms of energy transfer through marine food webs, and can be a reserve product which is drawn upon for lipid synthesis, particularly under nutrient-depleted conditions (Ahn et al., 2019; Hu, 2004). Along with lipid content, carbohydrate is also an essential component of cell membranes (Bhavya et al., 2019; Finkel et al., 2016). In addition, carbohydrate plays a role in protein synthesis, and protein content has a key role in all enzymatic processes vital for growth and survival, as the source of amino acids and regulators of metabolic pathways (Ruess & Müller-Navarra, 2019; Wu, 2010). In particular, microalgae are the source of essential amino acids, such as leucine and methionine, which cannot be synthesised *de novo* by consumers (Ruess & Müller-Navarra, 2019). Similarly, microalgae are the only source of the vital omega-3 fatty acids, eicosapentaenoic acid (EPA) and docosahexaenoic acid (DHA) (Ackman, 1989; Ruess & Müller-Navarra, 2019), and microalgal dietary provision of polyunsaturated (PUFA), monounsaturated (MUFA) and saturated fatty acids (SAFA) has been shown to directly influence the consumers growth and fitness (Jónasdóttir et al., 2005; Jónasdóttir et al., 2009; Kunisch et al., 2021; Leu et al., 2006a; Søreide et al., 2013).

Evidently, the biomolecular composition of microalgae is important as it directly influences the functioning of primary consumers, thereby indirectly affecting the entire food web. The partitioning of cellular biomolecular content is primarily determined by changes in the environment such as light (Duncan et al., 2024a; Van Oijen et al., 2004), temperature (Teoh et al., 2004; Torstensson et al., 2019) and nutrient availability (Mock & Kroon, 2002a; Pogorzelec et al., 2022), with shifts in environmental parameters affecting the biomolecular composition in different ways (see Chapter 2). It is through these changes to microalgae biomolecular composition, that environmental change can

have a significant influence on energy and essential compounds supplied to the marine food web, ultimately impacting marine ecosystem structure and functioning.

### **1.6. Climate change driven environmental perturbations and potential implications for polar microalgae**

The polar regions are some of the fastest changing environments on the planet (Meredith et al., 2019) and the climate change driven environmental shifts are complex (Fig. 1.4). The degrees and direction of the changes are variable across time and space, and the interconnected nature of many of the stressors amplify effects (Gutt et al., 2015). The central changes affecting polar marine microbial communities, and therefore the structure and functioning of marine ecosystems, are briefly reviewed below.

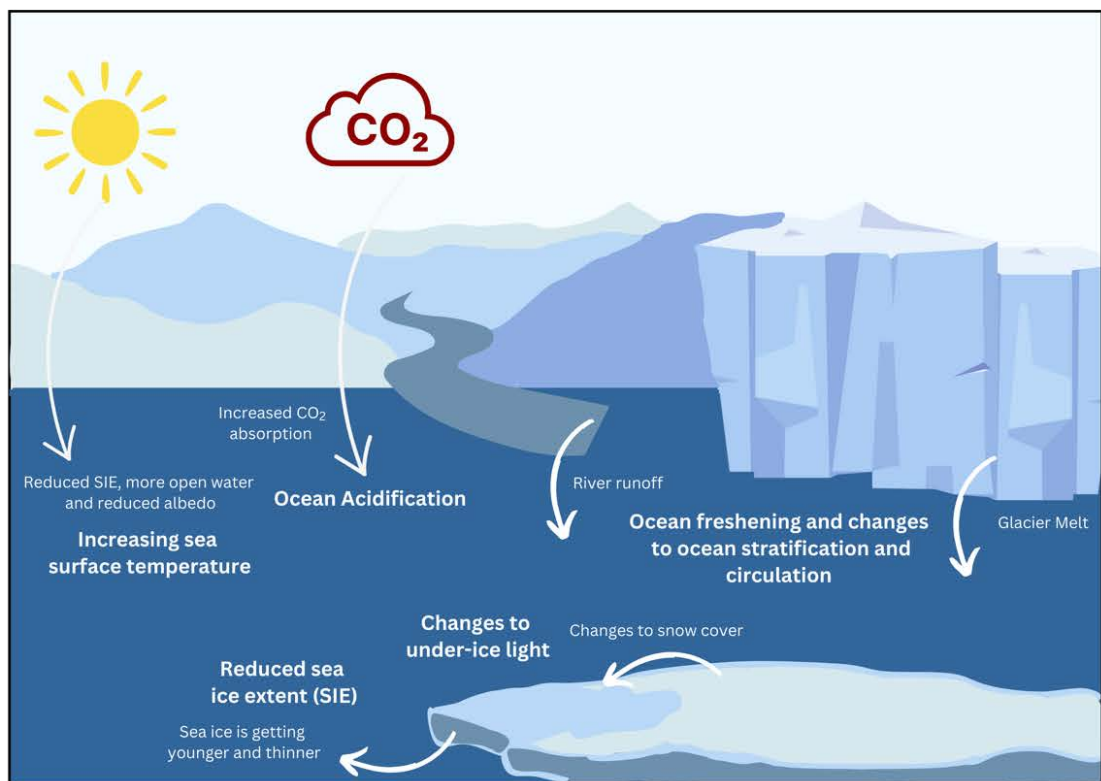


**Figure 1.4:** Overview of the key climate change driven environmental changes affecting polar microalgae. Some of the main drivers are provided in roman text and the major environmental changes are given in bold text.

### 1.6.1 Sea Ice

The most visible manifestation of climate change in the polar regions is the decline in sea-ice extent. In conjunction with a decline in spatial area, the melt season is extending and sea ice is becoming younger, thinner and more transient, particularly in the Arctic (Kacimi & Kwok, 2022; Parkinson, 2014a; Stroeve & Notz, 2018). In the Arctic, the average September (minimum) sea-ice extent has declined at ~12.8% per decade over the past four decades (Onarheim et al., 2018) (Fig. 1.5). In the Antarctic, the situation is more nuanced with no trend observed between 1979 and 2018 (Ludescher et al., 2019), followed by a recent precipitous rate of decline (Parkinson, 2019) including four record-low events in 2017, 2022, 2023 and 2024 (NSIDC, 2024; Purich & Doddridge, 2023). This trend of decline is expected to continue over the coming decades (Roach et al., 2020).

In the Arctic, concomitant with the decline in sea-ice extent, is a dramatic loss of ice thickness (Itkin et al., 2017; Renner et al., 2014; Yu et al., 2014). This is linked to a trend toward younger sea ice (Tschudi et al., 2016), with the Arctic now dominated by first-year ice (Stroeve et al., 2012). Land-fast ice, in particular, has been declining at up to twice the rate of pack ice (Li et al., 2019). For example, in Svalbard, where much of the research in this thesis was conducted, land-fast ice extent in 2005-2019 was at 50% of the extent recorded in 1973-2000, with projections that the extent will decline to only 12% in the next 10-20 years (Urbański & Litwicka, 2022). In addition to a decline in extent, the duration of sea-ice cover has shortened by 5 – 65 days per decade across the Arctic (Markus et al., 2009; Parkinson, 2014b), with an increasing expanse of open water in summer, and predictions that the AO will have ice-free summers by 2050 (Jahn et al., 2024; Notz & Community, 2020). In Svalbard specifically, the duration of sea-ice coverage has reduced by up to four months since 2005 (Urbański & Litwicka, 2022). Increasing periods of open water are directly linked to increased sea surface warming (Section 1.6.3) and amplification of further sea-ice loss (Letterly et al., 2018; Stroeve et al., 2014; Timmermans et al., 2018) (see Section 1.6.3).

These changes to sea ice have major ecological implications (Post et al., 2013) and profound effects for microalgae as the base of the marine food web. With more open-water, there are predictions of increased primary productivity through stronger and longer pelagic blooms (Arrigo & van Dijken, 2015; Forest et al., 2011b; Lewis et al., 2020).



However, a decline in sea-ice extent means less surface area for sea-ice algal blooms to occupy, and a shorter ice-cover duration means the incorporation of sea-ice assemblages into the ice is delayed and bloom termination occurs earlier. Given the important role of sea-ice algae in providing an early season nutrient source that matches zooplankton reproductive cycles (Section 1.4), an overall increase in primary production through pelagic blooms does not necessarily abate concerns of potential phenological mismatches between microalgae and zooplankton. Such mismatches could severely impact zooplankton reproduction and fundamentally alter the functioning of polar marine food webs.

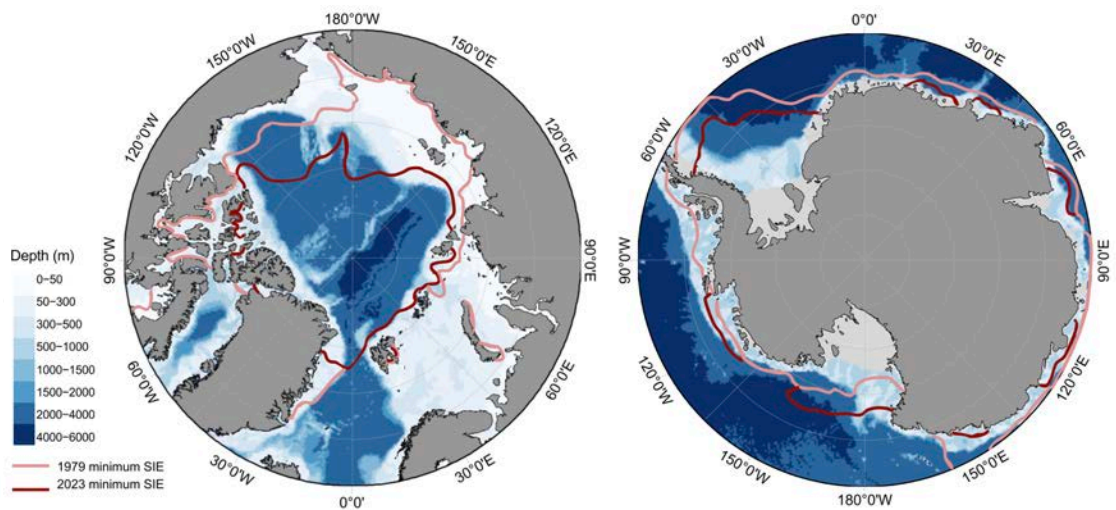


**Figure 1.5:** The Arctic (left) and Southern (right) oceans, including ocean floor depth indicated through colour gradient. Approximate minimum sea-ice extent (SIE) is given for 1979 (light pink) and 2023 (dark pink). Maps generated in R Studio (v. 2023.09.0463) using ggOceanMaps (v.2.1.1). Sea ice extents are adapted from National Snow and Ice Data Center sea ice extent data (NSIDC, 2023).

## 1.6.2 Snow Fall and Under-Ice Light

Much of the Arctic is experiencing a decline in snow fall (Callaghan et al., 2011; Kacimi & Kwok, 2022), with snow depth on sea-ice thinning up to 56% over the past 100 years in some areas (Webster et al., 2014) (Fig. 1.2). In addition, some areas of the Arctic are experiencing an increased proportion of precipitation falling as rain rather than snow (Screen & Simmonds, 2012). However, the direction and extent of change is variable temporally and spatially, with some parts of the Arctic experiencing increased snowfall over recent decades (Lam et al., 2023; van Pelt et al., 2016). This is likely due to increased storm activity and more open water leading to increased precipitation (Liu et al., 2012), and such trends in these areas can be expected to continue particularly in the short to medium term. The situation is more nuanced again in the Antarctic, with no clear trends in changes to snow depth determined, primarily due to challenges obtaining base line data such as extensive surface flooding and heavy snow fall events year-round (Webster et al., 2018).

Snowfall has a significant impact on ocean dynamics, as the depth of snow on sea-ice influences the melting rate of ice, and the amount of light that can travel to the ice-water interface (Fig. 1.6). This is because snow can have a much higher albedo than ice alone, meaning it can reflect nearly all of the incoming photosynthetically available radiation (PAR), reducing visible light transmission to <5% of incoming PAR (Perovich, 2007). Snow-free ice, on the other hand, can transmit up to 80% of incoming PAR (Hamre et al., 2004; Taskjelle et al., 2017). Therefore, a reduction in snow depth and sea-ice thickness would result in higher under-ice light intensity and conversely, an increase in snow depth would lead to a lower-light environment at the ice-water interface. As the microalgae inhabiting the bottom-ice environment are photosynthetic primary producers, the under-ice light climate directly determines biological productivity, microbial community composition (Chapter 3), and algal cellular carbon allocation (Chapter 4). As such, snow depth is one of the most significant factors in determining ice algal bloom phenology (Leu et al., 2015) and nutritional value (Chapter 2), and is therefore crucial in influencing marine ecosystem functioning (Section 1.4).

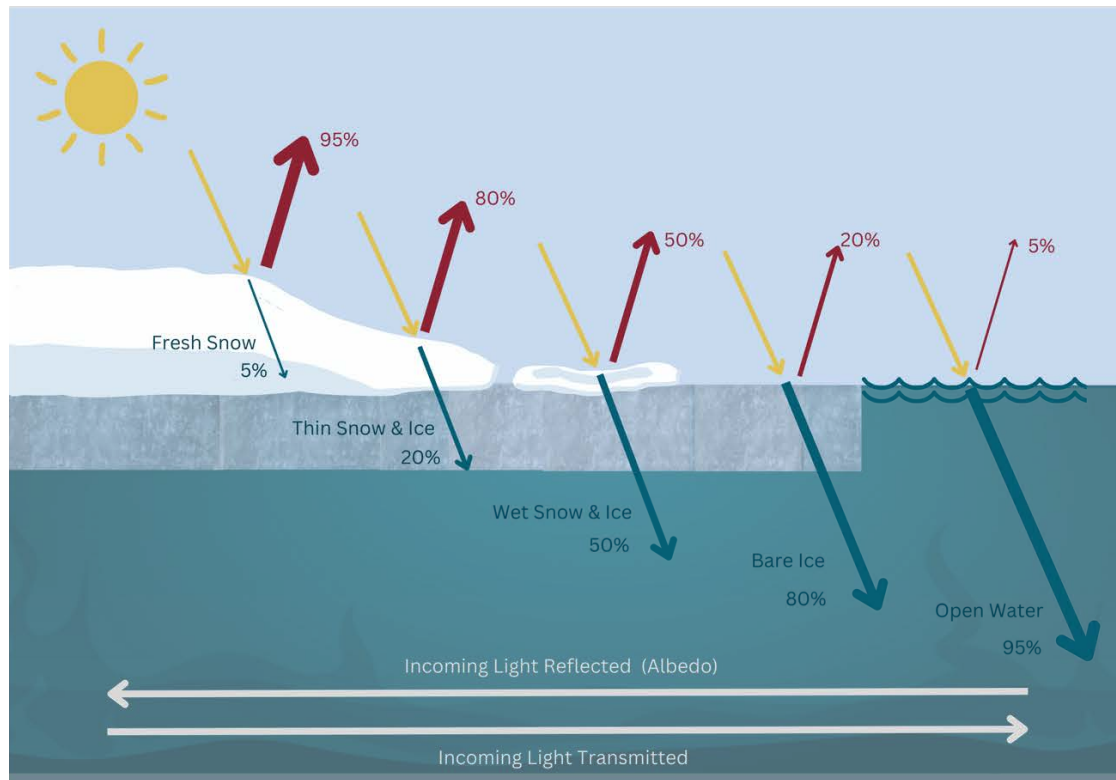


**Figure 1.6:** Conceptual figure of albedo (the fraction of incoming light that is reflected) of different surfaces, based on Hamre et al., 2004; Perovich et al., 2007. Incoming light is denoted in yellow, with the approximate percentage of reflected light denoted in red, and approximate percentage of light transmitted to the ocean denoted in blue. The grey arrows (bottom) denote that albedo is highest for fresh snow and lowest for open water, and that the amount of incoming light transmitted to the water increases, as albedo decreases.

### 1.6.3 Warming Temperatures

The Arctic near-surface atmosphere has warmed four times faster than any other region on Earth since 1979 (Rantanen et al., 2022), with winter temperature anomalies of +6 °C (relative to 1981-2010) recorded in recent years (Meredith et al., 2019). Whilst such severe air-temperature warming trends have not been observed over the entire Antarctic region, West Antarctica has warmed significantly (Meredith et al., 2019; Nicolas & Bromwich, 2014; Turner et al., 2020). Sea surface temperatures (SST) of the polar oceans, and in particular, the SO, have steadily increased over the previous decades (Auger et al., 2021; Gille, 2008; Liu & Curry, 2010; Schmidtko, 2014). Whilst spatially variable, the

increase is up to 0.5 °C per decade (Meredith et al., 2019), with expectation of a 2 °C rise by the end of the century (IPCC, 2023) (Fig. 1.4). These temperature increases are most pronounced in the SO, which accounted for 45-62% of global heat gain between 2005 and 2017 (Meredith et al., 2019), despite only occupying 25% of ocean area.

Increasing SSTs are anticipated to have substantial effects on polar marine ecosystems. Estimates suggest that warming polar oceans will bring an overall increase in pelagic bloom productivity (Arrigo & van Dijken, 2015; Moreau et al., 2015). However, the optimum temperature for microalgae growth is expected to be exceeded during summer by 2100, threatening phytoplankton blooms (Coello-Camba & Agustí, 2017). In addition, warming waters are driving shifts in microbial community composition, to a dominance of smaller cells (Moline et al., 2004; Montes-Hugo et al., 2009; Sugie et al., 2020; Tremblay et al., 2012). Such changes in community structure have direct consequences for many primary consumers (e.g. Antarctic krill) which can only efficiently graze microalgae over a certain size (Boyd et al., 1984; Moline et al., 2001). Changes to pelagic microalgal contributions coincide with serious implications for sympagic microalgal primary production, as warmer waters drive earlier ice-melt and reduce sea-ice formation (Section 1.6.1). These environmental changes are therefore anticipated to reduce sea-ice algal contribution to marine food webs, undermining their important phenological links with consumer reproduction (Tedesco et al., 2019; Section 1.4). Warmer waters are also expected to directly alter microalgal nutritional value to consumers through influencing their cellular carbon allocation (Chapters 2 and 5) and potentially influence the over-winter survival of many key ice algal taxa (Figueroa et al., 2011; McMinn & Martin, 2013; Reeves et al., 2011; Chapter 5).

#### **1.6.4 Ocean Freshening**

The polar oceans are freshening, through increased freshwater input from thinning ice shelves (Jacobs et al., 2022; Schmidtke, 2014), glacial melt (Pan et al., 2022; Silvano et al., 2018), sea-ice loss (Li & Fedorov, 2021; Wang et al., 2018) and increased freshwater river input, which is accelerated in the Arctic due to increased permafrost thawing (Brown et al., 2020; Peterson et al., 2002) (Fig. 1.4). Such freshening is anticipated to accelerate, with projections that by 2100 under RCP 8.5 (IPCC, 2021), the AO surface salinity is

expected to decline by 1.5 psu (Shu et al., 2018) and, depending on the rate of ice sheet melt, could decline by up to 5 psu in the Southern Ocean (Sadai et al., 2020).

Of particular significance in regard to primary production, is the way in which ocean freshening alters ocean stratification, which impacts nutrient supply. By strengthening the upper-ocean stratification, the addition of freshwater has been shown to deepen the nitracline and reduce nutrient supply, negatively impacting primary production (Boone et al., 2018; Coupel et al., 2015; Zhuang et al., 2021). For near-shore communities, some of this effect is abated by the increased nutrient input from river runoff, which has been shown to drive increases in local primary production (Terhaar et al., 2019), including fuelling blooms (Forest et al., 2011b). Similarly, sea ice and ice-sheet melt and has been shown to increase nutrient supply, linked to boosts in primary production (Arrigo et al., 2017; Hawkings et al., 2014; McGillicuddy Jr et al., 2015). The complex interplay of several potentially counterbalancing effects means there are significant uncertainties regarding the future nutrient dynamics of polar oceans (Brown et al., 2020; Lannuzel et al., 2020), and the subsequent effects on microalgae bloom dynamics and primary production (Ardyna & Arrigo, 2020; Cota et al., 1991; Ko et al., 2020).

### **1.6.5 Ocean Acidification**

With rapidly increasing anthropogenic CO<sub>2</sub> emissions (currently reaching ~37 gigatonnes per year (IEA, 2023; Liu et al., 2023)), the polar oceans are increasingly absorbing carbon, which reduces surface ocean pH and carbonate ion concentrations, resulting in ocean acidification (OA) (Haugan & Drange, 1996) (Fig. 1.4). This is particularly the case in the SO, as due to increased CO<sub>2</sub> solubility at low water temperatures, the deep, cool waters of the SO sequester disproportionate amounts of carbon (i.e. 40% of global uptake despite accounting for only 10% of the surface area) (Sabine et al., 2004). OA is expected to significantly worsen over the coming decades. If CO<sub>2</sub> emissions continue unabated (RCP 8.5), atmospheric CO<sub>2</sub> concentrations are estimated to rise to > 1000 ppmv by 2100. This would result in a further decline of the average ocean pH by an additional 0.4 pH units, equivalent to a 150% increase in acidity, declining from 8.2 (pre-industrial) to 7.7 (2100) (IPCC, 2023; Jiang et al., 2023).

OA has well-documented negative impacts on a broad range of marine life, particularly those relying on calcium carbonate to build shells or skeletal structures (Feely et al., 2004; Hancock et al., 2020; Orr et al., 2005). The negative acidification response extends beyond calcified organisms to polar microalgae, and particularly diatoms, with OA shown to have range of interconnected detrimental effects. An OA-induced limitation in growth rate has been observed in cultured polar diatoms (Andrew et al., 2022; Torstensson et al., 2015) and within a natural SO microbial community (Deppeler et al., 2018). OA has also been shown to inhibit photosynthetic performance of polar microalgae (Deppeler et al., 2018; Hoppe et al., 2015), including increasing sensitivity to light stress (Beszteri et al., 2018; Kvernvik et al., 2020) and alter phytoplankton community composition (Feng et al., 2010; Leu et al., 2013). Further, OA has been shown to reduce silicification rates in polar diatoms (Petrou et al., 2019) and alter nutritional content of a number of dominant polar dinoflagellates (Wynn-Edwards et al., 2014) and diatoms (Chapter 6).

### **1.7 Knowledge Gaps**

Despite the significant, rapid environmental changes taking place in the polar marine ecosystems, they remain under-studied. Countless questions remain about how these systems function, and how they may be expected to be impacted by climate change. This is a function of both the complexity of the ecosystems and the issues they face, and the logistical challenges associated with sampling in these extreme environments. Field-based research is often opportunistic and lacking spatiotemporal resolution. Because of this, it is particularly challenging to investigate seasonal dynamics, compare geographic locations or obtain repeated samples to decipher the influence of natural variability.

To understand how polar marine food webs are likely to be affected by environmental change, it is critical to understand the extant diversity and plasticity in microalgal biomolecular composition and equally, explore how the nutritional value of the base of the food web will be impacted. To date, limited studies investigating shifts in nutritional content of polar microalgae have been conducted (sympagic studies are listed and reviewed in Chapter 2). Of those, only a handful have used natural communities (e.g. Lee et al., 2008a, 2008b; Leu et al., 2010; Lund-Hansen et al., 2020; Mock & Gradinger, 2000; Palmisano & Sullivan, 1985; Smith & Herman, 1992) and these studies have typically focused on shifts observed across the entire microbial community, thereby lacking taxon-

specific resolution. Moreover, whilst some sea-ice algal studies have investigated land-fast ice communities (e.g. Leu et al., 2010; Lund-Hansen et al., 2020; Pogorzelec et al., 2022; Søreide et al., 2010), they have often been conducted on communities obtained from the drift ice (Van Leeuwe et al., 2018 and references therein). There is therefore a distinct lack of knowledge regarding microalgal species-specific plasticity in response to environmental change, and few insights into land-fast ice microbial communities. Particularly with land-fast ice rapidly diminishing, it is important to bridge these gaps.

As species-specific responses can vary substantially in their direction, speed and magnitude, understanding the ‘who, why and how’ of microalgal species impacted by environmental change is vital to truly understanding the future dynamics of the polar marine ecosystems. Typically, species-specific insights are gleaned through laboratory experiments and whilst these have some advantages, they generally focus on a small range of taxa and do not account for the natural variability within the communities, or the multi-factorial nature of the natural environment. Thus, the value of single-cell analyses on natural mixed communities is that they provide a unique insight into the extent to which a member of the community is affected. By providing detail on the diverse, taxon-specific responses, unprecedented detail is delivered on the potential physiological and ecological implications of environmental change.

Microalgal community composition also plays a significant role in determining the nutritional value of primary production, and in biogeochemical cycling through the marine food web (Van Leeuwe et al., 2018; Vancoppenolle et al., 2013). However, our understanding of the environmentally and seasonally driven shifts in pelagic and sympagic microalgal community composition is also limited. Again, the few studies that exist cover a relatively small spatiotemporal resolution. Of the ~30 investigations into sympagic communities, approximately half are based in the Arctic and approximately half again investigate land-fast ice communities (reviewed in Van Leeuwe et al., 2018). In addition, information on community composition throughout microalgal studies has often been provided to the taxonomic level of ‘Order’ or ‘Class’ only, i.e. dividing the composition into pennate diatoms, centric diatoms and dinophyceae, without providing genus or species information. Our knowledge of polar microalgal community compositions is therefore incomplete. Increasingly, microbial community composition is being investigated using high-throughput sequencing of ribosomal DNA and RNA (e.g.

Kong et al., 2023; Kramer et al., 2024; Oldenburg et al., 2024). Whilst these techniques have an important role in allowing for rapid, larger scale investigations, they are restricted by issues including; the reference databases are generally limited, they can over-represent certain species with higher gene copy number, and they provide relative abundance only (Godhe et al., 2008; Zhu et al., 2005). Until such short-falls are resolved, traditional microscopy-based approaches therefore remain invaluable.

The research contained in this thesis starts to address some of these critical knowledge gaps through extensive field sampling of AO land-fast sea-ice microalgal communities, and experimental manipulation of a natural SO pelagic community. The conceptual framework and specific research aims are outlined below.

### **1.8 Thesis Aims, Objectives and Outline**

The overarching aim of this PhD project was to assess how environmental conditions influenced polar marine food web nutrition, via quantitative analyses on community composition and species-specific biomolecular plasticity. However, to put the research in context, it was important to first determine known directions and magnitudes of change established in previous work (typically whole community analyses or lab-based culture studies) and compare and contrast the usefulness of alternative methodologies for investigating nutritional content at fine-scale taxonomic resolution. **Aim 1: To synthesise the current knowledge on how environmental conditions influence biomolecular partitioning in sea-ice algae, and evaluate and compare the techniques used to interrogate their biomolecular composition (Chapter 2).**

Anticipated changes to sea-ice extent and snow cover from climate change will alter the quality and quantity of light transmitted to the ice-water interface. Changes to under ice light climate changes sea-ice microalgal community composition, as photosynthetic rates will need to adjust favouring certain taxa more than others. Potential changes to microalgae community dynamics are significant for polar waters, as the community composition affects biogeochemical cycling, zooplankton grazing efficiency and carbon export. **Aim 2: To determine how under-ice light conditions, from varying ice thickness and snow conditions, affects land-fast sea-ice microalgal community composition (Chapter 3).**



Changes to sea-ice and snow cover already occurring in Arctic waters are expected to alter the allocation of photosynthetically derived carbon within polar sea-ice microalgae, determining their biomolecular (i.e. lipid, carbohydrate, fatty acids, and protein) composition. Due to the important role sea-ice algae play in providing an early season nutrient source for zooplankton reproduction, understanding changes to biomolecular composition of sea-ice algae in response to light availability is critical to determining the energy available to the polar marine food web under environmental change. **Aim 3: To provide quantifiable changes in biomolecular stores in individual, key sea-ice microalgal species from communities exposed to different environmental conditions, including changes to under-ice light conditions from changes to snow and sea-ice thickness (Chapter 4).**

In highly seasonal polar environments, microalgae are exposed to rapidly changing environmental conditions over relatively short time scales. It is therefore important to trace the seasonal progression in sea-ice microalgae biomolecular content, to determine how changing light, temperature, salinity and nutrient regimes may influence metabolism and carbon allocation, and therefore the supply of essential molecules to the polar food web. In addition, investigating the biomolecular composition of sea-ice algae at the end of the productive season reveals potential physiological strategies for winter survival. **Aim 4: To trace the seasonal progression of nutritional content in a key sea-ice microalgae taxa: characterising shifts in energy allocation that may link to survival during polar darkness, and future environmental change (Chapter 5).**

Despite OA disproportionately impacting the SO, and the importance of the phytoplankton–zooplankton link in the Antarctic pelagic food web, little is known about how OA is expected to affect the nutritional content of polar microalgae. To elucidate how the quality and quantity of carbon supplied to the marine food web may change under OA, it is crucial to understand how the biomolecular partitioning of key pelagic phytoplankton taxa is likely to be affected. **Aim 5: To present a snapshot into the effects of OA on the partitioning of biomolecular content by individual pelagic diatoms, offering new insight into the potential implications of CO<sub>2</sub>-induced changes to energy availability and transfer through the Antarctic marine food web (Chapter 6).**

Cumulatively, these five research aims explored in the following chapters provide new knowledge on species-specific metabolic carbon allocation and shifts in community composition under variable environmental conditions. These insights into microalgal plasticity are vital to elucidate the winners and losers within the microbial community under climate change. Moreover, the outcomes of this research are necessary for predicting how future ocean conditions may manifest in altered ecosystem functionality and the subsequent trophic implications for the polar marine food web. This new knowledge is synthesised in Chapter 7 where the research is summarised, the key findings are integrated and potential directions for future research are identified

## Chapter 2

### **Biomolecular Composition of Sea Ice Microalgae and Its Influence on Marine Biogeochemical Cycling and Carbon Transfer through Polar Marine Food Webs**

*Published in Geosciences as:*

**Duncan, R. J., & Petrou, K. (2022).** Biomolecular Composition of Sea Ice Microalgae and Its Influence on Marine Biogeochemical Cycling and Carbon Transfer through Polar Marine Food Webs. *Geosciences*, 12 (1), 38. DOI: 10.3390/geosciences12010038

*Author contributions:*

R.J.D. and K.P designed the study, determined the methodology and undertook the investigation, R.J.D undertook the data curation and formal analysis and performed the original draft preparation and K.P. undertook review and editing, visualization and supervision.

Production Note:

Signature removed prior to publication.

R. Duncan

Production Note:

Signature removed prior to publication.

K. Petrou

---

Chapter 2 provides a literature review of the plasticity of biomolecular composition in sea-ice algae from the Arctic and Antarctic, and a methodological comparison on the different approaches for investigating biomolecular composition in microalgae. This manuscript was written for a special issue on sea-ice biogeochemistry and as such, the literature review is focused on sea-ice microbial communities. The methodologies explored within this chapter are equally relevant for investigating the biomolecular composition of both sea-ice and pelagic microalgae.



## **Abstract**

Microalgae growing on the underside of sea ice are key primary producers in polar marine environments. Their nutritional status, determined by their biomolecular composition, contributes to the region's biochemistry and the unique temporal and spatial characteristics of their growth makes them essential for sustaining polar marine food webs. Here, we review the plasticity and taxonomic diversity of sea-ice microalgae biomolecular composition, with a focus on how different environmental conditions influence biomolecular production and partitioning within cells and communities. The advantages and disadvantages of methodologies for assessing biomolecular composition are presented, including techniques that provide high throughput, whole biomolecular profile and/or species-specific resolution, which are particularly recommended for future studies. The directions of environmentally driven biomolecular changes are discussed, alongside anticipated consequences on nutrients supplied to the polar marine ecosystem. Given that polar regions are facing accelerated rates of environmental change, it is argued that a climate change signature will become evident in the biochemical composition of sea-ice microalgal communities, highlighting the need for further research to understand the synergistic effects of multiple environmental stressors. The importance of sea-ice microalgae as primary producers in polar marine ecosystems means that ongoing research into climate change driven biomolecular phenotyping is critical to understanding the implications for the regions biochemical cycling and carbon transfer.

## **2.1 Introduction**

Ice-covered seas account for approximately 10% of the global ocean surface area ( $34 \times 10^6 \text{ km}^2$ ) annually, with the seasonal formation and decay of sea ice playing a key role in global ocean turnover. Sea ice forms during the dark winter months reaching its maximum extent as spring commences. Therefore, in the Arctic, the maximum extent of sea ice ( $\sim 15.2 \times 10^6 \text{ km}^2$ ) occurs in March, while in the Antarctic, sea-ice extent reaches a maximum ( $\sim 18.5 \times 10^6 \text{ km}^2$ ) in September (Parkinson, 2014a) (Fig. 2.1). Despite their asynchrony, combined, these two regions form a significant biome, providing essential habitat for many marine organisms, including diverse communities of bacteria, protists, and meiofauna (Arrigo, 2014; Deming & Collins, 2017).

The organisms that thrive in these vast expanses of frozen seawater, underpin polar marine biodiversity and biochemistry. In particular, photosynthetic microalgae, which become engrained into the ice as it forms (Fig. 2.1), support polar marine food webs, and, together with heterotrophic bacteria, are principal players in the biochemical cycling of elements within the marine and sea-ice environments (Arrigo, 2014). Sea-ice primary productivity and nutrient cycling is important for understanding the dynamics of seawater biochemistry, as the biomolecular composition of sea-ice microalgae and the cycling of nutrients that occurs within sea-ice microbial communities influences the biochemistry of seawater (Belt, 2018; Kohlbach et al., 2021). However, biochemical components can be sensitive to physical processes, including photooxidation from UV, which is determined by ice thickness or mixing depth (Rontani et al., 2021; Rontani et al., 2016), potentially reshaping the biochemical signature of the seawater (Bélanger et al., 2006; Massicotte et al., 2021).

The ecological importance of sea-ice microalgae is attributed to their role in primary production during the frozen winter and in spring as the ice begins to melt. During the early spring, sea-ice microalgae grow within the brine channel network under very low irradiances, and as the solar angle increases, spring blooms commence, marked by an increase in biomass on the underside of the ice (Johnsen & Hegseth, 1991; Leu et al., 2015). The total biomass that accumulates depends on the amount of light transmitted and therefore the thickness of the ice and snow cover, as well as the duration of the growth season, with substratum melt and ice breakup ultimately forcing the end of the sea-ice algae growth season (Cota et al., 1991; Selz et al., 2018)

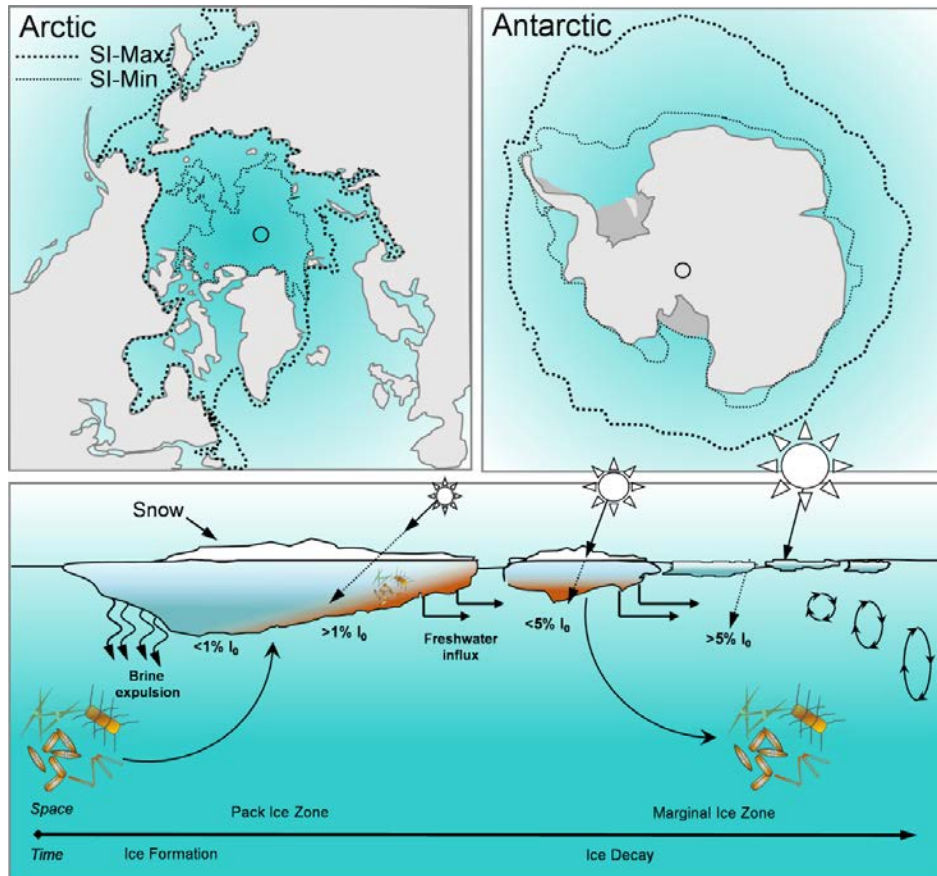


**Figure 2.1.** Sea-ice zones in both polar regions. Stippled lines indicate the maximum (SI-Max) and minimum (SI-Min) extent of sea ice in the Arctic (top left) and Southern Ocean (top right). Black open circles indicate the poles. Schematic of the spatial and temporal evolution and decay of sea ice in polar marine ecosystems. Arrows indicate seasonal changes in salinity from brine extrusion and freshwater melt, as well as light attenuation, solar angle, and mixing depth. The entrainment of microalgae into the sea ice as it forms, its proliferation and re-release into the water column during melt is also shown.  $I_0$  = percent incident irradiance.

Sea-ice microalgal communities can make significant contributions to primary production in polar regions, accounting for up to 25% of total primary production in seasonally ice-covered waters and up to ~60% in perennially ice-covered Arctic waters (Fernández-Méndez et al., 2015; Gosselin et al., 1997; Gradinger, 2009; Legendre et al., 1992). However, their precise contribution to primary production varies depending on time of year and geographic location. For example, sea-ice algae contributed as little as <math><1\%</math> to primary production in Young Sound, Greenland in 2002 (Rysgaard et al., 2001) yet contributed ~70% of primary production in Barrow, Alaska in 2003 (Lee et al., 2008b). Whilst the contribution of sea-ice microalgae to total primary productivity is generally

less than that of pelagic phytoplankton, the divergence in their timing and distribution means that the sea-ice microalgae subsist as an important source of food and energy to the marine food web (Fernández-Méndez et al., 2015; Lizotte, 2001). Indeed, their presence extends biological production in polar waters by up to three months (Cota et al., 1991), because they are the primary source of organic carbon for pelagic consumers during the ice-covered winter (Legendre et al., 1992; Michel et al., 1996; Riedel et al., 2008). Specifically, sea-ice microalgae form a critical food source for copepods, amphipods, and euphausiids (Arrigo et al., 2014a; Kohlbach et al., 2016), where the availability and nutritional quality of the microalgae have been shown to play an important role in the timing of zooplankton reproduction and, therefore, the quantity and quality of secondary production (Durbin & Casas, 2014; Leu et al., 2011; Søreide et al., 2010). As the ice begins to melt, the ecological function of sea-ice microalgae extends to seeding phytoplankton blooms in the marginal ice zone (Garrison et al., 1987; Haecky et al., 1998; Jin et al., 2007; Michel et al., 1993; Szymanski & Gradinger, 2016; Tedesco et al., 2012). Through shaping the initial phytoplankton community (Haecky et al., 1998; Selz et al., 2018) and influencing the timing of the pelagic bloom and secondary production (Tedesco et al., 2012), sea-ice microalgae can strongly influence pelagic processes, and thus exert significant influence over food web dynamics and biochemical cycling in the polar marine environment.

As primary producers, sea-ice microalgae convert solar energy into carbon via photosynthesis, making light a principal driver of sea-ice productivity. Photosynthates are converted into a variety of biochemical components including proteins, lipids, and carbohydrates; biomolecules that make up the majority of the cell biomass. The allocation of the photosynthetically derived carbon is largely determined by environmental conditions and is therefore dynamic, whereby the biomolecular composition of the microalgal cell reflects its physiological status (Bhavya et al., 2019). Shifts in biochemical composition in response to environmental conditions, while important for the physiology and nutritional status of the sea-ice microalgae itself, also strongly influence the productivity and nutritional value of primary consumers. For example, sea-ice microalgae have been shown to contribute up to ~146% of the energy budget of Antarctic krill during the winter (Bernard et al., 2019). Similarly, adequate lipid supply has been shown to be critical to the survival and reproduction of zooplankton (Graeve et al., 1994; Lee et al., 2006). Over winter, large lipid reserves are particularly important for

zooplankton when pelagic primary production is low (Falk-Petersen et al., 2009; Hagen & Auel, 2001; Kohlbach et al., 2018). The biomolecular stores of primary producers are therefore the cornerstone of productive marine ecosystems, and changes in the partitioning of these critical biomolecules contained in microalgae inevitably alters the supply of energy and essential compounds to higher trophic levels.

Planetary warming is causing polar environments to change rapidly (Meredith et al., 2019), and the significant decline in sea ice is of major ecological concern (Parkinson, 2014a; Post et al., 2013). For the past four decades, the most profound and consistent sea-ice decline has been measured in the Arctic (Mallett et al., 2021; Meredith et al., 2019; Parkinson, 2014a), which has experienced a decline in average September sea-ice extent of ~10.1% per decade (NSIDC, 2023; Post et al., 2019). Concomitant with the decline in extent is a dramatic loss of thicker multi-year ice, increasing the expanse of open water in summer, with predictions of sea ice-free summers within decades (Haine & Martin, 2017; Mallett et al., 2021; Overland & Wang, 2013). The situation in the Antarctic is more nuanced, as the southern hemisphere sea-ice extent experienced a gradual rate of increase between 1981 and 2014, after which it has been experiencing a precipitous rate of decline (Parkinson, 2019) amounting to a 27% reduction between 2010 and 2017 (NSIDC, 2023). Given that the growing season for sea-ice microalgae is already constrained to within a few months each year and seems likely to be further shortened as oceans warm and ice extent continues to decline (Cota et al., 1991; Mallett et al., 2021; Stroeve & Notz, 2018), it is probable that in the future we will see reduced accumulation of biomass, disrupting the critical early-season food supply for the region's primary consumers. Furthermore, as polar regions warm, light climate under the sea ice is expected to change, influencing productivity. A reduction in snow cover and declining sea-ice thickness would result in higher under-ice light intensity (Leu et al., 2015); conversely, where precipitation is expected to increase (more snow), light transmission may decline. In addition, sea surface temperatures are rising (Timmermans & Marshall, 2020), polar oceans are acidifying (Meredith et al., 2019; Terhaar et al., 2020), and there is an increase in freshwater input due to glacial retreat and run off (Terhaar et al., 2019). These shifts in ecosystem condition will influence future community composition (Archer et al., 1996; Becquevort et al., 2009) and biomolecular partitioning of sea-ice microalgae (Leu et al., 2010; Mock & Kroon, 2002a; Pogorzelec et al., 2017; Sackett et al., 2013; Sackett et al., 2016; Sheehan et al., 2020). Therefore, accurate assessment of the direction



and magnitude of these cellular changes is necessary to better understand the impact on marine biogeochemistry and carbon transfer through the polar marine food web.

## **2.2 Biomolecular Composition of Sea-Ice Algae from Polar Regions**

Microalgae are the primary source of biomolecules (protein, lipids, and carbohydrates) in marine ecosystems. In cells, proteins play a key role in all enzymatic processes and growth, while lipids and carbohydrates are essential components of cell membranes and form important energy reservoirs (Bhavya et al., 2019; Finkel et al., 2016; Hagen & Auel, 2001). Particular to sea-ice microalgae, lipids and antifreeze amino acids such as proline have been important evolutionary adaptations to tolerating the freezing and hypersaline conditions of the ice matrix (Morgan-Kiss et al., 2006; Thomas & Dieckmann, 2002a). The biomolecular composition of sea-ice microalgae in both absolute amounts and relative proportions vary between species, making community composition a strong determinant of overall nutritional status of primary producers.

Lipids are the most energy-rich biomolecules and, as such, contain much of the energy that is transferred among trophic levels (Hagen & Auel, 2001). Carbohydrates, which contribute less to energy transfer (Hagen & Auel, 2001), have an important role in supplying the cellular carbon pool (Finkel et al., 2016), and are integral for protein synthesis (Van Oijen et al., 2004). Proteins are the predominant source of amino acids (Ruess & Müller-Navarra, 2019) and form a cellular nitrogen reservoir (Finkel et al., 2016). They are a key source of nutrition for higher trophic levels (Hagen & Auel, 2001). In terms of carbon transfer through trophic webs, proteins have the highest relative efficiency (Bhavya et al., 2019; Lindqvist & Lignell, 1997; Scott, 1980), thus making protein rich species of potentially greater value in supporting secondary production. However, specific to polar regions, microalgae with high lipid content have been shown to be important for zooplankton fecundity (Leu et al., 2011; Søreide et al., 2010; Swalethorp et al., 2011).

Investigations into the biochemical composition of pelagic phytoplankton from the two polar regions have revealed differences in biomolecular characteristics, with Arctic waters shown to be dominated by lipid-rich cells (Kim et al., 2015; Yun et al., 2015), possibly a result of low nitrogen status. In contrast, Antarctic phytoplankton are generally found to be rich in protein (Fabiano et al., 1999; Kim et al., 2016; Smith Jr et al., 1996).

The high protein production by these primary producers, is likely supported by the high nitrogen concentrations in the seawater (Nelson & Smith Jr, 1986; Pollard et al., 2006), resulting in a nitrogen-rich food source for primary consumers and thus able to support a highly productive ecosystem. One study however, found high concentrations of carbohydrates during a summer bloom in the Amundsen Sea (Kim et al., 2018a). This was attributed to high densities of the haptophyte *Phaeocystis antarctica*, which is a common bloom-forming species in Antarctic waters (Alderkamp et al., 2007; Kim et al., 2018b). It is important to note, however, that while these patterns highlight differences between the Arctic and Antarctic, these general trends for pelagic phytoplankton are derived from only a few studies, representing low temporal and spatial coverage, and thus may not capture any potential seasonal and spatial variability. While numerous studies have investigated the biomolecular composition of sea-ice microalgae from both polar regions (Table 2.1), to date, no similar overall patterns have been observed for sea-ice microalgae. However, given the propensity for sea-ice microalgae to seed pelagic blooms, similar differences in key biochemical characteristics may exist for the ice communities from the two regions.

One of the strongest determinants of biomolecular composition is taxonomic composition. Phylogenetically distinct microalgal groups have been shown to vary in their proportional allocation of biomolecules. Diatoms (Orcophyta: Bacillariophyceae), for example, generally have higher lipid and lower carbohydrate content than other microalgal phyla, such as the chlorophytes and haptophytes (Finkel et al., 2016). More specifically, pennate diatoms within the sea ice have been shown to have higher lipid, fatty acid, and carbohydrate content than the centric diatoms from the same community (Sheehan et al., 2020). Similarly, diatoms with a smaller cell volume (such as pennate diatoms) have been shown to have higher carbohydrate content than larger volume diatoms (Hitchcock, 1982). At the taxonomic level of species, differentiation is more subtle, but nevertheless has been shown (Duncan et al., 2022; Sackett et al., 2013; Sheehan et al., 2020; Stehfest et al., 2005). However, by far most knowledge on species-specific biomolecular profiles is derived from single-species culture studies, providing a poor representation of what may be true for natural mixed communities. It is therefore important that studies on natural communities start to discriminate biomolecular profiles of individual taxa within a community if we are to improve our understanding of taxonomic biomolecular diversity.

**Table 2.1.** Compilation of studies that have measured biomolecules in sea-ice microalgae in the Arctic and Antarctic. N/A: Sampling date not available.

	Study	Taxa	Location	Latitude, Longitude	Sampling Date	Biomolecules Investigated
	An et al., 2013	<i>Chlamydomonas</i> sp. ICE-L	Zhongshan Research Station	69° S, 77° E	N/A	Fatty acids
	Cade-Menun & Paytan, 2010	<i>Fragilariopsis curta</i> , <i>Fragilariopsis cylindrus</i> , <i>Nitzschia subcurvata</i> , <i>Phaeocystis antarctica</i> , <i>Thalassiosira weissflogii</i> , <i>Dunaliella tertiolecta</i> , <i>Synechoccus</i> sp.	Culture	N/A	N/A	Lipid, protein, carbohydrate
Antarctica	Gleitz & Kirst, 1991	Diatom-dominated mixed community, primarily <i>Nitzschia</i> sp., <i>Chaetoceros</i> sp., <i>Navicula</i> sp., <i>Corethron</i> sp., <i>Rhizosolenia</i> sp., <i>Amphiprora</i> sp., <i>Dactyliosolen</i> sp., <i>Synedropsis</i> sp., <i>Tropidoneis</i> and <i>Phaeocystis pouchetii</i>	Weddell Sea	58–63° S, 55–45° W	1988/1989	Lipid, amino acid, carbohydrate
	Mock & Kroon, 2002a	<i>Fragilariopsis curta</i> , <i>Navicula gelida</i> var.-antarctica, <i>Nitzschia medioconstricta</i>	Weddell Sea	70°02' S, 06°00' W	March–May 1999	Lipid, protein
	Mock & Kroon, 2002b	<i>Fragilariopsis curta</i> , <i>Navicula gelida</i> var.-antarctica, <i>Nitzschia medioconstricta</i>	Weddell Sea	70°02' S, 06°00' W	March–May 1999	Lipid, protein

	Palmisano & Sullivan, 1985	Diatom-dominated mixed community, primarily <i>Pleurosigma</i> sp., <i>Nitzschia stellata</i> , <i>Berkeleya</i> sp., <i>Amphiprora kuferathii</i> , <i>Phaeocystis</i> spp. and small centrics.	McMurdo Sound	77° S, 166° W	November–December 1983	Lipid, protein, polysaccharide
	Teoh et al., 2004	<i>Chlamydomonas</i> sp. and <i>Navicula</i> sp.	Windmill Islands	66°17' S, 110°29' E	N/A	Lipid, protein, carbohydrate, fatty acids
	Sackett et al., 2013	<i>Fragilariopsis cylindrus</i> , <i>Chaetoceros simplex</i> and <i>Pseudo-nitzschia subcurvata</i>	Southern Ocean and Prydz Bay	66° S, 147° E, 68° S, 73° E	N/A	Lipid, protein, carbohydrate, fatty acids, amino acids
	Xu et al., 2014	<i>Chlamydomonas</i> sp. ICE-L	Zhongshan Research Station	69° S, 77° E	N/A	Lipid, fatty acids
Arctic	Lee et al., 2008a	Mixed community dominated by large chain-forming diatoms	Barrow, Alaska	71°20' N, 156°39' W	April–June 2003	Lipid, protein, polysaccharide
	Lee et al., 2008b	Mixed community dominated by large chain-forming diatoms	Barrow, Alaska	71°20' N, 156°39' W	February–June 2003	Lipid, protein, polysaccharide
	Leu et al., 2006	<i>Thalassiosira antarctica</i> var. <i>borealis</i>	Ny-Ålesund, Svalbard	78°55' N, 11°56' E	May–June 2004	Fatty acids
	Leu et al., 2010	Diatom-dominated mixed community, primarily <i>Nitzschia frigida</i> , <i>Navicula septentrionalis</i> and <i>Fragilariopsis cylindrus</i> .	Ripfjorden, Svalbard	80° N, 22° E	March–July 2007	Fatty acids
	Lund-Hansen et al., 2020	Mixed diatom-dominated community. Primarily <i>Nitzschia frigida</i> , <i>Nitzschia longissima</i> and <i>Thalassiosira</i> sp.	Kangerlussuaq West Greenland	66°57' N, 50°57' W	March 2016	Fatty acids

Mock & Gradinger, 2000	Mixed community dominated by <i>Nitzschia</i> sp., <i>Fragilariopsis</i> sp. and <i>Chaetoceros</i> sp.	Barents Sea	77°10' N, 34°04' E	May–June 1997	Lipid, protein, polysaccharides
Pogorzelec et al., 2017	<i>Nitzschia frigida</i> , pennate ribbon colonies and <i>Attheya</i> sp.	Dease Strait, Nunavut, Canada	69°1' N, 105°19' W	March–May 2014	Lipid, protein
Smith et al., 1987	Mixed community	Resolute Passage, Canada	74°41' N, 95°50' W	April–June 1985	Lipid, protein, polysaccharides
Smith et al., 1989	Diatom-dominated mixed community, primarily <i>Nitzschia frigida</i> and <i>Nitzschia grunowii</i>	Central Canadian Arctic	74°40' N, 94°54' W	April–May 1985; 1986	Lipid, protein, amino acid, polysaccharide
Smith et al., 1993	Diatom-dominated mixed community	Resolute Passage, Canada	74°41' N, 95°50' W	March–June 1989	Lipid
Smith & Herman, 1992	Diatom-dominated mixed community	Resolute Passage, Canada	74°41' N, 95°50' W	May 1987, May–June 1988	Lipid, protein, polysaccharide
Søreide et al., 2010	Diatom-dominated mixed community	Ripfjorden, Svalbard	80°27' N, 22°29' E	March–July 2007	Fatty acids
Torstensson et al., 2013	<i>Nitzschia lecointei</i>	Amundsen Sea	N/A	January 2011	Fatty acids
Torstensson et al., 2019	<i>Nitzschia lecointei</i>	Amundsen Sea	N/A	N/A	Lipid, protein carbohydrate, fatty acids

### **2.3 Measuring Biochemical Composition in Microalgae**

Quantification of the biomolecular composition of sea-ice microalgae is central to assessing biochemical cycling and carbon transfer through the polar marine food web. Numerous studies have quantified the principal constituents of cells, including lipids, carbohydrates, and proteins in sea-ice microalgae, using a variety of methods (Table 2.2). Chromatography techniques, including High Performance/Thin Layer Chromatography (HPTLC/TLC) and Gas Chromatography (GC), are popular in sea-ice microalgal studies because they are accurate, reproducible, sensitive, and rapid methods to separate and measure components within a given sample. The predominant method used in earlier studies of sea-ice microalgal nutrition was HPTLC/TLC (Gleitz & Kirst, 1991; Henderson et al., 1998; Leu et al., 2010; Mock & Kroon, 2002a; Smith et al., 1993); however GC, which is more widely available, is generally favored now (An et al., 2013; Leu et al., 2006a; Lund-Hansen et al., 2020; Mock & Kroon, 2002a; Teoh et al., 2004; Torstensson et al., 2013; Torstensson et al., 2019; Xu et al., 2014). These methods have both been used to measure proteins, lipids, carbohydrates, and fatty acids (Table 2.2). A more detailed analysis of fatty acid content (i.e., polyunsaturated (PUFA), monounsaturated (MUFA), and saturated fatty acids (SFA)) is commonly included in sea-ice microalgal studies, because fatty acids can be characteristic for specific taxonomic groups and can therefore be used as trophic markers (Leu et al., 2006a). Determining the proportion of PUFAs within microalgae is important for the polar food webs, as they are synthesized *de novo* only by photosynthetic organisms, yet are essential for many primary and secondary consumers (Sargent et al., 1985), playing a key role in successful egg production, hatching and larval development of zooplankton (Jónasdóttir et al., 2009; Mock & Kroon, 2002a; Sargent et al., 1985). Therefore, one of the major advantages of these chromatographic methods is their ability to determine specific fatty acid composition. Another significant advantage of these chromatographic methods is the capacity to measure carbon isotope signatures of individual lipids, specifically those with enhanced  $^{13}\text{C}$  values, such as sterols and highly branched isoprenoid alkenes (Belt, 2018; Belt et al., 2017; Brown et al., 2014; Johns et al., 1999). The signature of these specific lipids can then be used to determine the biochemical contribution of sea-ice algae to the water column (Belt, 2018; Kohlbach et al., 2021).

Radioisotope labelling is a relatively easy and reliable method to measure lipid, protein, polysaccharides, and amino acid content, and has been used extensively in sea-ice microalgal studies (Mock & Gradinger, 2000; Palmisano & Sullivan, 1985; Smith et al., 1987; Smith & Herman, 1992). However, this method requires biomolecular classes to be extracted prior to analysis (Li et al., 1980) and only provides information on the proportion of primary productivity allocated to a particular biomolecular pool, and not absolute concentrations, making it less quantitative than chromatographic methods.

Spectroscopic techniques have been broadly used in sea-ice microalgal research for determining lipid, protein, and carbohydrate contributions, as they have the advantage of being inexpensive and easy to use. In some cases, it may be necessary to extract the biomolecule prior to spectroscopy, for example, with the Sulpho-phospho-vanillin (SPV) reaction employed to measure lipid content (Smith et al., 1989). A potentially easier and more effective way to measure lipid content *in vivo* is by utilizing fluorescent dyes, such as BODIPY 505/515 (Xu et al., 2014). This form of live staining, however, has not been used for determination of protein or carbohydrate content in sea-ice microalgae, which are instead routinely measured using the Lowry and Smith assay (Mock & Kroon, 2002a; Smith et al., 1989; Torstensson et al., 2019) and phenol-sulfuric acid method (Smith et al., 1989; Torstensson et al., 2019), respectively. Spectroscopy techniques are limited, however, in that they are unable to determine specific fatty acid contributions. However, with  $^{13}\text{C}$  Nuclear Magnetic Resonance (NMR) spectroscopy, a quantitative measure of all biomolecules within the sample simultaneously can be obtained, with the added benefit of providing finer detail on the types of lipids, proteins, and carbohydrates present (Cade-Menun & Paytan, 2010). Due to its low sensitivity however, this technique has not been widely used in sea-ice microalgal biochemical studies (Cade-Menun & Paytan, 2010).

**Table 2.2:** Summary of the various analytical techniques that have been used to measure biomolecules (proteins and amino acids, lipids, and fatty acids, carbohydrates, and polysaccharides) in sea-ice microalgae, their advantages, and disadvantages.

Method	Biomolecules Investigated	Advantages	Disadvantages	Example Studies with Sea-Ice Algae
High Performance/Thin Layer Chromatography (HPTLC/TLC)	Lipid Fatty acid Amino Acid Carbohydrate	Rapid and easy to run multiple samples in parallel. Useful for complex lipids (therefore most marine lipids). Can be used for small quantity of sample.	Reproducibility can be unreliable. Temperature gradients can exist across the plate resulting in partial distillation of the sample. The silica plate is not reusable.	Gleitz & Kirst, 1991; Henderson et al., 1998; Mock & Kroon, 2002a; Smith et al., 1993
Gas Chromatography (GC)	Lipid Fatty acid Protein Carbohydrate	Highly sensitive. Accurate and reproducible. Easy to couple with detection and quantification techniques. Can analyze all biomolecular classes at once. Effective with a very small amount of sample.	Requires sample to be volatile and therefore lipids need to be derivatized into Fatty Acid Methyl Esters (FAMES).	An et al., 2013; Leu et al., 2006a; Leu et al., 2006b; Leu et al., 2007; Leu et al., 2010; Lund-Hansen et al., 2020; Nichols et al., 1989; Søreide et al., 2010; Teoh et al., 2004; Torstensson et al., 2013; Torstensson et al., 2019; Xu et al., 2014
Mass Spectrometry (MS)	Lipid Protein Polysaccharide	Sensitive. Accurate and reproducible.	Less sensitive than GC. Requires coupling with another technique, e.g., HPLC or radioisotope labelling.	Lee et al., 2008a, 2008b
Radioisotope Labelling	Lipid Protein Amino Acid	Highly sensitive. Accurate and reproducible.	Requires additional measurements to determine absolute concentrations.	McConville et al., 1985; Mock & Gradinger, 1999; Palmisano et al., 1988;



	Polysaccharide	Rapid and easy to run multiple samples in parallel.	Requires extraction of biomolecular classes. Requires correction for quenching. Requires training and precautions due to radioactive materials.	Palmisano & Sullivan, 1985; Smith et al., 1987; Smith & Herman, 1992
Fluorescent Dye (BIODIPY 505/515)	Lipid	Rapid. Inexpensive. Performed in vivo. Has lipid specificity, only binding to lipid bodies and chloroplasts and no other cytoplasmic compartments.	Does not stain all microalgae successfully. Can be issues associated with fading (i.e., fluorescence extinction).	Xu et al., 2014
Sulpho-phospho-vanillin (SPV) reaction	Lipid	Rapid. High throughput. Relatively easy to implement. Relatively cheap. Requires a small amount of sample.	Requires a reference standard. Color intensity varies between different lipids. Requires a two-step reaction.	Smith et al., 1989
Lowry and Smith Assays	Protein	Highly sensitive. Produces a linear response curve. Low protein-to-protein variation meaning higher accuracy in unknown protein samples. Widely used and well characterized.	Susceptible to interference by some common chemicals present in samples. Time sensitive during analysis. Lowry is more complicated with more steps than the Smith Assay. Destructive to proteins.	Mock & Kroon, 2002b; Smith et al., 1989; Torstensson et al., 2019
Phenol-Sulfuric Acid Method	Carbohydrate	Rapid. Relatively easy to implement. Accurate and reproducible.	Phenol is a toxic compound posing health risks. Non-stoichiometric method, meaning a calibration curve using	Smith et al., 1989; Torstensson et al., 2019

		Widely used and well characterized.	a series of standards must be generated, limiting the analysis of more complex carbohydrates.	
Carbon-13 Nuclear Magnetic Resonance ( <sup>13</sup> C NMR) Spectroscopy	Lipid Protein Carbohydrate	Can analyze all biomolecular classes at once. Provides intramolecular detail.	Low sensitivity. Long duration of analysis.	Cade-Menun & Paytan, 2010
FTIR-microspectroscopy	Lipid Fatty acid Protein Amino acid Carbohydrate	Highly sensitive. Can be used to analyze single cells giving species-specific results. Nondestructive. Ability to obtain data at multiple wavelengths simultaneously. Can analyze all biomolecular classes at once. Effective with a very small amount of sample.	Small size mounting chamber. Synchrotron light source is not readily available and is expensive.	Pogorzelec et al., 2017; Sackett et al., 2013; Sheehan et al., 2020

As with NMR and GC analyses, Fourier Transform Infrared (FTIR) microspectroscopy is a technique that measures the whole biomolecular profile at once, enabling each sample to be spectrally defined based on a biochemical fingerprint (Heraud et al., 2005). This spectroscopic approach has the benefits of being sensitive, high throughput, quantitative, and rapid (Dean et al., 2012; Fanesi et al., 2019; Heraud et al., 2007; Heraud et al., 2005; Sackett et al., 2013; Sackett et al., 2016). Coupled with a Synchrotron light source, FTIR microspectroscopy becomes more sensitive and can deliver much higher resolution ( $\sim 3$   $\mu\text{m}$ ) spectral imaging (Reffner et al., 1995). This technique has the significant advantage that it can be performed on individual cells and subcellular compartments, allowing for unique insight into the response of individual taxa within a natural community. Moreover, with micrometer resolution, it can be used to localize and measure specific organelles within larger cells or tissues. The ability to understand specifically which species within the community is affected by environmental change and in what way is unique to this biomolecular method. In nonpolar marine microalgae, it has been used widely to investigate biomolecular responses to environmental change (Giordano et al., 2001; Heraud et al., 2005; Sigeo et al., 2007; Wagner et al., 2010). To date however, very few studies have looked at the nutritional value of natural sea-ice assemblages at the species level, with only two studies investigating the effects of light on biomolecular composition of Arctic diatoms (Findlay et al., 2017; Pogorzelec et al., 2017) and one describing the biomolecular profiles of four Antarctic sea-ice diatoms (Sheehan et al., 2020). Synchrotron-based FTIR-microspectroscopy has been used successfully to investigate changes in biomolecular composition as a result of ocean acidification in Antarctic diatoms (Duncan et al., 2022) and biomolecular changes as a result of iron enrichment in Antarctic microalgae (Sackett et al., 2014). As the only biochemical method that delivers species-level resolution, it is an attractive technique for resolving questions related to response diversity within natural communities and tracking potential shifts in trophic carbon transfer.

#### **2.4 Environmental Factors That Influence Biomolecular Composition**

The sea-ice environment exposes microorganisms that live within it to strong gradients in temperature, salinity, and light (Boetius et al., 2013; Morgan-Kiss et al., 2006; Thomas & Dieckmann, 2002a). From the extreme hypersaline brine channels (salinities up to 145 ppt), freezing temperatures ( $-2$  –  $-20$   $^{\circ}\text{C}$ ) and high light conditions ( $>100$   $\mu\text{mol m}^{-2} \text{s}^{-1}$ ) near the ice surface (Gleitz & Thomas, 1993), to the relatively mild and stable conditions

for the microalgae living at the ice–water interface (temperature:  $\sim 1.8$  °C; irradiance:  $3.5\text{--}40 \mu\text{mol m}^{-2} \text{s}^{-1}$ ) (Cota et al., 1991; Thomas & Dieckmann, 2002b). These steep environmental gradients, which vary over the seasonal formation and decay of the ice, mean that the organisms living and thriving in this habitat have evolved specialized physiological strategies, including biomolecular adjustments, to cope with rapid and extreme changes in their living conditions (Morgan-Kiss et al., 2006). It is worth noting that growth rate is also expected to influence biomolecular storage; however, this is not explored further below as it cannot be measured or controlled for within natural community studies.

### 2.4.1 Temperature

At the ice–water interface, temperature generally remains around  $-1.8$  °C throughout spring, however as sea surface temperatures rise with the onset of ocean warming (Timmermans & Marshall, 2020), it is possible that warmer temperatures will alter the biochemical composition of the algae, drive an earlier ice melt, and ultimately inhibit sea-ice microalgal growth completely (Leu et al., 2015; Mallett et al., 2021). Limited work has been completed on the effects of temperature on the biochemical composition of sea-ice algae, but from these few studies some patterns have emerged. Extreme subzero temperatures ( $-20$  °C) have been associated with a decline in fatty acids, especially PUFA content (An et al., 2013). A decline in fatty acids has been observed also under moderate temperature increases (from  $-1.8$  °C to  $3$  °C), as well as in temperature increases well beyond the natural range ( $\sim 15$  °C) (An et al., 2013; Teoh et al., 2004; Torstensson et al., 2013; Torstensson et al., 2019) (Fig. 2.2A). In several Antarctic sea-ice diatoms, an increase in relative protein content and decrease in carbohydrate content have been observed with exposure to warmer (up to  $3$  °C) temperatures (Torstensson et al., 2019), including temperatures well above ( $\sim 20$  °C) the natural range for sea-ice microalgae (Teoh et al., 2004). These data indicate that optimal temperatures for maximum fatty acid content lies around  $-1.8$  °C, and that increases in temperature will likely see reductions in PUFA and carbohydrate content but increases in protein.

### 2.4.2 Salinity

Salinity within sea ice follows a steep gradient, from hyper-saline conditions within the brine channels ( $>70$  ppt) to seawater ( $\sim 35$  ppt) and meltwater ( $<30$  ppt) salinity levels at the ice–water interface. In hypersaline environments, such as sea-ice brine channels, lipid

and amino acid content have been shown to be higher than at lower salinity (~35 ppt) (Sackett et al., 2013). On the other hand, decreasing salinity (i.e., 10–20 ppt, compared to ambient levels) have resulted in increased protein (Gleitz & Kirst, 1991), amino acid (Sackett et al., 2013), fatty acid (Torstensson et al., 2019), and carbohydrate content (Torstensson et al., 2019) (Fig. 2.2B). These changes in response to hyposaline conditions provide insight into some of the possible changes to nutritional status of microalgae with increased freshening from ice melt and glacial runoff. Whilst further research is needed, these results suggest that ongoing ocean freshening (Brown et al., 2020; Jacobs et al., 2002) may lead to a decline in lipid, yet increase in protein and carbohydrate content.

### 2.4.3 Light

Being photosynthetic organisms, light transmittance is one of the key factors driving sea-ice microalgal community productivity and composition (Cota et al., 1991; Leu et al., 2015), playing a defining role in the commencement of the spring under ice bloom. It has been shown repeatedly to determine the nutritional quality in sea-ice microalgae, although the direction of change in biomolecular composition varies depending on the magnitude of change in light intensity (Fig. 2.2C). Primarily, a seasonally relevant change in light intensity as a result of low and high snow cover (Findlay et al., 2017; Pogorzelec et al., 2017; Smith et al., 1989) and through naturally manipulated light levels (Lee et al., 2008a), have been found to increase lipid synthesis over the duration of the spring bloom (Lee et al., 2008b; Smith et al., 1993; Smith et al., 1987; Smith & Herman, 1992), with one study finding no significant correlation (Palmisano & Sullivan, 1985). On the other hand, light intensity beyond the expected natural range ( $>100 \mu\text{mol m}^{-2} \text{s}^{-1}$ ) has been found to cause a decrease in lipid content (Cade-Menun & Paytan, 2010; Gleitz & Kirst, 1991) possibly due to photoinhibition limiting photosynthetic energy production and thereby biomolecular synthesis. In contrast to the general overall lipid response, PUFAs have consistently been found to decline with increasing light intensity (Fig. 2.2C). Decline in PUFAs have been observed in natural sea-ice microalgal communities with increase in irradiance, with minimal and dense snow cover (Leu et al., 2010), when exposed to in situ light manipulation (Lund-Hansen et al., 2020) and experimentally, using a unialgal culture of *Thalassiosira antarctica* var. *borealis* (Leu et al., 2006b) or when light adjusted sea-ice algae are subjected to continuous darkness (Xu et al., 2014). In Arctic open water phytoplankton communities, PUFAs have also been observed to decline with increasing light during the spring period (Leu et al., 2006a).

Changes in irradiance have also been shown to influence protein, amino acid, and carbohydrate content (Fig. 2.2C). In mixed microalgae communities, protein and amino acids have generally been found to decrease with increasing light intensity over a realistic spring light range (3.5–40  $\mu\text{mol m}^{-2} \text{s}^{-1}$ ), largely concomitant with an increase in lipid content (Lee et al., 2008a, 2008b; Palmisano & Sullivan, 1985; Smith et al., 1987; Smith et al., 1989). Declines in protein have also been observed at light levels exceeding those expected in situ (40–100  $\mu\text{mol m}^{-2} \text{s}^{-1}$ ; Gleitz & Kirst, 1991); however, at higher light levels (125–250  $\mu\text{mol m}^{-2} \text{s}^{-1}$ ), protein allocation has been shown to increase (Cade-Menun & Paytan, 2010). Importantly however, some studies found no effect on protein and amino acid content in response to increasing irradiance (Mock & Kroon, 2002b; Pogorzelec et al., 2017; Smith & Herman, 1992). For carbohydrates, sea-ice microalgae have been shown to increase their allocation of carbon to carbohydrates in response to natural environmental increases in irradiance (Smith et al., 1989), controlled incubations within the natural light range (Mock & Kroon, 2002b; Smith et al., 1987) and to higher than naturally expected under-ice irradiance intensities (42–106  $\mu\text{mol m}^{-2} \text{s}^{-1}$ , compared with 3–19  $\mu\text{mol m}^{-2} \text{s}^{-1}$ ; Gleitz & Kirst, 1991), with only one study finding no significant effect on carbohydrate content as a result of increasing light intensity (Lee et al., 2008b).

#### 2.4.5 Nutrient limitation

Another key factor well known for shaping sea-ice microalgal biomolecular composition is nutrient availability. Nutrient limitation can occur within the narrow brine channels, where the microalgae can exhaust some or all of the available nutrients. This may partly explain why some lipids measured in sea-ice microalgae are enriched with  $^{13}\text{C}$  (Budge et al., 2008; Kohlbach et al., 2016). Nutrient limitation is less of a problem at the ice–water interface, where nutrients are continually replenished from the seawater. However, nitrogen limitation, which is a defining constraint on growth and development (Lavoie et al., 2005; Leu et al., 2015; Róžańska et al., 2009) and is expected to intensify with increasing ocean stratification (Slagstad et al., 2015; Vancoppenolle et al., 2013), commonly leads to increased lipid and decreased protein content in microalgae (e.g. Chen et al., 2014; Chokshi et al., 2017; Jiang et al., 2012; Rehman & Anal, 2019). This is because nutrient stress induces the algae to favor energy storage in lieu of growth and photosynthetic efficiency (Berges et al., 1996; Berges & Falkowski, 1998; Dean et al., 2010; Giordano et al., 2001). These trends have been observed in sea-ice microalgae, which were shown to increase in relative lipid (Mock & Gradinger, 2000; Mock & Kroon,

2002a) and PUFA content (Mock & Kroon, 2002a), concomitant with a decline in protein and carbohydrate allocation (Mock & Gradinger, 2000; Mock & Kroon, 2002a) (Fig. 2.2D) with nitrogen limitation. Given that vast expanses of the Arctic are nitrogen poor, it is possible that this low nitrogen environment, which underpins the lipid-rich sea-ice microalgae (Kim et al., 2015; Yun et al., 2015), is partially responsible for driving an evolutionary dependence on lipids for the successful egg hatching and reproduction of Arctic zooplankton (Peltomaa et al., 2017; Søreide et al., 2010).

#### 2.4.6 pH

With ocean warming, nutrient limitation will likely occur heterogeneously; dissolved inorganic carbon availability, however, from atmospheric CO<sub>2</sub> absorption by seawater, is increasing ubiquitously. Ocean acidification poses a real and imminent threat to marine life in the polar regions, including microalgae (Hancock et al., 2020; Meredith et al., 2019; Petrou et al., 2016); however, limited work has been undertaken to understand its effect on sea-ice microalgal growth and biochemical composition. To date few studies have compared biochemical composition of sea-ice microalgae under current *p*CO<sub>2</sub> levels (~390 µatm) and those projected for 2100 (~1000 µatm; IPCC, 2014). Elevated *p*CO<sub>2</sub> levels (~1000 µatm) over a period of ≥14 days resulted in reduced lipid (Xu et al., 2014) and fatty acid content (Torstensson et al., 2013), whilst shorter exposure (6 days) at the same *p*CO<sub>2</sub> levels was found to have no significant effect on protein, fatty acid, or carbohydrate content (Torstensson et al., 2019), suggesting that length of exposure influences physiological response (Fig. 2.2E). A recent study on Antarctic coastal diatoms found that high *p*CO<sub>2</sub> levels resulted in a decrease in lipid content for the two largest taxa and an increase in protein content across all five taxa investigated (Duncan et al., 2022). Although conducted on polar pelagic algae, this study indicates that species-specific responses likely exist within sea-ice communities, which has the potential to affect food web dynamics and carbon transfer in polar regions.

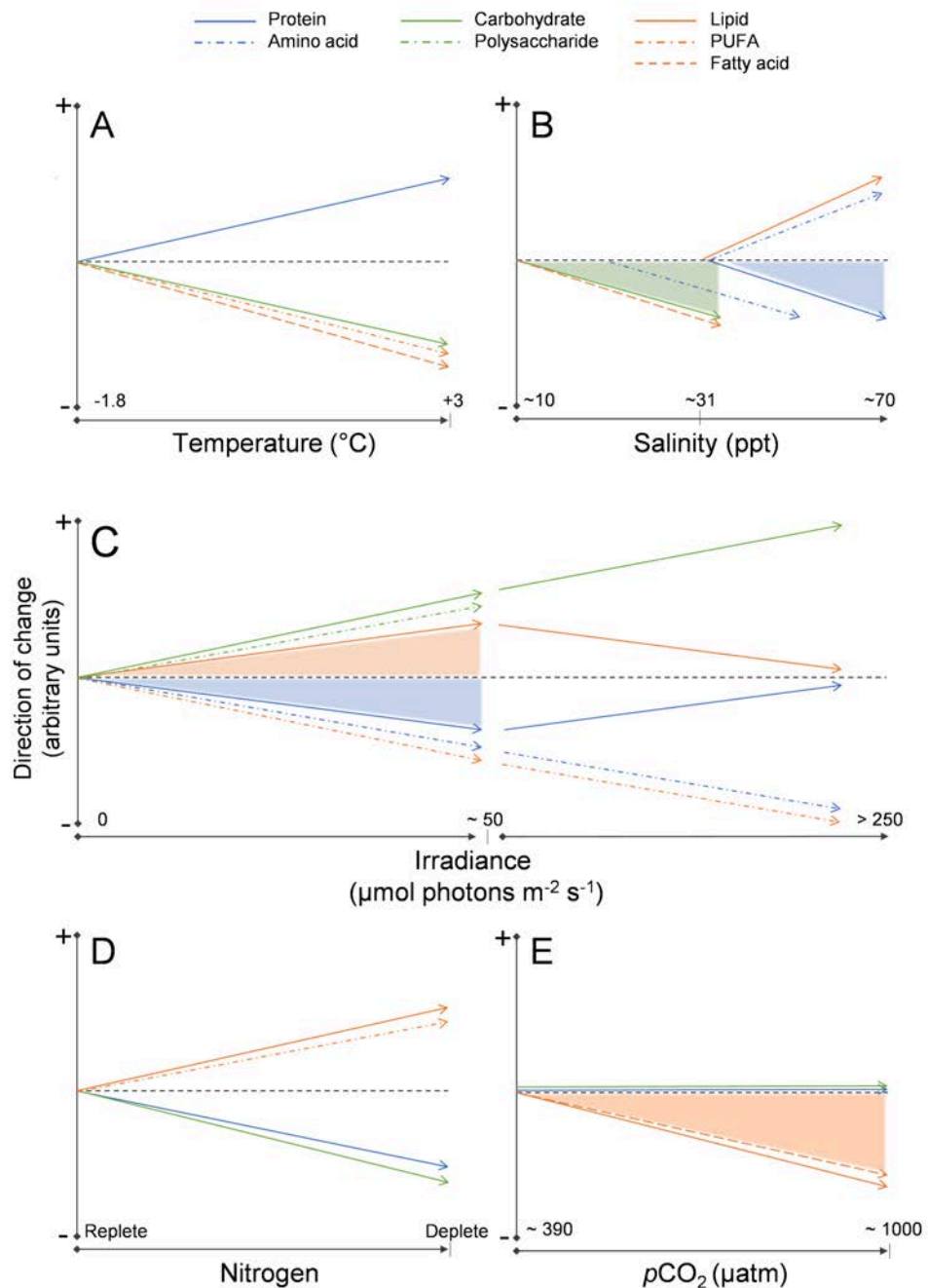


**Figure 2.2.** Schematic showing the direction of change (increase or decrease) in biomolecules in sea-ice microalgae exposed to variations in (A) temperature, (B) salinity, (C) irradiance, (D) nitrogen concentration, and (E)  $p\text{CO}_2$ . Changes are not indicative of magnitude. The different biomolecules are coded by color and line type as described in the legend. Shaded areas indicate where results from studies have revealed both a change and no change with environmental perturbation. Data were obtained from the studies listed in Table 2.1.



## **2.5 Sea-Ice Microalgae Biochemistry and Carbon Transfer through the Polar**

### **Marine Food Web with Climate Change**

Climate change has the potential to alter biodiversity and, therefore, ecosystem functioning. Multi-species assemblages are considered more resilient to environmental fluctuations. This is because the differences in the individuals' phenotypic plasticity and tolerance, as well as the inherent complexity of species interactions, result in greater response diversity within the community. For natural phytoplankton communities, biodiversity has been shown to be important for maintenance of overall ecosystem functioning in variable environments (Bestion et al., 2021), meaning that a reduction in biodiversity may reduce ecosystem productivity and resilience. We know from studies looking at biomolecular profiles of individual sea-ice diatoms that there is considerable diversity in cellular carbon allocation between species (Pogorzelec et al., 2017; Sackett et al., 2013; Sheehan et al., 2020). Similarly, while exploring the role of climate change on biomolecular partitioning, it has been shown that CO<sub>2</sub> enrichment of natural Antarctic diatom communities resulted in species-specific biochemical responses (Duncan et al., 2022). These studies highlight the potential importance of species richness and response diversity within sea-ice microalgal communities for the resilience of the polar ecosystem to climate change. Natural community studies on the nutritional value of sea-ice algae have primarily been completed on whole communities, which is valuable in that it can show an overall shift in food quality, but only by investigating individuals within a community, such as with synchrotron-based FTIR microspectroscopy, is it possible to determine the diverse taxon-specific responses, thereby elucidating the strength and direction of change and determining the winners and losers of environmental change.

There are indications that with the ongoing ecosystem changes in the polar regions, microalgal communities will shift toward smaller taxa and no longer be dominated by larger diatoms. This has already been observed in both Arctic and Antarctic communities in response to ocean acidification (Hancock et al., 2018; Sugie et al., 2020), ocean freshening (Li et al., 2009; Moline et al., 2004; Sugie et al., 2020), reduced sea-ice extent (Montes-Hugo et al., 2009; Neeley et al., 2018) and sea surface warming (Sugie et al., 2020). Such a shift is anticipated to have a significant effect on trophic energy transfer, where a community dominated by smaller cells would generally mean a reduction in grazing efficiency by zooplankton (Boyd et al., 1984; Moline et al., 2001; Moline et al., 2004; Quetin & Ross, 1985). There is also evidence of climate change altering taxonomic

dominance, for example, increased light transmittance has been shown to favor diatoms over flagellates (Róžańska et al., 2009), specifically favoring centric rather than pennate diatoms (Campbell et al., 2018). In sympagic and pelagic phytoplankton blooms, nanoflagellate dominance has been observed along with ocean freshening (Moline et al., 2004; Neeley et al., 2018; Saggiomo et al., 2021) and post-bloom meltwater conditions (Róžańska et al., 2009). While these shifts in microalgal community composition will be heterogeneous and geographically dependent, any persistent changes or losses in species will invariably have trophic and biogeochemical implications. For example, shifts that favor taxa of poorer nutritional quality, such as species with reduced lipid or protein content, would result in less energy available for transfer through the marine food web. Specifically, a decline in lipid content may alter the growth and reproduction of primary and secondary consumers (Hygum et al., 2000; Peltomaa et al., 2017; Søreide et al., 2010). Similarly, environmental conditions that favor one taxonomic group such as a shift toward nanoflagellate dominated communities at the expense of diatoms, may see strong alterations to regional carbon and silicon cycling (Finkel et al., 2016; Krause et al., 2018; Thingstad et al., 2008). It is clear, therefore, that as communities change or become less complex, we can expect to see altered marine biochemistry and ecosystem functioning.

Geographic variation in climate change effects means that changes to community composition and, therefore, biochemical composition of primary producers at the community level cannot be expected to be uniform. Since the 1970s, Arctic land-fast ice regions have seen a much more rapid decline in sea-ice extent of 10.5% per decade, compared to 5.2% per decade for Arctic pack-ice regions (Li et al., 2019), and recent studies have revealed similar trends of accelerated land-fast ice retreat in Antarctica (Kim et al., 2018b; Turner et al., 2017). As such, these coastal areas will likely experience an increased reliance on open water pelagic phytoplankton blooms sooner than perennial multi-year ice regions (Arrigo & van Dijken, 2015; Palmer et al., 2014). While we have seen a ~3 month increase in annual sea-ice free period since 1980 at both polar regions, the change is occurring in different ways. In the Arctic, sea-ice retreat is occurring on average two months earlier, with the advance one month later, whilst the Antarctic Peninsula is experiencing the average sea-ice retreat one month earlier and the advance two months later (Stammerjohn et al., 2012). With predictions of ice-free periods becoming more prolonged (Lee et al., 2017; Overland & Wang, 2013) we may see increases in total primary production (Arrigo & van Dijken, 2015; Lewis et al., 2020;

Slagstad et al., 2015; Vancoppenolle et al., 2013). However, there are concerns that a heavily reduced sea-ice season will result in a timing mismatch between the primary producers and the consumers who rely on the earlier sea-ice microalgal bloom for reproduction (Dünweber et al., 2010; Kahru et al., 2011; Koeller et al., 2009; Leu et al., 2011; McConnell et al., 2012; Søreide et al., 2010). In addition, for both the Arctic and Antarctic, reduced sea-ice production and increased glacial melt has amplified ocean freshening particularly in enclosed fjordic systems (Brown et al., 2020; Henley et al., 2019; Jacobs et al., 2002), altering phytoplankton community composition (Moline et al., 2004; Montes-Hugo et al., 2009; Saggiomo et al., 2021). Taken together, broad changes in sea-ice microalgal community structure, phenology, and species-specific carbon allocation, could significantly alter carbon transfer and biochemical characteristics of polar marine ecosystems.

## **2.6 Conclusions**

Knowledge of sea-ice microalgal biochemical composition and understanding the influence of environmental factors on their cellular carbon partitioning is critical to determining the nutritional quality of primary production in polar regions and the broader effects on energy transfer through the marine food web. As light is a primary driver of algal primary productivity, many studies to date have focused on the effect of irradiance on biomolecular composition, with trends indicating that an increase in total irradiance dose would drive an increase in lipid and carbohydrate content but a decrease in PUFA and protein content. Studies have also shown, however, that warmer temperatures will increase protein content, and nitrogen limitation will enhance lipid and PUFA production at the expense of all other biomolecules. Across the environmental effects considered here, changes in response to different environmental factors were not unidirectional, and as such, the overall direction of change likely to occur in the ecosystem under future conditions remains unclear. Further research is therefore recommended to better tease apart discrete and synergistic effects on sea-ice microalgal biochemistry. While understanding any degree of change across sea-ice microalgal communities is important, biochemical changes appear to have a degree of species specificity, and, therefore, future studies would benefit also from employing methodologies that allow for the determination of species-specific biomolecular characterization. With the accelerated pace of climate change rapidly reshaping the physical and chemical marine environment

(warmer temperatures causing reductions in sea-ice extent, thickness and longevity, ocean stratification and increasing atmospheric CO<sub>2</sub> concentrations causing seawater acidification), it is anticipated that changes to sea-ice microalgal community structure and biochemical composition will ensue. As shown here, these changes will likely alter the allocation of carbon to different biomolecules by sea-ice microalgae resulting in significant shifts in biochemical cycling and carbon transfer through polar marine food webs, the effects of which could have far-reaching consequences for polar marine ecosystems.

**Acknowledgements:**

R.J.D. is supported by an Australian Government Research Training Program Scholarship and an AINSE Ltd. Postgraduate Research Award (PGRA).

# Chapter 3

## Spatio-temporal dynamics in microalgal communities in Arctic land-fast sea ice

*Published in Progress in Oceanography as:*

**Duncan, R. J.**, Søreide, J. E., Varpe, Ø., Wiktor, J., Pitusi, V., Runge, E., & Petrou, K. (2024). Spatio-temporal dynamics in microalgal communities in Arctic land-fast sea ice. *Progress in Oceanography*. 224, 103248.  
DOI: 10.1016/j.pocean.2024.103248

*Author contributions:*

R.J.D., J.E.S., O.V., and K.P. conceptualised the study and determined the methodology. R.J.D. performed the investigation, data curation, formal analysis, data visualisation and wrote the original draft. D.N. assisted with the methodology, investigation and designed the code for spectroscopy data curation. J.E.S., V.P., E.R. and K.P. contributed to the investigation, and resources were supplied by J.E.S. Validation of taxonomic data was given by J.W. Supervision of R.J.D. was performed by J.E.S, O.V and K.P. Funding was acquired by R.J.D. and J.E.S. All authors contributed to reviewing and editing the original draft written by R.J.D.

Production Note: Signature removed prior to publication.	Production Note: Signature removed prior to publication.	Production Note: Signature removed prior to publication.	Production Note: Signature removed prior to publication.	Production Note: Signature removed prior to publication.	Production Note: Signature removed prior to publication.	Production Note: Signature removed prior to publication.
R. Duncan	J.E. Søreide	Ø. Varpe	J. Wiktor	V. Pitusi	E. Runge	K. Petrou

Chapter 3 investigates the relationship between land-fast sea-ice algal community composition and light transmissivity over the spring season in Svalbard, as changes to Arctic sea-ice extent and snow cover as a result of climate change will drive shifts in the light transmitted to the bottom-ice community. Spatial dynamics were captured through the sampling of six geographically different fjords, and temporal dynamics and seasonality were investigated through a repeated transect within one fjord.

**Abstract**

Sea-ice microalgae are an important source of energy for the polar marine food web, representing the primary carbon source prior to pelagic phytoplankton blooms. Here we investigate community dynamics of sea-ice microalgal communities in land-fast sea ice across six different fjords in high-Arctic Svalbard, Norway, during Spring (April – May). We found that light ( $0.1 - 23\%$  incoming PAR /  $0.1 - 193 \mu\text{mol photons m}^{-2}\text{s}^{-1}$ ) played a central role in determining community composition, with more diverse assemblages observed in sites with more light transmitted to the bottom ice community. In April, microalgal assemblages were similar when under-ice light transmittance was similar, independent of geographical location, however this light-derived separation of community structure was not evident in May. At all sites, assemblages were dominated by pennate diatoms, with the most abundant taxon being *Nitzschia frigida*. However, with increasing under-ice light transmittance, we saw an increase in the relative abundance of Dinophyceae, *Navicula* spp. and *Thalassiosira* spp. A positive relationship between light and  $\delta^{13}\text{C}$  enrichment and C:N ratios in the ice algal biomass demonstrated the effect of light on the biochemical composition of ice algae. Light did not correlate with cell abundance or chlorophyll *a* concentration. With anticipated changes to Arctic sea-ice extent and snow cover as a result of climate change, we will see shifts in the light transmitted to the bottom ice community. These shifts, whether caused by reduced light transmittance from increased snow cover or increased light transmittance from thinning ice, snow depth or increased rainfall, will likely alter sea-ice microalgal community composition, which in turn, may influence the success of secondary production and biogeochemical cycling in polar waters.

## **Introduction**

The sea ice-ocean interface forms a unique environment that provides a habitat for microalgae and micrograzers to live within a network of brine channels and tubes that exist on the bottom of the ice (Arrigo, 2014). This space-limited environment is characterised by sub-zero temperatures, changing nutrient availability, variable salinity and low light, frequently receiving < 10% incoming (incident) irradiance (Arrigo, 2014). The specialised photosynthetic sea-ice biota that thrive in these dynamic physiochemical conditions are an important contribution to polar primary production. During spring, the biomass of the bottom ice assemblages can be up to ten times higher than for the adjacent seawater (Comeau et al., 2013; Michel et al., 1996), with values above 25 g C m<sup>-2</sup> yr<sup>-1</sup> often recorded (Smith et al., 1988). Thus, sea-ice microalgal communities are an important source of energy for the polar marine food web (Kunisch et al., 2021; Michel et al., 1996).

The contribution of sea-ice microalgae to primary production varies across time and space, ranging from 1 - 60% in ice-covered Arctic waters (Fernández-Méndez et al., 2015; Gosselin et al., 1997; Gradinger, 2009), and are a primary source of organic carbon for pelagic consumers in the early spring, extending biological production in polar waters by up to three months (Cota et al., 1991; Ji et al., 2013). In providing this initial food source during the early phases of seasonal zooplankton reproduction, sea-ice algae play an important role in the quantity and quality of secondary production (Durbin & Casas, 2014; Leu et al., 2011; Søreide et al., 2010). In addition, sea-ice algae are intricately linked with pelagic primary producers. With some taxa able to thrive in both the sympagic and pelagic environment, they may play a role in seeding the late spring /early summer pelagic phytoplankton blooms (Michel et al., 1993; Runge & Ingram, 1991; Tedesco et al., 2012). The sea-ice algal cells not consumed in the water column, will often deposit on the sea floor and shallow littoral zone in a dormant or vegetative state, before being resuspended the following winter and spring (Vonnahme, 2021). In deeper areas, sea-ice algal biomass is exported to depth where it is deposited on the ocean floor or remineralized (Boetius et al., 2013).

Diatoms (Bacillariophyceae) dominate sea-ice algal communities (Arrigo, 2014; Hop et al., 2020; Horner, 1985). However, diversity within ice algal communities can vary from fewer than 20 taxa to over 150 taxa (Arrigo, 2014; Poulin et al. 2011; Campbell et al.,

2018; Hop et al., 2020), where the composition is controlled largely by species-specific responses to temperature, salinity, light, and nutrients (Campbell et al., 2018; Hop et al., 2020). For example, taxonomic diversity has been shown to increase with reduced sea-ice thickness, related to a weakened dominance of *Nitzschia frigida* as the ice thins (Hegseth & von Quillfeldt, 2022). Similarly, centric diatoms can increase their relative abundance compared to pennate diatoms under higher light conditions (Campbell et al., 2018), whereas flagellates tend to outcompete diatoms when light is severely restricted (Róžańska et al., 2009). These dynamics in community composition affect carbon and nutrient cycling, as regulation of photosynthetic state (Kvernvik et al., 2021; Petrou & Ralph, 2011) and nutritional content are species specific in polar microalgae (Duncan et al., 2024; Duncan et al., 2022; Sackett et al., 2013). Furthermore, sea-ice algal size structure influences nutrient uptake efficiency by primary consumers (Quetin & Ross, 1985) and nutrient supply and transfer to higher trophic levels (Hitchcock, 1982). Sea ice associated taxa are generally larger and more often chain-forming than open-oceanic phytoplankton (Arrigo, 2014). A community of larger cells in conjunction with the presence of aggregated chains, impacts the grazing efficiency due to micro- and mesozooplankton having a defined prey size range within which they can effectively graze (Berggreen et al., 1988; Quetin & Ross, 1985). In addition, in the early season when grazing pressure in the pelagic zone is minimal, the aggregated chains sink more quickly than single cells (Riebesell et al., 1991) to the ocean floor becoming an important food source for the benthos (McMahon et al., 2006). Taken together, community characteristics of size structure, nutritional content, growth rate and photosynthetic state are key to determining the extent to which the sea-ice algae support the polar marine food web.

Thickness and areal coverage of land-fast ice has been declining rapidly for the past four decades across the Arctic (Yu et al., 2014) and in some areas, it has been reported to be declining at twice the rate of pack ice (Li et al., 2019). In Svalbard, land-fast ice extent in 2005-2019 was at 50% of the extent recorded in 1973-2000, with projections that the extent will decline to only 12% in the next 10-20 years (Urbański & Litwicka, 2022). In addition, the duration of sea-ice coverage in Svalbard has reduced by up to four months since 2005 (Urbański & Litwicka, 2022), meaning the incorporation of sea-ice assemblages into the ice is delayed and bloom termination and end of season ice melting occurs earlier. To understand the implications of such a decline in land-fast ice extent and



duration on marine biodiversity and ecosystem function, it is important to understand how land-fast ice algal communities are affected by environmental change. To date, most studies into the composition of sea-ice algal communities and their dynamics have focussed on pack ice communities. However, a handful of studies comparing algal communities between pack and land-fast ice (Archer et al., 1996; Comeau et al., 2013; Ratkova & Wassmann, 2005) found significant compositional differences between habitats, suggesting that our understanding of land-fast ice algal community dynamics is incomplete.

This study investigates the relationship between land-fast sea-ice algal community composition and light transmissivity over the spring season (April-May) in Svalbard, Norway. Land-fast ice within six geographically distinct fjords was sampled to investigate spatial dynamics, while one fjord (Van Mijenfjorden) was sampled repeatedly throughout the spring to capture seasonality. The first hypothesis that is investigated is that sites with less snow cover and ice thickness, and therefore higher light transmissivity (higher under-ice light climate), would have a more abundant and taxonomically diverse algal community, with increased contributions of common pelagic taxa. The second hypothesis tested is that algal abundance and diversity would increase with the progression of spring until late spring, after which the advection of warmer waters would result in ice melt, attenuating community diversity and abundance.

### **Study Area**

This study was conducted within six fjords in Svalbard, Norway (Fig. 3.1; Table S3.1) between April-May 2021. The sampling locations covered the west, north and east coasts of Spitsbergen; Van Mijenfjorden, Tempelfjorden, Billefjorden, Austfjorden, Agardhbukta and Inglefieldbukta. Whilst the sampling sites are relatively close by land access, they are not close oceanographically and are influenced by different water masses, meaning they are markedly different in their conditions. Van Mijenfjorden (70 km long and 10 km wide) is located on the south western coast. It is comprised of an inner basin with an approximate depth of 70 m and an outer basin approximately 120 m deep (Høyland, 2009). It is a partially enclosed fjord due to the presence of Akseløya Island at the fjord mouth (Høyland, 2009), which minimises the advection of warm, saline Atlantic water transported to the area by the West Spitsbergen Current (WSC). The rather shallow and isolated fjord is efficiently cooled when air temperatures drop so the conditions are

favourable for seasonal ice formation from January to June (Høyland, 2009). Tempelfjorden (14 km long and 5 km wide) is the innermost branch of Isfjorden, located in the central west coast and is divided into two basins; a smaller, glacial fed basin in the inner fjord up to 70 m deep and a central-outer basin up to 110 m deep (Forwick et al., 2010). Petuniabukta (6 km long and 3.5 km wide) is the innermost bay of another branch of Isfjorden - Billefjorden. A shallow sill prevents much of the advection of warm, Atlantic water penetrating the main area of Isfjorden, meaning sea-ice cover generally persists from December-June in inner Billefjorden (Søreide et al., 2022). Austfjorden (35 km long and 5 km wide) is the innermost part of the 75 km long Wijdefjorden (totalling 110 km long), located on the north coast. The long, narrow nature of this fjord, and limited water exchange with offshore area due a cross-fjord sill, ensures reliable sea-ice cover throughout January-May (Allaart et al., 2020). Inglefieldbukta (2.5 km wide bay) and Agardhbukta (8 km wide bay) are located on the south eastern coast of Spitsbergen and are exposed to cold Arctic water masses passing through adjacent Storfjorden. In addition, Inglefieldbukta receives glacial runoff from Inglefieldbreen. These sites have extensive snow and ice cover during December - July (Haarpaintner et al., 2001).

## **Materials & Methods**

### **Sample Collection**

Samples of sea-ice algae were collected using a Kovacs core barrel (9 cm diameter; Kovacs Enterprise, USA). The bottom 3 cm of the sea ice was retained only (Smith et al., 1988). At each sampling site, six cores were taken approximately 1 m apart, with care taken to ensure the coring location was not disturbed. Cores were then pooled into triplicates, as cores 1-2, 3-4 and 5-6. Locally acquired filtered seawater (100 mL of 0.7  $\mu\text{m}$  GF/F, Whatman, England) was added for each cm of core, to minimise osmotic stress (Campbell et al., 2019) and samples allowed to melt in darkness for 24 h at 4 °C. From each of the three pooled cores, subsamples of known volume were taken for determination of community composition, particulate organic carbon and nitrogen (C:N) and chlorophyll *a* (chl *a*), with correction for dilution with filtered seawater applied. At each sampling event (date and station), under-ice water (0.5 m) was collected using a 5L Niskin water sampler (KC Denmark, Silkeborg) and subsampled for chl *a*, particulate organic C:N and nutrient (nitrate plus nitrite ( $\text{NO}_3^- + \text{NO}_2^-$ ), phosphate ( $\text{PO}_4^{3-}$ ) and silicic acid ( $\text{Si}(\text{OH})_4$ ) and ammonium ( $\text{NH}_4^+$ )) analyses.

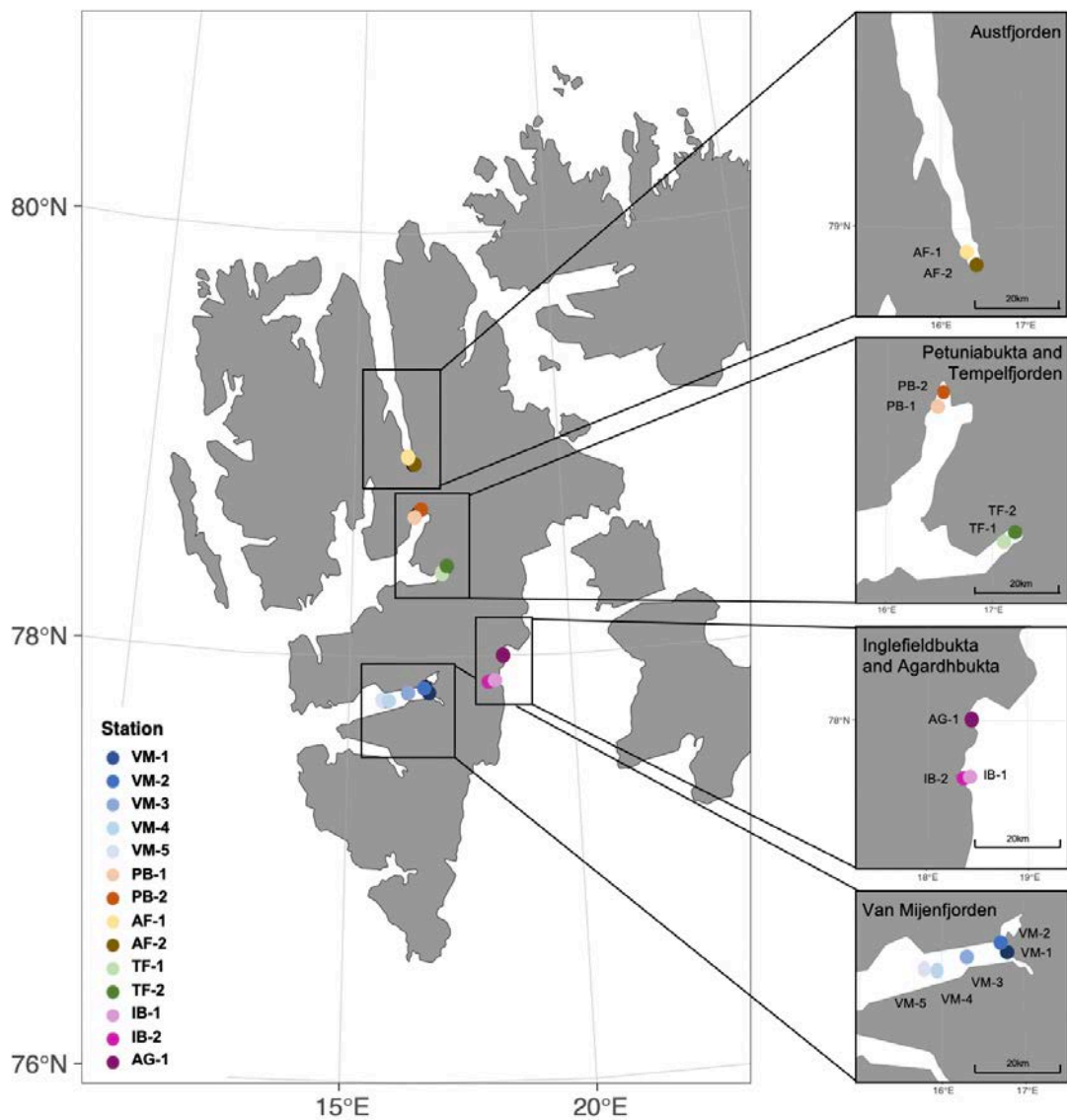


**Figure 3.1:** Land-fast sea ice sampling locations visited between April - May 2021, within various fjords of Svalbard, Norway.

### Physical and Chemical Variables

Prior to each core extraction, three snow depth measurements were taken using a standard ruler to determine snow depth in close vicinity to the planned core. Following core extraction, ice thickness was measured using a Kovacs ice thickness gauge (Kovacs Enterprise, Oregon, USA). Freeboard was measured at each core hole using a standard ruler. At each sampling event, two additional ice cores were taken to measure a salinity and temperature profile of the sea-ice column. The temperature profile was measured *in situ*, in 10 cm intervals along the core. Following complete melting of separate 10 cm sections, salinity of each section was measured (Thermo Scientific Orion Versa Star Pro). At each sampling site, approximately 100 mL of the water collected from the under-ice

water interface was put into acid washed bottles and stored at -20 °C until nutrient analyses were performed. The  $\text{NO}_3^- + \text{NO}_2^-$ ,  $\text{PO}_4^{3-}$ ,  $\text{Si}(\text{OH})_4$  and  $\text{NH}_4^+$  concentrations ( $\mu\text{M}$ ) were measured simultaneously on a San++ 5000 automated analyzer (Skalar: Breda, Netherlands), with separate channels for the four nutrients. The detection limits were 0.02  $\mu\text{M}$  for  $\text{NO}_3^- + \text{NO}_2^-$ , 0.01  $\mu\text{M}$  for  $\text{PO}_4^{3-}$ , 0.25  $\mu\text{M}$  for  $\text{Si}(\text{OH})_4$  and 0.3  $\mu\text{M}$  for  $\text{NH}_4^+$ . At most sampling locations, a full temperature and salinity profile was measured of the water column below the ice using a CTD probe (STD/CTD SD204, SAIV A/S: Bergen, Norway). Brine salinity and volume were calculated according to (Cox & Weeks, 1983).

For the C:N and  $\delta^{13}\text{C}$  and  $\delta^{15}\text{N}$  stable isotope analysis, all six ice cores from each sampling point were pooled to obtain a minimum weight of 20  $\mu\text{g}$  of N per filter, ensuring values were well above detection limits. Following complete melting, subsamples (300–1600 mL) of the ice cores and under-ice water (500–3000 mL) were filtered onto pre-combusted (400 °C for 8 h) filters (GF/F, 0.7  $\mu\text{m}$ ). The filtration was performed until visible colouration was observed and filters stored at -20 °C until analysis (within 12 months). Filters were dried at 60 °C within sterile glass petri dishes, acid fumed (37% (w/w) HCl for 8 h), dried at 60 °C and placed into a tin cup. Samples were analysed at the Stable Isotope Facility at the University of California, Davis in an elemental analyser isotope ratio mass spectrometry (EA-IRMS) system, according to Barrie et al. (1989). The detection limits were 100  $\mu\text{g}$  C for  $\delta^{13}\text{C}$  and 20  $\mu\text{g}$  N for  $\delta^{15}\text{N}$ .

### **Light Measurements and Modelling**

At each sampling event, both incoming and transmitted photosynthetically active radiation (PAR) measurements were taken at the ice-ocean interface and snow-covered surface. For each measurement, a LI-190 quantum air corrected sensor was placed on the surface of the snow facing south. In the vicinity, a small hole was made using a 10 cm diameter auger. A LI-192 underwater quantum sensor on a weighted frame was lowered through the hole, under the sea ice. To avoid shadowing of the measurement area, all sensors faced south with operations performed north, and the area was undisturbed. Measurements from both sensors were collected simultaneously using a LI-1500 Data Logger (LI-COR, Nebraska, USA). These measurements were then compared to modelled data (Table S3.2) using the equation:

Equation 1: 
$$E_z = E_0 \cdot \exp(-K_d \cdot Z)$$

where ( $E_z$ ) is irradiance at sampling depth,  $E_0$  is the incoming (incident) irradiance ( $\mu\text{mol photons m}^{-2}\text{s}^{-1}$ ),  $K_d$  is the diffuse light attenuation coefficient ( $\text{m}^{-1}$ ), and  $Z$  is the sampling depth (m). The PAR at the ice-ocean interface was estimated using *in-situ* measured irradiance at the top of snow and ice, and then attenuation through snow and ice was modelled using attenuation coefficients ( $K_d$ ) of  $20 \text{ m}^{-1}$  for snow,  $5 \text{ m}^{-1}$  for the top 10 cm of ice, and  $1 \text{ m}^{-1}$  for ice below the top 10 cm (Perovich, 1996; Varpe et al., 2015).

To account for the fact that *in situ* measurements were taken at different times of day and with a range of cloud coverage conditions, percent incoming PAR was used as a proxy for under ice light at a given location, providing an estimate of the attenuation effects of the sea ice and snow depth at each site, as the differences in light conditions that the bottom ice algae communities were exposed to was determined primarily by the attenuating effects of snow depth and ice thickness. Because solar angle has a substantial effect on light quantity (Connan-McGinty et al., 2022) and cloud cover can reduce light intensity by up to 90% (Pfister et al., 2003), using percent incoming PAR allowed us to determine how effective ice and snow depth was at blocking incoming irradiance to the bottom ice community. This allowed us to utilise our unique *in situ* measurements, rather than a reliance on weather station data, which is either not available or not truly representative of the conditions in the fjords sampled. In this study, we therefore use light transmissivity to describe the percent incoming PAR under given snow and ice thicknesses.

### **Biological Parameters**

Chlorophyll *a* concentration:

Following complete melting, subsamples (60–450 mL) of each sea ice triplicate and a volume (500–2200 mL) of under-ice water were filtered (GF/F,  $0.7 \mu\text{m}$ ). The filtration was performed until visible colouration of the filter and the filters were stored frozen ( $-80 \text{ }^\circ\text{C}$ ) until extraction. Extractions were performed within three months of collection. Analyses were performed according to Holm-Hansen & Riemann (1978). Briefly, filters were extracted in 10 mL 100% methanol and kept refrigerated for 24 h prior to extraction. Chl *a* content was measured with a calibrated 10-AU-005-CE fluorometer (Turner, California, USA), before and after acidifying the solution with 5% HCl (Parsons et al. 1984). For the sea-ice samples, chl *a* content was converted to chl *a* biomass per unit ice surface area ( $\text{mg m}^{-2}$ ).

### Species Composition by Light Microscopy:

From each sampling site and date, subsamples (100 mL) were collected into a brown bottle and preserved with gluteraldehyde (2% final conc.). Between 4 and 10 mL (depending on cell abundance) of the well-mixed subsamples were poured into a 10 mL Utermöhl cylinder (KC Denmark, Silkeborg, Denmark) and the cells were allowed to settle for 6–24 h, depending on volume (Edler & Elbrächter, 2010). Cells were counted at 400x magnification and identified to lowest taxonomic level possible. The identification of species and groups was primarily based on the work of Tomas (1997) and Wiktor et al. (1995). It is unlikely that all pico- or nanoflagellates were captured. To ensure rare taxa were captured as much as possible, a whole chamber counting approach was employed. Qualitative and quantitative analyses were conducted under Nikon TS100 microscope, within 9 months of sample collection.

### Data Analyses

To determine patterns in under ice community composition, similarity matrices were constructed using the Bray-Curtis coefficient on square root-transformed data (Sommerfield et al., 2021) and visualised using non-metric multidimensional scaling (nMDS). The community composition of all sampled sites was contrasted between high light transmissivity (HLT) (>4% incoming PAR) and low light transmissivity (LLT) (< 3% incoming PAR) sites throughout the sampling period (14<sup>th</sup> April 2021 – 25<sup>th</sup> May 2021) by analysis of similarities (ANOSIM, Clarke & Warwick 1994), with the groupings established by ANOSIM, to determine if community composition was similar within similar light levels, independent of geographic location. The light groupings were determined based on the potential for photoinhibition in some ice-algal taxa beyond ~3% incoming PAR/ 20  $\mu\text{mol photons m}^{-2}\text{s}^{-1}$  (Palmisano et al., 1985; Ryan et al., 2011) and ensured sufficient replication for statistical comparison. To avoid temporal confounding between samples taken during different periods of the spring season while accounting for all sampling events, samples were divided into ‘April’ (14<sup>th</sup> – 30<sup>th</sup> April) and ‘May’ (4<sup>th</sup> – 25<sup>th</sup> May). The specific taxa contributing most to similarities/dissimilarities between the HLT and LLT sites were determined using similarity percentage analysis (SIMPER). To determine correlations between the community contribution of specific taxa, a correlation plot was created, using a correlation matrix of the percentage of community contribution of each taxon.

To establish relationships between percentage contribution to community composition of taxonomic groups (Figs. 3.2-3.3) and percent incoming PAR, a linear regression (95% confidence interval) was applied to each taxonomic group, including all sampling events. In cases in which the data were poorly explained by a linear fit, a second order polynomial regression was applied. The Shapiro–Wilks (Shapiro & Wilk, 1965) test for normality showed that the modelled light and cell abundance data required  $\log_{10}$  transformation before analysis. Regressions were tested for overall model significance using the  $F$  statistic ( $P < 0.05$ ) and strength of fit using  $R^2$ . The residuals of all regressions were verified for homoscedasticity. Differences in cell abundance between HLT and LLT sampling sites in April and in May were determined using PERMANOVA. Differences between C:N and stable isotopes of particulate organic carbon and nitrogen between HLT and LLT sites were determined using a Welch t-test. To investigate which environmental variables account for a significant difference in the species composition, redundancy analysis (RDA) was performed, constrained to environmental variables ( $n = 15$ ) with Monte Carlo permutations (999), and only significant vectors are displayed. The percent incoming PAR levels used throughout all statistical analyses were taken from the modelled light, to ensure consistency and avoid any data gaps. All analyses were performed using RStudio v. 2022.02.03 (RStudio Team, 2022) and the add-on packages ‘vegan’ v.2.5-7 (Oksanen et al., 2013), ‘ggplot2’ v.3.3.6 (Wickham et al., 2016) and ‘dplyr’ v.1.0.8 (Wickham et al., 2019).

## **Results**

### **Physical Characteristics**

Across all sampling sites, sea-ice thickness ranged from 30–104 cm (Table 3.1) and snow depth from 3–36 cm (Table 3.1; Figs. 3.2-3.3). The temperature of the bottom 3 cm of ice (at the ice-water interface) ranged from -1.9 to -3.6 °C (Table 3.1), and bulk ice salinity from 1.7–10.7 ppt (Table 3.1). The brine salinity ranged from 33.9–62.8 ppt (Table 3.1) and the brine volume ranged from 3.4–25.4 % ice volume (Table 3.1). Water temperature and salinity (0.5 m below ice) varied only minimally across all sites, with temperature ranging from -1.4 °C to -1.9 °C and salinity ranging from 33–34.5 ppt (Table S3.3). At all sites, the seawater was nutrient replete, with mean  $\text{NO}_3^- + \text{NO}_2^-$ ,

$\text{PO}_4^{3-}$  and  $\text{Si}(\text{OH})_4$  concentrations of  $2.01 \pm 0.5 \mu\text{M}$ ,  $0.21 \pm 0.0 \mu\text{M}$ ,  $2.53 \pm 0.51 \mu\text{M}$ , and, respectively, and  $\text{NH}_4^+$  levels generally  $<1 \mu\text{M}$  (Table S3.3).

### **Chlorophyll *a*, Carbon and Nitrogen**

Bottom ice chl *a* ranged from 0.15–7.2 mg m<sup>-2</sup> (Table 3.1; Figs. 3.2-3.3), while chl *a* in the water column directly below the sea ice ranged from 0.04–1.94 mg /m<sup>3</sup> (Table S3.3). We observed a positive relationship between cell abundance and chl *a* ( $F_{1,28} = 28.68$ ,  $p < 0.05$ ;  $R^2 = 0.51$ ), but we found no relationship between light transmission through sea ice and bottom ice chl *a* ( $F_{1,28} = 0.00$ ,  $p > 0.05$ ;  $R^2 = 0.00$ ) or water column chl *a* ( $F_{1,28} = 3.20$ ,  $p > 0.05$ ;  $R^2 = 0.10$ ).

Molar ratios of C:N ranged from 4.53–13.80 in samples taken of the sea ice (Table 3.1) and 2.24–13.20 in under-ice water (Table S3.3). The C:N ratio was significantly higher in the sea ice at HLT compared to LLT sites in April ( $t(7) = 2.5$ ,  $p < 0.05$ ), but did not differ in May ( $t(5) = 1.31$ ,  $p > 0.05$ ). We found no difference in under-ice water C:N between HLT and LLT sites in either April or May.

Sea-ice stable isotope of organic carbon ( $\delta^{13}\text{C}_{\text{VPDB}}$ ) ranged from to -27.05 to -14.34 ‰ (Table 3.1) and organic nitrogen ( $\delta^{15}\text{N}_{\text{Air}}$ ) ranged from 1.92–6.34 ‰ (Table 3.1). Under-ice water  $\delta^{13}\text{C}$  ranged from -24.99 to -28.41 ‰ (Table S3.2) and  $\delta^{15}\text{N}$  ranged from 1.68 to 8.54 ‰ (Table S3.3). The samples taken from the sea ice at HLT sites were significantly more carbon enriched than those taken from the LLT sites in April ( $t(7) = 3.5$ ,  $p < 0.05$ ) and in May ( $t(5) = 2.95$ ,  $p < 0.05$ ). We found a positive correlation between under-ice light and  $\delta^{13}\text{C}$  throughout April and May ( $F_{1,28} = 23.96$ ,  $p < 0.05$ ;  $R^2 = 0.46$ ), however no correlation was detected between  $\delta^{13}\text{C}$  values and cell abundance or chl *a*. There was no difference in nitrogen enrichment between HLT and LLT sites in April ( $t(8) = -2.56$ ,  $p > 0.05$ ), however the LLT sites did have higher nitrogen enrichment in May ( $t(10) = -2.45$ ,  $p < 0.05$ ). A negative correlation was observed between  $\delta^{15}\text{N}$  values and cell abundance ( $F_{1,28} = 30.59$ ,  $p < 0.05$ ;  $R^2 = 0.52$ ) and  $\delta^{15}\text{N}$  values and chl *a* ( $F_{1,28} = 28.54$ ,  $p < 0.05$ ;  $R^2 = 0.50$ ), but no correlation was detected between  $\delta^{15}\text{N}$  values and under-ice light. Unlike  $\delta^{13}\text{C}$  values,  $\delta^{15}\text{N}$  increased as the season progressed ( $F_{1,28} = 7.27$ ,  $p < 0.05$ ;  $R^2 = 0.21$ ). There was no difference in carbon or nitrogen enrichment in under-ice water between HLT and LLT in either April or May.



**Table 3.1:** Parameters measured associated with sea-ice core extraction; snow depth (cm) ( $\pm$  SD,  $n = 18$ ), ice thickness (cm) ( $\pm$  SD,  $n = 6$ ) and within the bottom 3 cm of sea-ice core; ice temperature ( $^{\circ}$ C) salinity (ppt), brine salinity (ppt), brine volume (% of ice volume), chlorophyll *a* concentration ( $\text{mg m}^{-2}$ ) ( $n = 3$ ), daylight hours at time of sampling, carbon:nitrogen (C:N) molar ratio, carbon isotope ratio ( $\delta^{13}\text{C}_{\text{VPDB}}$  (‰)) and nitrogen isotope ratio ( $\delta^{15}\text{N}_{\text{Air}}$  (‰)). ND represents measurement not taken.

Date	Station	Snow Depth	Ice Thickness	Ice Temperature	Bulk Ice Salinity	Brine Salinity	Brine Volume	Chlorophyll <i>a</i>	Daylight	C:N	$\delta^{13}\text{C}$	$\delta^{15}\text{N}$
14.4.21	VM-1	36.4 $\pm$ 1.9	72 $\pm$ 1.4	-2.3	8.6	40.77	18.85	0.15 $\pm$ 0.0	15.09	4.61	-25.61	5.28
14.4.21	VM-2	12.6 $\pm$ 1.8	64 $\pm$ 1.1	-2.5	8.9	44.16	17.99	0.86 $\pm$ 0.16	15.09	4.69	-24.68	4.57
14.4.21	VM-3	25.5 $\pm$ 2.5	65 $\pm$ 3.8	-3.6	9.8	62.38	13.91	1.98 $\pm$ 0.90	15.09	5.51	-25.09	3.14
14.4.21	VM-4	16.9 $\pm$ 2.4	41 $\pm$ 1.0	-2.5	1.7	44.16	3.44	6.74 $\pm$ 0.46	15.09	4.65	-24.29	1.92
21.4.21	PB-1	9.5 $\pm$ 0.6	39 $\pm$ 1.1	-2.3	4.7	40.77	10.30	3.49 $\pm$ 2.89	19.55	5.50	-24.37	3.56
21.4.21	PB-2	10.6 $\pm$ 0.4	38 $\pm$ 0.5	-2.3	4.7	40.77	10.30	7.24 $\pm$ 0.85	19.55	6.53	-18.82	3.64
22.4.21	AF-1	14.2 $\pm$ 0.8	53 $\pm$ 2.2	-2.3	7.2	40.77	15.78	7.05 $\pm$ 1.02	19.59	5.28	-24.22	3.41
22.4.21	AF-2	10.9 $\pm$ 2.9	47 $\pm$ 1.2	-2.7	3.8	47.53	7.13	5.11 $\pm$ 2.64	19.59	5.64	-23.25	4.07
27.4.21	VM-4	2.8 $\pm$ 2.0	54 $\pm$ 4.7	-2.0	9.6	35.64	24.12	3.46 $\pm$ 1.88	20.36	7.19	-18.08	3.73
27.4.21	VM-5	5.0 $\pm$ 1.0	54 $\pm$ 1.9	-2.1	10.6	37.36	25.39	1.80 $\pm$ 0.47	20.36	4.99	-22.97	3.79
28.4.21	VM-1	13.2 $\pm$ 1.7	88 $\pm$ 1.3	-2.0	9.2	35.64	23.12	0.33 $\pm$ 0.26	20.36	4.53	-24.73	5.75
28.4.21	VM-2	22.7 $\pm$ 2.9	68 $\pm$ 1.5	-2.1	9.6	37.36	23.00	1.24 $\pm$ 0.40	20.36	5.96	-24.43	5.32
28.4.21	VM-3	19.8 $\pm$ 6.1	66 $\pm$ 5.4	-2.2	3.2	39.07	7.33	1.36 $\pm$ 0.35	20.36	5.26	-26.88	3.35
30.4.21	TF-1	3.9 $\pm$ 1.1	30 $\pm$ 2.8	-2.2	3.2	39.07	7.33	0.61 $\pm$ 0.22	20.47	7.52	-14.34	4.39
30.4.21	TF-2	3.4 $\pm$ 0.7	38 $\pm$ 1.1	-2.7	9.2	47.53	17.25	4.47 $\pm$ 1.59	20.47	10.18	-15.90	4.57
4.5.21	VM-3	10.0 $\pm$ 0.9	74 $\pm$ 2.6	-2.2	10.4	39.07	23.81	3.11 $\pm$ 1.13	21.05	6.02	-25.27	3.42
4.5.21	VM-4	7.0 $\pm$ 3.2	50 $\pm$ 2.2	-2.1	5.6	37.36	13.42	1.01 $\pm$ 0.24	21.05	7.50	-21.05	4.73
4.5.21	VM-5	4.8 $\pm$ 3.8	52 $\pm$ 3.6	-2.2	6.2	39.07	12.82	1.70 $\pm$ 0.52	21.05	6.92	-15.31	3.04

5.5.21	VM-1	14.3 ± 0.7	92 ± 3.2	-2.1	6.5	37.36	15.57	0.55 ± 0.35	21.05	6.09	-24.99	6.34
5.5.21	VM-2	15.8 ± 2.1	78 ± 3.0	-2.2	10.7	39.07	24.49	0.35 ± 0.07	21.05	5.73	-24.30	5.31
13.5.21	VM-1	21.2 ± 1.0	94 ± 3.3	-2.1	9.5	37.36	22.76	1.14 ± 0.53	24	7.57	-24.64	4.49
13.5.21	VM-5	11.0 ± 1.7	52 ± 5.2	-2	ND	ND	ND	0.77 ± 0.31	24	10.99	-17.13	4.41
21.5.21	VM-1	21.2 ± 1.4	78 ± 0.9	-2	7.9	35.64	19.85	2.18 ± 0.90	24	5.83	-24.61	5.06
21.5.21	VM-5	5.3 ± 1.6	42 ± 0.7	-2	ND	ND	ND	1.52 ± 0.93	24	13.80	-15.90	4.65
24.5.21	AG-1	21.7 ± 0.5	90 ± 2.5	-2.5	5	44.16	10.10	0.25 ± 0.10	24	11.15	-27.05	6.27
24.5.21	IB-1	23.5 ± 3.0	84 ± 2.3	-1.9	9.2	33.92	24.31	4.04 ± 1.18	24	6.02	-26.74	3.48
24.5.21	IB-2	26.5 ± 2.5	107 ± 1.3	-1.9	6.6	33.92	17.44	0.50 ± 0.22	24	5.54	-24.98	6.29
25.5.21	VM-1	15.9 ± 1.0	70 ± 2.3	-2	7.9	35.64	19.85	2.39 ± 0.74	24	7.13	-23.09	5.24
25.5.21	VM-2	22.1 ± 0.7	75 ± 2.1	-2	7.4	35.64	18.59	3.14 ± 1.56	24	6.48	-24.20	5.42
25.5.21	VM-3	14.2 ± 1.6	72 ± 1.7	-2	9.5	35.64	23.87	3.59 ± 0.71	24	8.54	-21.84	3.96

### Under-ice Light Transmissivity

Measured percent incoming PAR varied from 0.02–6.10 % ( $0.1\text{--}50 \mu\text{mol photons m}^{-2}\text{s}^{-1}$ ) across 21 of 30 sites and dates, and measured incident irradiance varied from 387–1314  $\mu\text{mol photons m}^{-2}\text{s}^{-1}$ . Modelled percent incoming PAR varied from 0.02–23.18% incoming PAR ( $0.1\text{--}193$ ,  $\bar{X} = 35 \pm 52 \mu\text{mol photons m}^{-2}\text{s}^{-1}$ ) across all 30 sites and times (Table S3.2; Figs. 3.2–3.3). Based on the average incoming irradiance of  $750 \mu\text{mol photons m}^{-2}\text{s}^{-1}$ , the percentage of light transmitted equates to a range of  $0.1\text{--}204 \mu\text{mol photons m}^{-2}\text{s}^{-1}$  transmitted to the bottom ice community. For the locations where *in situ* light measurements were obtained (21 out of 30), these values closely resembled the modelled light measurements, with the modelled light values slightly higher +1.25% ( $\pm 3.21\%$ ) on average, than the measured light levels (Table S3.2). The total variance in the modelled % incoming PAR was -4.7 to 10.3%. When plotted against each other, the modelled and measured values were significantly correlated ( $r_{19} = 0.5$ ,  $p < 0.05$ ).

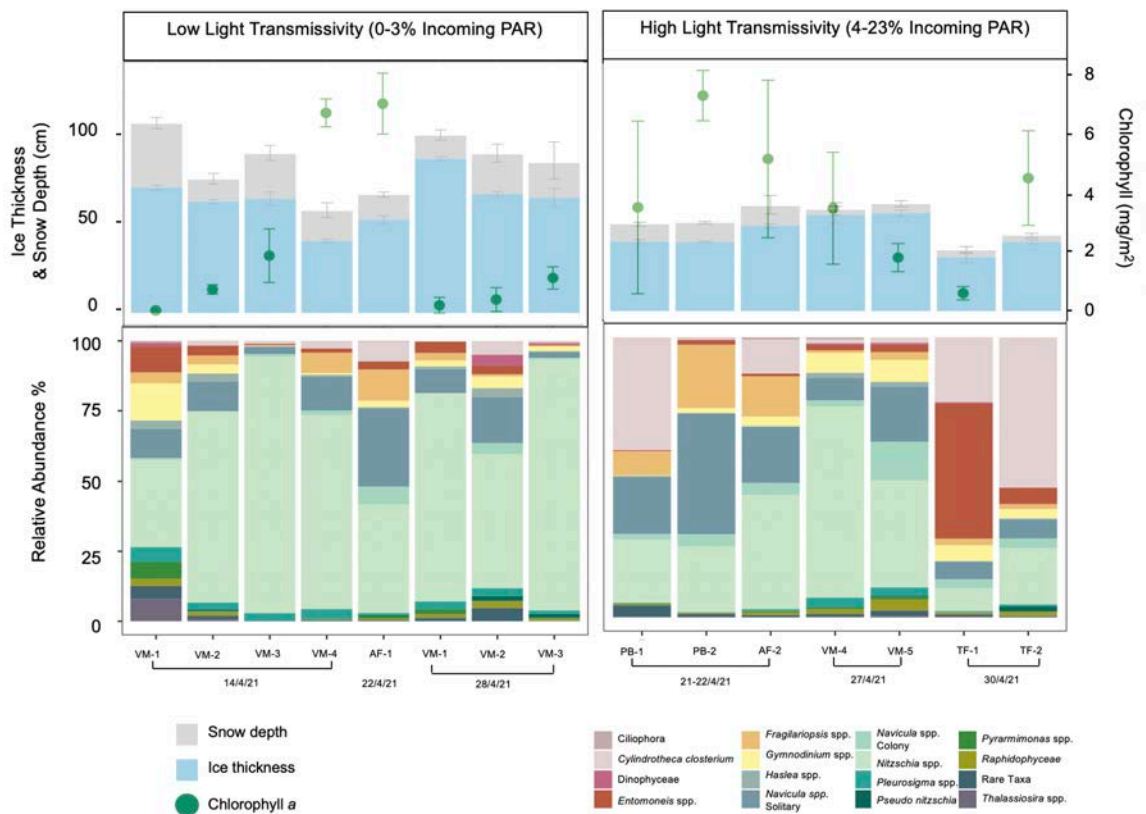


**Figure 3.2:** Bottom ice microalgal community composition from low light transmissivity (left) and high light transmissivity (right) sites sampled during April 2021, in Svalbard, Norway. Snow depth (grey), ice thickness (blue), and chlorophyll a concentration ( $\text{mg m}^{-2}$ ) (green circles) are displayed in the upper panels  $\pm$  SD ( $n = 18$ ,  $n = 6$  and  $n = 3$ , respectively), relative abundance (%) of taxonomic groups are shown in the lower panels.

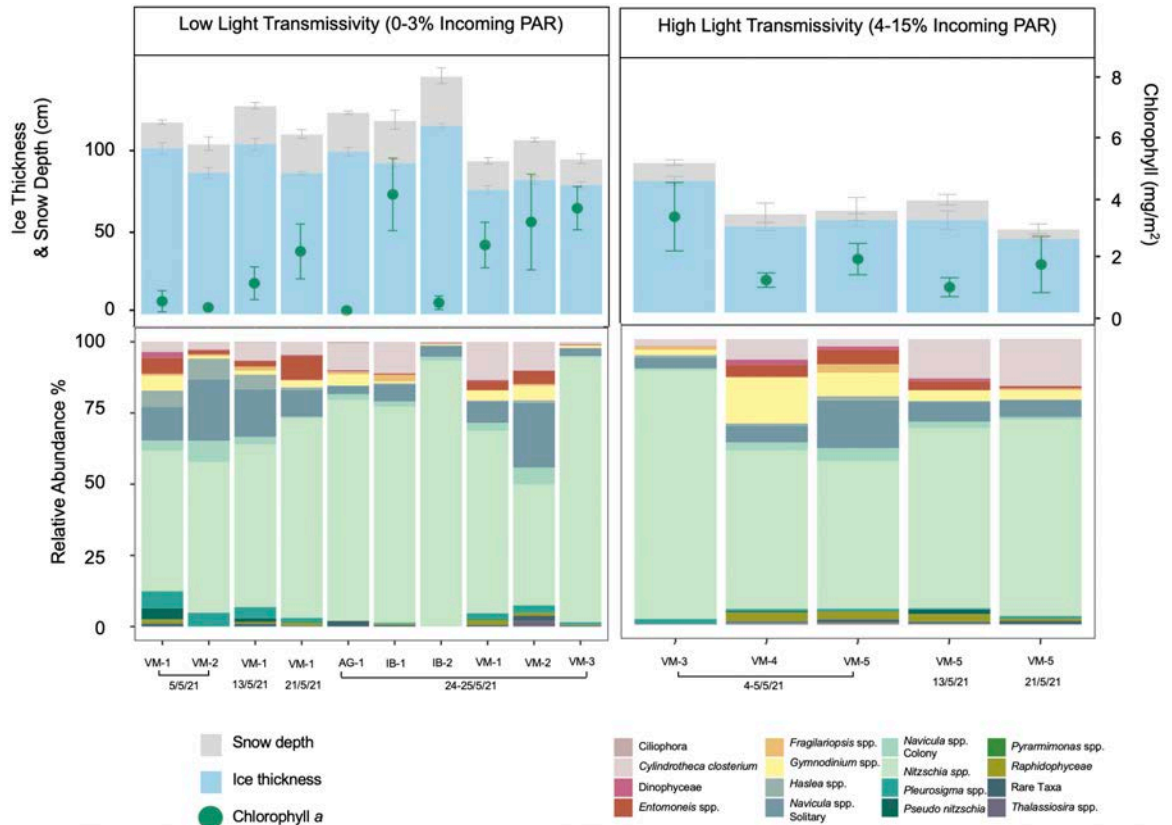


**Figure 3.3:** Bottom ice microalgal community composition from low light transmissivity (left) and high light transmissivity (right) sites sampled during May 2021, in Svalbard, Norway. Snow depth (grey), ice thickness (blue), and chlorophyll *a* concentration ( $\text{mg m}^{-2}$ ) (green circles) are displayed in the upper panels  $\pm$  SD ( $n = 18$ ,  $n = 6$  and  $n = 3$ , respectively), relative abundance (%) of taxonomic groups are shown in the lower panels.

### Species Composition

We identified a total of 55 taxa (to species or genus level), corresponding to seven phylogenetically distinct groups, with Bacillariophyceae accounting for 42 species (76% of the total), Dinophyceae accounting for six species (11%) and Pyramimonadophyceae being represented by three species (5%) (Tables S3.4–S3.5). Raphidophyceae, Cryptophyceae, Euglenoidea and Ciliophora were identified to class level only. Of the identified diatoms, 40 species (95%) were from the order Pennales, while only two species belonged to the Centrales (5%). At all sites, the community was dominated by *Nitzschia* spp. (Figs. 3.2–3.3; Table 3.1). The *Nitzschia* spp. group, while dominated by colonial *N. frigida*, was represented also by colonial *N. promare*, *N. arctica*, *N. laevisissima*, *N. brebissoni*, and *N. polaris*. Similarly, for the solitary *Navicula* group, *N.*

*directa* was the most common and abundant, however, *N. distans*, *N. kariana*, *N. transitas*, *N. algida*, *N. valida* and *N. pellucida* were also present. The colony forming (ribbon) *Navicula* group consisted of *N. pelagica*, *N. septentrionalis*, *N. granii* and *N. vanhoefenii*. The Dinophyceae group was primarily identified to class level but also included *Peridiniella catenata* and *Peridiniella* spp. *Gymnodinium* spp. was not included in the Dinophyceae group as it was included as a separate grouping at genus level. The *Fragilariopsis* spp. group was dominated by *F. cylindrus* but included *F. reginae-jahniae* and *F. oecania*. The *Thalassiosira* spp. group was primarily identified to genus level but included *T. nordenskiöldii*. The ‘Rare Taxa’ group included euglenophytes, uncommon diatom taxa and haptophytes (Table S3.4).

While *Nitzschia* spp. dominated the communities during April–May from both the HLT and LLT sites, there were clear shifts in percentage contribution of scarcer taxa with increased irradiance. For example, *Cylindrotheca closterium* and colony forming *Navicula* spp. became more prominent when incoming PAR was >4% during April (Figs. 3.2–3.3). In addition, throughout April, *Entomoneis* spp. was generally found in higher relative abundance in the LLT sites, with the exception of TF-1 where it was found to be the dominant taxa (Fig. 3.2). During May, *Gymnodinium* spp. tended to have a higher relative abundance at sites with HLT (Fig. 3.3).

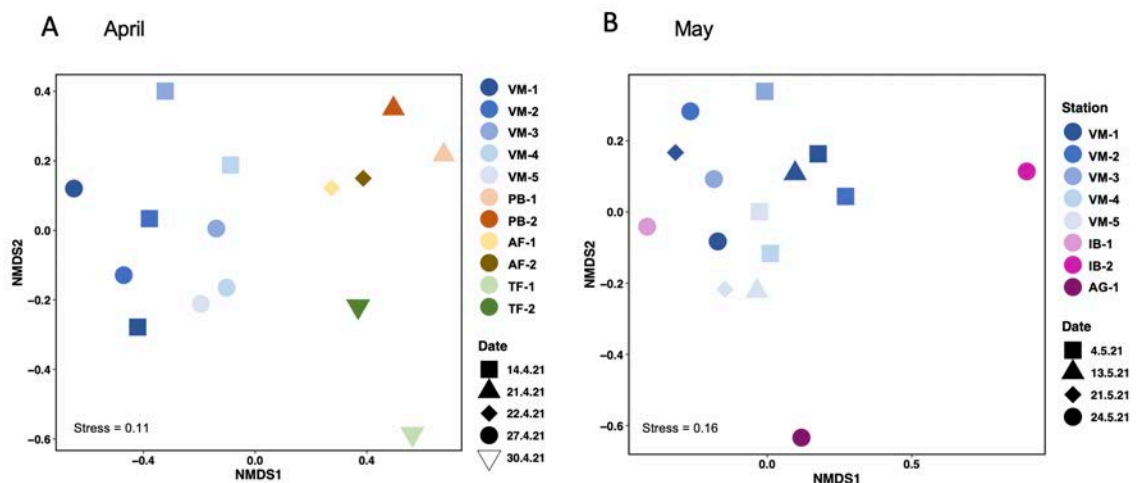


**Figure 3.4:** Non-metric multidimensional scaling (nMDS) of microalgal communities for (A) April and (B) May, based on resemblance using Bray-Curtis similarity. Sample sites are shown by colour and dates by shapes. The 2D stress is shown in the lower left.

### Influence of Light Transmissivity on Protist Community Composition

Spatial and temporal differences, associated with differing under-ice light climates, related to community composition during April, but not during May (Fig. 3.4A–B). When compared, HLT sites differed in community composition from the LLT sites during April (ANOSIM  $R = 0.26$ ,  $p < 0.05$ ; Fig. 3.2), with the LLT ( $< 3\%$  incoming PAR /  $< 20 \mu\text{mol photons m}^{-2}\text{s}^{-1}$ ) generally dominated by *Nitzschia* spp. (primarily *N. frigida*), compared to a more diverse community in the high light sites ( $> 4\%$  incoming PAR /  $> 21 \mu\text{mol photons m}^{-2}\text{s}^{-1}$ ) with an increased contribution of various *Navicula* spp., *C. closterium* and *Fragilariopsis* spp. (Fig. 3.2). The cumulative contribution to this dissimilarity between HLT and LLT sites was from *Nitzschia* spp. (11%), *C. closterium* (21%) *N. transitas* (27%), *F. cylindrus* (31%), *N. septentrionalis* (35%), *F. oecania* (39%), *Entomoneis* spp. (43%), *P. taeniata* (47%) and *Gymnodinium* spp.  $< 10\mu\text{m}$  (50%). In May, however, the HLT and LLT assemblages were similar, indicating that community composition was similar irrespective of light climate, sampling location or sampling date (2D Stress = 0.16, Fig. 3.4B). In May, the community composition of both HLT and LLT sites (ANOSIM  $R = 0.00$ ,  $p > 0.05$ ; Fig. 3.3) were dominated by *Nitzschia* spp., specifically, *N. frigida* (Fig. 3.3).

At an individual species level, we found significant relationships between the relative abundance and light transmissivity for five taxa (Fig. 3.5). For the most predominant species, *N. frigida*, the percentage contribution to the community decreased as light transmissivity increased ( $F_{1,28} = 6.30$ ,  $p < 0.05$ ;  $R^2 = 0.18$ ). In contrast, for the other four taxa, *Gymnodinium* spp. ( $F_{1,26} = 13.77$ ,  $p < 0.05$ ;  $R^2 = 0.35$ ), colony-forming *Navicula* spp. ( $F_{1,23} = 11.36$ ,  $p < 0.05$ ;  $R^2 = 0.33$ ), Dinophyceae ( $F_{1,27} = 6.58$ ,  $p < 0.05$ ;  $R^2 = 0.20$ ) and *Thalassiosira* spp. ( $F_{1,24} = 14.05$ ,  $p < 0.05$ ;  $R^2 = 0.37$ ), their percentage contribution to the community increased as under-ice light transmissivity increased. No trend between under ice light and contribution to the community was found for the other taxonomic groups (Table S3.6).

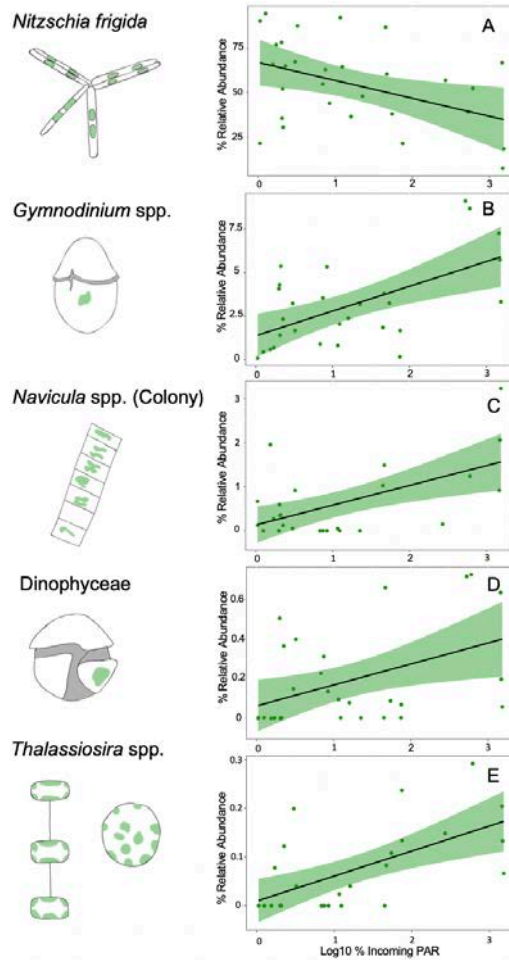


**Figure 3.5:** Significant relationships for relative contribution to community composition vs. Log10 percent (%) incoming PAR during April and May, (A) *Nitzschia frigida*, (B) *Gymnodinium* spp., (C) Colony forming *Navicula* spp., (D) Dinophyceae and (E) *Thalassiosira* spp. Data are fitted using linear regression with 95% confidence intervals (shading).

During April and May, we detected patterns in species occurrences. While there was a consistently negative correlation between *Nitzschia* spp. and all other taxa (Fig. 3.6A), we did detect strong positive correlations between the presence of *Thalassiosira* spp., *Raphidophyceae* spp. and *Pyramimonas* spp., high co-occurrence of *Pleurosigma* spp. and *Haslea* spp., as well as high co-occurrence of *Fragilariopsis* spp. with solitary *Navicula* spp. (Fig. 3.6B). Environmental conditions explained 58.7% (on two canonical axes) of the variability in community composition ( $F_{15} = 3.37$ ,  $p < 0.05$ , Fig. 3.6B). Abundance of *N. frigida* and *Thalassiosira* spp. was most strongly associated with chl *a* concentration, whilst the prevalence of *Entomoneis* spp., *C. closterium*, *Navicula* spp. (solitary and colony forming), *Gymnodinium* spp. and *Fragilariopsis* spp. was explained by percent incoming PAR more than any other variable (Fig. 3.6B). Brine salinity was the most explanatory variable for the presence of *Pleurosigma* spp., while the contribution from Dinophyceae appeared to be linked to  $\delta^{15}\text{N}$  (Fig. 3.6B).

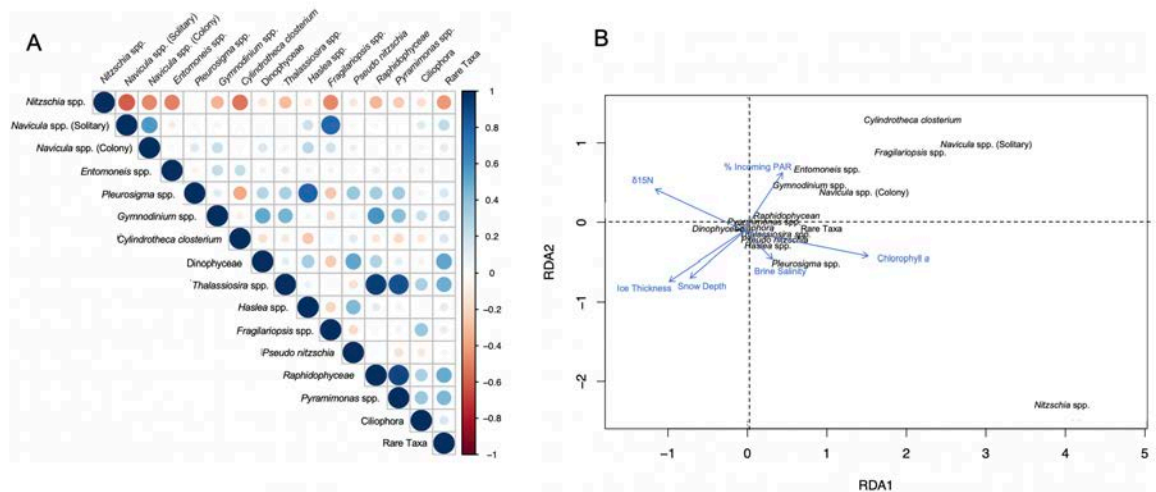


**Figure 3.6:** (A) Correlation matrix of the relative abundance of main taxonomic groups found throughout April and May 2021, in land-fast ice, Svalbard, Norway. The strength of the positive (blue) and negative (red) correlations is displayed according to dot size. (B) Redundancy analysis (RDA) biplot of the relative abundance of taxonomic groups with environmental variables. Only significant vectors are shown.

### Relationships between Light Transmissivity and Community Diversity

Accounting for all sampling events across time and space (both April and May), sea-ice algal species diversity increased with increasing percent incoming PAR ( $F_{1,28} = 4.6$ ,  $p < 0.05$ ;  $R^2 = 0.14$ ; Fig. 3.7B). However, we detected a decline in diversity from April to May. Using the five-time repeated transect from the outermost (VM-5) to the innermost



(VM-1) part of Van Mijenfjorden (Fig. 3.1), we found that diversity at the outer site (VM-5) declined significantly through time ( $F_{1,2} = 29.17$ ,  $p < 0.05$ ;  $R^2 = 0.94$ ; Fig. 3.7B) as did the inner site (VM-1), with a sharp dip on the 27<sup>th</sup> April ( $F_{1,3} = 28.03$ ,  $p < 0.05$ ;  $R^2 = 0.90$ ; Fig. 3.7B). Interestingly, this temporal decline in diversity was independent of light transmissivity and the changes that resulted in lower diversity differed between sites. As time progressed, the community at the VM-5 site had an increase in the relative abundance of *N. frigida* and *C. closterium* concurrent with a decrease in *Gymnodinium* spp., *Haslea* spp., *Fragilariopsis* spp. and *Navicula* spp. In contrast, the community at VM-1 saw an increase in *N. frigida* and *C. closterium*, with a decline in *Gymnodinium* spp. and *Pleurosigma* spp. as the season progressed. Whilst light transmissivity was not linked to the diversity index within sites, light transmissivity likely influenced the differences in community composition between the two sites (ANOSIM R: 0.28,  $p < 0.05$ ), as the sampling sites within Van Mijenfjorden differed in modelled percent incoming PAR during the sampling period (ANOVA:  $F_{4,14} = 3.63$ ,  $p < 0.05$ ), with the greatest difference observed between VM-1 and VM-5 sites (Tukey's HSD:  $p < 0.05$ , 95% CI = [-0.04 – 3.53]). No relationship was found between cell abundance and percent incoming PAR ( $F_{1,28} = 4.27$ ,  $p > 0.05$ ;  $R^2 = 0.13$ ).

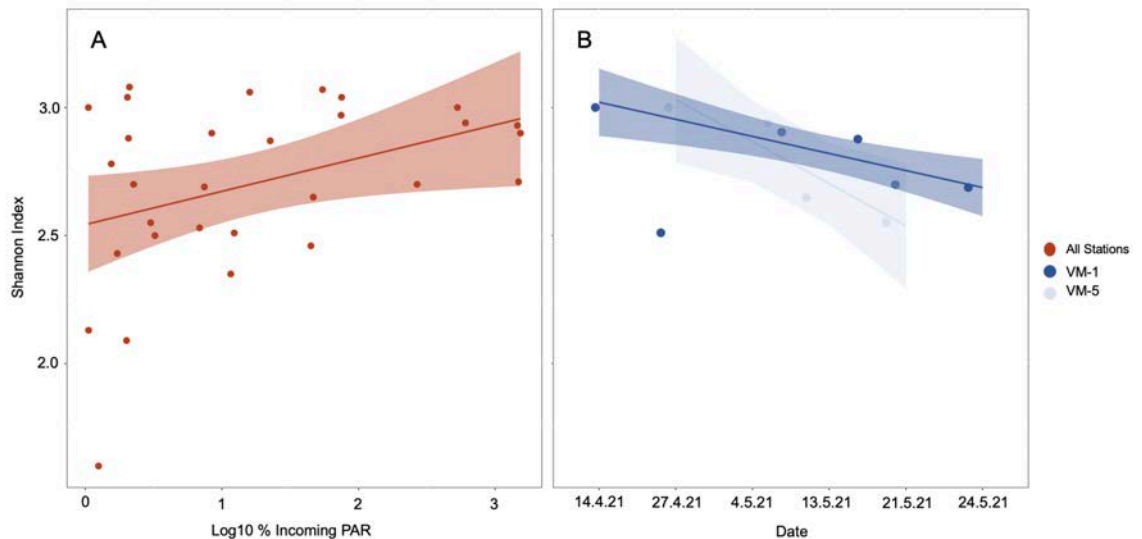


**Figure 3.7:** Spatial and temporal microalgal diversity dynamics (A) in relation to Log10 percent (%) incoming PAR for all data and (B) as a function of time for the outermost (VM-5) (light blue) and innermost (VM-1) (dark blue) sites within Van Mijenfjorden. Data are fitted using linear regression with 95% confidence intervals (shading). The outlier on 27<sup>th</sup> April has been excluded from the regression within the VM-1 site data.

## **Discussion**

In this study, we investigated bottom ice microalgal community composition in land-fast sea ice at both temporal and spatial scales. We evaluated under-ice light using a light transmittance model based on the physical parameters of ice thickness and snow depth. Validating against our *in situ* measurements, we found that modelled results were in good agreement with measured values and were thereby used to avoid the variability inherent in obtaining light data *in situ* that is complicated by time of day or variable weather conditions. Whilst it is difficult to directly compare under-ice light measurements with those measured in previous studies, as the light transmissivity is determined by snow depth and ice thickness which vary widely, the under-ice light values presented in this study ( $0 - 193$ ,  $\bar{X} = 35 \mu\text{mol photons m}^{-2}\text{s}^{-1}$ ) were primarily within the expected spring range in high latitudes for the observed sea ice and snow conditions (Campbell et al., 2016a; Leu et al., 2010). The few unusually high values ( $> 100 \mu\text{mol photons m}^{-2}\text{s}^{-1}$ ) recorded were taken at sites with snow depth  $< 5$  cm and ice thickness  $< 50$  cm.

Under-ice light transmittance, as a function of ice thickness and snow depth, was related with the sea-ice microalgal community composition. We found under-ice light transmittance to have a stronger association with community composition than other environmental variables, including temperature, ice salinity, brine volume and under-ice water nutrient concentration. Whilst initial community composition may play a role in determining the composition throughout the season, it was not able to be quantitatively evaluated as not all sampling sites were re-visited throughout the season. The association between under-ice light and community composition was particularly evident during the early-mid growth season. In April, the communities exposed to higher under-ice light conditions were typically more diverse, with higher relative abundance of common ice-associated taxa such as *Navicula* spp., *C. closterium* and *Fragilariopsis* spp. This may reflect that increased light transmitted to the bottom ice, until a threshold, drives an increased growth rate in many bottom ice taxa (Hegseth, 1992). Similar patterns of enhanced diversity with increased under-ice light transmittance have been observed previously in both the Arctic Ocean (Hop et al., 2020) and the Barents Sea (Hegseth & von Quillfeldt, 2022).

One of the most prevalent species throughout our study was *N. frigida*, a species endemic to sea-ice communities. This species has been found to form vast blooms throughout the

Arctic (Hegseth & von Quillfeldt, 2022; Hop et al., 2020). The relative abundance of *N. frigida* was negatively correlated with light and strongly associated with increased chl *a* concentration. These relationships were reflected in the onset of *N. frigida* blooms observed as the season progressed, coinciding with a reduction in under-ice light transmissivity, due to unusually high snow fall in the late spring (Norwegian Meteorological Institute, 2023). By early May, *N. frigida* dominated the communities at all sites, resulting in reduced overall diversity. This dominance by *N. frigida* during May could explain why no relationship was observed between under-ice light and diversity in May, and possibly indicates that light has a less distinct effect on the diversity of more established ice algal communities. When a higher proportion of incoming light was transmitted under the ice, a higher abundance of Dinophyceae overall was found (Fig. 3.5B), yet a contrasting temporal effect was also detected, with a relative increase in abundance during seasonal progression despite lower light transmission. This suggests that it was the lower nitrate concentrations later in the season, evidenced by the elevated  $\delta^{15}\text{N}$ , that favoured the Dinophyceae, potentially having a greater influence on their proliferation than light. This increase in Dinophyceae dominance with seasonal progression is consistent with the patterns suggested by other studies (Alou-Font et al., 2013; Hegseth & von Quillfeldt, 2022; Róžańska et al., 2009) and such seasonal successions in taxa are seen across a range of systems (e.g. McMinn & Hodgson, 1993; Winder & Varpe, 2020).

Concomitant with influencing the community composition, light transmissivity was positively correlated with  $\delta^{13}\text{C}$  enrichment and increased C:N, mirroring previous work (Gosselin et al., 1990; Lee et al., 2008a), and demonstrating how light directly affects the biochemical composition of ice algae. The  $\delta^{13}\text{C}$  values and C:N molar ratios within sea ice have been documented to range from -27 to -11‰ (Leu et al., 2020; Pineault et al., 2013), and 3 to 24 (Niemi & Michel, 2015), respectively, and our results are in line with these findings. Interestingly, we found no correlation between  $\delta^{13}\text{C}$  value and protist abundance or chl *a*, unlike the positive correlations observed previously (Gradinger, 2009; Pineault et al., 2013). In dense sea-ice assemblages which are highly productive and space limited, we expected to find enriched  $\delta^{13}\text{C}$  values due to preferential assimilation of  $^{12}\text{C}$  and minimal replenishment to the inorganic carbon pool (Pineault et al., 2013), so the lack of relationships between  $\delta^{13}\text{C}$  with either protist abundance or chl *a* within this study, could potentially be explained by the relatively low biomass

accumulated at the sites. Whilst the chl *a* concentrations are within the expected range for Arctic land-fast ice, they are on the lower end and do not represent a dense bloom scenario (Campbell et al., 2016a; Leu et al., 2020; Runge, 2021). In addition, the relationship between stoichiometric C:N ratios and under-ice light only, coupled with the fact that C:N molar ratios were typically at the Redfield Ratio of 6.6 or below, validates the greater influence of light than nutrient limitation at most sites (Campbell et al., 2016a; Gosselin et al., 1990). On the other hand,  $\delta^{15}\text{N}$  levels decreased with increasing protist abundance and were inversely related to the abundance of all taxa, particularly *N. frigida*. This relationship was not observed previously (Pineault et al., 2013). The observed decline in  $\delta^{15}\text{N}$  levels could suggest an increase in nutrient recycling, relative abundance of autotrophs or dissolved inorganic nitrogen reduction (Pineault et al., 2013) with higher algal density, thus the  $\delta^{15}\text{N}$  levels were not necessarily linked to under-ice light.

Based on the water column nutrient concentrations, the sites sampled were not nutrient limited, which differs from previous observations from late in the bottom ice algal season (Leu et al., 2020). This may be due to relatively low biomass accumulation at all sites, leaving a reservoir of unused nutrients. However, absolute values of nutrients within the sea-ice algal boundary layer were not obtained and therefore, we cannot say with certainty that the microalgal cells were not experiencing some level of nutrient stress. That said, the assemblages in Tempelfjorden in late April and VM-5 (the outermost site in VM) in mid-late May were experiencing enriched  $\delta^{13}\text{C}$  values between -14 and -17‰ and C:N ratios of >10, similar to those observed at high under-ice light sites in Van Mijenfjorden previously (Leu et al., 2020). Whilst it is possible that these sites were experiencing the onset of nutrient depletion within the ice, the under-water  $\text{NO}_3^- + \text{NO}_2^-$  concentrations were still replete at all sites with values >1.5  $\mu\text{M}$ . Rather than depletion of nitrate, it is possible that high light conditions could have resulted in a skewed uptake of C through the accumulation of C-rich storage compounds (Søreide et al., 2006), which can have significant consequences for transfer of energy through the marine food web (Hessen et al., 2008).

The unique community composition found at the TF-1 site (closest to the ice-edge) was unexpected and possibly a result of the site experiencing melting of the ice at the ice-ocean interface. It was characterised by high under-ice light (>100  $\mu\text{mol photons m}^{-2}\text{s}^{-1}$ ), low brine salinity, low chl *a* concentrations and seawater temperatures of -1.6 °C. These

conditions may explain why the dominant species was *Entomoneis* spp, a large cryobenthic diatom which has been shown to perform well in low salinity melt conditions (Ryan et al., 2004). It is important to note that when considering all sampling sites, *Entomoneis* spp. was not correlated to brine salinity, however another large solitary diatom, *Pleurosigma* spp., was positively correlated with brine salinity, thus brine salinity is unlikely to be the only driver of relatively high abundance of *Entomoneis* spp. at TF-1. A unique community composition was also observed in the assemblage at TF-2, with high relative abundance of *C. closterium*, however it did not appear to be melting out as the site had higher brine salinity and lower under ice water temperatures of -1.8 °C. Thus, based on the RDA it is likely that this assemblage is explained primarily by high light transmissivity (22% incoming PAR).

Previous studies have shown that the composition of the ice algal community can affect sympagic-pelagic-benthic coupling, as the melt community may seed the pelagic ecosystem, shaping the ensuing phytoplankton blooms (Jin et al., 2016; Michel et al., 1993; Pineault et al., 2013). An ice community dominated by colonial taxa forming aggregates has been shown to shift the dominance of the pelagic community from diatom to flagellate dominated, as the ice-associated aggregates of diatoms sink rapidly to the ocean floor (Tedesco et al., 2012). In addition, in the early season when grazing pressure in the pelagic zone is minimal, ice algae sinking to the ocean floor is an important food source for the benthos (McMahon et al., 2006) which may persist year round (Koch et al., 2023). Combined, these processes influence which taxa and nutrients are available to be transferred through trophic levels via pelagic and benthic pathways. The low  $\delta^{13}\text{C}$  values observed in the water column indicate that the ice-associated algae had not yet made a quantitatively significant contribution to the pelagic community, likely due to timing and the temperature of the ice, as most communities had not reached the end of season melt (i.e. under water ice temperatures remained at  $< -1.8$  °C, with some exceptions) and generally low light levels reaching the water column (i.e. 19 of 30 sites experienced  $< 20$   $\mu\text{mol photons m}^{-2}\text{s}^{-1}$ ).

The strong links between the availability of ice algae and reproduction in some zooplankton species reinforces the importance of ice algae to the extent of secondary production and nutrition supplied to the marine food web, with estimates of the carbon contribution derived from sea-ice algae to some zooplankton species being as high as

60% (Runge & Ingram, 1988; Søreide et al., 2006, 2013). For example, reproduction in *Calanus glacialis* has been shown to begin under the sea ice, prior to the pelagic blooms (Swailethorp et al., 2011), with availability of ice algae for grazing bringing forward oogenesis and oocyte maturation (Durbin & Casas, 2014). Ice algae availability can also boost fecundity, as the population reach higher numbers when the first feeding naupliar stage aligns with the subsequent pelagic phytoplankton bloom (Ringuette et al., 2002; Søreide et al., 2010) and it has been proposed that a longer ice-covered season could result in a longer spawning season and larger cohort for *C. glacialis* (Durbin & Casas, 2014). Copepods have also been observed to preferentially consume ice algae over pelagic phytoplankton during the reproductive period (Durbin & Casas, 2014). This is likely due to a preference for cells containing higher lipid content, such as has often been measured in sea-ice algae at the end of the spring season (Lee et al., 2008b; Smith et al., 1993).

The rapidly declining expanse and duration of land-fast ice in the Arctic means that communities reliant on this icy habitat are experiencing an ecosystem in flux, where snow and ice thickness are likely to vary across space and time. The implications of this instability will be highly variable light transmissivity, which in turn alters ice algal community composition, and thus likely the sea ice and pelagic primary and secondary production, as well as benthic productivity (Currie et al., 2021). Under a future scenario of warmer water and air temperatures, Arctic sea ice and snow depth are projected to be thinner (Kacimi & Kwok, 2022; Renner et al., 2014; Webster et al., 2014), thereby permitting greater light transmittance through the ice. Whilst our findings are constrained to correlative relationships, if our data are indicative of broader Arctic bottom ice communities, then these data suggest that a higher light under-ice environment could reshape the bottom ice algal communities towards higher diversity, with a greater contribution of dinoflagellates. Any shift away from diatoms and towards dinoflagellates would have trophic and biogeochemical implications, influencing both the transfer of energy through the food web and oceanic mineral cycling. For example, copepods and especially *Calanus* spp., the dominant zooplankton in Arctic waters, have a strong reliance on carbon derived from a diatom-based diet (Søreide et al., 2008). A reduced relative contribution of diatoms and a higher relative abundance of dinoflagellates would affect the fatty acid content available to higher trophic levels, as diatoms are high in C16 PUFA, essential fatty acids (20:5n-3) and omega-7 fatty acids (16:1n-7), whilst dinoflagellates are high in C18 and C22 PUFA (Dalsgaard et al., 2003). In addition, a

shift to a dinoflagellate dominated community would alter ocean biogeochemistry, as diatoms have a unique siliceous cell structure that acts as ballast, making them effective at exporting carbon to ocean depths and key players in biogenic silicon cycling (Baines et al., 2010). That said, the high, late-season snowfall observed during this study meant that light transmissivity declined as time progressed, highlighting how the stochasticity of snow fall adds a layer of complexity to the seasonality of light (which generally increases with the onset of Arctic summer). As lower light transmissivity correlated with a less diverse ice algal community, depending on the dominating taxa, this too would influence carbon transfer through the food web. A community dominated by colonial species such as *N. frigida*, or larger solitary species such as *Pleurosigma* spp. or *Entomoneis* spp. affects grazing efficiency in smaller copepod species, whereas smaller algal taxa reduce grazing efficiency in larger copepod species (Levinsen et al., 2000). Such a shift has been observed in the Antarctic krill *Euphausia superba*, which showed only 50% grazing efficiency for phytoplankton < 20  $\mu\text{m}$  (Boyd et al., 1984). Given the potential for higher precipitation (snowfall) to occur in the Arctic in the short-medium term (Liu et al., 2012; van Pelt et al., 2016), which would invariably reduce light transmittance to under ice communities (Perovich, 2007), we may see ice algal communities that are less diverse. Should the increased precipitation come as rain however, which is increasing in parts of the Arctic (Hansen et al., 2014), the snow cover would be reduced and the light transmittance would increase, potentially resulting in a more diverse ice algae community, as described above. Such conditions would also likely limit ice algae community establishment and biomass due to bottom ablation (Juhl & Krembs, 2010). While continuing and rapid environmental change is an established component of global warming, due to the many complexities of interactions and feedback mechanisms, the direction of the change is less decided.

This seasonal study has offered a unique insight into algal community composition in Arctic land-fast sea ice across broad temporal and spatial scales and examined the relationship between the community structure and environmental variables with a particular focus on the under-ice light environment. We showed that the bottom ice community composition was strongly correlated with under-ice light transmissivity, with algal assemblages generally exhibiting greater species diversity when experiencing more light early in the productive season. These findings are important, because shifts in ice algal community composition can have both trophic effects through changes to size and

food quality, and biogeochemical implications. Furthermore, these data intimate that the tight coupling between ice algae abundance and zooplankton reproductive success would be affected by alterations to sea-ice thickness and snow cover, with the precise direction of change being interwoven with the extent and direction of environmental change. Through revealing the importance of light availability on shaping Arctic land-fast ice algal communities, we have provided baseline data that can help inform predictive models to better constrain the ecological impacts of environmental change to polar marine food webs, which depend on these ice-based organisms.

**Acknowledgements:**

R.J.D is supported by an Australian Government Research Training Program Scholarship, an AINSE Ltd. Postgraduate Research Award (PGRA) and an Arctic Field Grant (310664) provided by the Research Council of Norway (RCN). E.R. was also supported with an Arctic Field Grant (310692). Further, funding was provided through the 2017-2018 Belmont Forum and BiodivERsA joint call for research proposals, under the BiodivScen ERA-Net COFUND programme, and with the funding organisations RCN (296836) and National Science Centre Poland (UMO-2015/17/B/NZ8/02473).



**Supplementary Information****Table S3.1:** *Sampling locations including fjord, site name, location coordinates (latitude, longitude) and dates sampled.*

<b>Location</b>	<b>Site</b>	<b>N</b>	<b>E</b>	<b>Sampling Dates</b>
<b>Van Mijenfjorden*</b>	VM-1	77.84918	16.7078	14.4.21; 28.4.21; 5.5.21; 13.5.21; 21.5.21; 25.5.21
	VM-2	77.86545	16.70532	14.4.21; 28.4.21; 5.5.21; 25.5.21
	VM-3	77.83154	16.30812	14.4.21; 28.4.21; 4.5.21; 25.5.21
	VM-4	77.79405	15.8085	14.4.21; 27.4.21; 4.5.21
	VM-5	77.79996	15.7583	4.5.21; 13.5.21; 21.5.21
<b>Petuniabukta</b>	PB-1	78.68988	16.55717	21.4.21
	PB-2	78.67344	16.47996	21.4.21
<b>Austfjorden</b>	AF-1	78.93678	16.32022	22.4.21
	AF-2	78.90926	16.41073	22.4.21
<b>Tempelfjorden</b>	TF-1	78.41145	17.14749	30.4.21
	TF-2	78.43113	17.22808	30.4.21
<b>East Coast</b>	AG-1	78.00874	18.44778	24.5.21
	IB-1	77.88842	18.26567	24.5.21
	IB-2	77.8881	18.23018	24.5.21

\*Three sites in Van Mijenfjorden were sampled during the FAABulous project (Future Arctic Algae Blooms—and their role in the context of climate change) (Kvernvik, 2019; Leu et al., 2020); however the naming system differs here. VM-1, VM-2 and VM-3 within this study are the previously known VMF-Main Station, VMF-IM and VMF-2 respectively.

**Table S3.2:** Comparison of irradiance measurements ( $\mu\text{mol photons m}^{-2}\text{s}^{-1}$ ) taken in situ using Li-COR under and above the ice and modelled irradiance measurements, including conversion to percent (%) incoming PAR values.

Date	Station	Time	Measured Irradiance Under Ice ( $\mu\text{mol m}^{-2}\text{s}^{-1}$ )	Measured Irradiance Surface ( $\mu\text{mol m}^{-2}\text{s}^{-1}$ )	Measured % Incoming PAR (Transmissivity)	Modelled Irradiance Under Ice	Modelled % Incoming PAR (Transmissivity)	Difference Incoming PAR (%)
14.4.21	VM-1	12:00	0.16	677	0.02	0.15	0.02	0.00
14.4.21	VM-2	10:10	1.01	609	0.17	17.48	2.87	2.71
14.4.21	VM-3	14:40	0.33	629.8	0.05	0.15	0.02	-0.03
14.4.21	VM-4	16:30	1.36	485.3	0.28	1.02	0.21	-0.07
21.4.21	PB-1	-	Failed	592	Failed	32.59	5.51	-
21.4.21	PB-2	16:30	3.84	645	0.97	21.91	5.53	4.56
22.4.21	AF-1	12:30	8.97	895	1.00	20.88	2.33	1.33
22.4.21	AF-2	-	Failed	895	Failed	41.87	4.68	-
27.4.21	VM-4	-	Failed	856.4	Failed	193.98	22.65	-
27.4.21	VM-5	-	Failed	898	Failed	127.90	14.24	-
28.4.21	VM-1	-	Failed	687	Failed	13.57	1.98	-
28.4.21	VM-2	-	Failed	797.7	Failed	2.88	0.36	-
28.4.21	VM-3	-	Failed	564.1	Failed	3.75	0.67	-
30.4.21	TF-1	-	Failed	789.4	Failed	180.40	22.85	-
30.4.21	TF-2	-	Failed	449.5	Failed	104.19	23.18	-
4.5.21	VM-3	18:20	0.66	406.7	0.16	17.14	4.22	4.05
4.5.21	VM-4	14:30	22.23	661.9	3.37	68.17	10.34	6.97

4.5.21	VM-5	13:00	31.93	647	4.88	99.29	15.17	10.29
5.5.21	VM-1	11:00	4.25	822.3	0.52	12.52	1.52	1.01
5.5.21	VM-2	9:30	4.76	662.4	0.72	8.66	1.31	0.59
13.5.21	VM-1	16:45	30.59	602.5	5.08	2.24	0.37	-4.71
13.5.21	VM-5	13:45	50.42	821.4	6.10	35.60	4.31	-1.79
21.5.21	VM-1	11:45	1.73	1158	0.15	4.91	0.42	0.27
21.5.21	VM-5	17:30	21.74	687.2	3.10	4.30	0.61	-2.49
24.5.21	AG-1	13:20	0.19	1183	0.02	4.17	0.35	0.34
24.5.21	IB-1	15:55	2.33	960.7	0.24	2.53	0.26	0.02
24.5.21	IB-2	17:50	1.00	906.1	0.11	0.92	0.10	-0.01
25.5.21	VM-1	11:10	10.61	1314	0.81	18.28	1.39	0.58
25.5.21	VM-2	16:30	1.14	387.7	0.29	1.48	0.38	0.09
25.5.21	VM-3	17:00	0.94	1022	0.09	19.41	1.90	1.81

**Table S3.3:** Physical, chemical, and biological variables measured in under-ice water (0.5 m below ice) at each sampling site and date including ammonium, silicic acid, nitrate and phosphate concentrations ( $\mu\text{M}$ ), chlorophyll *a* concentration ( $\text{mg m}^{-3}$ ), water temperature ( $^{\circ}\text{C}$ ), water salinity (ppt), C:N molar ratios and bottom depth (m) of the sampling site. NA represents data not available.

Date	Station	Ammonium	Silicic Acid	Nitrate	Phosphate	Chlorophyll <i>a</i>	Water Temperature	Water Salinity	Bottom Depth	C:N	$\delta^{13}\text{C}_{\text{VPDB}}$	$\delta^{15}\text{N}_{\text{Air}}$
14.4.21	VM-1	<1	2.50	2.06	0.20	0.04	-1.89	34.1	56.2	6.50	-26.48	7.31
14.4.21	VM-2	<1	2.50	2.16	0.20	0.16	NA	NA	56.2	3.90	-25.36	5.35
14.4.21	VM-3	<1	2.60	2.14	0.21	0.06	NA	NA	64.1	3.92	-28.41	3.00
14.4.21	VM-4	<1	2.60	2.18	0.21	0.20	-1.85	34.1	89.1	9.07	-27.18	5.02
21.4.21	PB-1	<1	2.91	2.31	0.24	0.47	-1.81	33.2	52.2	9.73	-26.61	5.67
21.4.21	PB-2	<1	2.71	2.08	0.23	0.77	NA	NA	NA	9.93	-26.43	5.53
22.4.21	AF-1	<1	2.81	2.00	0.22	0.21	-1.85	34.2	160.4	9.59	-26.70	5.96
22.4.21	AF-2	<1	2.91	1.97	0.22	1.27	NA	NA	NA	7.98	-26.46	4.78
27.4.21	VM-4	<1	2.91	2.19	0.23	1.06	-1.57	34.4	89.1	9.50	-26.79	5.47
27.4.21	VM-5	<1	2.91	2.21	0.24	0.65	-1.45	34.4	83.1	6.79	-26.40	4.82
28.4.21	VM-1	<1	2.39	2.06	0.20	0.05	-1.8	34.5	52.8	3.47	-26.33	4.61
28.4.21	VM-2	<1	2.60	2.10	0.20	0.20	NA	NA	56.2	13.20	-25.91	7.27
28.4.21	VM-3	<1	2.81	2.13	0.21	0.05	NA	NA	64.1	9.71	-26.61	3.07
30.4.21	TF-1	<1	2.91	2.13	0.22	0.70	-1.6	34.5	77.4	6.69	-25.49	4.82
30.4.21	TF-2	<1	2.71	1.92	0.20	0.72	-1.8	34.5	46.8	5.05	-28.05	3.93
4.5.21	VM-3	<1	2.71	2.14	0.21	0.76	-1.81	34.5	64.1	5.48	-25.71	5.84
4.5.21	VM-4	<1	2.81	2.18	0.23	1.01	-1.61	32.6	89.1	7.09	-25.37	3.30
4.5.21	VM-5	<1	2.81	2.14	0.23	0.73	NA	NA	83.1	7.07	-26.55	3.03
5.5.21	VM-1	<1	2.50	2.10	0.20	0.22	-1.71	34.5	52.8	2.84	-25.71	2.23

5.5.21	VM-2	<1	2.60	2.08	0.20	0.11	-1.86	34.4	56.2	2.24	-25.91	1.68
13.5.21	VM-1	<1	2.60	2.10	0.20	0.64	-1.70	34.0	52.8	8.78	-26.07	5.51
13.5.21	VM-5	<1	2.50	1.97	0.22	0.91	-1.64	33.7	83.1	5.49	-27.22	2.24
21.5.21	VM-1	<1	1.56	1.53	0.19	1.08	NA	NA	52.8	10.09	-26.98	4.22
21.5.21	VM-5	<1	0.83	0.79	0.13	1.94	NA	NA	83.1	5.77	-25.87	3.39
24.5.21	AG-1	NA	NA	NA	NA	0.21	NA	NA	NA	4.63	-25.92	3.67
24.5.21	IB-1	<1	2.91	2.08	0.20	0.82	NA	NA	NA	6.33	-26.65	6.12
24.5.21	IB-2	<1	2.81	2.13	0.20	0.31	NA	NA	NA	8.71	-27.36	8.54
25.5.21	VM-1	<1	1.14	1.40	0.16	1.25	NA	NA	52.8	4.64	-24.99	3.86
25.5.21	VM-2	<1	2.39	1.89	0.20	0.48	NA	NA	56.2	7.49	-26.65	4.61
25.5.21	VM-3	NA	NA	NA	NA	0.69	NA	NA	64.1	4.43	-26.68	2.81

**Table S3.4:** Relative percentage (%) contribution of species to the bottom ice algae community at each sampling site and date

This large table is available at: [doi.org/10.1016/j.pocean.2024.103248](https://doi.org/10.1016/j.pocean.2024.103248)

**Table S3.5:** Counts per mL per species present in the bottom ice algae community at each sampling site and date.

This large table is available at: [doi.org/10.1016/j.pocean.2024.103248](https://doi.org/10.1016/j.pocean.2024.103248)

**Table S3.6:** Statistical output of the regression models of taxa group and Log10 percent (%) incoming PAR, including multiple  $R^2$ , adjusted  $R^2$ ,  $F$  statistic, associated degrees of freedom (DF) and  $P$ -value model. Statistically significant  $P$ -values ( $< 0.05$ ) are marked in bold.

Taxa	Multiple $R^2$	Adjusted $R^2$	$F$ Statistic	DF	$P$ Value
Ciliophora	0.01	0.00	0.26	1,25	0.61
<i>Cylindrotheca closterium</i>	0.03	0.00	0.69	1,26	0.41
<i>Dinoflagellate</i> spp.	0.20	0.17	6.58	1,27	<b>0.02</b>
<i>Entomoneis</i> spp.	0.01	0.00	0.27	1,27	0.61
<i>Fragilariopsis</i> spp.	0.01	0.00	0.14	1,24	0.72
<i>Gymnodinium</i> spp.	0.35	0.32	13.77	1,26	<b><math>9.9 \times 10^{-4}</math></b>
<i>Haslea</i> spp.	0.00	0.00	0.15	1,25	0.91
<i>Navicula</i> spp. (Solitary)	0.00	0.00	0.03	1,28	0.86
<i>Navicula</i> spp. (Colony)	0.33	0.30	11.36	1,23	<b><math>2.6 \times 10^{-3}</math></b>
<i>Nitzschia frigida</i>	0.18	0.15	6.30	1,28	<b>0.02</b>
<i>Nitzschia</i> spp.	0.04	0.01	1.14	1,25	0.30
<i>Pauliella taeniata</i>	0.12	0.10	3.89	1,28	0.06
<i>Pleurosigma</i> spp.	0.06	0.03	1.93	1,28	0.18
<i>Pseudo-nitzschia</i>	0.00	0.00	0.03	1,24	0.87
<i>Pyramimonas</i> spp.	0.06	0.02	1.59	1,24	0.22
<i>Raphidiphyceae</i>	0.13	0.10	3.87	1,27	0.06
Rare Taxa*	0.03	0.00	0.85	1,25	0.37
<i>Thalassiosira</i> spp.	0.37	0.34	14.05	1,24	<b><math>9.94 \times 10^{-4}</math></b>

\*Rare Taxa includes: *Anisonema* spp., *Bacillaria paxillifera*, *Chaetoceros* spp., *Coccolithus pelagicus*, *Commation cryoporinum*, *Cryptophyceae* spp., *Diploneis littoralis*, *Euglena* spp., *Halosphaera* spp., *Manguinea rigida*, *Pinnularia quatratarea*, *Plagiotropis* spp., *Stenoneis inconspicua*, *Tropidoneis* spp.

## Chapter 4

### **Biomolecular profiles of Arctic sea-ice diatoms highlight the role of under-ice light in cellular energy allocation**

*Published in ISME Communications as:*

**Duncan, R. J.**, Nielsen, D., Søreide, J. E., Varpe, Ø., Tobin, M. J., Pitusi, V., Heraud, P., & Petrou, K. (2024). Biomolecular profiles of Arctic Sea-ice diatoms highlight the role of under-ice light in cellular energy allocation. *ISME Communications*, 10 (4), 1. DOI: 10.1093/ismeco/ycad010

*Author contributions:*

R.J.D., J.E.S., O.V. and K.P. conceptualised the study and determined the methodology. R.J.D. performed the investigation, data curation, formal analysis, data visualisation and wrote the original draft. D.N. assisted with the methodology, investigation and designed the code for spectroscopy data curation. J.E.S., V.P. and K.P. contributed to the investigation, and resources were supplied by J.E.S. Validation of spectroscopic data was given by M.T. and P.H. Supervision of R.J.D. was performed by J.E.S, O.V., M.T. and K.P. Funding was acquired by R.J.D., J.E.S and K.P. All authors contributed to reviewing and editing the original draft written by R.J.D.

Production Note: Signature removed prior to publication.	Production Note: Signature removed prior to publication.	Production Note: Signature removed prior to publication.	Production Note: Signature removed prior to publication.	Production Note: Signature removed prior to publication.	Production Note: Signature removed prior to publication.	Production Note: Signature removed prior to publication.	Production Note: Signature removed prior to publication.
R. Duncan	D. Nielsen	J.E. Søreide	Ø. Varpe	M.J. Tobin	V. Pitusi	P. Heraud	K. Petrou

Chapter 4 provides species-specific insights on the changes to biomolecular allocation in dominant sea-ice microalgal species, from land-fast sea-ice communities exposed to different environmental conditions. This chapter takes samples from the same field campaigns analysed in the previous chapter, specifically from the most frequently sampled fjord (Van Mijenfjorden), and during the peak time of spring productivity. With Chapter 3 providing insights into the community composition shifts, and this chapter providing taxon-specific nutritional information, together they provide two crucial pieces of the puzzle.

**Abstract**

Arctic sea-ice diatoms fuel polar marine food webs as they emerge from winter darkness into spring. Through their photosynthetic activity they manufacture the nutrients and energy that underpin secondary production. Sea-ice diatom abundance and biomolecular composition vary in space and time. With climate change causing short-term extremes and long-term shifts in mean environmental conditions, understanding how and in what way diatoms adjust biomolecular stores with environmental perturbation is important to gain insight into future ecosystem energy production and nutrient transfer. Using synchrotron-based Fourier Transform Infra-Red microspectroscopy, we examined the biomolecular composition of five dominant sea-ice diatom taxa from land-fast ice communities covering a range of under-ice light conditions during spring, in Svalbard, Norway. In all five taxa we saw a doubling of lipid and fatty acid content when light transmitted to the ice-water interface was >5% but <15% (85 - 95% attenuation through snow and ice). We determined a threshold around 15% light transmittance after which biomolecular synthesis plateaued, likely due to photoinhibitory effects, except for *Navicula* spp., which continued to accumulate lipids. Increasing under-ice light availability led to increased energy allocation towards carbohydrates, but this was secondary to lipid synthesis, while protein content remained stable. It is predicted that under-ice light availability will change in the Arctic, increasing due to sea-ice thinning and potentially decreasing with higher snowfall. Our findings show that the nutritional content of sea-ice diatoms are taxon-specific and linked to these changes, highlighting potential implications for future energy and nutrient supply for the polar marine food web.



## **Introduction**

The ecosystem within and directly below Arctic sea ice is highly seasonal, with light playing a critical role in its structure and functioning, through its influence on the productivity of the under-ice photosynthetic primary producers. The formation of land-fast ice typically occurs in winter when darkness persists for 24 h. During this time, the early microbial community of sea-ice microalgae are captured within the brine pockets of the sea ice (Leu et al., 2015). As the light returns to high latitudes in the early spring, dormant and vegetative sea-ice microalgae become active and begin to photosynthesise (Hancke et al., 2018). Early spring is characterised by sufficient inorganic nutrients supplied from the water below, but low light levels, which limit microalgal biomass and primary production (Cota et al., 1991; Leu et al., 2015). As spring progresses, light becomes abundant, resulting in peak productivity where ice algae can bloom, forming a key source of energy and nutrients for zooplankton and benthic reproductive cycles (Durbin & Casas, 2014; Renaud et al., 2007; Søreide et al., 2010). At our study sites at 78°N, the transition from perpetual darkness to constant daylight (the midnight sun) is rapid and occurs inside 42 days (Cohen et al., 2020). During this period, light reaching the sea-ice algae changes from being limiting to potentially harmful, if snow cover is absent (Leu et al., 2015; Mock & Thomas, 2005). As summer approaches, despite abundant light, the lower nutrient concentrations (Cota et al., 1987, 1990), increasing water temperatures and rapid brine drainage (Campbell et al., 2014; Mundy et al., 2005), start to limit sea-ice algal productivity and, ultimately the higher summer temperature causes the ice to melt completely, releasing the microbial community living within the brine channels into the pelagic and benthic zones below (Renaud et al., 2007).

The amount of light reaching the ice-water interface is dependent on snow depth and sea-ice thickness, which can be highly variable in space and time. As global temperatures rise with climate change, it is expected that snow and ice dynamics will change (Callaghan et al., 2011; van Pelt et al., 2016; Yu et al., 2014), and consequently the seasonal progression of the bottom-ice community will change as well. Whilst it is well-established that Arctic sea-ice extent is declining (Comiso et al., 2008; Meredith et al., 2019; Parkinson, 2014a; Stroeve et al., 2007) and becoming thinner (Itkin et al., 2017; Renner et al., 2014; Willmes & Heinemann, 2015), which alone would drive higher under-ice light levels, it is possible that the Arctic may experience increased precipitation in the form of higher snowfall in the short to medium term, due to increased storms and more open water (Liu et al., 2012;

van Pelt et al., 2016). The influence of snow depth on light attenuation is far greater than sea ice alone. Snow-free ice can transmit up to 80% of incoming photosynthetically available radiation (PAR) (Hamre et al., 2004; Taskjelle et al., 2017), whereas a 10 cm layer of fresh snow can effectively block light, reducing visible light transmission to <5% of incoming PAR (Perovich, 2007). As such, if the sea ice covered areas of the Arctic were to experience higher snowfall with global warming, despite thinner ice, under-ice light levels could be significantly reduced, modifying the growth conditions for the microalgae below.

Environmental conditions affect the allocation of photosynthetically derived carbon within polar ice algae, determining their biomolecular (i.e. lipid, carbohydrate, fatty acids, and protein) composition (Duncan & Petrou, 2022, and references within). In turn, the biomolecular composition of ice algae determines the energy and nutrients available to the polar marine food web (Smith et al., 1987). In actively growing ice algae, lipid may constitute up to 20% of dry weight and 60% of particulate organic matter composition (Falk-Petersen et al., 1998; Smith et al., 1989). Lipids are the most energy-rich biomolecule with a caloric value of approximately twice that of carbohydrate and protein (Hagen & Auel, 2001; Kim et al., 2015) and transfer much of the energy between levels of the food web. Lipid content available at the primary production level is important for development, growth rate (Hygum et al., 2000) the amount of secondary production (Peltomaa et al., 2017). Due to the synthesis of FAs, in particular polyunsaturated fatty acids (PUFA), being tightly coupled to photosynthesis, eukaryotic algae are the main source of FAs to the marine food web (Guschina & Harwood, 2009; Ruess & Müller-Navarra, 2019). In sea-ice associated ecosystems, ice algae have been shown to be responsible for up to 50% of the fatty acids (FA) present in higher trophic levels including fish, seals, and seabirds (Amiriaux et al., 2023; Budge et al., 2008). In particular, FAs, including saturated (SAFA), monounsaturated (MUFA) fatty acids, and PUFAs, impact zooplankton fecundity and larval development (Jónasdóttir et al., 2005, 2009), as they are critical for membrane development, growth and reproduction (Ruess & Müller-Navarra, 2019). Their importance is evident from the high efficiency with which they are transferred through the trophic levels, with PUFAs shown to be transferred twice as efficiently from primary to secondary trophic levels compared to bulk carbon (Gladyshev et al., 2011; Mayor et al., 2011). Carbohydrates are also important biomolecules in terms of energy transfer (Hagen & Auel, 2001), and play an important role in contributing to

the cellular carbon pool (2016). Particularly under nutrient-depleted conditions, carbohydrates are a reserve product which can be drawn upon for lipid synthesis (Ahn et al., 2019; Hu, 2004). Proteins are important for providing cellular nitrogen reserves and are the primary source of amino acids (AA) (2016), which are vital for organism growth and survival, as regulators of metabolic pathways and as the structural elements of enzymes (Wu, 2010). For heterotrophic organisms, non-essential AAs can be synthesised *de novo*, however essential AAs must be provided by diet of which microalgae are the primary source in marine ecosystems (Ruess & Müller-Navarra, 2019). While polar ice algae typically have a relatively reduced photosynthate allocation to protein compared to other biomolecules (Palmisano & Sullivan, 1985; Smith et al., 1987), they have a high transfer efficiency through food webs (Bhavya et al., 2019).

In the highly seasonal environment of the Arctic, in which productivity is severely restricted for much of the year, the provision of biomolecular energy from sea-ice algae is important for the transfer of energy through the polar marine ecosystem (Campbell et al., 2022). The value of sea-ice algae as food is linked also to the time in which they bloom. They are the primary source of carbon in the early spring (Michel et al., 1996; Selz et al., 2018; Tourangeau & Runge, 1991) before pelagic phytoplankton proliferate (Ji et al., 2013), and some Arctic zooplankton have evolved to temporally align their reproductive cycle with this early food availability.

Studies on natural sea-ice algal communities have investigated nutrient content (e.g. lipid and protein content) at the community scale (Duncan & Petrou, 2022, and references within), with only two studies looking at the effects of light on the biomolecular composition of Arctic diatoms at a taxon-specific level (Findlay et al., 2017; Pogorzelec et al., 2017). Our study investigates the influence of the under-ice light conditions on the allocation of biomolecules, including lipids, proteins, and carbohydrates, in five Arctic ice-associated pennate diatoms; *N. frigida* (colonial), *Pleurosigma* spp. (solitary), *Navicula* spp. (solitary), *Haslea* spp. (solitary), and *Entomoneis* spp. (solitary), taken from natural communities within the land-fast sea ice in Svalbard, Norway. Using synchrotron-based Fourier Transform Infrared (s-FTIR) microspectroscopy (Fig. 4.1) to analyse individual cells, we uncover taxon-specific patterns in biomolecular production and allocation, providing insight into how sea-ice algae nutritional content may change with climate-driven shifts in community composition.

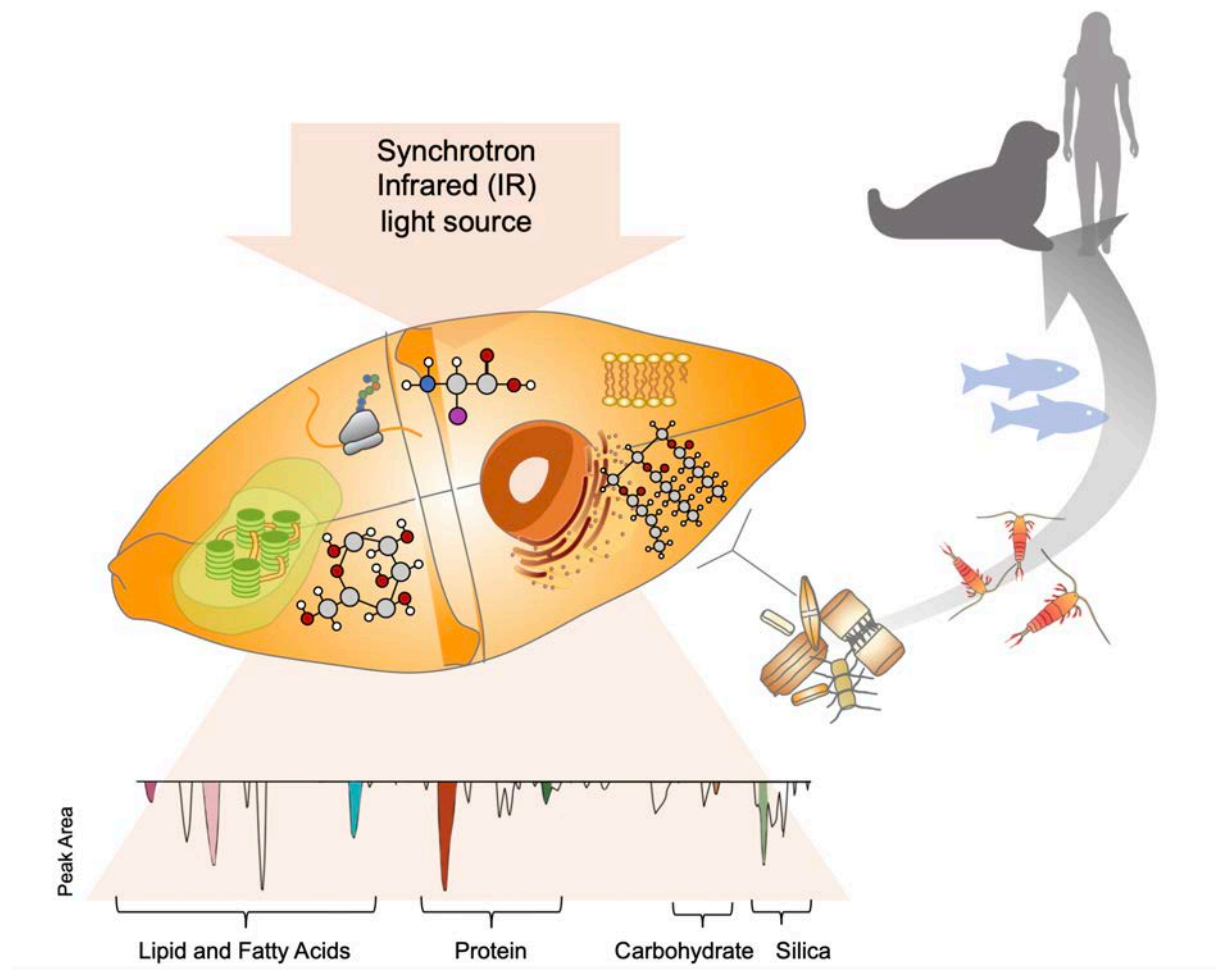


**Figure 4.1:** Conceptual model of the synchrotron infrared light source measuring and the biomolecules within an individual cell, and the corresponding wavelengths on the infrared (IR) spectrum (second derivative transformed) (bottom), in which the coloured sections represent the peak area of the biomolecules studied. A simplified overview of the transfer of these biomolecules up the polar marine food chain is displayed (right).

## **Materials & Methods**

### **Study Area**

This study was conducted within Tempelfjorden and Van Mijenfjorden in Svalbard, Norway (Fig. 4.2; Table S4.1) on the 30<sup>th</sup> of April and 4-5<sup>th</sup> of May, 2021, respectively. Within Van Mijenfjorden, five sites were sampled once along a transect from the inner to the outer fjord (VM-1, VM-2, VM-3, VM-4, VM-5), capturing a gradient of ice thickness and snow depth. A site from Tempelfjorden (TF-2) was sampled once and included due

to its thinner sea ice and snow depth, providing data from an environment of higher light transmissivity to the ice-water interface. Both fjords are located on the west coast of Svalbard and are influenced by glacial run-off (Høyland, 2009). Additionally, both fjords are comprised of an outer basin up to 120 m deep and inner basin up to 70 m deep (Van Mijenfjorden) and 60 m deep (Tempelfjorden). However, unlike Tempelfjorden, Van Mijenfjorden is a partially enclosed fjord meaning it has longer and more predictable sea-ice cover (Høyland, 2009). Detailed analysis of the under-ice protist community composition at all sites is available in Duncan et al. (2024b).

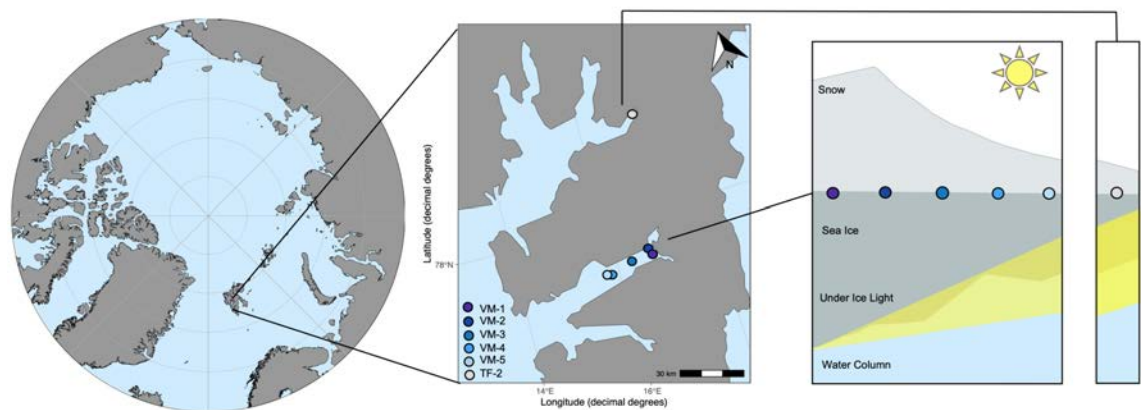


**Figure 4.2:** Location of Svalbard, Norway, within the Arctic (left), sampling locations visited between April-May 2021 in Svalbard (middle), overview of the snow depth, sea-ice thickness, and under-ice light at each of the sampling stations (right).

### Sample Collection

At each sampling site, six ice cores were extracted approximately 0.5-1 m apart, using a Kovacs core barrel (9 cm diameter; Kovacs Enterprise, Oregon, USA). The bottom 3 cm (at the ice-water interface) of each core was retained, as this is where the microbial community was concentrated (Kvernvik et al., 2021; Lee et al., 2008a; Smith et al., 1988). Cores were then pooled into triplicates, as cores 1-2, 3-4 and 5-6, and 100 mL of filtered sea water (GF/F, 0.7  $\mu\text{m}$ , Whatman, England) was added for every centimetre of core to minimise osmotic stress (Campbell et al., 2019; Garrison & Buck, 1986) after which the samples were allowed to melt in darkness for 24 h at 4  $^{\circ}\text{C}$ . To concentrate the cells, 100 mL from each of the three samples was centrifuged at 1000 rpm (Universal 320, Hettich, Germany) for 4 min and the supernatant removed. The remaining sample was then transferred to 2 mL Eppendorf tubes and centrifuged at 1000 rpm (Mikro 185, Hettich)

for 2 min before the supernatant was removed, and the sample was fixed by addition of formalin (5% v/v) in filtered sea water (FSW) for later analysis.

### **Environmental Parameters**

#### Physical Parameters:

Three snow depth measurements were taken to the nearest 0.5 cm using a standard ruler, to determine the average snow depth per core. Ice thickness was measured using a Kovacs ice thickness gauge. Water temperature was measured 0.5 m below the ice-water interface using a CTD probe (STD/CTD SD204, SAIV A/S: Bergen, Norway). At each sampling site, approximately 100 mL of the water from directly below the ice surface was collected in acid washed bottles for nutrient analysis. The samples were frozen until analysis, when they were melted and 4M H<sub>2</sub>SO<sub>4</sub> was added for preservation in transport for analysis at Akvaplan-niva, Norway. The nitrate plus nitrite (NO<sub>3</sub><sup>-</sup> + NO<sub>2</sub><sup>-</sup>) (NO<sub>x</sub>), phosphate (PO<sub>4</sub><sup>3-</sup>), silicic acid (Si(OH)<sub>4</sub>), and ammonium (NH<sub>4</sub>) concentrations (μM) were measured simultaneously on a San++ 5000 automated analyzer (Skalar: Breda, Netherlands), with separate analysis channels for the four nutrients. The detection limits were 0.02 μM for NO<sub>x</sub>, 0.01 μM for phosphate, 0.25 μM for silicic acid, and 0.3 μM for ammonium. Stable isotope analysis of the 0-3 cm section of sea ice was performed in an elemental analyser isotope ratio mass spectrometry (EA-IRMS) system, as previously published (Barrie et al., 1989).

#### Light Measurements and Modelling:

Incoming photosynthetically active radiation (PAR) was measured at each sampling site in Van Mijenfjorden using a LI-190 quantum air sensor placed on the sea-ice surface and a LI-192 underwater quantum sensor placed on a weighted frame positioned through a 10 cm hole in the sea ice, with measurements collected using a LI-1500 Data Logger (LI-COR, Nebraska, USA). To avoid shadowing of the measurement area, all sensors faced south with operations performed north, and the area was undisturbed. However, at Tempelfjorden, the underwater quantum sensor failed. Therefore, to ensure light transmittance values were available from all sampled sites and determined using a consistent methodology, and to utilise our unique *in situ* surface light measurements, the under-ice light measurements were modelled. Light at the ice-water interface under the sea ice was estimated using *in-situ* measured irradiance at the top of snow and ice, and then attenuation through snow and ice was modelled using attenuation coefficients of 20

$\text{m}^{-1}$  for snow,  $5 \text{ m}^{-1}$  for the top 10 cm of ice and  $1 \text{ m}^{-1}$  for ice below the top 10 cm (Perovich, 1996; Varpe et al., 2015), using the following equation:

$$\text{Equation 1: } E_Z = E_0 \cdot \exp(-K_d \cdot Z)$$

where ( $E_Z$ ) is irradiance at sampling depth,  $E_0$  is the surface irradiance ( $\mu\text{mol photons m}^{-2}\text{s}^{-1}$ ),  $K_d$  is the diffuse light attenuation coefficient ( $\text{m}^{-1}$ ), and  $Z$  is the sampling depth (m). Light values at the ice-water interface were converted to percent incoming PAR to account for the measured in situ irradiance above-ice being taken at various times of day and with a range of cloud coverage conditions, which have a substantial effect on light levels (Connan-McGinty et al., 2022; Matuszko, 2012). Below we use light transmissivity as a descriptive term for percent incoming PAR and have divided the sites into those receiving  $< 5\%$  incoming PAR as low light transmissivity (LLT) sites, and those receiving  $> 5\%$  incoming PAR as high light transmissivity (HLT) sites.

### **Species-specific Biomolecular Composition by FTIR**

The biomolecular composition of five selected taxa (*N. frigida*, *Pleurosigma* spp., *Navicula* spp., *Haslea* spp., and *Entomoneis* spp.) (Table S4.2) was determined using synchrotron-based FTIR microspectroscopy on hydrated, formalin-fixed (5% v/v final concentration) cells. All cells were measured as single cells, i.e. not dividing or associated with a chain. The *Navicula* spp. group consisted primarily of *N. transitas*, *N. directa*, and *N. valida*. Samples were loaded (3  $\mu\text{l}$ ) directly into a micro-compression cell between two 13 mm diameter 0.5 mm thick  $\text{CaF}_2$  windows (Tobin et al., 2010). Using the Infrared (IR) Microspectroscopy Beamline at the Australian Synchrotron, Victoria, spectral data of individual cells (between 1-20 cells per taxon per site, Table S4.3) were collected in transmission mode. Each biomolecule absorbs a specific range of IR wavelengths, and a set of well-defined absorbance bands between  $3050\text{-}2800 \text{ cm}^{-1}$ , and  $1770\text{-}1100 \text{ cm}^{-1}$  have been determined (Table 4.1). Spectra were acquired over the measurement range  $4000\text{-}800 \text{ cm}^{-1}$  with a Vertex 80v FTIR spectrometer (Bruker Optic, Ettlingen, Germany) in conjunction with an IR microscope (Hyperion 3000, Bruker) fitted with a narrow-band mercury cadmium telluride detector cooled with liquid nitrogen. The use of hydrated cells as opposed to desiccated samples have been shown to limit light scattering effects (Bamberg et al., 2012). Co-added interferograms (sample  $n = 32$ , background  $n = 64$ ) were collected at a wavenumber resolution of  $4 \text{ cm}^{-1}$ . To allow for measurements of

individual cells, all measurements were made in transmission mode, using a measuring aperture diameter of 6.9  $\mu\text{m}$  (area = 37.4  $\mu\text{m}^2$ ) for the smaller taxa (*N. frigida*, *Navicula* spp., and *Haslea* spp.) and 12.5  $\mu\text{m}$  (area = 122.7  $\mu\text{m}^2$ ) for the larger taxa (*Pleurosigma* spp. and *Entomoneis* spp.). All cells were measured with multiple points across the cell surface to account for heterogeneity in the cell structure and distribution of biomolecules (Fig. 4.3). Spectral acquisition and instrument control were achieved using Opus 7.5 software (Bruker). Analyses were performed within 6 months of samples being collected and fixed. All samples were kept refrigerated between fixation and analysis.

**Table 4.1:** Infrared (IR) band assignments for *s*-FTIR microspectroscopy used in this study.

Wave number ( $\text{cm}^{-1}$ )	Band Assignment	Reference
~3011	$\nu(\text{C-H})$ of cis $\text{C}=\text{CH-}$ from unsaturated lipids	Vongsvivut et al. 2013
~2960	$\nu_{\text{as}}(\text{C-H})$ from methyl ( $-\text{CH}_3$ ) groups of lipids and proteins	Vongsvivut et al. 2013
~2921	$\nu_{\text{as}}(\text{C-H})$ from methylene ( $-\text{CH}_2$ ) from saturated lipids	Vongsvivut et al. 2013
~2852	$\nu_{\text{s}}(\text{C-H})$ from methylene ( $-\text{CH}_2$ ) from saturated lipids	Vongsvivut et al. 2013
~1744	$\nu(\text{C=O})$ from ester carbonyl group from lipid triglycerides and fatty acids	Vongsvivut et al. 2013
~1549	Amide II mode from proteins; mainly $\delta(\text{N-H})$ of amides	Heraud et al., 2007
~1400	$\nu_{\text{s}}(\text{COO}^-)$ from carboxylated molecules	Sackett et al., 2014
~1377	$\delta_{\text{s}}(\text{CH}_3)$ and $\delta_{\text{s}}(\text{CH}_2)$ of lipids and proteins	Heraud et al., 2005
~1241	$\nu_{\text{as}}(\text{PO}_2^-)$ of the phosphodiester backbone of nucleic acids, phosphorylated proteins, and phosphorylated lipids	Whelan et al. 2011 Sackett et al., 2014
~1146	$\nu_{\text{s}}(\text{C-O})$ from carbohydrates	Heraud et al., 2008
~1080	$\nu_{\text{s}}(\text{Si-O})$ from silica	Beardall et al., 2001; Sackett et al., 2016



### Data Analyses

Infrared spectral data were analysed in R v4.2.2 (RStudio Team, 2022). Data were smoothed (4 pts either side) and second derivative (3rd order polynomial) transformed using the Savitzky-Golay algorithm from the *prospectr* package (Stevens & Ramirez-Lopez, 2014) and then normalised using Standard Normal Variate (SNV) (mean centered and standard deviation of 1) (Fig. 4.3). Biomolecular content for each measured cell was estimated based on integrating the area under each assigned peak (Table 4.1), using the Beer-Lambert Law, which assumes a direct relationship between absorbance and analyte concentration to determine metabolite content (Wagner et al., 2010).

Relationships between biomolecular content and environmental variables (% incoming PAR, nitrate and silicic acid concentration in the water at ice-water interface, bottom-ice temperature and salinity and water temperature at the ice-water interface) were investigated using Spearman's correlation (Table S4.4). As % incoming PAR was the most highly correlated with the biomolecular profile, relationships between biomolecular content and percent incoming PAR were estimated using principal component analyses (PCA) and with linear regressions applied to the mean peak area at each incoming % PAR level (i.e. each sampling site) ( $\pm$  95% confidence interval) for each taxon. Due to the difference in absorption properties of biomolecules, the integrated peak areas provide relative changes between samples, meaning any quantitative measure of change can only be applied within compounds. The Shapiro-Wilks (Shapiro & Wilk, 1965) test for normality showed the data required  $\log_{10}$  transformation before analysis. The number of cells measured ranged from 1 to 20 per taxa, per site (Table S4.3). Due to the low abundance of *Haslea* spp. and *Pleurosigma* spp. at TF-2, however, no confidence interval was applied to the linear regressions beyond 15.2% incoming PAR. Relationships between lipid and protein content, lipid and carbohydrate content and carbohydrate and protein content, with increasing light reaching the ice-water interface, were also investigated using linear regression. Fixed factor linear regression models, with under-ice light level (HLT vs LLT) as the factor, were used to determine that these regressions were improved when separated according to HLT sites (VM-4, VM-5, TF-2) and LLT sites (VM-1, VM-2, VM-3) sites. Statistical significance of the regressions was concluded based on the F statistic ( $p < 0.05$ ) and strength of fit estimated using  $R^2$ . The residuals of all regressions were verified for homoscedasticity. All analyses were performed using R Studio v. 2023.09.0 (RStudio Team, 2022) and the add-on packages *ggplot* v. 3.3.6

(Wickham et al., 2016), dplyr v. 1.0.8 (Wickham et al., 2015), corrplot (Wei et al., 2017) and vegan v. 2.6-4 (Oksanen et al., 2013).

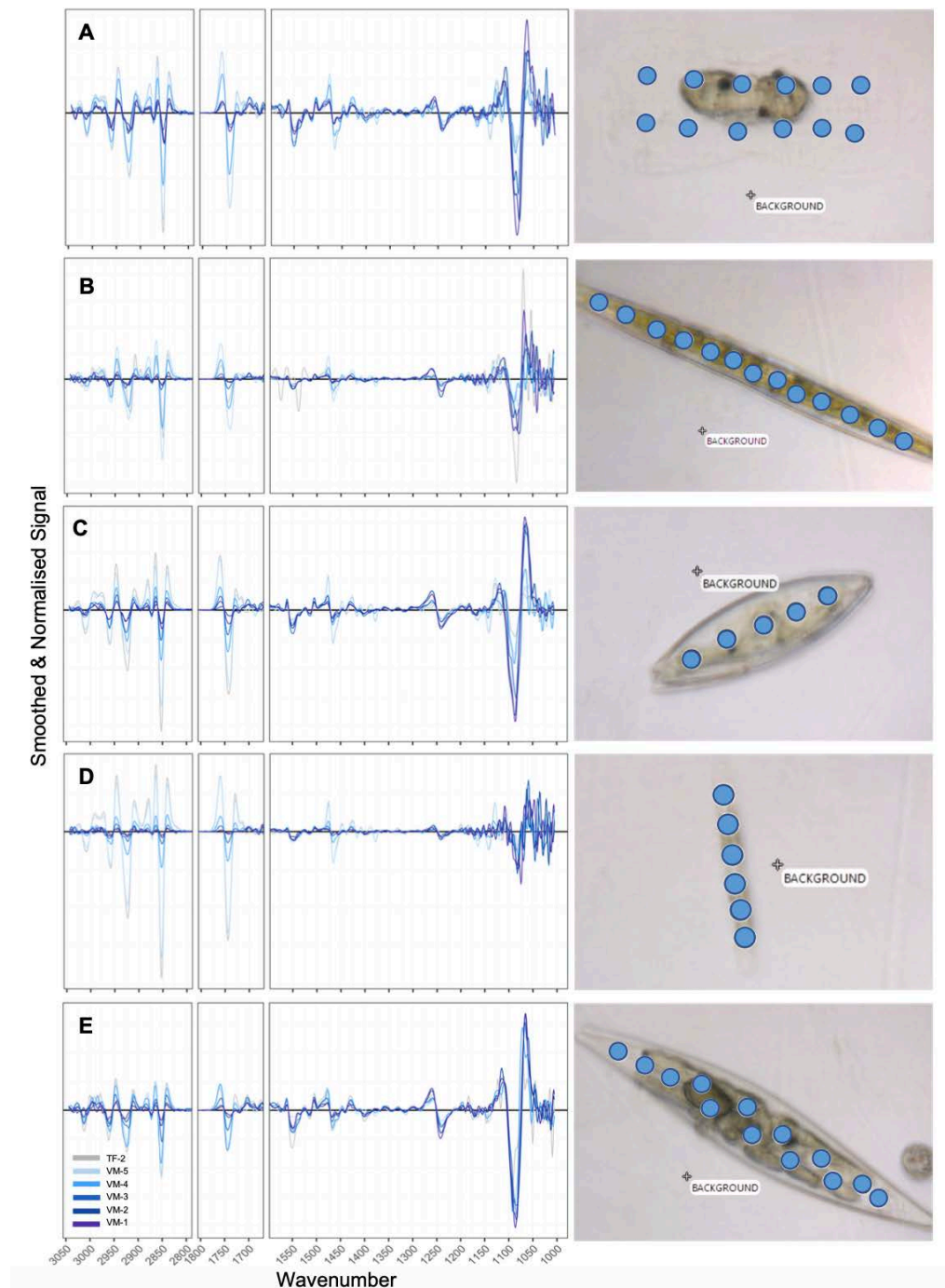


**Figure 4.3:** Smoothed and normalised spectra of each of the five taxa, (A) *Entomoneis* spp., (B) *Haslea* spp., (C) *Navicula* spp., (D) *N. frigida*, (E) *Pleurosigma* spp., with each site denoted in colour. Images of example cells of each taxa (right) with blue dots denoting the S-FTIR measurement points (where the aperture (actual measuring area) for each point was larger than the point indicated), demonstrating the entire cell contents were measured.

## **Results**

### **Physical Parameters**

Within Van Mijenfjorden, snow depth and ice thickness decreased towards the fjord opening. The outermost site (VM-5) had ice thickness of  $52 \pm 3.5$  cm and a snow depth of  $4.8 \pm 3.5$  cm, allowing 15% incoming PAR at the ice-water interface, and the innermost site (VM-1) had ice thickness of  $92 \pm 3.2$  cm and snow depth of  $14.3 \pm 0.7$ , allowing 1.5% incoming PAR (for data on all sites, see Table 2). The Tempelfjorden site (TF-2) had the highest incoming PAR at 23%, with an ice thickness of  $38 \pm 1.1$  cm and snow depth of  $3.4 \pm 0.7$  cm. Based on the average incoming PAR of  $640 \mu\text{mol m}^{-2} \text{s}^{-1}$ , measured in situ at the snow surface of the sampling sites, this equates to a range of  $8 - 148 \mu\text{mol m}^{-2} \text{s}^{-1}$  transmitted through the snow and ice to the bottom ice community. In mid-April, all VM sites experienced <3% incoming PAR however by late April, VM-4 and VM-5 experienced 23% and 14% incoming PAR respectively (Duncan et al. 2024b). Seawater nutrient concentrations were relatively high, with nitrate concentrations ranging from  $2.18 \mu\text{M}$  (VM-4) to  $1.92 \mu\text{M}$  (TF-2) (Table 2) and silicic acid concentrations ranging from  $2.81 \mu\text{M}$  (VM-4 and VM-5) to  $2.5 \mu\text{M}$  (VM-1). Taken from the sea ice, stable isotope of carbon ( $\delta^{13}\text{C}_{\text{VPDB}}$  (‰)) was more enriched at HLT sites ( $t(2) = 4.02$ ,  $p < 0.05$ ), averaging  $-17.42 \pm 3.2$  at the HLT sites (TF-2, VM-4, VM-5) and  $-24.85 \pm 0.5$  at the LLT sites (VM-1, VM-2, VM-3). Ice temperature in the 0-3 cm section was between  $-2.1$  and  $-2.2$  °C at all VM sites and  $-2.7$  at TF-2, whilst the under-ice water temperature ranged from  $-1.61$  °C (VM-4) to  $-1.86$  (VM-2). Bottom ice salinity ranged from 10.7 (VM-2) to 3.7 (VM-4). Given that bottom ice temperature was consistently below the seawater freezing point ( $-1.7$  °C), brine volume remained well within the reasonable range for communities to inhabit sea ice (>5%) (Golden et al., 2007) and all sites were nutrient replete ( $>1.9 \mu\text{M}$ ), these environmental variables were unlikely significant drivers for any observed metabolomic changes. In contrast, under-ice light transmittance (through snow and ice), was the most variable environmental variable across sites, but also the one that correlated most strongly and consistently with biomolecular content (Table S4.5) and therefore the focus of this study. For more details and further physical parameters, see Table 4.2 and Duncan et al. (2024b).

**Table 4.2:** Parameters measured associated with sea-ice core extraction; snow depth (cm) ( $\pm$  SD,  $n = 18$ ), ice thickness (cm) ( $\pm$  SD,  $n = 6$ ), % incoming PAR and under ice light ( $\mu\text{mol m}^{-2} \text{s}^{-1}$ ). Measurements from within the bottom 3 cm of sea-ice core; temperature ( $^{\circ}\text{C}$ ), salinity (ppt), brine salinity (ppt), brine volume (% of ice volume), chlorophyll a concentration ( $\text{mg m}^{-2}$ ) ( $n = 3$ ), particulate organic carbon (POC) to particulate organic nitrogen (PON) molar ratio (C:N). Parameters measured in under-ice water at each sampling site; ammonium ( $\text{NH}_4$ ), silicic acid ( $\text{Si}(\text{OH})_4$ ), nitrate ( $\text{NO}_3$ ) and phosphate ( $\text{PO}_4$ ) concentrations ( $\mu\text{M}$ ) and temperature ( $^{\circ}\text{C}$ ), where N.D. denotes not measured.

Date	Station	Sea Ice										Under-Ice Water				
		Snow Depth	Ice Thickness	% Incoming PAR	Light	Ice Temperature	Ice Salinity	Brine Salinity	Brine Volume	Chlorophyll	C:N	$\text{NH}_4$	$\text{Si}(\text{OH})_4$	$\text{NO}_3$	$\text{PO}_4$	Temperature
5.5.21	VM-1	14.3 $\pm$ 0.7	92 $\pm$ 3.2	1.5	12.52	-2.1	6.5	37.36	15.57	0.48 $\pm$ 0.3	6.09	<1	2.50	2.10	0.20	-1.71
5.5.21	VM-2	15.8 $\pm$ 2.1	78 $\pm$ 3.0	1.3	8.66	-2.2	10.7	39.07	24.49	0.29 $\pm$ 0.0	5.73	<1	2.60	2.08	0.20	-1.86
4.5.21	VM-3	10.0 $\pm$ 0.9	74 $\pm$ 2.6	4.2	17.14	-2.2	10.4	39.07	23.81	1.90 $\pm$ 0.2	6.02	<1	2.71	2.14	0.21	-1.81
4.5.21	VM-4	7.0 $\pm$ 3.2	50 $\pm$ 2.2	10.3	68.17	-2.1	3.7	37.36	8.86	0.63 $\pm$ 0.1	7.50	<1	2.81	2.18	0.23	-1.61
4.5.21	VM-5	4.8 $\pm$ 3.5	52 $\pm$ 3.5	15.2	99.29	-2.2	5.6	39.07	12.82	0.86 $\pm$ 0.2	6.92	<1	2.81	2.14	0.23	N.D.
30.4.21	TF-2	3.4 $\pm$ 0.7	38 $\pm$ 1.1	23.2	104.1 9	-2.7	9.2	47.53	17.25	2.82 $\pm$ 1.0	10.18	<1	2.71	1.92	0.20	-1.80

### Species-specific biomolecular composition

Across all five taxa, lipid (ester carbonyl) and carbohydrate content generally increased with increasing percent incoming PAR until 15% surface irradiance, after which, the content plateaued or declined in all taxa except for *Navicula* spp. which saw a continued increase up to 23% incoming PAR (Fig. 4.4, Table S4.5). The other photosynthetically derived biomolecules including unsaturated fatty acids, saturated fatty acids, saturated lipid and lipid (CH-stretch II) followed the same increasing trend with percent incoming PAR until ~15% (Fig. 4.4, Table S4.5). We saw no clear trend associated with percent incoming PAR for the other functional biomolecules i.e. protein (amide II) and phosphorylated molecules (Fig. 4.4, Table S4.5). Carboxylated molecules experienced a decline with increasing percent incoming PAR in all taxa except *Pleurosigma* spp. (Fig. 4.4).

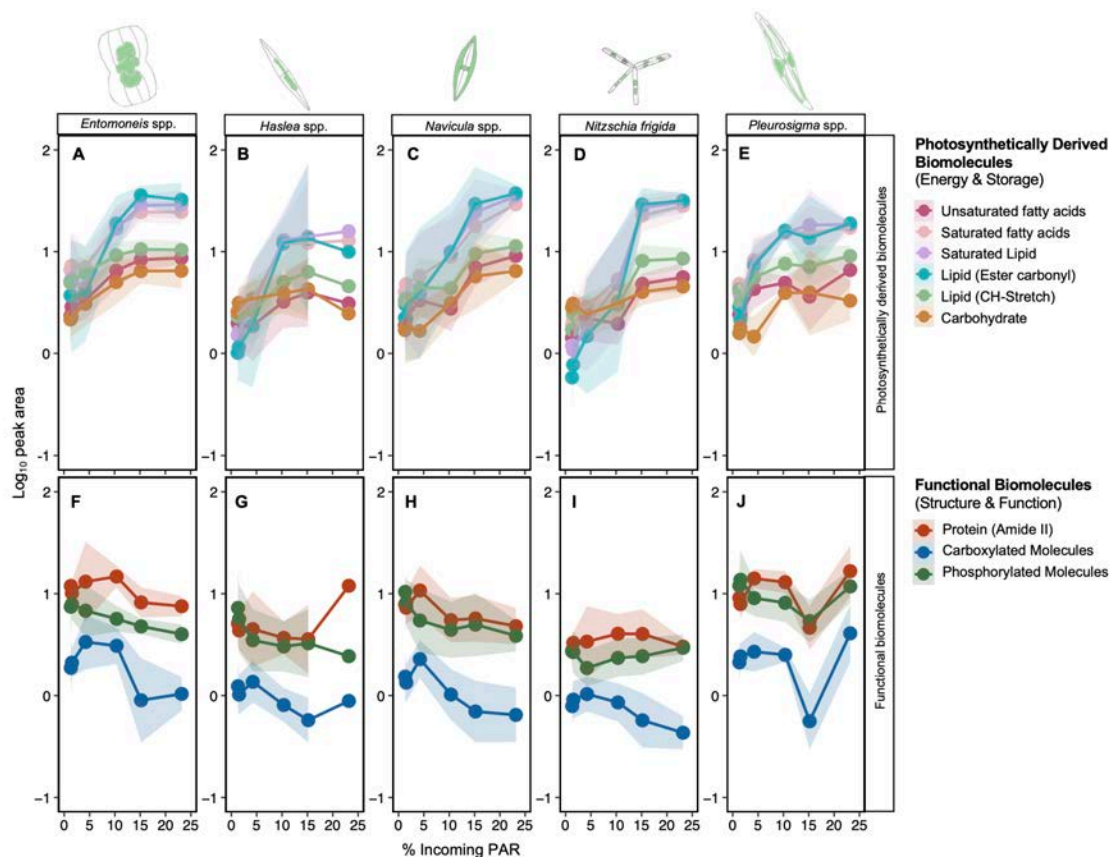


**Figure 4.4:** Mean cell-specific biomolecular content (based on normalised peak areas – see Table 4.1) for photosynthetically derived (energy-rich, storage) biomolecules (unsaturated fatty acids, saturated fatty acids, saturated lipid, lipid (ester carbonyl), lipid (CH-stretch II) and carbohydrate) (A) *Entomoneis* spp., (B) *Haslea* spp., (C) *Navicula* spp., (D) *N. frigida*, (E) *Pleurosigma* spp., and functional (structural and cell function) biomolecules (protein (amide II), carboxylated molecules, phosphorylated molecules)

(F) *Entomoneis* spp., (G) *Haslea* spp., (H) *Navicula* spp., (I) *N. frigida*, (J) *Pleurosigma* spp. as a function of the proportion of light reaching the ice-water interface. Coloured shading indicates 95% confidence intervals, applied to log-transformed data.

The correlation matrix shows clear separation in the relationships between photosynthetically derived and structural biomolecules (Fig. 4.5A). We saw strong positive correlations ( $>0.75$ ) amongst the lipid compounds (ester carbonyl, saturated lipids, saturated and unsaturated fatty acids), and moderate positive correlations with carbohydrates ( $>0.50$ , Fig. 4.5A). Furthermore, these photosynthetically-derived biomolecules were only weakly correlated with protein and phosphorylated molecule content ( $< 0.3$ ), and negatively correlated with carboxylated molecules ( $<-0.3$ ). Structural biomolecules (protein, phosphorylated molecules, carboxylated molecules) were positively correlated with one another ( $>0.6$ , Fig. 4.5A).

Analysing all peak areas of all five taxa from all sites, we found clustering according to a light gradient (Fig. 4.5B), with PC1 explaining 61.9% of the variation in biomolecular content, correlating with the gradient in percent incoming PAR. The difference observed across PC1 was driven by lipid, saturated lipid, saturated fatty acid, unsaturated fatty acid, lipid (CH-stretch II) and carbohydrate bands, corresponding with their measured increase with increasing transmitted irradiance (Fig. 4.4). The next main source of variation along the PC-2 was driven by the difference in protein (amide II), carboxylated molecules and phosphorylated molecule content, explaining 28% of the variation (Fig. 4.5B). Separation of the data by taxa reveals that this variation is likely species derived, with *N. frigida* and *Haslea* spp., clustering separately to *Navicula* spp., *Pleurosigma* spp., and *Entomoneis* spp., particularly within the LLT sites (Fig. 4.5B).

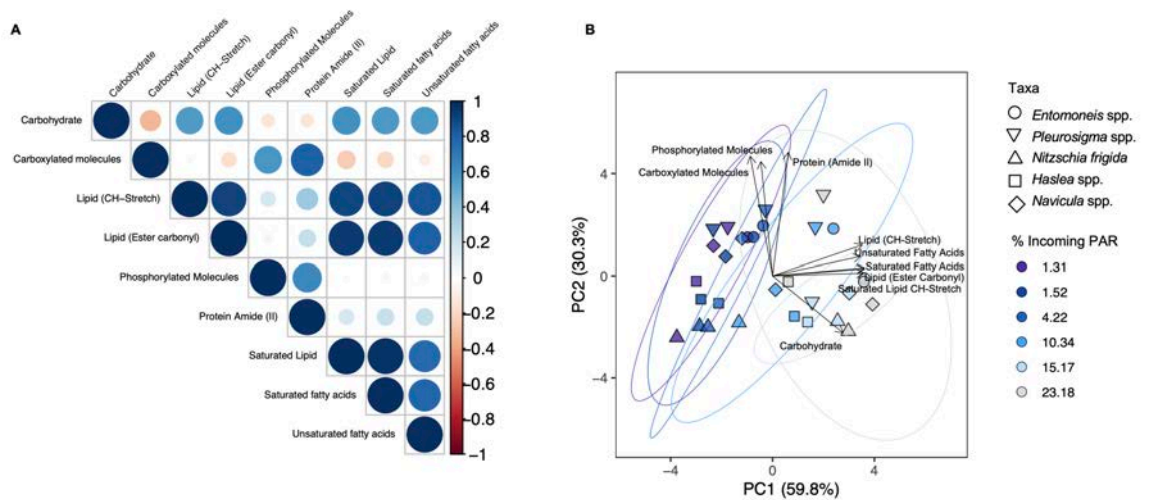


**Figure 4.5:** (A) Correlation plot based on Spearman's rank correlation coefficient for biomolecular content across all taxa and sampling sites where dark blue represents a strong positive correlation and dark red represents a strong negative correlation. (B) Principal component analysis (PCA) of biomolecular content at each under-ice light level for all taxa combined (*Entomoneis* spp., *Haslea* spp., *Navicula* spp., *N. frigida*, and *Pleurosigma* spp.). Direction and strength of individual biomolecules are displayed with ordination bi-plot overlay.

To estimate the key changes to biomolecular content and carbon allocation in the cell, the relationships between lipid, protein, and carbohydrate were investigated for each taxon using linear models. Including low (<5% incoming PAR) and high (>5% incoming PAR) light as fixed factors improved the model outcome, resulting in two regressions for each comparison. A positive correlation between lipid and carbohydrate was observed at HLT conditions only ( $F_{1,182} = 92.95$ ,  $p < 0.05$ ;  $R^2 = 0.34$ , Fig 4.6A) and the same correlation was observed for each species individually (Table S4.5). No correlation between lipid and carbohydrate was observed at LLT sites when all species were considered together (Fig. 4.6A). We saw a positive correlation between lipid and protein in all species under LLT conditions ( $F_{1,98} = 271.8$ ,  $p < 0.05$ ;  $R^2 = 0.58$ , Fig 4.6B, Table S4.5). This was also observed at HLT when all species were considered together ( $F_{1,182} = 10.15$ ,  $p < 0.05$ ;  $R^2 = 0.06$ , Fig. 4.6B), driven by the positive correlations in *Entomoneis* spp. and *Haslea* spp. only (Table S4.5). A strong parallel shift in increasing lipid content from LLT to HLT conditions was observed in all five taxa (Fig. S4.1). For carbohydrate, a weak negative correlation relationship with protein content was observed in the LLT sites when all species were considered together (Fig 4.6C), whereas a positive correlation was observed

at HLT sites. Similar to lipids, *Entomoneis* spp. and *Haslea* spp. only exhibited increases in carbohydrate content under HLT, with minimal changes to protein content (Table S4.5).

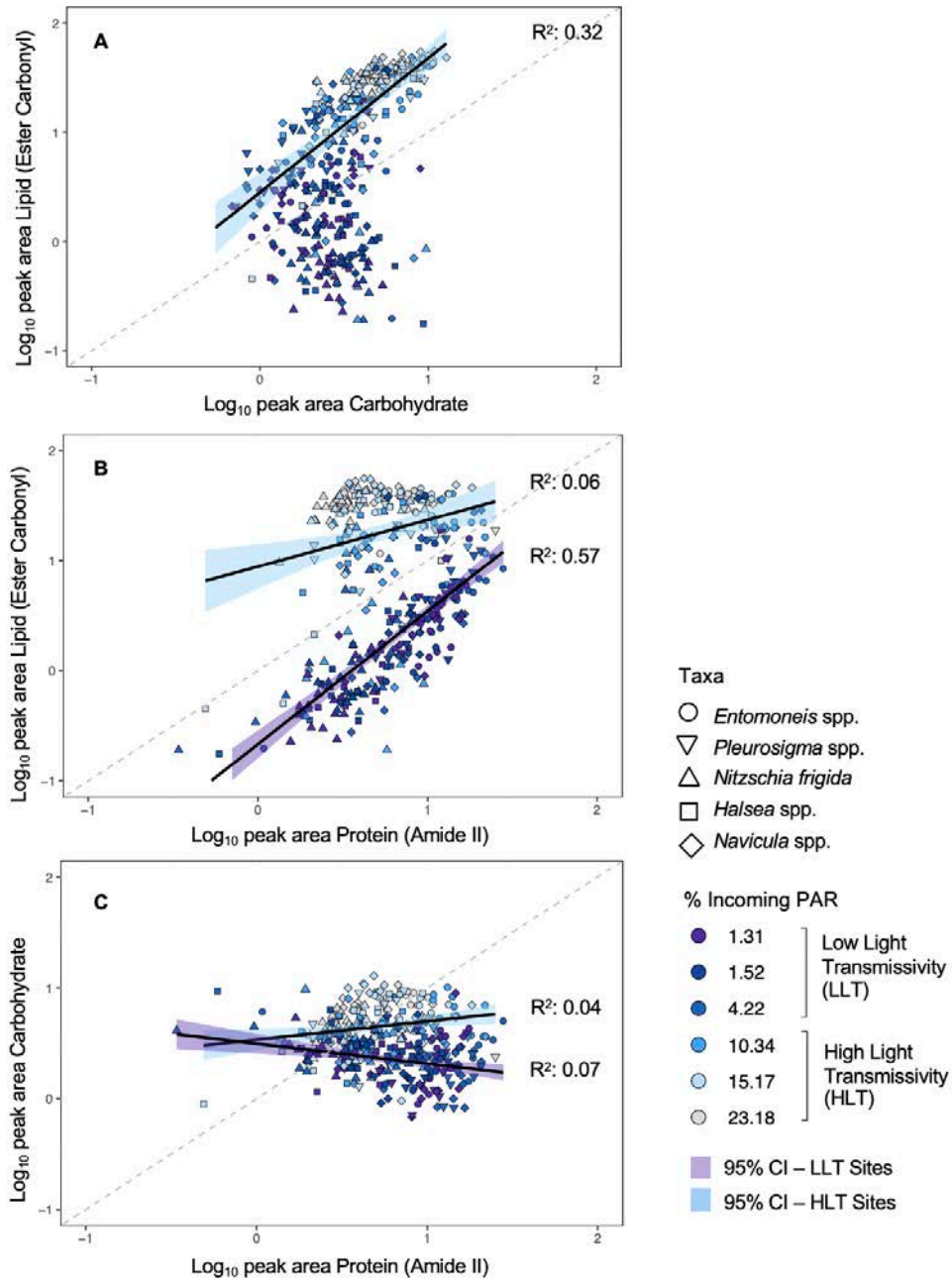


**Figure 4.6:** (A) Lipid (Ester carbonyl) vs. Carbohydrate content, (B) Lipid (Ester carbonyl) vs. Protein (Amide II) content and (C) Carbohydrate vs Protein content, based on normalised peak areas, for all taxa combined and data are divided into HLT sites (VM-4, VM-5, TF-2) and LLT sites (VM-1, VM-2, VM-3), with light levels indicated with colour fill and taxa are denoted by shape. The data are fitted with linear regressions, with 95% confidence intervals (coloured shading), applied to log-transformed data. Only statistically significant regressions are shown.



Integration of the silica peaks (maxima at 1080  $\text{cm}^{-1}$ ) for each species and site, revealed that silica concentration declined with declining incoming PAR in all species (Fig. 4.7A-E). For *Entomoneis* spp. ( $F_{1,66} = 44.94$ ,  $p < 0.05$ ;  $R^2 = 0.41$ ), *Haslea* spp., ( $F_{1,55} = 14.77$ ,  $p < 0.05$ ;  $R^2 = 0.22$ ), *Navicula* spp. ( $F_{1,104} = 107.6$ ,  $p < 0.05$ ;  $R^2 = 0.51$ ), and *Pleurosigma* spp. ( $F_{1,40} = 21.67$ ,  $p < 0.05$ ;  $R^2 = 0.35$ ), the decline in silica content was linear with declining incoming PAR whereas for *N. frigida* ( $F_{2,106} = 26.2$ ,  $p < 0.05$ ;  $R^2 = 0.33$ ) the decline was observed until  $\sim 15\%$  incoming PAR, after which it plateaued, suggesting a minimum level of silicification had been reached.

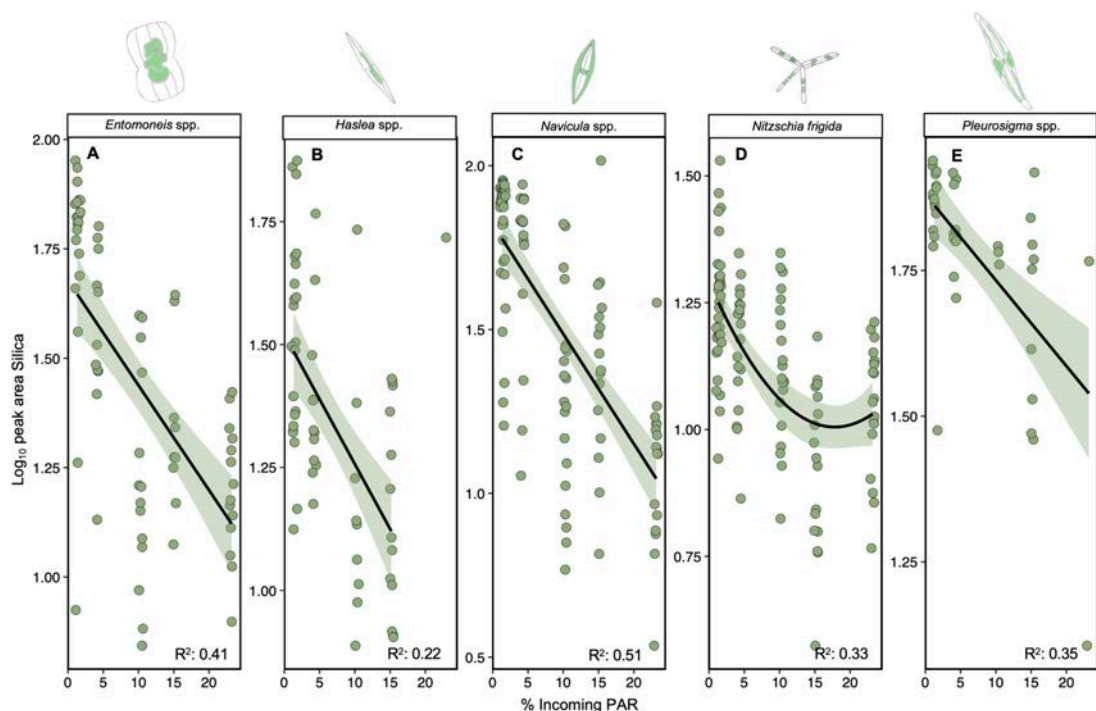


**Figure 4.7:** Silica content (based on normalised peak areas) with increasing % photosynthetically active radiation (PAR) reaching the ice-water interface, per taxa. Each data point represents one measured cell. The data are fitted with linear regressions, with 95% confidence intervals (coloured shading), applied to log-transformed data. Only statistically significant regressions are shown.

### **Discussion**

Biomolecules supplied by sea-ice microalgae to the polar marine food web are important, particularly as the primary food supply early in the season, but also as a source of essential fatty acids for zooplankton reproduction. Microalgal biomolecular composition however, is environmentally determined (Duncan & Petrou, 2022) and therefore even subtle shifts

in the physio-chemical conditions of the surrounding environment can affect the nutritional content supplied to the marine food web. In this study, key environmental variables (temperature, nutrients, salinity, etc.) varied minimally across the sites and were generally within the expected range for spring (Arrigo, 2014), whereas snow and sea-ice thickness varied more and the resulting under-ice light transmittance strongly correlated with biomolecular changes.

Across all five taxa, we found that increasing under-ice light availability led to an increase in lipids, fatty acids and carbohydrates, and that lipid accumulation was preferentially allocated over carbohydrates at higher irradiances. In most cases the increases in lipid, fatty acids and carbohydrate were observed until ~15% incoming PAR, at which point saturation occurred. This observed threshold could be due to the highest irradiances causing photoinhibition and thus limiting further biomolecular production (Cade-Menun & Paytan, 2010; Gleitz & Kirst, 1991; Lund-Hansen et al., 2020), as the measured irradiances for VM-5 and TF-2 were outside the typical spring bloom range ( $> 20\%$  incoming PAR or  $> 100 \mu\text{mol m}^{-2}\text{s}^{-1}$ ) (Duncan & Petrou, 2022). Evidence of photoinhibition has been observed in sea-ice microalgae at similar light levels (Leu et al., 2016; Lund-Hansen et al., 2020; Petrou et al., 2010) and is generally a result of synthesis of photoprotective pigments, changes to chlorophyll content and down-regulation of photosystem II (PSII) (Petrou et al., 2010). The greatest increase in lipid content with increasing under-ice light was observed in *N. frigida* until 15% incoming PAR, which aligns with previous observations that *N. frigida* accumulated higher lipid stores than *Attheya* spp. and pennate ribbon colonies (Pogorzelec et al., 2017). The exception to the observed light threshold was *Navicula* spp., which continued to increase lipid and carbohydrate content beyond 15% incoming PAR, suggesting morphological or photophysiological differences in this taxon. One explanation for this difference could be that *Navicula* spp. often have large central regions with chloroplasts concentrated along the cell wall (Poulin & Cardinal, 1982) and low intracellular chlorophyll under high light conditions as a photoadaptive strategy (Robinson et al., 1997), minimising photoinhibition and leaving substantial space for lipid accumulation in oil droplets within the cytoplasm (Maeda et al., 2017). In Antarctic sea-ice microalgal communities, *Navicula* spp. were found also to have a higher lipid content compared to other taxa (Priscu et al., 1990; Whitaker & Richardson, 1980).

There are several plausible explanations for the conserved response of the relative increases in lipid, fatty acids and carbohydrate with increasing light transmittance, these include: 1) increased growth rate (assuming a pre-bloom phase), 2) increased requirement for carbon storage in preparation for dormancy (assuming a post-bloom phase); or 3) the onset of nutrient limitation as a result of increasing algal biomass restricting nutrient influx within the ice. It is likely that the higher light communities (HLT) were experiencing higher growth rates relative to the LLT communities, due to the greater light availability driving more photosynthesis (Welch & Bergmann, 1989). The samples from the HLT sites were also more enriched with  $^{13}\text{C}$ , a parameter often associated with higher growth rates in microalgal species (Fry & Wainright, 1991), lending further support to the idea that the increased lipid and carbohydrates were a result of higher growth rates. Whilst surrounding  $\text{CO}_2$  concentrations were not evaluated, they were unlikely to have influenced  $^{13}\text{C}$  enrichment, as the  $\text{CO}_2$  concentration in brine channels is typically determined by temperature, which was consistent across our sites (McMinn, 2017). Under the assumption that the  $^{13}\text{C}$  is due to higher growth rates, the increase in lipid content may be attributed primarily to structural lipids, as microalgae tend to accumulate structural (polar), over storage (neutral), lipids alongside an increase in growth rate and as a response to early-season light intensification (Smith et al., 1989). An increase in growth rate and structural lipid content may explain the concurrent increase observed in other biomolecules including carboxylated molecules (Gong & Miao, 2019) and unsaturated fatty acids, as PUFA's are found primarily in structural lipids (Leu et al., 2010).

An additional explanation for the increased lipid content with higher light transmittance lies with the fact that many sea-ice algal species have a dormancy strategy for overwintering, in which the cells increase their carbon reserves while reducing cellular metabolic activity and pigment content (Niemi et al., 2011; Palmisano & Sullivan, 1982). This well-described strategy means that the increase in lipid, fatty acids and carbohydrate measured in the cells from HLT sites in this study, may reflect a response to increased light at the end of the growth season, when energy storage becomes a priority (Wagner et al., 2017). This physiological response may also explain the higher allocation to protein content relative to lipid and carbohydrate observed at LLT sites, as cell growth and division may have had lower priority at the HLT sites. The end-of-season response of reduced growth and increased allocation to storage molecules such as lipid, carbohydrate

(specifically triacyl glycerides and the polysaccharide storage polymer, glucan) and MUFA content has been observed previously in ice algal communities in response to increasing irradiance and decreasing nutrients characteristic of a post-bloom phase (Gleitz & Kirst, 1991; Leu et al., 2010; Smith et al., 1997; Smith et al., 1993). While nutrients were not limiting in the water under the ice at any of the sampling sites in this study, nor did we detect any decline over time (Duncan et al., 2024b), nutrient limitation within the boundary layer of the bottom-ice community cannot be ruled out, especially as cell densities increased. That said, the relatively low biomass accumulation at all sites, supported by the low chlorophyll *a* values (Campbell et al., 2016a; Leu et al., 2020), in addition with the ice C:N ratios being close to Redfield (6.6) in all sites except VM-4 and TF-2, makes the onset of nutrient limitation within the ice community, and therefore the third possible explanation, less likely. It is possible, that instead of one specific driver underpinning the measured response, a blend or cascade of these processes were at play, as both saturated and unsaturated FAs increased and responses were often species-specific, as well as spatially and temporally diverse. Of note, we observed large lipid droplets within cells from HLT sites during microspectroscopic measurements (personal observation), indicating that lipid was being accumulated for storage in some cells. Such changes in biomolecular content have been observed in different organisms as an adaptation to seasonality in resource availability and life stage requirements (Varpe, 2017). Most importantly however, whether driven by changes in energy allocation towards higher growth rates or increased energy storage in preparation for dormancy, the change in biomolecular content correlated with under-ice light environment, signifying the importance of light in determining food and essential nutrient availability to primary consumers.

The biomolecules more closely associated with functional cellular components were shown to vary with light transmissivity and across species, with some evidence of size-class grouping. Lipid (CH-stretch II) content increased with light in all taxa. Conversely, in all taxa, except *N. frigida*, we saw a decrease in phosphorylated molecules with increasing light. We saw a more nuanced response in protein across the five taxa, with four taxa showing no change in cellular protein content with light, whereas for one of the smallest taxa, *Navicula* spp., protein content was negatively correlated with under-ice light availability (up to 15% incoming PAR). The lack of protein changes in the larger taxa corresponds with a previous study that showed protein content in sea-ice algae to

remain stable, independent of light conditions (Pogorzelec et al., 2017). In contrast to our findings, earlier work observed higher protein content under low light conditions (Falkowski & LaRoche, 1991; Smith et al., 1987), but this was attributed to higher nutrients in the surrounding environment, rather than the low light conditions (Mock & Kroon, 2002a). This finding may indicate a potential size-specific biomolecular response, in which smaller taxa have a reduced requirement to allocate energy into protein compared with larger taxa.

In addition, we found silica content declined with increasing light transmittance in all five taxa with the exception of an upturn in silica content at the highest light level in *N. frigida*. Similar trends in decline have been observed previously in light levels up to  $150 \mu\text{mol m}^{-2} \text{s}^{-1}$  (Taylor, 1985), while the opposite direction of change has been shown at particularly elevated light levels ( $300 \mu\text{mol m}^{-2} \text{s}^{-1}$ ) (Su et al., 2018), meaning that there may be different mechanisms at play with respect to changes in diatom silicification and making the insights from this natural community study an important addition. The decrease in silica content observed with higher light conditions in this study could be attributed to higher growth rates. Changes in silicification has the potential to affect zooplankton grazing efficiency, as zooplankton have been shown to preferentially graze on less silicified diatoms (Liu et al., 2016) and reduced silica content may also mean the diatoms are more buoyant and therefore able to remain in the photic zone for longer when released from the sea ice, suggestive of potential changes to carbon flux.

The relationships between both photosynthetically derived and functional biomolecules and under-ice light have implications on energy supplied to the marine food web. In considering the prediction that parts of the Arctic may experience higher snowfall in the short-medium term (Liu et al., 2012; van Pelt et al., 2016), and therefore less light under the sea ice, our results indicate that such environmental conditions would be concomitant with a shorter productive season, lower growth rates, and biomass accumulation, as well as a lower lipid, carbohydrate, fatty acid, and lipid (CH-stretch II) content in Arctic sea-ice algae. This would have significant implications for secondary production and beyond, with a reduced supply of organic carbon. In addition, critical biomolecules that are produced *de novo*, such as saturated fatty acids, would likely be reduced, limiting supply to higher trophic levels (Leu et al., 2010). Such reductions would be expected to have ramifications on secondary production and zooplankton fecundity

(Søreide et al., 2010). Counter to the forecast of higher snowfall, if the increased precipitation comes in the form of rain or equally, as the warming ocean and air temperatures reduce ice thickness, then the under-ice light climate would increase. According to our data, the Arctic sea-ice algal communities could be expected to reduce silica content whilst increasing their lipid, carbohydrate and fatty acid stores, at least until a certain threshold of incoming irradiance, beyond which could lead to photoinhibition, limiting photosynthetic energy production and thereby biomolecular synthesis (Cade-Menun & Paytan, 2010). Higher under-ice light is likely to result in a higher relative abundance of *Navicula* spp., at the expense of the typically more dominant *N. frigida* (Duncan et al., 2024b), meaning that we might see even greater stores of lipid and carbohydrate with increasing under-ice light (beyond the threshold of 15% incoming PAR). Whilst higher under-ice light conditions may result in a community which is more calorific and nutrient rich, thinner sea-ice conditions, and warmer ocean temperatures would likely shorten the ice-covered duration and/or result in earlier release of the community from the brine channels and therefore could result in a mismatch of energy supply for zooplankton reproduction (Søreide et al., 2010). In the most extreme case, where warming prevents sea ice from forming, the lack of substrate for sea-ice algae communities to develop would mean that this energy source would no longer be available to fuel polar marine food webs as they emerge from winter darkness.

Our study has revealed the importance of characterising taxonomically resolved biochemical changes under varying environmental conditions. This is particularly pertinent for Arctic marine ecosystems where the effects of climate change are already occurring. While uncertainty remains about the direction and magnitude of change to future under-ice light regimes, the results herein indicate that the nutritional content of key ice algae taxa will vary in response to shifts in under-ice light conditions may result in a net loss of nutritional output. In combination with environmentally driven shifts in Arctic sea-ice microalgal community composition, season duration and biomass accumulation, these changes will have implications for the quality and quantity of energy supplied to the polar marine food web.

### **Acknowledgements**

R.J.D. is supported by an Australian Government Research Training Program Scholarship and an Australian Institute of Nuclear Science and Engineering (AINSE Ltd.) Postgraduate Research Award (PGRA). This research was supported by an Australian Research Council grant DP210101360 awarded to K.P. Part of this work was funded by the Australian Synchrotron through merit-based beamtime awarded on the Infrared Microscopy (IRM) beamline at the Australian Synchrotron, part of the Australian Nuclear Science and Technology Organisation (ANSTO) (AS213/IRM/17447). Funding was also provided by the Research Council of Norway (RCN) through an Arctic Field Grant in 2020 (310664), the ACCES Project (296836), and the 2017–18 Belmont Forum and BiodivERsA joint call for research proposals, under the BiodivScen ERA-Net COFUND programme (296836/E40). The authors would like to thank Stuart Thomson and Elaine Runge for their valuable assistance with the field sampling.

### **Data Availability:**

All data and processing scripts are available in the open repository Figshare. DOI: 10.6084/m9.figshare.24629718.

**Supplementary Information****Table S4.1:** Location and dates of sampling events, with longitude and latitude provided in decimal degrees.

Location	Site	Longitude (N)	Latitude (E)	Sampling Date
Tempelfjorden	TF-2	78.43113	17.22808	30.4.21
Van Mijenfjorden	VM-1	77.84918	16.7078	5.5.21
	VM-2	77.86545	16.70532	5.5.21
	VM-3	77.83154	16.30812	4.5.21
	VM-4	77.79405	15.8085	4.5.21
	VM-5	77.79996	15.7583	4.5.21

**Table S4.2:** Approximate cell length and width of the five taxa analysed

Taxa	Typical Length Range ( $\mu\text{m}$ )	Typical Width Range ( $\mu\text{m}$ )	Colonial/Solitary	Reference
<i>Entomoneis</i> spp.	60-140	30-50	Solitary	Poulin & Cardinal, 1983
<i>Haslea</i> spp.	50-120	9-15	Solitary	Sterrenburg et al., 2015
<i>Navicula</i> spp.	<i>N. Directa</i> : 72-105 <i>N. Transitas</i> : 50-105 <i>N. Valida</i> : 40-60	<i>N. Directa</i> : 7-10 <i>N. Transitas</i> : 13-23 <i>N. Valida</i> : 15-25	Solitary	Poulin & Cardinal, 1982; Tomas, 1997
<i>Nitzschia frigida</i>	45-75	5-7	Colonial	Medlin & Hasle, 1990
<i>Pleurosigma</i> spp.	100-300	15-30	Solitary	Poulin & Cardinal, 1982



**Table S4.3:** Number of cells measured via synchrotron-based Fourier transform infrared microspectroscopy (s-FTIR) per site, per taxa

Site	Taxa	Cells Measured
VM-1	<i>Entomoneis</i> spp.	10
	<i>Haslea</i> spp.	10
	<i>Navicula</i> spp.	18
	<i>Nitzschia frigida</i>	17
	<i>Pleurosigma</i> spp.	7
VM-2	<i>Entomoneis</i> spp.	11
	<i>Haslea</i> spp.	12
	<i>Navicula</i> spp.	20
	<i>Nitzschia frigida</i>	17
	<i>Pleurosigma</i> spp.	9
VM-3	<i>Entomoneis</i> spp.	11
	<i>Haslea</i> spp.	12
	<i>Navicula</i> spp.	15
	<i>Nitzschia frigida</i>	20
	<i>Pleurosigma</i> spp.	12
VM-4	<i>Entomoneis</i> spp.	14
	<i>Haslea</i> spp.	9
	<i>Navicula</i> spp.	20
	<i>Nitzschia frigida</i>	20
	<i>Pleurosigma</i> spp.	3
VM-5	<i>Entomoneis</i> spp.	9
	<i>Haslea</i> spp.	13
	<i>Navicula</i> spp.	17
	<i>Nitzschia frigida</i>	17
	<i>Pleurosigma</i> spp.	9
TF-2	<i>Entomoneis</i> spp.	14
	<i>Haslea</i> spp.	1
	<i>Navicula</i> spp.	17
	<i>Nitzschia frigida</i>	19
	<i>Pleurosigma</i> spp.	2

**Table S4.4:** Output of Spearman's rank correlation coefficient ( $\rho$  (rho)) and associated  $p$ -values) between environmental variables (% incoming photosynthetically active radiation (PAR), nitrite + nitrate ( $\text{NO}_3^- + \text{NO}_2^-$ ) ( $\text{NO}_x$ ) concentration in the water at ice-water interface, silicic acid ( $\text{Si}(\text{OH})_4$ ) concentration in the water at ice-water interface, ice temperature ( $^\circ\text{C}$ ), under ice water temperature ( $^\circ\text{C}$ ) and bulk ice salinity ( $^\circ\text{C}$ )) and biomolecular content (based on mean of each of the five taxa, per each set of pooled cores (total  $n = 86$ ). Statistically significant  $p$ -values ( $< 0.05$ ) and  $R^2$  exceeding 0.5 or -0.5 are marked in bold. Mean ( $\bar{x}$ )  $\pm$  standard deviation ( $\sigma$ ) for each environmental variable is provided in brackets.

	% Incoming PAR		$\text{NO}_3$ ( $\mu\text{M}$ )		$\text{Si}(\text{OH})_4$ ( $\mu\text{M}$ )		Ice Temperature ( $^\circ\text{C}$ )		Under-Ice Water Temperature ( $^\circ\text{C}$ )		Bulk Ice Salinity	
	$\rho$	$P$	$\rho$	$P$	$\rho$	$P$	$\rho$	$P$	$\rho$	$P$	$\rho$	$P$
	$(\bar{x} = 9.3, \sigma = \pm 9.0)$		$(\bar{x} = 2.1, \sigma = \pm 0.1)$		$(\bar{x} = 2.7, \sigma = \pm 0.1)$		$(\bar{x} = -2.3, \sigma = \pm 0.2)$		$(\bar{x} = -1.8, \sigma = \pm 0.1)$		$(\bar{x} = 7.7, \sigma = \pm 2.8)$	
Carbohydrate	-0.42	<b>&lt;0.01</b>	-0.36	<b>&lt;0.01</b>	0.31	<b>&lt;0.05</b>	0.23	<b>0.03</b>	0.03	0.78	0.11	0.30
Carboxylated Molecules	-0.46	<b>&lt;0.01</b>	-0.34	<b>&lt;0.01</b>	0.38	<b>&lt;0.05</b>	0.28	<b>0.01</b>	0.01	0.92	0.17	0.11
Lipid (ester carbonyl)	<b>0.81</b>	<b>&lt;0.01</b>	0.38	<b>&lt;0.01</b>	-0.21	0.05	-0.45	<b>&lt;0.01</b>	0.26	<b>&lt;0.01</b>	-0.37	<b>&lt;0.01</b>
Phosphorylated Molecules	-0.34	<b>&lt;&lt;0.01</b>	-0.15	0.17	0.01	0.94	0.17	0.11	-0.12	0.34	0.13	0.23
Protein (amide II)	-0.11	0.30	-0.13	0.23	0.17	0.12	0.05	0.64	-0.01	0.96	0.08	0.49
Lipid (CH-stretch II)	<b>0.72</b>	<b>&lt;0.01</b>	0.34	<b>&lt;0.01</b>	-0.23	<b>0.04</b>	-0.44	<b>&lt;0.01</b>	0.15	0.22	-0.27	<b>0.01</b>
Saturated Fatty Acids	<b>0.82</b>	<b>&lt;0.01</b>	0.34	<b>&lt;0.01</b>	-0.19	0.08	-0.48	<b>&lt;0.01</b>	0.22	0.07	-0.33	<b>&lt;0.01</b>
Saturated Lipid	<b>0.83</b>	<b>&lt;0.01</b>	0.37	<b>&lt;0.01</b>	-0.21	0.05	-0.47	<b>&lt;0.01</b>	0.24	0.05	-0.35	<b>&lt;0.01</b>
Silica	<b>-0.52</b>	<b>&lt;0.01</b>	-0.19	0.08	0.05	0.63	0.29	<b>0.01</b>	-0.18	0.13	0.23	<b>0.04</b>
Unsaturated fatty acids	<b>0.74</b>	<b>&lt;0.01</b>	0.28	<b>0.01</b>	-0.19	0.08	-0.49	<b>&lt;0.01</b>	0.12	0.32	-0.22	<b>0.04</b>

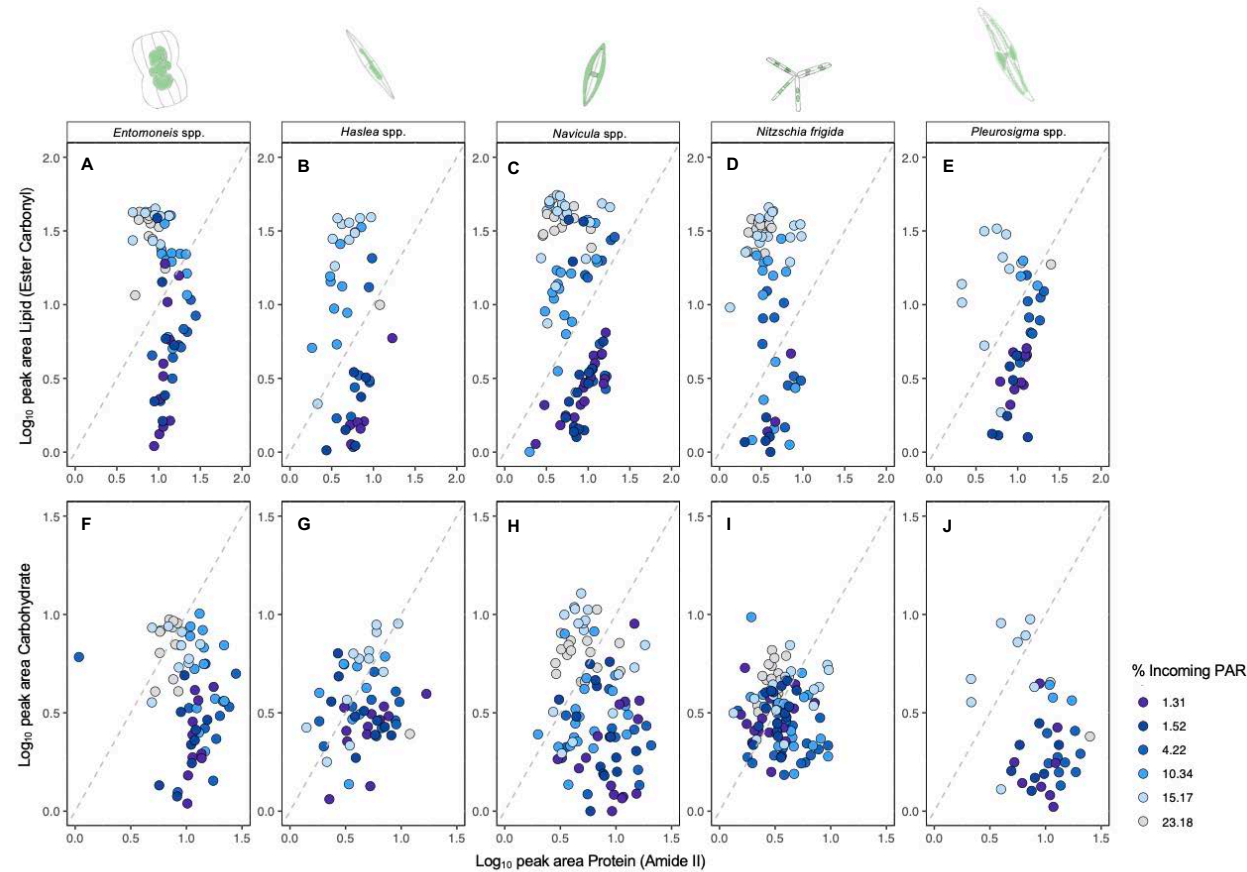
**Table S4.5:** Statistical output of the species-specific regression models for each biomolecular compound vs. under-ice light. Multiple  $R^2$ , adjusted  $R^2$ ,  $F$  statistic, associated degrees of freedom (DF) and  $p$ -value, Spearman's rank correlation coefficient ( $\rho$ ) and associated  $p$ -value. Statistically significant  $p$ -values ( $< 0.05$ ) are marked in bold.

		Multiple $R^2$	Adjusted $R^2$	F Statistic	DF	$P$ Value	Spearman's Correlation	$P$ Value (Spearman's)
<i>Entomoneis</i> spp.	Carbohydrate	0.45	0.44	52.91	1,66	<b>5.27 x 10<sup>-10</sup></b>	0.70	<b>2.18 x 10<sup>-11</sup></b>
	Carboxylated Molecules	0.21	0.19	17.11	1,66	<b>1.02 x 10<sup>-4</sup></b>	-0.44	<b>1.49 x 10<sup>-4</sup></b>
	Lipid (CH-stretch II)	0.44	0.43	52.37	1,66	<b>6.14 x 10<sup>-10</sup></b>	0.71	<b>1.09 x 10<sup>-11</sup></b>
	Lipid (ester carbonyl)	0.52	0.51	71.53	1,66	<b>4.02 x 10<sup>-12</sup></b>	0.78	<b>6.75 x 10<sup>-15</sup></b>
	Phosphorylated Molecules	0.28	0.27	26.23	1,66	<b>2.83 x 10<sup>-6</sup></b>	-0.62	<b>1.24 x 10<sup>-8</sup></b>
	Protein (amide II)	0.12	0.11	9.35	1,66	<b>0.01</b>	-0.41	<b>4.46 x 10<sup>-4</sup></b>
	Saturated Fatty Acids	0.51	0.50	68.08	1,66	<b>9.44 x 10<sup>-12</sup></b>	0.74	<b>6.73 x 10<sup>-13</sup></b>
	Saturated Lipid	0.54	0.53	77.41	1,66	<b>9.94 x 10<sup>-13</sup></b>	0.75	<b>1.52 x 10<sup>-13</sup></b>
	Unsaturated Fatty Acids	0.61	0.60	101.3	1,66	<b>5.86 x 10<sup>-15</sup></b>	0.80	<b>2.20 x 10<sup>-16</sup></b>
<i>Haslea</i> spp.	Carbohydrate	0.08	0.06	4.70	1,55	<b>0.03</b>	0.34	<b>0.01</b>
	Carboxylated Molecules	0.25	0.24	18.48	1,55	<b>7.08 x 10<sup>-5</sup></b>	-0.44	<b>5.97 x 10<sup>-4</sup></b>
	Lipid (CH-stretch II)	0.27	0.25	20.09	1,55	<b>3.80 x 10<sup>-5</sup></b>	0.52	<b>3.12 x 10<sup>-5</sup></b>
	Lipid (ester carbonyl)	0.46	0.45	46.49	1,55	<b>7.48 x 10<sup>-9</sup></b>	0.64	<b>8.18 x 10<sup>-8</sup></b>
	Phosphorylated Molecules	0.12	0.10	7.53	1,55	<b>8.18 x 10<sup>-3</sup></b>	-0.37	<b>0.005</b>
	Protein (amide II)	0.00	0.00	0.54	1,55	0.47	-0.09	0.52
	Saturated Fatty Acids	0.39	0.38	35.67	1,55	<b>1.78 x 10<sup>-7</sup></b>	0.60	<b>8.92 x 10<sup>-7</sup></b>
	Saturated Lipid	0.44	0.43	43.51	1,55	<b>1.73 x 10<sup>-8</sup></b>	0.64	<b>1.03 x 10<sup>-7</sup></b>
	Unsaturated Fatty Acids	0.18	0.16	12.01	1,55	<b>1.03 x 10<sup>-3</sup></b>	0.42	<b>8.48 x 10<sup>-4</sup></b>
<i>Navicula</i> spp.	Carbohydrate	0.42	0.42	77.19	1,105	<b>3.26 x 10<sup>-14</sup></b>	0.65	<b>5.56 x 10<sup>-14</sup></b>
	Carboxylated Molecules	0.28	0.28	41.74	1,105	<b>3.32 x 10<sup>-9</sup></b>	-0.49	<b>1.17 x 10<sup>-7</sup></b>

	Lipid (CH-stretch II)	0.46	0.46	90.31	1,105	<b>7.80 x 10<sup>-16</sup></b>	0.65	<b>2.08 x 10<sup>-14</sup></b>
	Lipid (ester carbonyl)	0.53	0.53	119.6	1,105	<b>2.2 x 10<sup>-16</sup></b>	0.74	<b>2.20 x 10<sup>-16</sup></b>
	Phosphorylated Molecules	0.21	0.20	27.82	1,105	<b>7.20 x 10<sup>-7</sup></b>	-0.55	<b>9.37 x 10<sup>-10</sup></b>
	Protein (amide II)	0.14	0.13	16.67	1,105	<b>8.69 x 10<sup>-5</sup></b>	-0.35	<b>2.68 x 10<sup>-4</sup></b>
	Saturated Fatty Acids	0.52	0.51	109.6	1,105	<b>2.20 x 10<sup>-16</sup></b>	0.72	<b>2.20 x 10<sup>-16</sup></b>
	Saturated Lipid	0.54	0.54	124.2	1,105	<b>2.20 x 10<sup>-16</sup></b>	0.75	<b>2.20 x 10<sup>-16</sup></b>
	Unsaturated Fatty Acids	0.59	0.58	149.6	1,105	<b>2.20 x 10<sup>-16</sup></b>	0.74	<b>2.20 x 10<sup>-16</sup></b>
	Carbohydrate	0.26	0.25	37.79	1,108	<b>1.35 x 10<sup>-8</sup></b>	0.47	<b>1.66 x 10<sup>-7</sup></b>
	Carboxylated Molecules	0.26	0.26	38.88	1,108	<b>8.95 x 10<sup>-9</sup></b>	-0.43	<b>2.71 x 10<sup>-6</sup></b>
	Lipid (CH-stretch II)	0.63	0.62	182.4	1,108	<b>2.20 x 10<sup>-16</sup></b>	0.76	<b>2.20 x 10<sup>-16</sup></b>
	Lipid (ester carbonyl)	0.68	0.68	230.6	1,108	<b>2.20 x 10<sup>-16</sup></b>	0.82	<b>2.20 x 10<sup>-16</sup></b>
<i>Nitzschia frigida</i>	Phosphorylated Molecules	0.02	0.00	2.07	1,108	0.15	0.07	0.44
	Protein (amide II)	0.00	0.00	0.27	1,108	0.61	0.08	0.41
	Saturated Fatty Acids	0.72	0.72	278.0	1,108	<b>2.20 x 10<sup>-16</sup></b>	0.80	<b>2.20 x 10<sup>-16</sup></b>
	Saturated Lipid	0.72	0.72	280.6	1,108	<b>2.20 x 10<sup>-16</sup></b>	0.82	<b>2.20 x 10<sup>-16</sup></b>
	Unsaturated Fatty Acids	0.40	0.38	70.49	1,108	<b>1.98 x 10<sup>-13</sup></b>	0.65	<b>2.47 x 10<sup>-14</sup></b>
	Carbohydrate	0.28	0.26	15.52	1,40	<b>3.19 x 10<sup>-4</sup></b>	0.47	<b>0.002</b>
	Carboxylated Molecules	0.18	0.16	9.04	1,40	<b>0.005</b>	-0.30	0.06
	Lipid (CH-stretch II)	0.36	0.33	21.62	1,40	<b>3.59 x 10<sup>-5</sup></b>	0.60	<b>2.79 x 10<sup>-5</sup></b>
	Lipid (ester carbonyl)	0.48	0.46	36.21	1,40	<b>2.47 x 10<sup>-7</sup></b>	0.75	<b>1.04 x 10<sup>-8</sup></b>
<i>Pleurosigma spp.</i>	Phosphorylated Molecules	0.17	0.15	8.17	1,40	<b>0.007</b>	-0.47	<b>0.001</b>
	Protein (amide II)	0.06	0.04	2.6	1,40	0.11	-0.07	0.63
	Saturated Fatty Acids	0.48	0.46	36.58	1,40	<b>4.04 x 10<sup>-7</sup></b>	0.69	<b>2.62 x 10<sup>-7</sup></b>
	Saturated Lipid	0.54	0.53	46.36	1,40	<b>3.46 x 10<sup>-8</sup></b>	0.73	<b>2.63 x 10<sup>-8</sup></b>
	Unsaturated Fatty Acids	0.11	0.09	5.06	1,40	<b>0.03</b>	0.39	<b>0.01</b>

**Table S4.6:** Statistical output of the biomolecular regression models at low light transmissivity and high light transmissivity conditions. Multiple  $R^2$ , adjusted  $R^2$ ,  $F$  statistic, associated degrees of freedom (DF) and  $p$ -value. Statistically significant  $p$ -values ( $< 0.05$ ) are marked in bold. The low light transmissivity sites include VM-1, VM-2 and VM-3 and the high light transmissivity sites include VM-4, VM-5 and TF-2.

		Multiple $R^2$	Adjusted $R^2$	F Statistic	DF	$P$ Value
<b>Lipid vs. Protein</b> <i>Low Light</i>	<i>Entomoneis</i> spp.	0.44	0.42	22.48	1,29	<b>5.21 x 10<sup>-5</sup></b>
	<i>Haslea</i> spp.	0.66	0.65	62.34	1,32	<b>5.21 x 10<sup>-9</sup></b>
	<i>Navicula</i> spp.	0.34	0.33	26.5	1,51	<b>4.27 x 10<sup>-6</sup></b>
	<i>Nitzschia frigida</i>	0.35	0.34	28.55	1,52	<b>2.05 x 10<sup>-6</sup></b>
	<i>Pleurosigma</i> spp.	0.62	0.61	41.76	1,26	<b>7.56 x 10<sup>-7</sup></b>
<b>Lipid vs. Protein</b> <i>High Light</i>	<i>Entomoneis</i> spp.	0.20	0.18	9.00	1,35	<b>0.005</b>
	<i>Haslea</i> spp.	0.62	0.60	34.59	1,21	<b>7.73 x 10<sup>-6</sup></b>
	<i>Navicula</i> spp.	0.01	0.00	0.61	1,52	0.44
	<i>Nitzschia frigida</i>	0.00	0.00	0.30	1,54	0.58
	<i>Pleurosigma</i> spp.	0.03	0.00	0.38	1,12	0.55
<b>Lipid vs. Carbohydrate</b> <i>Low Light</i>	<i>Entomoneis</i> spp.	0.15	0.12	5.23	1,29	<b>0.03</b>
	<i>Haslea</i> spp.	0.00	0.00	0.01	1,32	0.91
	<i>Navicula</i> spp.	0.08	0.06	4.44	1,51	<b>0.04</b>
	<i>Nitzschia frigida</i>	0.03	0.01	1.67	1,52	0.21
	<i>Pleurosigma</i> spp.	0.00	0.00	0.10	1,26	0.75
<b>Lipid vs. Carbohydrate</b> <i>High Light</i>	<i>Entomoneis</i> spp.	0.62	0.61	57.84	1,35	<b>6.34 x 10<sup>-9</sup></b>
	<i>Haslea</i> spp.	0.57	0.55	28.29	1,21	<b>2.83 x 10<sup>-5</sup></b>
	<i>Navicula</i> spp.	0.35	0.33	27.81	1,52	<b>2.63 x 10<sup>-6</sup></b>
	<i>Nitzschia frigida</i>	0.17	0.16	11.19	1,54	<b>0.001</b>
	<i>Pleurosigma</i> spp.	0.87	0.86	83.18	1,12	<b>9.56 x 10<sup>-7</sup></b>
<b>Carbohydrate vs. Protein</b> <i>Low Light</i>	<i>Entomoneis</i> spp.	0.00	0.00	0.07	1,29	0.79
	<i>Haslea</i> spp.	0.04	0.01	1.34	1,32	0.26
	<i>Navicula</i> spp.	0.00	0.00	0.24	1,51	0.63
	<i>Nitzschia frigida</i>	0.06	0.04	3.10	1,52	0.08
	<i>Pleurosigma</i> spp.	0.00	0.00	0.01	1,26	<b>0.90</b>
<b>Carbohydrate vs. Protein</b> <i>High Light</i>	<i>Entomoneis</i> spp.	0.11	0.09	4.36	1,35	<b>0.04</b>
	<i>Haslea</i> spp.	0.40	0.36	13.58	1,21	<b>0.001</b>
	<i>Navicula</i> spp.	0.00	0.00	0.00	1,52	0.94
	<i>Nitzschia frigida</i>	0.03	0.00	1.40	1,54	0.24
	<i>Pleurosigma</i> spp.	0.00	0.00	0.05	1,12	0.82



**Supplementary Figure S4.1:** Lipid (ester carbonyl) to protein (amide II) ratios (top) and carbohydrate to protein (amide II) ratios (bottom) for (A, F) *Entomoneis* spp., (B, G) *Haslea* spp., (C, H) *Navicula* spp., (D, I) *Nitzschia frigida* and (E, J) *Pleurosigma* spp. All data are  $\log(10)$  transformed and each data point represents a cell. % incoming PAR levels are represented by colour.

## Chapter 5

### Seasonal environmental transitions and metabolic plasticity in a sea-ice alga from an individual cell perspective

*Published in Scientific Reports as:*

**Duncan, R. J.**, Søreide, J. E., Nielsen, D., Varpe, Ø., Wiktor, J., Tobin, M. J., Pitusi, V., & Petrou, K. (2024). Seasonal environmental transitions and metabolic plasticity in a sea-ice alga from an individual cell perspective. *Scientific Reports*, 14, 14984.

*Author contributions:*

R.J.D., J.E.S., O.V. and K.P. conceptualised the study and determined the methodology. R.J.D. performed the investigation, data curation, formal analysis, data visualisation and wrote the original draft. D.N. assisted with the methodology, investigation and designed the code for spectroscopy data curation. J.E.S., V.P. and K.P. contributed to the investigation, and resources were supplied by J.E.S and K.P.. Validation of spectroscopic data was given by M.T. and validation of the taxonomic analysis was provided by J.W. Supervision of R.J.D. was performed by J.E.S, O.V., M.T. and K.P. Funding was acquired by R.J.D., J.E.S and K.P. All authors contributed to reviewing and editing the original draft written by R.J.D.

Production Note: Signature removed prior to publication.	Production Note: Signature removed prior to publication.	Production Note: Signature removed prior to publication.	Production Note: Signature removed prior to publication.	Production Note: Signature removed prior to publication.	Production Note: Signature removed prior to publication.	Production Note: Signature removed prior to publication.	Production Note: Signature removed prior to publication.
R. Duncan	J.E. Søreide	D. Nielsen	Ø. Varpe	J. Wiktor	M.J. Tobin	V. Pitusi	K. Petrou

Chapter 5 explores the seasonal progression of biomolecular content in a dominant sea-ice diatom (*Nitzschia frigida*) taken from natural land-fast sea-ice communities. By sampling at an inner and outer fjord site, over 6 weeks, this chapter adds a crucial layer of temporal resolution to the taxon-specific nutritional content data. In this way, the study elucidates seasonal shifts, giving clues to how the taxa may perform with future climate change scenarios, and provides insights into how biomolecular allocation influences survival through polar darkness.

**Abstract**

Sea-ice microalgae are a key source of energy and nutrient supply to polar marine food webs, particularly during spring, prior to open-water phytoplankton blooms. The nutritional quality of microalgae as a food source depends on their biomolecular (lipid:protein:carbohydrate) composition. In this study, we used synchrotron-based Fourier transform infra-red microspectroscopy (s-FTIR) to measure the biomolecular content of a dominant sea-ice taxa, *Nitzschia frigida*, from natural land-fast ice communities throughout the Arctic spring season. Repeated sampling over six weeks from an inner (relatively stable) and an outer (relatively dynamic) fjord site revealed high intra-specific variability in biomolecular content, elucidating the plasticity of *N. frigida* to adjust to the dynamic sea ice and water conditions. Environmental triggers indicating the end of productivity in the ice and onset of ice melt, including nitrogen limitation and increased water temperature, drove an increase in lipid and fatty acids stores, and a decline in protein and carbohydrate content. In the context of climate change and the predicted Atlantification of the Arctic, dynamic mixing and abrupt warmer water advection could truncate these important end-of-season environmental shifts, causing the algae to be released from the ice prior to adequate lipid storage, influencing carbon transfer through the polar marine system.



**Introduction:**

The last half century has seen ocean temperatures rise and circulation patterns shift, resulting in a rapid decline in Arctic sea-ice extent, thickness and area (Kwok, 2018; Stroeve & Notz, 2018; Yu et al., 2014). The increasing temperatures and advection of warmer, more saline Atlantic waters (AW) into the Arctic means that sea ice has become more prone to summer melting (Årthun et al., 2019), which has resulted in a decline in multi-year sea ice (MYI; sea ice which has survived multiple summers) (Perovich et al., 2018). Since 1999, the extent of MYI has diminished by ~50% (Comiso, 2012; Kwok, 2018), and now covers less than a third of the Arctic Ocean (AO) (Maslanik et al., 2011), meaning that first year ice (FYI; sea ice which completely melts each summer), which is thinner and more sensitive to changes in the physical environment, now dominates the Arctic (Kacimi & Kwok, 2022; Kwok, 2018; Stroeve & Notz, 2018). Warmer surface water temperatures impede Arctic sea-ice formation delaying freezing while also causing earlier melting (Stroeve & Notz, 2018). This contracted period of FYI, with shortened timeframes between ice formation (late winter), substantial daylight returning to the Arctic (early spring) and melting of the ice from below (late spring/summer) (Leu et al., 2015), results in a reduced window of productivity for sea-ice associated ecosystems. These warming-associated changes in Arctic sea-ice conditions have implications for the seasonal productivity and ecology of the polar marine ecosystem (Post et al., 2013; Varpe et al., 2015).

Sea ice forms an important habitat for microalgae, which represent the primary source of energy for the marine ecosystem in the early spring, in the absence of other sources of primary production and prior to the late-spring/summer open-water phytoplankton blooms (Leu et al., 2015; Mundy et al., 2014). Through prolonging polar marine biological production (Cota et al., 1991; Ji et al., 2013) and this provision of food during the early phases of seasonal zooplankton reproduction, sea-ice microalgae are an important factor in the quality and quantity of secondary production (Durbin & Casas, 2014; Kohlbach et al., 2016; Søreide et al., 2010). The nutritional quality of microalgae as a food source is dependent on which species are present and their individual elemental stoichiometry, which reflects their biomolecular (lipid:protein:carbohydrate) composition (Finkel et al., 2016). Cell stoichiometry, and thus biomolecular composition, is sensitive to changes in environment, such as light (Duncan et al., 2024a),

temperature (Teoh et al., 2004; Torstensson et al., 2019) and nutrient availability (Mock & Kroon, 2002a; Pogorzelec et al., 2022), with shifts in each parameter affecting biomolecular stores in different ways. In sea-ice microalgae, increasing irradiance transmitted through the ice can increase lipid production (Duncan et al., 2024a), nutrient limitation has been shown to decrease protein and increase fatty acid (FA) content (Mock & Gradinger, 2000; Mock & Kroon, 2002a), whilst increasing ocean temperatures have been observed to increase protein content and decrease FA content (An et al., 2013; Teoh et al., 2004; Torstensson et al., 2019). As such, shifts in the biomolecular composition of sea-ice microalgae as a result of changing sea ice-surface ocean conditions, invariably influences Arctic food webs, local biogeochemistry and plays a vital role in determining the productivity of polar marine ecosystems (Duncan & Petrou, 2022) and references therein.

In natural systems, microalgal communities form complex functional networks, making it challenging to obtain knowledge on species' phenomes and metabolomes in a dynamic and multivariate environment. Species and communities adapt to changing environmental conditions either through phenotypic plasticity or genetically (Merilä & Hendry, 2014). Seasonally, it is phenotypic adjustments to changes in environment that dominate, but the capacity for such plasticity varies across and within species. Therefore, to gain a systematic understanding of metabolic plasticity and uncover the phenome (set of traits modifiable for enhanced growth and survival) in natural biological systems, we need single-celled multiparameter measurements that can probe the changes occurring in individual cells in response to environmental shifts.

Here we use synchrotron-based Fourier transform infra-red microspectroscopy to measure the biomolecular content of *Nitzschia frigida* from natural sea-ice habitat over the Arctic spring. *N. frigida* is one of the most prolific and ubiquitous Arctic sea-ice diatoms, typically dominating first year sea-ice assemblages (Duncan et al., 2024b; Gosselin et al., 1997; Leu et al., 2015; Syvertsen, 1991). It is a colony-forming pennate diatom which can often be observed as single cells early in the spring, increasingly creating arborescent colonies as spring progresses. In contrast to taxa such as *Chaetoceros* spp., *Thalassiosira* spp. and dinoflagellates that create resting spores to survive the long winter darkness (Hargraves, 1983; Palmisano & Sullivan, 1983), *N. frigida* are thought to survive the winter in the epibenthic region, primarily through storing energy and

reducing metabolic rate (Palmisano & Sullivan, 1983; Qing et al., 2003). This energy storage strategy means that in addition to contributing substantially to spring primary production in the ice, following their release during ice melt, they strongly contribute to carbon flux as they are either consumed during descent (Tremblay et al., 1989) or exported to the benthos (Aumack & Juhl, 2015; McMahon et al., 2006). In this study, we investigated changes in the biomolecular content of *N. frigida* throughout the spring sea-ice season until ice-melt (March to May), tracing the seasonal progression of nutritional content to document potential shifts in energy allocation that may link to survival during polar darkness.

## **Materials & Methods**

### **Study Area**

This study was conducted within Van Mijenfjorden in Svalbard, Norway (Fig. 5.1A) throughout April – May 2022. Two sites, one at the inner fjord (inner site; 77.80194 N, 15.76916 E) and one at the outer fjord (outer site; 77.84918 N, 16.7078 E), were sampled regularly (6-7.4.22; Week 1 (W1), 20-21.4.22; Week 3 (W3), 29-30.4.22; Week 4 (W4) and 12-13.5.22; Week 6 (W6)) to investigate seasonal changes in the biomolecular content of *N. frigida*, under different environmental conditions. Van Mijenfjorden is a partially enclosed fjord, with an inner basin approximately 70 m deep and an outer basin up to 120 m deep, located on the west coast of Spitsbergen, Svalbard, Norway (Høyland, 2009). The fjord experiences advection of warm, saline Atlantic water transported to the area by the West Spitsbergen Current (WSC), however this is substantially abated by the presence of the island Akseløya at the fjord mouth which allows for sea-ice formation in winter. For further information on the conditions in Van Mijenfjorden see (Duncan et al., 2024a; 2024b). Sea-ice had been formed in the fjord since January, with closed drift-ice observed at the inner site from the 17.1.22 and from 24.1.22 at the outer site (Norwegian Ice Service, 2022).

### **Sample Collection**

For each sampling event, six ice cores were extracted approximately 0.5 m apart, with a Kovacs core barrel (9 cm diameter; Kovacs Enterprise, Oregon, USA). The bottom 3 cm (at the ice-water interface) was retained, due to the microbial community being concentrated in this section of the ice (Lee et al., 2008a; Smith et al., 1988). The six ice cores were then pooled into triplicates, as cores 1-2, 3-4 and 5-6, and 100 mL of filtered

sea water (FSW) (Glass Fibre Filter (GF/F), nominal pore size 0.7  $\mu\text{m}$ , Whatman, England) per centimetre of core was added to minimise osmotic stress (Campbell et al., 2019; Garrison & Buck, 1986). The samples were then allowed to melt in darkness for 24 h at 4 °C. Cells were concentrated before biomolecular analysis; 100 mL from each of the three pooled samples was centrifuged at 1000 rpm (Universal 320, Hettich, Germany) for 4 min and the supernatant removed. The aliquot was then transferred to 2 mL Eppendorf tubes and centrifuged at 1000 rpm (Mikro 185, Hettich) for a further 2 min. The supernatant was again removed and the sample fixed by addition of formaldehyde (5% v/v) for later analysis. Additional cores were extracted for ice temperature (measured *in situ*), for bulk ice salinity (sectioned into 0-3 cm for bottom-ice and then 10 cm sections) and bulk ice nutrients (without the addition of FSW).

### **Biological variables**

Chlorophyll *a* concentration:

Once the ice samples were completely melted, triplicate subsamples (150–400 mL) and a sample of under-ice water (500-1250 mL) were filtered (GF/F, 0.7  $\mu\text{m}$ ) until visible colouration was observed on the filter. The filters were stored frozen (–80 °C) until extraction and the extractions were performed within three months of collection. The analyses were performed according to (Holm-Hansen & Riemann, 1978). Briefly, filters were extracted in 10 mL methanol and kept refrigerated at 4 °C for 24 h prior to extraction, after which Chl *a* content was measured, accounting for FSW dilution, with a calibrated Trilogy fluorometer (Turner, California, USA), before and after acidifying the extracts with 5% HCl (Parsons et al., 1984).

Community Composition:

From each sampling event, subsamples (100 mL) of the melted triplicate cores were collected into a brown bottle and preserved with glutaraldehyde (2% final conc.). Species composition was determined through the use of light microscopy; between 3–6 mL (depending on cell abundance) of the well-mixed subsamples were poured into an Utermöhl chamber with sedimentation cylinder (KC Denmark, Silkeborg, Denmark) (Utermöhl, 1958) and the cells were allowed to settle for up to 24 h (Edler & Elbrächter, 2010). Cells were counted at 400x magnification and identified to lowest possible taxonomic level. A whole chamber counting approach was employed to ensure rare taxa

were captured. These analyses were conducted under Nikon TS100 microscope within six months of sample collection.

#### Fatty Acid Composition:

Samples from six pooled cores from each site on their final sampling date (inner site: 12.5.22 and outer site: 13.5.22) were filtered onto pre-combusted GF/F filters, until coloration was visible (300 mL from the outer site and 470 mL from the inner site). The filters were placed in glass vials with Teflon-lined caps and 8 mL of Methanol:dichloromethane was added and the vials were stored at  $-80\text{ }^{\circ}\text{C}$  until analysis. Total lipid was extracted according to Folch et al. 1957, at Akvaplan Niva AS, Norway.

### **Environmental Variables**

#### Physical Variables:

Snow depth was measured three times in the close vicinity of the ice core extraction using a standard ruler, prior to core extraction. Ice thickness was measured at every core hole, after the core extraction, using a Kovacs ice thickness gauge. Additional cores were extracted for ice temperature (measured *in situ*) and for bulk ice salinity (sectioned into 0-3 cm for bottom-ice and then 10 cm sections). Following complete melting of separate 10 cm sections, salinity of each section was measured (Thermo Scientific Orion Versa Star Pro). Based on these measurements, brine salinity and volume fractions were calculated according to (Cox & Weeks, 1983). A subsample of each pooled, melted ice cores was filtered onto pre-combusted GF/F filters until coloration was visible, for particulate organic carbon and particulate organic nitrogen (POC:PON) analysis. With each sampling event, a 0-3 cm section of an ice core was melted without the addition of FSW and then transferred to an acid washed bottle for bulk ice nutrient analysis and frozen until analysis. Also at each sampling event, approximately 100 mL of the water from directly below the ice-bottom surface was collected using a 5 L Niskin bottle (Hydro-Bios, Germany) and transferred to acid washed bottles for nutrient analysis. The nitrate plus nitrite ( $\text{NO}_3^- + \text{NO}_2^-$ ) ( $\text{NO}_x$ ), phosphate ( $\text{PO}_4^{3-}$ ) and silicic acid ( $\text{Si}(\text{OH})_4$ ) concentrations ( $\mu\text{M}$ ) for ice and surface water were measured simultaneously on a QuAAtro 39 nutrient analyzer (SEAL Analytical, United Kingdom), with separate analysis channels for the three nutrients. The detection limits were  $0.01\ \mu\text{M}$  for  $\text{NO}_x$ ,  $0.02\ \mu\text{M}$  for phosphate and  $0.02\ \mu\text{M}$  for silicic acid. POC:PON analysis and stable isotope analysis on the bottom-ice and surface water was performed at the UC Davis Stable

Isotope Facility in an EA-IRMS system, according to (Barrie et al., 1989). The detection limits were 100  $\mu\text{g C}$  for  $\delta^{13}\text{C}$  and 20  $\mu\text{g N}$  for  $\delta^{15}\text{N}$ .

#### Light Measurements:

At each sampling site, incoming photosynthetically active radiation (PAR) was measured using a LI-192 spherical underwater quantum sensor placed on a weighted frame moored  $\sim 0.5$  m below the ice (from 26.3.22 until 13.5.22) recording PAR (400-700 nm) every minute (RBR*solo*<sup>3</sup> PAR; rbr-global.com). Further, a temperature sensor (RBR*solo*<sup>3</sup> T, accuracy of  $\pm 0.002$  °C) with every 0.5 min logger intervals were placed at the same depth. Albedo was calculated on each sampling date as snow reflected PAR as proportion (%) of reflected PAR and incoming PAR to the snow surface, using a LI-190 quantum air sensor placed on the snow/sea-ice surface to measure incoming PAR, and held level 1m above the snow surface, facing the snow, to measure snow reflected PAR.

#### Species-specific biomolecular content by synchrotron-FTIR:

The biomolecular composition of *N. frigida* was determined using synchrotron based FTIR microspectroscopy on formalin-fixed (5% v/v final concentration) cells. To ensure true replication, all cells measured were single cells and not dividing or associated with another cell. Samples were loaded directly into a micro-compression cell between two 13 mm diameter 0.5 mm thick BaF<sub>2</sub> windows and spectral data of individual cells ( $\bar{x}$  = 26 cells per site, Table S5.1) obtained on the Infrared (IR) Microspectroscopy Beamline at the Australian Synchrotron, Melbourne. Each biomolecule absorbs a specific range of IR wavelengths, and a set of well-defined absorbance bands between 3050-2800  $\text{cm}^{-1}$ , and 1770-1100  $\text{cm}^{-1}$  have been determined (Table 15). Spectra were acquired over the measurement range 4000–800  $\text{cm}^{-1}$  with a Vertex 80v FTIR spectrometer (Bruker Optic, Ettlingen, Germany) in conjunction with an IR microscope (Hyperion 3000, Bruker) fitted with a narrow-band mercury cadmium telluride detector cooled with liquid nitrogen. To limit the light scattering effects, the measurements were performed on hydrated cells (Bamberg et al., 2012). Co-added interferograms (sample  $n = 32$ , background  $n = 64$ ) were collected at a wavenumber resolution of 4  $\text{cm}^{-1}$ . All measurements were made in transmission mode, using a measuring aperture diameter of 6.9  $\mu\text{m}$  (area = 37.4  $\mu\text{m}^2$ ). Cell compression was consistent ensuring the path length was uniform to account for any variation in cell size. To account for heterogeneity in the cell structure and distribution of biomolecules, all cells were measured with multiple points across the cell surface. Opus 8.0 software (Bruker) was used for both spectral acquisition

and instrument control. Analyses were performed in July 2022 (within 6 months of samples being collected and fixed). All samples were kept refrigerated between fixation and analysis.

### **Data analyses**

Biomolecular content for each measured cell was determined by integrating the area under each assigned peak (Table 5.1), applying the Beer-Lambert Law assuming a direct relationship between absorbance and analyte concentration (Wagner et al., 2010). Data were smoothed (4 pts either side) and second derivative (3rd order polynomial) transformed using the Savitzky-Golay algorithm from the `prospectr` package (Stevens & Ramirez-Lopez, 2014). Data were then normalised using Standard Normal Variate (SNV).

The community composition of all samples per site was contrasted by analysis of similarities (ANOSIM, Clarke & Warwick 1994), to determine if community composition was different between the inner and outer sites. Relationships between biomolecular content and sampling date and site were estimated using principal component analyses (PCA) and key biomolecular content per date was visualised using violin plots. To investigate which environmental variables account for a significant difference in the biomolecular content, redundancy analysis (RDA) was performed constrained to environmental variables ( $n = 6$ ) with Monte Carlo permutations (999), following model optimisation, and only significant vectors displayed. Further redundancy analyses were performed, constrained to the stable isotopes ( $n = 4$ ), to determine the effect on the differences in biomolecular composition. Regressions were tested for overall model significance of RDA analyses using the  $F$  statistic ( $P < 0.05$ ) and strength of fit using  $R^2$ . The residuals of all regressions were verified for homoscedasticity. The correlations between stable isotope of carbon ( $\delta^{13}\text{C}_{\text{VPDB}}$  (‰)) and lipid (ester carbonyl) and protein (amide II) content were visualised using boxplots. The Shapiro–Wilks (Shapiro & Wilk, 1965) test for normality showed that the biomolecular content required  $\log_{10}$  transformation before analysis. All analyses were performed using RStudio v. 2023.09.463 (RStudio Team, 2022) and the add-on packages ‘`vegan`’ v.2.5-7 (Oksanen et al., 2013), ‘`ggplot2`’ v.3.3.6 (Wickham et al., 2016), ‘`dplyr`’ v.1.0.8 (Wickham et al., 2019), ‘`ggbreak`’ v.0.1.2 (Xu et al., 2021).

**Table 5.1:** Infrared (IR) band assignments for *s*-FTIR microspectroscopy used in this study

Wave number (cm <sup>-1</sup> )	Band Assignment	Reference
~3011	$\nu(\text{CH})$ – from unsaturated fatty acids	
~2852	$\nu_s(\text{C-H})$ from methylene ( $-\text{CH}_2$ ) from saturated lipids (CH-Stretch IV)	Vongsvivut et al., 2013
~2921	$\nu_{\text{as}}(\text{C-H})$ from methylene ( $-\text{CH}_2$ ) from saturated fatty acids	
~1744	$\nu(\text{C=O})$ ester carbonyl group from lipid triglycerides and fatty acids	
~1549	Protein (Amide II mode); mainly $\delta(\text{N-H})$ of amides	Heraud et al., 2007
~1400	$\nu_s(\text{COO}^-)$ from carboxylated molecules	Sackett et al., 2014
~1241	$\nu_{\text{as}}(\text{PO}_2^-)$ of the phosphodiester backbone of nucleic acids, phosphorylated proteins and lipids	Sackett et al., 2014; Whelan et al., 2011
~1191 - 1146	$\nu_s(\text{C-O})$ from carbohydrates	Heraud et al., 2008
~1080	$\nu_s(\text{Si-O})$ from silica	Beardall et al., 2001; Sackett et al., 2016



## **Results**

### **Physical and Chemical Environment**

Under ice light at the outer site oscillated between 0 and 7  $\mu\text{mol/s/m}^2$  until 21 April (W3), when it abruptly declined by  $\sim 50\%$  (range 0 and  $\sim 3 \mu\text{mol/s/m}^2$ ), a shift coincident with a doubling of snow depth from  $15 \pm 0.7 \text{ cm}$  (W1) to  $27 \pm 2 \text{ cm}$  (W2) (Fig. 5.1B). Albedo was highest (94%) on W3, increasing from 76% during early April (W1) (Table 5.2) due to changes in snow properties. For the inner site, under ice light remained constantly low (0 - 3  $\mu\text{mol/s/m}^2$ ) for the entire sampling period, consistent with minimal changes in snow ( $\bar{x} = 27 \pm 2 \text{ cm}$ ) and ice depth (Fig. 5.1B, Table 5.2). We measured abrupt increases in water temperature over the sampling period at both sites (Fig. 5.1C). However, for the outer site, under ice temperature reached expected sea-ice melting point ( $> -1.7 \text{ }^\circ\text{C}$ ) in W3, followed by oscillations between freezing and thawing temperatures, whereas warming occurred after W4 at the inner site, with a steady increase to  $-1.5 \text{ }^\circ\text{C}$  (Fig. 5.1C). Sea-ice thickness gradually increased with time at the outer site, ranging from  $64 \pm 1 \text{ cm}$  (W1) to  $74 \pm 1 \text{ cm}$  (W6), and increased from  $83 \pm 2 \text{ cm}$  (W1) to  $90 \pm 1 \text{ cm}$  (W4) at the inner site, before declining to  $85 \pm 3 \text{ cm}$  (W6). The bulk salinity in the bottom of the ice was similar between the two sites, ranging from 12.33 to 7.34 ( $\bar{x} = 10.1$ ) at the outer site and 13.14 to 8.9 ( $\bar{x} = 11.2$ ) at the inner site, with both sites experiencing the fresher conditions during W6 (Table 5.2). Brine volume did not vary between the two sites, ranging from 24% to 14% ( $\bar{x} = 20\%$ ) at the outer site and 28% to 19% ( $\bar{x} = 24\%$ ) at the inner site, with both sites experiencing the lowest brine volume during W6 (Table 5.2).

**Table 5.2:** *Parameters measured associated with sea ice core extraction (white) and under-ice water (grey); snow depth ( $\pm \text{SD}$ ,  $n = 18$ ), albedo (%), ice thickness ( $\pm \text{SD}$ ,  $n = 6$ ), temperature ( $^\circ\text{C}$ ), bulk ice salinity (ppt), brine salinity (ppt), brine volume (% of ice volume), chlorophyll a concentration (ice:  $\text{mg m}^{-2}$ ,  $n = 3$  and water:  $\text{mg m}^{-3}$ ), particulate organic carbon (POC) to particulate organic nitrogen (PON) molar ratio (C:N), stable isotope of carbon  $\delta^{13}\text{C}_{\text{VPDB}}$  (‰), stable isotope of nitrogen  $\delta^{15}\text{N}_{\text{VPDB}}$  (‰), silicic acid ( $\text{Si}(\text{OH})_4$ ), nitrate + nitrite ( $\text{NO}_x$ ), phosphate ( $\text{PO}_4$ ) concentrations ( $\mu\text{M}$ ) and average water temperature at the ice-water interface ( $^\circ\text{C}$ ).*

Date	Station	Snow Depth	Albedo	Ice Thickness	Ice Temperature	Ice Salinity	Brine Salinity	Brine Volume	Chlorophyll <i>a</i>	C:N	$\delta^{13}\text{C}_{\text{VPDB}}$	$\delta^{15}\text{N}_{\text{VPDB}}$	$\text{Si(OH)}_4$	$\text{NO}_3^- + \text{NO}_2^-$	$\text{PO}_4$	Average Water Temperature
6.4.22 Week 1	Outer	15 ± 0.7	76	64 ± 1	-2.3	10.80	40.78	24	0.52 ± 1.0	6.14	-25.01	3.81	N.D.	0.98	0.24	
									0.29	4.95	-31.31	2.04	15.61	7.46	0.51	-1.79
7.4.22 Week 1	Inner	22 ± 2	95	83 ± 2	-2.1	9.74	37.36	23	0.31 ± 1.9	2.75	-26.81	3.26	2.51	2.46	0.34	
									0.02	3.99	-28.91	2.56	15.37	7.62	0.51	-1.79
20.4.22 Week 3	Inner	27 ± 4	77	85 ± 0.5	-2.6	13.14	45.85	26	2.00 ± 0.1	5.40	-21.95	2.49	3.93	5.65	0.47	
									0.04	3.16	-26.5	2.18	9.62	5.52	0.40	-1.87
21.4.22 Week 3	Outer	27 ± 2	94	70 ± 1	-2.7	12.33	47.53	23	0.49 ± 0.3	2.62	-27.14	1.48	N.D.	3.19	0.30	
									0.31	2.57	-26.86	4.69	14.48	7.22	0.53	-1.85
29.4.22 Week 4	Outer	19 ± 5	90	73 ± 3	-2.5	9.78	44.15	19	1.32 ± 0.2	4.79	-22.65	2.88	0.38	2.01	0.40	
									0.25	5.67	-24.83	4.03	11.33	5.70	0.45	-1.65
30.4.22 Week 4	Inner	28 ± 0.5	93	90 ± 1	-2.3	13.00	40.78	28	2.91 ± 0.8	3.24	-22.92	0.96	1.38	9.90	0.60	
									0.28	4.85	-26.08	3.49	12.84	7.17	0.41	-1.87
12.5.22 Week 6	Inner	32 ± 1.5	78	85 ± 3	-2.3	8.90	40.78	19	2.03 ± 0.5	4.04	-23.41	3.05	0.45	1.79	0.65	
									0.27	7.15	-24.73	4.25	12.13	6.44	0.47	-1.50
13.5.22 Week 6	Outer	9 ± 1	88	74 ± 1	-2.6	7.34	45.85	14	4.33 ± 1.6	11.51	-16.29	4.24	1.37	0.60	1.62	
									0.88	6.33	-25.17	4.6	3.86	2.52	0.31	-1.67

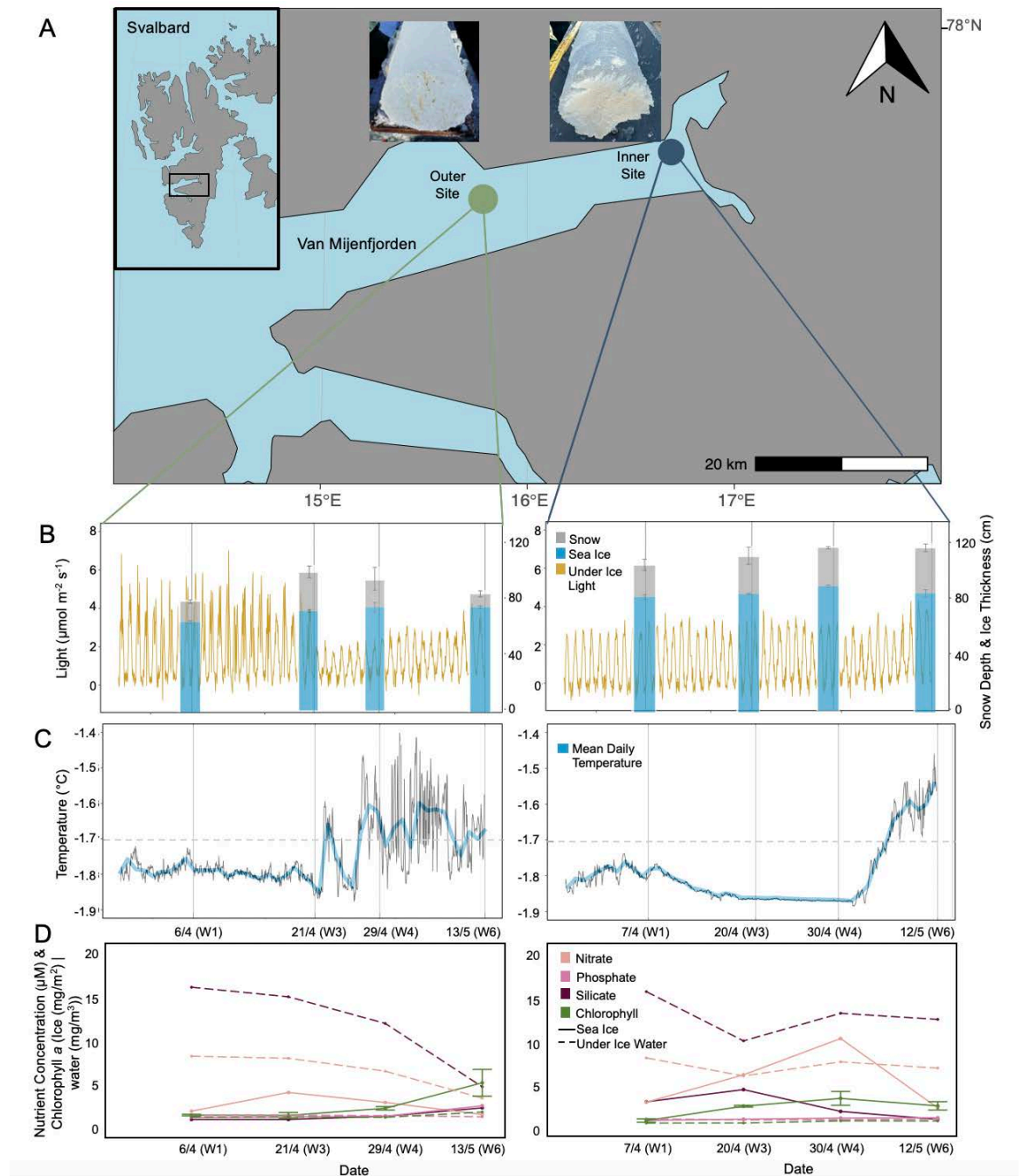


**Figure 5.1:** Location of sampling sites (A) visited between April-May 2022; inner site – blue dot and outer site – green dot, in Van Mijenfjorden, within Svalbard, Norway, generated in R Studio (v. 2023.09.0463) using ggOceanMaps (v.2.1.1) (inset box). Photographs of bottom ice cores collected from the inner and outer site on the 12.5.22 and 13.5.22 respectively, demonstrate more heterogeneity and lumping of biomass at the outer site. (B) Snow depth (cm)  $\pm$  SD (grey bars), sea-ice thickness (cm)  $\pm$  SD (blue bars) and photosynthetically active radiation (PAR) ( $\mu\text{mol photons m}^{-2}\text{s}^{-1}$ ), measured by the light sensor deployed under the ice throughout the season (yellow line). (C) Under water

*temperature (black line) as measured by the temperature sensor deployed alongside the light sensor, solid line indicates average temperature (blue). (D) Nutrients and chlorophyll a concentration are displayed (bottom panel), including nitrate (light pink), phosphate (medium pink), silicic acid (dark pink) and chlorophyll a concentration (green) in the sea ice (solid line) and under-ice water (dashed line), on all sampling dates at the outer site (left) and inner site (right).*

Ice  $\text{NO}_x$  concentrations peaked ( $3.2 \mu\text{M}$ ) in W3 at the outer site, before declining to potentially limiting levels ( $0.6 \mu\text{M}$ ) by W6. In contrast, concentrations of  $\text{NO}_x$  were higher at the inner site (averaging  $5.0 \pm 3.7 \mu\text{M}$  throughout the study), with a peak concentration of  $9.9 \mu\text{M}$  in W4 (Fig. 5.1D). For the outer site,  $\text{Si(OH)}_4$  concentration in the ice was not detected until W5 when it was low ( $0.4 \mu\text{M}$ ), while  $\text{PO}_4^{3-}$  increased to  $1.6 \mu\text{M}$  in W6 (Table 5.2). Unlike the outer site, ice  $\text{Si(OH)}_4$  concentrations were consistently detectable at the inner site, with the concentration ranging from  $0.5 \mu\text{M} - 3.9 \mu\text{M}$  (Fig. 5.1D). Chl *a* concentrations within the bottom ice gradually increased with time at both sites, peaking at W6 for the outer site and W4 for the inner site (Fig. 5.1D; Table 5.2). There was a visible change in the chl *a* biomass within the bottom-ice following the melting period at the outer site (Fig. 5.1D), in which the biomass was heterogenous and forming visible lumps. Under-ice water chl *a* concentrations remained low throughout, increasing to  $0.9$  and  $0.3 \text{ mg m}^{-3}$  by W6 at both the outer and inner site, respectively (Table 5.3; Fig 5.1). Seawater  $\text{NO}_x$  and  $\text{Si(OH)}_4$  concentrations decreased with time at the outer site, but remained replete ( $\text{NO}_x$ :  $2.5-7.5$  and  $\text{Si(OH)}_4$ :  $0.9-3.8 \mu\text{M}$ , respectively).  $\text{PO}_4^{3-}$  concentration remained constant ( $0.3-0.5 \mu\text{M}$ ) and replete. For the inner site, concentrations of  $\text{NO}_x$  and  $\text{Si(OH)}_4$  and  $\text{PO}_4^{3-}$  in the seawater remained relatively constant and replete ( $\text{NO}_x$ :  $6.4-7.6 \mu\text{M}$ ,  $\text{Si(OH)}_4$ :  $9.6-15.4 \mu\text{M}$  and  $\text{PO}_4^{3-}$ :  $0.4-0.5 \mu\text{M}$ ) throughout the study (Fig. 5.1D). Molar ratios of C:N did not differ between sites (Table 5.2). However, there was a greater range in C:N ( $2.62 - 11.51$ ) at the outer site than the inner site ( $2.75 - 5.40$ ). Molar ratios of N:Si taken from the ice ranged between  $1.0$  and  $12.1$  at the outer site and  $2.23$  and  $16.25$  at the inner site, whilst the molar ratio of Si:P was  $0.2$  at the outer site and ranged from  $0.2$  to  $2.0$  at the inner site (Table 5.2). Bottom-ice POC and Chl *a* were found to be positively correlated at the outer site only ( $F_{1,2} = 51.72$ ,  $p < 0.05$ ,  $R^2 = 0.96$ ) and POC:Chl *a* did not exhibit a relationship with time at either site.

### Protist Community Composition

*N. frigida* was the most abundant taxa at all sites and all time points, making up between 31% of the community at the inner site during W4 and 56% at the outer site during W6 (Fig. 5.2), with an increase in abundance towards the end of the season. Sea-ice community composition was similar across the two sites and all time points (ANOSIM  $R = 0.03$ ,  $p > 0.05$ ), although some apparent decline in the proportion of *Navicula* spp. and *Pleurosigma/Gyrosigma* spp., in conjunction with an increase in the proportion of dinoflagellates, including *Gymnodinium* spp. is evident at the outer site by W6 (Fig. 5.2).

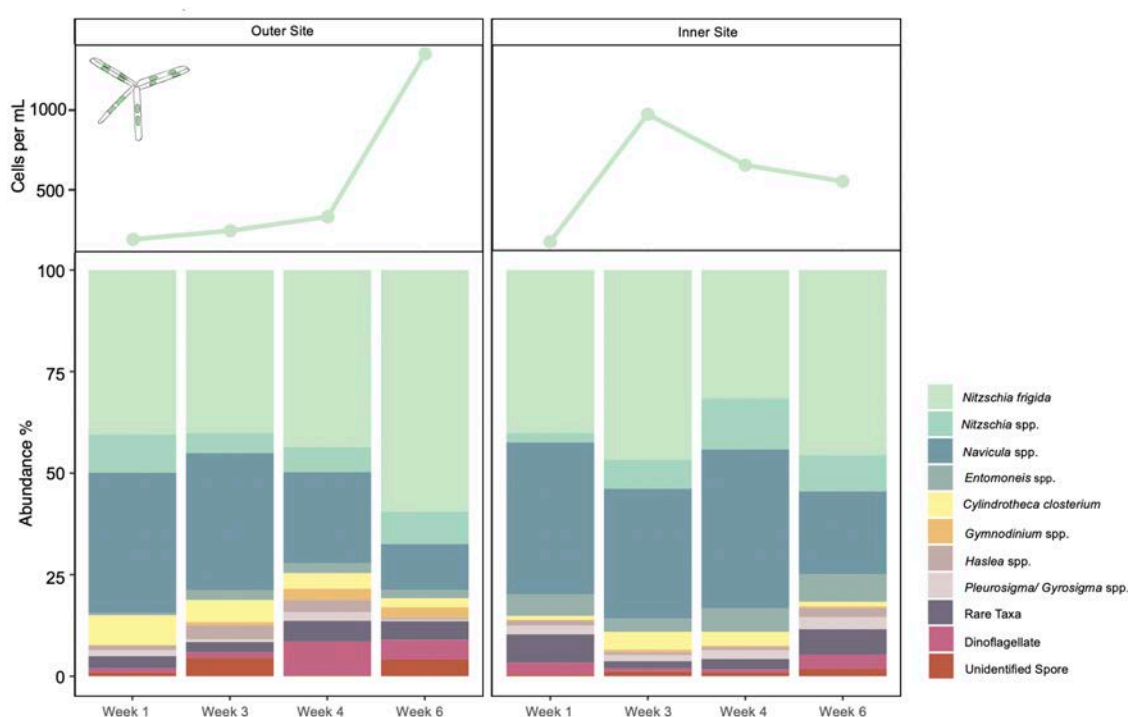


**Figure 5.2:** Bottom ice microalgal community composition from outer site (left) and inner site (right) sampled during April-May 2022, in Van Mijenfjorden, Svalbard, Norway. Raw counts of *Nitzschia frigida* cells per mL are displayed in the top panels, and the relative abundance (%) of taxonomic groups are shown in the lower panels. *Nitzschia* spp. includes all *Nitzschia* species identified with the exception of *Nitzschia frigida*. Rare Taxa includes: *Hantzchia* spp., *Diploneis littoralis*, *Stenoneis inconspicua*, *Pinnularia quadratarea*, *Plagiotropis* spp., *Manguinea rigida*, *Tropidoneis* spp.

### Biomolecular Composition

Spectral analyses revealed strong trends and differences in key biomolecular peaks across time for both sites (Fig. 5.3A-B). Principle component analysis on the nine selected biomolecular peaks of *N. frigida* from the outer site showed separation with time of

sampling along PC1, explaining 68.2% of the variation (Fig. 5.3C). The temporal trend was primarily driven by relative increases in lipids and FAs at the last sampling time point (W6). For the inner site, PC1 explained 42.9% of the variation, with evidence of a temporal effect driven by increases in lipid and saturated FAs (Fig. 5.3D).

Integrated peak areas for selected biomolecules revealed high cell-specific variability in *N. frigida* from both sites (Fig. 5.4A-D). We detected a significant shift in biomolecular composition of *N. frigida* at the end time point for the outer site (Fig. 5.4A-D), where differences observed were driven by an increase in allocation to storage biomolecules i.e. lipid (ester carbonyl) ( $F_{1,93}= 148.6$ ,  $p < 0.05$ ,  $R^2 = 0.62$ ; Fig. 5.4B), saturated fatty acids (SFA) and unsaturated fatty acids (USFA) (Table S5.2). These increases were concomitant with a decrease in protein (amide II) ( $F_{1,94}= 60.16$ ,  $p < 0.05$ ,  $R^2 = 0.39$ ; Fig. 5.4C), carbohydrates ( $F_{1,93}= 26.54$ ,  $p < 0.05$ ,  $R^2 = 0.22$ ; Fig. 5.4A), phosphodiester and carboxylated molecules (Table S5.2). In contrast, *N. frigida* cells from the inner site, showed a significant shift in biomolecular profiles from early April (W1) and the final time point (Fig. 5.4E-H), primarily driven by a relative increase in protein (amide II) ( $F_{1,100}= 44.19$ ,  $p < 0.05$ ,  $R^2 = 0.31$ ; Fig. 5.4G) and decrease in carbohydrate content ( $F_{1,100}= 44.19$ ,  $p < 0.05$ ,  $R^2 = 0.31$ ; Fig. 5.4E). A significant increase in lipids (ester carbonyl) ( $F_{1,99}= 26.99$ ,  $p < 0.05$ ,  $R^2 = 0.21$ ; Fig. 5.4F) and SFAs were also observed (Table S5.2). In addition to interrogating the biomolecules in the cell, we also looked for any changes in the silica peak at  $1150\text{ cm}^{-1}$ . Unexpectedly, we saw a significant decline in biogenic silica in cells from the outer site by W6 (Fig. 5.4D), corresponding with the other significant changes in biomolecular components. No change in silica content was detected for *N. frigida* cells from the inner site (Fig. 5.4H).

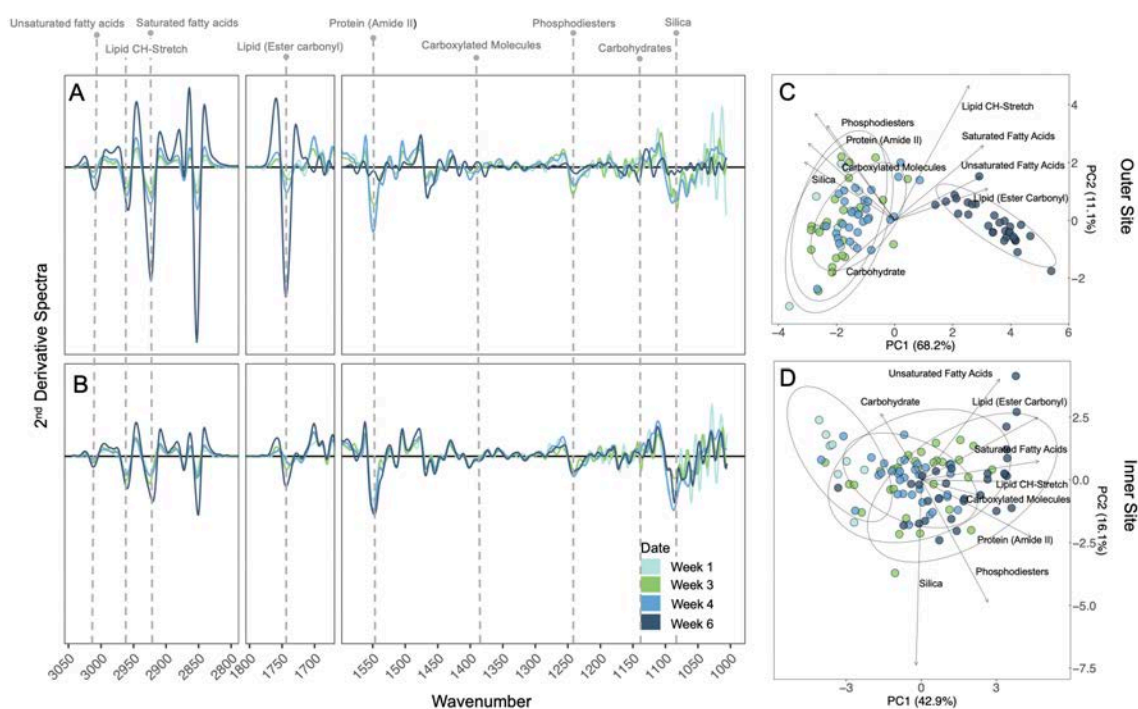


**Figure 5.3:** Smoothed and normalised 2<sup>nd</sup> derivative spectra for *Nitzschia frigida* at the (A) outer and (B) inner site with each sampling week denoted by colour gradient. Dashed vertical lines indicate respective wavenumber for peaks of interest. Principal component analysis (PCA) of biomolecular content at the (C) outer and (D) inner site with sampling week denoted by colour, in which each dot represents the measurements of one cell. Direction and strength of individual biomolecules are displayed with ordination bi-plot overlay.

Redundancy analysis revealed that the environmental parameters of brine volume, bottom-ice salinity and ice nitrate concentration combined explained 77% of the variability in biomolecular content across the two sites, while seawater temperature explained 11% of the variability ( $F_6 = 2.92$ ,  $p < 0.05$ , Fig. 5.4E). Photosynthetically derived biomolecules (e.g. lipids and FAs) were negatively correlated with brine volume, bottom-ice salinity and ice nitrate, yet showed a positive relationship with these environmental parameters for the functional biomolecules (e.g. protein, phosphodiesteres and silica content) and carbohydrate content. Water temperature (i.e. freezing or melting the bottom of the sea ice) was shown to have the greatest positive effect on lipid (CH-stretch) content and an inverse relationship with carbohydrate content (Fig. 5.4E). Previous studies have found increasing light to drive increases in lipid and FA allocation in sea-ice algae (Duncan et al., 2024a; Smith et al., 1993; Smith & Herman, 1992) but the

typical increase light transmitted to the bottom-ice toward the end of the productive season was not observed in this study, excluding light as a significant driver in determining biomolecular changes.

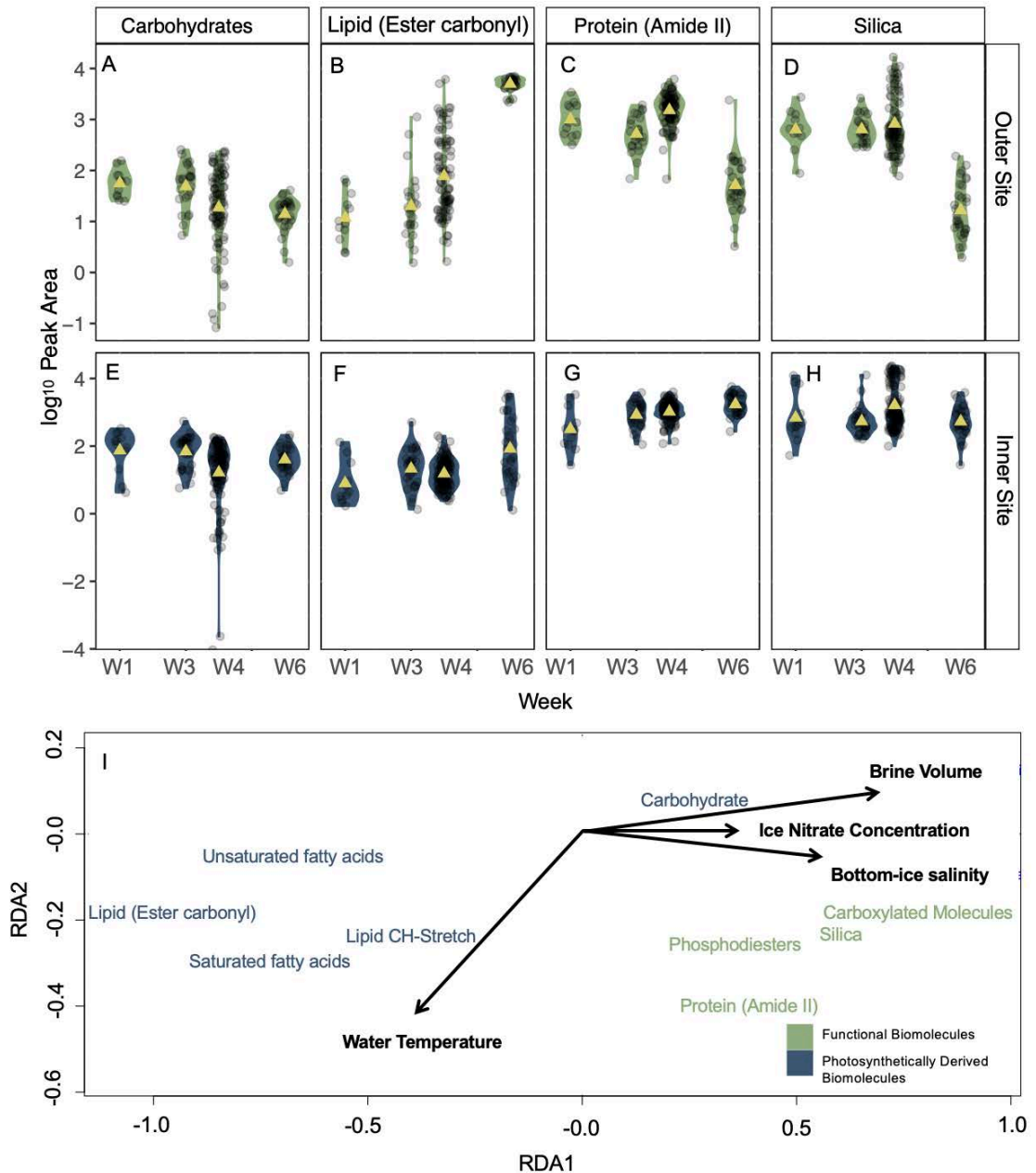


**Figure 5.4:** Biomolecular content based on normalised peak areas of specific biomolecules, for *Nitzschia frigida* per sampling week for the outer (A-D) and inner site (E-H); specifically (A,E) Carbohydrate (B,F) Lipid (ester carbonyl), (C,G) Protein (amide II) and (D,H) Silica content. Data are presented as violin plots where coloured shading indicates SE and yellow triangle represents the mean, individual cells are shown by transparent dots. Site location is represented with colour; outer site (green; top



panels) and inner site (blue; bottom panels). Redundancy analysis (RDA) biplot (I) of the mean biomolecular content (divided into functional biomolecules (cell structure and function) and photosynthetically derived biomolecules (energy and storage), denoted by colour) from each sampling site and date with environmental variables displayed with ordination bi-plot overlay. Only significant vectors are shown and RDA model is significant ( $p < 0.05$ ).

### Fatty Acid Composition

Total fatty acid (FA) content of the outer site community was double (54% total lipid of dry matter) that of the inner site community (25% total lipid of dry matter) (Fig 5.5A). The predominant FA at both sites was 16:1 n-7, followed by 16:0, 20:5 n-3 and 14:0 (Table 5.2), together accounting for 83.5% and 56.5% of FA content at the outer and inner sites, respectively. As a proportion of total FA content, both sites had a similar relative proportion of SAFA content (30% FA: inner site, 35% FA: outer site). However, the inner site had a relatively higher proportion of PUFA content (28% FA: inner site, 16% FA: outer site) and a lower proportion of MUFA content (38% FA: inner site, 54% FA: outer site) compared with the outer site (Fig. 5.5A). In addition, the proportion of omega-3 FA EPA+DHA (polyunsaturated eicosapentaenoic acid and docosahexaenoic acid) was almost double at the inner site (13% FA) compared to the outer site (7.8% FA). Comparing SAFA and USFA content from the total community analysis with the FTIR samples from the final time point, we see that in both *N. frigida* and the total community, the total FA content was substantially higher at the outer site (Fig. 5.5B). There was a strong relationship between SAFA and USFA content at the outer site ( $F_{1,28} = 16.35$ ,  $p < 0.05$ ,  $R^2 = 0.37$ ) but not at the inner site ( $F_{1,28} = 2.4$ ,  $p > 0.05$ ,  $R^2 = 0.08$ ), where more variability was observed (Fig. 5.5B).

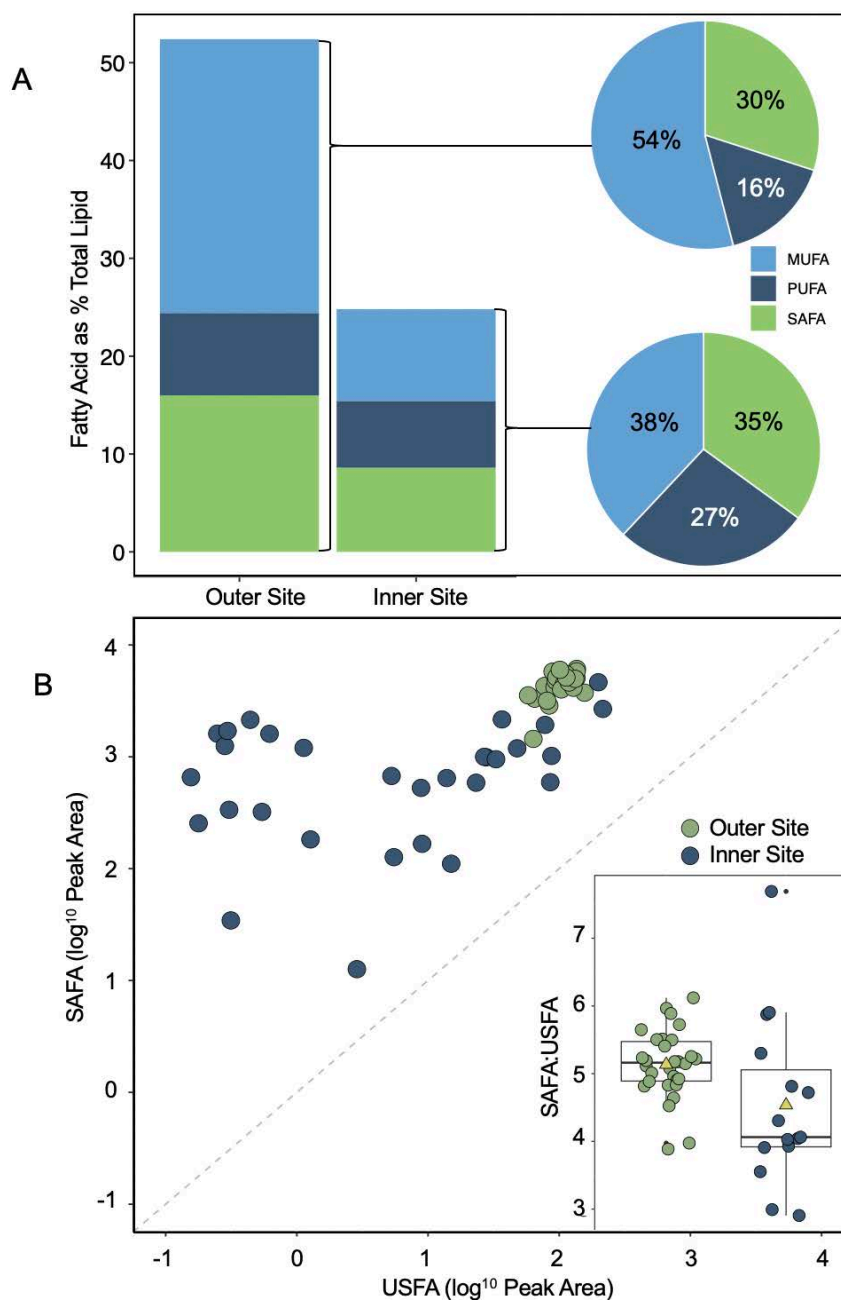


**Figure 5.5:** Fatty acid (FA) content as % total lipid content of the whole bottom ice community at the outer and inner site (A), during week 6. The different FA types, monounsaturated fatty acid (MUFA), polyunsaturated fatty acid (PUFA) and saturated fatty acid (SAFA) per site, are denoted by colour. Site-specific FA content as a proportion of total FA are presented in pie charts (right). Cell-specific SAFA vs. unsaturated fatty acid (USFA) content of *Nitzschia frigida*, as determined by *s*-FTIR (B), with site denoted by colour. The ratio of SAFA:USFA content per cell is displayed (inset), as a boxplot with yellow triangles representing the mean.

**Table 5.3:** Fatty acid (FA) composition of entire sea ice algae community at the inner and outer site of Van Mijenfjorden, Svalbard on the 12<sup>th</sup> May and 13<sup>th</sup> May 2022, respectively, as % total FA displayed (with SUM % total lipid dry matter (DM) displayed in brackets), for 6 ice cores pooled. FAs accounting for <0.1% of total in both sites are not displayed. FA: Fatty acids, PUFA: polyunsaturated fatty acids, MUFA: monounsaturated fatty acids, SAFA: saturated fatty acids, EPA: eicosapentaenoic acid and DHA: docosahexaenoic acid.

	Outer Site % FA	Inner Site % FA
14:0	7.5	5.5
15:0	0.3	0.4
16:0	20	19
16:1 n-9	2.7	8.5
16:1 n-7	49	22
16:1 n-5	0.6	1.5
17:0 Phytanic	0.1	0.4
17:0	0.1	0.5
16:2 n-7	0.9	1.9
16:3 n-4	0.5	1.9
18:0	1.4	6.2
16:4 n-1	1.4	3.1
18:1 n-9	1	1.5
18:1 n-7	0.3	0.7
18:2 n-6	0.6	0.6
18:3 n-6	1.9	1
18:3 n-3	0.3	0.4
20:0	0.2	0.4
18:4 n-3	1.4	2.1
20:4 n-6	0.8	3.4
20:3 n-3	0.2	0.3
22:0	0.1	0.4
20:4 n-3	0.2	0.3
22:1 n-9	0.4	3.3
20:5 n-3	6.9	10
22:6 n-3	0.9	2.1
SUM FA of DM	52	25
SUM SAFA	30 (16)	35 (8.6)
SUM MUFA	54 (28)	38 (9.4)
SUM PUFA	16 (8.4)	28 (6.8)
SUM omega-3 FA	10 (5.2)	16 (3.9)
SUM omega-6 FA	3.3 (1.7)	5 (1.3)
SUM omega-9 FA	4.1 (2.1)	13 (3.3)
SUM EPA + DHA	7.8 (4.1)	13 (3.1)

### $\delta^{13}\text{C}$ and $\delta^{15}\text{N}$ Stable Isotopes

Neither ice nor seawater  $\delta^{15}\text{N}_{\text{Air}}$  (‰) differed between sites, and showed no distinct pattern nor relationship to chl *a* concentrations (Fig. 5.6A-B). Conversely, under-ice seawater at both sites, and ice at the outer site, showed increased carbon-enrichment over time, with  $\delta^{13}\text{C}_{\text{VPDB}}$  (‰) ranging from -31.31 to -25.17 ‰ in the water and -25.01 to -16.29 ‰ in the ice at the outer site (Fig. 5.6A-B). Unlike the  $\delta^{15}\text{N}_{\text{Air}}$  (‰),  $\delta^{13}\text{C}$  values from the ice mirrored the patterns observed in the ice chl *a* concentration (Fig. 5.6A-B). There was no significant difference in carbon enrichment between the sites for the ice or under-ice water (Fig. 5.6A-B). Carbon enrichment was positively associated with storage biomolecular content (i.e. lipid and FAs), and inversely related to protein, carbohydrate, silica, carboxylated molecule and phosphodiester content (Fig. 5.6C). These relationships were driven by changes at the outer site only, where peak carbon enrichment was associated with the highest lipid content and lowest protein content (Fig. 5.6D).

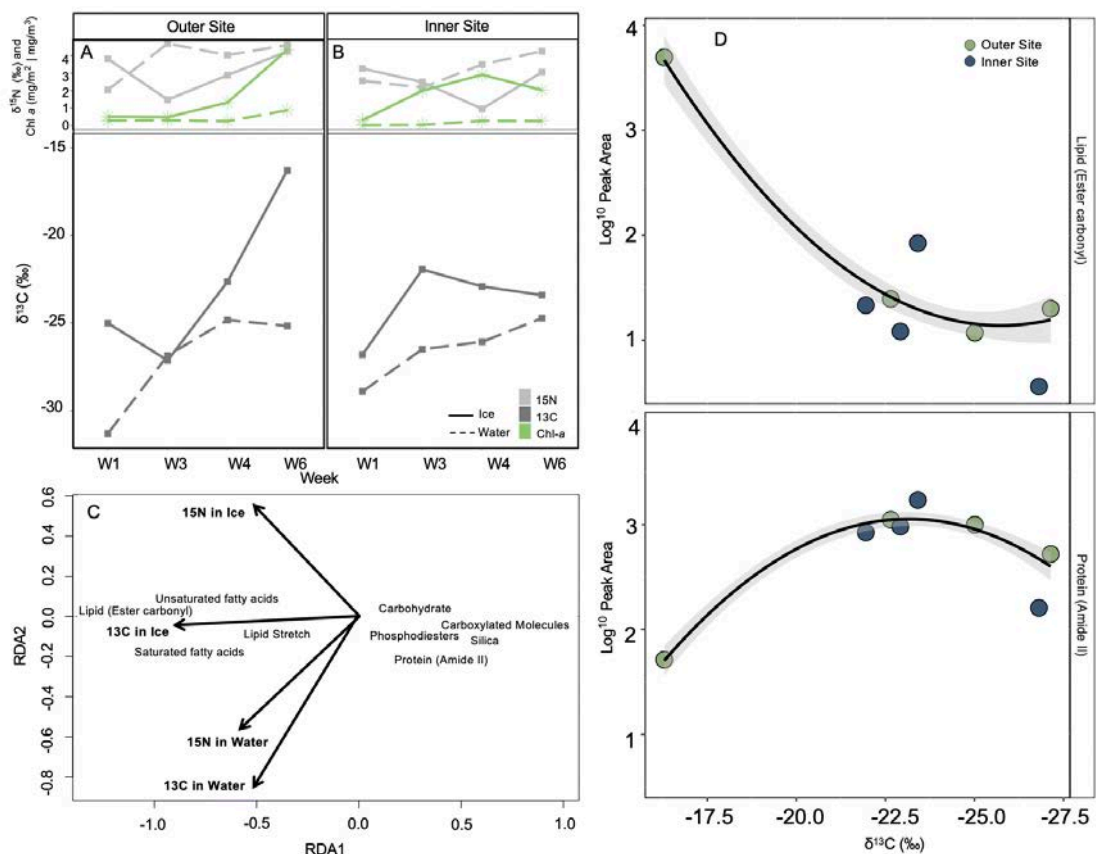


**Figure 5.6:**  $\delta^{15}\text{N}$  (light grey square),  $\delta^{13}\text{C}$  (dark grey square) and chlorophyll *a* concentration (green star) from the bottom-ice (solid line) and water directly below ice (stippled line) at the (A) outer site and (B) inner site, across all sampling weeks. Redundancy analysis (RDA) biplot (C) of the mean biomolecular content of *Nitzschia frigida* cells from each sampling site and time point with  $\delta^{13}\text{C}$  and  $\delta^{15}\text{N}$  stable isotope

values from the sea ice and water below displayed with ordination bi-plot overlay, only significant vectors are shown and RDA model is significant ( $p < 0.05$ ). **(D)** Content of lipid (ester carbonyl; top panel) and protein (amide II) (bottom panel) vs.  $\delta^{13}\text{C}$  values, at the outer site (green) and inner site (blue). The data (both locations combined) are fitted with linear regressions, with 95% confidence intervals (coloured shading).

## **Discussion**

Our study followed the seasonal progression in biomolecular composition of the key sea-ice diatom, *N. frigida*. By sampling from two locations at four separate time points spanning five weeks during spring, we were able to capture spatial and temporal dynamics in environmental conditions from an inner (more stable) and an outer (more dynamic) fjord site and look at them in relation to plasticity in biomolecular properties. Furthermore, by analysing individual cells we revealed high plasticity and individual variability in *N. frigida* cell content, with major changes becoming evident with the onset of seasonal melt. Close examination of the biomolecular profiles in relation to environmental variables, revealed that nitrogen limitation, in conjunction with warming sea temperatures and decreased brine volume, corresponded with increased lipid and FAs stores, and a decline in protein and carbohydrate. These shifts in metabolic energy allocation may be representative of energy storage becoming a priority (Wagner et al., 2017) in *N. frigida* cells, in preparation for overwintering as the Arctic summer advances.

Increasing ocean temperature is a key environmental trigger for initiating the seasonal transition from spring into Arctic summer. There was a two-week difference in the timing of warming between our two sites, making evident the influence ice melt can have on *N. frigida* populations. Throughout the study, the community was dominated by diatoms (predominantly *N. frigida*). Our microscopy findings were supported by the FA composition analyses, which showed 20:5n3, C16 PUFAs and 16:1n7 – the diatom-marker FAs (Leu et al., 2010) as the primary constituents. From the onset of under-ice melt, we measured an increase in *N. frigida* numbers, as well as an increase in the proportion of dinoflagellates at the outer site, mirroring trends previously observed with seasonal progression (Duncan et al., 2024b; Hegseth & von Quillfeldt, 2022; Mundy et al., 2011; Róžańska et al., 2009). Further, at the outer site with slightly younger ice, the under-ice melt resulted in a decrease in the proportion of *Navicula* spp. and increase in unidentified spores during mid-April (W3). The early warming at the outer site (starting

W3), was followed by a series of temperature oscillations between freezing and thawing until mid-May (W6), causing physical changes to the bottom of the sea ice (i.e. removal of skeletal layer) and a reduction in brine volume (i.e. space for community colonisation). Interestingly, despite the loss of skeletal layer and reduction in brine volume from W4 onwards, the chl-*a* content within the ice increased at the outer site, forming a patchy distribution of biomass, still dominated by *N. frigida*. This ability for *N. frigida* to grow as large aggregates, likely provides a competitive advantage to *N. frigida* as it forms dendroid colonies, allowing it to remain on the bottom-ice, even in the absence of a skeletal-ice layer and expansive brine channel network. In addition, *N. frigida*, along with many other pennate diatoms, can produce exopolysaccharides (EPSs), creating a viscous biofilm and increasing cell adhesion to the bottom-ice (Krembs et al., 2011). These adaptations explain the sympagic biomass increase despite less advantageous sea-ice conditions. The predominance of such aggregates has implications for secondary production and carbon export (Fernández-Méndez et al., 2014) with zooplankton unable to graze on larger food packages as effectively (Koski et al., 2017) and the aggregates falling to the sea floor more quickly (Riebesell et al., 1991), enhancing carbon deposition.

Our single-celled approach revealed high intra-specific variability in biomolecular content, suggesting that *N. frigida* possess many plastic traits able to adjust to the dynamic spring sea ice and water conditions, providing a plausible evolutionary explanation for its ecological success in the sea ice and dominance throughout the entire productive season (Fig. 6.3, 6.4). We also detected considerable reduced variability in expressed lipid content at the last time point for the outer site, which could be indicative of strong environmental forcing causing cellular stress, whereby cells reach their phenotypic limit, in this case maximum production and storage of lipids. These changes coincided with significant decrease in protein and silica, supporting the idea of possible stress-induced changes in metabolic homeostasis. This type of latent stress response is often typical of variations in temperature (Torstensson et al., 2019), such as the observed warming, reduced nitrogen availability (Pogorzelec et al., 2022), and/or salinity (Forgereau et al., 2023).

Alongside warming, nitrogen depletion, following its consumption by primary production, often signals the end of the productive ice-algae season (Demers et al., 1989; Różańska et al., 2009), and typically occurs with the beginning of the ice-breakup. As

such, microalgal cells respond to nitrogen limitation by increasing lipid stores in preparation for dormancy (Mock & Kroon, 2002a; Smith & Herman, 1992). Therefore, the rapid and significant increase in lipid accumulation by *N. frigida*, could be indicative of reduction in nitrogen availability (Pogorzelec et al., 2017). The Redfield ratio for sea-ice algae (amended to include the silicate requirement for diatoms) is generally accepted to be 106C:16N:15Si:1P (Parsons et al. 1961). Based on these requirements, in our study, nitrogen at the outer site could only have become limiting in mid-May, coinciding with the strongest biomolecular changes. The relatively constant and replete nitrogen levels within the other samples was likely due to exchange with seawater below the ice (Cota et al., 1991), and/or remineralisation and nitrification (Clark et al., 2020; Fripiat et al., 2014) within the ice. Nitrate replenishment is indicated by low  $\delta^{15}\text{N}$  values and the relatively low chl *a* content and biomass, supported by the generally low C:N values (indicating low carbon), observed at the other sampling points throughout the season. Another indication of possible temperature and nitrogen stress, was the observed decline in cellular energy allocation to protein and reduced carbohydrate content, such shifts have been previously observed in nitrogen limited sea-ice algal communities (Mock & Kroon, 2002a; Pogorzelec et al., 2022; Smith & Herman, 1992). The biomolecular shifts in energy allocation toward lipid storage, suggest that under warmer, nitrogen limiting conditions, further growth is not prioritised.

While the inner site showed little variation over our seasonal sampling, the outer site community was found to have approximately double the total FA content than the inner site, with proportionally higher MUFA content on the final sampling date. This is consistent with increases in neutral lipids under nitrate limitation, and as primarily storage lipids, this demonstrates a response to stress and preparation for dormancy (Johnsen et al., 2020; Zhang et al., 1998). In addition, the outer site had substantially higher 16:1 n7 content, an indicator of the cell entering a storage and survival phase. The community from the inner site on the final sampling date was indicative of a community in exponential growth with proportionally more PUFAs (and specifically higher proportions of 20:5 n-3 and 16:4 n-1) (Leu et al., 2006a), and which is consistent with nitrate limited cells taken post-bloom (Leu et al., 2006a; Leu et al., 2010; Schmidt et al., 2024). The availability of PUFA content has been shown to determine zooplankton production and growth (Jónasdóttir et al., 2005; Jónasdóttir et al., 2009; Søreide et al., 2010). The omega-3 FAs (PUFAs) EPA and DHA are essential for growth and reproduction in all marine

organisms and are key indicators of how nutrient rich a food source is, yet are produced exclusively by marine algae (Ackman, 1989). Furthermore, the increase in lipid observed in *N. frigida*, corresponding with an increase in total carbon enrichment ( $\delta^{13}\text{C}$ ) within the ice (Lee et al., 2008a), indicates that the biomolecular response of *N. frigida* could be representative of many taxa in the sea-ice algae community. Taken together, the species-specific spectroscopy and community FA composition and carbon enrichment results from the outer site elucidate how end of season nitrate limitation alters the nutritional quality of food available to higher trophic levels.

In response to seasonal warming, another environmental change signalling the end of the ice season is a decrease in brine volume and associated freshening of the bottom-ice. While this process can occur during ice growth, drainage is often triggered by either warming at the ice surface (air temperature), or melting at the ice-water interface (water temperature) (Griewank & Notz, 2013). The hypersaline brine drains out to the ocean below and fresh meltwater from the ice percolates through the brine network, replacing the brine (Notz & Worster, 2009) and lowering interstitial salinity. In this study, we measured a decrease in brine volume and freshening of ice at the outer site on the last sampling time point, coinciding with detected changes in biomolecular profiles. Whilst the bulk ice salinity was within expected ranges for the end of the ice season (e.g. Forgereau et al., 2023; Leu et al., 2020; Róžańska et al., 2009) and brine volume remained above the 5% threshold necessary for colonisation (Golden et al., 2007), the changes appeared to be sufficient to create environmental stress for the *N. frigida* cells. The move toward hypoosmotic conditions, which have been found to significantly lower photosynthetic efficiency in pennate ice diatoms (Forgereau et al., 2023), could have induced strong increases in lipid storage and decreases in carbohydrate production as a means to prioritise energy storage over growth and development, in readiness for a period of dormancy (Johnsen et al., 2020; Mock & Kroon, 2002a). Such adaptations to seasonality are commonly observed in many animals (Varpe, 2017), but are to a lesser degree documented for phytoplankton. Zooming in on individual properties of microalgae cells, as done in this study, adds much power when aiming to identify the extent of such adaptations in diatoms and other single cell organisms in the ocean. At the same time, the decrease in carbohydrate content and increase in lipid could be attributed also to the enduring higher average water temperatures ( $-1.65\text{ }^{\circ}\text{C}$ , a temperature expected to melt sea ice from below) from the end of April. Similar biomolecular changes have been observed



previously, albeit over a greater temperature change, e.g. between  $-1.8\text{ }^{\circ}\text{C}$  and  $+3\text{ }^{\circ}\text{C}$  (Torstensson et al., 2019). This is the first time such changes have been reported at the boundary temperature between melting and freezing. Given the above, it is likely that the combination of a decrease in brine volume, freshening of the bottom-ice and warmer under-ice water temperature contributed to creating a multi-stressor environment, and when combined with nitrogen limitation, directed metabolism and photosynthate allocation toward increased energy storage rather than continue growth and development.

Unlike nitrate, silicic acid was limiting at both sites throughout the season, with N:Si higher than Redfield (1.07) and Si:P lower than Redfield (15) at both sites (Brzezinski, 1985). As silicate is necessary for building and maintenance of diatom frustules (Martin-Jézéquel et al., 2000), under limitation, biogenic silica formation and therefore diatom growth, is constrained (Gosselin et al., 1990). Our data showed a strong decline of biogenic silica in *N. frigida* at the final time point, which may be explained by the additional stress on the cells experiencing end of season conditions, compromising their growth and frustule formation.

The results from this study demonstrate how environmental conditions that lead to the sea-ice algae community being ‘released’ from the ice, are important in terms of the cell’s viability for surviving ice free conditions, for carbon export, and for energy supply to the marine food web. With the onset of warming, the biggest environmental changes to influence *N. frigida* physiology, morphology and metabolism, were reduced brine volume and the onset of nitrogen limitation. The sea-ice algal community, and *N. frigida* in particular, showed high phenotypic diversity and plasticity throughout the sea-ice season, and appeared to ‘tolerate’ the dynamic freeze/thaw cycles, continuing to grow, independently or perhaps because of the variable conditions. Variability in the phenome of *N. frigida* was reduced as the season progressed towards ice-free conditions. We saw large changes in biomolecular composition, specifically an increase in lipid and FA storage, at the expense of protein and carbohydrate stores, associated with the onset of nitrogen limitation, marking the end of the sea-ice algal growth season. As lipid stores and reduced metabolic rate are thought to be the key to the ability of *N. frigida* to survive summer and the six months of darkness that follow, these findings highlight the importance of this seasonal metabolic cascade for Arctic food web dynamics and carbon export. Our study revealed a significant decline in cell-specific silica content as the

community approached the end of the cascade. This reduction in cell-specific silica content, has the potential to alter *N. frigida* sinking rates and grazability, thereby influencing carbon transfer. Conversely, these changes may be countered by the increased aggregation by *N. frigida*, which would likely result in a net increase in population sinking rate and provide additional protection from potential grazers. In the context of climate change, the predicted Atlantification of the Arctic would bring warmer water advection earlier in the season and/or create a more abrupt transition to the melting phase. This transition earlier in the season could obviate these important end-of-season environmental shifts, causing the algae to be released from the ice prior to significant biomass accumulation and sufficient lipid build-up and storage, with the onset of nitrogen limitation. Reduced biomass would likely alter food web dynamics, changing the quality and quantity of the food source at a critical time of development and seasonal growth, while diminished lipid stores upon melt-out could result in fewer cells surviving dormancy. As lipids are the most energy dense of all biomolecules, taken together, such changes at the primary production level could result in less carbon transfer through the polar marine ecosystem.

### **Acknowledgements**

R.J.D. is supported by an Australian Government Research Training Program Scholarship and an AINSE Ltd. Postgraduate Research Award (PGRA). Funding was also provided through the 2017-2018 Belmont Forum and BiodivErsA joint call for research proposal, under the BiodivScen ERA-Net COFUND programme, and with the funding organisations Research Council of Norway (RCN; 296836) and National Science Centre Poland (NSC; UMO2015/17/B/NZ8/02473). In addition, RCN allocated funding through an Arctic Field Grant to R.J.D. (33156) and V.P (350579). This research was supported by an Australian Research Council grant DP210101360 awarded to KP. Part of this work was funded by the Australian Synchrotron through merit-based beamtime awarded on the Infrared Microscopy (IRM) beamline at the Australian Synchrotron, part of ANSTO (AS222/IRM/18486) awarded to K.P. The authors would like to thank Stuart Thomson, Einar Bergland and Stina Skånhoff for their valuable assistance with the field sampling.

### **Data Availability**

Data are available in the open repository Figshare. DOI: 10.6084/m9.figshare.25222808

**Supplementary Information:****Table S5.1:** Number of *Nitzschia frigida* cells measured per site, per date

Site	Date	Cells Measured
Inner Site	6.4.22	12
	21.4.22	34
	29.4.22	30
Outer Site	13.5.22	30
	7.4.22	9
	20.4.22	30
	30.4.22	33
	12.5.22	30

**Table S5.2:** Statistical output from regression models of *Nitzschia frigida* biomolecular content with time. Multiple  $R^2$ , adjusted  $R^2$ ,  $F$  statistic, associated degrees of freedom (DF) and  $p$ -value. Statistically significant  $p$ -values ( $< 0.05$ ) are marked in bold.

	Multiple $R^2$	Adjusted $R^2$	F Statistic	DF	P Value	
Outer Site	Carbohydrates	0.22	0.21	26.54	1,93	<b><math>1.42 \times 10^{-6}</math></b>
	Carboxylated Molecules	0.60	0.58	135.9	1,93	<b><math>2.2 \times 10^{-16}</math></b>
	Lipid CH Stretch	0.36	0.36	53.28	1,94	<b><math>9.12 \times 10^{-11}</math></b>
	Lipid (ester carbonyl)	0.62	0.61	148.6	1,93	<b><math>2.2 \times 10^{-16}</math></b>
	Phosphodiesteres	0.38	0.37	55.86	1,92	<b><math>4.12 \times 10^{-11}</math></b>
	Protein (amide II)	0.39	0.39	60.16	1,94	<b><math>1.04 \times 10^{-11}</math></b>
	Saturated Fatty Acids	0.57	0.56	122.6	1,94	<b><math>2.2 \times 10^{-16}</math></b>
	Silica	0.60	0.59	135.7	1,93	<b><math>2.2 \times 10^{-16}</math></b>
	Unsaturated Fatty Acids	0.52	0.52	102.5	1,94	<b><math>2.2 \times 10^{-16}</math></b>
Inner Site	Carbohydrates	0.14	0.13	15.61	1,100	<b><math>1.45 \times 10^{-4}</math></b>
	Carboxylated Molecules	0.00	0.00	0.13	1,99	0.72
	Lipid CH Stretch	0.26	0.25	34.89	1,100	<b><math>4.87 \times 10^{-8}</math></b>
	Lipid (ester carbonyl)	0.21	0.21	26.99	1,99	<b><math>1.10 \times 10^{-6}</math></b>
	Phosphodiesteres	0.12	0.10	13.11	1,100	<b><math>4.63 \times 10^{-4}</math></b>
	Protein (amide II)	0.31	0.30	44.19	1,100	<b><math>1.59 \times 10^{-9}</math></b>
	Saturated Fatty Acids	0.40	0.40	67.34	1,100	<b><math>8.18 \times 10^{-13}</math></b>
	Silica	0.01	0.00	1.18	1,100	0.28
	Unsaturated Fatty Acids	0.07	0.06	7.97	1,100	<b><math>5.74 \times 10^{-3}</math></b>

# Chapter 6

## Ocean acidification alters the nutritional value of Antarctic diatoms

*Published in* New Phytologist *as:*

**Duncan, R. J.**, Nielsen, D. A., Sheehan, C. E., Deppeler, S., Hancock, A. M., Schulz, K. G., Davidson, A. T., & Petrou, K. (2022). Ocean acidification alters the nutritional value of Antarctic diatoms. *New Phytologist*, 233(4), 1813-1827. DOI: 10.1111/nph.17868

*Author contributions:*

A.T.D and K.P. conceptualised the study and K.P. determined the methodology. C.E.S., S.D., A.M.H., K.G.S., A.T.D. and K.P. undertook the investigation and D.N. was responsible for data curation. R.J.D. performed the formal analysis, data visualisation and wrote the original draft. D.N., S.D., A.M.H., K.G.S., A.T.D. and K.P. reviewed and edited the original draft. K.P. assisted with data visualisation and was responsible for supervision of R.J.D. A.T.D and K.P. were responsible for funding acquisition.

Production Note: Signature removed prior to publication.	Production Note: Signature removed prior to publication.	Production Note: Signature removed prior to publication.	Production Note: Signature removed prior to publication.	Production Note: Signature removed prior to publication.	Production Note: Signature removed prior to publication.	Production Note: Signature removed prior to publication.	Production Note: Signature removed prior to publication.
R. Duncan	D. Nielsen	C.E. Sheehan	S. Deppeler	A.M. Hancock	K.G. Schulz	A.T. Davidson	K. Petrou

Chapter 6 presents data from a mesocosm study which exposed a natural pelagic community to a range of ocean acidification (OA) scenarios, providing a species-specific snapshot into the effects of OA on Southern Ocean diatoms. This chapter was the result of a contingency plan after scheduled fieldwork was cancelled during the global travel shutdown of the COVID-19 pandemic in 2020. It is a valuable addition to the previous chapters, as it provides an important Southern Ocean perspective and investigates pelagic taxa, which are the principal players in primary production. In addition, through experimental manipulation on natural communities, this research allowed for investigation into the effects of OA on microalgal biomolecular content, which is a persistent and ubiquitous environmental threat.

**Abstract**

Primary production in the Southern Ocean (SO) is dominated by diatom-rich phytoplankton assemblages, whose individual physiological characteristics and community composition are strongly shaped by the environment, yet knowledge on how diatoms allocate cellular energy in response to ocean acidification (OA) is limited. Understanding such changes in allocation is integral to determining the nutritional quality of diatoms and the subsequent impacts on the trophic transfer of energy and nutrients. Using synchrotron-based FTIR-microspectroscopy, we analysed the macromolecular content of selected individual diatom taxa from a natural Antarctic phytoplankton community exposed to a gradient of  $f\text{CO}_2$  levels (288 – 1263  $\mu\text{atm}$ ). Strong species-specific differences in macromolecular partitioning were observed under OA. Large taxa showed preferential energy allocation towards proteins, while smaller taxa increased both lipid and protein stores at high  $f\text{CO}_2$ . If these changes are representative of future Antarctic diatom physiology, we may expect a shift away from lipid rich large diatoms towards a community dominated by smaller taxa, but with higher lipid and protein stores than their present-day contemporaries, a response that could have cascading effects on food web dynamics in the Antarctic marine ecosystem.

## **Introduction**

Ocean acidification (OA) is one of the most prodigious and ubiquitous threats to the structure and function of marine life (Hancock et al., 2020; Kroeker et al., 2013; Ross et al., 2011). Since the beginning of the industrial era, the world's oceans have sequestered ~30 % of anthropogenic CO<sub>2</sub> emissions (Denman et al., 2007; Le Quéré et al., 2018; Sabine et al., 2004). As a result, the average ocean surface water pH has fallen from approximately 8.21 to 8.10 (IPCC, 2014), equivalent to a 29% increase in hydrogen ion (H<sup>+</sup>) concentrations. If CO<sub>2</sub> emissions continue unabated (RCP8.5), atmospheric CO<sub>2</sub> concentrations are estimated to rise from the current ~410 ppmv to >1000 ppmv by 2100 (IPCC, 2014), with the average ocean pH expected to further decline by up to 0.4 pH units (IPCC, 2014). The cold waters of the Southern Ocean (SO) result in higher than average CO<sub>2</sub> uptake in this region (Frölicher et al., 2015; Khatiwala et al., 2009) and the naturally low saturation state (McNeil & Matear, 2008) renders the Antarctic marine ecosystem and its biota immediately vulnerable to the effects of OA.

Phytoplankton provide the nutritional base that underpins the wealth of life in the oceans. Their growth and productivity have been shown to be positively (Baragi et al., 2015; Chen et al., 2015; Tew et al., 2014; Wu et al., 2010), negatively (Chen & Durbin, 1994; Hoppe et al., 2015; Shi et al., 2017) and neutrally (Beardall & Raven, 2004; Berge et al., 2010) affected by increased CO<sub>2</sub> concentrations. Similarly, no definitive taxonomic or size-related shifts in phytoplankton community composition in response to OA have been determined (Bach & Taucher, 2019; Eggers et al., 2014; Feng et al., 2010; Feng et al., 2009; Nielsen et al., 2010). This variability in phytoplankton community response to CO<sub>2</sub> has been suggested to result from differences in the concentrations tested, where low CO<sub>2</sub> enhancement promotes growth with increased passive transfer of CO<sub>2</sub> for photosynthesis, while higher CO<sub>2</sub> inhibits growth in some taxa, possibly due to high energy costs associated with greater dependence on H<sup>+</sup> pumps (Deppeler et al., 2018; Paul & Bach, 2020). Nevertheless, the range in CO<sub>2</sub>-driven responses to productivity and community composition, highlights the presence of interspecific differences in tolerance. Thus, uncovering the tolerance and thresholds of individual species is essential for understanding species and community responses to the projected ocean acidification.

In pelagic food webs, the effects of small changes in nutrient availability at the primary production level can have broad, cascading effects on higher trophic organisms (Moline

et al., 2001). Lipids, which are the most energy rich macromolecules, contain much of the energy that is transferred among trophic levels (Hagen & Auel, 2001). Adequate lipid supply has been shown to be critical to the survival and reproduction of zooplankton (Graeve et al., 1994; Lee et al., 2006), particularly for Antarctic krill (Hagen & Auel, 2001) that require large lipid reserves over winter when primary production is scarce. Proteins are also a key source of energy (Hagen & Auel, 2001), the predominant source of amino acids (Ruess & Müller-Navarra, 2019), and a cellular nitrogen reservoir (Finkel et al., 2016) for higher trophic levels. Macromolecular stores of primary producers are the cornerstone of productive marine ecosystems and changes in the partitioning of critical macromolecules contained in phytoplankton, such as proteins and lipids, inevitably alters the supply of energy and essential compounds to higher trophic levels.

Diatoms dominate much of the primary production in the Southern Ocean (Eggers et al., 2014; Wolf et al., 2013; Wright et al., 2010), particularly in coastal areas and along sea-ice margins (Kang & Fryxell, 1993; Wright et al., 2010). Diatoms form dense, siliceous cell walls known as frustules by converting soluble silicic acid into biogenic silica (Martin-Jézéquel et al., 2000). These frustules provide the cell with ballast (Tréguer et al., 2018), and afford the cell some defence against grazers (Hamm et al., 2003). Despite this protective armour, the relatively high growth rates and generally larger cell sizes make diatoms a favourite food source for krill and other large zooplankton, delivering both quality and quantity of proteins and lipids necessary for growth and reproduction (Bhavya et al., 2019; Cowles et al., 1988; Litchman et al., 2007). Indeed, Antarctic krill and copepods have been shown to selectively feed on diatoms (Cowles et al., 1988; Haberman et al., 2003; Head & Harris, 1994; Turner et al., 2001) with a strong preference for less silicified diatoms, which have been shown to benefit copepod growth rate, egg production and hatching (Liu et al., 2016). Enrichment of seawater with CO<sub>2</sub> has been shown to stimulate carbon fixation in diatoms, thereby reducing the nutrient content relative to carbon (Bellerby et al., 2008; Engel et al., 2008; Urabe et al., 2003) and thus food quality for zooplankton, yet little is known about the effects of OA on diatom macromolecular composition. In one study, acidification (750  $\mu$ atm) resulted in a decline in total fatty acids (FAs) in the discoid centric diatom *Thalassiosira weissflogii* that translated to a 10-fold decline in FAs in the fed copepods, causing significant declines in copepod somatic growth and egg production (Rossoll et al., 2012). Given the importance of the diatom-zooplankton link in the Antarctic pelagic food web, these results emphasise

the importance for understanding how OA may influence the nutritional quality of key primary producers.

Understanding which species within the phytoplankton community are affected by environmental change requires a depth of study that broader community analyses do not provide. Single-cell analyses on natural mixed communities provides a unique insight into the extent to which a member of the community is affected, delivering unprecedented detail on potential physiological and ecological implications. In a parallel study on the same phytoplankton community, we used single-cell analyses to investigate the effects of OA on the silicification rates of several Antarctic marine diatoms from within a natural mixed community (Petrou et al., 2019). This study uncovered species-specific sensitivities to acidification and revealed a potential threat of OA to diatoms. In another study, single-cell analyses were used to differentiate diatoms from contrasting Antarctic marine habitats based on the taxonomic-specific macromolecular fingerprint (Sheehan et al., 2020). However, to date, no study has looked at the macromolecular profiles of individual diatoms from a natural, phytoplankton assemblage in response to increasing CO<sub>2</sub> concentration. Knowledge of species-specific macromolecular partitioning under high CO<sub>2</sub> may help elucidate potential changes to the nutritional quality of primary producers and in combination with information on lower trophic feeding links, may refine our understanding of the role of diatoms in secondary production.

Using Synchrotron-based Fourier Transform InfraRed (FTIR) microspectroscopy, we determine the macromolecular composition of selected Antarctic marine diatoms from amongst a natural community following 18-days exposure to different  $f\text{CO}_2$  levels, delivering a snapshot of carbon partitioning as a response to ocean acidification. In our experiment, large volume mesocosms were used, ensuring the inclusion of the entire microbial community –phytoplankton, bacteria, viruses– and the influence of these interactions (predation, competition) among and between these trophic levels, improving our ability to extrapolate to natural systems (Cottingham et al., 2005; Kreyling et al., 2018). Further, by exposing the communities to a gradient of increasing  $f\text{CO}_2$ , we enhance the predictive strength of our data (Havenhand et al., 2010). Through single-cell analyses, we show differential effects of OA on the partitioning of macromolecules by individual diatom taxa, offering insight into potential implications of  $f\text{CO}_2$ -induced changes to energy availability and transfer through the Antarctic marine food web.



## **Materials and Methods**

### **Experimental Design and Mesocosm Set Up**

Mesocosm set up and conditions were as described previously (Deppeler et al., 2018; Hancock et al., 2018; Petrou et al., 2019; Table S6.1). Briefly, a near-shore, natural Antarctic microbial community was collected from an ice-free area among broken fast ice approximately 1 km offshore from Davis Station, Antarctica (68° 35' S, 77° 58' E) on 19 November 2014. This community was incubated in 6 x 650 L polyurethane tanks (mesocosms) across a gradient of  $f\text{CO}_2$  levels (343, 506, 634, 953, 1140 and 1641  $\mu\text{atm}$ ; denoted M1 – M6). These  $f\text{CO}_2$  levels corresponded to pH values ranging from 8.17 to 7.57 (Table S6.1). The seawater was initially gravity fed through a 200  $\mu\text{m}$  Arkal filter to exclude metazooplankton. Unavoidably, this filtration may also have removed some of the larger chain-forming diatom taxa as well. Temperature was maintained at  $0.0\text{ }^\circ\text{C} \pm 0.5\text{ }^\circ\text{C}$  and the mesocosms were stirred continuously by a central auger (15 r.p.m.) for gentle mixing and covered with an air-tight lid. Irradiance was initially kept low ( $0.8 \pm 0.2\ \mu\text{mol photons m}^{-2}\text{s}^{-1}$ ), while cell physiology was left to acclimate to increasing  $f\text{CO}_2$  levels (over 5 days). When target  $f\text{CO}_2$  levels were reached in all six mesocosms, light was gradually increased (days 5-8) to  $89 \pm 16\ \mu\text{mol photons m}^{-2}\text{s}^{-1}$  on a 19 h:5 h light:dark cycle, to mimic current natural conditions. To generate the gradient in carbonate chemistry, filtered seawater saturated with  $\text{CO}_2$  was added to five of the mesocosms. One mesocosm remained at ambient levels, with regular filtered seawater (unenriched with  $\text{CO}_2$ ), to control for the physical disturbance and dilution from the  $\text{CO}_2$ -enriched seawater additions to the other mesocosms. Daily measurements were taken to monitor pH and dissolved inorganic carbon (DIC). The former was measured using the indicator dye m-cresol purple on a GBC UV-vis 916 spectrophotometer in a 10 cm temperature-controlled ( $25\text{ }^\circ\text{C}$ ) cuvette (Dickson et al., 2007). DIC was measured on an Apollo SciTech AS-C3 by infrared absorption and calibrated against certified reference material batch CRM127 (Dickson, 2010). Practical alkalinity (PA) was calculated at  $25\text{ }^\circ\text{C}$ , as per Deppeler et al., (2018). For details of  $f\text{CO}_2$  manipulations, analytical procedures and calculations see Deppeler et al., (2018). Samples for physiological and macromolecular measurements in this study were taken on day 18, at the end of the incubation period (Deppeler et al., 2018).

### Macronutrient analyses

Samples for macronutrient concentration for this study were obtained from each mesocosm on day 18, filtered through 0.45 µm cellulose ester filters (Millipore) and frozen at -20 °C. Concentrations of nitrate + nitrite (NO<sub>x</sub>), soluble reactive phosphorus (SRP) and molybdate re-active silica (hereafter, silica) were determined following analysis described previously (Davidson et al., 2016). Operational detection limits for NO<sub>x</sub>, SRP and Si were 0.14, 0.10 and 1.66 µM, respectively.

### Diatom Community Structure

Samples for community structure and abundance were collected from each mesocosm on days 1, 3, 5, 8, 10, 12, 14, 16 and 18. These were microscopically analysed within two years of collection as described in Hancock et al., (2018). Briefly, between 2 and 10 mL of refrigerated Lugol's concentrated fixed samples were placed in an Utermöhl cylinder (Hydro-Bios) and cells allowed to settle overnight. A stratified counting procedure was employed to capture both small and large cells, with all cells > 20 µm identified and quantified at 200× magnification, whilst those < 20 µm were assessed at 400× magnification. Size categories were established via visual inspection with assistance of a graticule in the ocular or the light microscope. To determine growth condition (active or stationary) closest to time of macromolecular profiling (day 18), cell counts from days 14-18 for each taxon from each mesocosm (see Hancock et al., 2018) were used to estimate specific growth rates on day 18 (for complete growth curves, see Hancock et al., 2018). Due to limitations in species identification for some taxa during FTIR microspectroscopy measurements, some species were grouped. Selected taxa for determination of macromolecular composition in this study included *Chaetoceros* spp. (predominantly comprised of chains of *C. castracanei*, but also *C. tortissimus* and *C. bulbosus*), *Fragilariopsis cylindrus*, *Proboscia truncata*, *Stellarima microtrias* and large Discoid centric (>20 µm) diatoms (including *Thalassiosira ritscheri* and unidentified large discoid centric diatoms (>20 µm), predominantly from the genus *Thalassiosira*). These taxa were selected for analyses, as they were the most prevalent large (>10-15 µm) diatoms to be found in all six tanks (Hancock et al., 2018; Table S6.3) and together, they represent up to 11% of the diatom dominated community (Hancock et al., 2018; Table S6.3). While their numerical contribution may be relatively minor, being the largest cells within the community, their contribution to the community macromolecular pool is

significant. Furthermore, in analysing multiple taxa, we can uncover potential response diversity of macromolecular partitioning in diatoms to ocean acidification.

### **Cell Volume and Photophysiological Status**

Cell volume was determined for selected taxa from M1 and M6 via light microscopy. Cells were imaged on a calibrated microscope (Nikon Eclipse Ci-L, Japan) and length, width and height (24-77 cells per taxa) determined using ImageJ software (Schneider et al., 2012). Biovolume was then calculated according to the cell morphology and corresponding equations described by Hillebrand et al. (1999). To establish photophysiological status of individual taxa, maximum quantum yield of Photosystem II ( $F_v/F_m$ ) was measured on individual cells as described in Petrou et al., (2019). Briefly, mesocosm samples were loaded into a flow cell (Biotech) and chlorophyll-*a* fluorescence measurements made on randomly selected diatom cells using a pulse amplitude modulated fluorometer (Imaging PAM IMAG-K4, Walz GmbH, Germany) mounted on a compound microscope (AxioStar plus, Zeiss, Germany). Following 10 min dark-adaptation, minimum fluorescence was recorded and then a saturating pulse of light was applied (SP width = 0.8s; SP intensity = 10; using the special SP-routine) to obtain maximum fluorescence. From these two parameters  $F_v/F_m$  was calculated. All measurements were taken at x200 magnification, with blue excitation light (440 nm) and at 0 °C.

### **Species-specific Macromolecular Content by FTIR**

The macromolecular composition of the selected diatom taxa sampled from all six mesocosms on day 18 was determined using Synchrotron based FTIR microspectroscopy on formalin-fixed (2% v/v final concentration) cells. Samples were fixed directly after being taken from the mesocosm, kept refrigerated and analysed within nine months. Measurements were made on hydrated cells, a method shown to limit light scattering effects (Bambery et al., 2012) and processed according to previous studies (Sackett et al., 2014; Sackett et al., 2013; Sheehan et al., 2020). Briefly, fixed cells were loaded directly onto a micro-compression cell with a 0.3 mm thick CaF<sub>2</sub> window (Tobin et al., 2010). Spectral data of individual cells (between 15-49 cells per taxon per mesocosm; Table S6.2) were collected in transmission mode, using the Infrared Microspectroscopy Beamline at the Australian Synchrotron, Melbourne, in November 2015. Spectra (one per cell) were acquired over the measurement range 4000– 800 cm<sup>-1</sup> with a Vertex 80v FTIR

spectrometer (Bruker Optics) in conjunction with an IR microscope (Hyperion 2000, Bruker) fitted with a mercury cadmium telluride detector cooled with liquid nitrogen. To reduce water vapor interference, the microscope stage was contained within a box flushed with dehumidified air. Co-added interferograms ( $n = 64$ ) were collected at a wavenumber resolution of  $6 \text{ cm}^{-1}\text{s}$ . To allow for measurements of individual cells, all measurements were made in transmission mode, using a measuring area aperture size of  $5 \times 5 \text{ }\mu\text{m}$ . Spectral acquisition and instrument control were achieved using Opus 6.5 software (Bruker). All cells were identified and inspected visually to ensure consistency across spectral measurements. In cases where the taxon was much larger than the aperture, three scans from different areas of the cell were taken and averaged, ensuring full coverage of cellular components.

Normalised spectra of biologically relevant regions revealed absorbance bands representative of key macromolecules, from which five previously verified band assignments were selected for comparison within taxon and treatment (Table 6.1). In this study, the amide II band ( $\sim 1540 \text{ cm}^{-1}$ ) was used as an indicator of cellular protein content, as the other major protein band, amide I was masked by water absorption. Lipids were primarily determined using the integrated peak of the ester carbonyl from lipids ( $\sim 1745 \text{ cm}^{-1}$ ) as described previously (Heraud et al., 2005), but with associated changes to saturated fatty acids. Carbohydrates were not measured, as the silica from diatoms overlaps with these bands.

### **Data Analyses**

Infra-red spectral data were analysed using custom made scripts in R (RStudio Team 2021). The regions of  $3050\text{-}2800$ ,  $1770\text{-}1100 \text{ cm}^{-1}$ , which contain the major biological bands (Table 6.1), were selected for analysis. Spectral data were smoothed (4 pts either side) and second derivative (3rd order polynomial) transformed using the Savitzky-Golay algorithm from the *prospectr* package in R (Stevens & Ramirez-Lopez, 2014) and then normalised using the method of Single Normal Variate (SNV). Macromolecular content for individual taxon was estimated based on integrating the area under each assigned peak (Table 6.1), providing metabolite content according to the Beer-Lambert Law, which assumes a direct relationship between absorbance and relative analyte concentration (Wagner et al., 2010).

**Table 6.1:** Infrared (IR) band assignments for FTIR microspectroscopy used in this study.

Wave number (cm <sup>-1</sup> )	Frequency Range (cm <sup>-1</sup> )	Assignment	Compound Label	Reference
~2920	2939-2912	$\nu_{as}(\text{C-H})$ from methylene ( $-\text{CH}_2$ )	Saturated fatty acids	(Vongsvivut et al., 2012)
~1745	1745-1734	$\nu(\text{C=O})$ of ester functional groups, from membrane lipids and fatty acids	Ester carbonyl	(Murdock & Wetzel, 2009; Vongsvivut et al., 2012)
~1545	1556-1540	$\delta(\text{N-H})$ of amides associated with protein	Protein (amide II)	(Giordano et al., 2001)
~1452	1457-1446	$\delta_{as}(\text{CH}_3)$ and $\delta_{as}(\text{CH}_2)$ of proteins	Free amino acid	(Petrou et al., 2018)
~1375	1340-1407	$\Delta_s(\text{CH}_3)$ and $\delta_s(\text{CH}_2)$ of proteins, and $\nu_s(\text{C-O})$ of $\text{COO}^-$ groups (carboxylic group)	Carboxylates	(Giordano et al., 2001)

Regression analyses were used to explore the functional relationships between  $f\text{CO}_2$  and macromolecular content. Because of their superior interpolation potential, gradient designs are generally considered more useful for model parameterisation (Havenhand et al., 2010). They are also deemed more effective at exposing response patterns to environmental perturbation than replicated designs (Cottingham et al., 2005; Kreyling et al., 2018; Riebesell & Gattuso, 2015). Integrated peak areas provide relative changes in macromolecular content between samples. Because of the differences in absorption properties of macromolecules, peak areas can only be used as relative measure within compounds. Therefore, peak areas were visualised using free axes to improve readability and discourage comparison between macromolecules. To determine significant relationships between macromolecular content and  $f\text{CO}_2$  level, a linear regression at each  $f\text{CO}_2$  level ( $\pm 95\%$  confidence interval) was applied to each taxon. In cases where the data were poorly explained by a linear fit, a second order polynomial regression was applied. The Shapiro-Wilks (Shapiro & Wilk, 1965) test for normality showed the data required  $\log_{10}$  transformation before analysis. Regressions were tested for overall model significance using the F statistic ( $p < 0.05$ ) and strength of fit using  $R^2$ . The residuals of all regressions were verified for homoscedasticity. All analyses were performed using R

Studio Version 1.3.959 (RStudio Team 2021) and the add-on packages ggplot2 version 2.2.1 (Wickham et al., 2016) and dplyr version 1.0.0 (Wickham et al., 2020).

## **Results**

### **Chemistry, Cell Density and Photophysiology**

There was significant drawdown of macronutrients from phytoplankton growth in the mesocosms by day 18. NO<sub>x</sub> concentration began to decline from day 10, but did not fall below the limits of detection in any tank until day 18 (Deppeler et al., 2018). By day 18, SRP was lowest (0.10 µM) in M1 (control) and highest (0.19 µM) in M6 (highest *f*CO<sub>2</sub> treatment), whilst silica concentrations ranged from 85 µM (M3) – 99 µM (M6). Dissolved inorganic carbon (DIC) concentrations ranged from 2179 – 2360 µmol kg<sup>-1</sup> (M1- M6, respectively), matching a gradient in total pH from 8.17 to 7.57, while practical alkalinity (PA) remained relatively consistent across the pH gradient, dropping only 10 µmol kg<sup>-1</sup> (Table S6.1). Salinity and temperature were consistent across all mesocosms (Table S6.1).

For all species except *P. truncata*, cell abundance was lowest in the highest *f*CO<sub>2</sub> treatment with a general decreasing trend with increasing *f*CO<sub>2</sub> levels following a peak abundance at 427 µatm (Table S6.3). *P. truncata* had the lowest cell abundance at 547 µatm and peak abundance at 957 µatm. It is important to note that the five diatom taxa selected for this study comprised <11% of the total community in all *f*CO<sub>2</sub> treatments. Cell volume ranged from the 847±370 µm<sup>3</sup> for the smallest taxa, *Chaetoceros* spp., to 252 445±180 405 µm<sup>3</sup> for the largest taxa, Discoid centric (>20 µm) diatoms (Table S6.4). Broad indicators of the physiological state of the phytoplankton communities in the mesocosms showed that each community was photosynthetically active on day 18, where F<sub>v</sub>/F<sub>M</sub> values ranged between 0.61 and 0.70 (Table S6.3). There was however no apparent *f*CO<sub>2</sub> response.

### **Cell Specific Macromolecular Partitioning**

Spectral analyses revealed taxonomic differences in macromolecular content and diverse response patterns to acidification. Between 6-31% of the variance in macromolecular content was found to be explained by the variation in *f*CO<sub>2</sub> (Table S6.5). In *Chaetoceros* spp., all investigated macromolecules showed a u-shaped response to acidification, with an initial drop in macromolecular content at moderate *f*CO<sub>2</sub> enrichment, followed by an

increase towards maximum macromolecular content in cells grown at the highest  $f\text{CO}_2$  level (Fig. 6.1A-E; Table S6.5). This u-shaped pattern, although non-significant, was also observed in day 18 growth rates, where the *Chaetoceros* spp. in M3 and M4 had already entered stationary phase or were in decline (Fig. 6.1F). A consistent response pattern across all macromolecules was also detected for the pennate diatom *F. cylindrus*, but was the inverse of that seen for *Chaetoceros* spp., with an initial increase in macromolecular content with increased  $f\text{CO}_2$  and generally stabilising above 700  $\mu\text{atm}$ , indicating a possible threshold in  $f\text{CO}_2$ -induced synthesis of macromolecules (Fig. 6.2A-E; Table S6.5). Growth rates for *F. cylindrus* on day 18 were highest in M2-M4 and lower relative to M1 in the highest  $f\text{CO}_2$  conditions (Fig. 6.2F). In *P. truncata*, a positive relationship to increasing  $f\text{CO}_2$  was found for amide II, free amino acids, and carboxylates, with minimum protein content in cells from M1 and maximum protein content in cells from M6 (Fig. 6.3A-C; Table S6.5). In contrast, ester carbonyl and saturated fatty acids exhibited a bell-shaped response to  $f\text{CO}_2$ , with maximal lipid content at mid- $f\text{CO}_2$  (Fig. 6.3D-E; Table S6.5). We observed no significant effect of  $f\text{CO}_2$  on the growth rate of *P. truncata* (Fig. 6.3F).

The  $f\text{CO}_2$ -induced changes in macromolecules by the two discoid centric diatom groups, *S. microtrias* and the Discoid centric group, differed greatly among compounds with strong similarities in responses of the two taxa (Fig. 6.4, 6.5). For *S. microtrias*, protein from amide II exhibited a weak positive relationship ( $R^2 < 0.1$ ), while free amino acids showed a negative relationship and carboxylates a positive relationship with increasing  $f\text{CO}_2$  (Fig. 6.4A-C; Table S6.5). There was no response shown with saturated fatty acids, but a negative relationship was detected for ester carbonyl (Fig. 6.4D; Table S6.5). *S. microtrias* growth rates on day 18, showed the highest rate observed at the highest  $f\text{CO}_2$  level (Fig. 6.4F). For the large Discoid centric diatoms, protein showed a weak, but significant u-shaped relationship (Fig. 6.5A). Similar to *S. microtrias*, a negative relationship was observed in free amino acid (Fig. 6.5B; Table S6.5), while carboxylates exhibited a positive response to increasing  $f\text{CO}_2$  (Fig. 6.5C; Table S6.5). Negative relationships were observed with both ester carbonyl and saturated fatty acids (Fig. 6.5D-E; Table S6.5). These changes in macromolecular content occurred despite similar growth rates at all  $f\text{CO}_2$  concentrations (Fig 6.5F).

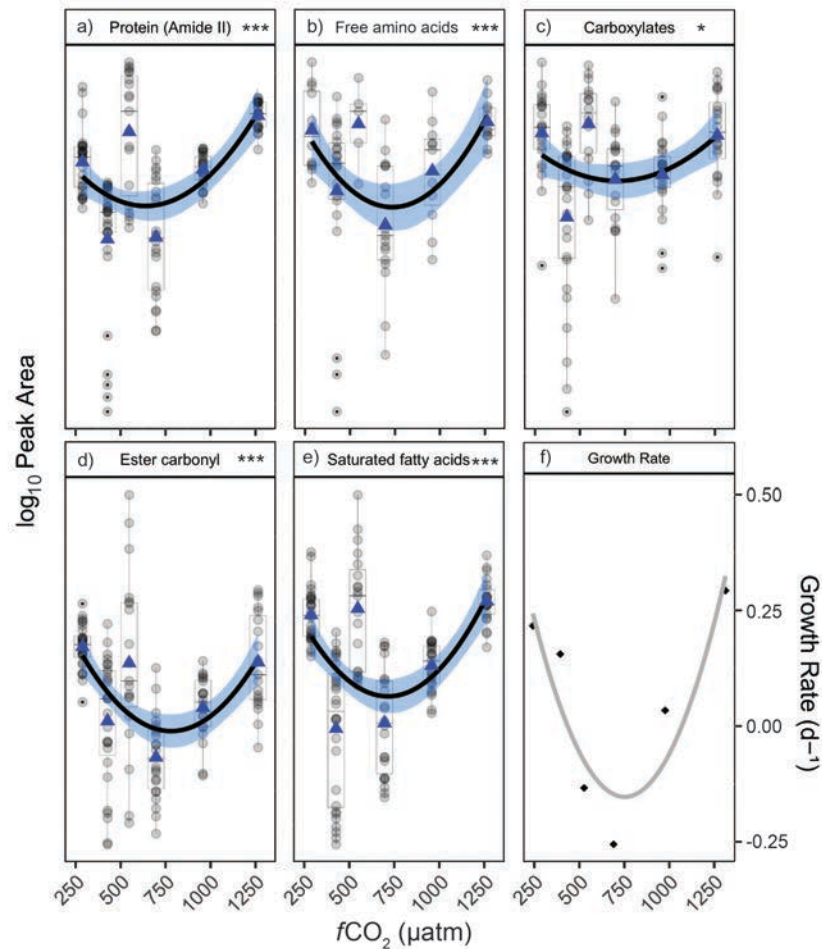


**Figure 6.1:** Cell specific macromolecular content (based on normalised peak areas) and growth rates for *Chaetoceros* spp.. (A-F) Relative content of selected macromolecules along an  $f\text{CO}_2$  gradient. Data are visualised using box plots with overlain grey dots showing the macromolecular content of individual cells from within  $f\text{CO}_2$  treatment mesocosm. Data are fitted with a second order polynomial regression, with 95% confidence intervals (dark blue shading), applied to log transformed data (\*  $p < 0.05$ , \*\*\*  $p < 0.0005$ ). The y-axis is free and units are arbitrary. Data means are displayed as blue triangles. (F) Growth rate ( $\text{d}^{-1}$ ) is displayed as diamonds, fitted with a second order polynomial regression (grey line).



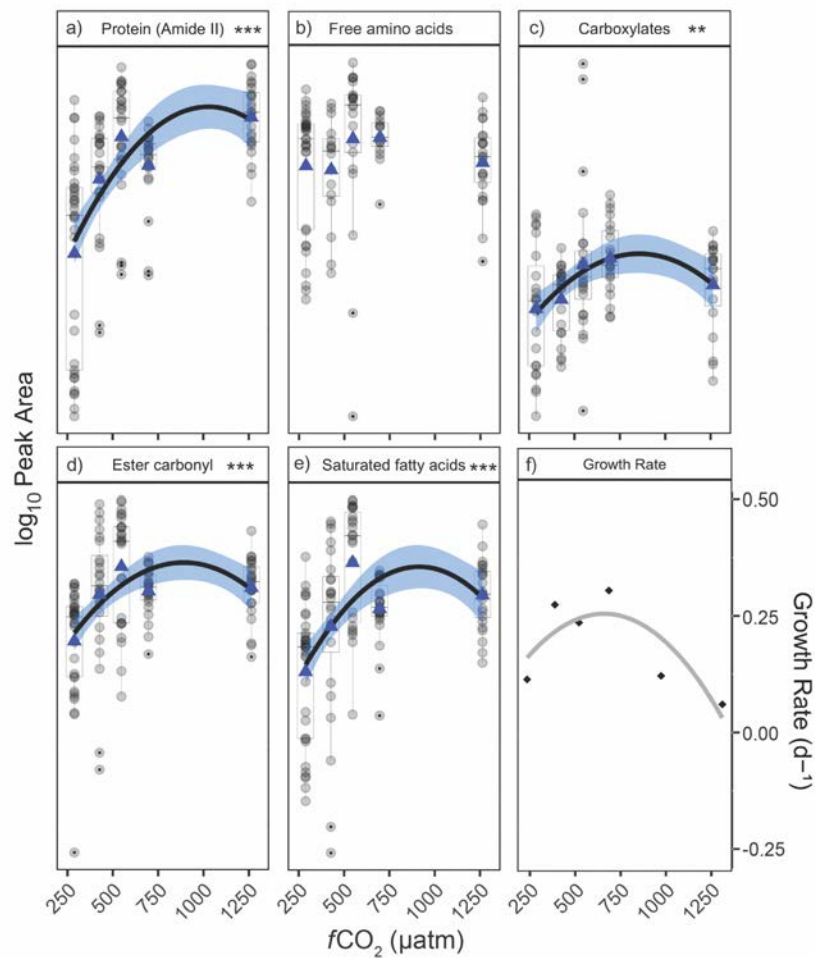


**Figure 6.2:** Cell specific macromolecular content (based on normalised peak areas) and growth rates for *Fragilariopsis cylindrus* (A-F) Relative content of selected macromolecules along an  $f\text{CO}_2$  gradient. Data are visualised using box plots with overlain grey dots showing the macromolecular content of individual cells from within  $f\text{CO}_2$  treatment mesocosm. Data are fitted with a second order polynomial regression, with 95% confidence intervals (dark blue shading), applied to log transformed data (\*\*  $p < 0.005$ , \*\*\*  $p < 0.0005$ ). The y-axis is free and units are arbitrary. Data means are displayed as blue triangles. (F) Growth rate ( $\text{d}^{-1}$ ) is displayed as diamonds, fitted with a second order polynomial regression (grey line).

## Lipid vs. Protein Content

To explore overall shifts in macromolecular partitioning we used the protein to lipid ratio, providing a snapshot of the principle changes to carbon allocation by the cell (Heraud et al., 2005). Lipids were positively correlated with protein in *Chaetoceros* spp. (Fig. 6.6A; Table S6.6), *F. cylindrus* (Fig. 6.6B; Table S6.6) and *P. truncata* (Fig. 6.6C; Table S6.6). Despite some grouping associated with an increase in protein with the highest  $f\text{CO}_2$  treatment, the lipid to protein ratio was largely unaffected by  $f\text{CO}_2$  in these taxa. We found no relationship between lipid and protein content for the two large discoid centric taxa, *S. microtrias* and Discoid centrics (Fig. 6.6D-E; Table S6.6).

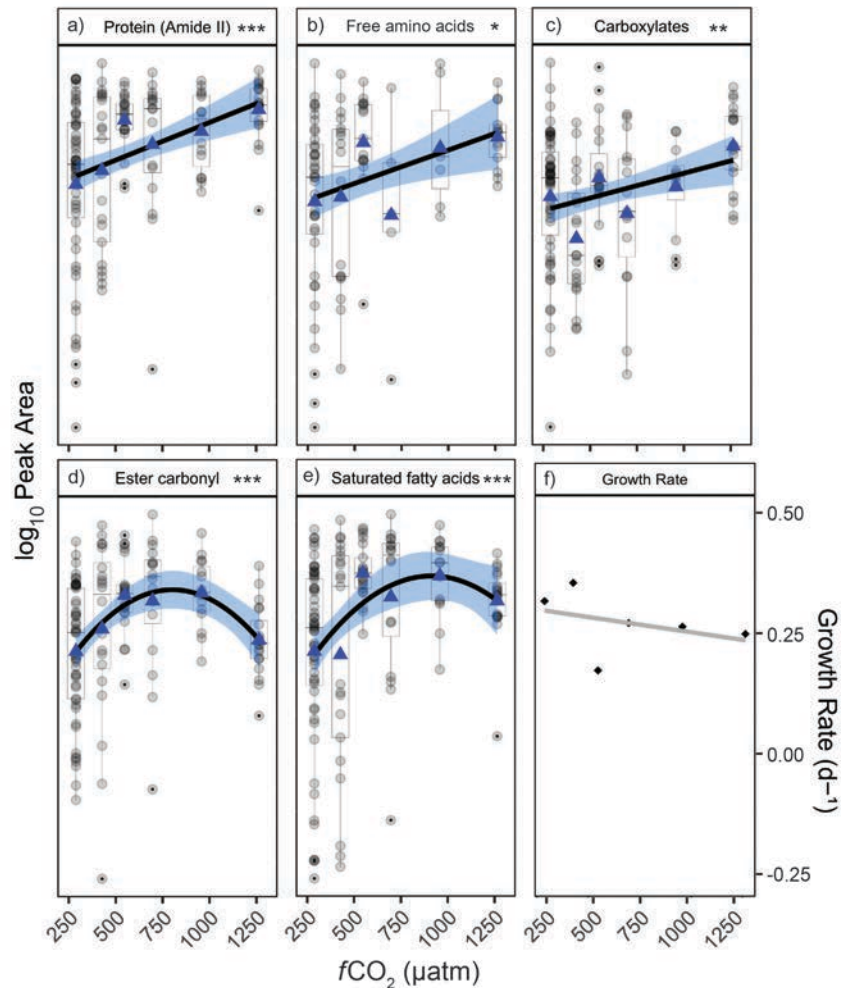


**Figure 6.3:** Cell specific macromolecular content (based on normalised peak areas) and growth rates for *Proboscia truncata* (A-F) Relative content of selected macromolecules along an  $f\text{CO}_2$  gradient. Data are visualised using box plots with overlain grey dots showing the macromolecular content of individual cells from within  $f\text{CO}_2$  treatment mesocosm. Data are fitted with a linear or a second order polynomial regression, with

95% confidence intervals (dark blue shading), applied to log transformed data (\*  $p < 0.05$ , \*\*  $p < 0.005$ , \*\*\*  $p < 0.0005$ ). The y-axis is free and units are arbitrary. Data means are displayed as blue triangles. **(F)** Growth rate ( $d^{-1}$ ) is displayed as diamonds, fitted with linear regression (grey line).

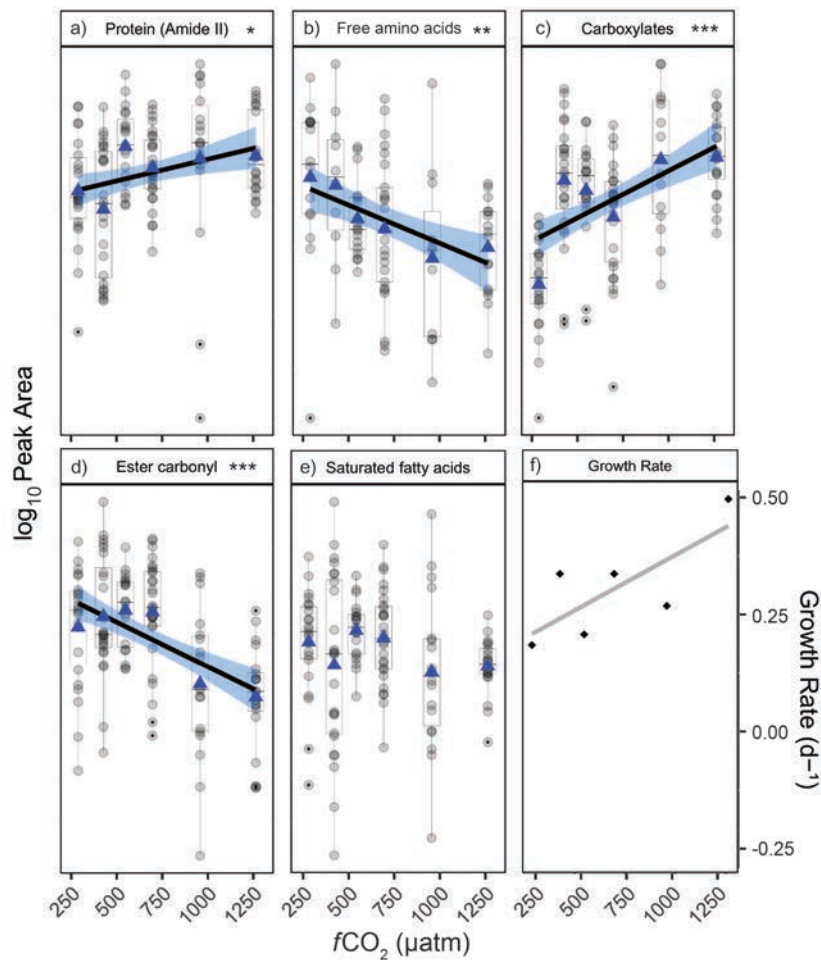


**Figure 6.4:** Cell specific macromolecular content (based on normalised peak areas) and growth rates for *Stellarima microtrias* (A-F). Relative content of selected macromolecules along an  $fCO_2$  gradient. Data are visualised using box plots with overlain grey dots showing the macromolecular content of individual cells from within  $fCO_2$  treatment mesocosm. Data are fitted with linear regression, with 95% confidence intervals (dark blue shading), applied to log transformed data (\*  $p < 0.05$ , \*\*  $p < 0.005$ , \*\*\*  $p < 0.0005$ ). The y-axis is free and units are arbitrary. Data means are displayed as blue triangles. **(F)** Growth rate ( $d^{-1}$ ) is displayed as diamonds, fitted with linear regression (grey line).

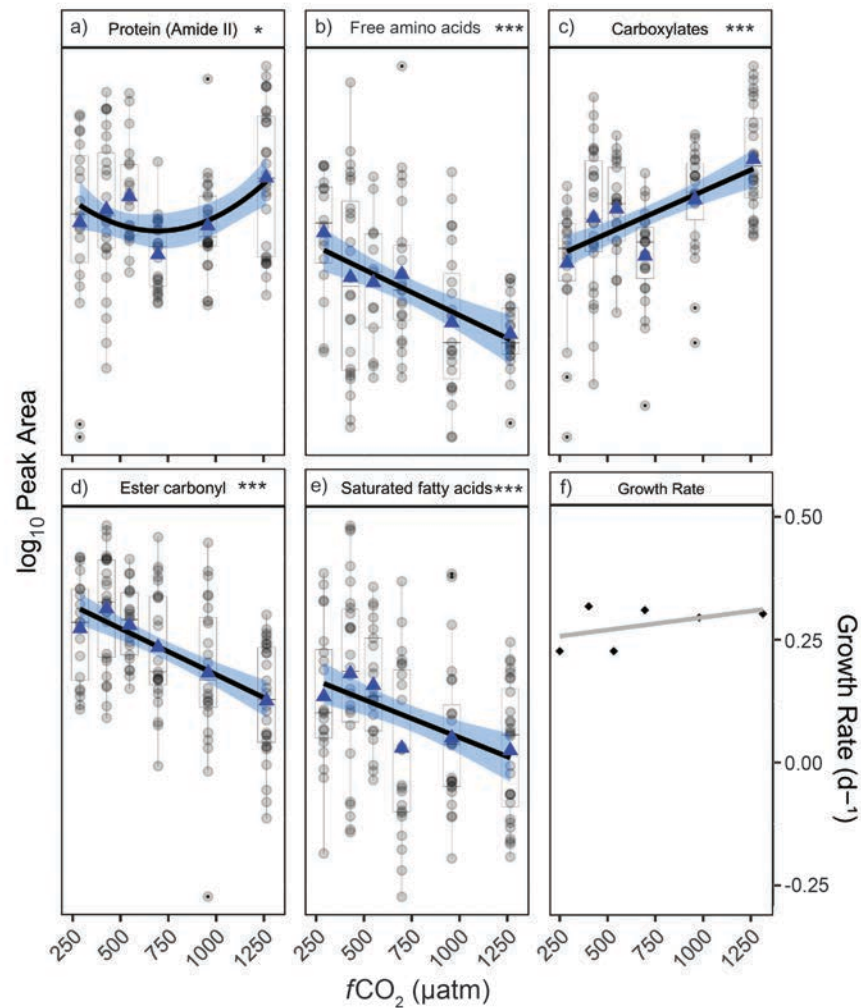


**Figure 6.5:** Cell specific macromolecular content (based on normalised peak areas) and growth rates for *Discoid centric diatoms*  $>20 \mu\text{M}$  (A-F). Relative content of selected macromolecules along an  $f\text{CO}_2$  gradient. Data are visualised using box plots with overlain grey dots showing the macromolecular content of individual cells from within  $f\text{CO}_2$  treatment mesocosm. Data are fitted with linear or second order polynomial regression, with 95% confidence intervals (dark blue shading), applied to log transformed data (\*  $p < 0.05$ , \*\*\*  $p < 0.0005$ ). The y-axis is free and units are arbitrary. Data means are displayed as blue triangles. (F) Growth rate ( $\text{d}^{-1}$ ) is displayed as diamonds, fitted with linear regression (grey line).

### Cell Volume vs. Lipid and Protein Content

Under the lowest  $f\text{CO}_2$  (M1), there was a positive relationship between mean taxon-specific cell volume and protein (Fig. 6.7A; Table S6.7, S6.8), however no relationship was observed for lipid (ester carbonyl) content (Fig. 6.7B; Table S6.7, S6.8). We did, however, find positive relationships between the mean cell volume and protein content (Fig. 6.7C; Table S6.7, S6.8) and a bell-shaped relationship between mean cell volume and lipid content in the highest  $f\text{CO}_2$  treatment (M6) (Fig. 6.7D; Table S6.7, S6.8).

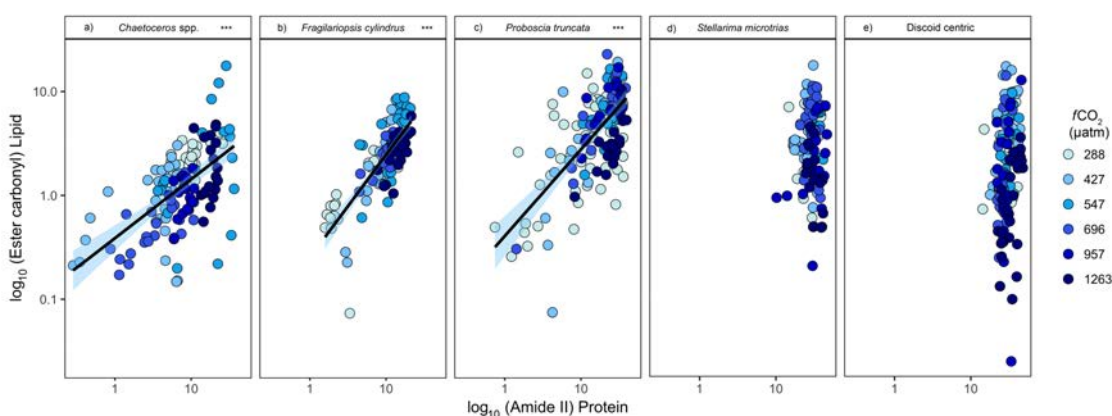


**Figure 6.6:** Lipid (ester carbonyl) to protein (amide II) ratios for (A) *Chaetoceros* spp., (B) *Fragilariopsis cylindrus*, (C) *Proboscia truncata*, (D) *Stellarima microtrias* and (E) *Discoid centric* diatoms  $>20 \mu\text{M}$ . All data are  $\log(10)$  transformed.  $f\text{CO}_2$  ( $\mu\text{atm}$ ) levels are represented by colour. Data are fitted with linear regression, with 95% confidence intervals (blue shading).

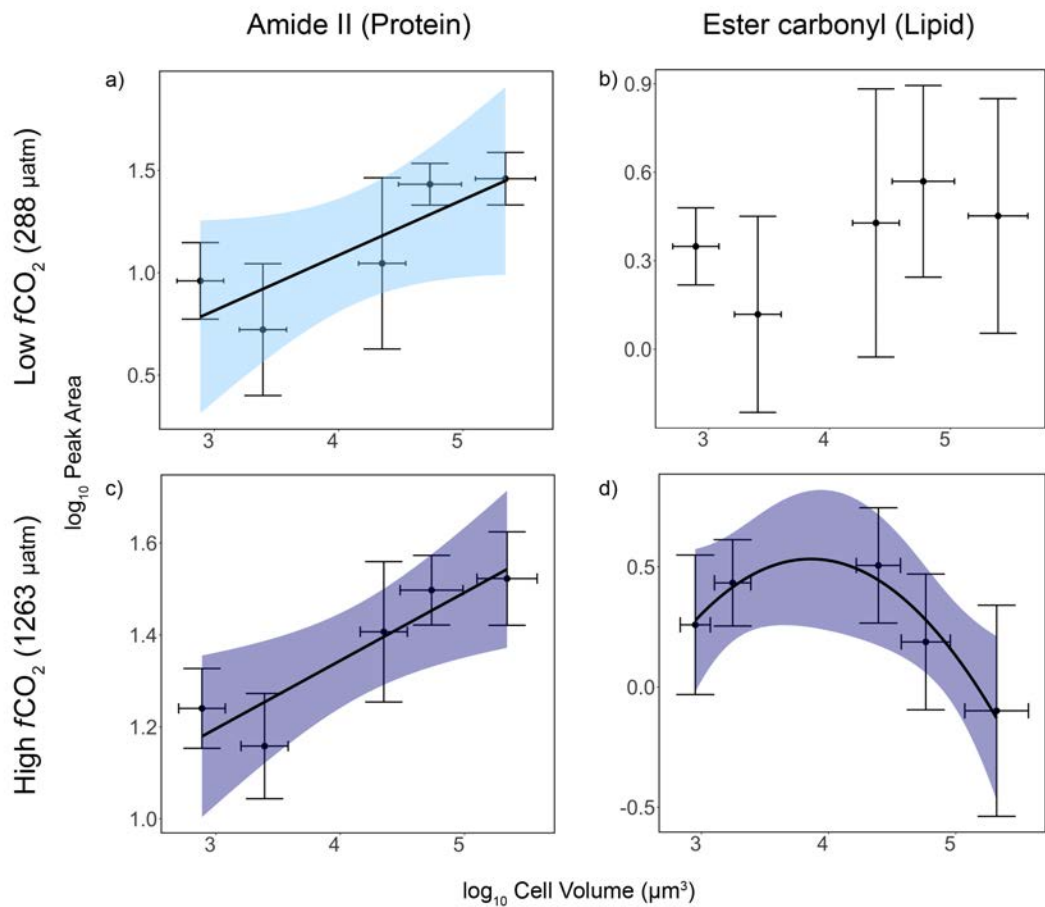


**Figure 6.7:** Cell volume ( $\mu\text{m}^3$ ) and protein (amide II) or lipid (ester carbonyl) content; (A) – (B) for diatoms in the low  $f\text{CO}_2$  treatment (288  $\mu\text{atm}$ ) and (C) – (D) high  $f\text{CO}_2$  treatment (1263  $\mu\text{atm}$ ). Data have been  $\log(10)$  transformed and fitted with linear or a second order polynomial regression with 95% confidence intervals (shading). The data represent mean  $\pm$  SD ( $n > 19$ ), with all regressions applied to the mean.

### Discussion

The diatom-zooplankton link of the food chain is the foundation of a productive marine ecosystem, whereby changes to food quality at the primary production level can have broad consequences for energy transfer through the food web (Arrigo, 2005; Rossoll et al., 2012). The effects of anthropogenic environmental change are already manifesting in some physicochemical properties of the ocean, including declining pH and increasing sea surface temperatures (Gille, 2002; IPCC, 2014). These changes are expected to be accelerated in the SO (Deppeler & Davidson, 2017; Larsen et al., 2014), where ocean pH is projected to exceed levels used in M3 before the end of the century (McNeil & Matear,

2008). Ocean acidification has been shown to influence the biochemical compositions of primary producers, and their subsequent nutrient transfer to higher trophic levels, potentially disrupting marine food webs (Jin et al., 2020; Nagelkerken et al., 2020). This study presents a snapshot of changes to macromolecular stores in Antarctic diatoms in response to short-term exposure to increases in  $f\text{CO}_2$ . We found that elevated  $f\text{CO}_2$  concentrations altered the way diatoms partition macromolecular content and that this partitioning differed among taxa, revealing some size-dependent relationships. Given the short duration of the study (18 days), it is unclear whether these results would be different under longer-term exposure, however, these data provide insight into the short-term response diversity within diatoms to acidification. Species-specific differences in resource partitioning between macromolecule storage, photosynthesis and growth, ultimately determine the quality and quantity of food available for higher trophic levels (Arrigo, 2005; Sackett et al., 2016). It has been shown that acidifying ocean conditions can select for both small ( $<20 \mu\text{m}$ ) (Brussaard et al., 2013; Davidson et al., 2016; Hoppe et al., 2015; Hoppe et al., 2017; Husherr et al., 2017; Sugie et al., 2020) and large ( $> 20 \mu\text{m}$ ) diatoms (Bach & Taucher, 2019; Eggers et al., 2014; Feng et al., 2010; Tortell et al., 2008) depending on the starting community, duration of exposure and  $\text{CO}_2$  concentrations, and Southern Ocean taxa appear to be more sensitive to these OA effects than equivalent Arctic taxa (Hoppe et al., 2015). In light of the evidence that OA will select for particular phytoplankton taxa and/or size class (Hancock et al., 2018; Sugie et al., 2020), size-related changes to macromolecular stores could have significant implications for the trophic transfer of energy and nutrients through the marine food web.

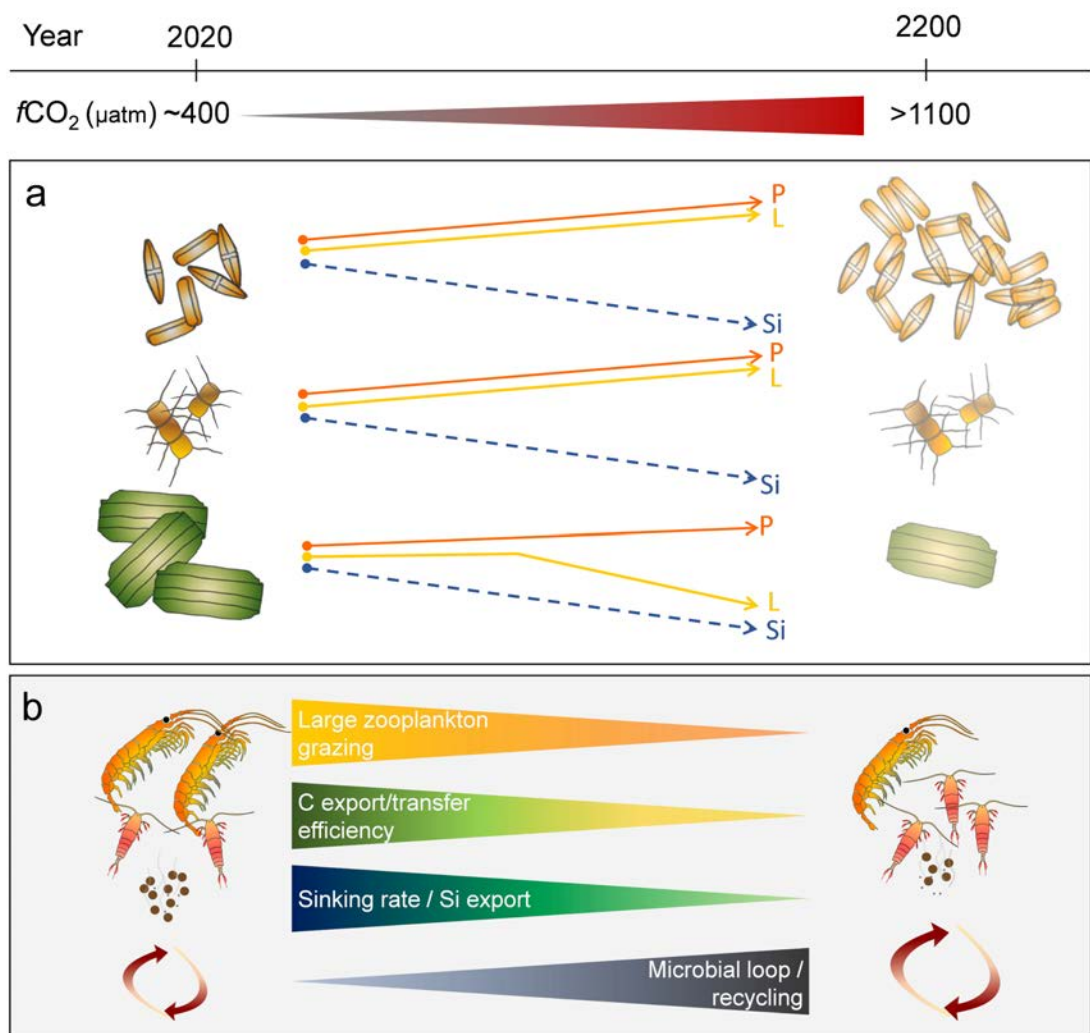


**Figure 6.8:** Summary of measured changes to diatoms under high  $f\text{CO}_2$  and expected ecological implications. **(A)** Projected increase in  $\text{CO}_2$  by the end of next century (2200) results in a shift in dominance towards smaller diatom species with increased lipid and protein content, but reduced silicification, while larger diatoms become scarce with lower lipid content and reduced silica content. **(B)** These changes alter food quality and availability for large zooplankton species such as krill and large copepods, affecting zooplankton growth and fecundity. A reduction in large diatoms and large zooplankton grazing would likely reduce carbon and silica export efficiency and alter energy transfer through to higher trophic organisms. Lowered silica production may alleviate some of this loss by increasing grazing on the abundant lipid and protein rich small diatoms by smaller zooplankton. Smaller cells and high grazing rates by smaller zooplankton would likely increase microbial loop activity and nutrient recycling in surface waters. Solid lines represent measured changes to relative protein (P) and lipid (L) content, while stippled



lines represent the measured decline in silicification ( $Si$ ) in the same diatoms from a parallel study (Petrou et al., 2019).

In all five diatom groups, we saw an increase in protein content between M1 and M6. For *P. truncata* and *S. microtrias* the increase was linear, however for *F. cylindrus* the increase was linear only until M3, after which it plateaued. Both *Chaetoceros* spp. and the Discoid centric group had highest protein content in M6, however they exhibited a u-shaped response to increasing  $fCO_2$ . The unexpected trend towards decline in growth rate despite increased protein content observed in *F. cylindrus*, may suggest increased energy use for protein synthesis and growth under higher  $fCO_2$ . This seems counterintuitive, as increasing  $CO_2$  has previously been shown to reduce gross metabolism in constantly growing diatoms (Hennon et al., 2015) because of the energy savings associated with downregulation of CCM activity (Hennon et al., 2015; 2017) but this response may only hold true under low-moderate  $CO_2$  enrichment (Deppeler et al., 2018). Carboxylates and amino acids are the major functional groups associated with cellular protein (Bromke, 2013). We saw similar responses for carboxylate content to increasing  $fCO_2$  in all taxa and consistent trends, within taxa, between free amino acids and proteins for *Chaetoceros* spp., and *P. truncata*, reflecting the role of amino acids in the synthesis of proteins and as precursors for metabolites with multiple functions in growth (Bromke, 2013). For the larger diatoms, *S. microtrias* and the Discoid centric group, amino acids declined. Larger diatoms generally have substantial amino acid pools relative to protein content, where amino acids can act as a nitrogen reservoir when availability is limiting (Admiraal et al., 1986). Thus, the decline of free amino acids with increasing  $fCO_2$  in the larger diatoms could suggest use of this nitrogen reservoir for protein generation (Dortch, 1982; Marañón et al., 2013). Because protein content in primary producers is an important source of energy and amino acids for higher trophic levels, ecologically, its overall increase between the lowest and highest  $fCO_2$  concentrations measured, suggests protein availability for secondary production may increase under OA.

The measured changes in lipids and fatty acid content in response to  $fCO_2$  between taxa were more variable than those for protein. We found that increasing  $fCO_2$  resulted in decreased relative lipid content for the larger diatoms compared to a bell-shaped increase in lipid content for the smaller diatoms *F. cylindrus* and *P. truncata*. Because the effect for *Chaetoceros* spp. closely followed growth rate, it is likely that the response was

related to growth phase and/or nutrient limitation rather than  $f\text{CO}_2$ , limiting the interpretation of  $f\text{CO}_2$  effects on macromolecular partitioning for *Chaetoceros* spp. particularly for M3 and M4 where cells had reached stationary phase. These size-specific trends may be due to the larger diatoms in this study having a greater need to prioritise protein synthesis over lipid storage (although it is important to note that we did not differentiate between storage and structural lipid types in the analyses). In the two large discoid centric diatoms (*S. microtrias* and Discoid centrics), the  $f\text{CO}_2$ -related decline in lipids was accompanied by an increase in relative protein content suggesting a shift in macromolecular energy partitioning with acidification. This loss in lipid content is congruent with a previous study that found total fatty acid content declined significantly in the discoid centric diatom *Thalassiosira weissflogii* at high  $\text{CO}_2$  (Rossoll et al., 2012). An increase in protein content at the expense of ester carbonyl, could be explained by the fact that ester carbonyl acts as a fixed carbon reservoir for protein biosynthesis in cells (Stehfest et al., 2005; Terry et al., 1985). Thus, its degradation and decline could be directly linked to increased protein production. Alternatively, changes to lipid content could be a strategy for regulating cell ballast. In a parallel study from the same mesocosm experiment, we measured significant declines in the silicification rates of these two taxa with acidification (Petrou et al., 2019). We found that at the highest  $f\text{CO}_2$  (M6) treatment, silicification declined 59% and 39% in *S. microtrias* and Discoid centrics, respectively (Petrou et al., 2019). Extent of silicification contributes to diatom sinking rate (Miklasz & Denny, 2010), and therefore any reduction in silicification may increase diatom buoyancy. By decreasing cellular lipid content, the diatoms may counteract this loss in ballast, increasing their density, and thus decreasing buoyancy (Smayda, 1970), enabling the diatoms to regulate their depth within the water column.

In both *P. truncata* and *F. cylindrus*, an  $f\text{CO}_2$  threshold for increasing lipid content was observed, where lipids increased until about  $\sim 950 \mu\text{atm}$ , after which they declined. This initial increase in lipid reserves at moderate  $f\text{CO}_2$  enrichment, may reflect a boosted investment into energy stores, as the cells are relieved from potential carbon limitation (Halsey & Jones, 2015). However, as protein content continued to increase for both species beyond  $\sim 950 \mu\text{atm}$ , the threshold response of lipid content likely indicates that, once the CCMs are saturated, lipids are preferentially catabolised for energy to synthesise proteins and support growth (Halsey & Jones, 2015; Stehfest et al., 2005). Alternatively, the shift could be due to higher energy requirements to support increased proton pumping

at high  $f\text{CO}_2$  (Deppeler et al., 2018). This shift towards higher energy consumption indicates that  $\text{CO}_2$  concentrations  $>1000 \mu\text{atm}$ , which are predicted by 2100 (IPCC, 2014), could be a critical point of change for these species, a finding supported by our parallel mesocosm study (Deppeler et al., 2018), which reported significant declines in carbon production by these taxa at  $f\text{CO}_2$  concentrations  $>1140 \mu\text{atm}$ .

Our inability to detect any  $\text{NO}_x$  by day 18 alerted us to the possibility of nitrogen limitation in our mesocosms, which has the potential to confound any  $f\text{CO}_2$ -induced macromolecular responses. Indeed, in three of the mesocosms, the  $\text{NO}_x$  concentrations were strongly diminished by day 16; M1, M3 ( $1.5 \mu\text{M}$ ) and M4 ( $0.2 \mu\text{M}$ ) (Deppeler et al., 2018), yet while these concentrations are low for Southern Ocean waters, they are within the normal range of most oceanic waters and not generally considered limiting for microalgae (Voss et al., 2013). Notwithstanding these low  $\text{NO}_x$  values, our data did not exhibit signs of limitation. Instead, the diatoms studied were still actively growing on day 18 (except *Chaetoceros* spp. from M3 and M4) and therefore unlikely have been nutrient limited, possibly supported by luxury uptake of nitrate at an earlier stage (Behrenfeld et al., 2021). Further support for the unlikelihood that our data were affected by nutrient limitation is provided by the fact that removal of the data points for the mesocosms in which nitrate concentrations were low on day 16 (M1, M3 and M4) has little or no effect on the observed trends.

If our snapshot of macromolecular profiles in response to  $f\text{CO}_2$  enrichment is representative of the broader effect on phytoplankton nutritional quality in nature, selection for smaller diatoms (as was the case in our mesocosm community study, see Hancock et al., 2018), with increased lipid and protein content per cell could translate to increased energy available for secondary production. Availability and transfer of lipids through the trophic web are particularly important, as lipids are the most energy-rich macromolecules, with an energy storage capacity of  $39.4 \text{ J mg}^{-1}$ , compared to  $23.6 \text{ J mg}^{-1}$  for proteins (Hagen & Auel, 2001). High lipid content in primary producers is essential to sustain growth, reproduction and ensure the survival of the aphotic Antarctic winter of higher trophic levels, from zooplankton to marine mammals and birds (Breteler et al., 2005; Jones & Flynn, 2005; Kattner et al., 2007). Thus, OA may result in higher secondary production. However, an increase in available lipid in small cells does not directly imply an increase in the calories transferred to higher trophic levels. Antarctic

krill exhibit only 50% grazing efficiency for phytoplankton  $< 20 \mu\text{m}$  (Boyd et al., 1984; Moline et al., 2004; Quetin & Ross, 1985), meaning a shift to a community dominated by small diatoms may have significant impacts on krill populations and the organisms that depend on them. Further, krill and other large zooplankton have been demonstrated to have a grazing preference for larger cells (Meyer et al., 2003; Meyer & El-Sayed, 1983; Quetin & Ross, 1985), which means that the decline in lipid measured in the larger diatoms in this study could directly affect large zooplankton populations. Indeed, copepod diets low in lipid content have been shown to cause significant declines in growth and fecundity (Rossoll et al., 2012; Shin et al., 2003). Considering the multiplicity of responses, the opposing effects of increased available lipid content have to be weighed up with overall changes to trophic efficiency, which will likely be influenced by a shift in community composition, a decrease or change in average cell size (Hancock et al., 2018) and reduced silicification (Petrou et al., 2019), all of which affect grazing preference and efficiency. As such, an increase in energy available to secondary production under OA will not necessarily translate to increased energy transferred to higher trophic levels.

Taking a single cell approach, we were able to differentiate diatom species responses to OA with increasing  $f\text{CO}_2$ . We saw clear species-specific trends in macromolecular stores despite high within-treatment variability. The variability observed between diatom populations may be attributed to differences in cell size and thus differences in cellular nutrient requirement (Sarhou et al., 2005), cell shape, which can also affect diffusion rates (Mitchell et al., 2013; Pahlow et al., 1997) (or some other underlying physiological variant, such as photosynthesis and carbon acquisition strategies (Hennon et al., 2017)), however, none of these parameters were tested here. Instead, this species-specific variability reveals the adaptive potential of each taxon, and thus the potential resilience of that taxon to environmental change. Similarly, the broad within-species spread in macromolecular responses suggests large phenotypic plasticity in the taxa studied. Interestingly, we saw a general decrease in within-treatment variability with increasing  $f\text{CO}_2$ , suggesting a possible convergence of cell responses and thus potential for reduced within-species plasticity. Ecologically, this could have implications for resilience to environmental change in future populations. Contrary to the commonly observed shift towards larger cells, the highest  $f\text{CO}_2$  levels of our community study selected for smaller diatoms (Hancock et al., 2018). This loss of larger diatoms from the community could

reduce the efficiency of energy transfer, as smaller cell sizes may be more difficult to graze on for some larger zooplankton. From a trophic energy perspective, reduced grazing efficiency or smaller krill populations due to a community dominated by smaller diatoms, despite a per cell increase in protein and lipid content, may in fact reduce the transfer efficiency of nutrients to higher predators (Fig. 6.8). This may be enhanced by concurrent sea surface temperature increases, which have been shown to contribute to polar phytoplankton communities being dominated by smaller cells (Coello-Camba et al., 2014; Mendes et al., 2018; Mendes et al., 2013). Alternatively, when viewed in combination with reduced silicification in the taxonomic groups studied here, not only diatom sinking rates would be reduced, but also protection against grazing (Liu et al., 2016), potentially increasing diatom predation in surface waters. Such a shift could counter some of the energy loss that might ensue with a trend towards a community dominated by smaller cells, while increasing recycling of carbon and silica via increased microbial loop activity. Deriving precise trophic projections based on the taxonomic variability in macromolecular responses described here is challenging due to the uncertainty around OA driven changes to community composition and size structure. However, if our results hold true, they indicate that as the community becomes dominated by smaller, less silicified taxa under OA, the increased protein and lipid may benefit some grazers, but may not be as effectively conveyed to higher trophic levels due to overall less efficient large zooplankton grazing (Fig. 6.8). Concurrently, the remaining large taxa would have less lipid, resulting in less energy available to large zooplankton, with biogeochemical consequences of reduced carbon export and increase nutrient remineralisation (Fig. 6.8). Thus, whilst determining the net effects of OA on trophic energy transfer is inherently complex, it is clear that OA drives changes in diatom macromolecular partitioning with the potential for significant implications on nutrient and energy supply to the Antarctic pelagic food web.

### **Acknowledgements**

We thank the Australian Synchrotron Principal Beamline Scientists Drs. Mark Tobin and Jitra-porn Vongsvivut for technical support in synchrotron IR microspectroscopy data acquisition. Part of this work was funded by the Australian Synchrotron through merit-based beamtime awarded on the Infrared Microscopy (IRM) beamline (AS153/IRM/10005) awarded to KP. Field support and sample collection was conducted as part of Australian Antarctic Science Project 4026 awarded to ATD. Samples were imported under permit no. IP13019928. RJD is supported by an Australian Government Research Training Program Scholarship and an AINSE Ltd. Postgraduate Research Award (PGRA), and research funding was provided by the School of Life Sciences, University of Technology Sydney.

### **Data Availability**

Data are available in Supplementary Information and via the Australian Antarctic Division Data Centre DOI:10.26179/ej5x-2h37).

**Supplementary Information**

**Table S6.1:** Summary of initial seawater (*T0*) conditions (*italicised*) and mesocosm conditions on day 18. Fugacity of carbon dioxide ( $f\text{CO}_2$ ), nitrogen ( $\text{NO}_x$ ), soluble reactive phosphorous (SRP), silica, dissolved inorganic carbon (DIC), total pH ( $\text{pH}_T$ ), practical alkalinity (PA), salinity and temperature, across the six mesocosms. Where measurements were below detection limits, it is marked not detected (ND). Full physiochemical parameters can be found in Deppeler et al., (2018).

Mesocosm	$f\text{CO}_2$ ( $\mu\text{atm}$ )	Nitrogen ( $\mu\text{M}$ )	SRP ( $\mu\text{M}$ )	Silica ( $\mu\text{M}$ )	DIC ( $\mu\text{mol kg}^{-1}$ )	$\text{pH}_T$	PA ( $\mu\text{mol kg}^{-1}$ )	Salinity	Temperature ( $^\circ\text{C}$ )
<i>T0</i>	<i>356.00</i>	<i>26.19</i>	<i>1.74</i>	<i>60.75</i>	<i>2187.00</i>	<i>8.08</i>	<i>2317.00</i>	<i>34.30</i>	<i>-1.03</i>
1	288.02	ND	0.10	92.57	2178.60	8.17	2342.39	34.60	-0.30
2	427.19	ND	0.13	96.13	2234.60	8.01	2340.27	34.60	-0.30
3	547.53	ND	0.13	85.45	2265.70	7.91	2341.04	34.60	0.10
4	696.59	ND	0.13	89.01	2291.50	7.81	2336.00	34.60	0.00
5	957.79	ND	0.13	96.13	2332.20	7.68	2338.44	34.60	0.00
6	1263.84	ND	0.19	99.69	2360.00	7.57	2332.30	34.60	0.10

**Table S6.2** Summary of number of cells, per taxa, per mesocosm, measured for species-specific macromolecular content using FTIR-microspectroscopy. For each, the total number of cells measured (*n*) and the mean number of cells measured across all taxon per mesocosm is supplied. For Mesocosm 5 (M5), *Fragilariopsis cylindrus* was not analysed.

Mesocosm	Taxon	n	Mean
M1	<i>Chaetoceros</i> spp.	28	30
	<i>Fragilariopsis cylindrus</i>	33	
	<i>Proboscia truncata</i>	49	
	<i>Stellarima microtrias</i>	22	
	Discoid centric >20 µm	20	
M2	<i>Chaetoceros</i> spp.	27	24
	<i>Fragilariopsis cylindrus</i>	24	
	<i>Proboscia truncata</i>	20	
	<i>Stellarima microtrias</i>	24	
	Discoid centric >20 µm	26	
M3	<i>Chaetoceros</i> spp.	21	21
	<i>Fragilariopsis cylindrus</i>	25	
	<i>Proboscia truncata</i>	21	
	<i>Stellarima microtrias</i>	19	
	Discoid centric >20 µm	21	
M4	<i>Chaetoceros</i> spp.	22	22
	<i>Fragilariopsis cylindrus</i>	23	
	<i>Proboscia truncata</i>	16	
	<i>Stellarima microtrias</i>	27	
	Discoid centric >20 µm	23	
M5	<i>Chaetoceros</i> spp.	20	19
	<i>Fragilariopsis cylindrus</i>	-	
	<i>Proboscia truncata</i>	15	
	<i>Stellarima microtrias</i>	18	
	Discoid centric >20 µm	24	
M6	<i>Chaetoceros</i> spp.	19	22
	<i>Fragilariopsis cylindrus</i>	24	
	<i>Proboscia truncata</i>	20	
	<i>Stellarima microtrias</i>	20	
	Discoid centric >20 µm	28	



**Table S6.3:** Cell density and community photosynthetic efficiency on day 18. Cell density of selected diatoms (cells/L<sup>-1</sup>), total cell density of whole phytoplankton community and % diatoms of whole phytoplankton community, across the 6 mesocosms. Maximum quantum yield of PSII (F<sub>V</sub>/F<sub>M</sub>) ± the standard deviation (SD) of three pseudo-triplicated measurements taken from each of the six mesocosms on day 18.

Mesocosm	<i>Chaetoceros</i> spp.	<i>Fragilariopsis cylindrus</i>	<i>Proboscia truncata</i>	<i>Stellarima microtrias</i>	Discoid centric >20 µm	Total cells	Diatoms (listed) % of community	F <sub>V</sub> /F <sub>M</sub> (± SD)
1	140 504	110 110	84 597	152 409	69 155	8 334 650	6.68	0.63 ± 0.01
2	380 536	114 699	103 348	228 800	79 751	12 673 208	7.16	0.70 ± 0.00
3	177 789	113 823	36 687	150 509	46 564	19 190 981	2.74	0.64 ± 0.04
4	129 285	93 553	58 471	102 648	74 387	9 648 883	4.75	0.60 ± 0.05
5	377 086	57 508	106 800	101 871	57 918	6 526 246	10.74	0.61 ± 0.04
6	94 182	40 802	47 898	57 360	44 942	8 565 493	3.33	0.63 ± 0.03

**Table S6.4** Mean cell volume (µm<sup>3</sup>) on day 18 for taxa from Mesocosms 1 (M1) and Mesocosm 6 (M6). For each taxa, per mesocosm, the mean cell volume, standard deviation (SD), number of cells analysed (n) and difference between mean in M1 and M6 ± standard deviation (SD) is supplied.

Taxon	Mean cell volume (µm <sup>3</sup> )		SD		n		Difference of means ± SD
	M1	M6	M1	M6	M1	M6	
<i>Chaetoceros</i> spp.	847	927	370	254	55	41	-80 ± 64
<i>Fragilariopsis cylindrus</i>	2713	1849	1291	570	53	24	864 ± 211
<i>Proboscia truncata</i>	24 558	26 414	10 824	9544	39	35	-1856 ± 2367
<i>Stellarima microtrias</i>	63 290	64 198	33 365	30 354	77	75	-908 ± 5171
Discoid centric >20 µm	258 154	252 445	161184	180 405	32	41	5708 ± 40071

**Table S6.5** Statistical output of the species-specific regression models (Figures 6.1-6.5). Multiple  $R^2$ , adjusted  $R^2$ ,  $F$  statistic, associated degrees of freedom (DF),  $p$ -value and equation of regression model. Statistically significant  $p$ -values ( $< 0.05$ ) are marked in bold.

		Multiple $R^2$	Adjusted $R^2$	F Statistic	DF	$P$ Value	Regression Equation
<i>Chaetoceros</i> spp.	Protein (amide II)	0.21	0.20	18.04	2, 139	<b><math>1.08 \times 10^{-7}</math></b>	$y=0.15x^2 + 1.60x + 0.85$
	Free Amino Acids	0.19	0.17	8.79	2, 75	<b><math>3.73 \times 10^{-4}</math></b>	$y=0.28x^2 + 1.11x + 1.00$
	Saturated Fatty Acids	0.22	0.21	19.19	2, 138	<b><math>4.44 \times 10^{-8}</math></b>	$y=0.80x^2 + 2.19x + 0.50$
	Ester Carbonyl	0.20	0.19	16.5	2, 132	<b><math>4.02 \times 10^{-7}</math></b>	$y=-0.24x^2 + 2.00x + 0.08$
	Carboxylates	0.06	0.04	3.75	2, 124	<b>0.03</b>	$y=0.36x^2 + 0.75x + 0.03$
	Growth Rate	0.81	0.69	6.54	2, 3	0.08	$y=0.10x^2 + 0.55x + 0.08$
<i>Fragilariopsis cylindrus</i>	Protein (amide II)	0.31	0.30	28.07	2, 126	<b><math>8.27 \times 10^{-11}</math></b>	$y=1.43x^2 - 0.85x + 0.97$
	Free Amino Acids	0.03	0.02	1.82	2, 102	0.17	$y=0.05x^2 - 0.53x + 0.28$
	Saturated Fatty Acids	0.20	0.19	15.26	2, 124	<b><math>1.19 \times 10^{-6}</math></b>	$y=0.93x^2 - 1.05x + 0.69$
	Ester Carbonyl	0.16	0.15	11.75	2, 125	<b><math>2.11 \times 10^{-5}</math></b>	$y=0.86x^2 - 1.21x + 0.37$
	Carboxylates	0.11	0.09	6.47	2, 106	<b><math>2.23 \times 10^{-3}</math></b>	$y=0.36x^2 - 0.88x + 0.00$
	Growth Rate	0.69	0.48	3.27	2, 3	0.18	$y=-0.15x^2 - 0.20x + 0.26$
<i>Proboscia truncata</i>	Protein (amide II)	0.12	0.11	19.77	1, 146	<b><math>1.72 \times 10^{-5}</math></b>	$y=0.0004x + 0.9810$
	Free Amino Acids	0.08	0.07	7.94	1, 96	<b><math>5.88 \times 10^{-3}</math></b>	$y=0.0002x + 0.3159$
	Saturated Fatty Acids	0.12	0.11	9.89	2, 146	<b><math>9.38 \times 10^{-5}</math></b>	$y=1.43x^2 - 1.17x + 0.98$
	Ester Carbonyl	0.13	0.18	10.25	2, 138	<b><math>7.08 \times 10^{-5}</math></b>	$y=0.66x^2 - 1.78x + 0.60$
	Carboxylates	0.06	0.06	9.24	1, 137	<b><math>2.85 \times 10^{-3}</math></b>	$y=0.0002x + 0.0414$
	Growth Rate	0.14	-0.08	0.63	1, 4	0.47	$y=-0.0008x + 0.4382$
<i>Stellarima microtrias</i>	Protein (amide II)	0.06	0.05	7.44	1, 128	<b><math>7.26 \times 10^{-3}</math></b>	$y=0.0008x + 1.4110$
	Free Amino Acids	0.12	0.11	12.04	1, 92	<b><math>7.93 \times 10^{-4}</math></b>	$y=0.0002x + 0.6608$
	Saturated Fatty Acids	0.02	0.01	2.09	1, 128	0.15	$y=-0.0007x + 1.0320$

	Ester Carbonyl	0.19	0.19	30.21	1, 128	<b>2.02 x10<sup>-7</sup></b>	y=-0.0005x+0.8412
	Carboxylates	0.19	0.19	29.05	1, 121	<b>3.54 x10<sup>-7</sup></b>	y=0.0002x+0.3190
	Growth Rate	0.57	0.46	5.30	1, 4	0.08	y=0.0003x+0.2116
<b>Discoid centric (&gt;20 µm)</b>	Protein (amide II)	0.07	0.05	4.92	2, 139	<b>8.66 x10<sup>-3</sup></b>	y=0.17x <sup>2</sup> + 0.24x + 1.47
	Free Amino Acids	0.15	0.15	21.58	1, 119	<b>8.83 x10<sup>-6</sup></b>	y=0.0004x+1.4420
	Saturated Fatty Acids	0.10	0.09	15.64	1, 140	<b>1.21 x10<sup>-4</sup></b>	y=0.0004x+0.6396
	Ester Carbonyl	0.22	0.22	40.21	1, 140	<b>2.94 x10<sup>-9</sup></b>	y=-0.0007x+0.8063
	Carboxylates	0.19	0.18	31.75	1, 139	<b>9.39 x10<sup>-8</sup></b>	y=0.0002x + 0.1645
	Growth Rate	0.23	0.04	1.20	1, 4	0.33	y=0.0007x + 0.3589

**Table S6.6:** Statistical output of the lipid (ester carbonyl) to protein (amide II) ratios models (Figure 6.6). Multiple R<sup>2</sup>, adjusted R<sup>2</sup>, F statistic, associated degrees of freedom (DF), p-value and equation of regression model. Statistically significant p-values (< 0.05) are marked in bold.

Taxon	Multiple R <sup>2</sup>	Adjusted R <sup>2</sup>	F Statistic	DF	P Value	Regression Equation
<i>Chaetoceros</i> spp.	0.35	0.35	72.74	1, 133	<b>&lt;0.001</b>	y=0.63x + 0.80
<i>Fragilariopsis cylindrus</i>	0.60	0.60	191.9	1, 126	<b>&lt;0.001</b>	y=0.62x + 0.75
<i>Proboscia truncata</i>	0.45	0.45	113.7	1, 139	<b>&lt;0.001</b>	y=0.54x + 0.86
<i>Stellarima microtrias</i>	0.00	0.00	0.38	1, 128	0.54	y=0.02x + 1.46
Discoid centric >20 µm	0.05	0.04	7.49	1, 140	0.07	y=0.04x + 1.46

**Table S6.7:** Data corresponding to cell volume ( $\mu\text{m}^3$ ) and protein (amide II) or lipid (ester carbonyl) content; for diatoms in the low  $f\text{CO}_2$  treatment (288  $\mu\text{atm}$ ) in Mesocosm 1 (M1) and high  $f\text{CO}_2$  treatment (1263  $\mu\text{atm}$ ) in Mesocosm 6 (M6). For all taxa investigated, the mean, standard deviation (SD), total number of cells analysed ( $n$ ) and standard error (SE) are supplied.

Macromolecule	Mesocosm	Taxon	$\log_{10}$ Cell Volume ( $\mu\text{m}^3$ )			$\log_{10}$ Peak Area		
			Mean	SD	n	Mean	SD	n
Protein (amide II)	M1	<i>Chaetoceros</i> spp.	2.89	0.19	55	0.96	0.19	28
		<i>Fragilariopsis cylindrus</i>	3.40	0.19	53	0.72	0.32	33
		<i>Proboscia truncata</i>	4.35	0.19	39	1.05	0.42	55
		<i>Stellarima microtrias</i>	4.73	0.25	77	1.43	0.10	22
		Discoid centric >20 $\mu\text{m}$	5.34	0.24	32	1.46	0.13	20
	M6	<i>Chaetoceros</i> spp.	2.89	0.19	55	1.24	0.09	21
		<i>Fragilariopsis cylindrus</i>	3.40	0.19	53	1.16	0.11	24
		<i>Proboscia truncata</i>	4.35	0.19	39	1.41	0.15	20
		<i>Stellarima microtrias</i>	4.73	0.25	77	1.50	0.08	20
		Discoid centric >20 $\mu\text{m}$	5.34	0.24	32	1.52	0.10	28
Ester Carbonyl	M1	<i>Chaetoceros</i> spp.	2.88	0.19	55	0.35	0.13	23
		<i>Fragilariopsis cylindrus</i>	3.39	0.19	53	0.12	0.33	32
		<i>Proboscia truncata</i>	4.35	0.19	39	0.43	0.45	49
		<i>Stellarima microtrias</i>	4.73	0.25	32	0.57	0.32	22
		Discoid centric >20 $\mu\text{m}$	5.34	0.24	77	0.45	0.40	20
	M6	<i>Chaetoceros</i> spp.	2.95	0.12	41	0.26	0.29	19
		<i>Fragilariopsis cylindrus</i>	3.25	0.14	24	0.42	0.18	24
		<i>Proboscia truncata</i>	4.39	0.17	35	0.50	0.24	20
		<i>Stellarima microtrias</i>	4.76	0.19	75	0.19	0.28	20
		Discoid centric >20 $\mu\text{m}$	5.32	0.25	41	0.00	0.44	28

**Table S6.8:** Statistical output of the cell volume ( $\mu\text{m}^3$ ) and protein (amide II) or lipid (ester carbonyl) content models (Figure 6.7). Multiple  $R^2$ , adjusted  $R^2$ ,  $F$  statistic, associated degrees of freedom (DF),  $p$ -value and equation of regression model. Statistically significant  $p$ -values ( $< 0.05$ ) are marked in bold.

Mesocosm	Macromolecule	Multiple $R^2$	Adjusted $R^2$	F Statistic	DF	$P$ Value	Regression Equation
<b>M1</b>	Protein (amide II)	0.77	0.70	10.19	1, 3	<b>0.05</b>	$y=2.80x + 1.00$
	Ester Carbonyl	0.44	0.26	2.37	1, 3	0.22	$y= 3.94x + 2.63$
<b>M6</b>	Protein (amide II)	0.85	0.80	17.00	1, 3	<b>0.03</b>	$y=5.74x - 3.69$
	Ester Carbonyl	0.94	0.88	15.47	2, 2	<b>0.05</b>	$y=-0.28x^2 - 0.37x + 0.26$

## **Chapter 7: Synthesis of Results, Future Directions and Conclusions**

Sea-ice algae and phytoplankton form the base of productive polar marine food webs, responsible for the energy and nutrients supplied to higher trophic levels, and for structuring ocean biogeochemical dynamics. Through their photosynthetic activity, microalgae manufacture the nutrients and energy that underpin secondary production, and their nutritional quality as a food source depends on their biomolecular (lipid:protein:carbohydrate) composition. This thesis demonstrates that changes in sea-ice condition and ocean acidification alter microalgal biomolecular content and community composition, and highlights the potential for cascading effects on the marine ecosystem.

This research was motivated by the need to better understand individual species contributions to polar food webs and how the nutritional value of the base of polar marine food web may be impacted by climate change driven environmental perturbations. Through a series of field campaigns sampling varied sea-ice conditions and a manipulative study, this project aimed to determine how changes to environmental conditions influence sympagic and pelagic microalgal community composition and individual species' nutritional content, both of which have consequences for marine biogeochemical cycling and energy supply to consumers.

At the outset, an initial review of the current state of knowledge of how environmental conditions shape the biomolecular content of sea-ice algal communities was completed, including an evaluation of the relevant analytical techniques and approaches (Chapter 2). This review highlighted broad plasticity in microalgal biomolecular composition in regulating cellular metabolism to meet the needs of altered environmental conditions to maintain cell homeostasis. In presenting the current evidence for carbon allocation alteration, it was clear that there are also species-specific responses with respect to strength and direction of effect. Given the above, we concluded that techniques able to provide high-throughput, whole biomolecular profiling of individual cells within natural communities were important for future studies.

Using s-FTIR to analyse natural microbial communities from Arctic land-fast sea ice, we were able to show that increasing light transmitted to the bottom-ice, up to a threshold of ~15%, significantly alters the biomolecular content of key sea-ice microalgae, specifically through an increase in lipid and fatty acid storage (Chapter 4). A higher under-ice light environment, as a result of declining ice and snow thickness, was also shown to alter sea-ice microalgal community composition resulting in higher diversity in early spring from a relative increase in *Navicula* spp. and Dinophyceae, and decrease in *N. frigida* abundance (Chapter 3). Together, this work suggests that with continued decline in sea ice and snow coverage until a certain threshold, we may see sea-ice algal communities dominated by flagellates and *Navicula* spp., and a nutritional contribution shifted toward high energy molecules, as the species-specific physiologies lead to changes in the competitive hierarchy.

When following a key sea-ice microalgal taxon over a seasonal cycle we observed that environmental triggers indicating the end of productivity in the ice and onset of ice melt, such as nitrogen limitation and increased water temperature, corresponded with an increase in sea-ice algal lipid and fatty acids content in *N. frigida* (Chapter 5). This work sheds light on the survival strategies that this key taxon uses to survive the dark winter outside of the sea ice, and indicates that if sea ice is abruptly melted from below through an influx of warm water, the sympagic community could be released to the pelagic zone prior to accumulating adequate lipid storage for winter, impacting carbon transfer through the polar marine system.

In the final chapter, we had the opportunity to explore the influence of ocean acidification on the biomolecular profiles of key coastal Antarctic phytoplankton. We found species-specific biomolecular profiles and varying levels of plasticity both under controlled conditions and with acidification across five key taxa. This work revealed that ocean acidification levels projected for 2100 could alter SO pelagic communities, with a shift towards a community dominated by lipid and protein enriched smaller taxa (Chapter 6).

Taken together, the major findings presented in this thesis provide new insights into the extant phenotypic plasticity of selected sympagic and pelagic microalgae, elucidating how polar marine ecosystem dynamics are accounted for by the physiology of its inhabitants. The variability in species biomolecular profiles indicates an evolutionary

adaptation to acclimate to changeable environmental conditions. In the context of climate change, this research has shown what might be expected to shift with respect to community composition and nutritional content under altered sea ice and ocean conditions and seawater chemistry. A synthesis of the importance of these findings is presented below, and future directions are also addressed within this final chapter.

**Under-ice light strongly influences sea-ice microalgal community composition:**

Through extensive field sampling of land-fast ice in six different Arctic fjords, during spring (April-May) of 2021 and 2022, the community composition of 38 sampling events was analysed, identifying 55 different sea-ice microalgal taxa. Light transmitted to the bottom-ice communities ranged from 0.1 – 193  $\mu\text{mol photons m}^{-2}\text{s}^{-1}$  and was found to play a central role in determining the community composition, as more diverse communities were found in higher light environments. The influence of under-ice light was particularly evident earlier in the development of communities (i.e. earlier in the productive season), when community composition was similar at similar under-ice light transmittance, independent of geographical location. The role of light in determining community composition was strengthened in the seasonal assemblages collected in 2022. During this campaign, all the communities were exposed to relatively stable, low light environments, and all were determined to have similar overall compositions, with *Nitzschia* spp., and *Navicula* spp., generally making up over 80% of the community. While comparable patterns of enhanced sympagic microalgal diversity with higher under-ice light have been observed previously in the Arctic Ocean (Hop et al., 2020) and Barents Sea (Hegseth & von Quillfeldt, 2022), this research expands the spatio-temporal resolution of taxonomic data collected to date, greatly augmenting our species level coverage (Fig. 7.1). These relatively rare, fine-scale, data sets are important contributions to baseline data, which are valuable for future comparative studies to determine how these communities have changed, and are likely to change.

Sea-ice communities were dominated by pennate diatoms, in particular the colonial species *Nitzschia frigida*, which made up 56% [7% - 95%] of the community composition on average, a finding consistent with other land-fast ice communities across the Arctic (Hegseth & von Quillfeldt, 2022; Hop et al., 2020; Róžańska et al., 2009). Other taxa including *Navicula* spp., *Entomoneis* spp., *Cylindrotheca closterium* and Dinophyceae were ubiquitous in all samples. Whilst these data are important for understanding spatial



and temporal dynamics in influencing sympagic community composition, it does not clearly tease apart any temporal effects between years or spatial effects across ~ 10,000 km<sup>2</sup> geographical distances (Fig. 7.1A). However, combining the sympagic assemblages from both seasons with environmental parameters, patterns emerged between the dominance of certain taxa and specific environmental drivers, namely under-ice light, nutrient depletion and initiation of ice-melt (Fig. 7.1B). We found that higher under-ice light, as a function of reduced snow and ice thickness, was associated with higher community diversity, through positive correlation with the contribution of taxa such as Dinophyceae, *Navicula* spp., *Fragilariopsis* spp. and *Cylindrotheca closterium* (Chapter 3; Fig 7.1). An increase in relative abundance of Dinophyceae was likely also linked to this group being favoured by lower nitrate concentrations at times observed at the higher light sites (Chapter 3; Fig 7.1), which fits with this taxa being observed to increase with seasonal progression toward high light and nutrient limitation in other areas of the Arctic (Alou-Font et al., 2013; Hegseth & von Quillfeldt, 2022; Mundy et al., 2011; Róžańska et al., 2009).

Lower nitrate within the bottom-ice, combined with warmer ice temperature (i.e. toward melting), were also associated with a higher prevalence of key taxa including *Navicula* spp., *Pleurosigma* spp., and *Nitzschia* spp., (Fig. 7.1B), in particular, *N. frigida* (Chapter 5). Despite these associations, a decline in *Navicula* spp. and *Pleurosigma* spp. abundance was observed with time (Chapter 5), which corresponds with previously observed trends in *Navicula* spp. (Róžańska et al., 2009). These findings may reflect that *N. frigida* has a competitive advantage over other key taxa under these end-of-season conditions.

Together, these data would suggest that higher under-ice light elicits greater productivity and increased growth rates among many taxa, which breaks down competitive hierarchies and increases community diversity. Toward the end of the productive season, however, the conditions become more physiochemically challenging and particular taxa, such as Dinophyceae and *N. frigida*, are better adapted than others. More difficult growth conditions appear to create a competitive advantage for *N. frigida*, as a specialised ice-taxa with a particular ability to maximise growth at low light levels (Croteau et al., 2022), produce EPS and proliferate in dendroid colonies, which together ameliorates chemical stress and provides good ability to attach to the ice surface (Medlin & Hasle, 1990; Mundy & Meiners, 2021). Thus, in low-light (Chapter 3) and nitrate limited environments

(Chapter 5), and with minimal skeletal layer in the bottom-ice (Chapter 5), *N. frigida* was relatively more abundant and was the dominating taxa of the community through its physiological adaptations to challenging physiochemical environments.

The environmental changes facing polar marine ecosystems (Chapter 1) will therefore inevitably lead to shifts in species abundance. Such shifts could have potentially far reaching implications. For example, *Pleurosigma* spp. abundance was observed to decrease with time and brine salinity, as brine salinity is higher with ice-formation than ice-melt. In the context of freshening polar waters (Chapter 1) and/or rapid under-ice melt, we may therefore see a decline in *Pleurosigma* spp. abundance, and as this species is one the largest diatom taxa, this may contribute to shaping a community dominated by smaller taxa with implications for grazing efficiency (Boyd et al., 1984).

If our data on the influences on community composition are indicative of broader sympagic communities, then projected environmental changes of decline in sea-ice extent and snow cover leading to increased light transmitted under the ice, may shape communities to be more diverse, with a greater contribution of *Navicula* spp., *Fragilariopsis* spp., *Cylindrotheca closterium* and Dinophyceae. However, if communities face physiochemically stressful conditions associated with warming oceans, including bottom-ice melt and nitrate limitation, the assemblages may be less diverse with an increased contribution from *N. frigida*. Such changes would have significant biogeochemical implications, as Dinophyceae predominantly cycle S and P whilst diatoms are key players in the Si cycle. In addition, alterations to microalgal community size structure and abundance of aggregate chains vs. solitary cells would inevitably have implications for energy supplied to the food web and carbon export (Levinsen et al., 2000).

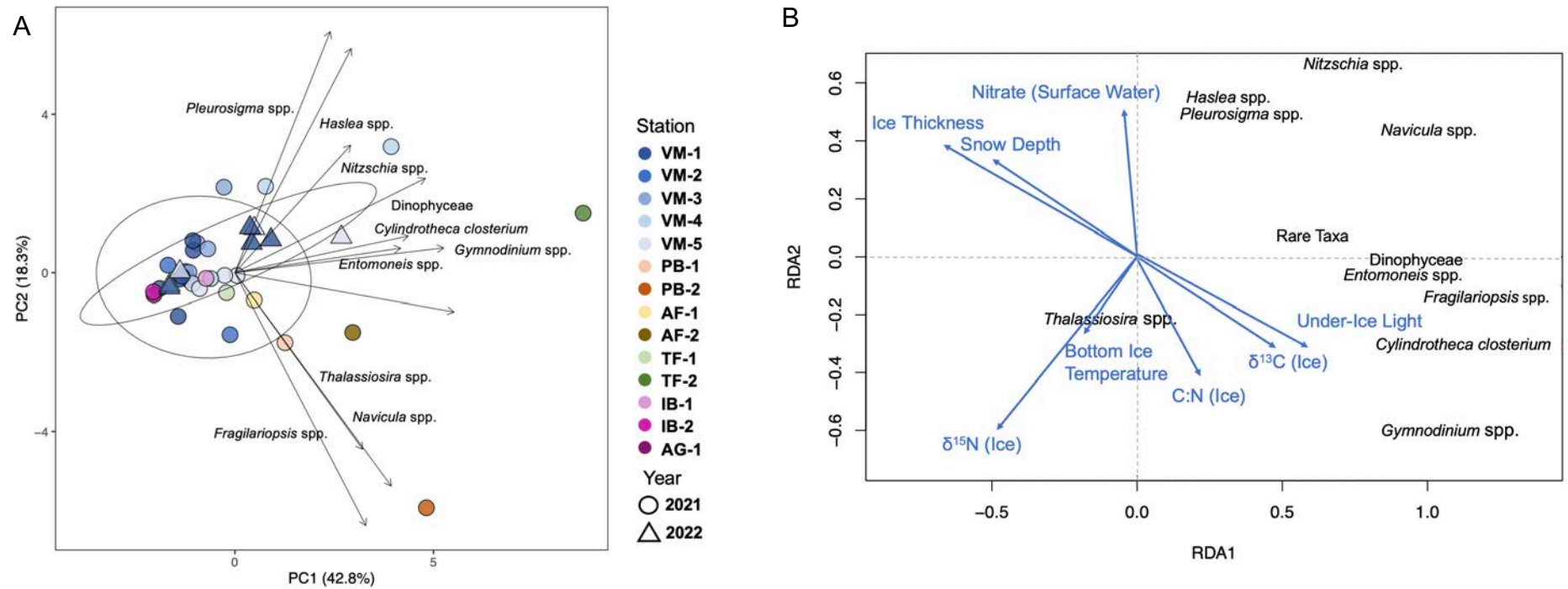


**Figure 7.1:** (A) Principal component analysis (PCA) of community composition in 2021 (circles) and 2022 (triangles) with station denoted by colour. Direction and strength of species composition are displayed with ordination bi-plot overlay. (B) Redundancy analysis (RDA) biplot of the relative abundance of taxonomic groups constrained to environmental variables ( $n=7$ ) with Monte Carlo permutations (999), model is significant ( $F_8=9.793$ ,  $p < 0.05$ ) following model optimisation in which insignificant variables were removed.

### **Environmental conditions determine biomolecular content of sea-ice microalgae exposing species specific metabolic plasticity**

Using s-FTIR, we examined the biomolecular composition of five dominant sea-ice diatom taxa from Arctic land-fast ice communities within gradients of environmental conditions, and five pelagic diatom taxa from a Southern Ocean community exposed to OA scenarios. All taxa were found to exhibit plasticity in how they shifted their carbon compounds with different environmental conditions, but the direction and strength of the changes varied across taxa.

Firstly, under-ice light was found to be a key determinant of carbon allocation into biomolecules of sea-ice algae. Of the five taxa examined, all showed a doubling of lipid and fatty acid content when light transmitted to the bottom-ice communities was >5% but <15% incoming PAR. Secondary to lipid synthesis, all five taxa also increased energy allocation toward carbohydrates, whilst protein content remained stable. Lipid content plateaued in four of the five taxa beyond the threshold of 15% incoming PAR, possibly due to photo-inhibitory effects. Given that protein content remained stable, and a loss or decline in protein is often an indicator of stress, it is also possible that once light reached a threshold in which photosynthesis was maximised, lipid production became saturated. Interestingly, *Navicula* spp. continued to accumulate lipids beyond 15% incoming light (Chapter 4) and was more dominant at higher light sites (Chapter 3). These findings indicate that species from this genus may be better adapted to high-light than many of their contemporaries, and future work should look into the photophysiological properties of this species comparatively with others. Moreover, these results suggest that assemblages exposed to increased incoming light, as a result of a decline in snow depth or ice thickness, may be more likely to be dominated by lipid-rich, energy dense *Navicula* spp. cells. This is one of the few studies that can separate species plasticity and their responses within the sea-ice environment, showing that not all taxa react the same to environmental change. These findings highlight the importance of single-cell interrogation of natural microalgal communities for realising how shifts in species dominance will ultimately impact the nutritional value of the community at the base of the polar marine food web.

To capture temporal dynamics in community structure and nutritional content, we conducted a seasonal study of the most prevalent bottom-ice taxa, *N. frigida*. The findings from this study elucidated additional environmental factors that determine shifts in sea-ice algal nutritional content, as there was minimal variability in light transmittance for the duration of the study. The plasticity of *N. frigida* was revealed, as this species was shown to have high intra-specific variability in biomolecular content depending on environmental conditions. These types of temporal studies in polar sea ice are uncommon, due to logistical constraints, making the knowledge derived from this study important and a rare contribution to the field. By using single cell analysis, we were able to isolate and target a single taxon within its natural environment. This ensures that the species of interest is exposed to multivariable influences (environmental and biological), providing important and unique insight into the metabolic adjustment that *N. frigida* undergo within a natural setting. This repeated measures approach allowed us to capture seasonal progression towards the end of the productive sea-ice season, indicated by warming seawater temperatures and low nutrient conditions. These conditions resulted in an increase in lipid and fatty acids stores, and a decline in protein and carbohydrate content in *N. frigida* (Chapter 5). The observed shifts in metabolic energy allocation by this taxon alone greatly influences energy supplied to polar marine food webs, as *N. frigida* was shown to contribute up to 95% of the sympagic community (Chapter 3), especially late in the productive season (Chapters 3 & 5). Increased lipid stores have implications for microalgal inter-annual survival, as lipid storage is expected to be used by *N. frigida* to allow the cells to survive the dark winter outside of sea-ice (Palmisano & Sullivan, 1983; Zhang et al., 1998). The increased lipid allocation also has implications for carbon export to the ocean floor. Whilst lipid-rich cells provide high energy food to hungry food webs, they are more buoyant and therefore slower to sink to depths, with a higher likelihood of being consumed in the pelagic zone, thereby reducing and slowing carbon export (Harvey & Johnston, 1995; Parrish et al., 2005). Through this work, we were able to show the natural seasonal progression in cell-specific biomolecular content of *N. frigida*, bringing to light new understanding of the overwintering strategies of this dominant taxon.

In the context of climate change driven environmental perturbations, it is generally predicted that under-ice light availability will change, particularly in the Arctic, due to sea-ice thinning and changes in snowfall trends. Our findings show that the nutritional content of sea-ice diatoms is taxon-specific and can be linked to such changes. If our

findings are ubiquitous across other sea-ice microalgal communities, we may anticipate assemblages with higher lipid, fatty acid and carbohydrate content, as light transmitted to the bottom-ice and ocean temperatures increase. However, this research has also shown that these increases are finite and carbon storage molecules reach a threshold, at intensities already experienced by sea-ice communities. If conditions exceed ~15% of incoming PAR transmitted to the bottom-ice, the accumulation of energy within cells appears to plateau, with the exception of *Navicula* spp. Therefore, with thinning ice and snow, the threshold of incoming irradiance may be reached earlier in the productive season meaning that lipid production and peak net primary productivity occur earlier. Depending on the magnitude and extent of early productivity boom, this may counter potential losses from an earlier sea-ice break up. On the other hand, if the ecosystem experiences very limited sea-ice growth and snowfall, or rain-on-snow events early in the season, the community may not have time to become established and proliferate before the light transmitted to the bottom-ice is above the tolerated threshold observed for several key species, or before the warming breaks up the ice. Either scenario could be detrimental to the development of sympagic blooms and their peak productivity and similarly to their growth and preparation for overwintering.

As with under-ice light conditions, the impact of ocean warming is complex and difficult to predict. Increased sea-surface temperatures and associated changes to ocean circulation patterns could bring abrupt warmer water advection triggering an early end-of-season sea-ice melt. Under a scenario where the sea-ice melt occurs earlier, it is possible that this could trigger a trophic mismatch with zooplankton who have evolved their reproductive cycles to allow adults to make use of the lipid-rich sea-ice assemblage for reproduction, ensuring the juveniles are at a feeding stage by the summer pelagic blooms (Søreide et al., 2006, 2008, 2010). It is unclear whether key zooplankton species could adapt their life strategy to be successful with sympagic and pelagic blooms arriving earlier, or in the absence of sympagic blooms entirely. The rapidity of the under-ice melt is also anticipated to impact sea-ice algal communities and carbon export. If sea-ice is rapidly and prematurely melted from below through an abrupt influx of warm water, or through rain and atmospheric heatwave events (Fortier et al. 2002), the sympagic community could be released to the pelagic zone prior to accumulating adequate lipid storage to survive the winter. On the other hand, if the bottom-ice melt simply occurs earlier, but

not abruptly, the community could have time to accumulate the necessary lipid for winter storage but not be phenologically matched to supply this lipid to zooplankton.

Ocean acidification (OA) presents one of the most salient threats to marine life and the SO, because of its cool, well mixed waters, is one of the biggest CO<sub>2</sub> sinks, making its biota some of the most vulnerable to OA. While many studies have explored the effects of OA on phytoplankton, none to date have looked at the effect OA has on biomolecular composition of species within natural phytoplankton communities, making this work a unique contribution to the field of OA research. Through exposing a natural Antarctic phytoplankton community to a gradient of  $f\text{CO}_2$  levels (288 – 1263  $\mu\text{atm}$ ), we found that there are species-specific differences in the metabolic plasticity of diatoms in response to OA. Our findings demonstrate that under the acidification levels projected for 2100, larger taxa preferentially allocated energy towards proteins, while smaller taxa increased both lipid and protein stores. If these changes are representative of future SO diatom physiology, we may therefore expect the community to be dominated by smaller taxa, but with higher lipid and protein allocation than present-day contemporaries, inevitably having cascading effects on food web dynamics in the Antarctic marine ecosystem. However, it is unknown whether these findings are consistent beyond the five Antarctic taxa measured. Further work is therefore required to determine how widespread and heterogenous these responses are, both across SO species and taxa from different oceanic regions.

The biomolecular research presented in this thesis has delivered novel insights into the nutritional diversity of polar sympagic and pelagic microalgae, their individual plasticity and responses. Through this work, it has provided new knowledge on climate change driven environmental perturbations that may impact polar microalgal community composition, species-specific biomolecular allocation and ultimately the quantity and quality of energy supplied to polar marine food webs.

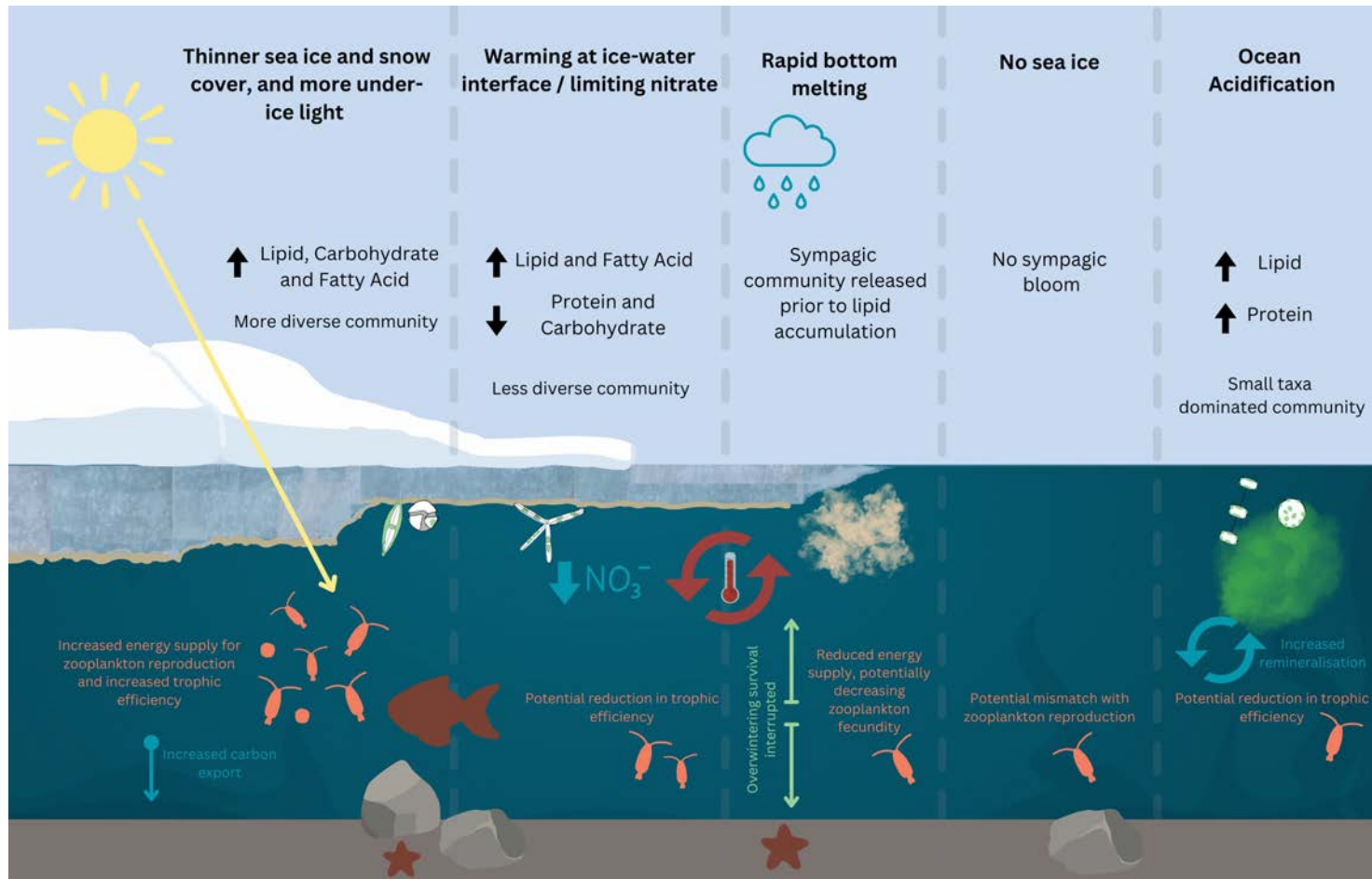


**Figure 7.2:** Conceptual overview of biomolecular and community composition changes under different projected environmental scenarios (bold text), and some potential impacts on trophic transfer, secondary production (orange), diatom over-wintering (green) and nutrient cycling (blue).



## Future Directions

### *Cellular Level Changes:*

The single celled analyses (microscopy and s-FTIR microspectroscopy) employed throughout this research demonstrate how harnessing such techniques are essential for disentangling taxon-specific changes from community wide effects. In providing cell-specific biomolecular profiles in an ecologically relevant setting, we can better determine the potential winners of environmental change, and accurately predict biochemical cycling and the nutritional quality of the energy that is transferred through food webs. Ongoing research into climate change driven biomolecular phenotyping is therefore essential to obtaining a comprehensive and fine-scale understanding of future polar marine ecosystem dynamics. As such, single celled techniques, including the s-FTIR used in these studies, are projected to be essential tools and techniques in future studies.

Advancements in this field that could help us to better understand the physiological mechanism behind the changes in carbon allocation include combining measurements of microalgal nutritional content with productivity rates and photophysiology. The relationships between these variables are important for disentangling stress responses from peak productivity or limitation and teasing apart species competition. This could be explored by combining the single-cell analysis techniques presented in this thesis with tools such as, single-celled microscopy-based pulse amplitude modulation (PAM) fluorometry (providing insights into the photosynthetic activity) and/or stable isotope probing (elucidating the pathway of carbon through photosynthesis, respiration and biosynthesis).

It would also be of great interest to investigate the role of trace metal bioavailability in determining sea-ice microalgal biomolecular profiles, particularly in the SO where iron is well-established to be a limiting element for photosynthetic activity (Boyd, 2002; Lannuzel et al., 2020), with seasonal and spatial variability. One potential approach to investigate this is combining s-FTIR with synchrotron-based X-ray fluorescence microscopy, which allows imaging the elemental concentration and distribution in cells at sub-micron level spatial scale. When used together, this would provide a comprehensive 2D cellular map of macro- and micro-nutrient acquisition, storage and cycling by sea-ice algae at a taxon-specific level.

As the ‘omics’ fields continue to improve, these technologies are increasingly useful in providing insights into microalgal distribution, physiological condition and metabolic activities. Metaproteomics and metatranscriptomics are fields of particular interest for polar algal research, as they explore microalgal functionality by characterising protein and gene expression, respectively, at a defined point in time. These approaches can therefore determine microalgal adaptive responses, resource allocation strategies and capacity to shifting environmental conditions (McCain et al., 2022; Salazar et al., 2019; Wang et al., 2014). Metabolomic analyses would also make a valuable addition to the single-cell analyses presented in this thesis (Behrendt et al., 2018), as this technique elucidates the metabolic pathways occurring when microalgae are exposed to different environmental conditions, which would therefore provide important insights into why the observed shifts in biomolecular allocation take place.

#### *Trophic-level Changes and Alterations to Food Web Dynamics*

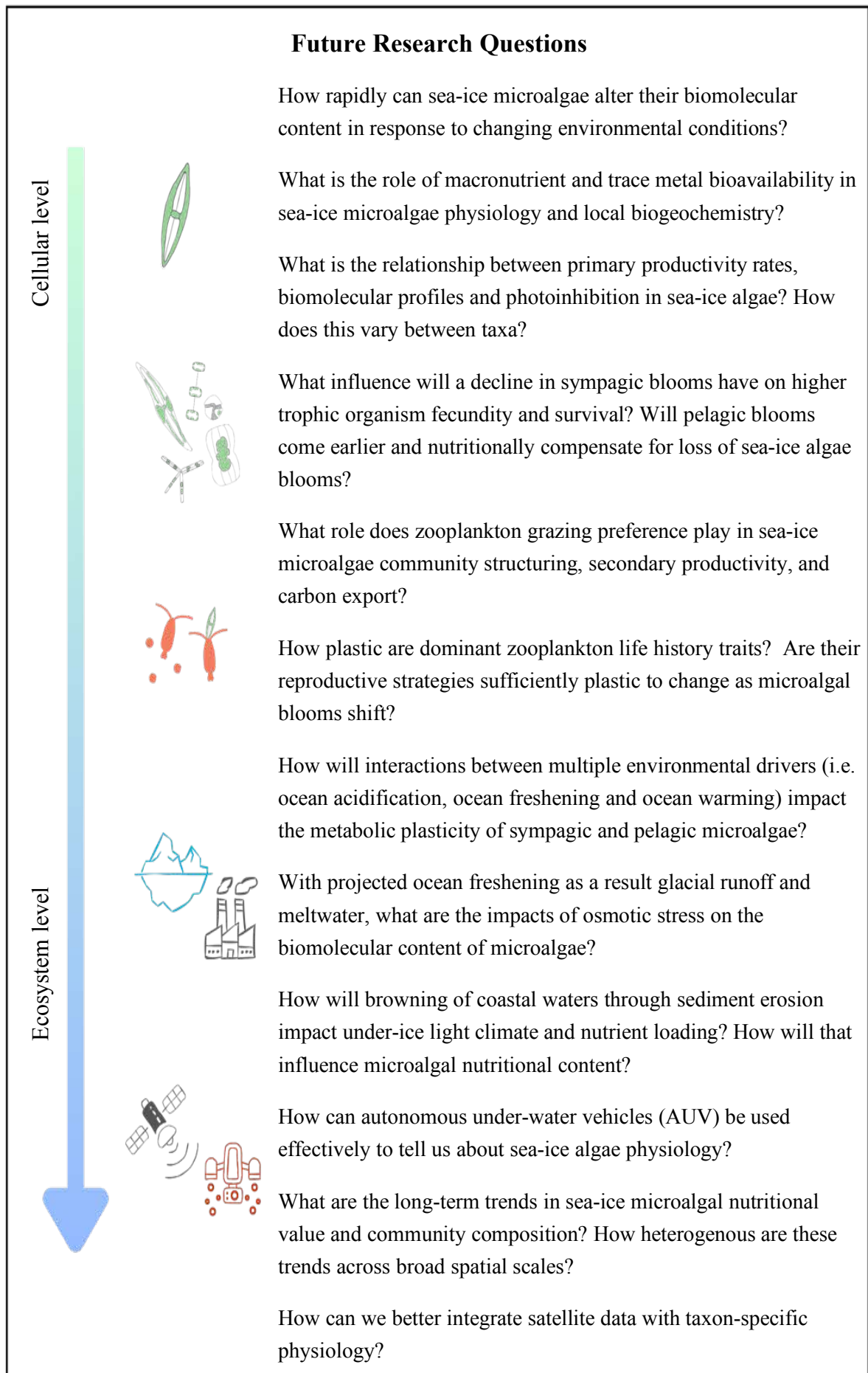
To adequately interpret the changes to polar microalgae in an ecological context, the linkages within the marine food webs need further investigation. Zooplankton are the main consumer of microalgae and are themselves an important prey for many predators such as fish and birds (Lønne & Gulliksen, 1989; Trathan & Hill, 2016; Wold et al., 2011). Therefore, understanding how dominant zooplankton species, such as *Calanus* spp. in the AO and *Euphausia superba* in the SO, are impacted by changes to microalgal quality and bloom timing, is vital to understanding the flows of carbon and energy through the marine system. It is therefore essential for future studies to target how the nutritional content and timing of blooms may change, and the plasticity of zooplankton life history traits.

Firstly, it is unclear how zooplankton grazing preferences will impact secondary productivity and carbon export, as microalgal community composition and nutritional content shift. Whilst some insights into zooplankton preferences of microalgal size (Campbell et al., 2009, 2016b) and species (Durbin & Casas, 2014) have been ascertained, further work on additional dominant zooplankton species is needed. It also remains unknown how microalgal nutritional content influences zooplankton consumption. Therefore, grazing experiments, potentially involving exposure to projected environmental stressors, coupled with gut content analysis of natural communities under

variable environmental conditions, through next-generation sequencing of 18S rDNA (Cleary et al., 2017; Durbin & Casas, 2014), would be valuable.

Secondly, with sympagic and pelagic bloom timing anticipated to shift with changing sea-ice conditions, it is critical to ascertain if earlier pelagic blooms can nutritionally compensate for changes to, or loss of, sea-ice algae blooms. Whilst considerable work has been done on the trophic links of ice-algal derived carbon (Amiriaux et al., 2023; Kohlbach et al., 2018; Leu et al., 2020; Søreide et al., 2006, 2013), the adaptability of zooplankton life history traits to meet reproductive nutritional requirements under new environmental regimes is unclear. Variation has been observed between the life strategies between different *Calanus* spp. in the Arctic (Swalethorp et al., 2011), however it remains unclear if each *Calanus* spp. could adjust their own traits to match bloom timing, and if so, what the trade-offs would be. This could be achieved through individual based modelling (Ji et al., 2012) on the key *Calanus* species, to determine if alterations to their reproductive timing to match earlier and shorter blooms is possible. Such studies should be linked to ground-truthing data on ‘when’ zooplankton are consuming ‘what’ microalgal blooms currently in natural systems, determined through techniques such as stable isotope tracing (Forest et al. 2011a; Kohlbach et al., 2016). With increasing awareness of the importance of under-ice blooms (pelagic blooms below sea ice) (Ardyna et al., 2020; Arrigo et al., 2012), it would be of particular interest to apply stable isotope trophic-marker studies (Clement Kinney et al., 2020) to determine the role that these blooms can and will play in providing energy to the marine food web.

If zooplankton life history traits lack the necessary plasticity to adapt to the changing bloom timing, patterns of species dominance amongst zooplankton may change as food availability changes (i.e. smaller zooplankton species dominating if smaller microalgal species dominate). Here, studies utilising molecular probes and DNA metabarcoding are useful to determine species composition, size and discriminate between what life histories are present at different times coinciding with blooms (Kiesling et al., 2002). In addition, targeted and non-targeted metabolomics and metaproteomics (reviewed in Amato & Carotenuto, 2018; Matos et al., 2020) are increasingly valuable to determine shifts in zooplankton metabolic potential, nutritional value and energy transfer through food webs (Wang et al., 2016).



*Broad Temporal and Spatial Scales, and Effects of Multi-Drivers*

With the nature of the environmental changes facing the polar regions being so complex and interconnected, ongoing research needs to be conducted into the synergistic effects of multiple environmental stressors, ideally on many species. With natural community sampling, this emphasises the need to collect as much ancillary environmental data as possible, and employ multivariate analysis techniques to ensure all possible environmental drivers are considered as agents for change. Outside of field-based research, potential valuable approaches to tackle the understanding of synergistic effects include network interaction models, which consider the interactions of multiple, interactive and hierarchical effects on a system (Arrigo et al., 2020). Further multivariate manipulative studies would also be particularly useful (Spilling et al., 2015; Xu et al., 2014) to directly test climate change drivers in a controlled manner to elucidate how different environmental perturbations may interact with each other in eliciting physiological and community based changes.

Research in the polar regions requires a multi-faceted approach. The large, often inaccessible and inhospitable, spatial scales mean that spatially broad techniques need to be applied. Tools such as aerial remote sensing can be beneficial for addressing large scale questions (i.e. pan-Arctic, Antarctic or polar) such as spatial and temporal changes to primary productivity, sea-ice extent, incoming light to the water column, ocean colour and sediment inflows (e.g. IOCCG, 2015; Petrenko et al., 2013; Singh et al., 2022). However, the important finer scale, general mechanistic questions require different approaches. The use of remote technologies therefore does not preclude or supplant the need to sample natural communities and capture ecological variation or obtain ground-truthing data. Thus, whilst field sampling is logistically difficult and has an environmental cost, analysis of natural communities and collection of field observations remains critical and should not be neglected.

One valuable approach, combining field sampling with remote data collection, is the use of autonomous under-water vehicles (AUV). This technology offers exciting prospects including sampling and *in situ* monitoring without disturbing the environment, and for mapping microalgal distribution across the bottom-ice surface (Cimoli et al., 2017; Forrest et al., 2019; Lund-Hansen et al., 2018). The rapid advancement of robotic auto-sampling will increasingly lead to AUV's equipped with instrumentation and samplers

facilitating remote and extensive data and sample collection (Yamahara et al., 2019). With the potential for long-term deployments, this technology would also allow for more data to be collected, providing greater spatial and temporal resolution. Future studies would benefit from combining analysis techniques discussed here and presented in this thesis, with emerging technologies, enabling targeted sample collection and/or monitoring from autonomous underwater vehicles (AUVs) (Zhang et al., 2019). With this framework, these remote technologies could collect data on broad spatial and temporal scales, whilst facilitating analyses on a small cell or subcellular scale. Finding the balance and link between these small-scale tools and broad scale approaches is a vital step in obtaining a complete understanding of polar ecosystems and how they are changing.

### **Concluding Remarks**

This thesis addresses critical knowledge gaps by providing much needed insights into taxon-specific microalgal metabolic plasticity, including demonstrating anticipated shifts in nutritional value under climate change driven environmental change. This was achieved through extensive field sampling of AO land-fast sea-ice microalgal communities, and experimental manipulation of a natural SO pelagic community. Through incorporating repeated transects over time, seasonal data has also been captured which is crucial to our understanding of these fragile ecosystems. Valuable insights into anticipated community composition shifts with climate change are presented, through spatiotemporally expansive data. Together, these results provide new insights into how the expected environmental changes may manifest in the nutritional value and community dynamics of polar microalgae. Such insights are essential in determining the future of the polar oceans, revealing shifts in ocean biogeochemistry and the success of zooplankton, food-webs and the wider polar marine ecosystem.

## References:

- Aagaard, K. (1981). On the deep circulation in the Arctic Ocean. *Deep Sea Research Part A. Oceanographic Research Papers*, 28(3), 251-268.
- Ackman, R. G. (1989). *Marine biogenic lipids, fats and oils* (Vol. 2). CRC press, Boca Raton, FL, U.S.A.
- Ahn, S. H., Whitley, T. E., Stockwell, D. A., Lee, J. H., & Lee, S. H. (2019). The biochemical composition of phytoplankton in the Laptev and East Siberian seas during the summer of 2013. *Polar Biology*, 42(1), 133-148.
- Alderkamp, A.-C., Buma, A. G., & van Rijssel, M. (2007). The carbohydrates of *Phaeocystis* and their degradation in the microbial food web. *Biogeochemistry*, 83, 99-118.
- Alou-Font, E., Mundy, C.-J., Roy, S., Gosselin, M., & Agustí, S. (2013). Snow cover affects ice algal pigment composition in the coastal Arctic Ocean during spring. *Marine Ecology Progress Series*, 474, 89-104.
- Amato, A., & Carotenuto, Y. (2018). Planktonic calanoids embark into the “omics” era. In M. Uttieri (Ed.) *Trends in Copepod Studies—Distribution, Biology and Ecology*, (pp. 287-314), Nova Science Publishers, Hauppauge, NY, U.S.A.
- Amiriaux, R., Mundy, C., Pierrejean, M., Niemi, A., Hedges, K. J., Brown, T. A., Ehn, J. K., Elliott, K. H., Ferguson, S. H., & Fisk, A. T. (2023). Tracing carbon flow and trophic structure of a coastal Arctic marine food web using highly branched isoprenoids and carbon, nitrogen and sulfur stable isotopes. *Ecological Indicators*, 147, 109938.
- An, M., Mou, S., Zhang, X., Ye, N., Zheng, Z., Cao, S., Xu, D., Fan, X., Wang, Y., & Miao, J. (2013). Temperature regulates fatty acid desaturases at a transcriptional level and modulates the fatty acid profile in the Antarctic microalga *Chlamydomonas* sp. ICE-L. *Bioresource technology*, 134, 151-157.
- Andrew, S. M., Strzepek, R. F., Branson, O., & Ellwood, M. J. (2022). Ocean acidification reduces the growth of two Southern Ocean phytoplankton. *Marine Ecology Progress Series*, 682, 51-64.
- Archer, S. D., Leakey, R. J., Burkill, P. H., Sleigh, M. A., & Appleby, C. J. (1996). Microbial ecology of sea ice at a coastal Antarctic site: community composition, biomass and temporal change. *Marine Ecology Progress Series*, 135, 179-195.
- Ardyna, M., & Arrigo, K. R. (2020). Phytoplankton dynamics in a changing Arctic Ocean. *Nature Climate Change*, 10(10), 892-903.
- Ardyna, M., Gosselin, M., Michel, C., Poulin, M., & Tremblay, J.-É. (2011). Environmental forcing of phytoplankton community structure and function in the Canadian High Arctic: contrasting oligotrophic and eutrophic regions. *Marine Ecology Progress Series*, 442, 37-57.
- Ardyna, M., Mundy, C., Mayot, N., Matthes, L. C., Oziel, L., Horvat, C., Leu, E., Assmy, P., Hill, V., & Matrai, P. A. (2020). Under-ice phytoplankton blooms: Shedding light on the “invisible” part of Arctic primary production. *Frontiers in Marine Science*, 7, 608032.
- Armbrust, E. V. (2009). The life of diatoms in the world's oceans. *Nature*, 459(7244), 185-192.
- Arndt, S., Meiners, K. M., Ricker, R., Krumpfen, T., Katlein, C., & Nicolaus, M. (2017). Influence of snow depth and surface flooding on light transmission through Antarctic pack ice. *Journal of Geophysical Research: Oceans*, 122(3), 2108-2119.

- Arrigo, K., van Dijken, G. L., Cameron, M., van der Grient, J., Wedding, L., Hazen, L., Leape, J., Leonard, G., Merkl, A., & Micheli, F. (2020). Synergistic interactions among growing stressors increase risk to an Arctic ecosystem. *Nature Communications*, *11*(1), 6255.
- Arrigo, K. R. (2005). Marine microorganisms and global nutrient cycles. *Nature*, *437*(7057), 349-355.
- Arrigo, K. R. (2014). Sea ice ecosystems. *Annual review of marine science*, *6*, 439-467.
- Arrigo, K. R., Brown, Z. W., & Mills, M. M. (2014a). Sea ice algal biomass and physiology in the Amundsen Sea, Antarctica. *Elementa*, *2*, 000028.
- Arrigo, K. R., Perovich, D. K., Pickart, R. S., Brown, Z. W., Van Dijken, G. L., Lowry, K. E., Mills, M. M., Palmer, M. A., Balch, W. M., & Bahr, F. (2012). Massive phytoplankton blooms under Arctic sea ice. *Science*, *336*(6087), 1408-1408.
- Arrigo, K. R., Perovich, D. K., Pickart, R. S., Brown, Z. W., Van Dijken, G. L., Lowry, K. E., Mills, M. M., Palmer, M. A., Balch, W. M., & Bates, N. R. (2014b). Phytoplankton blooms beneath the sea ice in the Chukchi Sea. *Deep Sea Research Part II: Topical Studies in Oceanography*, *105*, 1-16.
- Arrigo, K. R., Mills, M. M., & Juranek, L. W. (2024). The Arctic Ocean Nitrogen Cycle. *Biogeosciences*, *129*(7), e2024JG008088.
- Arrigo, K. R., & van Dijken, G. L. (2011). Secular trends in Arctic Ocean net primary production. *Journal of Geophysical Research: Oceans*, *116*, C09011.
- Arrigo, K. R., & van Dijken, G. L. (2015). Continued increases in Arctic Ocean primary production. *Progress in Oceanography*, *136*, 60-70.
- Arrigo, K. R., van Dijken, G. L., & Bushinsky, S. (2008). Primary production in the Southern Ocean, 1997–2006. *Journal of Geophysical Research: Oceans*, *113*, C08004.
- Arrigo, K. R., van Dijken, G. L., Castelao, R. M., Luo, H., Rennermalm, Å. K., Tedesco, M., Mote, T. L., Oliver, H., & Yager, P. L. (2017). Melting glaciers stimulate large summer phytoplankton blooms in southwest Greenland waters. *Geophysical Research Letters*, *44*(12), 6278-6285.
- Arrigo, K. R., Worthen, D., Schnell, A., & Lizotte, M. P. (1998). Primary production in Southern Ocean waters. *Journal of Geophysical Research: Oceans*, *103*(C8), 15587-15600.
- Arrigo, K. R., Worthen, D. L., Lizotte, M. P., Dixon, P., & Dieckmann, G. (1997). Primary production in Antarctic sea ice. *Science*, *276*(5311), 394-397.
- Arteaga, L. A., Boss, E., Behrenfeld, M. J., Westberry, T. K., & Sarmiento, J. L. (2020). Seasonal modulation of phytoplankton biomass in the Southern Ocean. *Nature Communications*, *11*(1), 5364.
- Årthun, M., Eldevik, T., & Smedsrud, L. H. (2019). The role of Atlantic heat transport in future Arctic winter sea ice loss. *Journal of Climate*, *32*(11), 3327-3341.
- Auger, M., Morrow, R., Kestenare, E., Sallée, J.-B., & Cowley, R. (2021). Southern Ocean in-situ temperature trends over 25 years emerge from interannual variability. *Nature Communications*, *12*(1), 514.
- Aumack, C., & Juhl, A. (2015). Light and nutrient effects on the settling characteristics of the sea ice diatom *Nitzschia frigida*. *Limnology and Oceanography*, *60*(3), 765-776.
- Bach, L. T., & Taucher, J. (2019). CO<sub>2</sub> effects on diatoms: a synthesis of more than a decade of ocean acidification experiments with natural communities. *Ocean Science*, *15*(4), 1159-1175.



- Bamberg, K. R., Wood, B. R., & McNaughton, D. (2012). Resonant Mie scattering (RMieS) correction applied to FTIR images of biological tissue samples. *Analyst*, 137(1), 126-132.
- Baragi, L. V., Khandeparker, L., & Anil, A. C. (2015). Influence of elevated temperature and pCO<sub>2</sub> on the marine periphytic diatom *Navicula distans* and its associated organisms in culture. *Hydrobiologia*, 762, 127-142.
- Barlow, R., Gosselin, M., Legendre, L., Therriault, J.-C., Demers, S., Mantoura, R., & Llewellyn, C. (1988). Photoadaptive strategies in sea-ice microalgae. *Marine Ecology Progress Series*, 45, 145-152.
- Barrie, A., Davies, J., Park, A., & Workman, C. (1989). Continuous-flow stable isotope analysis for biologists. *Spectroscopy*, 4(7), 42-52.
- Beardall, J., & Raven, J. A. (2004). The potential effects of global climate change on microalgal photosynthesis, growth and ecology. *Phycologia*, 43(1), 26-40.
- Beardall, J., Berman, T., Heraud, P., Omo Kadiri, M., Light, B. R., Patterson, G., Roberts, G., Sulzberger, B., Sahan, E., Uehlinger, U. & Wood, B. (2001). A comparison of methods for detection of phosphate limitation in microalgae. *Aquatic Sciences*, 63(1), 107-121.
- Becquevort, S., Dumont, I., Tison, J.-L., Lannuzel, D., Sauvée, M.-L., Chou, L., & Schoemann, V. (2009). Biogeochemistry and microbial community composition in sea ice and underlying seawater off East Antarctica during early spring. *Polar Biology*, 32(6), 879-895.
- Behrendt, L., Raina, J.-B., Lutz, A., Kot, W., Albertsen, M., Halkjær-Nielsen, P., Sørensen, S. J., Larkum, A. W., & Kühl, M. (2018). In situ metabolomic-and transcriptomic-profiling of the host-associated cyanobacteria *Prochloron* and *Acaryochloris marina*. *The ISME journal*, 12(2), 556-567.
- Behrenfeld, M. J., Halsey, K. H., Boss, E., Karp-Boss, L., Milligan, A. J., & Peers, G. (2021). Thoughts on the evolution and ecological niche of diatoms. *Ecological Monographs*, 91(3), e01457.
- Bélangier, S., Xie, H., Krotkov, N., Larouche, P., Vincent, W. F., & Babin, M. (2006). Photomineralization of terrigenous dissolved organic matter in Arctic coastal waters from 1979 to 2003: Interannual variability and implications of climate change. *Global Biogeochemical Cycles*, 20(4), GB4005.
- Bellerby, R., Schulz, K. G., Riebesell, U., Neill, C., Nondal, G., Heegaard, E., Johannessen, T., & Brown, K. (2008). Marine ecosystem community carbon and nutrient uptake stoichiometry under varying ocean acidification during the PeECE III experiment. *Biogeosciences*, 5(6), 1517-1527.
- Belt, S. T. (2018). Source-specific biomarkers as proxies for Arctic and Antarctic sea ice. *Organic geochemistry*, 125, 277-298.
- Belt, S. T., Brown, T. A., Smik, L., Tatarek, A., Wiktor, J., Stowasser, G., Assmy, P., Allen, C. S., & Husum, K. (2017). Identification of C25 highly branched isoprenoid (HBI) alkenes in diatoms of the genus *Rhizosolenia* in polar and sub-polar marine phytoplankton. *Organic Geochemistry*, 110, 65-72.
- Benkort, D., Daewel, U., Heath, M., & Schrum, C. (2020). On the role of biogeochemical coupling between sympagic and pelagic ecosystem compartments for primary and secondary production in the Barents Sea. *Frontiers in Environmental Science*, 8, 548013.
- Berge, J., Renaud, P. E., Darnis, G., Cottier, F., Last, K., Gabrielsen, T. M., Johnsen, G., Seuthe, L., Weslawski, J. M., & Leu, E. (2015). In the dark: a review of ecosystem processes during the Arctic polar night. *Progress in Oceanography*, 139, 258-271.

- Berge, T., Daugbjerg, N., Andersen, B. B., & Hansen, P. J. (2010). Effect of lowered pH on marine phytoplankton growth rates. *Marine Ecology Progress Series*, 416, 79-91.
- Berges, J. A., Charlebois, D. O., Mauzerall, D. C., & Falkowski, P. G. (1996). Differential effects of nitrogen limitation on photosynthetic efficiency of photosystems I and II in microalgae. *Plant Physiology*, 110(2), 689-696.
- Berges, J. A., & Falkowski, P. G. (1998). Physiological stress and cell death in marine phytoplankton: induction of proteases in response to nitrogen or light limitation. *Limnology and Oceanography*, 43(1), 129-135.
- Bernard, K. S., Gunther, L. A., Mahaffey, S. H., Qualls, K. M., Sugla, M., Saenz, B. T., Cossio, A. M., Walsh, J., & Reiss, C. S. (2019). The contribution of ice algae to the winter energy budget of juvenile Antarctic krill in years with contrasting sea ice conditions. *ICES Journal of Marine Science*, 76(1), 206-216.
- Bestion, E., Haegeman, B., Alvarez Codesal, S., Garreau, A., Huet, M., Barton, S., & Montoya, J. M. (2021). Phytoplankton biodiversity is more important for ecosystem functioning in highly variable thermal environments. *Proceedings of the National Academy of Sciences*, 118(35), e2019591118.
- Beszteri, S., Thoms, S., Benes, V., Harms, L., & Trimborn, S. (2018). The response of three Southern Ocean phytoplankton species to ocean acidification and light availability: a transcriptomic study. *Protist*, 169(6), 958-975.
- Bhavya, P., Kim, B. K., Jo, N., Kim, K., Kang, J. J., Lee, J. H., Lee, D., Lee, J. H., Joo, H., & Ahn, S. H. (2019). A review on the macromolecular compositions of phytoplankton and the implications for aquatic biogeochemistry. *Ocean Science Journal*, 54(1), 1-14.
- Boetius, A., Albrecht, S., Bakker, K., Bienhold, C., Felden, J., Fernández-Méndez, M., Hendricks, S., Katlein, C., Lalande, C., & Krumpen, T. (2013). Export of algal biomass from the melting Arctic sea ice. *Science*, 339(6126), 1430-1432.
- Boone, W., Rysgaard, S., Carlson, D. F., Meire, L., Kirillov, S., Mortensen, J., Dmitrenko, I., Vergeynst, L., & Sejr, M. K. (2018). Coastal freshening prevents fjord bottom water renewal in Northeast Greenland: a mooring study from 2003 to 2015. *Geophysical Research Letters*, 45(6), 2726-2733.
- Boyd, C. M., Heyraud, M., & Boyd, C. N. (1984). Feeding of the Antarctic krill *Euphausia superba*. *Journal of Crustacean Biology*, 4(5), 123-141.
- Boyd, P. W. (2002). Environmental factors controlling phytoplankton processes in the Southern Ocean. *Journal of Phycology*, 38(5), 844-861.
- Boyd, P. W., Claustre, H., Levy, M., Siegel, D. A., & Weber, T. (2019). Multi-faceted particle pumps drive carbon sequestration in the ocean. *Nature*, 568(7752), 327-335.
- Breteler, W. K., Schogt, N., & Rampen, S. (2005). Effect of diatom nutrient limitation on copepod development: role of essential lipids. *Marine Ecology Progress Series*, 291, 125-133.
- Bromke, M. A. (2013). Amino acid biosynthesis pathways in diatoms. *Metabolites*, 3(2), 294-311.
- Brown, K. A., Holding, J. M., & Carmack, E. C. (2020). Understanding regional and seasonal variability is key to gaining a pan-Arctic perspective on Arctic Ocean freshening. *Frontiers in Marine Science*, 7, 606.
- Brown, T. A., Belt, S. T., Tatarek, A., & Mundy, C. (2014). Source identification of the Arctic sea ice proxy IP25. *Nature Communications*, 5(1), 4197.

- Brown, T. A., Galicia, M. P., Thiemann, G. W., Belt, S. T., Yurkowski, D. J., & Dyck, M. G. (2018). High contributions of sea ice derived carbon in polar bear (*Ursus maritimus*) tissue. *PLoS one*, *13*(1), e0191631.
- Brussaard, C., Noordeloos, A., Witte, H., Collenteur, M., Schulz, K., Ludwig, A., & Riebesell, U. (2013). Arctic microbial community dynamics influenced by elevated CO<sub>2</sub> levels. *Biogeosciences*, *10*(2), 719-731.
- Brzezinski, M. A. (1985). The Si: C: N ratio of marine diatoms: interspecific variability and the effect of some environmental variables. *Journal of Phycology*, *21*(3), 347-357.
- Budge, S., Wooller, M., Springer, A., Iverson, S. J., McRoy, C., & Divoky, G. (2008). Tracing carbon flow in an arctic marine food web using fatty acid-stable isotope analysis. *Oecologia*, *157*(1), 117-129.
- Bunt, J., & Lee, C. (1972). Data on the composition and dark survival of four sea-ice microalgae. *Limnology and Oceanography*, *17*(3), 458-461.
- Cade-Menun, B. J., & Paytan, A. (2010). Nutrient temperature and light stress alter phosphorus and carbon forms in culture-grown algae. *Marine Chemistry*, *121*(1-4), 27-36.
- Callaghan, T. V., Johansson, M., Brown, R. D., Groisman, P. Y., Labba, N., Radionov, V., Barry, R. G., Bulygina, O. N., Essery, R. L., & Frolov, D. (2011). The changing face of Arctic snow cover: A synthesis of observed and projected changes. *Ambio*, *40*, 17-31.
- Campbell, K., Matero, I., Bellas, C., Turpin-Jelfs, T., Anhaus, P., Graeve, M., Fripiat, F., Tranter, M., Landy, J. C., & Sanchez-Baracaldo, P. (2022). Monitoring a changing Arctic: Recent advancements in the study of sea ice microbial communities. *Ambio*, *51*(2), 318-332.
- Campbell, K., Mundy, C., Belzile, C., Delaforge, A., & Rysgaard, S. (2018). Seasonal dynamics of algal and bacterial communities in Arctic sea ice under variable snow cover. *Polar Biology*, *41*(1), 41-58.
- Campbell, K., Mundy, C., Juhl, A. R., Dalman, L. A., Michel, C., Galley, R. J., Else, B. E., Geilfus, N. X., & Rysgaard, S. (2019). Melt procedure affects the photosynthetic response of sea ice algae. *Frontiers in Earth Science*, *7*, 21.
- Campbell, K., Mundy, C., Landy, J., Delaforge, A., Michel, C., & Rysgaard, S. (2016a). Community dynamics of bottom-ice algae in Dease Strait of the Canadian Arctic. *Progress in Oceanography*, *149*, 27-39.
- Campbell, K., Mundy, C. J., Barber, D. G., Gosselin, M., & Giguère, N. (2014). Remote estimates of ice algae biomass and their response to environmental conditions during spring melt. *Arctic*, *67*(3), 375-387.
- Campbell, R. G., Ashjian, C. J., Sherr, E. B., Sherr, B. F., Lomas, M. W., Ross, C., Alatalo, P., Gelfman, C., & Van Keuren, D. (2016b). Mesozooplankton grazing during spring sea-ice conditions in the eastern Bering Sea. *Deep Sea Research Part II: Topical Studies in Oceanography*, *134*, 157-172.
- Campbell, R. G., Sherr, E. B., Ashjian, C. J., Plourde, S., Sherr, B. F., Hill, V., & Stockwell, D. A. (2009). Mesozooplankton prey preference and grazing impact in the western Arctic Ocean. *Deep Sea Research Part II: Topical Studies in Oceanography*, *56*(17), 1274-1289.
- Chen, C. Y., & Durbin, E. G. (1994). Effects of pH on the growth and carbon uptake of marine phytoplankton. *Marine Ecology-Progress Series*, *109*, 83-83.
- Chen, G., Zhao, L., & Qi, Y. (2015). Enhancing the productivity of microalgae cultivated in wastewater toward biofuel production: a critical review. *Applied Energy*, *137*, 282-291.

- Chen, J.-J., Li, Y.-R., & Lai, W.-L. (2014). Application of experimental design methodology for optimization of biofuel production from microalgae. *Biomass and Bioenergy*, *64*, 11-19.
- Chokshi, K., Pancha, I., Ghosh, A., & Mishra, S. (2017). Nitrogen starvation-induced cellular crosstalk of ROS-scavenging antioxidants and phytohormone enhanced the biofuel potential of green microalga *Acutodesmus dimorphus*. *Biotechnology for biofuels*, *10*, 1-12.
- Cimoli, E., Meiners, K. M., Lund-Hansen, L. C., & Lucieer, V. (2017). Spatial variability in sea-ice algal biomass: an under-ice remote sensing perspective. *Advances in Polar Science*, *28*(4), 268-296.
- Clark, S., Granger, J., Mastorakis, A., Aguilar-Islas, A., & Hastings, M. (2020). An investigation into the origin of nitrate in Arctic sea ice. *Global Biogeochemical Cycles*, *34*(2), e2019GB006279.
- Cleary, A. C., Søreide, J. E., Freese, D., Niehoff, B., & Gabrielsen, T. M. (2017). Feeding by *Calanus glacialis* in a high arctic fjord: potential seasonal importance of alternative prey. *ICES Journal of Marine Science*, *74*(7), 1937-1946.
- Clement Kinney, J., Maslowski, W., Osinski, R., Jin, M., Frants, M., Jeffery, N., & Lee, Y. J. (2020). Hidden production: On the importance of pelagic phytoplankton blooms beneath Arctic sea ice. *Journal of Geophysical Research: Oceans*, *125*(9), e2020JC016211.
- Codispoti, L., Kelly, V., Thessen, A., Matrai, P., Suttles, S., Hill, V., Steele, M., & Light, B. (2013). Synthesis of primary production in the Arctic Ocean: III. Nitrate and phosphate based estimates of net community production. *Progress in Oceanography*, *110*, 126-150.
- Coello-Camba, A., & Agustí, S. (2017). Thermal thresholds of phytoplankton growth in polar waters and their consequences for a warming polar ocean. *Frontiers in Marine Science*, *4*, 168.
- Coello-Camba, A., Agustí, S., Holding, J., Arrieta, J. M., & Duarte, C. M. (2014). Interactive effect of temperature and CO<sub>2</sub> increase in Arctic phytoplankton. *Frontiers in Marine Science*, *1*, 49.
- Cohen, J., Berge, J., Moline, M., Johnsen, G., & Zolich, A. (2020). Light in the Polar Night. In J. Berge, G. Johnsen, & J. Cohen (Eds.), *POLAR NIGHT Marine Ecology - life and light at the dead of night*, vol. 4 (pp. 37-67). Springer Nature, Switzerland.
- Comeau, A. M., Philippe, B., Thaler, M., Gosselin, M., Poulin, M., & Lovejoy, C. (2013). Protists in Arctic drift and land-fast sea ice. *Journal of Phycology*, *49*(2), 229-240.
- Comiso, J. (2010). Fundamental characteristics of the Polar Oceans and their sea ice cover. *Polar Oceans from Space*, vol. 41 (pp. 19-71). Atmospheric and Oceanographic Sciences Library; Springer, New York, NY.
- Comiso, J. C. (2012). Large decadal decline of the Arctic multiyear ice cover. *Journal of Climate*, *25*(4), 1176-1193.
- Comiso, J. C., Parkinson, C. L., Gersten, R., & Stock, L. (2008). Accelerated decline in the Arctic sea ice cover. *Geophysical Research Letters*, *35*(1), L01703.
- Connan-McGinty, S., Banas, N. S., Berge, J., Cottier, F., Grant, S., Johnsen, G., Kopec, T. P., Porter, M., & McKee, D. (2022). Midnight sun to Polar Night: A model of seasonal light in the Barents Sea. *J. Adv. Model. Earth Syst.*, *14*(10), e2022MS003198.

- Cota, G., Legendre, L., Gosselin, M., & Ingram, R. (1991). Ecology of bottom ice algae: I. Environmental controls and variability. *Journal of Marine Systems*, 2(3-4), 257-277.
- Cota, G., Pomeroy, L. R., Harrison, W., Jones, E., Peters, F., Sheldon Jr, W., & Weingartner, T. (1996). Nutrients, primary production and microbial heterotrophy in the southeastern Chukchi Sea: Arctic summer nutrient depletion and heterotrophy. *Marine Ecology Progress Series*, 135, 247-258.
- Cota, G., Prinsenberg, S., Bennett, E., Loder, J., Lewis, M., Anning, J., Watson, N., & Harris, L. (1987). Nutrient fluxes during extended blooms of Arctic ice algae. *Journal of Geophysical Research: Oceans*, 92(C2), 1951-1962.
- Cota, G. F. (1985). Photoadaptation of high Arctic ice algae. *Nature*, 315(6016), 219-222.
- Cota, G. F., Anning, J. L., Harris, L. R., Harrison, W. G., & Smith, R. E. (1990). Impact of ice algae on inorganic nutrients in seawater and sea ice in Barrow Strait, NWT, Canada, during spring. *Can. J. Fish. Aquat. Sci.*, 47(7), 1402-1415.
- Cottingham, K. L., Lennon, J. T., & Brown, B. L. (2005). Knowing when to draw the line: designing more informative ecological experiments. *Frontiers in Ecology and the Environment*, 3(3), 145-152.
- Coupe, P., Ruiz-Pino, D., Sicre, M.-A., Chen, J., Lee, S., Schiffrine, N., Li, H., & Gascard, J.-C. (2015). The impact of freshening on phytoplankton production in the Pacific Arctic Ocean. *Progress in Oceanography*, 131, 113-125.
- Cowles, T., Olson, R., & Chisholm, S. (1988). Food selection by copepods: discrimination on the basis of food quality. *Marine biology*, 100, 41-49.
- Cox, G. F., & Weeks, W. F. (1983). Equations for determining the gas and brine volumes in sea-ice samples. *Journal of Glaciology*, 29(102), 306-316.
- Croteau, D., Lacour, T., Schiffrine, N., Morin, P. I., Forget, M. H., Bruyant, F., Ferland, J., Lafond, A., Campbell, D. A., & Tremblay, J. É. (2022). Shifts in growth light optima among diatom species support their succession during the spring bloom in the Arctic. *Journal of Ecology*, 110(6), 1356-1375.
- Danielson, S. L., Eisner, L., Ladd, C., Mordy, C., Sousa, L., & Weingartner, T. J. (2017). A comparison between late summer 2012 and 2013 water masses, macronutrients, and phytoplankton standing crops in the northern Bering and Chukchi Seas. *Deep Sea Research Part II: Topical Studies in Oceanography*, 135, 7-26.
- Davidson, A. T., McKinlay, J., Westwood, K., Thomson, P. G., van den Enden, R., de Salas, M., Wright, S., Johnson, R., & Berry, K. (2016). Enhanced CO<sub>2</sub> concentrations change the structure of Antarctic marine microbial communities. *Marine Ecology Progress Series*, 552, 93-113.
- Dean, A. P., Nicholson, J. M., & Sigee, D. C. (2012). Changing patterns of carbon allocation in lake phytoplankton: an FTIR analysis. *Hydrobiologia*, 684, 109-127.
- Dean, A. P., Sigee, D. C., Estrada, B., & Pittman, J. K. (2010). Using FTIR spectroscopy for rapid determination of lipid accumulation in response to nitrogen limitation in freshwater microalgae. *Bioresource technology*, 101(12), 4499-4507.
- Demers, S., Legendre, L., Maestrini, S. Y., Rochet, M., & Grant Ingram, R. (1989). Nitrogenous nutrition of sea-ice microalgae. *Polar Biology*, 9, 377-383.
- Deming, J. W., & Eric Collins, R. (2017). Sea ice as a habitat for bacteria, archaea and viruses, In D.N. Thomas (Ed.), *Sea Ice*, (pp. 326-351), John Wiley & Sons, Ltd., Chichester, UK.

- Denman, K., Brasseur, G., Chidthaisong, A., Ciais, P., Cox, P., Dickinson, R., Hauglustaine, D., Heinze, C., Holland, E., & Jacob, D. (2007). *Couplings between changes in the climate system and biogeochemistry*, In S. Solomon, D. Qin, M. Manning, Z. Chen, M. Marquis, K.B. Averyt, M. Tignor, H.L. Miller (Eds.) *Climate change 2007: the physical science basis. Contribution of Working Group I to the fourth assessment report of the Intergovernmental Panel on Climate Change, Issue*, (pp. 499–563), Cambridge University Press, Cambridge, UK and New York, NY, USA.
- Deppeler, S., Petrou, K., Schulz, K. G., Westwood, K., Pearce, I., McKinlay, J., & Davidson, A. (2018). Ocean acidification of a coastal Antarctic marine microbial community reveals a critical threshold for CO<sub>2</sub> tolerance in phytoplankton productivity. *Biogeosciences*, *15*(1), 209-231.
- Deppeler, S. L., & Davidson, A. T. (2017). Southern Ocean phytoplankton in a changing climate. *Frontiers in Marine Science*, *4*, 40.
- Dickson, A. G. (2010). Standards for ocean measurements. *Oceanography*, *23*(3), 34-47.
- Dickson, A. G., Sabine, C. L., & Christian, J. R. (Eds.) (2007). *Guide to best practices for ocean CO<sub>2</sub> measurements*. PICES Special Publication 3, North Pacific Marine Science Organization.
- Dortch, Q. (1982). Effect of growth conditions on accumulation of internal nitrate, ammonium, amino acids, and protein in three marine diatoms. *Journal of Experimental Marine Biology and Ecology*, *61*(3), 243-264.
- Duncan, R. J., Nielsen, D., Søreide, J. E., Varpe, Ø., Tobin, M. J., Pitusi, V., Heraud, P., & Petrou, K. (2024a). Biomolecular profiles of Arctic Sea-ice diatoms highlight the role of under-ice light in cellular energy allocation. *ISME Communications*, *4*(1), ycad010.
- Duncan, R. J., Nielsen, D. A., Sheehan, C. E., Deppeler, S., Hancock, A. M., Schulz, K. G., Davidson, A. T., & Petrou, K. (2022). Ocean acidification alters the nutritional value of Antarctic diatoms. *New Phytologist*, *233*(4), 1813-1827.
- Duncan, R. J., & Petrou, K. (2022). Biomolecular Composition of Sea Ice Microalgae and Its Influence on Marine Biogeochemical Cycling and Carbon Transfer through Polar Marine Food Webs. *Geosciences*, *12*(1), 38.
- Duncan, R. J., Søreide, J. E., Varpe, Ø., Wiktor, J., Pitusi, V., Runge, E., & Petrou, K. (2024b). Spatio-temporal dynamics in microalgal communities in Arctic land-fast sea ice. *Progress in Oceanography*, *224*, 103248.
- Dünweber, M., Swalethorp, R., Kjellerup, S., Nielsen, T. G., Arendt, K. E., Hjorth, M., Tønnesson, K., & Møller, E. F. (2010). Succession and fate of the spring diatom bloom in Disko Bay, western Greenland. *Marine Ecology Progress Series*, *419*, 11-29.
- Durbin, E. G., & Casas, M. C. (2014). Early reproduction by *Calanus glacialis* in the Northern Bering Sea: the role of ice algae as revealed by molecular analysis. *Journal of Plankton Research*, *36*(2), 523-541.
- Edler, L., & Elbrächter, M. (2010). The Utermöhl method for quantitative phytoplankton analysis. *Microscopic and molecular methods for quantitative phytoplankton analysis*, *110*, 13-20.
- Eggers, S. L., Lewandowska, A. M., Barcelos e Ramos, J., Blanco-Ameijeiras, S., Gallo, F., & Matthiessen, B. (2014). Community composition has greater impact on the functioning of marine phytoplankton communities than ocean acidification. *Global Change Biology*, *20*(3), 713-723.

- Eicken, H. (2003). From the microscopic, to the macroscopic, to the regional scale: growth, microstructure and properties of sea ice. In D.N. Thomas & G.S. Dieckmann, *Sea ice: an introduction to its physics, chemistry, biology and geology*, (pp. 22-81), Blackwell Publishing, Oxford, U.K.
- Engel, A., Schulz, K. G., Riebesell, U., Bellerby, R., Delille, B., & Schartau, M. (2008). Effects of CO<sub>2</sub> on particle size distribution and phytoplankton abundance during a mesocosm bloom experiment (PeECE II). *Biogeosciences*, 5(2), 509-521.
- Eriksen, R., Trull, T. W., Davies, D., Jansen, P., Davidson, A. T., Westwood, K., & van den Enden, R. (2018). Seasonal succession of phytoplankton community structure from autonomous sampling at the Australian Southern Ocean Time Series (SOTS) observatory. *Marine Ecology Progress Series*, 589, 13-31.
- Fabiano, M., Danovaro, R., & Povero, P. (1999). Vertical distribution and biochemical composition of pico-and microparticulate organic matter in the Ross Sea (Antarctica). In *Oceanography of the Ross Sea Antarctica* (pp. 233-246). Springer, Milan.
- Falk-Petersen, S., Mayzaud, P., Kattner, G., & Sargent, J. R. (2009). Lipids and life strategy of Arctic *Calanus*. *Marine Biology Research*, 5(1), 18-39.
- Falk-Petersen, S., Sargent, J., Henderson, J., Hegseth, E., Hop, H., & Okolodkov, Y. (1998). Lipids and fatty acids in ice algae and phytoplankton from the Marginal Ice Zone in the Barents Sea. *Polar Biology*, 20(1), 41-47.
- Falkowski, P. G., & LaRoche, J. (1991). Acclimation to spectral irradiance in algae. *Journal of Phycology*, 27(1), 8-14.
- Fanesi, A., Wagner, H., Birarda, G., Vaccari, L., & Wilhelm, C. (2019). Quantitative macromolecular patterns in phytoplankton communities resolved at the taxonomical level by single-cell Synchrotron FTIR-spectroscopy. *BMC plant biology*, 19, 1-14.
- Feely, R. A., Sabine, C. L., Lee, K., Berelson, W., Kleypas, J., Fabry, V. J., & Millero, F. J. (2004). Impact of anthropogenic CO<sub>2</sub> on the CaCO<sub>3</sub> system in the oceans. *Science*, 305(5682), 362-366.
- Feng, Y., Hare, C., Rose, J., Handy, S., DiTullio, G., Lee, P., Smith Jr, W., Peloquin, J., Tozzi, S., & Sun, J. (2010). Interactive effects of iron, irradiance and CO<sub>2</sub> on Ross Sea phytoplankton. *Deep Sea Research Part I: Oceanographic Research Papers*, 57(3), 368-383.
- Feng, Y., Hare, C. E., Leblanc, K., Rose, J. M., Zhang, Y., DiTullio, G. R., Lee, P. A., Wilhelm, S. W., Rowe, J. M., & Sun, J. (2009). Effects of increased pCO<sub>2</sub> and temperature on the North Atlantic spring bloom. I. The phytoplankton community and biogeochemical response. *Marine Ecology Progress Series*, 388, 13-25.
- Fernández-Méndez, M., Katlein, C., Rabe, B., Nicolaus, M., Peeken, I., Bakker, K., Flores, H., & Boetius, A. (2015). Photosynthetic production in the central Arctic Ocean during the record sea-ice minimum in 2012. *Biogeosciences*, 12(11), 3525-3549.
- Fernández-Méndez, M., Wenzhöfer, F., Peeken, I., Sørensen, H. L., Glud, R. N., & Boetius, A. (2014). Composition, buoyancy regulation and fate of ice algal aggregates in the Central Arctic Ocean. *PLoS One*, 9(9), e107452.
- Figueroa, R. I., Vazquez, J. A., Massanet, A., Murado, M. A., & Bravo, I. (2011). Interactive effects of salinity and temperature on planozygote and cyst formation of *Alexandrium minutum* (dinophyceae) in culture. *Journal of Phycology*, 47(1), 13-24.

- Findlay, C., Morrison, J., Mundy, C., Sedlmair, J., Hirschmugl, C. J., & Gough, K. M. (2017). Thermal source Fourier transform infrared microtomography applied to Arctic sea ice diatoms. *Analyst*, *142*(4), 660-669.
- Finkel, Follows, M., Liefer, J., Brown, C., Benner, I., & Irwin, A. (2016). Phylogenetic diversity in the macromolecular composition of microalgae. *PLoS One*, *11*(5), e0155977.
- Finkel, Z., Follows, M., & Irwin, A. (2016). Size-scaling of macromolecules and chemical energy content in the eukaryotic microalgae. *Journal of Plankton Research*, *38*(5), 1151-1162.
- Forest, A., Galindo, V., Darnis, G., Pineault, S., Lalonde, C., Tremblay, J.-É., & Fortier, L. (2011a). Carbon biomass, elemental ratios (C: N) and stable isotopic composition ( $\delta^{13}\text{C}$ ,  $\delta^{15}\text{N}$ ) of dominant calanoid copepods during the winter-to-summer transition in the Amundsen Gulf (Arctic Ocean). *Journal of Plankton Research*, *33*(1), 161-178.
- Forest, A., Tremblay, J.-É., Gratton, Y., Martin, J., Gagnon, J., Darnis, G., Sampei, M., Fortier, L., Ardyna, M., & Gosselin, M. (2011b). Biogenic carbon flows through the planktonic food web of the Amundsen Gulf (Arctic Ocean): A synthesis of field measurements and inverse modeling analyses. *Progress in Oceanography*, *91*(4), 410-436.
- Forgereau, Z. L., Lange, B. A., Gradinger, R. R., Assmy, P. K. W., Osanen, J., Martín, L., Søreide, J., Granskog, M., Leu, E., & Campbell, K. L. (2023). Photophysiological responses of bottom sea-ice algae to fjord dynamics and rapid freshening. *Frontiers in Marine Science*, *10*, 1221639.
- Forrest, A. L., Lund-Hansen, L. C., Sorrell, B. K., Bowden-Floyd, I., Lucieer, V., Cossu, R., Lange, B. A., & Hawes, I. (2019). Exploring spatial heterogeneity of antarctic sea ice algae using an autonomous underwater vehicle mounted irradiance sensor. *Frontiers in Earth Science*, *7*, 169.
- Fortier, M., Fortier, L., Michel, C., & Legendre, L. (2002). Climatic and biological forcing of the vertical flux of biogenic particles under seasonal Arctic sea ice. *Marine Ecology Progress Series*, *225*, 1-16.
- Fripiat, F., Sigman, D. M., Fawcett, S. E., Rafter, P. A., Weigand, M. A., & Tison, J. L. (2014). New insights into sea ice nitrogen biogeochemical dynamics from the nitrogen isotopes. *Global Biogeochemical Cycles*, *28*(2), 115-130.
- Frölicher, T. L., Sarmiento, J. L., Paynter, D. J., Dunne, J. P., Krasting, J. P., & Winton, M. (2015). Dominance of the Southern Ocean in anthropogenic carbon and heat uptake in CMIP5 models. *Journal of Climate*, *28*(2), 862-886.
- Fry, B., & Wainright, S. C. (1991). Diatom sources of  $^{13}\text{C}$ -rich carbon in marine food webs. *Marine Ecology Progress Series*, *76*, 149-157.
- Garrison, D. L., & Buck, K. R. (1986). Organism losses during ice melting: a serious bias in sea ice community studies. *Polar Biology*, *6*, 237-239.
- Garrison, D. L., Buck, K. R., & Fryxell, G. A. (1987). Algal assemblages in Antarctic pack ice and in ice-edge plankton. *Journal of Phycology*, *23*(4), 564-572.
- Gille, S. T. (2008). Decadal-scale temperature trends in the Southern Hemisphere ocean. *Journal of Climate*, *21*(18), 4749-4765.
- Giordano, M., Kansiz, M., Heraud, P., Beardall, J., Wood, B., & McNaughton, D. (2001). Fourier transform infrared spectroscopy as a novel tool to investigate changes in intracellular macromolecular pools in the marine microalga *Chaetoceros muellerii* (Bacillariophyceae). *Journal of Phycology*, *37*(2), 271-279.



- Gladyshev, M. I., Sushchik, N. N., Anishchenko, O. V., Makhutova, O. N., Kolmakov, V. I., Kalachova, G. S., Kolmakova, A. A., & Dubovskaya, O. P. (2011). Efficiency of transfer of essential polyunsaturated fatty acids versus organic carbon from producers to consumers in a eutrophic reservoir. *Oecologia*, *165*(2), 521-531.
- Gleitz, M., & Kirst, G. (1991). Photosynthesis-irradiance relationships and carbon metabolism of different ice algal assemblages collected from Weddell Sea pack ice during austral spring (EPOS 1). *Polar Biology*, *11*(6), 385-392.
- Gleitz, M., & Thomas, D. N. (1993). Variation in phytoplankton standing stock, chemical composition and physiology during sea-ice formation in the southeastern Weddell Sea, Antarctica. *Journal of Experimental Marine Biology and Ecology*, *173*(2), 211-230.
- Gleitz, M., vd Loeff, M. R., Thomas, D. N., Dieckmann, G. S., & Millero, F. J. (1995). Comparison of summer and winter inorganic carbon, oxygen and nutrient concentrations in Antarctic sea ice brine. *Marine Chemistry*, *51*(2), 81-91.
- Godhe, A., Asplund, M. E., Härnström, K., Saravanan, V., Tyagi, A., & Karunasagar, I. (2008). Quantification of diatom and dinoflagellate biomasses in coastal marine seawater samples by real-time PCR. *Applied and environmental microbiology*, *74*(23), 7174-7182.
- Golden, K. M., Eicken, H., Heaton, A., Miner, J., Pringle, D., & Zhu, J. (2007). Thermal evolution of permeability and microstructure in sea ice. *Geophysical Research Letters*, *34*(16), L16501.
- Gong, Y., & Miao, X. (2019). Short chain fatty acid biosynthesis in microalgae *Synechococcus* sp. PCC 7942. *Marine drugs*, *17*(5), 255.
- Gosselin, M., Legendre, L., Therriault, J.-C., Demers, S., & Rochet, M. (1986). Physical control of the horizontal patchiness of sea-ice microalgae. *Marine Ecology Progress Series*, *29*, 289-298.
- Gosselin, M., Legendre, L., Therriault, J. C., & Demers, S. (1990). Light and nutrient limitation of sea-ice microalgae (Hudson Bay, Canadian Arctic). *Journal of Phycology*, *26*(2), 220-232.
- Gosselin, M., Levasseur, M., Wheeler, P. A., Horner, R. A., & Booth, B. C. (1997). New measurements of phytoplankton and ice algal production in the Arctic Ocean. *Deep Sea Research Part II: Topical Studies in Oceanography*, *44*(8), 1623-1644.
- Goutte, A., Charrassin, J.-B., Cherel, Y., Carravieri, A., De Grissac, S., & Massé, G. (2014). Importance of ice algal production for top predators: new insights using sea-ice biomarkers. *Marine Ecology Progress Series*, *513*, 269-275.
- Gradinger, R. (2009). Sea-ice algae: Major contributors to primary production and algal biomass in the Chukchi and Beaufort Seas during May/June 2002. *Deep Sea Research Part II: Topical Studies in Oceanography*, *56*(17), 1201-1212.
- Graeve, M., Kattner, G., & Hagen, W. (1994). Diet-induced changes in the fatty acid composition of Arctic herbivorous copepods: experimental evidence of trophic markers. *Journal of Experimental Marine Biology and Ecology*, *182*(1), 97-110.
- Granskog, M., Kaartokallio, H., & Shirasawa, K. (2003). Nutrient status of Baltic Sea ice: Evidence for control by snow-ice formation, ice permeability, and ice algae. *Journal of Geophysical Research: Oceans*, *108*(C8), 3253.
- Griewank, P. J., & Notz, D. (2013). Insights into brine dynamics and sea ice desalination from a 1-D model study of gravity drainage. *Journal of Geophysical Research: Oceans*, *118*(7), 3370-3386.

- Gruber, N. (2008). The marine nitrogen cycle: overview and challenges. *Nitrogen in the Marine Environment*, 2, 1-50.
- Guschina, I. A., & Harwood, J. L. (2009). Algal lipids and effect of the environment on their biochemistry. In M. Kainz, M.T. Brett, M.T. Arts, *Lipids in aquatic ecosystems* (pp. 1-24), Springer New York, NY.
- Gutt, J., Bertler, N., Bracegirdle, T. J., Buschmann, A., Comiso, J., Hosie, G., Isla, E., Schloss, I. R., Smith, C. R., & Tournadre, J. (2015). The Southern Ocean ecosystem under multiple climate change stresses-an integrated circumpolar assessment. *Global Change Biology*, 21(4), 1434-1453.
- Haberman, K. L., Ross, R. M., & Quetin, L. B. (2003). Diet of the Antarctic krill (*Euphausia superba* Dana): II. Selective grazing in mixed phytoplankton assemblages. *Journal of Experimental Marine Biology and Ecology*, 283(1-2), 97-113.
- Haecky, P., Jonsson, S., & Andersson, A. (1998). Influence of sea ice on the composition of the spring phytoplankton bloom in the northern Baltic Sea. *Polar Biology*, 20(1), 1-8.
- Hagen, W., & Auel, H. (2001). Seasonal adaptations and the role of lipids in oceanic zooplankton. *Zoology*, 104(3-4), 313-326.
- Hagen, W., Van Vleet, E. S., & Kattner, G. (1996). Seasonal lipid storage as overwintering strategy of Antarctic krill. *Marine Ecology Progress Series*, 134, 85-89.
- Haine, T. W., & Martin, T. (2017). The Arctic-Subarctic sea ice system is entering a seasonal regime: Implications for future Arctic amplification. *Scientific Reports*, 7(1), 4618.
- Halsey, K. H., & Jones, B. M. (2015). Phytoplankton strategies for photosynthetic energy allocation. *Annual review of marine science*, 7, 265-297.
- Hamm, C. E., Merkel, R., Springer, O., Jurkojc, P., Maier, C., Prectel, K., & Smetacek, V. (2003). Architecture and material properties of diatom shells provide effective mechanical protection. *Nature*, 421(6925), 841-843.
- Hamre, B., Winther, J. G., Gerland, S., Stamnes, J. J., & Stamnes, K. (2004). Modeled and measured optical transmittance of snow-covered first-year sea ice in Kongsfjorden, Svalbard. *Journal of Geophysical Research: Oceans*, 109, C10006.
- Hancke, K., Lund-Hansen, L. C., Lamare, M. L., Højlund Pedersen, S., King, M. D., Andersen, P., & Sorrell, B. K. (2018). Extreme low light requirement for algae growth underneath sea ice: A case study from Station Nord, NE Greenland. *Journal of Geophysical Research: Oceans*, 123(2), 985-1000.
- Hancock, A. M., Davidson, A. T., McKinlay, J., McMinn, A., Schulz, K. G., & van den Enden, R. L. (2018). Ocean acidification changes the structure of an Antarctic coastal protistan community. *Biogeosciences*, 15(8), 2393-2410.
- Hancock, A. M., King, C. K., Stark, J. S., McMinn, A., & Davidson, A. T. (2020). Effects of ocean acidification on Antarctic marine organisms: A meta-analysis. *Ecology and Evolution*, 10(10), 4495-4514.
- Hargraves, P. (1983). Diatom resting spores: Significance and strategies. *Survival strategies of the algae*, 49-68. Cambridge University Press, Cambridge, U.K.
- Harvey, H. R., & Johnston, J. R. (1995). Lipid composition and flux of sinking and size-fractionated particles in Chesapeake Bay. *Organic Geochemistry*, 23(8), 751-764.
- Haugan, P. M., & Drange, H. (1996). Effects of CO<sub>2</sub> on the ocean environment. *Energy conversion and management*, 37(6-8), 1019-1022.

- Havenhand, J., Dupont, S., & Quinn, G. P. (2010). Designing ocean acidification experiments to maximise inference. *Guide to best practices for ocean acidification research and data reporting*, (pp. 67-80), Publications Office of the European Union, Luxembourg.
- Hawkings, J. R., Wadham, J. L., Tranter, M., Raiswell, R., Benning, L. G., Statham, P. J., Tedstone, A., Nienow, P., Lee, K., & Telling, J. (2014). Ice sheets as a significant source of highly reactive nanoparticulate iron to the oceans. *Nature Communications*, 5(1), 1-8.
- Head, E., & Harris, L. (1994). Feeding selectivity by copepods grazing on natural mixtures of phytoplankton determined by HPLC analysis of pigments. *Marine Ecology Progress Series*, 110, 75-75.
- Hegseth, E. N., & von Quillfeldt, C. (2022). The Sub-Ice Algal Communities of the Barents Sea Pack Ice: Temporal and Spatial Distribution of Biomass and Species. *Journal of Marine Science and Engineering*, 10(2), 164.
- Henderson, R., Hegseth, E., & Park, M. (1998). Seasonal variation in lipid and fatty acid composition of ice algae from the Barents Sea. *Polar Biology*, 20, 48-55.
- Henley, S. F., Schofield, O. M., Hendry, K. R., Schloss, I. R., Steinberg, D. K., Moffat, C., Peck, L. S., Costa, D. P., Bakker, D. C., & Hughes, C. (2019). Variability and change in the west Antarctic Peninsula marine system: research priorities and opportunities. *Progress in Oceanography*, 173, 208-237.
- Hennon, G. M., Ashworth, J., Groussman, R. D., Berthiaume, C., Morales, R. L., Baliga, N. S., Orellana, M. V., & Armbrust, E. (2015). Diatom acclimation to elevated CO<sub>2</sub> via cAMP signalling and coordinated gene expression. *Nature Climate Change*, 5(8), 761-765.
- Hennon, G. M., Hernández Limón, M. D., Haley, S. T., Juhl, A. R., & Dyhrman, S. T. (2017). Diverse CO<sub>2</sub>-induced responses in physiology and gene expression among eukaryotic phytoplankton. *Frontiers in Microbiology*, 8, 306803.
- Heraud, P., Wood, B. R., Tobin, M. J., Beardall, J., & McNaughton, D. (2005). Mapping of nutrient-induced biochemical changes in living algal cells using synchrotron infrared microspectroscopy. *FEMS Microbiology Letters*, 249(2), 219-225.
- Heraud, P., Wood, B. R., Beardall, J., & McNaughton, D. (2007). Probing the influence of the environment on microalgae using infrared and raman spectroscopy. *New approaches in biomedical spectroscopy*, 963, 85-106.
- Heraud, P., Stojkovic, S., Beardall, J., McNaughton, D. and Wood, B. R. (2008). Intercolonial variability in macromolecular composition in p-starved and p-replete *Scenedesmus* populations revealed by infrared microspectroscopy. *Journal of Phycology*, 44(5), 1335-1339.
- Hirche, H.-J., & Kosobokova, K. (2003). Early reproduction and development of dominant calanoid copepods in the sea ice zone of the Barents Sea—need for a change of paradigms? *Marine biology*, 143, 769-781.
- Hitchcock, G. L. (1982). A comparative study of the size-dependent organic composition of marine diatoms and dinoflagellates. *Journal of Plankton Research*, 4(2), 363-377.
- Holm-Hansen, O., & Riemann, B. (1978). Chlorophyll a determination: improvements in methodology. *Oikos*, 30(3), 438-447.
- Hop, H., Vihtakari, M., Bluhm, B. A., Assmy, P., Poulin, M., Gradinger, R., Peeken, I., von Quillfeldt, C., Olsen, L. M., & Zhitina, L. (2020). Changes in sea-ice protist diversity with declining sea ice in the Arctic Ocean from the 1980s to 2010s. *Frontiers in Marine Science*, 7, 243.

- Hoppe, C. J., Holtz, L. M., Trimborn, S., & Rost, B. (2015). Ocean acidification decreases the light-use efficiency in an Antarctic diatom under dynamic but not constant light. *New Phytologist*, 207(1), 159-171.
- Hoppe, C. J., Schuback, N., Semeniuk, D. M., Maldonado, M. T., & Rost, B. (2017). Functional redundancy facilitates resilience of subarctic phytoplankton assemblages toward ocean acidification and high irradiance. *Frontiers in Marine Science*, 4, 229.
- Horner, R. (Ed.). (1985). *Sea Ice Biota* (1st edition ed.). CRC Press, Boca Raton, FL, U.S.A.
- Horner, R., & Schrader, G. (1982). Relative contributions of ice algae, phytoplankton, and benthic microalgae to primary production in nearshore regions of the Beaufort Sea. *Arctic*, 35(4), 485-503.
- Høyland, K. V. (2009). Ice thickness, growth and salinity in Van Mijenfjorden, Svalbard, Norway. *Polar Research*, 28(3), 339-352.
- Hu, Q. (2004). *Environmental effects on cell composition* In A. Richmond, Q. Hu (Eds.) *Handbook of Microalgal Culture: Biotechnology and Applied Phycology*, (pp. 114-122), Blackwell Science Ltd, Oxford, U.K.
- Hussherr, R., Levasseur, M., Lizotte, M., Tremblay, J.-É., Mol, J., Thomas, H., Gosselin, M., Starr, M., Miller, L. A., & Jarniková, T. (2017). Impact of ocean acidification on Arctic phytoplankton blooms and dimethyl sulfide concentration under simulated ice-free and under-ice conditions. *Biogeosciences*, 14(9), 2407-2427.
- Hygum, B., Rey, C., Hansen, B. W., & Tande, K. (2000). Importance of food quantity to structural growth rate and neutral lipid reserves accumulated in *Calanus finmarchicus*. *Marine biology*, 136(6), 1057-1073.
- International Energy Agency (IEA). (2023). *CO2 Emissions in 2022*. <https://www.iea.org/reports/co2-emissions-in-2022>
- IOCCG. (2015). *Ocean Colour Remote Sensing in Polar Seas*. Babin, M., Arrigo, K., Bélanger, S. and Forget, M-H. (eds.), IOCCG Report Series, No. 16, International Ocean Colour Coordinating Group, Dartmouth, Canada
- IPCC. (2014). *Climate Change 2014: Impacts, Adaptation, and Vulnerability. Part A: Global and Sectoral Aspects. Contribution of Working Group II to the Fifth Assessment Report of the Intergovernmental Panel on Climate Change*. C.B. Field, V.R. Barros, D.J. Dokken, K.J. Mach, M.D. Mastrandrea, T.E. Bilir, M. Chatterjee, K.L. Ebi, Y.O. Estrada, R.C. Genova, B. Girma, E.S. Kissel, A.N. Levy, S. MacCracken, P.R. Mastrandrea, and L.L. White (Eds.), Cambridge University Press, Cambridge, U.K.
- IPCC. (2021), *Climate Change 2021: The Physical Science Basis. Contribution of Working Group I to the Sixth Assessment Report of the Intergovernmental Panel on Climate Change*, V. Masson-Delmotte, P. Zhai, A. Pirani, S.L. Connors, C. Péan, S. Berger, N. Caud, Y. Chen, L. Goldfarb, M.I. Gomis, M. Huang, K. Leitzell, E. Lonnoy, J.B.R. Matthews, T.K. Maycock, T. Waterfield, O. Yelekçi, R. Yu, and B. Zhou (Eds.) Cambridge University Press, Cambridge, United Kingdom and New York, NY, USA.
- IPCC. (2023). *Sections. In: Climate Change 2023: Synthesis Report. Contribution of Working Groups I, II and III to the Sixth Assessment Report of the Intergovernmental Panel on Climate Change*, Core Writing Team, H. Lee and J. Romero (Eds.), (pp. 35-115), IPCC, Geneva, Switzerland.
- Itkin, P., Spreen, G., Cheng, B., Doble, M., Girard-Arduin, F., Haapala, J., Hughes, N., Kaleschke, L., Nicolaus, M., & Wilkinson, J. (2017). Thin ice and storms: Sea

- ice deformation from buoy arrays deployed during N-ICE 2015. *Journal of Geophysical Research: Oceans*, 122(6), 4661-4674.
- Jacobs, S., Giulivi, C., & Dutrieux, P. (2022). Persistent Ross Sea freshening from imbalance West Antarctic ice shelf melting. *Journal of Geophysical Research: Oceans*, 127(3), e2021JC017808.
- Jacobs, S., Giulivi, C., & Mele, P. (2002). Freshening of the Ross Sea during the late 20th century. *Science*, 297(5580), 386-389.
- Jahn, A., Holland, M. M., & Kay, J. E. (2024). Projections of an ice-free Arctic Ocean. *Nature Reviews Earth & Environment*, 5, 164-176.
- Ji, R., Ashjian, C. J., Campbell, R. G., Chen, C., Gao, G., Davis, C. S., Cowles, G. W., & Beardsley, R. C. (2012). Life history and biogeography of *Calanus* copepods in the Arctic Ocean: an individual-based modeling study. *Progress in Oceanography*, 96(1), 40-56.
- Ji, R., Jin, M., & Varpe, Ø. (2013). Sea ice phenology and timing of primary production pulses in the Arctic Ocean. *Global Change Biology*, 19(3), 734-741.
- Jiang, L. q., Dunne, J., Carter, B. R., Tjiputra, J. F., Terhaar, J., Sharp, J. D., Olsen, A., Alin, S., Bakker, D. C., & Feely, R. A. (2023). Global surface ocean acidification indicators from 1750 to 2100. *Journal of Advances in Modeling Earth Systems*, 15(3), e2022MS003563.
- Jiang, Y., Yoshida, T., & Quigg, A. (2012). Photosynthetic performance, lipid production and biomass composition in response to nitrogen limitation in marine microalgae. *Plant physiology and biochemistry*, 54, 70-77.
- Jin, M., Deal, C., Wang, J., Alexander, V., Gradinger, R., Saitoh, S. i., Iida, T., Wan, Z., & Stabeno, P. (2007). Ice-associated phytoplankton blooms in the southeastern Bering Sea. *Geophysical Research Letters*, 34(6), L06612.
- Jin, P., Hutchins, D. A., & Gao, K. (2020). The impacts of ocean acidification on marine food quality and its potential food chain consequences. *Frontiers in Marine Science*, 7, 543979.
- Johns, L., Wraige, E., Belt, S., Lewis, C., Massé, G., Robert, J.-M., & Rowland, S. (1999). Identification of a C25 highly branched isoprenoid (HBI) diene in Antarctic sediments, Antarctic sea-ice diatoms and cultured diatoms. *Organic Geochemistry*, 30(11), 1471-1475.
- Johnsen, G., & Hegseth, E. N. (1991). Photoadaptation of sea-ice microalgae in the Barents Sea. *Polar Biology*, 11, 179-184.
- Johnsen, G., Leu, E., & Gradinger, R. (2020). Marine micro-and macroalgae in the polar night. In J. Berge, G. Johnsen, J. Cohen, *Polar night marine ecology: life and light in the dead of night*, vol. 4, (pp. 67-112), Springer, Cham.
- Jónasdóttir, S. H., Trung, N. H., Hansen, F., & Gärtner, S. (2005). Egg production and hatching success in the calanoid copepods *Calanus helgolandicus* and *Calanus finmarchicus* in the North Sea from March to September 2001. *Journal of Plankton Research*, 27(12), 1239-1259.
- Jónasdóttir, S. H., Visser, A. W., & Jespersen, C. (2009). Assessing the role of food quality in the production and hatching of *Temora longicornis* eggs. *Marine Ecology Progress Series*, 382, 139-150.
- Jónasdóttir, S. H., Visser, A. W., Richardson, K., & Heath, M. R. (2015). Seasonal copepod lipid pump promotes carbon sequestration in the deep North Atlantic. *Proceedings of the National Academy of Sciences*, 112(39), 12122-12126.
- Jones, R. H., & Flynn, K. J. (2005). Nutritional status and diet composition affect the value of diatoms as copepod prey. *Science*, 307(5714), 1457-1459.

- Kacimi, S., & Kwok, R. (2022). Arctic Snow Depth, Ice Thickness, and Volume From ICESat-2 and CryoSat-2: 2018–2021. *Geophysical Research Letters*, *49*(5), e2021GL097448.
- Kahru, M., Brotas, V., Manzano-Sarabia, M., & Mitchell, B. (2011). Are phytoplankton blooms occurring earlier in the Arctic? *Global Change Biology*, *17*(4), 1733-1739.
- Kang, S.-H., & Fryxell, G. (1993). Phytoplankton in the Weddell Sea, Antarctica: composition, abundance and distribution in water-column assemblages of the marginal ice-edge zone during austral autumn. *Marine biology*, *116*, 335-348.
- Kattner, G., & Hagen, W. (2009). Lipids in marine copepods: latitudinal characteristics and perspective to global warming. In M. Kainz, M.T. Brett, M.T. Arts, *Lipids in aquatic ecosystems* (pp. 257-280), Springer New York, NY.
- Kattner, G., Hagen, W., Lee, R. F., Campbell, R., Deibel, D., Falk-Petersen, S., Graeve, M., Hansen, B. W., Hirche, H.-J., & Jónasdóttir, S. H. (2007). Perspectives on marine zooplankton lipids. *Canadian Journal of Fisheries and Aquatic Sciences*, *64*(11), 1628-1639.
- Kennedy, F., Martin, A., Bowman, J. P., Wilson, R., & McMinn, A. (2019). Dark metabolism: a molecular insight into how the Antarctic sea-ice diatom *Fragilariopsis cylindrus* survives long-term darkness. *New Phytologist*, *223*(2), 675-691.
- Khatiwala, S., Primeau, F., & Hall, T. (2009). Reconstruction of the history of anthropogenic CO<sub>2</sub> concentrations in the ocean. *Nature*, *462*(7271), 346-349.
- Kiesling, T. L., Wilkinson, E., Rabalais, J., Ortner, P. B., McCabe, M. M., & Fell, J. W. (2002). Rapid identification of adult and naupliar stages of copepods using DNA hybridization methodology. *Marine Biotechnology*, *4*, 30-39.
- Kim, B. K., Lee, J. H., Joo, H., Song, H. J., Yang, E. J., Lee, S. H., & Lee, S. H. (2016). Macromolecular compositions of phytoplankton in the Amundsen Sea, Antarctica. *Deep Sea Research Part II: Topical Studies in Oceanography*, *123*, 42-49.
- Kim, B. K., Lee, J. H., Yun, M. S., Joo, H., Song, H. J., Yang, E. J., Chung, K. H., Kang, S.-H., & Lee, S. H. (2015). High lipid composition of particulate organic matter in the northern Chukchi Sea, 2011. *Deep Sea Research Part II: Topical Studies in Oceanography*, *120*, 72-81.
- Kim, B. K., Lee, S., Ha, S. Y., Jung, J., Kim, T. W., Yang, E. J., Jo, N., Lim, Y. J., Park, J., & Lee, S. H. (2018a). Vertical distributions of macromolecular composition of particulate organic matter in the water column of the Amundsen Sea Polynya during the summer in 2014. *Journal of Geophysical Research: Oceans*, *123*(2), 1393-1405.
- Kim, S., Saenz, B., Scanniello, J., Daly, K., & Ainley, D. (2018b). Local climatology of fast ice in McMurdo Sound, Antarctica. *Antarctic Science*, *30*(2), 125-142.
- Kirst, G. O., & Wiencke, C. (1995). Ecophysiology of polar algae. *Oceanographic Literature Review*, *12*(42), 1094.
- Ko, E., Gorbunov, M. Y., Jung, J., Joo, H. M., Lee, Y., Cho, K. H., Yang, E. J., Kang, S. H., & Park, J. (2020). Effects of nitrogen limitation on phytoplankton physiology in the Western Arctic Ocean in summer. *Journal of Geophysical Research: Oceans*, *125*(11), e2020JC016501.
- Koch, C. W., Brown, T. A., Amiriaux, R., Ruiz-Gonzalez, C., MacCorquodale, M., Yunda-Guarin, G. A., Kohlbach, D., Loseto, L. L., Rosenberg, B., & Hussey, N. E. (2023). Year-round utilization of sea ice-associated carbon in Arctic ecosystems. *Nature communications*, *14*(1), 1964.

- Koeller, P., Fuentes-Yaco, C., Platt, T., Sathyendranath, S., Richards, A., Ouellet, P., Orr, D., Skúladóttir, U., Wieland, K., & Savard, L. (2009). Basin-scale coherence in phenology of shrimps and phytoplankton in the North Atlantic Ocean. *Science*, *324*(5928), 791-793.
- Kohlbach, D., Graeve, M., Lange, B., David, C., Peeken, I., & Flores, H. (2016). The importance of ice algae-produced carbon in the central Arctic Ocean ecosystem: Food web relationships revealed by lipid and stable isotope analyses. *Limnology and Oceanography*, *61*(6), 2027-2044.
- Kohlbach, D., Graeve, M., Lange, B. A., David, C., Schaafsma, F. L., van Franeker, J. A., Vortkamp, M., Brandt, A., & Flores, H. (2018). Dependency of Antarctic zooplankton species on ice algae-produced carbon suggests a sea ice-driven pelagic ecosystem during winter. *Global Change Biology*, *24*(10), 4667-4681.
- Kohlbach, D., Hop, H., Wold, A., Schmidt, K., Smik, L., Belt, S. T., Keck Al-Hababbeh, A., Woll, M., Graeve, M., & Dąbrowska, A. M. (2021). Multiple trophic markers trace dietary carbon sources in Barents Sea zooplankton during late summer. *Frontiers in Marine Science*, *7*, 610248.
- Kong, H., Yang, E.-J., Jiao, N., Lee, Y., Jung, J., Cho, K.-H., Moon, J.-K., Kim, J.-H., & Xu, D. (2023). RNA outperforms DNA-based metabarcoding in assessing the diversity and response of microeukaryotes to environmental variables in the Arctic Ocean. *Science of the Total Environment*, *876*, 162608.
- Koski, M., Boutorh, J., & de La Rocha, C. (2017). Feeding on dispersed vs. aggregated particles: the effect of zooplankton feeding behavior on vertical flux. *PloS one*, *12*(5), e0177958.
- Kramer, S.J., Bolaños, L.M., Catlett, D., Chase, A.P., Behrenfeld, M.J., Boss, E.S., Crockford, E.T., Giovannoni, S.J., Graff, J.R., Haëntjens, N., Karp-Boss, L., Peacock, E.E., Roesler, C.S., Sosik, H.M. and Siegel, D.A. (2024), Toward a synthesis of phytoplankton community composition methods for global-scale application. *Limnology and Oceanography Methods*, *22*, 217-240.
- Krause, J. W., Duarte, C. M., Marquez, I. A., Assmy, P., Fernández-Méndez, M., Wiedmann, I., Wassmann, P., Kristiansen, S., & Agustí, S. (2018). Biogenic silica production and diatom dynamics in the Svalbard region during spring. *Biogeosciences*, *15*(21), 6503-6517.
- Krembs, C., Eicken, H., & Deming, J. W. (2011). Exopolymer alteration of physical properties of sea ice and implications for ice habitability and biogeochemistry in a warmer Arctic. *Proceedings of the National Academy of Sciences*, *108*(9), 3653-3658.
- Kreyling, J., Schweiger, A. H., Bahn, M., Ineson, P., Migliavacca, M., Morel-Journel, T., Christiansen, J. R., Schtickzelle, N., & Larsen, K. S. (2018). To replicate, or not to replicate—that is the question: how to tackle nonlinear responses in ecological experiments. *Ecology Letters*, *21*(11), 1629-1638.
- Kroeker, K. J., Kordas, R. L., Crim, R., Hendriks, I. E., Ramajo, L., Singh, G. S., Duarte, C. M., & Gattuso, J. P. (2013). Impacts of ocean acidification on marine organisms: quantifying sensitivities and interaction with warming. *Global Change Biology*, *19*(6), 1884-1896.
- Kunisch, E., Graeve, M., Gradinger, R., Haug, T., Kovacs, K. M., Lydersen, C., Varpe, Ø., & Bluhm, B. (2021). Ice-algal carbon supports harp and ringed seal diets in the European Arctic: evidence from fatty acid and stable isotope markers. *Marine Ecology Progress Series*, *675*, 181-197.
- Kvernvik, A. C. (2019). *Ecophysiological responses of sea ice algae and phytoplankton to a changing Arctic* [Doctoral Dissertation, University in Tromsø].

- Kvernvik, A. C., Hoppe, C. J. M., Greenacre, M., Verbiest, S., Wiktor, J. M., Gabrielsen, T. M., Reigstad, M., & Leu, E. (2021). Arctic sea ice algae differ markedly from phytoplankton in their ecophysiological characteristics. *Marine Ecology Progress Series*, 666, 31-55.
- Kvernvik, A. C., Hoppe, C. J. M., Lawrenz, E., Prášil, O., Greenacre, M., Wiktor, J. M., & Leu, E. (2018). Fast reactivation of photosynthesis in arctic phytoplankton during the polar night1. *Journal of Phycology*, 54(4), 461-470.
- Kvernvik, A. C., Rokitta, S. D., Leu, E., Harms, L., Gabrielsen, T. M., Rost, B., & Hoppe, C. J. (2020). Higher sensitivity towards light stress and ocean acidification in an Arctic sea-ice-associated diatom compared to a pelagic diatom. *New Phytologist*, 226(6), 1708-1724.
- Kwok, R. (2018). Arctic sea ice thickness, volume, and multiyear ice coverage: losses and coupled variability (1958–2018). *Environmental Research Letters*, 13(10), 105005.
- Lam, H. M., Geldsetzer, T., Howell, S. E., & Yackel, J. (2023). Snow depth on sea ice and on land in the Canadian Arctic from long-term observations. *Atmosphere-Ocean*, 61(4), 217-233.
- Lannuzel, D., Tedesco, L., Van Leeuwe, M., Campbell, K., Flores, H., Delille, B., Miller, L., Stefels, J., Assmy, P., & Bowman, J. (2020). The future of Arctic sea-ice biogeochemistry and ice-associated ecosystems. *Nature Climate Change*, 10(11), 983-992.
- Larsen, J., Anisimov, O., Constable, A., Hollowed, A., Maynard, N., Prestrud, P., Prowse, T., & Stone, J. (2014). Polar regions, In C.B. Field, V.R. Barros, D.J. Dokken, K.J. Mach, M.D. Mastrandrea, T.E. Bilir, M. Chatterjee, K.L. Ebi, Y.O. Estrada, R.C. Genova, B. Girma, E.S. Kissel, A.N. Levy, S. MacCracken, P.R. Mastrandrea, and L.L.White (Eds.), *Climate Change 2014: impacts, adaptation, and vulnerability. Part B: Regional aspects. Contribution of Working Group II to the fifth assessment report of the Intergovernmental Panel on Climate Change*, (pp. 1567 – 1612), Cambridge University Press, Cambridge, U.K.
- Lavoie, D., Denman, K., & Michel, C. (2005). Modeling ice algal growth and decline in a seasonally ice-covered region of the Arctic (Resolute Passage, Canadian Archipelago). *Journal of Geophysical Research: Oceans*, 110, C11009.
- Le Quéré, C., Andrew, R. M., Friedlingstein, P., Sitch, S., Pongratz, J., Manning, A. C., Korsbakken, J. I., Peters, G. P., Canadell, J. G., & Jackson, R. B. (2018). Global carbon budget 2017. *Earth System Science Data*, 10(1), 405-448.
- Lee, J. R., Raymond, B., Bracegirdle, T. J., Chadès, I., Fuller, R. A., Shaw, J. D., & Terauds, A. (2017). Climate change drives expansion of Antarctic ice-free habitat. *Nature*, 547(7661), 49-54.
- Lee, R. F., Hagen, W., & Kattner, G. (2006). Lipid storage in marine zooplankton. *Marine Ecology Progress Series*, 307, 273-306.
- Lee, S. H., Whitley, T. E., & Kang, S.-H. (2008a). Carbon uptake rates of sea ice algae and phytoplankton under different light intensities in a landfast sea ice zone, Barrow, Alaska. *Arctic*, 281-291.
- Lee, S. H., Whitley, T. E., & Kang, S.-H. (2008b). Spring time production of bottom ice algae in the landfast sea ice zone at Barrow, Alaska. *Journal of Experimental Marine Biology and Ecology*, 367(2), 204-212.
- Legendre, L., Ackley, S. F., Dieckmann, G. S., Gulliksen, B., Horner, R., Hoshiai, T., Melnikov, I. A., Reeburgh, W. S., Spindler, M., & Sullivan, C. W. (1992). Ecology of sea ice biota. *Polar Biology*, 12(3), 429-444.



- Letterly, A., Key, J., & Liu, Y. (2018). Arctic climate: changes in sea ice extent outweigh changes in snow cover. *The Cryosphere*, 12(10), 3373-3382.
- Leu, E., Brown, T. A., Graeve, M., Wiktor, J., Hoppe, C. J., Chierici, M., Fransson, A., Verbiest, S., Kvernvik, A. C., & Greenacre, M. J. (2020). Spatial and temporal variability of ice algal trophic markers—with recommendations about their application. *Journal of Marine Science and Engineering*, 8(9), 676.
- Leu, E., Daase, M., Schulz, K. G., Stuhr, A., & Riebesell, U. (2013). Effect of ocean acidification on the fatty acid composition of a natural plankton community. *Biogeosciences*, 10(2), 1143-1153.
- Leu, E., Falk-Petersen, S., & Hessen, D. O. (2007). Ultraviolet radiation negatively affects growth but not food quality of arctic diatoms. *Limnology and Oceanography*, 52(2), 787-797.
- Leu, E., Falk-Petersen, S., Kwaśniewski, S., Wulff, A., Edvardsen, K., & Hessen, D. O. (2006a). Fatty acid dynamics during the spring bloom in a High Arctic fjord: importance of abiotic factors versus community changes. *Canadian Journal of Fisheries and Aquatic Sciences*, 63(12), 2760-2779.
- Leu, E., Graeve, M., & Wulff, A. (2016). A (too) bright future? Arctic diatoms under radiation stress. *Polar Biology*, 39, 1711-1724.
- Leu, E., Mundy, C., Assmy, P., Campbell, K., Gabrielsen, T., Gosselin, M., Juul-Pedersen, T., & Gradinger, R. (2015). Arctic spring awakening—Steering principles behind the phenology of vernal ice algal blooms. *Progress in Oceanography*, 139, 151-170.
- Leu, E., Søreide, J., Hessen, D., Falk-Petersen, S., & Berge, J. (2011). Consequences of changing sea-ice cover for primary and secondary producers in the European Arctic shelf seas: timing, quantity, and quality. *Progress in Oceanography*, 90(1-4), 18-32.
- Leu, E., Wängberg, S.-Å., Wulff, A., Falk-Petersen, S., Ørbæk, J. B., & Hessen, D. O. (2006b). Effects of changes in ambient PAR and UV radiation on the nutritional quality of an Arctic diatom (*Thalassiosira antarctica* var. *borealis*). *Journal of Experimental Marine Biology and Ecology*, 337(1), 65-81.
- Leu, E., Wiktor, J., Søreide, J., Berge, J., & Falk-Petersen, S. (2010). Increased irradiance reduces food quality of sea ice algae. *Marine Ecology Progress Series*, 411, 49-60.
- Levinsen, H., Turner, J. T., Nielsen, T. G., & Hansen, B. W. (2000). On the trophic coupling between protists and copepods in Arctic marine ecosystems. *Marine Ecology Progress Series*, 204, 65-77.
- Lewis, K., Arntsen, A., Coupel, P., Joy-Warren, H., Lowry, K., Matsuoka, A., Mills, M., Van Dijken, G., Selz, V., & Arrigo, K. (2019). Photoacclimation of Arctic Ocean phytoplankton to shifting light and nutrient limitation. *Limnology and Oceanography*, 64(1), 284-301.
- Lewis, K., Van Dijken, G., & Arrigo, K. R. (2020). Changes in phytoplankton concentration now drive increased Arctic Ocean primary production. *Science*, 369(6500), 198-202.
- Li, H., & Fedorov, A. V. (2021). Persistent freshening of the Arctic Ocean and changes in the North Atlantic salinity caused by Arctic sea ice decline. *Climate Dynamics*, 57(11), 2995-3013.
- Li, W., Glover, H., & Morris, I. (1980). Physiology of carbon photoassimilation by *Oscillatoria thiebautii* in the Caribbean Sea. *Limnology and Oceanography*, 25(3), 447-456.

- Li, W. K., McLaughlin, F. A., Lovejoy, C., & Carmack, E. C. (2009). Smallest algae thrive as the Arctic Ocean freshens. *Science*, *326*(5952), 539-539.
- Li, Z., Zhao, J., Su, J., Li, C., Cheng, B., Hui, F., Yang, Q., & Shi, L. (2019). Spatial and temporal variations in the extent and thickness of arctic landfast ice. *Remote Sensing*, *12*(1), 64.
- Lindqvist, K., & Lignell, R. (1997). Intracellular partitioning of  $^{14}\text{CO}_2$  in phytoplankton during a growth season in the northern Baltic. *Marine Ecology Progress Series*, *152*, 41-50.
- Litchman, E., Klausmeier, C. A., Schofield, O. M., & Falkowski, P. G. (2007). The role of functional traits and trade-offs in structuring phytoplankton communities: scaling from cellular to ecosystem level. *Ecology letters*, *10*(12), 1170-1181.
- Liu, H., Chen, M., Zhu, F., & Harrison, P. J. (2016). Effect of diatom silica content on copepod grazing, growth and reproduction. *Frontiers in Marine Science*, *3*, 89.
- Liu, J., & Curry, J. A. (2010). Accelerated warming of the Southern Ocean and its impacts on the hydrological cycle and sea ice. *Proceedings of the National Academy of Sciences*, *107*(34), 14987-14992.
- Liu, J., Curry, J. A., Wang, H., Song, M., & Horton, R. M. (2012). Impact of declining Arctic sea ice on winter snowfall. *PNAS*, *109*(11), 4074-4079.
- Liu, Z., Deng, Z., Davis, S., & Ciais, P. (2023). Monitoring global carbon emissions in 2022. *Nature Reviews Earth & Environment*, *4*(4), 205-206.
- Lizotte, M. P. (2001). The contributions of sea ice algae to Antarctic marine primary production. *American zoologist*, *41*(1), 57-73.
- Lønne, O., & Gulliksen, B. (1989). Size, age and diet of polar cod, *Boreogadus saida* (Lepechin 1773), in ice covered waters. *Polar Biology*, *9*, 187-191.
- Ludescher, J., Yuan, N., & Bunde, A. (2019). Detecting the statistical significance of the trends in the Antarctic sea ice extent: an indication for a turning point. *Climate dynamics*, *53*, 237-244.
- Lund-Hansen, L. C., Hawes, I., Hancke, K., Salmansen, N., Nielsen, J. R., Balslev, L., & Sorrell, B. K. (2020). Effects of increased irradiance on biomass, photobiology, nutritional quality, and pigment composition of Arctic sea ice algae. *Marine Ecology Progress Series*, *648*, 95-110.
- Lund-Hansen, L. C., Juul, T., Eskildsen, T. D., Hawes, I., Sorrell, B., Melvad, C., & Hancke, K. (2018). A low-cost remotely operated vehicle (ROV) with an optical positioning system for under-ice measurements and sampling. *Cold Regions Science and Technology*, *151*, 148-155.
- Lyon, B. R., & Mock, T. (2014). Polar microalgae: new approaches towards understanding adaptations to an extreme and changing environment. *Biology*, *3*(1), 56-80.
- Maeda, Y., Nojima, D., Yoshino, T., & Tanaka, T. (2017). Structure and properties of oil bodies in diatoms. *Philos. Trans. R. Soc. Lond., B, Biol. Sci.*, *372*(1728), 20160408.
- Mallett, R. D., Stroeve, J. C., Tsamados, M., Landy, J. C., Willatt, R., Nandan, V., & Liston, G. E. (2021). Faster decline and higher variability in the sea ice thickness of the marginal Arctic seas when accounting for dynamic snow cover. *The Cryosphere*, *15*(5), 2429-2450.
- Marañón, E., Cermeño, P., López-Sandoval, D. C., Rodríguez-Ramos, T., Sobrino, C., Huete-Ortega, M., Blanco, J. M., & Rodríguez, J. (2013). Unimodal size scaling of phytoplankton growth and the size dependence of nutrient uptake and use. *Ecology letters*, *16*(3), 371-379.

- Markus, T., Stroeve, J. C., & Miller, J. (2009). Recent changes in Arctic sea ice melt onset, freezeup, and melt season length. *Journal of Geophysical Research: Oceans*, 114(C12).
- Martin-Jézéquel, V., Hildebrand, M., & Brzezinski, M. A. (2000). Silicon metabolism in diatoms: implications for growth. *Journal of Phycology*, 36(5), 821-840.
- Maslanik, J., Stroeve, J., Fowler, C., & Emery, W. (2011). Distribution and trends in Arctic sea ice age through spring 2011. *Geophysical Research Letters*, 38(13).
- Massicotte, P., Amon, R. M., Antoine, D., Archambault, P., Balzano, S., Bélanger, S., Benner, R., Boeuf, D., Bricaud, A., & Bruyant, F. (2021). The MALINA oceanographic expedition: how do changes in ice cover, permafrost and UV radiation impact biodiversity and biogeochemical fluxes in the Arctic Ocean? *Earth System Science Data*, 13(4), 1561-1592.
- Matos, A., Ledoux, J.-B., Domínguez-Pérez, D., Almeida, D., & Antunes, A. (2020). Omics advances in the study of zooplankton: Big data for small drifting organisms. In M.A. Teodosio, A.M. Branco Barboza, *Zooplankton Ecology*, (pp. 264-277), CRC Press, Boca Raton, FL, U.S.A.
- Matuszko, D. (2012). Influence of the extent and genera of cloud cover on solar radiation intensity. *Int. J. Climatol.*, 32(15), 2403-2414.
- Mayor, D. J., Cook, K., Thornton, B., Walsham, P., Witte, U. F., Zuur, A. F., & Anderson, T. R. (2011). Absorption efficiencies and basal turnover of C, N and fatty acids in a marine Calanoid copepod. *Functional Ecology*, 25(3), 509-518.
- McCain, J. S. P., Allen, A. E., & Bertrand, E. M. (2022). Proteomic traits vary across taxa in a coastal Antarctic phytoplankton bloom. *The ISME journal*, 16(2), 569-579.
- McConnell, B., Gradinger, R., Iken, K., & Bluhm, B. A. (2012). Growth rates of arctic juvenile *Scolecopsis squamata* (Polychaeta: Spionidae) isolated from Chukchi Sea fast ice. *Polar Biology*, 35, 1487-1494.
- McConville, M., Mitchell, C., & Wetherbee, R. (1985). Patterns of carbon assimilation in a microalgal community from annual sea ice, East Antarctica. *Polar Biology*, 4(3), 135-141.
- McGillicuddy Jr, D., Sedwick, P. N., Dinniman, M. S., Arrigo, K., Bibby, T., Greenan, B., Hofmann, E. E., Klinck, J. M., Smith Jr, W. O., & Mack, S. (2015). Iron supply and demand in an Antarctic shelf ecosystem. *Geophysical Research Letters*, 42(19), 8088-8097.
- McMahon, K. W., Ambrose Jr, W. G., Johnson, B. J., Sun, M.-Y., Lopez, G. R., Clough, L. M., & Carroll, M. L. (2006). Benthic community response to ice algae and phytoplankton in Ny Ålesund, Svalbard. *Marine Ecology Progress Series*, 310, 1-14.
- McMinn, A. (2017). Reviews and syntheses: Ice acidification, the effects of ocean acidification on sea ice microbial communities. *Biogeosciences*, 14(17), 3927-3935.
- McMinn, A., & Martin, A. (2013). Dark survival in a warming world. *Proceedings of the Royal Society B: Biological Sciences*, 280(1755), 20122909.
- McNeil, B. I., & Matear, R. J. (2008). Southern Ocean acidification: A tipping point at 450-ppm atmospheric CO<sub>2</sub>. *Proceedings of the National Academy of Sciences*, 105(48), 18860-18864.
- Medlin, L. K., & Hasle, G. R. (1990). Some *Nitzschia* and related diatom species from fast ice samples in the Arctic and Antarctic. *Polar Biology*, 10, 451-479.
- Medlin, L. K., & Priddle, J. (1990). *Polar marine diatoms*. British Antarctic Survey, Cambridge, U.K.

- Meiners, K., Gradinger, R., Fehling, J., Civitarese, G., & Spindler, M. (2003). Vertical distribution of exopolymer particles in sea ice of the Fram Strait (Arctic) during autumn. *Marine Ecology Progress Series*, 248, 1-13.
- Meiners, K., Krembs, C., & Gradinger, R. (2008). Exopolymer particles: microbial hotspots of enhanced bacterial activity in Arctic fast ice (Chukchi Sea). *Aquatic Microbial Ecology*, 52(2), 195-207.
- Meiners, K. M., Vancoppenolle, M., Thanassekos, S., Dieckmann, G. S., Thomas, D. N., Tison, J. L., Arrigo, K. R., Garrison, D., McMinn, A., & Lannuzel, D. (2012). Chlorophyll a in Antarctic sea ice from historical ice core data. *Geophysical Research Letters*, 39(21), L216022.
- Mendes, C. R. B., Tavano, V. M., Dotto, T. S., Kerr, R., De Souza, M. S., Garcia, C. A. E., & Secchi, E. R. (2018). New insights on the dominance of cryptophytes in Antarctic coastal waters: a case study in Gerlache Strait. *Deep Sea Research Part II: Topical Studies in Oceanography*, 149, 161-170.
- Mendes, C. R. B., Tavano, V. M., Leal, M. C., de Souza, M. S., Brotas, V., & Garcia, C. A. E. (2013). Shifts in the dominance between diatoms and cryptophytes during three late summers in the Bransfield Strait (Antarctic Peninsula). *Polar Biology*, 36, 537-547.
- Meredith, M., Sommerkorn, M., Cassotta, S., Derksen, C., Ekaykin, A., Hollowed, A., Kofinas, G., Mackintosh, A., Melbourne-Thomas, J., & Muelbert, M. (2019). Polar Regions. In H.-O. Pörtner, D.C. Roberts, V. Masson-Delmotte, P. Zhai, M. Tignor, E. Poloczanska, K. Mintenbeck, A. Alegría, M. Nicolai, A. Okem, J. Petzold, B. Rama, N.M. Weyer (Eds.), *IPCC Special Report on the Ocean and Cryosphere in a Changing Climate*, Cambridge University Press, Cambridge, U.K. and New York, NY, U.S.A.
- Merilä, J., & Hendry, A. P. (2014). Climate change, adaptation, and phenotypic plasticity: the problem and the evidence. *Evolutionary applications*, 7(1), 1-14.
- Meyer, B., Atkinson, A., Blume, B., & Bathmann, U. V. (2003). Feeding and energy budgets of larval Antarctic krill *Euphausia superba* in summer. *Marine Ecology Progress Series*, 257, 167-178.
- Meyer, M. A., & El-Sayed, S. (1983). Grazing of *Euphausia superba* Dana on natural phytoplankton populations. *Polar Biology*, 1, 193-197.
- Michel, C., Legendre, L., Ingram, R., Gosselin, M., & Levasseur, M. (1996). Carbon budget of sea-ice algae in spring: Evidence of a significant transfer to zooplankton grazers. *Journal of Geophysical Research: Oceans*, 101(C8), 18345-18360.
- Michel, C., Legendre, L., Therriault, J.-C., Demers, S., & Vandeveld, T. (1993). Springtime coupling between ice algal and phytoplankton assemblages in southeastern Hudson Bay, Canadian Arctic. *Polar Biology*, 13(7), 441-449.
- Miklasz, K. A., & Denny, M. W. (2010). Diatom sinkings speeds: Improved predictions and insight from a modified Stokes' law. *Limnology and Oceanography*, 55(6), 2513-2525.
- Mitchell, J. G., Seuront, L., Doubell, M. J., Losic, D., Voelcker, N. H., Seymour, J., & Lal, R. (2013). The role of diatom nanostructures in biasing diffusion to improve uptake in a patchy nutrient environment. *PLoS One*, 8(5), e59548.
- Mock, T., & Gradinger, R. (1999). Determination of Arctic ice algal production with a new in situ incubation technique. *Marine Ecology Progress Series*, 177, 15-26.
- Mock, T., & Gradinger, R. (2000). Changes in photosynthetic carbon allocation in algal assemblages of Arctic sea ice with decreasing nutrient concentrations and irradiance. *Marine Ecology Progress Series*, 202, 1-11.

- Mock, T., & Kroon, B. M. (2002a). Photosynthetic energy conversion under extreme conditions—I: important role of lipids as structural modulators and energy sink under N-limited growth in Antarctic sea ice diatoms. *Phytochemistry*, *61*(1), 41-51.
- Mock, T., & Kroon, B. M. (2002b). Photosynthetic energy conversion under extreme conditions—II: the significance of lipids under light limited growth in Antarctic sea ice diatoms. *Phytochemistry*, *61*(1), 53-60.
- Mock, T., & Thomas, D. N. (2005). Recent advances in sea-ice microbiology. *Environmental Microbiology*, *7*(5), 605-619.
- Moline, M. A., Claustre, H., Frazer, T. K., Grzyski, J., & Vernet, M. (2001). Changes in phytoplankton assemblages along the Antarctic Peninsula and potential implications for the Antarctic food web. In: W. Davidson, C. Howard-Williams, P. Broady (Eds). *Antarctic ecosystems: models for wider ecological understanding*, (pp. 263–271), Canterbury University, New Zealand.
- Moline, M. A., Claustre, H., Frazer, T. K., Schofield, O., & Vernet, M. (2004). Alteration of the food web along the Antarctic Peninsula in response to a regional warming trend. *Global Change Biology*, *10*(12), 1973-1980.
- Montes-Hugo, M., Doney, S. C., Ducklow, H. W., Fraser, W., Martinson, D., Stammerjohn, S. E., & Schofield, O. (2009). Recent changes in phytoplankton communities associated with rapid regional climate change along the western Antarctic Peninsula. *Science*, *323*(5920), 1470-1473.
- Moore, J. K., Doney, S. C., Glover, D. M., & Fung, I. Y. (2001). Iron cycling and nutrient-limitation patterns in surface waters of the World Ocean. *Deep Sea Research Part II: Topical Studies in Oceanography*, *49*(1-3), 463-507.
- Moreau, S., Boyd, P. W., & Strutton, P. G. (2020). Remote assessment of the fate of phytoplankton in the Southern Ocean sea-ice zone. *Nature Communications*, *11*(1), 3108.
- Moreau, S., Mostajir, B., Bélanger, S., Schloss, I. R., Vancoppenolle, M., Demers, S., & Ferreyra, G. A. (2015). Climate change enhances primary production in the western Antarctic Peninsula. *Global Change Biology*, *21*(6), 2191-2205.
- Morgan-Kiss, R. M., Priscu, J. C., Pockock, T., Gudynaite-Savitch, L., & Huner, N. P. (2006). Adaptation and acclimation of photosynthetic microorganisms to permanently cold environments. *Microbiology and Molecular Biology Reviews*, *70*(1), 222-252.
- Mundy, C., Barber, D., & Michel, C. (2005). Variability of snow and ice thermal, physical and optical properties pertinent to sea ice algae biomass during spring. *Journal of Marine Systems*, *58*(3-4), 107-120.
- Mundy, C., Barber, D., Michel, C., & Marsden, R. (2007). Linking ice structure and microscale variability of algal biomass in Arctic first-year sea ice using an in situ photographic technique. *Polar Biology*, *30*, 1099-1114.
- Mundy, C., & Meiners, K. M. (2021). Ecology of Arctic Sea Ice. In D.N. Thomas (Ed.) *Arctic Ecology*, (pp. 261-288). John Wiley & Sons, Ltd., Chichester, UK.
- Mundy, C. J., Gosselin, M., Ehn, J. K., Belzile, C., Poulin, M., Alou, E., Roy, S., Hop, H., Lessard, S., Papakyriakou, T. N., Barber, D. G., & Stewart, J. (2011). Characteristics of two distinct high-light acclimated algal communities during advanced stages of sea ice melt. *Polar Biology*, *34*(12), 1869-1886.
- Mundy, C. J., Gosselin, M., Gratton, Y., Brown, K., Galindo, V., Campbell, K., Lévassieur, M., Barber, D., Papakyriakou, T., & Bélanger, S. (2014). Role of environmental factors on phytoplankton bloom initiation under landfast sea ice in Resolute Passage, Canada. *Marine Ecology Progress Series*, *497*, 39-49.

- Murdock, J. N., & Wetzel, D. L. (2009). FT-IR microspectroscopy enhances biological and ecological analysis of algae. *Applied Spectroscopy Reviews*, 44(4), 335-361. NASA Goddard Space Flight Center, Ocean Ecology Laboratory, Ocean Biology Processing Group, 2024. Moderate-resolution Imaging Spectroradiometer (MODIS) Aqua Level 3 Mapped Data; NASA OB.DAAC, Greenbelt, MD, USA. doi: 10.5067/AQUA/MODIS/L3M/CHL/2022.
- Nagelkerken, I., Goldenberg, S. U., Ferreira, C. M., Ullah, H., & Connell, S. D. (2020). Trophic pyramids reorganize when food web architecture fails to adjust to ocean change. *Science*, 369(6505), 829-832.
- Neeley, A., Harris, L., & Frey, K. (2018). Unraveling phytoplankton community dynamics in the northern Chukchi Sea under sea-ice-covered and sea-ice-free conditions. *Geophysical Research Letters*, 45(15), 7663-7671.
- Nelson, D. M., & Smith Jr, W. O. (1986). Phytoplankton bloom dynamics of the western Ross Sea ice edge—II. Mesoscale cycling of nitrogen and silicon. *Deep Sea Research Part A. Oceanographic Research Papers*, 33(10), 1389-1412.
- Nichols, P. D., Palmisano, A. C., Rayner, M. S., Smith, G. A., & White, D. C. (1989). Changes in the lipid composition of Antarctic sea-ice diatom communities during a spring bloom: an indication of community physiological status. *Antarctic Science*, 1(2), 133-140.
- Nicolas, J. P., & Bromwich, D. H. (2014). New reconstruction of Antarctic near-surface temperatures: Multidecadal trends and reliability of global reanalyses. *Journal of Climate*, 27(21), 8070-8093.
- Nielsen, L. T., Jakobsen, H. H., & Hansen, P. J. (2010). High resilience of two coastal plankton communities to twenty-first century seawater acidification: Evidence from microcosm studies. *Marine Biology Research*, 6(6), 542-555.
- Niemi, A., Michel, C., Hille, K., & Poulin, M. (2011). Protist assemblages in winter sea ice: setting the stage for the spring ice algal bloom. *Polar Biology*, 34, 1803-1817.
- Norwegian Ice Service. (2022). *Ice Service Charts*. Norwegian Meteorological Institute. <https://cryo.met.no/en/latest-ice-charts>
- Notz, D., & Community, S. (2020). Arctic sea ice in CMIP6. *Geophysical Research Letters*, 47(10), e2019GL086749.
- Notz, D., & Worster, M. G. (2009). Desalination processes of sea ice revisited. *Journal of Geophysical Research: Oceans*, 114, C5, C05006.
- NSIDC. (2023). *Sea Ice Index*. National Snow & Ice Data Center [https://nsidc.org/data/seaice\\_index/](https://nsidc.org/data/seaice_index/)
- NSIDC. (2024). *Antarctic Daily Image Update*. National Snow & Ice Data Center <https://nsidc.org/arcticseaicenews/antarctic-daily-image-update/>
- Oksanen, J., Blanchet, F. G., Kindt, R., Legendre, P., Minchin, P. R., O'hara, R., Simpson, G. L., Solymos, P., Stevens, M. H. H., & Wagner, H. (2013). Package 'vegan': Community Ecology Package, Version 2.4.3 <https://cran.r-project.org>, <https://github.com/vegandevs/vegan>
- Oldenburg, E., Popa, O., Wietz, M., von Appen, W.-J., Torres-Valdes, S., Bienhold, C., Ebenhöf, O., & Metfies, K. (2024). Sea-ice melt determines seasonal phytoplankton dynamics and delimits the habitat of temperate Atlantic taxa as the Arctic Ocean atlantifies. *ISME ommunications*, 4(1), ycae027.
- Onarheim, I. H., Eldevik, T., Smedsrud, L. H., & Stroeve, J. C. (2018). Seasonal and regional manifestation of Arctic sea ice loss. *Journal of Climate*, 31(12), 4917-4932.

- Orr, J. C., Fabry, V. J., Aumont, O., Bopp, L., Doney, S. C., Feely, R. A., Gnanadesikan, A., Gruber, N., Ishida, A., & Joos, F. (2005). Anthropogenic ocean acidification over the twenty-first century and its impact on calcifying organisms. *Nature*, *437*(7059), 681-686.
- Overland, J. E., & Wang, M. (2013). When will the summer Arctic be nearly sea ice free? *Geophysical Research Letters*, *40*(10), 2097-2101.
- Pabi, S., van Dijken, G. L., & Arrigo, K. R. (2008). Primary production in the Arctic Ocean, 1998–2006. *Journal of Geophysical Research: Oceans*, *113*, C08005.
- Pahlow, M., Riebesell, U., & Wolf-Gladrow, D. A. (1997). Impact of cell shape and chain formation on nutrient acquisition by marine diatoms. *Limnology and Oceanography*, *42*(8), 1660-1672.
- Palmer, M. A., Saenz, B. T., & Arrigo, K. R. (2014). Impacts of sea ice retreat, thinning, and melt-pond proliferation on the summer phytoplankton bloom in the Chukchi Sea, Arctic Ocean. *Deep Sea Research Part II: Topical Studies in Oceanography*, *105*, 85-104.
- Palmisano, A. C., Lizotte, M. P., Smith, G. A., Nichols, P. D., White, D. C., & Sullivan, C. W. (1988). Changes in photosynthetic carbon assimilation in Antarctic sea-ice diatoms during spring bloom: variation in synthesis of lipid classes. *Journal of Experimental Marine Biology and Ecology*, *116*(1), 1-13.
- Palmisano, A. C., & Sullivan, C. W. (1982). Physiology of sea ice diatoms. I. Response of three polar diatoms to a simulated summer-winter transition. *Journal of Phycology*, *18*(4), 489-498.
- Palmisano, A. C., & Sullivan, C. W. (1983). Physiology of sea ice diatoms. II. Dark survival of three polar diatoms. *Canadian Journal of Microbiology*, *29*(1), 157-160.
- Palmisano, A. C., & Sullivan, C. W. (1985). Pathways of photosynthetic carbon assimilation in sea-ice microalgae from McMurdo Sound, Antarctica. *Limnology and Oceanography*, *30*(3), 674-678.
- Pan, X. L., Li, B. F., & Watanabe, Y. W. (2022). Intense ocean freshening from melting glacier around the Antarctica during early twenty-first century. *Scientific reports*, *12*(1), 383.
- Parkinson, C. L. (2014a). Global sea ice coverage from satellite data: Annual cycle and 35-yr trends. *Journal of Climate*, *27*(24), 9377-9382.
- Parkinson, C. L. (2014b). Spatially mapped reductions in the length of the Arctic sea ice season. *Geophysical Research Letters*, *41*(12), 4316-4322.
- Parkinson, C. L. (2019). A 40-y record reveals gradual Antarctic sea ice increases followed by decreases at rates far exceeding the rates seen in the Arctic. *Proceedings of the National Academy of Sciences*, *116*(29), 14414-14423.
- Parrish, C. C., Thompson, R. J., & Deibel, D. (2005). Lipid classes and fatty acids in plankton and settling matter during the spring bloom in a cold ocean coastal environment. *Marine Ecology Progress Series*, *286*, 57-68.
- Parsons, T. R., Maita, Y., & Lalli, C. M. (1984). *A manual of chemical & biological methods for seawater analysis*. Pergamon Press, Oxford, UK.
- Paul, A. J., & Bach, L. T. (2020). Universal response pattern of phytoplankton growth rates to increasing CO<sub>2</sub>. *New Phytologist*, *228*(6), 1710-1716.
- Peltomaa, E. T., Aalto, S. L., Vuorio, K. M., & Taipale, S. J. (2017). The importance of phytoplankton biomolecule availability for secondary production. *Front. Ecol. Evol.*, *5*, 128.
- Perovich, D., Meier, W., Tschudi, M., Farrell, S., Hendricks, S., Gerland, S., Haas, C., Krumpfen, T., Polashenski, C., Ricker, R., & Webster, M. (2018). *Sea Ice*,

- NOAA: Arctic Report Card. <https://arctic.noaa.gov/report-card/report-card-2018/sea-ice-5/>
- Perovich, D. K. (1996). *The optical properties of sea ice*. CRREL monograph 96-1, Office of Naval Research.
- Perovich, D. K. (2007). Light reflection and transmission by a temperate snow cover. *Journal of Glaciology*, 53(181), 201-210.
- Peterson, B. J., Holmes, R. M., McClelland, J. W., Vörösmarty, C. J., Lammers, R. B., Shiklomanov, A. I., Shiklomanov, I. A., & Rahmstorf, S. (2002). Increasing river discharge to the Arctic Ocean. *Science*, 298(5601), 2171-2173.
- Petrenko, D., Pozdnyakov, D., Johannessen, J., Counillon, F., & Syrov, V. (2013). Satellite-derived multi-year trend in primary production in the Arctic Ocean. *International Journal of Remote Sensing*, 34(11), 3903-3937.
- Petrou, K., Baker, K. G., Nielsen, D. A., Hancock, A. M., Schulz, K. G., & Davidson, A. T. (2019). Acidification diminishes diatom silica production in the Southern Ocean. *Nature Climate Change*, 9(10), 781-786.
- Petrou, K., Hill, R., Brown, C. M., Campbell, D. A., Doblin, M. A., & Ralph, P. J. (2010). Rapid photoprotection in sea-ice diatoms from the East Antarctic pack ice. *Limnology and Oceanography*, 55(3), 1400-1407.
- Petrou, K., Hill, R., Doblin, M. A., McMinn, A., Johnson, R., Wright, S. W., & Ralph, P. J. (2011). Photoprotection of sea-ice microalgal communities from the east antarctic pack ice 1. *Journal of Phycology*, 47(1), 77-86.
- Petrou, K., Kranz, S. A., Trimborn, S., Hassler, C. S., Ameijeiras, S. B., Sackett, O., Ralph, P. J., & Davidson, A. T. (2016). Southern Ocean phytoplankton physiology in a changing climate. *Journal of Plant Physiology*, 203, 135-150.
- Petrou, K., Nielsen, D. A., & Heraud, P. (2018). Single-cell biomolecular analysis of coral algal symbionts reveals opposing metabolic responses to heat stress and expulsion. *Frontiers in Marine Science*, 5, 110.
- Pogorzelec, N. M., Gough, K. M., Ha, S.-Y., Campbell, K., Else, B., Kim, K., Lee, S. H., & Mundy, C. (2022). FTIR autecological analysis of bottom-ice diatom taxa across a tidal strait in the Canadian Arctic. *Elementa: Science of the Anthropocene*, 10(1), 00094.
- Pogorzelec, N. M., Mundy, C., Findlay, C. R., Campbell, K., Diaz, A., Ehn, J. K., Rysgaard, S., & Gough, K. M. (2017). FTIR imaging analysis of cell content in sea-ice diatom taxa during a spring bloom in the lower Northwest Passage of the Canadian Arctic. *Marine Ecology Progress Series*, 569, 77-88.
- Pollard, R., Tréguer, P., & Read, J. (2006). Quantifying nutrient supply to the Southern Ocean. *Journal of Geophysical Research: Oceans*, 111, C05011.
- Post, E., Alley, R. B., Christensen, T. R., Macias-Fauria, M., Forbes, B. C., Gooseff, M. N., Iler, A., Kerby, J. T., Laidre, K. L., & Mann, M. E. (2019). The polar regions in a 2 C warmer world. *Science advances*, 5(12), eaaw9883.
- Post, E., Bhatt, U. S., Bitz, C. M., Brodie, J. F., Fulton, T. L., Hebblewhite, M., Kerby, J., Kutz, S. J., Stirling, I., & Walker, D. A. (2013). Ecological consequences of sea-ice decline. *Science*, 341(6145), 519-524.
- Poulin, M., & Cardinal, A. (1982). Sea ice diatoms from Manitounuk Sound, southeastern Hudson Bay (Quebec, Canada).: II. *Naviculaceae*, genus *Navicula*. *Canad. J. Bot.*, 60(12), 2825-2845.
- Poulin, M., & Cardinal, A. (1983). Sea ice diatoms from Manitounuk Sound, southeastern Hudson Bay (Quebec, Canada). III. *Cymbellaceae*, *Entomoneidaceae*, *Gomphonemataceae*, and *Nitzschiaceae*. *Canad. J. Bot.*, 61(1), 107-118.



- Poulin, M., Daugbjerg, N., Gradinger, R., Ilyash, L., Ratkova, T., and von Quillfeldt, C. (2011). The pan-Arctic biodiversity of marine pelagic and sea-ice unicellular eukaryotes: a first-attempt assessment. *Marine Biodiversity*, *41*, 13–28.
- Priscu, J. C., Priscu, L. R., Palmisano, A. C., & Sullivan, C. W. (1990). Estimation of neutral lipid levels in Antarctic sea ice microalgae by Nile red fluorescence. *Antarctic Science*, *2*(2), 149-155.
- Purich, A., & Doddridge, E. W. (2023). Record low Antarctic sea ice coverage indicates a new sea ice state. *Communications Earth & Environment*, *4*(1), 314.
- Qing, Z., Gradinger, R., & Qingsong, Z. (2003). Competition within the marine microalgae over the polar dark period in the Greenland Sea of high Arctic. *Acta Oceanologica Sinica*(2), 233-242.
- Quetin, L., & Ross, R. (1985). Feeding by Antarctic Krill, *Euphausia superba*: does size matter? In *Antarctic nutrient cycles and food webs* (pp. 372-377). Springer.
- Rantanen, M., Karpechko, A. Y., Lipponen, A., Nordling, K., Hyvärinen, O., Ruosteenoja, K., Vihma, T., & Laaksonen, A. (2022). The Arctic has warmed nearly four times faster than the globe since 1979. *Communications Earth & Environment*, *3*(1), 168.
- Reeves, S., McMinn, A., & Martin, A. (2011). The effect of prolonged darkness on the growth, recovery and survival of Antarctic sea ice diatoms. *Polar Biology*, *34*, 1019-1032.
- Reffner, J. A., Martoglio, P. A., & Williams, G. P. (1995). Fourier transform infrared microscopical analysis with synchrotron radiation: The microscope optics and system performance. *Review of Scientific Instruments*, *66*(2), 1298-1302.
- Rehman, Z. U., & Anal, A. K. (2019). Enhanced lipid and starch productivity of microalga (*Chlorococcum* sp. TISTR 8583) with nitrogen limitation following effective pretreatments for biofuel production. *Biotechnology Reports*, *21*, e00298.
- Renaud, P. E., Riedel, A., Michel, C., Morata, N., Gosselin, M., Juul-Pedersen, T., & Chiuchiolo, A. (2007). Seasonal variation in benthic community oxygen demand: a response to an ice algal bloom in the Beaufort Sea, Canadian Arctic? *Journal of Marine Systems*, *67*(1-2), 1-12.
- Renner, A. H., Gerland, S., Haas, C., Spreen, G., Beckers, J. F., Hansen, E., Nicolaus, M., & Goodwin, H. (2014). Evidence of Arctic sea ice thinning from direct observations. *Geophysical Research Letters*, *41*(14), 5029-5036.
- Riebesell, U., & Gattuso, J.-P. (2015). Lessons learned from ocean acidification research. *Nature Climate Change*, *5*(1), 12-14.
- Riebesell, U., Schloss, I., & Smetacek, V. (1991). Aggregation of algae released from melting sea ice: implications for seeding and sedimentation. *Polar Biology*, *11*, 239-248.
- Riedel, A., Michel, C., Gosselin, M., & LeBlanc, B. (2008). Winter–spring dynamics in sea-ice carbon cycling in the coastal Arctic Ocean. *Journal of Marine Systems*, *74*(3-4), 918-932.
- Roach, L. A., Dörr, J., Holmes, C. R., Massonnet, F., Blockley, E. W., Notz, D., Rackow, T., Raphael, M. N., O'Farrell, S. P., & Bailey, D. A. (2020). Antarctic sea ice area in CMIP6. *Geophysical Research Letters*, *47*(9), e2019GL086729.
- Robinson, D. H., Kolber, Z., & Sullivan, C. W. (1997). Photophysiology and photoacclimation in surface sea ice algae from McMurdo Sound, Antarctica. *Marine Ecology Progress Series*, *147*, 243-256.
- Rontani, J.-F., Amiraux, R., Smik, L., Wakeham, S. G., Paulmier, A., Vaultier, F., Sun-Yong, H., Jun-Oh, M., & Belt, S. T. (2021). Type II photosensitized oxidation in

- senescent microalgal cells at different latitudes: Does low under-ice irradiance in polar regions enhance efficiency? *Science of the Total Environment*, 779, 146363.
- Rontani, J.-F., Belt, S. T., Brown, T. A., Amiraux, R., Gosselin, M., Vaultier, F., & Mundy, C. J. (2016). Monitoring abiotic degradation in sinking versus suspended Arctic sea ice algae during a spring ice melt using specific lipid oxidation tracers. *Organic geochemistry*, 98, 82-97.
- Ross, P. M., Parker, L., O'Connor, W. A., & Bailey, E. A. (2011). The impact of ocean acidification on reproduction, early development and settlement of marine organisms. *Water*, 3(4), 1005-1030.
- Rossoll, D., Bermúdez, R., Hauss, H., Schulz, K. G., Riebesell, U., Sommer, U., & Winder, M. (2012). Ocean acidification-induced food quality deterioration constrains trophic transfer. *PLoS one*, 7(4), e34737.
- Róžańska, M., Gosselin, M., Poulin, M., Wiktor, J., & Michel, C. (2009). Influence of environmental factors on the development of bottom ice protist communities during the winter–spring transition. *Marine Ecology Progress Series*, 386, 43-59.
- RStudio Team. (2021). *RStudio: Integrated Development for R*. Version 2023.09.0), Posit Software PBC, Boston, MA, U.S.A. [Computer Software].
- RStudio Team. (2022). *RStudio: Integrated Development for R*. Version 1.3.959), Posit Software PBC, Boston, MA, U.S.A. [Computer Software].
- Ruess, L., & Müller-Navarra, D. C. (2019). Essential biomolecules in food webs. *Frontiers in Ecology and Evolution*, 7, 269.
- Runge, J., & Ingram, R. G. (1991). Under-ice feeding and diel migration by the planktonic copepods *Calanus glacialis* and *Pseudocalanus minutus* in relation to the ice algal production cycle in southeastern Hudson Bay, Canada. *Marine Biology*, 108, 217-225.
- Runge, E. (2021). *Timing and magnitude of sea ice algal blooms in Svalbard archipelago: synthesis of chlorophyll a and driving physical environmental variables from 2007 to 2021* [Master Thesis, University in Copenhagen].
- Rysgaard, S., Kühl, M., Glud, R. N., & Hansen, J. W. (2001). Biomass, production and horizontal patchiness of sea ice algae in a high-Arctic fjord (Young Sound, NE Greenland). *Marine Ecology Progress Series*, 223, 15-26.
- Rysgaard, S., Nielsen, T. G., & Hansen, B. W. (1999). Seasonal variation in nutrients, pelagic primary production and grazing in a high-Arctic coastal marine ecosystem, Young Sound, Northeast Greenland. *Marine Ecology Progress Series*, 179, 13-25.
- Sabine, C. L., Feely, R. A., Gruber, N., Key, R. M., Lee, K., Bullister, J. L., Wanninkhof, R., Wong, C., Wallace, D. W., & Tilbrook, B. (2004). The oceanic sink for anthropogenic CO<sub>2</sub>. *Science*, 305(5682), 367-371.
- Sackett, O., Armand, L., Beardall, J., Hill, R., Doblin, M., Connelly, C., Howes, J., Stuart, B., Ralph, P., & Heraud, P. (2014). Taxon-specific responses of Southern Ocean diatoms to Fe enrichment revealed by synchrotron radiation FTIR microspectroscopy. *Biogeosciences*, 11(20), 5795-5808.
- Sackett, O., Petrou, K., Reedy, B., De Grazia, A., Hill, R., Doblin, M., Beardall, J., Ralph, P., & Heraud, P. (2013). Phenotypic plasticity of southern ocean diatoms: key to success in the sea ice habitat? *PLoS one*, 8(11), e81185.
- Sackett, O., Petrou, K., Reedy, B., Hill, R., Doblin, M., Beardall, J., Ralph, P., & Heraud, P. (2016). Snapshot prediction of carbon productivity, carbon and

- protein content in a Southern Ocean diatom using FTIR spectroscopy. *The ISME journal*, 10(2), 416-426.
- Sadai, S., Condron, A., DeConto, R., & Pollard, D. (2020). Future climate response to Antarctic Ice Sheet melt caused by anthropogenic warming. *Science advances*, 6(39), eaaz1169.
- Saggiomo, M., Escalera, L., Saggiomo, V., Bolinesi, F., & Mangoni, O. (2021). Phytoplankton blooms below the Antarctic landfast ice during the melt season between late spring and early summer. *Journal of Phycology*, 57(2), 541-550.
- Sakshaug, E., Stein, R., & Macdonald, R. (2004). *The organic carbon cycle in the Arctic Ocean*, (pp. 57-81), Springer-Verlag, Berlin.
- Salazar, G., Paoli, L., Alberti, A., Huerta-Cepas, J., Ruscheweyh, H.-J., Cuenca, M., Field, C. M., Coelho, L. P., Cruaud, C., & Engelen, S. (2019). Gene expression changes and community turnover differentially shape the global ocean metatranscriptome. *Cell*, 179(5), 1068-1083. e1021.
- Sargent, J., Eilertsen, H., Falk-Petersen, S., & Taasen, J. (1985). Carbon assimilation and lipid production in phytoplankton in northern Norwegian fjords. *Marine biology*, 85, 109-116.
- Sarthou, G., Timmermans, K. R., Blain, S., & Tréguer, P. (2005). Growth physiology and fate of diatoms in the ocean: a review. *Journal of sea research*, 53(1-2), 25-42.
- Schmidt, K., Graeve, M., Hoppe, C. J., Torres-Valdes, S., Welteke, N., Whitmore, L. M., Anhaus, P., Atkinson, A., Belt, S. T., & Brenneis, T. (2024). Essential omega-3 fatty acids are depleted in sea ice and pelagic algae of the Central Arctic Ocean. *Global Change Biology*, 30(1), e17090.
- Schmidtko, S., Heywood, KJ, Thompson, AF, Aoki, S. (2014). Multidecadal warming of Antarctic waters. *Science*, 5(346:6214), 1227-1231.
- Scott, J. (1980). Effect of growth rate of the food alga on the growth/ingestion efficiency of a marine herbivore. *Journal of the Marine Biological Association of the United Kingdom*, 60(3), 681-702.
- Screen, J. A., & Simmonds, I. (2012). Declining summer snowfall in the Arctic: Causes, impacts and feedbacks. *Climate dynamics*, 38, 2243-2256.
- Selz, V., Laney, S., Arnsten, A. E., Lewis, K. M., Lowry, K. E., Joy-Warren, H. L., Mills, M. M., van Dijken, G. L., & Arrigo, K. R. (2018). Ice algal communities in the Chukchi and Beaufort Seas in spring and early summer: Composition, distribution, and coupling with phytoplankton assemblages. *Limnology and Oceanography*, 63(3), 1109-1133.
- Shapiro, S. S., & Wilk, M. B. (1965). An analysis of variance test for normality (complete samples). *Biometrika*, 52(3/4), 591-611.
- Sheehan, C. E., Nielsen, D. A., & Petrou, K. (2020). Macromolecular composition, productivity and dimethylsulfoniopropionate in Antarctic pelagic and sympagic microalgal communities. *Marine Ecology Progress Series*, 640, 45-61.
- Sherr, E. B., Sherr, B. F., Wheeler, P. A., & Thompson, K. (2003). Temporal and spatial variation in stocks of autotrophic and heterotrophic microbes in the upper water column of the central Arctic Ocean. *Deep Sea Research Part I: Oceanographic Research Papers*, 50(5), 557-571.
- Shi, Q., Xiahou, W., & Wu, H. (2017). Photosynthetic responses of the marine diatom *Thalassiosira pseudonana* to CO<sub>2</sub>-induced seawater acidification. *Hydrobiologia*, 788, 361-369.

- Shin, K., Jang, M.-C., Jang, P.-K., Ju, S.-J., Lee, T.-K., & Chang, M. (2003). Influence of food quality on egg production and viability of the marine planktonic copepod *Acartia omorii*. *Progress in Oceanography*, 57(3-4), 265-277.
- Shu, Q., Qiao, F., Song, Z., Zhao, J., & Li, X. (2018). Projected freshening of the Arctic Ocean in the 21st century. *Journal of Geophysical Research: Oceans*, 123(12), 9232-9244.
- Sigee, D. C., Bahrami, F., Estrada, B., Webster, R. E., & Dean, A. P. (2007). The influence of phosphorus availability on carbon allocation and P quota in *Scenedesmus subspicatus*: a synchrotron-based FTIR analysis. *Phycologia*, 46(5), 583-592.
- Silvano, A., Rintoul, S., Peña-Molino, B., Hobbs, W., van Wijk, E., Aoki, S., Tamura, T., & Williams, G. (2018). Freshening by glacial meltwater enhances melting of ice shelves and reduces formation of Antarctic Bottom Water. *Science advances*, 4(4), eaap9467.
- Singh, R. K., Vader, A., Mundy, C. J., Søreide, J. E., Iken, K., Dunton, K. H., Castro de la Guardia, L., Sejr, M. K., & Bélanger, S. (2022). Satellite-derived photosynthetically available radiation at the coastal Arctic seafloor. *Remote Sensing*, 14(20), 5180.
- Slagstad, D., Wassmann, P. F., & Ellingsen, I. (2015). Physical constraints and productivity in the future Arctic Ocean. *Frontiers in Marine Science*, 2, 85.
- Smith Jr, W. O., Nelson, D. M., DiTullio, G. R., & Leventer, A. R. (1996). Temporal and spatial patterns in the Ross Sea: phytoplankton biomass, elemental composition, productivity and growth rates. *Journal of Geophysical Research: Oceans*, 101(C8), 18455-18465.
- Smith, R., Anning, J., & Pierre Clement, G. (1988). Abundance and production of ice algae in Resolute Passage, Canadian Arctic. *Marine Ecology Progress Series*, 48, 251-263.
- Smith, R., Gosselin, M., & Taguchi, S. (1997). The influence of major inorganic nutrients on the growth and physiology of high arctic ice algae. *Journal of Marine Systems*, 11(1-2), 63-70.
- Smith, R. E., Cavaletto, J. F., Eadie, B., & Gardner, W. S. (1993). Growth and lipid composition of high Arctic ice algae during the spring bloom at Resolute, Northwest Territories, Canada. *Marine Ecology Progress Series*, 97, 19-29.
- Smith, R. E., Clement, P., Cota, G. F., & Li, W. K. (1987). Intracellular photosynthate allocation and the control of Arctic marine ice algal production *Journal of Phycology*, 23(2), 124-132.
- Smith, R. E., Clement, P., & Head, E. (1989). Biosynthesis and photosynthate allocation patterns of Arctic ice algae. *Limnology and Oceanography*, 34(3), 591-605.
- Smith, R. E., & Herman, A. W. (1992). In situ patterns of intracellular photosynthate allocation by sea ice algae in the Canadian High Arctic. *Polar Biology*, 12(6), 545-551.
- Søreide, J. E., Carroll, M. L., Hop, H., Ambrose Jr, W. G., Hegseth, E. N., & Falk-Petersen, S. (2013). Sympagic-pelagic-benthic coupling in Arctic and Atlantic waters around Svalbard revealed by stable isotopic and fatty acid tracers. *Marine Biology Research*, 9(9), 831-850.
- Søreide, J. E., Falk-Petersen, S., Hegseth, E. N., Hop, H., Carroll, M. L., Hobson, K. A., & Blachowiak-Samolyk, K. (2008). Seasonal feeding strategies of *Calanus* in the high-Arctic Svalbard region. *Deep Sea Research Part II: Topical Studies in Oceanography*, 55(20-21), 2225-2244.

- Søreide, J. E., Hop, H., Carroll, M. L., Falk-Petersen, S., & Hegseth, E. N. (2006). Seasonal food web structures and sympagic–pelagic coupling in the European Arctic revealed by stable isotopes and a two-source food web model. *Progress in Oceanography*, 71(1), 59-87.
- Søreide, J. E., Leu, E. V., Berge, J., Graeve, M., & Falk-Petersen, S. (2010). Timing of blooms, algal food quality and *Calanus glacialis* reproduction and growth in a changing Arctic. *Global Change Biology*, 16(11), 3154-3163.
- Spilling, K., Ylöstalo, P., Simis, S., & Seppälä, J. (2015). Interaction effects of light, temperature and nutrient limitations (N, P and Si) on growth, stoichiometry and photosynthetic parameters of the cold-water diatom *Chaetoceros wighamii*. *PLoS One*, 10(5), e0126308.
- Stammerjohn, S., Massom, R., Rind, D., & Martinson, D. (2012). Regions of rapid sea ice change: An inter-hemispheric seasonal comparison. *Geophysical Research Letters*, 39(6), L06501.
- Stehfest, K., Toepel, J., & Wilhelm, C. (2005). The application of micro-FTIR spectroscopy to analyze nutrient stress-related changes in biomass composition of phytoplankton algae. *Plant Physiology and biochemistry*, 43(7), 717-726.
- Sterrenburg, F. A., Tiffany, M. A., Hinz, F., Herwig, W. E., & Hargraves, P. E. (2015). Seven new species expand the morphological spectrum of *Haslea*. A comparison with *Gyrosigma* and *Pleurosigma* (Bacillariophyta). *Phytotaxa*, 207(2), 143-162.
- Stevens, A., & Ramirez-Lopez, L. (2014). An introduction to the prospectr package. In: GitHub.
- Stroeve, J., Holland, M. M., Meier, W., Scambos, T., & Serreze, M. (2007). Arctic sea ice decline: Faster than forecast. *Geophysical Research Letters*, 34(9), L09501, Article L09501.
- Stroeve, J., & Notz, D. (2018). Changing state of Arctic sea ice across all seasons. *Environmental Research Letters*, 13(10), 103001.
- Stroeve, J. C., Markus, T., Boisvert, L., Miller, J., & Barrett, A. (2014). Changes in Arctic melt season and implications for sea ice loss. *Geophysical Research Letters*, 41(4), 1216-1225.
- Stroeve, J. C., Serreze, M. C., Holland, M. M., Kay, J. E., Malanik, J., & Barrett, A. P. (2012). The Arctic's rapidly shrinking sea ice cover: a research synthesis. *Climatic change*, 110, 1005-1027.
- Su, Y., Lundholm, N., & Ellegaard, M. (2018). The effect of different light regimes on diatom frustule silicon concentration. *Algal research*, 29, 36-40.
- Sugie, K., Fujiwara, A., Nishino, S., Kameyama, S., & Harada, N. (2020). Impacts of temperature, CO<sub>2</sub>, and salinity on phytoplankton community composition in the Western Arctic Ocean. *Frontiers in Marine Science*, 6, 821.
- Svenning, J. B., Vasskog, T., Campbell, K., Bæverud, A. H., Myhre, T. N., Dalheim, L., Forgereau, Z. L., Osanen, J. E., Hansen, E. H., & Bernstein, H. C. (2024). Lipidome Plasticity Enables Unusual Photosynthetic Flexibility in Arctic vs. Temperate Diatoms. *Marine Drugs*, 22(2), 67.
- Swalethorp, R., Kjellerup, S., Dünweber, M., Nielsen, T. G., Møller, E. F., Rysgaard, S., & Hansen, B. W. (2011). Grazing, egg production, and biochemical evidence of differences in the life strategies of *Calanus finmarchicus*, *C. glacialis* and *C. hyperboreus* in Disko Bay, western Greenland. *Marine Ecology Progress Series*, 429, 125-144.
- Syvertsen, E. E. (1991). Ice algae in the Barents Sea: types of assemblages, origin, fate and role in the ice-edge phytoplankton bloom. *Polar Research*, 10(1), 277-288.

- Szymanski, A., & Gradinger, R. (2016). The diversity, abundance and fate of ice algae and phytoplankton in the Bering Sea. *Polar Biology*, 39(2), 309-325.
- Tarling, G. A., Belcher, A., Blackwell, M., Castellani, C., Cook, K. B., Cottier, F. R., Dewar-Fowler, V., Freer, J. J., Gerrish, L., & Johnson, M. L. (2022). Carbon and lipid contents of the copepod *Calanus finmarchicus* entering diapause in the Fram Strait and their contribution to the boreal and Arctic lipid pump. *Frontiers in Marine Science*, 9, 926462.
- Taskjelle, T., Granskog, M. A., Pavlov, A. K., Hudson, S. R., & Hamre, B. (2017). Effects of an Arctic under-ice bloom on solar radiant heating of the water column. *Journal of Geophysical Research: Oceans*, 122(1), 126-138.
- Taylor, N. (1985). Silica incorporation in the diatom *Coscinodiscus granii* as affected by light intensity. *British Phycological Journal*, 20(4), 365-374.
- Tedesco, L., Vichi, M., & Scoccimarro, E. (2019). Sea-ice algal phenology in a warmer Arctic. *Science Advances*, 5(5), eaav4830.
- Tedesco, L., Vichi, M., & Thomas, D. N. (2012). Process studies on the ecological coupling between sea ice algae and phytoplankton. *Ecol. Model.*, 226, 120-138.
- Teoh, M.-L., Chu, W.-L., Marchant, H., & Phang, S.-M. (2004). Influence of culture temperature on the growth, biochemical composition and fatty acid profiles of six Antarctic microalgae. *Journal of Applied Phycology*, 16, 421-430.
- Terhaar, J., Kwiatkowski, L., & Bopp, L. (2020). Emergent constraint on Arctic Ocean acidification in the twenty-first century. *Nature*, 582(7812), 379-383.
- Terhaar, J., Orr, J., Ethé, C., Regnier, P., & Bopp, L. (2019). Simulated Arctic Ocean response to doubling of riverine carbon and nutrient delivery. *Global Biogeochemical Cycles*, 33(8), 1048-1070.
- Terry, K. L., Hirata, J., & Laws, E. A. (1985). Light-, nitrogen-, and phosphorus-limited growth of *Phaeodactylum tricorutum* Bohlin strain TFX-1: Chemical composition, carbon partitioning, and the diel periodicity of physiological processes. *Journal of Experimental Marine Biology and Ecology*, 86(1), 85-100.
- Tew, K. S., Kao, Y.-C., Ko, F.-C., Kuo, J., Meng, P.-J., Liu, P.-J., & Glover, D. C. (2014). Effects of elevated CO<sub>2</sub> and temperature on the growth, elemental composition, and cell size of two marine diatoms: potential implications of global climate change. *Hydrobiologia*, 741, 79-87.
- Thingstad, T., Bellerby, R., Bratbak, G., Børsheim, K., Egge, J., Heldal, M., Larsen, A., Neill, C., Nejstgaard, J., & Norland, S. (2008). Counterintuitive carbon-to-nutrient coupling in an Arctic pelagic ecosystem. *Nature*, 455(7211), 387-390.
- Thomas, D., & Dieckmann, G. (2002a). Antarctic sea ice--a habitat for extremophiles. *Science*, 295(5555), 641-644.
- Thomas, D. N., & Dieckmann, G. S. (2002b). Biogeochemistry of Antarctic sea ice. In *Oceanography and Marine Biology* (pp. 151-156). CRC Press, Boca Raton, FL, U.S.A.
- Timmermans, M.-L., Toole, J., & Krishfield, R. (2018). Warming of the interior Arctic Ocean linked to sea ice losses at the basin margins. *Science advances*, 4(8), eaat6773.
- Timmermans, M. L., & Marshall, J. (2020). Understanding Arctic Ocean circulation: A review of ocean dynamics in a changing climate. *Journal of Geophysical Research: Oceans*, 125(4), e2018JC014378.
- Tobin, M. J., Puskar, L., Barber, R. L., Harvey, E. C., Heraud, P., Wood, B. R., Bamberg, K. R., Dillon, C. T., & Munro, K. L. (2010). FTIR spectroscopy of single live cells in aqueous media by synchrotron IR microscopy using microfabricated sample holders. *Vib. Spectrosc.*, 53(1), 34-38.

- Tomas, C. R. (Ed.) (1997). *Identifying marine phytoplankton*. Elsevier, San Diego, CA, U.S.A.
- Torstensson, A., Hedblom, M., Andersson, J., Andersson, M., & Wulff, A. (2013). Synergism between elevated pCO<sub>2</sub> and temperature on the Antarctic sea ice diatom *Nitzschia lecontei*. *Biogeosciences*, *10*(10), 6391-6401.
- Torstensson, A., Hedblom, M., Mattsdotter Björk, M., Chierici, M., & Wulff, A. (2015). Long-term acclimation to elevated p CO<sub>2</sub> alters carbon metabolism and reduces growth in the Antarctic diatom *Nitzschia lecontei*. *Proceedings of the Royal Society B: Biological Sciences*, *282*(1815), 20151513.
- Torstensson, A., Jiménez, C., Nilsson, A. K., & Wulff, A. (2019). Elevated temperature and decreased salinity both affect the biochemical composition of the Antarctic sea-ice diatom *Nitzschia lecontei*, but not increased pCO<sub>2</sub>. *Polar Biology*, *42*, 2149-2164.
- Tortell, P. D., Payne, C. D., Li, Y., Trimborn, S., Rost, B., Smith, W. O., Riesselman, C., Dunbar, R. B., Sedwick, P., & DiTullio, G. R. (2008). CO<sub>2</sub> sensitivity of Southern Ocean phytoplankton. *Geophysical Research Letters*, *35*(4).
- Tourangeau, S., & Runge, J. (1991). Reproduction of *Calanus glacialis* under ice in spring in southeastern Hudson Bay, Canada. *Marine biology*, *108*(2), 227-233.
- Trathan, P. N., & Hill, S. L. (2016). The importance of krill predation in the Southern Ocean. In V. Siegel (Ed.), *Biology and Ecology of Antarctic krill*, (pp. 321-350), Springer, Cham.
- Tréguer, P., Bowler, C., Moriceau, B., Dutkiewicz, S., Gehlen, M., Aumont, O., Bittner, L., Dugdale, R., Finkel, Z., & Iudicone, D. (2018). Influence of diatom diversity on the ocean biological carbon pump. *Nature Geoscience*, *11*(1), 27-37.
- Tremblay, C., Runge, J. A., & Legendre, L. (1989). Grazing and sedimentation of ice algae during and immediately after a bloom at the ice-water interface. *Marine Ecology Progress Series*, *56*(3), 291-300.
- Tremblay, J.-É., & Gagnon, J. (2009). The effects of irradiance and nutrient supply on the productivity of Arctic waters: a perspective on climate change. In J.C.J. Nihoul, A.G Kostianoy (Eds.), *Influence of climate change on the changing arctic and sub-arctic conditions* (pp. 73-93). Springer, Dordrecht
- Tremblay, J.-É., Robert, D., Varela, D. E., Lovejoy, C., Darnis, G., Nelson, R. J., & Sastri, A. R. (2012). Current state and trends in Canadian Arctic marine ecosystems: I. Primary production. *Climatic Change*, *115*, 161-178.
- Tschudi, M. A., Stroeve, J. C., & Stewart, J. S. (2016). Relating the age of Arctic sea ice to its thickness, as measured during NASA's ICESat and IceBridge campaigns. *Remote Sensing*, *8*(6), 457.
- Turner, J., Marshall, G. J., Clem, K., Colwell, S., Phillips, T., & Lu, H. (2020). Antarctic temperature variability and change from station data. *International Journal of Climatology*, *40*(6), 2986-3007.
- Turner, J., Phillips, T., Marshall, G. J., Hosking, J. S., Pope, J. O., Bracegirdle, T. J., & Deb, P. (2017). Unprecedented springtime retreat of Antarctic sea ice in 2016. *Geophysical Research Letters*, *44*(13), 6868-6875.
- Turner, J. T., Ianora, A., Miralto, A., Laabir, M., & Esposito, F. (2001). Decoupling of copepod grazing rates, fecundity and egg-hatching success on mixed and alternating diatom and dinoflagellate diets. *Marine Ecology Progress Series*, *220*, 187-199.
- Urabe, J., Togari, J., & Elser, J. J. (2003). Stoichiometric impacts of increased carbon dioxide on a planktonic herbivore. *Global Change Biology*, *9*(6), 818-825.

- Urbański, J. A., & Litwicka, D. (2022). The decline of Svalbard land-fast sea ice extent as a result of climate change. *Oceanologia*, 64(3), 535-545.
- Utermöhl, H. (1958). Zur vervollkommnung der quantitativen phytoplankton-methodik: Mit 1 Tabelle und 15 abbildungen im Text und auf 1 Tafel. *Internationale Vereinigung für theoretische und angewandte Limnologie: Mitteilungen*, 9(1), 1-38.
- Van Leeuwe, M. A., Tedesco, L., Arrigo, K. R., Assmy, P., Campbell, K., Meiners, K. M., Rintala, J.-M., Selz, V., Thomas, D. N., & Stefels, J. (2018). Microalgal community structure and primary production in Arctic and Antarctic sea ice: A synthesis. *Elementa: Science of the Anthropocene*, 6(4).
- Van Oijen, T., Van Leeuwe, M., Granum, E., Weissing, F., Bellerby, R., Gieskes, W., & De Baar, H. (2004). Light rather than iron controls photosynthate production and allocation in Southern Ocean phytoplankton populations during austral autumn. *Journal of Plankton Research*, 26(8), 885-900.
- van Pelt, W. J., Kohler, J., Liston, G., Hagen, J. O., Luks, B., Reijmer, C., & Pohjola, V. A. (2016). Multidecadal climate and seasonal snow conditions in Svalbard. *J. Geophys. Res. Earth Surf.*, 121(11), 2100-2117.
- Vancoppenolle, M., Bopp, L., Madec, G., Dunne, J., Ilyina, T., Halloran, P. R., & Steiner, N. (2013). Future Arctic Ocean primary productivity from CMIP5 simulations: Uncertain outcome, but consistent mechanisms. *Global Biogeochemical Cycles*, 27(3), 605-619.
- Varela, D. E., Crawford, D. W., Wrohan, I. A., Wyatt, S. N., & Carmack, E. C. (2013). Pelagic primary productivity and upper ocean nutrient dynamics across Subarctic and Arctic Seas. *Journal of Geophysical Research: Oceans*, 118(12), 7132-7152.
- Varpe, Ø. (2017). Life history adaptations to seasonality. *Integrative and comparative biology*, 57(5), 943-960.
- Varpe, Ø., Daase, M., & Kristiansen, T. (2015). A fish-eye view on the new Arctic lightscape. *ICES Journal of Marine Science*, 72(9), 2532-2538.
- Vongsivut, J., Heraud, P., Zhang, W., Kralovec, J. A., McNaughton, D., & Barrow, C. J. (2012). Quantitative determination of fatty acid compositions in micro-encapsulated fish-oil supplements using Fourier transform infrared (FTIR) spectroscopy. *Food chemistry*, 135(2), 603-609.
- Vongsivut, J., Heraud, P., Gupta, A., Puri, M., McNaughton, D. & Barrow C. J. (2013). FTIR microspectroscopy for rapid screening and monitoring of polyunsaturated fatty acid production in commercially valuable marine yeasts and protists, *Analyst*, 138(20), 6016-6031, 2013.
- Vonnahme, T. (2021). *Microbial diversity and ecology in the coastal Arctic seasonal ice zone* [Doctoral Dissertation, University in Tromsø].
- Voss, M., Bange, H. W., Dippner, J. W., Middelburg, J. J., Montoya, J. P., & Ward, B. (2013). The marine nitrogen cycle: recent discoveries, uncertainties and the potential relevance of climate change. *Philosophical Transactions of the Royal Society B: Biological Sciences*, 368(1621), 20130121.
- Wagner, H., Jakob, T., Fanesi, A., & Wilhelm, C. (2017). Towards an understanding of the molecular regulation of carbon allocation in diatoms: the interaction of energy and carbon allocation. *Philos Trans R Soc Lond, B, Biol Sci.*, 372(1728), 20160410.
- Wagner, H., Liu, Z., Langner, U., Stehfest, K., & Wilhelm, C. (2010). The use of FTIR spectroscopy to assess quantitative changes in the biochemical composition of microalgae. *Journal of biophotonics*, 3(8-9), 557-566.



- Wang, D.-Z., Kong, L.-F., Li, Y.-Y., & Xie, Z.-X. (2016). Environmental microbial community proteomics: status, challenges and perspectives. *International journal of molecular sciences*, 17(8), 1275.
- Wang, D.-Z., Xie, Z.-X., & Zhang, S.-F. (2014). Marine metaproteomics: current status and future directions. *Journal of proteomics*, 97, 27-35.
- Wang, Q., Wekerle, C., Danilov, S., Koldunov, N., Sidorenko, D., Sein, D., Rabe, B., & Jung, T. (2018). Arctic sea ice decline significantly contributed to the unprecedented liquid freshwater accumulation in the Beaufort Gyre of the Arctic Ocean. *Geophysical Research Letters*, 45(10), 4956-4964.
- Webster, M., Gerland, S., Holland, M., Hunke, E., Kwok, R., Lecomte, O., Massom, R., Perovich, D., & Sturm, M. (2018). Snow in the changing sea-ice systems. *Nature Climate Change*, 8(11), 946-953.
- Webster, M. A., Rigor, I. G., Nghiem, S. V., Kurtz, N. T., Farrell, S. L., Perovich, D. K., & Sturm, M. (2014). Interdecadal changes in snow depth on Arctic sea ice. *Journal of Geophysical Research: Oceans*, 119(8), 5395-5406.
- Wei, T., Simko, V., Levy, M., Xie, Y., Jin, Y., & Zemla, J. (2017). Package ‘corrplot’. *Statistician*, 56(316), e24.
- Welch, H. E., & Bergmann, M. A. (1989). Seasonal development of ice algae and its prediction from environmental factors near Resolute, NWT, Canada. *Can. J. Fish. Aquat. Sci.*, 46(10), 1793-1804.
- Whelan, D. R., Bamberg, K. R., Heraud, P., Tobin, M. J., Diem, M., McNaughton, D., & Wood, B. R. (2011). Monitoring the reversible B to A-like transition of DNA in eukaryotic cells using Fourier transform infrared spectroscopy. *Nucleic Acids Research*, 39(13), 5439-5448.
- Whitaker, T. M., & Richardson, M. G. (1980). Morphology and chemical composition of a natural population of an ice-associated Antarctic diatom *Navicula glaciei*. *Journal of Phycology*, 16(2), 250-257.
- Wickham, H., Averick, M., Bryan, J., Chang, W., McGowan, L. D. A., François, R., Grolemund, G., Hayes, A., Henry, L., & Hester, J. (2019). Welcome to the Tidyverse. *Journal of open source software*, 4(43), 1686.
- Wickham, H., Chang, W., & Wickham, M. H. (2016). Package ‘ggplot2’. *Create elegant data visualisations using the grammar of graphics. Version*, 2(1), 1-189.
- Wickham, H., François, R., Henry, L., & Müller, K. (2015). dplyr: A grammar of data manipulation. *R package version 0.4.3*, p156.
- Wickham, H., François, R., Henry, L., & Müller, K. (2020). dplyr: A grammar of data manipulation, R Package Version 0.8.4. <https://CRAN.R-project.org/package=dplyr>
- Willmes, S., & Heinemann, G. (2015). Sea-ice wintertime lead frequencies and regional characteristics in the Arctic, 2003–2015. *Remote Sensing*, 8(1), 4.
- Wold, A., Jæger, I., Hop, H., Gabrielsen, G. W., & Falk-Petersen, S. (2011). Arctic seabird food chains explored by fatty acid composition and stable isotopes in Kongsfjorden, Svalbard. *Polar Biology*, 34, 1147-1155.
- Wolf, C., Frickenhaus, S., Kiliyas, E. S., Peeken, I., & Metfies, K. (2013). Regional variability in eukaryotic protist communities in the Amundsen Sea. *Antarctic Science*, 25(6), 741-751.
- Wright, S. W., van den Enden, R. L., Pearce, I., Davidson, A. T., Scott, F. J., & Westwood, K. J. (2010). Phytoplankton community structure and stocks in the Southern Ocean (30–80 E) determined by CHEMTAX analysis of HPLC pigment signatures. *Deep Sea Research Part II: Topical Studies in Oceanography*, 57(9-10), 758-778.

- Wu, G. (2010). Functional amino acids in growth, reproduction, and health. *Advances in Nutrition*, 1(1), 31-37.
- Wu, Y., Gao, K., & Riebesell, U. (2010). CO<sub>2</sub>-induced seawater acidification affects physiological performance of the marine diatom *Phaeodactylum tricorutum*. *Biogeosciences*, 7(9), 2915-2923.
- Wynn-Edwards, C., King, R., Davidson, A., Wright, S., Nichols, P. D., Wotherspoon, S., Kawaguchi, S., & Virtue, P. (2014). Species-specific variations in the nutritional quality of Southern Ocean phytoplankton in response to elevated p CO<sub>2</sub>. *Water*, 6(6), 1840-1859.
- Xu, D., Wang, Y., Fan, X., Wang, D., Ye, N., Zhang, X., Mou, S., Guan, Z., & Zhuang, Z. (2014). Long-term experiment on physiological responses to synergetic effects of ocean acidification and photoperiod in the Antarctic sea ice algae *Chlamydomonas* sp. ICE-L. *Environmental science & technology*, 48(14), 7738-7746.
- Xu, S., Chen, M., Feng, T., Zhan, L., Zhou, L., & Yu, G. (2021). Use ggbreak to effectively utilize plotting space to deal with large datasets and outliers. *Frontiers in Genetics*, 12, 2122.
- Yamahara, K. M., Preston, C. M., Birch, J., Walz, K., Marin III, R., Jensen, S., Pargett, D., Roman, B., Ussler III, W., & Zhang, Y. (2019). In situ autonomous acquisition and preservation of marine environmental DNA using an autonomous underwater vehicle. *Frontiers in Marine Science*, 6, 373.
- Yu, Y., Stern, H., Fowler, C., Fetterer, F., & Maslanik, J. (2014). Interannual variability of Arctic landfast ice between 1976 and 2007. *Journal of Climate*, 27(1), 227-243.
- Yun, M. S., Lee, D. B., Kim, B. K., Kang, J. J., Lee, J. H., Yang, E. J., Park, W. G., Chung, K. H., & Lee, S. H. (2015). Comparison of phytoplankton macromolecular compositions and zooplankton proximate compositions in the northern Chukchi Sea. *Deep Sea Research Part II: Topical Studies in Oceanography*, 120, 82-90.
- Zhang, Q., Gradinger, R., & Spindler, M. (1998). Dark survival of marine microalgae in the high Arctic (Greenland Sea). *Polarforschung*, 65(3), 111-116.
- Zhang, Y., Ryan, J. P., Kieft, B., Hobson, B. W., McEwen, R. S., Godin, M. A., Harvey, J. B., Barone, B., Bellingham, J. G., & Birch, J. M. (2019). Targeted sampling by autonomous underwater vehicles. *Frontiers in Marine Science*, 6, 415.
- Zhu, F., Massana, R., Not, F., Marie, D., & Vaultot, D. (2005). Mapping of picoeucaryotes in marine ecosystems with quantitative PCR of the 18S rRNA gene. *FEMS microbiology ecology*, 52(1), 79-92.
- Zhuang, Y., Jin, H., Cai, W.-J., Li, H., Jin, M., Qi, D., & Chen, J. (2021). Freshening leads to a three-decade trend of declining nutrients in the western Arctic Ocean. *Environmental Research Letters*, 16(5), 054047.

## Appendix:

Publications as they appear in print, provided in the following order:

**Duncan, R. J., & Petrou, K. (2022).** Biomolecular Composition of Sea Ice Microalgae and Its Influence on Marine Biogeochemical Cycling and Carbon Transfer through Polar Marine Food Webs. *Geosciences*, *12*(1), 38.

**Duncan, R. J., Søreide, J. E., Varpe, Ø., Wiktor, J., Pitusi, V., Runge, E., & Petrou, K. (2024).** Spatio-temporal dynamics in microalgal communities in Arctic land-fast sea ice. *Progress in Oceanography*. *224*, 103248


**Duncan, R. J., Nielsen, D., Søreide, J. E., Varpe, Ø., Tobin, M. J., Pitusi, V., Heraud, P., & Petrou, K. (2024).** Biomolecular profiles of Arctic Sea-ice diatoms highlight the role of under-ice light in cellular energy allocation. *ISME Communications*, *10*(4), 1.

**Duncan, R. J., Nielsen, D. A., Sheehan, C. E., Deppeler, S., Hancock, A. M., Schulz, K. G., Davidson, A. T., & Petrou, K. (2022).** Ocean acidification alters the nutritional value of Antarctic diatoms. *New Phytologist*, *233*(4), 1813-1827.

**Duncan, R. J., Søreide, J. E., Nielsen, D., Varpe, Ø., Wiktor, J., Tobin, M. J., Pitusi, V. & Petrou, K. (2024).** Seasonal environmental transitions and metabolic plasticity in a sea-ice alga from an individual cell perspective. *Scientific Reports*, *14*, 14984.

Review

# Biomolecular Composition of Sea Ice Microalgae and Its Influence on Marine Biogeochemical Cycling and Carbon Transfer through Polar Marine Food Webs

Rebecca Julianne Duncan <sup>1,2,\*</sup>  and Katherina Petrou <sup>1,\*</sup><sup>1</sup> School of Life Sciences, University of Technology Sydney, Sydney, NSW 2007, Australia<sup>2</sup> Department of Arctic Biology, The University Centre in Svalbard, 9171 Longyearbyen, Norway

\* Correspondence: rebecca.duncan@uts.edu.au (R.J.D.); katherina.petrou@uts.edu.au (K.P.)

**Abstract:** Microalgae growing on the underside of sea ice are key primary producers in polar marine environments. Their nutritional status, determined by their macromolecular composition, contributes to the region's biochemistry and the unique temporal and spatial characteristics of their growth makes them essential for sustaining polar marine food webs. Here, we review the plasticity and taxonomic diversity of sea ice microalgae macromolecular composition, with a focus on how different environmental conditions influence macromolecular production and partitioning within cells and communities. The advantages and disadvantages of methodologies for assessing macromolecular composition are presented, including techniques that provide high throughput, whole macromolecular profile and/or species-specific resolution, which are particularly recommended for future studies. The directions of environmentally driven macromolecular changes are discussed, alongside anticipated consequences on nutrients supplied to the polar marine ecosystem. Given that polar regions are facing accelerated rates of environmental change, it is argued that a climate change signature will become evident in the biochemical composition of sea ice microalgal communities, highlighting the need for further research to understand the synergistic effects of multiple environmental stressors. The importance of sea ice microalgae as primary producers in polar marine ecosystems means that ongoing research into climate-change driven macromolecular phenotyping is critical to understanding the implications for the regions biochemical cycling and carbon transfer.

**Keywords:** sea ice; sympagic microalgae; lipid; protein; carbohydrates; biochemistry; trophic transfer; sea ice microalgae



**Citation:** Duncan, R.J.; Petrou, K. Biomolecular Composition of Sea Ice Microalgae and Its Influence on Marine Biogeochemical Cycling and Carbon Transfer through Polar Marine Food Webs. *Geosciences* **2022**, *12*, 38. <https://doi.org/10.3390/geosciences12010038>

Academic Editors: Mirko Severi and Jesus Martinez-Frias

Received: 8 November 2021

Accepted: 7 January 2022

Published: 13 January 2022

**Publisher's Note:** MDPI stays neutral with regard to jurisdictional claims in published maps and institutional affiliations.



**Copyright:** © 2022 by the authors. Licensee MDPI, Basel, Switzerland. This article is an open access article distributed under the terms and conditions of the Creative Commons Attribution (CC BY) license (<https://creativecommons.org/licenses/by/4.0/>).

## 1. Introduction

Ice-covered seas account for approximately 10% of the global ocean surface area ( $34 \times 10^6 \text{ km}^2$ ) annually, with the seasonal formation and decay of sea ice playing a key role in global ocean turnover. Sea ice forms during the dark winter months reaching its maximum extent as spring commences. Therefore, in the Arctic, the maximum extent of sea ice ( $\sim 15.2 \times 10^6 \text{ km}^2$ ) occurs in March, while in the Antarctic, sea ice extent reaches a maximum ( $\sim 18.5 \times 10^6 \text{ km}^2$ ) in September [1] (Figure 1). Despite their asynchrony, combined, these two regions form a significant biome, providing essential habitat for many marine organisms, including diverse communities of bacteria, protists, and meiofauna [2,3].

The organisms that thrive in these vast expanses of frozen seawater, underpin polar marine biodiversity and biochemistry. In particular, photosynthetic microalgae, which become engrained into the ice as it forms (Figure 1), support polar marine food webs, and, together with heterotrophic bacteria, are principal players in the biochemical cycling of elements within the marine and sea ice environments [2]. Sea ice primary productivity and nutrient cycling is important for understanding the dynamics of seawater biochemistry, as the biomolecular composition of sea ice microalgae and the cycling of nutrients that occurs within sea ice microbial communities influences the biochemistry of seawater [4,5].

However, biochemical components can be sensitive to physical processes, including photooxidation from UV, which is determined by ice thickness or mixing depth [6,7], potentially reshaping the biochemical signature of the seawater [8,9].

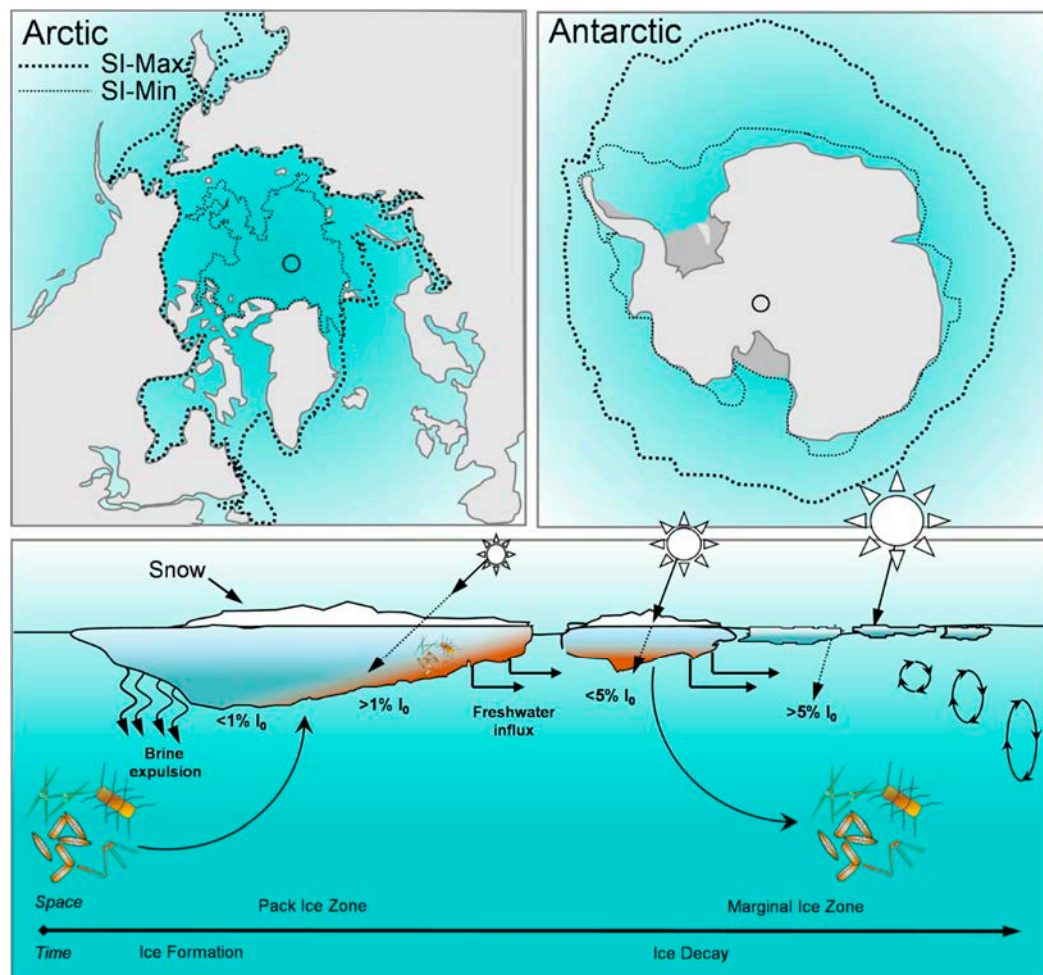


**Figure 1.** Sea ice zones in both polar regions. Stippled lines indicate the maximum (SI-Max) and minimum (SI-Min) extent of sea ice in the Arctic (**top left**) and Southern Ocean (**top right**). Black open circles indicate the poles. Schematic of the spatial and temporal evolution and decay of sea ice in polar marine ecosystems. Arrows indicate seasonal changes in salinity from brine extrusion and freshwater melt, as well as light attenuation, solar angle, and mixing depth. The entrainment of microalgae into the sea ice as it forms, its proliferation and re-release into the water column during melt is also shown.  $I_0$  = percent incident irradiance.

The ecological importance of sea ice microalgae is attributed to their role in primary production during the frozen winter and in spring as the ice begins to melt. During the early spring, sea ice microalgae grow within the brine channel network under very low irradiances [10,11], and as the solar angle increases, spring blooms commence, marked by an increase in biomass on the underside of the ice [10,11]. The total biomass that accumulates depends on the amount of light transmitted and therefore the thickness of the ice and snow cover, as well as the duration of the growth season, with substratum melt and ice breakup ultimately forcing the end of the sea ice algae growth season [12,13].

Sea ice microalgal communities can make significant contributions to primary production in polar regions, accounting for up to 25% of total primary production in seasonally ice-covered waters and up to ~60% in perennially ice-covered Arctic waters [14–17]. However, their precise contribution to primary production varies depending on time of year and geographic location. For example, sea ice algae contributed as little as <math>< 1\%</math> to primary

production in Young Sound, Greenland in 2002 [18] yet contributed ~70% of primary production in Barrow, Alaska in 2003 [19]. Whilst the contribution of sea ice microalgae to total primary productivity is generally less than that of pelagic phytoplankton, the divergence in their timing and distribution means that the sea ice microalgae subsist as an important source of nutrients and energy to the marine food web [17,20]. Indeed, their presence extends biological production in polar waters by up to three months [12], because they are the primary source of organic carbon for pelagic consumers during the ice-covered winter [15,21,22]. Specifically, sea ice microalgae form a critical food source for copepods, amphipods, and euphausiids [23,24], where the availability and nutritional quality of the microalgae have been shown to play an important role in the timing of zooplankton reproduction and, therefore, the quantity and quality of secondary production [25–27]. As the ice begins to melt, the ecological function of sea ice microalgae extends to seeding phytoplankton blooms in the marginal ice zone [28–33]. Through shaping the initial phytoplankton community [13,30] and influencing the timing of the pelagic bloom and secondary production [32], sea ice microalgae can strongly influence pelagic processes, and thus exert significant influence over food web dynamics and biochemical cycling in the polar marine environment.

As primary producers, sea ice microalgae convert solar energy into carbon via photosynthesis, making light a principal driver of sea ice productivity. Photosynthates are converted into a variety of biochemical components including proteins, lipids, and carbohydrates; biomolecules that make up the majority of the cell biomass. The allocation of the photosynthetically derived carbon is largely determined by environmental conditions and is therefore dynamic, whereby the biomolecular composition of the microalgal cell reflects its physiological status [34]. Shifts in biochemical composition in response to environmental conditions, while important for the physiology and nutritional status of the sea ice microalgae itself, also strongly influence the productivity and nutritional value of primary consumers. For example, sea ice microalgae have been shown to contribute up to ~146% of the energy budget of Antarctic krill during the winter [35]. Similarly, adequate lipid supply has been shown to be critical to the survival and reproduction of zooplankton [36,37]. Over winter, large lipid reserves are particularly important for zooplankton when pelagic primary production is low [38–40]. The biomolecular stores of primary producers are therefore the cornerstone of productive marine ecosystems, and changes in the partitioning of these critical biomolecules contained in microalgae inevitably alters the supply of energy and essential compounds to higher trophic levels.

Planetary warming is causing polar environments to change rapidly [41], and the significant decline in sea ice is of major ecological concern [1,42]. For the past four decades, the most profound and consistent sea ice decline has been measured in the Arctic [1,41,43], which has experienced a decline in average September sea ice extent of ~10.1% per decade [44,45]. Concomitant with the decline in extent is a dramatic loss of thicker multi-year ice, increasing the expanse of open water in summer, with predictions of sea ice-free summers within decades [43,46,47]. The situation in the Antarctic is more nuanced, as the southern hemisphere sea ice extent experienced a gradual rate of increase between 1981 and 2014, after which it has been experiencing a precipitous rate of decline [48] amounting to a 27% reduction between 2010 and 2017 [45]. Given that the growing season for sea ice microalgae is already constrained to within a few months each year and seems likely to be further shortened as oceans warm and ice extent continues to decline [12,43,49], it is probable that in the future we will see reduced accumulation of biomass, disrupting the critical early-season food supply for the region's primary consumers. Furthermore, as polar regions warm, light climate under the sea ice is expected to change, influencing productivity. A reduction in snow cover and declining sea ice thickness would result in higher under-ice light intensity [11]; conversely, where precipitation is expected to increase (more snow), light transmission may decline. In addition, sea surface temperatures are rising [50], polar oceans are acidifying [41,51], and there is an increase in freshwater input due to glacial retreat and run off [52]. These shifts in ecosystem condition will influence future

community composition [53,54] and biomolecular partitioning of sea ice microalgae [55–60]. Therefore, accurate assessment of the direction and magnitude of these cellular changes is necessary to better understand the impact on marine biogeochemistry and carbon transfer through the polar marine food web.

## 2. Biomolecular Composition of Sea Ice Algae from Polar Regions

Microalgae are the primary source of biomolecules (protein, lipids, and carbohydrates) in marine ecosystems. In cells, proteins play a key role in all enzymatic processes and growth, while lipids and carbohydrates are essential components of cell membranes and form important energy reservoirs [34,38,61]. Particular to sea ice microalgae, lipids and antifreeze amino acids such as proline have been important evolutionary adaptations to tolerating the freezing and hypersaline conditions of the ice matrix [62,63]. The biomolecular composition of sea ice microalgae in both absolute amounts and relative proportions vary between species, making community composition a strong determinant of overall nutritional status of primary producers.

Lipids are the most energy-rich biomolecules and, as such, contain much of the energy that is transferred among trophic levels [38]. Carbohydrates, which contribute less to energy transfer [38], have an important role in supplying the cellular carbon pool [64], and are integral for protein synthesis [65]. Proteins are the predominant source of amino acids [66] and form a cellular nitrogen reservoir [61]. They are a key source of nutrition for higher trophic levels [38]. In terms of carbon transfer through trophic webs, proteins have the highest relative efficiency [34,67,68], thus making protein rich species of potentially greater value in supporting secondary production. However, specific to polar regions, microalgae with high lipid content have been shown to be important for zooplankton fecundity [25,26,69].

Investigations into the biochemical composition of pelagic phytoplankton from the two polar regions have revealed differences in biomolecular characteristics, with Arctic waters shown to be dominated by lipid-rich cells [70,71], possibly a result of low nitrogen status. In contrast, Antarctic phytoplankton are generally found to be rich in protein [72–74]. The high protein production by these primary producers, is likely supported by the high nitrogen concentrations in the seawater [75,76], resulting in a nitrogen-rich food source for primary consumers and thus able to support a highly productive ecosystem. One study however, found high concentrations of carbohydrates during a summer bloom in the Amundsen Sea [77]. This was attributed to high densities of the haptophyte *Phaeocystis antarctica*, which is a common bloom-forming species in Antarctic waters [77,78]. It is important to note, however, that while these patterns highlight differences between the Arctic and Antarctic, these general trends for pelagic phytoplankton are derived from only a few studies, representing low temporal and spatial coverage, and thus may not capture any potential seasonal and spatial variability. While numerous studies have investigated the biomolecular composition of sea ice microalgae from both polar regions (Table 1), to date, no similar overall patterns have been observed for sea ice microalgae. However, given the propensity for sea ice microalgae to seed pelagic blooms, similar differences in key biochemical characteristics may exist for the ice communities from the two regions.

One of the strongest determinants of biomolecular composition is taxonomic composition. Phylogenetically distinct microalgal groups have been shown to vary in their proportional allocation of biomolecules. Diatoms (Orcophyta: Bacillariophyceae), for example, generally have higher lipid and lower carbohydrate content than other microalgal phyla, such as the Chlorophytes and Haptophytes [61]. More specifically, pennate diatoms within the sea ice have been shown to have higher lipid, fatty acid, and carbohydrate content than the centric diatoms from the same community [60]. Similarly, diatoms with a smaller cell volume (such as pennate diatoms) have been shown to have higher carbohydrate content than larger volume diatoms [79]. At the taxonomic level of species, differentiation is more subtle, but nevertheless has been shown [57,60,80,81]. However, by far most knowledge on species-specific biomolecular profiles is derived from single-species

culture studies, providing a poor representation of what may be true for natural mixed communities. It is therefore important that studies on natural communities start to discriminate biomolecular profiles of individual taxa within a community if we are to improve our understanding of taxonomic biomolecular diversity.

**Table 1.** Compilation of studies that have measured biomolecules in sea ice microalgae in the Arctic and Antarctic.

	Study	Taxa	Location	Latitude, Longitude	Sampling Date	Biomolecules Investigated
Antarctica	An et al., 2013	<i>Chlamydomonas</i> sp. ICE-L	Zhongshan Research Station	69° S, 77° E	N/A	Fatty acids
	Cade-Menun & Paytan 2010	<i>Fragilariopsis curta</i> , <i>Fragilariopsis cylindrus</i> , <i>Nitzschia subcurvata</i> , <i>Phaeocystis Antarctica</i> , <i>Thalassiosira weissflogii</i> , <i>Dunaliella tertiolecta</i> , <i>Synechococcus</i> sp.	Culture	N/A	N/A	Lipid, protein, carbohydrate
	Gleitz & Kirst 1991	Diatom-dominated mixed community, primarily <i>Nitzschia</i> sp., <i>Chaetoceros</i> sp., <i>Navicula</i> sp., <i>Corethron</i> sp., <i>Rhizosolenia</i> sp., <i>Amphiprora</i> sp., <i>Dactyliosolen</i> sp., <i>Synedropsis</i> sp., <i>Tropidoneis</i> and <i>Phaeocystis pouchetii</i>	Weddell Sea	58–63° S, 55–45° W	1988/1989	Lipid, amino acid, carbohydrate
	Mock & Kroon 2002a	<i>Fragilariopsis curta</i> , <i>Navicula gelida</i> var.-antarctica, <i>Nitzschia medioconstricta</i>	Weddell Sea	70°02' S, 06°00' W	March–May 1999	Lipid, protein
	Mock & Kroon 2002b	<i>Fragilariopsis curta</i> , <i>Navicula gelida</i> var.-antarctica, <i>Nitzschia medioconstricta</i>	Weddell Sea	70°02' S, 06°00' W	March–May 1999	Lipid, protein
	Palmisano & Sullivan 1985	Diatom-dominated mixed community, primarily <i>Pleurosigma</i> sp., <i>Nitzschia stellata</i> , <i>Berkeleya</i> sp., <i>Amphiprora kuferathii</i> , <i>Phaeocystis</i> sp. and small centrics.	McMurdo Sound	77° S, 166° W	November–December 1983	Lipid, protein, polysaccharide
	Teoh et al., 2004	<i>Chlamydomonas</i> sp. and <i>Navicula</i> sp.	Windmill Islands	66°17' S, 110°29' E	N/A	Lipid, protein, carbohydrate, fatty acids
	Sackett et al., 2013	<i>Fragilariopsis cylindrus</i> , <i>Chaetoceros simplex</i> and <i>Pseudo-nitzschia subcurvata</i>	Southern Ocean and Prydz Bay	66° S, 147° E, 68° S, 73° E	N/A	Lipid, protein, carbohydrate, fatty acids, amino acids
	Xu et al., 2014	<i>Chlamydomonas</i> sp. ICE-L	Zhongshan Research Station	69° S, 77° E	N/A	Lipid, fatty acids
	Arctic	Lee et al., 2008a	Mixed community dominated by large chain-forming diatoms	Barrow, Alaska	71°20' N, 156°39' W	April–June 2003
Lee et al., 2008b		Mixed community dominated by large chain-forming diatoms	Barrow, Alaska	71°20' N, 156°39' W	February–June 2003	Lipid, protein, polysaccharide
Leu et al., 2006b		<i>Thalassiosira antarctica</i> var. <i>borealis</i>	Ny-Ålesund, Svalbard	78°55' N, 11°56' E	May–June 2004	Fatty acids



Table 1. Cont.

Study	Taxa	Location	Latitude, Longitude	Sampling Date	Biomolecules Investigated
Leu et al., 2010	Diatom-dominated mixed community, primarily <i>Nitzschia frigida</i> , <i>Navicula septentrionalis</i> and <i>Fragilariopsis cylindrus</i> .	Ripfjorden, Svalbard	80° N, 22° E	March–July 2007	Fatty acids
Lund-Hansen et al., 2020	Mixed diatom-dominated community. Primarily <i>Nitzschia frigida</i> , <i>Nitzschia longissima</i> and <i>Thalassiosira</i> sp.	Kangerlussuaq West Greenland	66°57' N, 50°57' W	March 2016	Fatty acids
Mock & Gradinger 2000	Mixed community dominated by <i>Nitzschia</i> sp., <i>Fragilariopsis</i> sp. and <i>Chaetoceros</i> sp.	Barents Sea	77°10' N, 34°04' E	May–June 1997	Lipid, protein, polysaccharides
Pogorzelec et al., 2017	<i>Nitzschia frigida</i> , pennate ribbon colonies and <i>Attheya</i> sp.	Dease Strait, Nunavut, Canada	69°1' N, 105°19' W	March–May 2014	Lipid, protein
Smith et al., 1987	Mixed community	Resolute Passage, Canada	74°41' N, 95°50' W	April–June 1985	Lipid, protein, polysaccharides
Smith et al., 1989	Diatom-dominated mixed community, primarily <i>Nitzschia frigida</i> and <i>Nitzschia grunowii</i>	Central Canadian Arctic	74°40' N, 94°54' W	April–May 1985; 1986	Lipid, protein, amino acid, polysaccharide
Smith et al., 1993	Diatom-dominated mixed community	Resolute Passage, Canada	74°41' N, 95°50' W	March–June 1989	Lipid
Smith & Herman 1992	Diatom-dominated mixed community	Resolute Passage, Canada	74°41' N, 95°50' W	May 1987, May–June 1988	Lipid, protein, polysaccharide
Søreide et al., 2010	Diatom-dominated mixed community	Ripfjorden, Svalbard	80°27' N, 22°29' E	March–July 2007	Fatty acids
Torstensson et al., 2013	<i>Nitzschia lecontei</i>	Amundsen Sea	N/A	January 2011	Fatty acids
Torstensson et al., 2019	<i>Nitzschia lecontei</i>	Amundsen Sea	N/A	N/A	Lipid, protein carbohydrate, fatty acids

### 3. Measuring Biochemical Composition in Microalgae

Quantification of the biomolecular composition of sea ice microalgae is central to assessing biochemical cycling and carbon transfer through the polar marine food web. Numerous studies have quantified the principal constituents of cells, including lipids, carbohydrates, and proteins in sea ice microalgae, using a variety of methods (Table 2). Chromatography techniques, including High Performance/Thin Layer Chromatography (HPTLC/TLC) and Gas Chromatography (GC), are popular in sea ice microalgal studies because they are accurate, reproducible, sensitive, and rapid methods to separate and measure components within a given sample. The predominant method used in earlier studies of sea ice microalgal nutrition was HPTLC/TLC [56,82–85]; however GC, which is more widely available, is generally favored now [55,86–92]. These methods have both been used to measure proteins, lipids, carbohydrates, and fatty acids (Table 2). A more detailed analysis of fatty acid content (i.e., polyunsaturated (PUFA), monounsaturated (MUFA), and saturated fatty acids (SFA)) is commonly included in sea ice microalgal studies, because fatty acids can be characteristic for specific taxonomic groups and can therefore be used as

trophic markers [87]. Determining the proportion of PUFAs within microalgae is important for the polar food webs, as they are synthesized de novo only by photosynthetic organisms, yet are essential for many primary and secondary consumers [93], playing a key role in successful egg production, hatching and larval development of zooplankton [55,93,94]. Therefore, one of the major advantages of these chromatographic methods is their ability to determine specific fatty acid composition. Another significant advantage of these chromatographic methods is the capacity to measure carbon isotope signatures of individual lipids, specifically those with enhanced  $^{13}\text{C}$  values, such as sterols and highly branched isoprenoid alkenes [4,95–97]. The signature of these specific lipids can then be used to determine the biochemical contribution of sea ice algae to the water column [4,5].

Radioisotope labelling is a relatively easy and reliable method to measure lipid, protein, polysaccharides, and amino acid content, and has been used extensively in sea ice microalgal studies [98–101]. However, this method requires biomolecular classes to be extracted prior to analysis [102] and only provides information on the proportion of primary productivity allocated to a particular biomolecular pool, and not absolute concentrations, making it less quantitative than chromatographic methods.

**Table 2.** Summary of the various analytical techniques that have been used to measure biomolecules (proteins and amino acids, lipids, and fatty acids, carbohydrates, and polysaccharides) in sea ice microalgae, their advantages, and disadvantages.

Method	Biomolecules Investigated	Advantages	Disadvantages	Example Studies with Sea Ice Algae
High Performance/Thin Layer Chromatography (HPTLC/TLC)	Lipid Fatty acid Amino Acid Carbohydrate	Rapid and easy to run multiple samples in parallel. Useful for complex lipids (therefore most marine lipids). Can be used for small quantity of sample.	Reproducibility can be unreliable. Temperature gradients can exist across the plate resulting in partial distillation of the sample. The silica plate is not reusable.	Gleitz & Kirst 1991 Smith et al., 1993 Henderson et al., 1998 Mock & Kroon, 2002a,b
Gas Chromatography (GC)	Lipid Fatty acid Protein Carbohydrate	Highly sensitive Accurate and reproducible. Easy to couple with detection and quantification techniques. Can analyze all biomolecular classes at once. Effective with a very small amount of sample.	Requires sample to be volatile and therefore lipids need to be derivatized into Fatty Acid Methyl Esters (FAMES).	Nichols et al., 1989 [103] Teoh et al., 2004 Leu et al., 2006a,b; 2007 [104]; 2010 Søreide et al., 2010 An et al., 2013 Xu et al., 2014 Lund-Hansen et al., 2020 Torstensson et al., 2013; 2019
Mass Spectrometry (MS)	Lipid Protein Polysaccharide	Sensitive Accurate and reproducible.	Less sensitive than GC. Requires coupling with another technique, e.g., HPLC or radioisotope labelling	Lee et al., 2008a,b
Radioisotope Labelling	Lipid Protein Amino Acid Polysaccharide	Highly sensitive Accurate and reproducible. Rapid and easy to run multiple samples in parallel.	Requires additional measurements to determine absolute concentrations. Requires extraction of biomolecular classes. Requires correction for quenching. Requires training and precautions due to radioactive materials	McConville et al., 1985 [105] Palmisano & Sullivan 1985 Smith et al., 1987 Palmisano et al., 1988 Smith & Herman 1992 Mock & Gradinger 2000
Fluorescent Dye (BIODIPY 505/515)	Lipid	Rapid Inexpensive Performed in vivo Has lipid specificity, only binding to lipid bodies and chloroplasts and no other cytoplasmic compartments.	Does not stain all microalgae successfully. Can be issues associated with fading (i.e., fluorescence extinction)	Xu et al., 2014

Table 2. Cont.

Method	Biomolecules Investigated	Advantages	Disadvantages	Example Studies with Sea Ice Algae
Sulpho-phospho-vanillin (SPV) reaction	Lipid	Rapid High throughput Relatively easy to implement. Relatively cheap Requires a small amount of sample.	Requires a reference standard Color intensity varies between different lipids Requires a two-step reaction	Smith et al., 1989
Lowry and Smith Assays	Protein	Highly sensitive Produces a linear response curve. Low protein-to-protein variation meaning higher accuracy in unknown protein samples. Widely used and well characterized.	Susceptible to interference by some common chemicals present in samples. Time sensitive during analysis. Lowry is more complicated with more steps than the Smith Assay. Destructive to proteins.	Smith et al., 1989 Mock & Kroon 2002a Torstensson et al., 2019
Phenol-Sulfuric Acid Method	Carbohydrate	Rapid Relatively easy to implement. Accurate and reproducible. Widely used and well characterized.	Phenol is a toxic compound posing health risks Non-stoichiometric method, meaning a calibration curve using a series of standards must be generated, limiting the analysis of more complex carbohydrates.	Smith et al., 1989 Torstensson et al., 2019
Carbon-13 Nuclear Magnetic Resonance ( <sup>13</sup> C NMR) Spectroscopy	Lipid Protein Carbohydrate	Can analyze all biomolecular classes at once. Provides intramolecular detail.	Low sensitivity Long duration of analysis.	Cade-Menun & Paytan 2010
FTIR-microspectroscopy	Lipid Fatty acid Protein Amino acid Carbohydrate	Highly sensitive Can be used to analyze single cells giving species-specific results. Nondestructive. Ability to obtain data at multiple wavelengths simultaneously. Can analyze all biomolecular classes at once. Effective with a very small amount of sample.	Small size mounting chamber. Synchrotron light source is not readily available and is expensive.	Sackett et al., 2013 Pogorzelec et al., 2017 Sheehan et al., 2020

Spectroscopic techniques have been broadly used in sea ice microalgal research for determining lipid, protein, and carbohydrate contributions, as they have the advantage of being inexpensive and easy to use. In some cases, it may be necessary to extract the biomolecule prior to spectroscopy, for example, with the Sulpho-phospho-vanillin (SPV) reaction employed to measure lipid content [106]. A potentially easier and more effective way to measure lipid content in vivo is by utilizing fluorescent dyes, such as BODIPY 505/515 [91]. This form of live staining, however, has not been used for determination of protein or carbohydrate content in sea ice microalgae, which are instead routinely measured using the Lowry and Smith assay [85,90,106] and phenol-sulfuric acid method [90,106], respectively. Spectroscopy techniques are limited, however, in that they are unable to determine specific fatty acid contributions. However, with <sup>13</sup>C Nuclear Magnetic Resonance (NMR) spectroscopy, a quantitative measure of all biomolecules within the sample simultaneously can be obtained, with the added benefit of providing finer detail on the types of lipids, proteins, and carbohydrates present [107]. Due to its low sensitivity however, this technique has not been widely used in sea ice microalgal biochemical studies [107].

As with NMR and GC analyses, Fourier Transform Infrared (FTIR) microspectroscopy is a technique that measures the whole biomolecular profile at once, enabling each sample to be spectrally defined based on a biochemical fingerprint [108]. This spectroscopic approach has the benefits of being sensitive, high throughput, quantitative, and rapid [57,58,108–111]. Coupled with a Synchrotron light source, FTIR microspectroscopy becomes more sensitive and can deliver much higher resolution (~3 μm) spectral imaging [112]. This technique has the significant advantage that it can be performed on individual cells and subcellular

compartments, allowing for unique insight into the response of individual taxa within a natural community. Moreover, with micrometer resolution, it can be used to localize and measure specific organelles within larger cells or tissues. The ability to understand specifically which species within the community is affected by environmental change and in what way is unique to this biomolecular method. In nonpolar marine microalgae, it has been used widely to investigate biomolecular responses to environmental change [108,113–115]. To date however, very few studies have looked at the nutritional value of natural sea ice assemblages at the species level, with only two studies investigating the effects of light on biomolecular composition of Arctic diatoms [59,116] and one describing the biomolecular profiles of four Antarctic sea ice diatoms [60]. Synchrotron-based FTIR-microspectroscopy has been used successfully to investigate changes in biomolecular composition as a result of ocean acidification in Antarctic diatoms [81] and biomolecular changes as a result of iron enrichment in Antarctic microalgae [117]. As the only biochemical method that delivers species-level resolution, it is an attractive technique for resolving questions related to response diversity within natural communities and tracking potential shifts in trophic carbon transfer.

#### 4. Environmental Factors That Influence Biomolecular Composition

The sea ice environment exposes microorganisms that live within it to strong gradients in temperature, salinity, and light [62,63,118]. From the extreme hypersaline brine channels (salinities up to 145 ppt), freezing temperatures ( $-2$ – $-20$  °C) and high light conditions ( $>100$   $\mu\text{mol m}^{-2} \text{s}^{-1}$ ) near the ice surface [119], to the relatively mild and stable conditions for the microalgae living at the ice–water interface (temperature:  $\sim 1.8$  °C; irradiance:  $3.5$ – $40$   $\mu\text{mol m}^{-2} \text{s}^{-1}$ ) [12,120]. These steep environmental gradients, which vary over the seasonal formation and decay of the ice, mean that the organisms living and thriving in this habitat have evolved specialized physiological strategies, including biomolecular adjustments, to cope with rapid and extreme changes in their living conditions [63]. It is worth noting that growth rate is also expected to influence biomolecular storage; however, this is not explored further below as it cannot be measured or controlled for within natural community studies.

**Temperature:** At the ice–water interface, temperature generally remains around  $-1.8$  °C throughout spring, however as sea surface temperatures rise with the onset of ocean warming [50], it is possible that warmer temperatures will alter the biochemical composition of the algae, drive an earlier ice melt, and ultimately inhibit sea ice microalgal growth completely [11,43]. Limited work has been completed on the effects of temperature on the biochemical composition of sea ice algae, but from these few studies some patterns have emerged. Extreme subzero temperatures ( $-20$  °C) have been associated with a decline in fatty acids, especially PUFA content [88]. A decline in fatty acids has been observed also under moderate temperature increases (from  $-1.8$  °C to  $3$  °C), as well as in temperature increases well beyond the natural range ( $\sim 15$  °C) [86,88–90] (Figure 2A). In several Antarctic sea-ice diatoms, an increase in relative protein content and decrease in carbohydrate content have been observed with exposure to warmer (up to  $3$  °C) temperatures [90], including temperatures well above ( $\sim 20$  °C) the natural range for sea ice microalgae [86]. These data indicate that optimal temperatures for maximum fatty acid content lies around  $-1.8$  °C, and that increases in temperature will likely see reductions in PUFA and carbohydrate content but increases in protein.

**Salinity:** Salinity within sea ice follows a steep gradient, from hyper-saline conditions within the brine channels ( $>70$  ppt) to seawater and meltwater ( $\sim 30$  ppt) salinity levels at the ice–water interface. In hypersaline environments, such as sea ice brine channels, lipid and amino acid content have been shown to be higher than at lower salinity ( $\sim 35$  ppt) [57]. On the other hand, decreasing salinity (i.e.,  $10$ – $20$  ppt, compared to ambient levels) have resulted in increased protein [82], amino acid [57], fatty acid [90], and carbohydrate content [90] (Figure 2B). These changes in response to hyposaline conditions provide insight into some of the possible changes to nutritional status of microalgae with increased fresh-

ening from ice melt and glacial runoff. Whilst further research is needed, these results suggest that ongoing ocean freshening [121,122] may lead to a decline in lipid, yet increase in protein and carbohydrate content.

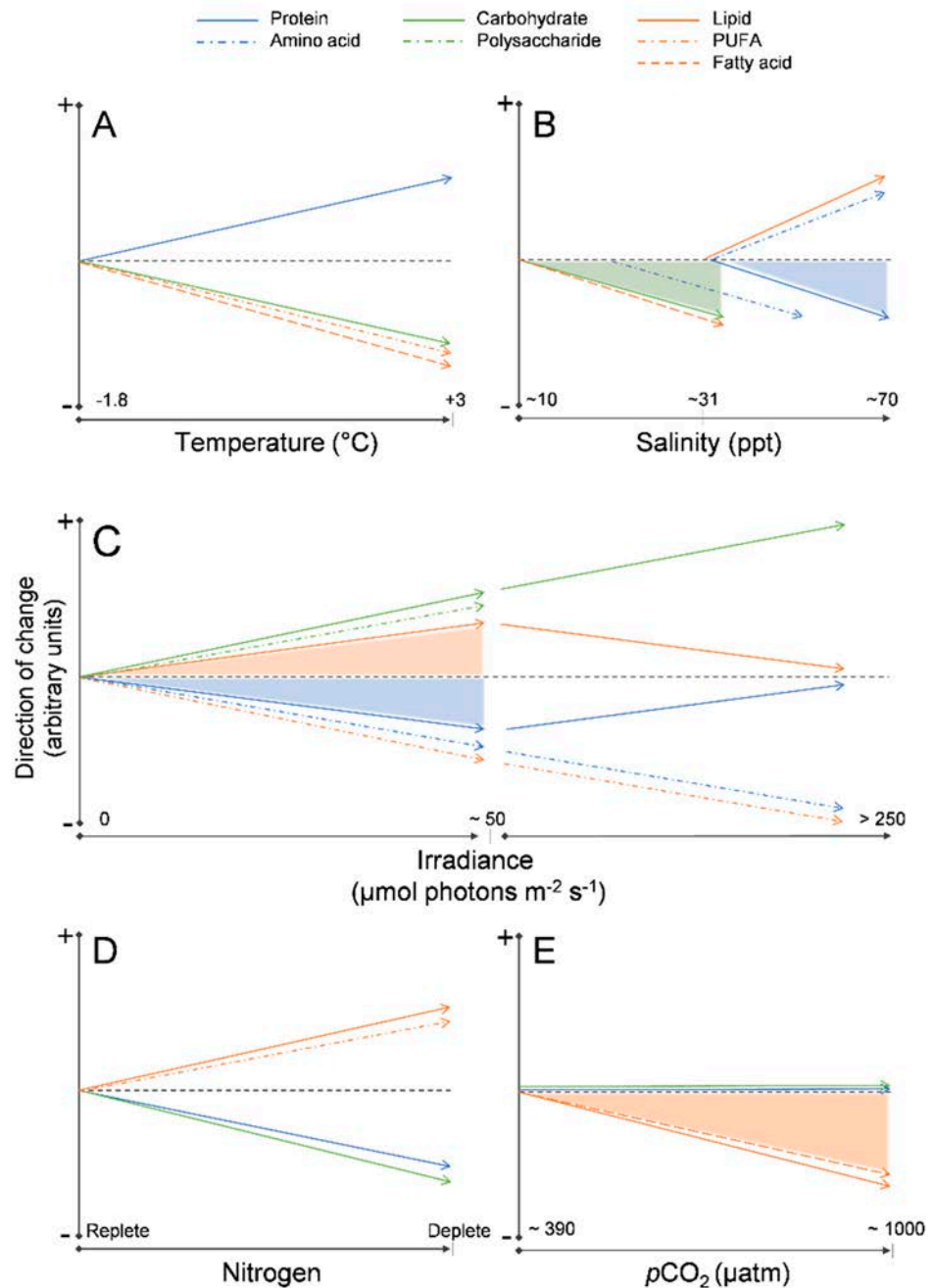


**Figure 2.** Schematic showing the direction of change (increase or decrease) in biomolecules in sea ice microalgae exposed to variations in (A) temperature, (B) salinity, (C) irradiance, (D) nitrogen concentration, and (E)  $p\text{CO}_2$ . Changes are not indicative of magnitude. The different biomolecules are coded by color and line type as described in the legend. Shaded areas indicate where results from studies have revealed both a change and no change with environmental perturbation. Data were obtained from the studies listed in Table 1.

**Light:** Being photosynthetic organisms, light transmittance is one of the key factors driving sea ice microalgal community productivity and composition [11,12], playing a defining role in the commencement of the spring under ice bloom. It has been shown repeatedly to determine the nutritional quality in sea ice microalgae, although the direction

of change in biomolecular composition varies depending on the magnitude of change in light intensity (Figure 2C). Primarily, a seasonally relevant change in light intensity as a result of low and high snow cover [59,106,116] and through naturally manipulated light levels [123], have been found to increase lipid synthesis over the duration of the spring bloom [19,83,99,100], with one study finding no significant correlation [98]. On the other hand, light intensity beyond the expected natural range ( $>100 \mu\text{mol m}^{-2} \text{s}^{-1}$ ) has been found to cause a decrease in lipid content [82,107] possibly due to photoinhibition limiting photosynthetic energy production and thereby biomolecular synthesis. In contrast to the general overall lipid response, PUFAs have consistently been found to decline with increasing light intensity (Figure 2C). Decline in PUFAs have been observed in natural sea ice microalgal communities with increase in irradiance, with minimal and dense snow cover [56], when exposed to in situ light manipulation [92] and experimentally, using a unialgal culture of *Thalassiosira antarctica* var. *borealis* [124] or when light adjusted sea ice algae are subjected to continuous darkness [91]. In Arctic open water phytoplankton communities, PUFAs have also been observed to decline with increasing light during the spring period [87].

Changes in irradiance have also been shown to influence protein, amino acid, and carbohydrate content (Figure 2C). In mixed microalgae communities, protein and amino acids have generally been found to decrease with increasing light intensity over a realistic spring light range ( $3.5\text{--}40 \mu\text{mol m}^{-2} \text{s}^{-1}$ ), largely concomitant with an increase in lipid content [19,98,99,106,123]. Declines in protein have also been observed at light levels exceeding those expected in situ ( $40\text{--}100 \mu\text{mol m}^{-2} \text{s}^{-1}$ ; [82]); however, at higher light levels ( $125\text{--}250 \mu\text{mol m}^{-2} \text{s}^{-1}$ ), protein allocation has been shown to increase [107]. Importantly however, some studies found no effect on protein and amino acid content in response to increasing irradiance [55,59,100]. For carbohydrates, sea ice microalgae have been shown to increase their allocation of carbon to carbohydrates in response to natural environmental increases in irradiance [106], controlled incubations within the natural light range [55,99] and to higher than naturally expected under-ice light intensities ( $42\text{--}106 \mu\text{mol m}^{-2} \text{s}^{-1}$ , compared with  $3\text{--}19 \mu\text{mol m}^{-2} \text{s}^{-1}$ ; [82]), with only one study finding no significant effect on carbohydrate content as a result of increasing light intensity [19].

**Nutrient limitation:** Another key factor well known for shaping sea ice microalgal biomolecular composition is nutrient availability. Nutrient limitation can occur within the narrow brine channels, where the microalgae can exhaust some or all of the available nutrients. This may partly explain why some lipids measured in sea ice microalgae are enriched with  $^{13}\text{C}$  [24,125]. Nutrient limitation is less of a problem at the ice–water interface, where nutrients are continually replenished from the seawater. However, nitrogen limitation, which is a defining constraint on growth and development [11,126,127] and is expected to intensify with increasing ocean stratification [128,129], commonly leads to increased lipid and decreased protein content in microalgae (e.g., [130–133]). This is because nutrient stress induces the algae to favor energy storage in lieu of growth and photosynthetic efficiency [113,134–136]. These trends have been observed in sea ice microalgae, which were shown to increase in relative lipid [85,101] and PUFA content [85], concomitant with a decline in protein and carbohydrate allocation [85,101] (Figure 2D) with nitrogen limitation. Given that vast expanses of the Arctic are nitrogen poor, it is possible that this low nitrogen environment, which underpins the lipid-rich sea ice microalgae [70,71], is partially responsible for driving an evolutionary dependence on lipids for the successful egg hatching and reproduction of arctic zooplankton [25,137].

**pH:** With ocean warming, nutrient limitation will likely occur heterogeneously; carbon availability, however, from atmospheric  $\text{CO}_2$  uptake by seawater, is increasing ubiquitously. Ocean acidification poses a real and imminent threat to marine life in the polar regions, including microalgae [41,138,139]; however, limited work has been undertaken to understand its effect on sea ice microalgal growth and biochemical composition. To date few studies have compared biochemical composition of sea ice microalgae under current  $p\text{CO}_2$  levels ( $\sim 390 \mu\text{atm}$ ) and those projected for 2100 ( $\sim 1000 \mu\text{atm}$ ; [140]). Elevated  $p\text{CO}_2$

levels (~1000  $\mu\text{atm}$ ) over a period of  $\geq 14$  days resulted in reduced lipid [91] and fatty acid content [89], whilst shorter exposure (6 days) at the same  $p\text{CO}_2$  levels was found to have no significant effect on protein, fatty acid, or carbohydrate content [90], suggesting that length of exposure influences physiological response (Figure 2E). A recent study on Antarctic coastal diatoms found that high  $p\text{CO}_2$  levels resulted in a decrease in lipid content for the two largest taxa and an increase in protein content across all five taxa investigated [81]. Although conducted on polar pelagic algae, this study indicates that species-specific responses likely exist within sea ice communities, which has the potential to affect food web dynamics and carbon transfer in polar regions.

### 5. Sea Ice Microalgae Biochemistry and Carbon Transfer through the Polar Marine Food Web with Climate Change

Climate change has the potential to alter biodiversity and, therefore, ecosystem functioning. Multi-species assemblages are considered more resilient to environmental fluctuations, as the differences in the individuals' phenotypic plasticity and tolerance, as well as the inherent complexity of species interactions, result in greater response diversity within the community. For natural phytoplankton communities, biodiversity has been shown to be important for maintenance of overall ecosystem functioning in variable environments [141], meaning that a reduction in biodiversity may reduce ecosystem productivity and resilience. We know from studies looking at biomolecular profiles of individual sea ice diatoms that there is considerable diversity in cellular carbon allocation between species [58–60]. Similarly, while exploring the role of climate change on biomolecular partitioning, it has been shown that  $\text{CO}_2$  enrichment of natural Antarctic diatom communities resulted in species-specific biochemical responses [81]. These studies highlight the potential importance of species richness and response diversity within sea ice microalgal communities for the resilience of the polar ecosystem to climate change. Natural community studies on the nutritional value of sea ice algae have primarily been completed on whole communities, which is valuable in that it can show an overall shift in food quality, but only by investigating individuals within a community, such as with synchrotron-based FTIR microspectroscopy, is it possible to determine the diverse taxon-specific responses, thereby elucidating the strength and direction of change and determining the winners and losers of environmental change.

There are indications that with the ongoing ecosystem changes in the polar regions, microalgal communities will shift toward smaller taxa and no longer be dominated by larger diatoms. This has already been observed in both Arctic and Antarctic communities in response to ocean acidification [142,143], ocean freshening [143–145], reduced sea ice extent [146,147], and sea surface warming [143]. Such a shift is anticipated to have a significant effect on trophic energy transfer, where a community dominated by smaller cells would generally mean a reduction in grazing efficiency by zooplankton [144,148–150]. There is also evidence of climate change altering taxonomic dominance, for example, increased light transmittance has been shown to favor diatoms over flagellates [127], specifically favoring centric rather than pennate diatoms [151]. In under ice and pelagic phytoplankton blooms, nanoflagellate dominance has been observed along with ocean freshening [144,147,152] and post-bloom meltwater conditions [127]. While these shifts in microalgal community composition will be heterogeneous and geographically dependent, any persistent changes or losses in species will invariably have trophic and biogeochemical implications. For example, shifts that favor taxa of poorer nutritional quality, such as species with reduced lipid or protein content, would result in less energy available for transfer through the marine food web. Specifically, a decline in lipid content may alter the growth and reproduction of primary and secondary consumers [25,137,153]. Similarly, environmental conditions that favor one taxonomic group such as a shift toward nanoflagellate dominated communities at the expense of diatoms, may see strong alterations to regional carbon and silicon cycling [61,154,155]. It is clear, therefore, that as communities change or become less complex, we can expect to see altered marine biochemistry and ecosystem functioning.

Geographic variation in climate change effects means that changes to community composition and, therefore, biochemical composition of primary producers at the community level cannot be expected to be uniform. Since the 1970s, Arctic landfast ice regions have seen a much more rapid decline in sea ice extent of 10.5% per decade, compared to 5.2% per decade for Arctic seas [156], and recent studies have revealed similar trends of accelerated landfast ice retreat in Antarctica [157,158]. As such, these coastal areas will likely experience an increased reliance on open water pelagic phytoplankton blooms sooner than perennial multi-year ice regions [159,160]. While we have seen a ~3 month increase in annual sea-ice free period since 1980 at both polar regions, the change is occurring in different ways. In the Arctic, sea ice retreat is occurring on average two months earlier, with the advance one month later, whilst the Antarctic Peninsula is experiencing the average sea ice retreat one month earlier and the advance two months later [161]. With predictions of ice-free periods becoming more prolonged [46,162] we may see increases in total primary production [128,129,160,163]. However, there are concerns that a heavily reduced sea ice season will result in a timing mismatch between the primary producers and the consumers who rely on the earlier sea ice microalgal bloom for reproduction [25,26,164–167]. In addition, for both the Arctic and Antarctic, reduced sea ice production and increased glacial melt has amplified ocean freshening particularly in enclosed fjordic systems [121,122,168], altering phytoplankton community composition [144,146,152]. Taken together, broad changes in sea ice microalgal community structure, phenology, and species-specific carbon allocation, could significantly alter carbon transfer and biochemical characteristics of polar marine ecosystems.

## 6. Conclusions

Knowledge of sea ice microalgal biochemical composition and understanding the influence of environmental factors on their cellular carbon partitioning is critical to determining the nutritional quality of primary production in polar regions and the broader effects on energy transfer through the marine food web. As light is a primary driver of sea ice microalgae primary productivity, many studies to date have focused on the effect of irradiance on biomolecular composition, with trends indicating that an increase in total irradiance dose would drive an increase in lipid and carbohydrate content but a decrease in PUFA and protein content. Studies have also shown, however, that warmer temperatures will increase protein content, and nitrogen limitation will enhance lipid and PUFA production at the expense of all other biomolecules. Across the environmental effects considered here, changes in response to different environmental factors were not unidirectional, and as such, the overall direction of change likely to occur in the ecosystem under future conditions remains unclear. Further research is therefore recommended to better tease apart discrete and synergistic effects on sea ice microalgal biochemistry. While understanding any degree of change across sea ice microalgal communities is important, biochemical changes appear to have a degree of species specificity, and, therefore, future studies would benefit also from employing methodologies that allow for the determination of species-specific biomolecular characterization. With the accelerated pace of climate change rapidly reshaping the physical and chemical marine environment (warmer temperatures causing reductions in sea ice extent, thickness and longevity, ocean stratification and increasing atmospheric CO<sub>2</sub> concentrations causing seawater acidification), it is anticipated that changes to sea ice microalgal community structure and biochemical composition will ensue. As shown here, these changes will likely alter the allocation of carbon to different biomolecules by sea ice microalgae resulting in significant shifts in biochemical cycling and carbon transfer through polar marine food webs, the effects of which could have far-reaching consequences for polar marine ecosystems.

**Author Contributions:** Conceptualization, R.J.D. and K.P.; methodology, R.J.D. and K.P.; formal analysis, R.J.D.; investigation, R.J.D. and K.P.; data curation, R.J.D.; writing—original draft preparation, R.J.D.; writing—review and editing, K.P.; visualization, K.P.; supervision, K.P. All authors have read and agreed to the published version of the manuscript.



**Funding:** R.J.D. is supported by an Australian Government Research Training Program Scholarship and an AINSE Ltd. Postgraduate Research Award (PGRA).

**Conflicts of Interest:** The authors declare no conflict of interest. The funders had no role in the design of the study; in the collection, analyses, or interpretation of data; in the writing of the manuscript, or in the decision to publish the paper.

## References

- Parkinson, C.L. Global Sea Ice Coverage from Satellite Data: Annual Cycle and 35-Yr Trends. *J. Clim.* **2014**, *27*, 9377–9382. [[CrossRef](#)]
- Arrigo, K.R. Sea ice as a habitat for primary producers. In *Sea Ice*, 3rd ed.; Thomas, D., Ed.; Wiley-Blackwell: Oxford, UK, 2017; pp. 352–369. [[CrossRef](#)]
- Deming, J.W.; Eric Collins, R. Sea ice as a habitat for bacteria, archaea and viruses. In *Sea Ice*, 3rd ed.; Thomas, D., Ed.; Wiley-Blackwell: Oxford, UK, 2017; pp. 326–351. [[CrossRef](#)]
- Belt, S.T. Source-specific biomarkers as proxies for Arctic and Antarctic sea ice. *Org. Geochem.* **2018**, *125*, 277–298. [[CrossRef](#)]
- Kohlbach, D.; Hop, H.; Wold, A.; Schmidt, K.; Smik, L.; Belt, S.T.; Al-Habahbeh, A.K.; Woll, M.; Graeve, M.; Dąbrowska, A.M.; et al. Multiple trophic markers trace dietary carbon sources in barents sea zooplankton during late summer. *Front. Mar. Sci.* **2021**, *7*, 1216. [[CrossRef](#)]
- Rontani, J.-F.; Belt, S.T.; Brown, T.; Amiraux, R.; Gosselin, M.; Vaultier, F.; Mundy, C.J. Monitoring abiotic degradation in sinking versus suspended Arctic sea ice algae during a spring ice melt using specific lipid oxidation tracers. *Org. Geochem.* **2016**, *98*, 82–97. [[CrossRef](#)]
- Rontani, J.-F.; Amiraux, R.; Smik, L.; Wakeham, S.G.; Paulmier, A.; Vaultier, F.; Sun-Yong, H.; Jun-Oh, M.; Belt, S.T. Type II photosensitized oxidation in senescent microalgal cells at different latitudes: Does low under-ice irradiance in polar regions enhance efficiency? *Sci. Total Environ.* **2021**, *779*, 146363. [[CrossRef](#)] [[PubMed](#)]
- Bélanger, S.; Xie, H.; Krotkov, N.; Larouche, P.; Vincent, W.F.; Babin, M. Photomineralization of terrigenous dissolved organic matter in Arctic coastal waters from 1979 to 2003: Interannual variability and implications of climate change. *Glob. Biogeochem. Cycles* **2006**, *20*, 1–13. [[CrossRef](#)]
- Massicotte, P.; Amon, R.M.W.; Antoine, D.; Archambault, P.; Balzano, S.; Bélanger, S.; Benner, R.; Boeuf, D.; Bricaud, A.; Bruyant, F.; et al. The MALINA oceanographic expedition: How do changes in ice cover, permafrost and UV radiation impact biodiversity and biogeochemical fluxes in the Arctic Ocean? *Earth Syst. Sci. Data* **2021**, *13*, 1561–1592. [[CrossRef](#)]
- Johnsen, G. Photoadaptation of sea-ice microalgae in the Barents Sea. *Polar Biol.* **1991**, *11*, 179–184. [[CrossRef](#)]
- Leu, E.; Mundy, C.; Assmy, P.; Campbell, K.; Gabrielsen, T.; Gosselin, M.; Juul-Pedersen, T.; Gradinger, R. Arctic spring awakening—Steering principles behind the phenology of vernal ice algal blooms. *Prog. Oceanogr.* **2015**, *139*, 151–170. [[CrossRef](#)]
- Cota, G.; Legendre, L.; Gosselin, M.; Ingram, R. Ecology of bottom ice algae: I. Environmental controls and variability. *J. Mar. Syst.* **1991**, *2*, 257–277. [[CrossRef](#)]
- Selz, V.; Laney, S.; Arnsten, A.E.; Lewis, K.M.; Lowry, K.E.; Joy-Warren, H.L.; Mills, M.M.; van Dijken, G.L.; Arrigo, K.R. Ice algal communities in the Chukchi and Beaufort Seas in spring and early summer: Composition, distribution, and coupling with phytoplankton assemblages. *Limnol. Oceanogr.* **2018**, *63*, 1109–1133. [[CrossRef](#)]
- Gosselin, M.; Levasseur, M.; Wheeler, P.A.; Horner, R.A.; Booth, B.C. New measurements of phytoplankton and ice algal production in the Arctic Ocean. *Deep Sea Res. Part II Top. Stud. Oceanogr.* **1997**, *44*, 1623–1644. [[CrossRef](#)]
- Legendre, L.; Ackley, S.F.; Dieckmann, G.S.; Horner, R.; Hoshiai, T.; Melnikov, I.A.; Reeburgh, W.S.; Spindler, M.; Sullivan, C.W. Ecology of sea ice biota. *Polar Biol.* **1992**, *12*, 429–444. [[CrossRef](#)]
- Gradinger, R. Sea-ice algae: Major contributors to primary production and algal biomass in the Chukchi and Beaufort Seas during May/June 2002. *Deep Sea Res. Part II Top. Stud. Oceanogr.* **2009**, *56*, 1201–1212. [[CrossRef](#)]
- Fernández-Méndez, M.; Katlein, C.; Rabe, B.; Nicolaus, M.; Peeken, I.; Bakker, K.; Flores, H.; Boetius, A. Photosynthetic production in the central Arctic Ocean during the record sea-ice minimum in 2012. *Biogeosciences* **2015**, *12*, 3525–3549. [[CrossRef](#)]
- Rysgaard, S.; Kühl, M.; Glud, R.N.; Hansen, J.W. Biomass, production and horizontal patchiness of sea ice algae in a high-Arctic fjord (Young Sound, NE Greenland). *Mar. Ecol. Prog. Ser.* **2001**, *223*, 15–26. [[CrossRef](#)]
- Lee, S.H.; Whittedge, T.E.; Kang, S.-H. Spring time production of bottom ice algae in the landfast sea ice zone at Barrow, Alaska. *J. Exp. Mar. Biol. Ecol.* **2008**, *367*, 204–212. [[CrossRef](#)]
- Lizotte, M.P. The contributions of sea ice algae to Antarctic marine primary production1. *Am. Zool.* **2001**, *41*, 57–73. [[CrossRef](#)]
- Michel, C.; Legendre, L.; Ingram, R.G.; Gosselin, M.; Levasseur, M. Carbon budget of sea-ice algae in spring: Evidence of a significant transfer to zooplankton grazers. *J. Geophys. Res. Earth Surf.* **1996**, *101*, 18345–18360. [[CrossRef](#)]
- Riedel, A.; Michel, C.; Gosselin, M.; LeBlanc, B. Winter–spring dynamics in sea-ice carbon cycling in the coastal Arctic Ocean. *J. Mar. Syst.* **2008**, *74*, 918–932. [[CrossRef](#)]
- Arrigo, K.R.; Brown, Z.W.; Mills, M.M. Sea ice algal biomass and physiology in the Amundsen Sea, Antarctica. *Elem. Sci. Anth.* **2014**, *2*, 28. [[CrossRef](#)]

24. Kohlbach, D.; Graeve, M.; Lange, B.A.; David, C.; Peeken, I.; Flores, H. The importance of ice algae-produced carbon in the central Arctic Ocean ecosystem: Food web relationships revealed by lipid and stable isotope analyses. *Limnol. Oceanogr.* **2016**, *61*, 2027–2044. [CrossRef]
25. Søreide, J.E.; Leu, E.; Berge, J.; Graeve, M.; Falk-Petersen, S. Timing of blooms, algal food quality and *Calanus glacialis* reproduction and growth in a changing Arctic. *Glob. Chang. Biol.* **2010**, *16*, 3154–3163. [CrossRef]
26. Leu, E.; Søreide, J.; Hessen, D.; Falk-Petersen, S.; Berge, J. Consequences of changing sea-ice cover for primary and secondary producers in the European Arctic shelf seas: Timing, quantity, and quality. *Prog. Oceanogr.* **2011**, *90*, 18–32. [CrossRef]
27. Durbin, E.G.; Casas, M.C. Early reproduction by *Calanus glacialis* in the Northern Bering Sea: The role of ice algae as revealed by molecular analysis. *J. Plankton Res.* **2014**, *36*, 523–541. [CrossRef]
28. Garrison, D.L.; Buck, K.R.; Fryxell, G.A. Algal assemblages in Antarctic pack ice and in ice-edge plankton 1. *J. Phycol.* **1987**, *23*, 564–572. [CrossRef]
29. Michel, C.; Legendre, L.; Therriault, J.-C.; Demers, S.; Vandeveld, T. Springtime coupling between ice algal and phytoplankton assemblages in southeastern Hudson Bay, Canadian Arctic. *Polar Biol.* **1993**, *13*, 441–449. [CrossRef]
30. Haecky, P.; Jonsson, S.; Andersson, A. Influence of sea ice on the composition of the spring phytoplankton bloom in the northern Baltic Sea. *Polar Biol.* **1998**, *20*, 1–8. [CrossRef]
31. Jin, M.; Deal, C.; Wang, J.; Alexander, V.; Gradinger, R.; Saitoh, S.-I.; Iida, T.; Wan, Z.; Stabeno, P. Ice-associated phytoplankton blooms in the southeastern Bering Sea. *Geophys. Res. Lett.* **2007**, *34*, L006612. [CrossRef]
32. Tedesco, L.; Vichi, M.; Thomas, D.N. Process studies on the ecological coupling between sea ice algae and phytoplankton. *Ecol. Model.* **2012**, *226*, 120–138. [CrossRef]
33. Szymanski, A.; Gradinger, R. The diversity, abundance and fate of ice algae and phytoplankton in the Bering Sea. *Polar Biol.* **2015**, *39*, 309–325. [CrossRef]
34. Bhavya, P.S.; Kim, B.K.; Jo, N.; Kim, K.; Kang, J.J.; Lee, J.H.; Lee, D.; Lee, J.H.; Joo, H.; Ahn, S.H.; et al. A Review on the Macromolecular compositions of phytoplankton and the implications for aquatic biogeochemistry. *Ocean Sci. J.* **2018**, *54*, 1–14. [CrossRef]
35. Bernard, K.S.; Gunther, L.A.; Mahaffey, S.H.; Qualls, K.M.; Sugla, M.; Saenz, B.T.; Cossio, A.M.; Walsh, J.; Reiss, C.S. The contribution of ice algae to the winter energy budget of juvenile Antarctic krill in years with contrasting sea ice conditions. *ICES J. Mar. Sci.* **2019**, *76*, 206–216. [CrossRef]
36. Graeve, M.; Kattner, G.; Hagen, W. Diet-induced changes in the fatty acid composition of Arctic herbivorous copepods: Experimental evidence of trophic markers. *J. Exp. Mar. Biol. Ecol.* **1994**, *182*, 97–110. [CrossRef]
37. Lee, R.; Hagen, W.; Kattner, G. Lipid storage in marine zooplankton. *Mar. Ecol. Prog. Ser.* **2006**, *307*, 273–306. [CrossRef]
38. Hagen, W.; Auel, H. Seasonal adaptations and the role of lipids in oceanic zooplankton. *Zoology* **2001**, *104*, 313–326. [CrossRef] [PubMed]
39. Falk-Petersen, S.; Mayzaud, P.; Kattner, G.; Sargent, J.R. Lipids and life strategy of Arctic *Calanus*. *Mar. Biol. Res.* **2009**, *5*, 18–39. [CrossRef]
40. Kohlbach, D.; Graeve, M.; Lange, B.A.; David, C.; Schaafsma, F.L.; Van Franeker, J.A.; Vortkamp, M.; Brandt, A.; Flores, H. Dependency of Antarctic zooplankton species on ice algae-produced carbon suggests a sea ice-driven pelagic ecosystem during winter. *Glob. Chang. Biol.* **2018**, *24*, 4667–4681. [CrossRef]
41. Meredith, M.; Sommerkorn, M.; Cassotta, S.; Derksen, C.; Ekaykin, A.; Hollowed, A.; Kofinas, G.; Macintosh, A.; Melbourne-Thomas, J.; Muelbert, M.M.C.; et al. Polar Regions. In *IPCC Special Report on the Ocean and Cryosphere in a Changing Climate*; Pörtner, H.-O., Roberts, D.C., Masson-Delmotte, V., Zhai, P., Tignor, M., Poloczanska, E., Mintenbeck, K., Alegria, A., Nicolai, M., Okem, A., et al., Eds.; Intergovernmental Panel on Climate Change (IPCC): Geneva, Switzerland, 2019.
42. Post, E.; Bhatt, U.S.; Bitz, C.M.; Brodie, J.F.; Fulton, T.L.; Hebblewhite, M.; Kerby, J.; Kutz, S.J.; Stirling, I.; Walker, D.A. Ecological consequences of sea-ice decline. *Science* **2013**, *341*, 519–524. [CrossRef]
43. Mallett, R.D.C.; Stroeve, J.C.; Tsamados, M.; Landy, J.C.; Willatt, R.; Nandan, V.; Liston, G.E. Faster decline and higher variability in the sea ice thickness of the marginal Arctic seas when accounting for dynamic snow cover. *Cryosphere* **2021**, *15*, 2429–2450. [CrossRef]
44. Post, E.; Alley, R.B.; Christensen, T.R.; Macias-Fauria, M.; Forbes, B.C.; Gooseff, M.N.; Iler, A.; Kerby, J.T.; Laidre, K.L.; Mann, M.E.; et al. The polar regions in a 2 °C warmer world. *Sci. Adv.* **2019**, *5*, eaaw9883. [CrossRef]
45. National Snow & Ice Data Center (NSIDC) Sea Ice Index. Available online: [https://nsidc.org/data/seaice\\_index/](https://nsidc.org/data/seaice_index/) (accessed on 14 September 2021).
46. Overland, J.E.; Wang, M. When will the summer Arctic be nearly sea ice free? *Geophys. Res. Lett.* **2013**, *40*, 2097–2101. [CrossRef]
47. Haine, T.W.N.; Martin, T. The Arctic-Subarctic sea ice system is entering a seasonal regime: Implications for future Arctic amplification. *Sci. Rep.* **2017**, *7*, 4618. [CrossRef] [PubMed]
48. Parkinson, C.L. A 40-y record reveals gradual Antarctic sea ice increases followed by decreases at rates far exceeding the rates seen in the Arctic. *Proc. Natl. Acad. Sci. USA* **2019**, *116*, 14414–14423. [CrossRef]
49. Stroeve, J.; Notz, D. Changing state of Arctic sea ice across all seasons. *Environ. Res. Lett.* **2018**, *13*, 103001. [CrossRef]
50. Timmermans, M.; Marshall, J. Understanding Arctic Ocean circulation: A review of ocean dynamics in a changing climate. *J. Geophys. Res. Oceans* **2020**, *125*, 1–35. [CrossRef]

51. Terhaar, J.; Kwiatkowski, L.; Bopp, L. Emergent constraint on Arctic Ocean acidification in the twenty-first century. *Nature* **2020**, *582*, 379–383. [[CrossRef](#)]
52. Terhaar, J.; Orr, J.C.; Ethé, C.; Regnier, P.; Bopp, L. Simulated Arctic Ocean response to doubling of riverine carbon and nutrient delivery. *Glob. Biogeochem. Cycles* **2019**, *33*, 1048–1070. [[CrossRef](#)]
53. Archer, S.; Leakey, R.; Burkill, P.; Sleight, M.; Appleby, C. Microbial ecology of sea ice at a coastal Antarctic site: Community composition, biomass and temporal change. *Mar. Ecol. Prog. Ser.* **1996**, *135*, 179–195. [[CrossRef](#)]
54. Becquevort, S.; Dumont, I.; Tison, J.-L.; Lannuzel, D.; Sauvée, M.-L.; Chou, L.; Schoemann, V. Biogeochemistry and microbial community composition in sea ice and underlying seawater off East Antarctica during early spring. *Polar Biol.* **2009**, *32*, 879–895. [[CrossRef](#)]
55. Mock, T.; Kroon, B.M. Photosynthetic energy conversion under extreme conditions—II: The significance of lipids under light limited growth in Antarctic sea ice diatoms. *Phytochemistry* **2002**, *61*, 53–60. [[CrossRef](#)]
56. Leu, E.; Wiktor, J.; Søreide, J.E.; Berge, J.; Falk-Petersen, S. Increased irradiance reduces food quality of sea ice algae. *Mar. Ecol. Prog. Ser.* **2010**, *411*, 49–60. [[CrossRef](#)]
57. Sackett, O.; Petrou, K.; Reedy, B.; De Grazia, A.; Hill, R.; Doblin, M.; Beardall, J.; Ralph, P.; Heraud, P. Phenotypic plasticity of southern ocean diatoms: Key to success in the sea ice habitat? *PLoS ONE* **2013**, *8*, e81185. [[CrossRef](#)]
58. Sackett, O.; Petrou, K.; Reedy, B.; Hill, R.; Doblin, M.; Beardall, J.; Ralph, P.; Heraud, P. Snapshot prediction of carbon productivity, carbon and protein content in a Southern Ocean diatom using FTIR spectroscopy. *ISME J.* **2015**, *10*, 416–426. [[CrossRef](#)] [[PubMed](#)]
59. Pogorzelec, N.; Mundy, C.; Findlay, C.; Campbell, K.; Diaz, A.; Ehn, J.; Rysgaard, S.; Gough, K. FTIR imaging analysis of cell content in sea-ice diatom taxa during a spring bloom in the lower northwest passage of the Canadian Arctic. *Mar. Ecol. Prog. Ser.* **2017**, *569*, 77–88. [[CrossRef](#)]
60. Sheehan, C.; Nielsen, D.A.; Petrou, K. Macromolecular composition, productivity and dimethylsulfoniopropionate in Antarctic pelagic and sympagic microalgal communities. *Mar. Ecol. Prog. Ser.* **2020**, *640*, 45–61. [[CrossRef](#)]
61. Finkel, Z.V.; Follows, M.J.; Liefer, J.; Brown, C.M.; Benner, I.; Irwin, A.J. Phylogenetic Diversity in the Macromolecular Composition of Microalgae. *PLoS ONE* **2016**, *11*, e0155977. [[CrossRef](#)]
62. Thomas, D.N.; Dieckmann, G.S. Antarctic sea ice—A habitat for extremophiles. *Science* **2002**, *295*, 641–644. [[CrossRef](#)]
63. Morgan-Kiss, R.M.; Priscu, J.C.; Pockock, T.; Gudynaite-Savitch, L.; Huner, N.P.A. Adaptation and acclimation of photosynthetic microorganisms to permanently cold environments. *Microbiol. Mol. Biol. Rev.* **2006**, *70*, 222–252. [[CrossRef](#)]
64. Finkel, Z.V.; Follows, M.J.; Irwin, A.J. Size-scaling of macromolecules and chemical energy content in the eukaryotic microalgae. *J. Plankton Res.* **2016**, *38*, 1151–1162. [[CrossRef](#)]
65. Van Oijen, T.; Van Leeuwe, M.A.; Granum, E.; Weissing, F.J.; Bellerby, R.G.J.; Gieskes, W.W.C.; De Baar, H.J.W. Light rather than iron controls photosynthate production and allocation in Southern Ocean phytoplankton populations during austral autumn. *J. Plankton Res.* **2004**, *26*, 885–900. [[CrossRef](#)]
66. Ruess, L.; Müller-Navarra, D.C. Essential Biomolecules in Food Webs. *Front. Ecol. Evol.* **2019**, *7*, 269. [[CrossRef](#)]
67. Scott, J.M. Effect of growth rate of the food alga on the growth/ingestion efficiency of a marine herbivore. *J. Mar. Biol. Assoc. UK* **1980**, *60*, 681–702. [[CrossRef](#)]
68. Lindqvist, K.; Lignell, R. Intracellular partitioning of  $^{14}\text{C}$  in phytoplankton during a growth season in the northern Baltic. *Mar. Ecol. Prog. Ser.* **1997**, *152*, 41–50. [[CrossRef](#)]
69. Swalethorp, R.; Kjellerup, S.; Dünweber, M.; Nielsen, T.G.; Møller, E.F.; Rysgaard, S.; Hansen, B. Grazing, egg production, and biochemical evidence of differences in the life strategies of *Calanus finmarchicus*, *C. glacialis* and *C. hyperboreus* in Disko Bay, western Greenland. *Mar. Ecol. Prog. Ser.* **2011**, *429*, 125–144. [[CrossRef](#)]
70. Kim, B.K.; Lee, J.H.; Yun, M.S.; Joo, H.; Song, H.J.; Yang, E.J.; Chung, K.H.; Kang, S.-H.; Lee, S.H. High lipid composition of particulate organic matter in the northern Chukchi Sea, 2011. *Deep Sea Res. Part II Top. Stud. Oceanogr.* **2015**, *120*, 72–81. [[CrossRef](#)]
71. Yun, M.S.; Lee, D.B.; Kim, B.K.; Kang, J.J.; Lee, J.H.; Yang, E.J.; Park, W.G.; Chung, K.H.; Lee, S.H. Comparison of phytoplankton macromolecular compositions and zooplankton proximate compositions in the northern Chukchi Sea. *Deep Sea Res. Part II Top. Stud. Oceanogr.* **2015**, *120*, 82–90. [[CrossRef](#)]
72. Smith, W.O.; Nelson, D.M.; DiTullio, G.R.; Leventer, A. Temporal and spatial patterns in the Ross Sea: Phytoplankton biomass, elemental composition, productivity and growth rates. *J. Geophys. Res. Space Phys.* **1996**, *101*, 18455–18465. [[CrossRef](#)]
73. Fabiano, M.; Danovaro, R.; Povero, P. Vertical distribution and biochemical composition of pico- and microparticulate organic matter in the Ross Sea (Antarctica). In *Oceanography of the Ross Sea Antarctica*; Springer: Milano, Italy, 1999; pp. 233–246. [[CrossRef](#)]
74. Kim, B.K.; Lee, J.H.; Joo, H.; Song, H.J.; Yang, E.J.; Lee, S.H. Macromolecular compositions of phytoplankton in the Amundsen Sea, Antarctica. *Deep Sea Res. Part II Top. Stud. Oceanogr.* **2016**, *123*, 42–49. [[CrossRef](#)]
75. Nelson, D.M.; Smith, W.O. Phytoplankton bloom dynamics of the western Ross Sea ice edge—II. Mesoscale cycling of nitrogen and silicon. *Deep Sea Res. Part A Oceanogr. Res. Pap.* **1986**, *33*, 1389–1412. [[CrossRef](#)]
76. Pollard, R.; Tréguer, P.; Read, J. Quantifying nutrient supply to the Southern Ocean. *J. Geophys. Res. Space Phys.* **2006**, *111*, C0501. [[CrossRef](#)]
77. Kim, B.K.; Lee, S.; Ha, S.-Y.; Jung, J.; Kim, T.W.; Yang, E.J.; Jo, N.; Lim, Y.J.; Park, J. Vertical distributions of macromolecular composition of particulate organic matter in the water column of the Amundsen sea polynya during the summer in 2014. *J. Geophys. Res. Oceans* **2018**, *123*, 1393–1405. [[CrossRef](#)]

78. Alderkamp, A.-C.; Buma, A.G.J.; van Rijssel, M. The carbohydrates of Phaeocystis and their degradation in the microbial food web. *Biogeochemistry* **2007**, *83*, 99–118. [[CrossRef](#)]
79. Hitchcock, G.L. A comparative study of the size-dependent organic composition of marine diatoms and dinoflagellates. *J. Plankton Res.* **1982**, *4*, 363–377. [[CrossRef](#)]
80. Stehfest, K.; Toepel, J.; Wilhelm, C. The application of micro-FTIR spectroscopy to analyze nutrient stress-related change in biomass composition of phytoplankton algae. *Plant Physiol. Biochem.* **2005**, *43*, 717–726. [[CrossRef](#)] [[PubMed](#)]
81. Duncan, R.J.; Nielsen, D.A.; Sheehan, C.E.; Deppeler, S.; Hancock, A.M.; Schulz, K.G.; Davidson, A.T.; Petrou, K. Ocean acidification alters the nutritional value of Antarctic diatoms. *New Phytol.* **2022**, *in press*. [[CrossRef](#)]
82. Gleitz, M.; Kirst, G. Photosynthesis-irradiance relationships and carbon metabolism of different ice algal assemblages collected from Weddell Sea pack ice during austral spring (EPOS 1). *Polar Biol.* **1991**, *11*, 385–392. [[CrossRef](#)]
83. Smith, R.; Cavaletto, J.; Eadie, B.; Gardner, W. Growth and lipid composition of high Arctic ice algae during the spring bloom at Resolute, Northwest Territories, Canada. *Mar. Ecol. Prog. Ser.* **1993**, *97*, 19–29. [[CrossRef](#)]
84. Henderson, R.J.; Hegseth, E.N.; Park, M.T. Seasonal variation in lipid and fatty acid composition of ice algae from the Barents Sea. *Polar Biol.* **1998**, *20*, 48–55. [[CrossRef](#)]
85. Mock, T.; Kroon, B.M. Photosynthetic energy conversion under extreme conditions—I: Important role of lipids as structural modulators and energy sink under N-limited growth in Antarctic sea ice diatoms. *Phytochemistry* **2002**, *61*, 41–51. [[CrossRef](#)]
86. Teoh, M.-L.; Chu, W.-L.; Marchant, H.; Phang, S.-M. Influence of culture temperature on the growth, biochemical composition and fatty acid profiles of six Antarctic microalgae. *J. Appl. Phycol.* **2004**, *16*, 421–430. [[CrossRef](#)]
87. Leu, E.; Falk-Petersen, S.; Kwaśniewski, S.; Wulff, A.; Edvardsen, K.; Hessen, D.O. Fatty acid dynamics during the spring bloom in a High Arctic fjord: Importance of abiotic factors versus community changes. *Can. J. Fish. Aquat. Sci.* **2006**, *63*, 2760–2779. [[CrossRef](#)]
88. An, M.; Mou, S.; Zhang, X.; Ye, N.; Zheng, Z.; Cao, S.; Xu, D.; Fan, X.; Wang, Y.; Miao, J. Temperature regulates fatty acid desaturases at a transcriptional level and modulates the fatty acid profile in the Antarctic microalga *Chlamydomonas* sp. *ICE-L. Bioresour. Technol.* **2013**, *134*, 151–157. [[CrossRef](#)]
89. Torstensson, A.; Hedblom, M.; Andersson, J.; Andersson, M.X.; Wulff, A. Synergism between elevated pCO<sub>2</sub> and temperature on the Antarctic sea ice diatom *Nitzschia lecontei*. *Biogeosciences* **2013**, *10*, 6391–6401. [[CrossRef](#)]
90. Torstensson, A.; Jiménez, C.; Nilsson, A.K.; Wulff, A. Elevated temperature and decreased salinity both affect the biochemical composition of the Antarctic sea-ice diatom *Nitzschia lecontei*, but not increased pCO<sub>2</sub>. *Polar Biol.* **2019**, *42*, 2149–2164. [[CrossRef](#)]
91. Xu, D.; Wang, Y.; Fan, X.; Wang, D.; Ye, N.; Zhang, X.; Mou, S.; Guan, Z.; Zhuang, Z. Long-Term Experiment on Physiological Responses to Synergetic Effects of Ocean Acidification and Photoperiod in the Antarctic Sea Ice Algae *Chlamydomonas* sp. *ICE-L. Environ. Sci. Technol.* **2014**, *48*, 7738–7746. [[CrossRef](#)] [[PubMed](#)]
92. Lund-Hansen, L.; Hawes, I.; Hancke, K.; Salmansen, N.; Nielsen, J.; Balslev, L.; Sorrell, B. Effects of increased irradiance on biomass, photobiology, nutritional quality, and pigment composition of Arctic sea ice algae. *Mar. Ecol. Prog. Ser.* **2020**, *648*, 95–110. [[CrossRef](#)]
93. Sargent, J.R.; Eilertsen, H.C.; Falk-Petersen, S.; Taasen, J.P. Carbon assimilation and lipid production in phytoplankton in northern Norwegian fjords. *Mar. Biol.* **1985**, *85*, 109–116. [[CrossRef](#)]
94. Jonasdottir, S.; Visser, A.; Jespersen, C. Assessing the role of food quality in the production and hatching of *Temora longicornis* eggs. *Mar. Ecol. Prog. Ser.* **2009**, *382*, 139–150. [[CrossRef](#)]
95. Johns, L.; Wraige, E.; Belt, S.; Lewis, C.; Massé, G.; Robert, J.-M.; Rowland, S. Identification of a C<sub>25</sub> highly branched isoprenoid (HBI) diene in Antarctic sediments, Antarctic sea-ice diatoms and cultured diatoms. *Org. Geochem.* **1999**, *30*, 1471–1475. [[CrossRef](#)]
96. Brown, T.; Belt, S.T.; Tatarek, A.; Mundy, C.J. Source identification of the Arctic sea ice proxy IP<sub>25</sub>. *Nat. Commun.* **2014**, *5*, 4197. [[CrossRef](#)]
97. Belt, S.T.; Brown, T.; Smik, L.; Tatarek, A.; Wiktor, J.; Stowasser, G.; Assmy, P.; Allen, C.S.; Husum, K. Identification of C<sub>25</sub> highly branched isoprenoid (HBI) alkenes in diatoms of the genus *Rhizosolenia* in polar and sub-polar marine phytoplankton. *Org. Geochem.* **2017**, *110*, 65–72. [[CrossRef](#)]
98. Palmisano, A.C.; Sullivan, C.W. Pathways of photosynthetic carbon assimilation in sea-ice microalgae from McMurdo Sound, Antarctica. *Limnol. Oceanogr.* **1985**, *30*, 674–678. [[CrossRef](#)]
99. Smith, R.E.H.; Clement, P.; Cota, G.F.; Li, W.K.W. Intracellular photosynthate allocation and the control of arctic marine ice algal production. *J. Phycol.* **2007**, *23*, 124–132. [[CrossRef](#)]
100. Smith, R.; Herman, A. In situ patterns of intracellular photosynthate allocation by sea ice algae in the Canadian high arctic. *Polar Biol.* **1992**, *12*, 545–551. [[CrossRef](#)]
101. Mock, T.; Gradinger, R. Changes in photosynthetic carbon allocation in algal assemblages of Arctic sea ice with decreasing nutrient concentrations and irradiance. *Mar. Ecol. Prog. Ser.* **2000**, *202*, 1–11. [[CrossRef](#)]
102. Li, W.K.W.; Glover, H.E.; Morris, I. Physiology of carbon photoassimilation by *Oscillatoria thiebautii* in the Caribbean Sea. *Limnol. Oceanogr.* **1980**, *25*, 447–456. [[CrossRef](#)]
103. Nichols, P.D.; Palmisano, A.C.; Rayner, M.S.; Smith, G.A.; White, D.C. Changes in the lipid composition of Antarctic sea-ice diatom communities during a spring bloom: An indication of community physiological status. *Antarct. Sci.* **1989**, *1*, 133–140. [[CrossRef](#)]

104. Leu, E.; Falk-Petersen, S.; Hessen, D.O. Ultraviolet radiation negatively affects growth but not food quality of arctic diatoms. *Limnol. Oceanogr.* **2007**, *52*, 787–797. [[CrossRef](#)]
105. McConville, M.J.; Mitchell, C.; Wetherbee, R. Patterns of carbon assimilation in a microalgal community from annual sea ice, east Antarctica. *Polar Biol.* **1985**, *4*, 135–141. [[CrossRef](#)]
106. Smith, R.E.H.; Clement, P.; Head, E. Biosynthesis and photosynthate allocation patterns of arctic ice algae. *Limnol. Oceanogr.* **1989**, *34*, 591–605. [[CrossRef](#)]
107. Cade-Menun, B.J.; Paytan, A. Nutrient temperature and light stress alter phosphorus and carbon forms in culture-grown algae. *Mar. Chem.* **2010**, *121*, 27–36. [[CrossRef](#)]
108. Heraud, P.; Wood, B.R.; Tobin, M.J.; Beardall, J.; McNaughton, D. Mapping of nutrient-induced biochemical changes in living algal cells using synchrotron infrared microspectroscopy. *FEMS Microbiol. Lett.* **2005**, *249*, 219–225. [[CrossRef](#)]
109. Heraud, P.; Wood, B.R.; Beardall, J.; McNaughton, D. Probing the Influence of the Environment on Microalgae Using Infrared and Raman Spectroscopy. *New Approaches Biomed. Spectrosc.* **2007**, *963*, 85–106. [[CrossRef](#)]
110. Dean, A.P.; Nicholson, J.M.; Sigeo, D.C. Changing patterns of carbon allocation in lake phytoplankton: An FTIR analysis. *Hydrobiologia* **2011**, *684*, 109–127. [[CrossRef](#)]
111. Fanesi, A.; Wagner, H.; Birarda, G.; Vaccari, L.; Wilhelm, C. Quantitative macromolecular patterns in phytoplankton communities resolved at the taxonomical level by single-cell Synchrotron FTIR-spectroscopy. *BMC Plant Biol.* **2019**, *19*, 142. [[CrossRef](#)] [[PubMed](#)]
112. Reffner, J.A.; Martoglio, P.A.; Williams, G.P. Fourier transform infrared microscopical analysis with synchrotron radiation: The microscope optics and system performance (invited). *Rev. Sci. Instrum.* **1995**, *66*, 1298–1302. [[CrossRef](#)]
113. Giordano, M.; Kansiz, M.; Heraud, P.; Beardall, J.; Wood, B.; McNaughton, D. Fourier transform infrared spectroscopy as a novel tool to investigate changes in intracellular macromolecular pools in the marine microalga *Chaetoceros muellerii* (bacillariophyceae). *J. Phycol.* **2001**, *37*, 271–279. [[CrossRef](#)]
114. Wagner, H.; Liu, Z.; Langner, U.; Stehfest, K.; Wilhelm, C. The use of FTIR spectroscopy to assess quantitative changes in the biochemical composition of microalgae. *J. Biophotonics* **2010**, *3*, 557–566. [[CrossRef](#)]
115. Sigeo, D.C.; Bahrami, F.; Estrada, B.; Webster, R.E.; Dean, A.P.; Elizabeth, R.; Peter Dean, A.; Sigeo, D.C.; Bahrami, F.; Estrada, B.; et al. The influence of phosphorus availability on carbon allocation and P quota in *Scenedesmus subspicatus*: A synchrotron-based FTIR analysis. *Phycologia* **2007**, *46*, 583–592. [[CrossRef](#)]
116. Findlay, C.; Morrison, J.; Mundy, C.J.; Sedlmair, J.; Hirschmugl, C.J.; Gough, K.M. Thermal source Fourier transform infrared microtomography applied to Arctic sea ice diatoms. *Analyst* **2017**, *142*, 660–669. [[CrossRef](#)] [[PubMed](#)]
117. Sackett, O.; Armand, L.; Beardall, J.; Hill, R.; Doblin, M.; Connelly, C.; Howes, J.; Stuart, B.; Ralph, P.; Heraud, P. Taxon-specific responses of Southern Ocean diatoms to Fe enrichment revealed by synchrotron radiation FTIR microspectroscopy. *Biogeosciences* **2014**, *11*, 5795–5808. [[CrossRef](#)]
118. Boetius, A.; Anesio, A.M.; Deming, J.M.; Mikucki, J.A.; Rapp, J.Z. Microbial ecology of the cryosphere: Sea ice and glacial habitats. *Nat. Rev.* **2015**, *13*, 677–690. [[CrossRef](#)]
119. Gleitz, M.; Thomas, D.N. Variation in phytoplankton standing stock, chemical composition and physiology during sea-ice formation in the southeastern Weddell Sea, Antarctica. *J. Exp. Mar. Biol. Ecol.* **1993**, *173*, 211–230. [[CrossRef](#)]
120. Thomas, D.N.; Dieckmann, G.S. Biogeochemistry of antarctic sea ice. In *Oceanography and Marine Biology, an Annual Review*; Gibson, R.N., Barnes, M., Atkinson, A., Taylor, R.J., Eds.; CRC Press: Boca Raton, FL, USA, 2002; Volume 40, pp. 151–156, ISBN 9780429217722.
121. Jacobs, S.S.; Giulivi, C.F.; Mele, P.A. Freshening of the ross sea during the late 20th century. *Science* **2002**, *297*, 386–389. [[CrossRef](#)]
122. Brown, K.A.; Holding, J.M.; Carmack, E.C. Understanding regional and seasonal variability is key to gaining a pan-arctic perspective on arctic ocean freshening. *Front. Mar. Sci.* **2020**, *7*, 606. [[CrossRef](#)]
123. Lee, S.H.; Whitley, T.E.; Kang, S.-H. Carbon uptake rates of sea ice algae and phytoplankton under different light intensities in a landfast sea ice zone, Barrow, Alaska. *Arctic* **2009**, *61*, 281–291. [[CrossRef](#)]
124. Leu, E.; Wängberg, S.-Å.; Wulff, A.; Falk-Petersen, S.; Ørbæk, J.B.; Hessen, D.O. Effects of changes in ambient PAR and UV radiation on the nutritional quality of an Arctic diatom (*Thalassiosira antarctica* var. *borealis*). *J. Exp. Mar. Biol. Ecol.* **2006**, *337*, 65–81. [[CrossRef](#)]
125. Budge, S.M.; Wooler, M.J.; Springer, A.M.; Iverson, S.J.; McRoy, C.P.; Divoky, G.J. Tracing carbon flow in an arctic marine food web using fatty acid-stable isotope analysis. *Oecologia* **2008**, *157*, 117–129. [[CrossRef](#)] [[PubMed](#)]
126. Lavoie, D.; Denman, K.; Michel, C. Modeling ice algal growth and decline in a seasonally ice-covered region of the Arctic (Resolute Passage, Canadian Archipelago). *J. Geophys. Res. Space Phys.* **2005**, *110*, 1–17. [[CrossRef](#)]
127. Rozanska, M.; Gosselin, M.; Poulin, M.; Wiktor, J.; Michel, C. Influence of environmental factors on the development of bottom ice protist communities during the winter–spring transition. *Mar. Ecol. Prog. Ser.* **2009**, *386*, 43–59. [[CrossRef](#)]
128. Vancoppenolle, M.; Bopp, L.; Madec, G.; Dunne, J.; Ilyina, T.; Halloran, P.R.; Steiner, N. Future Arctic Ocean primary productivity from CMIP5 simulations: Uncertain outcome, but consistent mechanisms. *Glob. Biogeochem. Cycles* **2013**, *27*, 605–619. [[CrossRef](#)]
129. Slagstad, D.; Wassmann, P.F.J.; Ellingsen, I. Physical constrains and productivity in the future Arctic Ocean. *Front. Mar. Sci.* **2015**, *2*, 85. [[CrossRef](#)]
130. Jiang, Y.; Yoshida, T.; Quigg, A. Photosynthetic performance, lipid production and biomass composition in response to nitrogen limitation in marine microalgae. *Plant Physiol. Biochem.* **2012**, *54*, 70–77. [[CrossRef](#)]

131. Chen, J.-J.; Li, Y.-R.; Lai, W.-L. Application of experimental design methodology for optimization of biofuel production from microalgae. *Biomass Bioenergy* **2014**, *64*, 11–19. [[CrossRef](#)]
132. Chokshi, K.; Pancha, I.; Ghosh, A.; Mishra, S. Nitrogen starvation-induced cellular crosstalk of ROS-scavenging antioxidants and phytohormone enhanced the biofuel potential of green microalga *Acutodesmus dimorphus*. *Biotechnol. Biofuels* **2017**, *10*, 60. [[CrossRef](#)] [[PubMed](#)]
133. Rehman, Z.U.; Anal, A.K. Enhanced lipid and starch productivity of microalga (*Chlorococcum* sp. TISTR 8583) with nitrogen limitation following effective pretreatments for biofuel production. *Biotechnol. Rep.* **2019**, *21*, e00298. [[CrossRef](#)]
134. Dean, A.P.; Sigee, D.C.; Estrada, B.; Pittman, J.K. Using FTIR spectroscopy for rapid determination of lipid accumulation in response to nitrogen limitation in freshwater microalgae. *Bioresour. Technol.* **2010**, *101*, 4499–4507. [[CrossRef](#)] [[PubMed](#)]
135. Berges, J.A.; Charlebois, D.O.; Mauzerall, D.C.; Falkowski, P.G. Differential Effects of Nitrogen Limitation on Photosynthetic Efficiency of Photosystems I and II in Microalgae. *Plant Physiol.* **1996**, *110*, 689–696. [[CrossRef](#)] [[PubMed](#)]
136. Berges, J.A.; Falkowski, P.G. Physiological stress and cell death in marine phytoplankton: Induction of proteases in response to nitrogen or light limitation. *Limnol. Oceanogr.* **1998**, *43*, 129–135. [[CrossRef](#)]
137. Peltomaa, E.T.; Aalto, S.L.; Vuorio, K.M.; Taipale, S.J. The Importance of Phytoplankton Biomolecule Availability for Secondary Production. *Front. Ecol. Evol.* **2017**, *5*, 128. [[CrossRef](#)]
138. Hancock, A.M.; King, C.K.; Stark, J.S.; McMinn, A.; Davidson, A.T. Effects of ocean acidification on Antarctic marine organisms: A meta-analysis. *Ecol. Evol.* **2020**, *10*, 4495–4514. [[CrossRef](#)]
139. Petrou, K.; Kranz, S.A.; Trimborn, S.; Hassler, C.S.; Blanco-Ameijeiras, S.; Sackett, O.; Ralph, P.J.; Davidson, A.T. Southern Ocean phytoplankton physiology in a changing climate. *J. Plant Physiol.* **2016**, *203*, 135–150. [[CrossRef](#)]
140. IPCC. *Climate Change 2014: Impacts, Adaptation, and Vulnerability. Part A: Global and Sectoral Aspects. Contribution of Working Group II to the Fifth Assessment Report of the Intergovernmental Panel on Climate Change*; Field, C.B., Barros, V.R., Dokken, D.J., Mach, K.J., Mastrandrea, M.D., Bilir, T.E., Chatterjee, M., Ebi, K.L., Estrada, Y.O., Genova, R.C., et al., Eds.; Cambridge University Press: Cambridge, UK; New York, NY, USA, 2014; pp. 411–484.
141. Bestion, E.; Haegeman, B.; Codesal, S.A.; Garreau, A.; Huet, M.; Barton, S.; Montoya, J.M. Phytoplankton biodiversity is more important for ecosystem functioning in highly variable thermal environments. *Proc. Natl. Acad. Sci. USA* **2021**, *118*, e2019591118. [[CrossRef](#)] [[PubMed](#)]
142. Hancock, A.M.; Davidson, A.T.; McKinlay, J.; McMinn, A.; Schulz, K.G.; Enden, R.L.V.D. Ocean acidification changes the structure of an Antarctic coastal protistan community. *Biogeosciences* **2018**, *15*, 2393–2410. [[CrossRef](#)]
143. Sugie, K.; Fujiwara, A.; Nishino, S.; Kameyama, S.; Harada, N. Impacts of temperature, CO<sub>2</sub>, and salinity on phytoplankton community composition in the Western Arctic Ocean. *Front. Mar. Sci.* **2020**, *6*, 821. [[CrossRef](#)]
144. Moline, M.A.; Claustre, H.; Frazer, T.K.; Schofield, O.; Vernet, M. Alteration of the food web along the Antarctic Peninsula in response to a regional warming trend. *Glob. Chang. Biol.* **2004**, *10*, 1973–1980. [[CrossRef](#)]
145. Li, W.K.W.; McLaughlin, F.A.; Lovejoy, C.; Carmack, E.C. Smallest Algae Thrive As the Arctic Ocean Freshens. *Science* **2009**, *326*, 539. [[CrossRef](#)]
146. Montes-Hugo, M.; Doney, S.C.; Ducklow, H.W.; Fraser, W.; Martinson, D.; Stammerjohn, S.E.; Schofield, O. Recent changes in phytoplankton communities associated with rapid regional climate change along the Western Antarctic Peninsula. *Science* **2009**, *323*, 1470–1473. [[CrossRef](#)] [[PubMed](#)]
147. Neeley, A.R.; Harris, L.A.; Frey, K.E. Unraveling phytoplankton community dynamics in the Northern Chukchi sea under sea-ice-covered and sea-ice-free conditions. *Geophys. Res. Lett.* **2018**, *45*, 7663–7671. [[CrossRef](#)]
148. Boyd, C.M.; Heyraud, M.; Boyd, C.N. Feeding of the Antarctic Krill *Euphausia superba*. *J. Crustac. Biol.* **1984**, *4*, 123–141. [[CrossRef](#)]
149. Quetin, L.B.; Ross, R.M. Feeding by Antarctic Krill, *Euphausia superba*: Does size matter? In *Antarctic Nutrient Cycles and Food Webs*; Springer: Berlin/Heidelberg, Germany, 1985; pp. 372–377. [[CrossRef](#)]
150. Moline, M.A.; Claustre, H.; Frazer, T.K.; Grzymiskj, J.O.E.; Schofield, O.; Verner, M. Changes in phytoplankton assemblages along the Antarctic Peninsula and potential implications for the antarctic food web. In *Antarctic Ecosystems: Models for Wider Ecological Understanding*; Davidson, W., Howard-Williams, C., Broady, P., Eds.; New Zealand Natural Sciences: Christchurch, New Zealand, 2001; pp. 263–271.
151. Campbell, K.; Mundy, C.J.; Belzile, C.; Delaforge, A.; Rysgaard, S. Seasonal dynamics of algal and bacterial communities in Arctic sea ice under variable snow cover. *Polar Biol.* **2018**, *41*, 41–58. [[CrossRef](#)]
152. Saggiomo, M.; Escalera, L.; Saggiomo, V.; Bolinesi, F.; Mangoni, O. Phytoplankton blooms below the antarctic landfast ice during the melt season between late spring and early summer. *J. Phycol.* **2020**, *57*, 541–550. [[CrossRef](#)] [[PubMed](#)]
153. Hygum, B.H.; Rey, C.; Hansen, B.W.; Tande, K. Importance of food quantity to structural growth rate and neutral lipid reserves accumulated in *Calanus finmarchicus*. *Mar. Biol.* **2000**, *136*, 1057–1073. [[CrossRef](#)]
154. Thingstad, T.F.; Bellerby, R.G.J.; Bratbak, G.; Børshheim, K.Y.; Egge, J.K.; Heldal, M.; Larsen, A.; Neill, C.; Nejtgaard, J.; Norland, S.; et al. Counterintuitive carbon-to-nutrient coupling in an Arctic pelagic ecosystem. *Nat. Cell Biol.* **2008**, *455*, 387–390. [[CrossRef](#)] [[PubMed](#)]
155. Krause, J.W.; Duarte, C.M.; Marquez, I.A.; Assmy, P.; Fernández-Méndez, M.; Wiedmann, I.; Wassmann, P.; Kristiansen, S.; Agustí, S. Biogenic silica production and diatom dynamics in the Svalbard region during spring. *Biogeosciences* **2018**, *15*, 6503–6517. [[CrossRef](#)]

156. Li, Z.; Zhao, J.; Su, J.; Li, C.; Cheng, B.; Hui, F.; Yang, Q.; Shi, L. Spatial and Temporal variations in the extent and thickness of Arctic landfast ice. *Remote Sens.* **2019**, *12*, 64. [[CrossRef](#)]
157. Turner, J.; Phillips, T.; Marshall, G.J.; Hosking, J.S.; Pope, J.O.; Bracegirdle, T.J.; Deb, P. Unprecedented springtime retreat of Antarctic sea ice in 2016. *Geophys. Res. Lett.* **2017**, *44*, 6868–6875. [[CrossRef](#)]
158. Kim, S.; Saenz, B.; Scanniello, J.; Daly, K.; Ainley, D. Local climatology of fast ice in McMurdo Sound, Antarctica. *Antarct. Sci.* **2018**, *30*, 125–142. [[CrossRef](#)]
159. Palmer, M.; Saenz, B.T.; Arrigo, K.R. Impacts of sea ice retreat, thinning, and melt-pond proliferation on the summer phytoplankton bloom in the Chukchi Sea, Arctic Ocean. *Deep Sea Res. Part II Top. Stud. Oceanogr.* **2014**, *105*, 85–104. [[CrossRef](#)]
160. Arrigo, K.R.; Van Dijken, G. Continued increases in Arctic Ocean primary production. *Prog. Oceanogr.* **2015**, *136*, 60–70. [[CrossRef](#)]
161. Stammerjohn, S.E.; Massom, R.; Rind, D.; Martinson, D.G. Regions of rapid sea ice change: An inter-hemispheric seasonal comparison. *Geophys. Res. Lett.* **2012**, *39*, 6501. [[CrossRef](#)]
162. Lee, J.; Raymond, B.; Bracegirdle, T.J.; Chadès, I.; Fuller, R.; Shaw, J.; Terauds, A. Climate change drives expansion of Antarctic ice-free habitat. *Nature* **2017**, *547*, 49–54. [[CrossRef](#)] [[PubMed](#)]
163. Lewis, K.M.; van Dijken, G.L.; Arrigo, K.R. Changes in phytoplankton concentration now drive increased Arctic Ocean primary production. *Science* **2020**, *369*, 198–202. [[CrossRef](#)]
164. Kahru, M.; Brotas, V.; Manzano-Sarabia, M.; Mitchell, B.G. Are phytoplankton blooms occurring earlier in the Arctic? *Glob. Chang. Biol.* **2010**, *17*, 1733–1739. [[CrossRef](#)]
165. McConnell, B.; Gradinger, R.; Iken, K.; Bluhm, B.A. Growth rates of arctic juvenile *Scolelepis squamata* (Polychaeta: Spionidae) isolated from Chukchi Sea fast ice. *Polar Biol.* **2012**, *35*, 1487–1494. [[CrossRef](#)]
166. Koeller, P.; Fuentes-Yaco, C.; Platt, T.; Sathyendranath, S.; Richards, A.; Ouellet, P.; Orr, D.; Skúladóttir, U.; Wieland, K.; Savard, L.; et al. Basin-scale coherence in phenology of shrimps and phytoplankton in the North Atlantic Ocean. *Science* **2009**, *324*, 791–793. [[CrossRef](#)]
167. Dünweber, M.; Swalethorp, R.; Kjellerup, S.; Nielsen, T.; Arendt, K.; Hjorth, M.; Tönnesson, K.; Møller, E.F. Succession and fate of the spring diatom bloom in Disko Bay, western Greenland. *Mar. Ecol. Prog. Ser.* **2010**, *419*, 11–29. [[CrossRef](#)]
168. Henley, S.F.; Schofield, O.; Hendry, K.; Schloss, I.R.; Steinberg, D.K.; Moffat, C.; Peck, L.S.; Costa, D.; Bakker, D.; Hughes, C.; et al. Variability and change in the west Antarctic Peninsula marine system: Research priorities and opportunities. *Prog. Oceanogr.* **2019**, *173*, 208–237. [[CrossRef](#)]



## Spatio-temporal dynamics in microalgal communities in Arctic land-fast sea ice

Rebecca J. Duncan<sup>a,b,\*</sup>, Janne E. Søreide<sup>b</sup>, Øystein Varpe<sup>c,d</sup>, Józef Wiktor<sup>e</sup>, Vanessa Pitusi<sup>b,f</sup>, Elaine Runge<sup>b,g</sup>, Katherina Petrou<sup>a</sup>

<sup>a</sup> School of Life Sciences, University of Technology Sydney, NSW, Australia

<sup>b</sup> Department of Arctic Biology, The University Centre in Svalbard, Longyearbyen, Norway

<sup>c</sup> Department of Biological Sciences, University of Bergen, Bergen, Norway

<sup>d</sup> Norwegian Institute for Nature Research, Bergen, Norway

<sup>e</sup> Institute of Oceanology, Polish Academy of Sciences, Sopot, Poland

<sup>f</sup> Department of Arctic and Marine Biology, University in Tromsø, Tromsø, Norway

<sup>g</sup> Department of Natural Sciences, University of Copenhagen, Copenhagen, Denmark

### ARTICLE INFO

#### Keywords:

Sea ice microalgae  
Svalbard  
*Nitzschia frigida*  
biogeochemical cycling  
under ice light transmittance

### ABSTRACT

Sea ice microalgae are an important source of energy for the polar marine food web, representing the primary carbon source prior to pelagic phytoplankton blooms. Here we investigate community dynamics of sea ice microalgal communities in land-fast sea ice across six different fjords in high-Arctic Svalbard, Norway, during Spring (April – May). We found that light (0.1 – 23% incoming PAR / 0.1 – 193  $\mu\text{mol photons m}^{-2}\text{s}^{-1}$ ) played a central role in determining community composition, with more diverse assemblages observed in sites with more light transmitted to the bottom ice community. In April, microalgal assemblages were similar when under-ice light transmittance was similar, independent of geographical location, however this light-derived separation of community structure was not evident in May. At all sites, assemblages were dominated by pennate diatoms, with the most abundant taxon being *Nitzschia frigida*. However, with increasing under-ice light transmittance, we saw an increase in the relative abundance of Dinophyceae, *Navicula* spp. and *Thalassiosira* spp.. A positive relationship between light and  $\delta^{13}\text{C}$  enrichment and C:N ratios in the ice algal biomass demonstrated the effect of light on the biochemical composition of ice algae. Light did not correlate with cell abundance or chlorophyll *a* concentration. With anticipated changes to Arctic sea ice extent and snow cover as a result of climate change, we will see shifts in the light transmitted to the bottom ice community. These shifts, whether caused by reduced light transmittance from increased snow cover or increased light transmittance from thinning ice, snow depth or increased rainfall, will likely alter sea ice microalgal community composition, which in turn, may influence the success of secondary production and biogeochemical cycling in polar waters.

### 1. Introduction:

The sea ice-ocean interface forms a unique environment that provides a habitat for microalgae and micrograzers to live within a network of brine channels and tubes that exist on the bottom of the ice (Arrigo, 2014). This space-limited environment is characterised by sub-zero temperatures, changing nutrient availability, variable salinity and low light, frequently receiving < 10% incoming (incident) irradiance (Arrigo, 2014). The specialised photosynthetic sea ice biota that thrive in these dynamic physiochemical conditions are an important contribution to polar primary production. During spring, the biomass of the

bottom ice assemblages can be up to ten times higher than for the adjacent seawater (Comeau et al., 2013; Michel et al., 1996), with values above 25 g C m<sup>-2</sup> yr<sup>-1</sup> often recorded (Smith et al., 1988). Thus, sea ice microalgal communities are an important source of energy for the polar marine food web (Kunisch et al., 2021; Michel et al., 1996).

The contribution of sea ice microalgae to primary production varies across time and space, ranging from 1 - 60% in ice-covered Arctic waters (Fernández-Méndez et al., 2015; Gosselin et al., 1997; Gradinger, 2009), and are a primary source of organic carbon for pelagic consumers in the early spring, extending biological production in polar waters by up to three months (Cota et al., 1991; Ji et al., 2013). In providing this initial

\* Corresponding author at: University Technology Sydney, Building 7, 67 Thomas St, Ultimo, NSW Australia 2007.

E-mail address: [rebecca.duncan@uts.edu.au](mailto:rebecca.duncan@uts.edu.au) (R.J. Duncan).

<https://doi.org/10.1016/j.pocean.2024.103248>

Received 6 April 2023; Received in revised form 8 February 2024; Accepted 24 March 2024

Available online 27 March 2024

0079-6611/© 2024 The Author(s). Published by Elsevier Ltd. This is an open access article under the CC BY license (<http://creativecommons.org/licenses/by/4.0/>).



food source during the early phases of seasonal zooplankton reproduction, sea ice algae play an important role in the quantity and quality of secondary production (Durbin & Casas, 2014; Leu et al., 2011; Søreide et al., 2010). In addition, sea ice algae are intricately linked with pelagic primary producers. With some taxa able to thrive in both the sympagic and pelagic environment, they may play a role in seeding the late spring/early summer pelagic phytoplankton blooms (Michel et al., 1993; Runge & Ingram, 1991; Tedesco et al., 2012). The sea ice algal cells not consumed in the water column, will often deposit on the sea floor and shallow littoral zone in a dormant or vegetative state, before being resuspended the following winter and spring (Vonnahme, 2021). In deeper areas, sea ice algal biomass is exported to depth where it is deposited on the ocean floor or remineralized (Boetius et al., 2013).

Diatoms (Bacillariophyceae) dominate sea ice algal communities (Arrigo, 2014; Hop et al., 2020; Horner, 1985). However, diversity within ice algal communities can vary from fewer than 20 taxa to over 150 taxa (Arrigo, 2014; Campbell et al., 2018; Hop et al., 2020), where the composition is controlled largely by species-specific responses to temperature, salinity, light, and nutrients (Campbell et al., 2018; Hop et al., 2020). For example, taxonomic diversity has been shown to increase with reduced sea ice thickness, related to a weakened dominance of *Nitzschia frigida* as the ice thins (Hegseth & von Quillfeldt, 2022). Similarly, centric diatoms can increase their relative abundance compared to pennate diatoms under higher light conditions (Campbell et al., 2018), whereas flagellates tend to outcompete diatoms when light is severely restricted (Rozanska et al., 2009). These dynamics in community composition affect carbon and nutrient cycling, as regulation of photosynthetic state (Kvernvik et al., 2021; Petrou & Ralph, 2011) and nutritional content are species specific in polar microalgae (Duncan et al., 2024; Duncan et al., 2022; Sackett et al., 2013). Furthermore, sea ice algal size structure influences nutrient uptake efficiency by primary consumers (Quetin & Ross, 1985) and nutrient supply and transfer to higher trophic levels (Hitchcock, 1982). Sea ice associated taxa are generally larger and more often chain-forming than open-oceanic phytoplankton (Arrigo, 2014). A community of larger cells in conjunction with the presence of aggregated chains, impacts the grazing efficiency due to micro- and mesozooplankton having a defined prey size range within which they can effectively graze (Berggreen et al., 1988; Quetin & Ross, 1985). In addition, in the early season when grazing pressure in the pelagic zone is minimal, the aggregated chains sink more quickly than single cells (Riebesell et al., 1991) to the ocean floor becoming an important food source for the benthos (McMahon et al., 2006). Taken together, community characteristics of size structure, nutritional content, growth rate and photosynthetic state are key to determining the extent to which the sea ice algae support the polar marine food web.

Thickness and areal coverage of land-fast ice has been declining rapidly for the past four decades across the Arctic (Yu et al., 2014) and in some areas, it has been reported to be declining at twice the rate of pack ice (Li et al., 2019). In Svalbard, land-fast ice extent in 2005-2019 was at 50% of the extent recorded in 1973-2000, with projections that the extent will decline to only 12% in the next 10-20 years (Urbański & Litwicka, 2022). In addition, the duration of sea ice coverage in Svalbard has reduced by up to four months since 2005 (Urbański & Litwicka, 2022), meaning the incorporation of sea ice assemblages into the ice is delayed and bloom termination and end of season ice melting occurs earlier. To understand the implications of such a decline in land-fast ice extent and duration on marine biodiversity and ecosystem function, it is important to understand how land-fast ice algal communities are affected by environmental change. To date, most studies into the composition of sea ice algal communities and their dynamics have focussed on pack ice communities. However, a handful of studies comparing algal communities between pack and land-fast ice (Archer et al., 1996; Comeau et al., 2013; Ratkova & Wassmann, 2005) found significant compositional differences between habitats, suggesting that our understanding of land-fast ice algal community dynamics is

incomplete.

This study investigates the relationship between land-fast sea ice algal community composition and light transmissivity over the spring season (April-May) in Svalbard, Norway. Land-fast ice within six geographically distinct fjords was sampled to investigate spatial dynamics, while one fjord (Van Mijenfjorden) was sampled repeatedly throughout the spring to capture seasonality. The first hypothesis that is investigated is that sites with less snow cover and ice thickness, and therefore higher light transmissivity (higher under-ice light climate), would have a more abundant and taxonomically diverse algal community, with increased contributions of common pelagic taxa. The second hypothesis tested is that algal abundance and diversity would increase with the progression of spring until late spring, after which the advection of warmer waters would result in ice melt, attenuating community diversity and abundance.

### 1.1. Study Area

This study was conducted within six fjords in Svalbard, Norway (Fig. 1; Table S1) between April-May 2021. The sampling locations covered the west, north and east coasts of Spitsbergen; Van Mijenfjorden, Tempelfjorden, Billefjorden, Austfjorden, Agardhbukta and Inglefieldbukta. Whilst the sampling sites are relatively close by land access, they are not close oceanographically and are influenced by different water masses, meaning they are markedly different in their conditions. Van Mijenfjorden (70 km long and 10 km wide) is located on the south western coast. It is comprised of an inner basin with an approximate depth of 70 m and an outer basin approximately 120 m deep (Høyland, 2009). It is a partially enclosed fjord due to the presence of Akseløya island at the fjord mouth (Høyland, 2009), which minimises the advection of warm, saline Atlantic water transported to the area by the West Spitsbergen Current (WSC). The rather shallow and isolated fjord is efficiently cooled when air temperatures drop so the conditions are favourable for seasonal ice formation from January to June (Høyland, 2009). Tempelfjorden (14 km long and 5 km wide) is the innermost branch of Isfjorden, located in the central west coast and is divided into two basins; a smaller, glacial fed basin in the inner fjord up to 70 m deep and a central-outer basin up to 110 m deep (Forwick et al., 2010). Petuniabukta (6 km long and 3.5 km wide), is the innermost bay of another branch of Isfjorden - Billefjorden. A shallow sill prevents much of the advection of warm, Atlantic water penetrating the main area of Isfjorden, meaning sea ice cover generally persists from December-June in inner Billefjorden (Søreide et al., 2022). Austfjorden (35 km long and 5 km wide) is the innermost part of the 75 km long Wijdefjorden (totalling 110 km long), located on the north coast. The long, narrow nature of this fjord, and limited water exchange with offshore area due a cross-fjord sill, ensures reliable sea ice cover throughout January-May (Allaart et al., 2020). Inglefieldbukta (2.5 km wide bay) and Agardhbukta (8 km wide bay) are located on the south eastern coast of Spitsbergen and are exposed to cold Arctic water masses passing through adjacent Storfjorden. In addition, Inglefieldbukta receives glacial runoff from Inglefieldbreen. These sites have extensive snow and ice cover during December - July (Haarpaintner et al., 2001).

## 2. Materials & Methods

### 2.1. Sample Collection

Samples of sea ice algae were collected from the ice-water interface using a Kovacs core barrel (9 cm diameter; Kovacs Enterprise, USA). The bottom 3 cm of the sea ice was retained only (Smith et al., 1988). At each sampling site, six cores were taken approximately 1 m apart, with care taken to ensure the coring location was not disturbed. Cores were then pooled into triplicates, as cores 1-2, 3-4 and 5-6. Filtered seawater (100 ml of 0.7 µm GF/F) was added for each cm of core, to minimise osmotic stress (Campbell et al., 2019) and samples allowed to melt in darkness

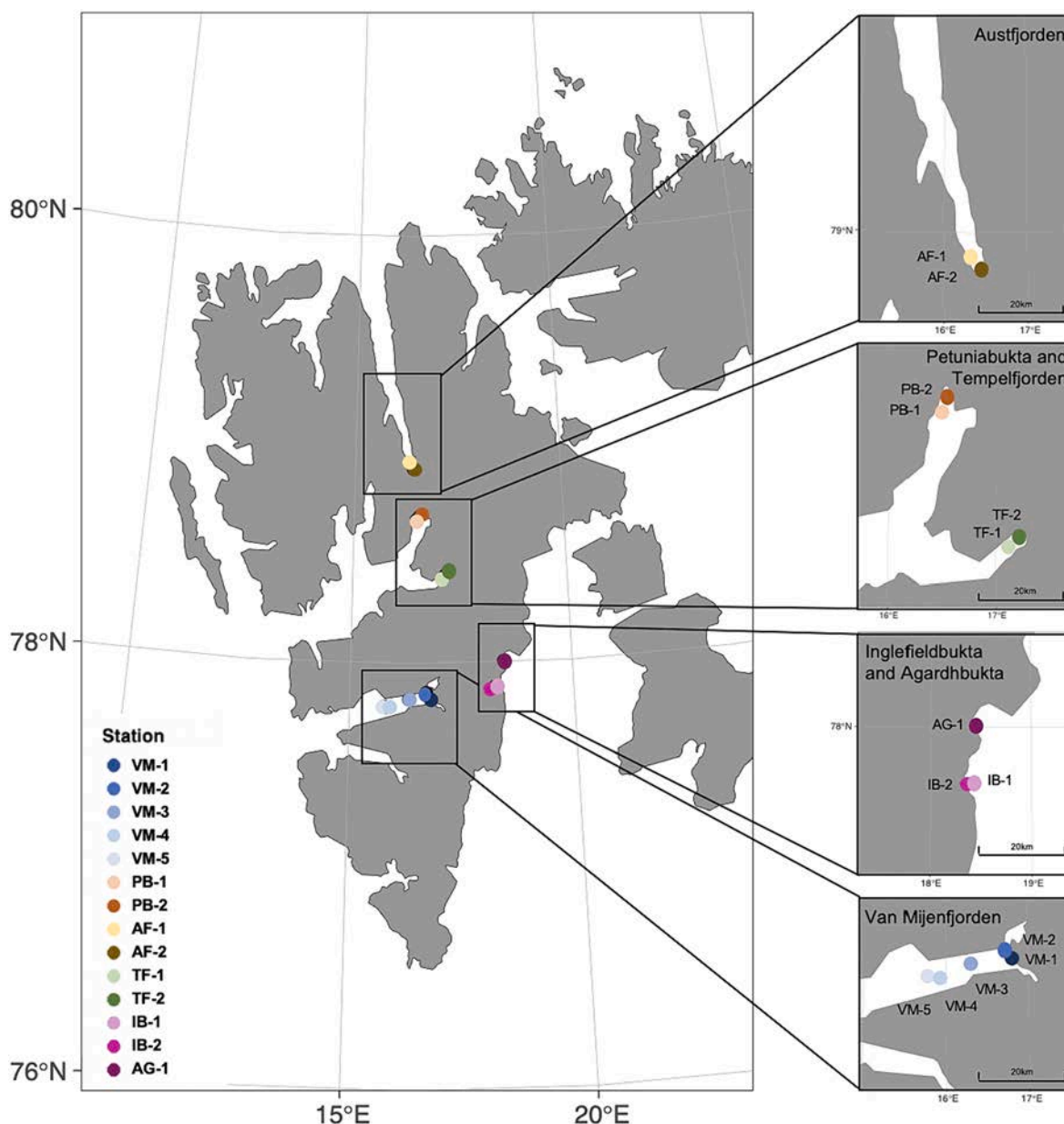


Fig. 1. Land-fast sea ice sampling locations visited between April- May 2021, within various fjords of Svalbard, Norway.

for 24 h at 4 °C. From each of the three pooled cores, subsamples of known volume were taken for determination of community composition, chlorophyll *a* (chl *a*) and particulate organic carbon and nitrogen (C:N). At each sampling event (date and station), under-ice water was collected using a 5L Niskin water sampler (KC Denmark, Silkeborg) and subsampled for chl *a*, particulate organic C:N and nutrient (nitrate plus nitrite ( $\text{NO}_3^- + \text{NO}_2^-$ ), phosphate ( $\text{PO}_4^{3-}$ ) and silicic acid ( $\text{Si}(\text{OH})_4$ ) and ammonium ( $\text{NH}_4^+$ )) analyses.

## 2.2. Physical Parameters

Prior to each core extraction, three snow depth measurements were taken using a standard ruler to determine snow depth in close vicinity to the planned core. Following core extraction, ice thickness was measured using a Kovacs ice thickness gauge (Kovacs Enterprise, Oregon, USA). Freeboard was measured at each core hole using a standard ruler. At each sampling event, two additional ice cores were taken to measure a salinity and temperature profile of the sea ice column. The temperature profile was measured *in situ*, in 10 cm intervals along the core. Following

complete melting of separate 10 cm sections, salinity of each section was measured (Thermo Scientific Orion Versa Star Pro). At each sampling site, approximately 100 ml of the water collected from the ice-water interface was put into acid washed bottles and stored at -20 °C until nutrient analyses were performed. The  $\text{NO}_3^- + \text{NO}_2^-$ ,  $\text{PO}_4^{3-}$ ,  $\text{Si}(\text{OH})_4$  and  $\text{NH}_4^+$  concentrations ( $\mu\text{M/L}$ ) were measured simultaneously on a San++ 5000 automated analyzer (Skalar: Breda, Netherlands), with separate channels for the four nutrients. The detection limits were 0.02  $\mu\text{M/L}$  for  $\text{NO}_3^- + \text{NO}_2^-$ , 0.01  $\mu\text{M/L}$  for  $\text{PO}_4^{3-}$ , 0.25  $\mu\text{M/L}$  for  $\text{Si}(\text{OH})_4$  and 0.3  $\mu\text{M/L}$  for  $\text{NH}_4^+$ . At most sampling locations, a full temperature and salinity profile was measured of the water column below the ice using a CTD probe (STD/CTD SD204, SAIV A/S: Bergen, Norway). Brine salinity and volume were calculated according to (Cox & Weeks, 1983).

For the C:N and  $\delta^{13}\text{C}$  and  $\delta^{15}\text{N}$  stable isotope analysis, all six ice cores from each sampling point were pooled to obtain a minimum weight of 20  $\mu\text{g}$  of N per filter, ensuring values were well above detection limits. Following complete melting, subsamples (300-1600 mL) of the ice cores and under-ice water (500-3000 mL) were filtered onto pre-combusted (400°C for 8h) filters (GF/F, 0.7  $\mu\text{m}$ , Whatman). The filtration was

performed until visible colouration was observed and filters stored at  $-20^{\circ}\text{C}$  until analysis (within 12 months). Filters were dried at  $60^{\circ}\text{C}$  within sterile glass petri dishes, acid fumed (37% HCL for 8h), dried at  $60^{\circ}\text{C}$  and placed into a tin cup. Samples were analysed at the Stable Isotope Facility at the University of California, Davis in an elemental analyser isotope ratio mass spectrometry (EA-IRMS) system, according to [Barrie et al. \(1989\)](#). The detection limits were  $100\ \mu\text{g C}$  for  $\delta^{13}\text{C}$  and  $20\ \mu\text{g N}$  for  $\delta^{15}\text{N}$ .

### 2.3. Light Measurements and Modelling

At each sampling event, both incoming and transmitted photosynthetic active radiation (PAR) measurements were taken at the ice-ocean interface and snow-covered surface. For each measurement, a LI-190 quantum air corrected sensor was placed on the surface of the snow facing south. In the vicinity, a small hole was made using a 10 cm diameter auger, to lower a LI-192 underwater quantum sensor on a weighted frame, under the sea ice. To avoid shadowing of the measurement area, all sensors faced south with operations performed north, and the area was undisturbed. Measurements from both sensors were collected simultaneously using a LI-1500 Data Logger (LI-COR, Nebraska, USA). These measurements were then compared to modelled data ([Table S2](#)) using the equation:

$$\text{Equation 1: } E_z = E_0 \cdot \exp(-K_d \cdot Z)$$

Where  $E_z$  is irradiance at sampling depth  $Z$  (m),  $E_0$  is the surface irradiance ( $\mu\text{mol photons m}^{-2}\text{s}^{-1}$ ) and  $K_d$  is the diffuse light attenuation coefficient ( $\text{m}^{-1}$ ). The PAR at the ice-ocean interface was estimated using *in-situ* measured irradiance at the top of snow and ice, and then attenuation through snow and ice was modelled using attenuation coefficients ( $K_d$ ) of  $20\ \text{m}^{-1}$  for snow,  $5\ \text{m}^{-1}$  for the top 10 cm of ice, and  $1\ \text{m}^{-1}$  for ice below the top 10 cm ([Perovich, 1996](#); [Varpe et al., 2015](#)).

To account for the fact that *in situ* measurements were taken at different times of day and with a range of cloud coverage conditions, percent incoming PAR was used as a proxy for under ice light at a given location, providing an estimate of the attenuation effects of the sea ice and snow depth at each site, as the differences in light conditions that the bottom ice algae communities were exposed to was determined primarily by the attenuating effects of snow depth and ice thickness. Because solar angle has a substantial effect on light quantity ([Connan-McGinty et al., 2022](#)) and cloud cover can reduce light intensity by up to 90% ([Pfister et al., 2003](#)), using percent incoming PAR allowed us to determine how effective ice and snow depth was at blocking incoming irradiance to the bottom ice community. This allowed us to utilise our unique *in situ* measurements, rather than a reliance on weather station data, which is either not available or not truly representative of the conditions in the fjords sampled. In this study, we therefore use light transmissivity to describe the percent incoming PAR under given snow and ice thicknesses.

### 2.4. Biological Parameters

#### 2.4.1. Chlorophyll *a* content

Following complete melting, subsamples (60–450 mL) of each sea ice triplicate and a volume (500–2200 mL) of under-ice water were filtered (GF/F,  $0.7\ \mu\text{m}$ , Whatman, England). The filtration was performed until visible colouration of the filter and the filters were stored frozen ( $-80^{\circ}\text{C}$ ) until extraction. Extractions were performed within three months of collection. Analyses were performed according to [Holm-Hansen & Riemann \(1978\)](#). Briefly, filters were extracted in 10 ml methanol and kept refrigerated for 24 h prior to extraction. Chl *a* content was measured with a calibrated 10-AU-005-CE fluorometer (Turner, California, USA), before and after acidifying the solution with 5% HCl ([Parsons, 2013](#)). For the sea ice samples, chl *a* content was converted to chl *a* biomass per unit ice surface area ( $\text{mg m}^{-2}$ ).

#### 2.4.2. Species Composition by Light Microscopy:

From each sampling site and date, subsamples (100 mL) were collected into a brown bottle and preserved with glutaraldehyde (2% final conc.). Between 4 and 10 mL (depending on cell density) of the well-mixed subsamples were poured into a 10 mL Utermöhl cylinder (KC Denmark, Silkeborg, Denmark) and the cells were allowed to settle for 6–24 h, depending on volume ([Edler & Elbrächter, 2010](#)). Cells were counted at 400x magnification and identified to lowest taxonomic level possible. The identification of species and groups was primarily based on the work of [Tomas \(1997\)](#) and [Wiktor et al. \(1995\)](#). It is unlikely that all pico- or nanoflagellates were captured. To ensure rare taxa were captured as much as possible, a whole chamber counting approach was employed. Qualitative and quantitative analyses were conducted under Nikon TS100 microscope, within 9 months of sample collection.

### 2.5. Data Analyses

To determine patterns in under ice community composition, similarity matrices were constructed using the Bray-Curtis coefficient on square root-transformed data ([Somerfield et al., 2021](#)) and visualised using non-metric multidimensional scaling (nMDS). The community composition of all sampled sites was contrasted between high light transmissivity (HLT) (>4% incoming PAR) and low light transmissivity (LLT) (< 3% incoming PAR) sites throughout the sampling period (14<sup>th</sup> April 2021 – 25<sup>th</sup> May 2021) by analysis of similarities (ANOSIM, [Clarke & Warwick 1994](#)), with the groupings established by ANOSIM, to determine if community composition was similar within similar light levels, independent of geographic location. The light groupings were determined based on the potential for photoinhibition in some ice-algal taxa beyond ~3% incoming PAR/  $20\ \mu\text{mol photons m}^{-2}\text{s}^{-1}$  ([Palmisano et al., 1985](#); [Ryan et al., 2011](#)) and ensured sufficient replication for statistical comparison. To avoid temporal confounding between samples taken during different periods of the spring season while accounting for all sampling events, samples were divided into ‘April’ (14<sup>th</sup> – 30<sup>th</sup> April) and ‘May’ (4<sup>th</sup> – 25<sup>th</sup> May). The specific taxa contributing most to similarities/dissimilarities between the HLT and LLT sites were determined using similarity percentage analysis (SIMPER). To determine correlations between the community contribution of specific taxa, a correlation plot was created, using a correlation matrix of the percentage of community contribution of each taxon.

To establish relationships between percentage contribution to community composition of taxonomic groups ([Fig. 2-3](#)) and percent incoming PAR, a linear regression (95% confidence interval) was applied to each taxonomic group, including all sampling events. In cases in which the data were poorly explained by a linear fit, a second order polynomial regression was applied. The Shapiro–Wilks ([Shapiro & Wilk, 1965](#)) test for normality showed that the modelled light and cell density data required  $\log_{10}$  transformation before analysis. Regressions were tested for overall model significance using the  $F$  statistic ( $P < 0.05$ ) and strength of fit using  $R^2$ . The residuals of all regressions were verified for homoscedasticity. Differences in cell density between HLT and LLT sampling sites in April and in May were determined using PERMANOVA. Differences between C:N and stable isotopes of organic carbon and nitrogen between HLT and LLT sites were determined using a Welch t-test. To investigate which environmental variables account for a significant difference in the species composition, redundancy analysis (RDA) was performed, constrained to environmental variables ( $n = 15$ ) with Monte Carlo permutations (999), and only significant vectors are displayed. The percent incoming PAR levels used throughout all statistical analyses were taken from the modelled light, to ensure consistency and avoid any data gaps. All analyses were performed using RStudio v. 2022.02.03 (R Core Team, 2022) and the add-on packages ‘vegan’ v.2.5-7 ([Oksanen et al., 2013](#)), ‘ggplot2’ v.3.3.6 ([Wickham et al., 2016](#)) and ‘dplyr’ v.1.0.8 ([Wickham et al., 2019](#)).

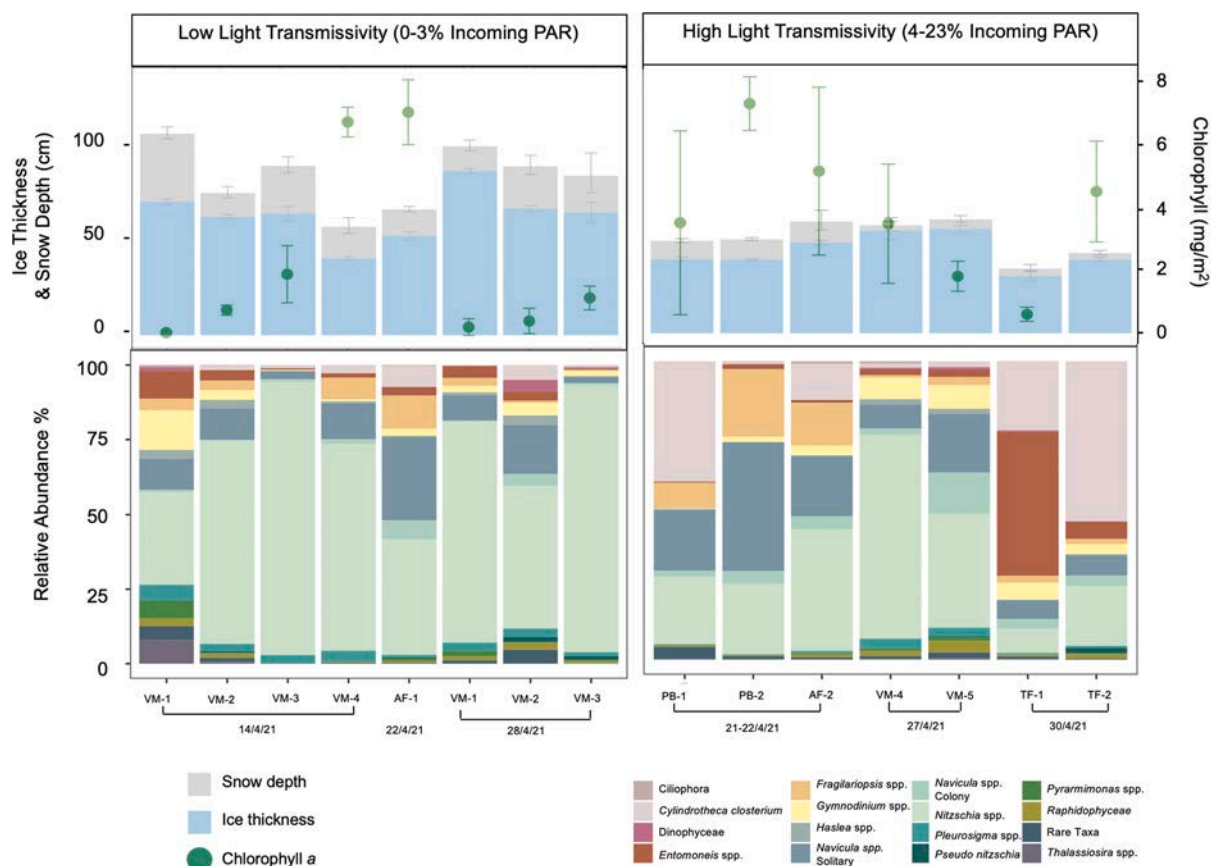


**Fig. 2.** Bottom ice microalgal community composition from low light transmissivity (left) and high light transmissivity (right) sites sampled during April 2021, in Svalbard, Norway. Snow depth (grey), ice thickness (blue), and chlorophyll *a* content (mg/m<sup>2</sup>) (green circles) are displayed in the upper panels +/- SD ( $n = 18$ ,  $n = 6$  and  $n = 3$ , respectively), relative abundance (%) of taxonomic groups are shown in the lower panels.

### 3. Results

#### 3.1. Physical Characteristics

Across all sampling sites, sea ice thickness ranged from 30–104 cm (Table 1) and snow depth from 3–36 cm (Table 1; Fig. 2-3). The temperature of the bottom 3 cm of ice (at the ice-water interface) ranged from -1.9 to -3.6 °C (Table 1), and bulk ice salinity from 1.7–10.7 ppt (Table 1). The brine salinity ranged from 33.9–62.8 ppt (Table 1) and the brine volume ranged from 3.4–25.4 % ice volume (Table 1). Water temperature and salinity varied only minimally across all sites, with temperature ranging from -1.4 °C to -1.9 °C and salinity ranging from 33–34.5 ppt (Table S3). At all sites, the seawater was nutrient replete, with mean  $\text{NO}_3^- + \text{NO}_2^-$ ,  $\text{PO}_4^{3-}$  and  $\text{Si(OH)}_4$  concentrations of 2.01 +/- 0.5  $\mu\text{M}$ , 2.01 +/- 0.3  $\mu\text{M}$ , and 0.21 +/- 0.0  $\mu\text{M}$ , respectively, and  $\text{NH}_4^+$  levels generally <1  $\mu\text{M}$  (Table S3).

#### 3.2. Chlorophyll *a*, carbon and nitrogen:

Bottom ice chl *a* ranged from 0.15–7.2 mg/m<sup>2</sup> (Table 1; Fig. 2-3), while chl *a* in the water column directly below the sea ice ranged from 0.04–1.94 mg /m<sup>3</sup> (Table S3). We observed a positive relationship between cell density and chl *a* ( $F_{1,28} = 28.68$ ,  $p > 0.05$ ;  $R^2 = 0.51$ ), but we found no relationship between under-ice light transmissivity and bottom ice chl *a* ( $F_{1,28} = 0.00$ ,  $p > 0.05$ ;  $R^2 = 0.00$ ) or water column chl *a* ( $F_{1,28} = 3.20$ ,  $p > 0.05$ ;  $R^2 = 0.10$ ).

Molar ratios of C:N ranged from 4.53–13.80 in samples taken of the sea ice (Table 1) and 2.24–13.20 in under-ice water (Table S3). The C:N ratio was significantly higher in the sea ice at HLT compared to LLT sites in April ( $t(7) = 2.5$ ,  $p < 0.05$ ), but did not differ in May ( $t(5) = 1.31$ ,  $p > 0.05$ ).

>0.05). We found no difference in under-ice water C:N between HLT and LLT sites in either April or May.

Sea ice stable isotope of organic carbon ( $\delta^{13}\text{C}_{\text{VPDB}}$ ) ranged from -27.05 to -14.34 ‰ (Table 1) and organic nitrogen ( $\delta^{15}\text{N}_{\text{AIR}}$ ) ranged from 1.92–6.34 ‰ (Table 1). Under-ice water  $\delta^{13}\text{C}$  ranged from -24.99 to -28.41 ‰ (Table S2) and  $\delta^{15}\text{N}$  ranged from 1.68 to 8.54 ‰ (Table S3). The samples taken from the sea ice at HLT sites were significantly more carbon enriched than those taken from the LLT sites in April ( $t(7) = 3.5$ ,  $p < 0.05$ ) and in May ( $t(5) = 2.95$ ,  $p < 0.05$ ). We found a positive correlation between under-ice light and  $\delta^{13}\text{C}$  throughout April and May ( $F_{1,28} = 23.96$ ,  $p < 0.05$ ;  $R^2 = 0.46$ ), however no correlation was detected between  $\delta^{13}\text{C}$  values and cell density or chl *a*. There was no difference in nitrogen enrichment between HLT and LLT sites in April ( $t(8) = -2.56$ ,  $p > 0.05$ ), however the LLT sites did have higher nitrogen enrichment in May ( $t(10) = -2.45$ ,  $p < 0.05$ ). A negative correlation was observed between  $\delta^{15}\text{N}$  values and cell density ( $F_{1,28} = 30.59$ ,  $p < 0.05$ ;  $R^2 = 0.52$ ) and  $\delta^{15}\text{N}$  values and chl *a* ( $F_{1,28} = 28.54$ ,  $p < 0.05$ ;  $R^2 = 0.50$ ), but no correlation was detected between  $\delta^{15}\text{N}$  values and under-ice light. Unlike  $\delta^{13}\text{C}$  values,  $\delta^{15}\text{N}$  increased as the season progressed ( $F_{1,28} = 7.27$ ,  $p < 0.05$ ;  $R^2 = 0.21$ ). There was no difference in carbon or nitrogen enrichment in under-ice water between HLT and LLT in either April or May.

#### 3.3. Under-ice Light Transmissivity

Measured percent incoming PAR varied from 0.02–6.10 % (0.1–50  $\mu\text{mol photons m}^{-2}\text{s}^{-1}$ ) across 21 of 30 sites and dates, and measured surface irradiance varied from 387–1314  $\mu\text{mol photons m}^{-2}\text{s}^{-1}$ . Modelled percent incoming PAR varied from 0.02–23.18% incoming PAR (0.1–193,  $X^- = 35 \pm 52 \mu\text{mol photons m}^{-2}\text{s}^{-1}$ ) across all 30 sites and

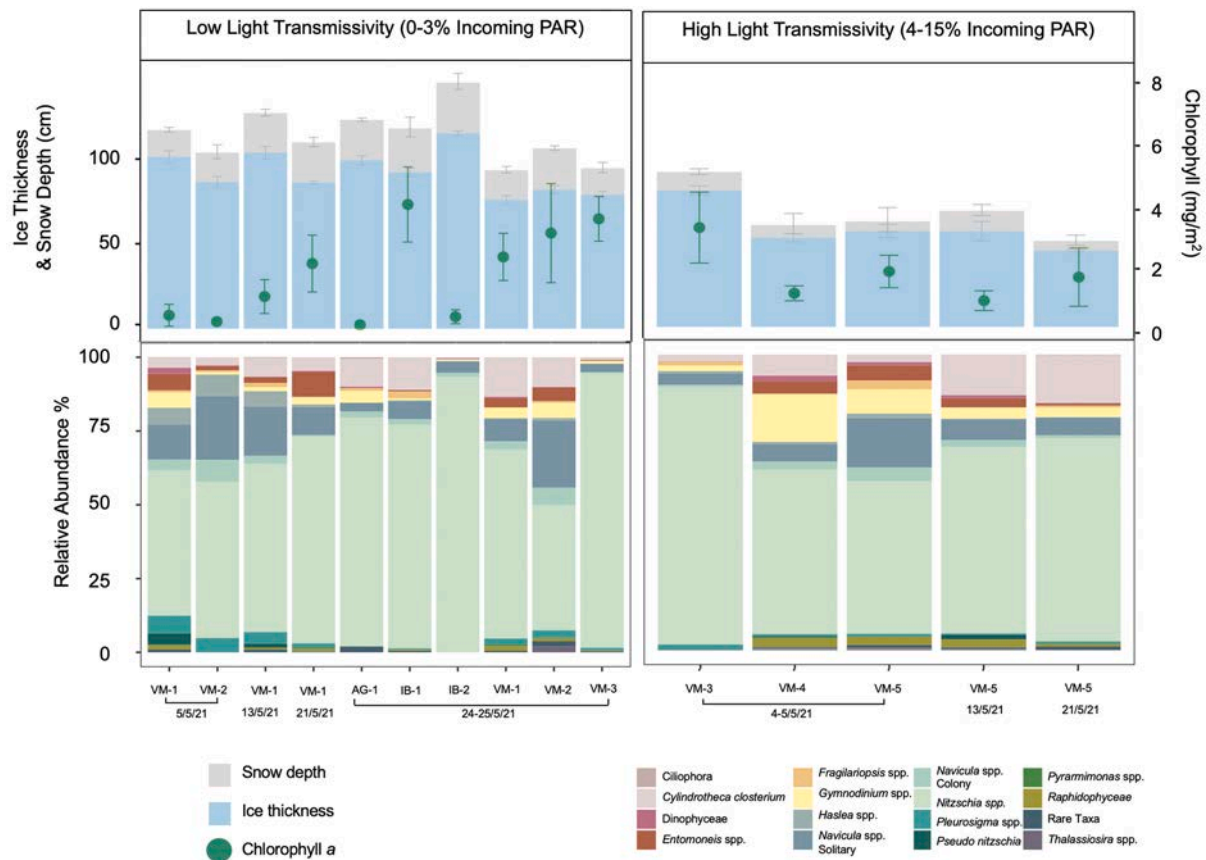


**Fig. 3.** Bottom ice microalgal community composition from low light transmissivity (left) and high light transmissivity (right) sites sampled during May 2021, in Svalbard, Norway. Snow depth (grey), ice thickness (blue), and chlorophyll *a* content ( $\text{mg}/\text{m}^2$ ) (green circles) are displayed in the upper panels  $\pm$  SD ( $n = 18$ ,  $n = 6$  and  $n = 3$ , respectively), relative abundance (%) of taxonomic groups are shown in the lower panels.

times (Table S2; Fig. 2–3). Based on the average incoming irradiance of  $750 \mu\text{mol photons m}^{-2}\text{s}^{-1}$ , the percentage of light transmitted equates to a range of  $0.1\text{--}204 \mu\text{mol photons m}^{-2}\text{s}^{-1}$  transmitted to the bottom ice community. For the locations where *in situ* light measurements were obtained (21 out of 30), these values closely resembled the modelled light measurements, with the modelled light values slightly higher  $+1.25\%$  ( $\pm 3.21\%$ ) on average, than the measured light levels (Table S2). The total variance in the modelled % incoming PAR was  $-4.7$  to  $10.3\%$ . When plotted against each other, the modelled and measured values were significantly correlated ( $r_{19} = 0.5$ ,  $p < 0.05$ ).

### 3.4. Species Composition

We identified a total of 55 taxa (to species or genus level), corresponding to seven phylogenetically distinct groups, with Bacillariophyceae accounting for 42 species (76% of the total), Dinophyceae accounting for six species (11%) and Pyramimonadophyceae being represented by three species (5%) (Table S4–S5). Raphidophyceae, Cryptophyceae, Euglenoidea and Ciliophora were identified to class level only. Of the identified diatoms, 40 species (95%) were from the order Pennales, while only two species belonged to the Centrales (5%). At all sites, the community was dominated by *Nitzschia* spp. (Figs. 2–3; Table 1). The *Nitzschia* spp. group, while dominated by colonial *N. frigida*, was represented also by colonial *N. promare*, *N. arctica*, *N. laevissima*, *N. brebissoni*, and *N. polaris*. Similarly, for the solitary *Navicula* group, *N. directa* was the most common and abundant, however, *N. distans*, *N. kariana*, *N. transitas*, *N. algida*, *N. valida* and *N. pellucida* were also present. The colony forming (ribbon) *Navicula* group consisted of *N. pelagica*, *N. septentrionalis*, *N. granii* and *N. vanhoefenii*. The Dinophyceae group was primarily identified to class level but also included

*Peridiniella catenata* and *Peridiniella* spp.. *Gymnodinium* spp. was not included in the Dinophyceae group as it was included as a separate grouping at genus level. The *Fragilariopsis* spp. group was dominated by *Fragilariopsis cylindrus* but included *F. reginae-jahniae* and *F. oecania*. The *Thalassiosira* spp. group was primarily identified to genus level but included *T. nordenskiöldii*. The ‘Rare Taxa’ group included euglenophytes, uncommon diatom taxa and haptophytes (Table S4).

While *Nitzschia* spp. dominated the communities during April–May from both the HLT and LLT sites, there were clear shifts in percentage contribution of scarcer taxa with increased irradiance. For example, *Cylindrotheca closterium* and colony forming *Navicula* spp. became more prominent when incoming PAR was  $>4\%$  during April (Figs. 2–3). In addition, throughout April, *Entomoneis* spp. was generally found in higher relative abundance in the LLT sites, with the exception of TF-1 where it was found to be the dominant taxa (Fig. 2). During May, *Gymnodinium* spp. tended to have a higher relative abundance at sites with HLT (Fig. 3).

### 3.5. Influence of Light Transmissivity on Protist Community Composition

Spatial and temporal differences, associated with differing under-ice light climates, related to community composition during April, but not during May (Fig. 4a–b). When compared, HLT sites differed in community composition from the LLT sites during April (ANOSIM  $R = 0.26$ ,  $p < 0.05$ ; Fig. 2), with the LLT ( $< 3\%$  incoming PAR /  $< 20 \mu\text{mol photons m}^{-2}\text{s}^{-1}$ ) generally dominated by *Nitzschia* spp. (primarily *N. frigida*), compared to a more diverse community in the high light sites ( $> 4\%$  incoming PAR /  $> 21 \mu\text{mol photons m}^{-2}\text{s}^{-1}$ ) with an increased contribution of various *Navicula* spp., *C. closterium* and *Fragilariopsis* spp. (Fig. 2). The cumulative contribution to this dissimilarity between HLT

**Table 1**

Parameters measured associated with sea ice core extraction; snow depth (+/- SD, n = 18), ice thickness (+/- SD, n = 6) and within the bottom 3cm of sea ice core; salinity (ppt), brine salinity (ppt), brine volume (% of ice volume), chlorophyll *a* concentration (mg/m<sup>2</sup>) (n = 3), daylight hours at time of sampling, carbon:nitrogen (C:N) ratio, carbon isotope ratio ( $\delta^{13}\text{C}_{\text{VPDB}}$  (‰)) and nitrogen isotope ratio ( $\delta^{15}\text{N}_{\text{Air}}$  (‰)).

Date	Station	Snow Depth (cm)	Ice Thickness (cm)	Ice Temperature (°C)	Salinity (ppt)	Brine Salinity (ppt)	Brine Volume (% ice volume)	Chlorophyll <i>a</i> (mg/m <sup>2</sup> )	Daylight (Hours)	C:N	$\delta^{13}\text{C}$ (‰)	$\delta^{15}\text{N}$ (‰)
14.4.21	VM-1	36.4 +/- 1.9	72 +/- 1.4	-2.3	8.6	40.77	18.85	0.15 +/- 0.0	15.09	4.61	-25.61	5.28
14.4.21	VM-2	12.6 +/- 1.8	64 +/- 1.1	-2.5	8.9	44.16	17.99	0.86 +/- 0.16	15.09	4.69	-24.68	4.57
14.4.21	VM-3	25.5 +/- 2.5	65 +/- 3.8	-3.6	9.8	62.38	13.91	1.98 +/- 0.90	15.09	5.51	-25.09	3.14
14.4.21	VM-4	16.9 +/- 2.4	41 +/- 1.0	-2.5	1.7	44.16	3.44	6.74 +/- 0.46	15.09	4.65	-24.29	1.92
21.4.21	PB-2	9.5 +/- 0.6	39 +/- 1.1	-2.3	4.7	40.77	10.30	3.49 +/- 2.89	19.55	5.50	-24.37	3.56
21.4.21	PB-3	10.6 +/- 0.4	38 +/- 0.5	-2.3	4.7	40.77	10.30	7.24 +/- 0.85	19.55	6.53	-18.82	3.64
22.4.21	AF-1	14.16 +/- 0.8	53 +/- 2.2	-2.3	7.2	40.77	15.78	7.05 +/- 1.02	19.59	5.28	-24.22	3.41
22.4.21	AF-2	10.9 +/- 2.9	47 +/- 1.2	-2.7	3.8	47.53	7.13	5.11 +/- 2.64	19.59	5.64	-23.25	4.07
27.4.21	VM-4	2.8 +/- 2.0	54 +/- 4.7	-2	9.6	35.64	24.12	3.46 +/- 1.88	20.36	7.19	-18.08	3.73
27.4.21	VM-5	5.0 +/- 1.0	54 +/- 1.9	-2.1	10.6	37.36	25.39	1.80 +/- 0.47	20.36	4.99	-22.97	3.79
28.4.21	VM-1	13.2 +/- 1.7	88 +/- 1.3	-2	9.2	35.64	23.12	0.33 +/- 0.26	20.36	4.53	-24.73	5.75
28.4.21	VM-2	22.7 +/- 2.9	68 +/- 1.5	-2.1	9.6	37.36	23.00	1.24 +/- 0.40	20.36	5.96	-24.43	5.32
28.4.21	VM-3	19.8 +/- 6.1	66 +/- 5.4	-2.2	3.2	39.07	7.33	1.36 +/- 0.35	20.36	5.26	-26.88	3.35
30.4.21	TF-1	3.9 +/- 1.1	30 +/- 2.8	-2.2	3.2	39.07	7.33	0.61 +/- 0.22	20.47	7.52	-14.34	4.39
30.4.21	TF-2	3.4 +/- 0.7	38 +/- 1.1	-2.7	9.2	47.53	17.25	4.47 +/- 1.59	20.47	10.18	-15.90	4.57
4.5.21	VM-3	10.0 +/- 0.9	74 +/- 2.6	-2.2	10.4	39.07	23.81	3.11 +/- 1.13	21.05	6.02	-25.27	3.42
4.5.21	VM-4	7.0 +/- 3.2	50 +/- 2.2	-2.1	5.6	37.36	13.42	1.01 +/- 0.24	21.05	7.50	-21.05	4.73
4.5.21	VM-5	4.8 +/- 3.8	52 +/- 3.6	-2.2	6.2	39.07	12.82	1.70 +/- 0.52	21.05	6.92	-15.31	3.04
5.5.21	VM-1	14.3 +/- 0.7	92 +/- 3.2	-2.1	6.5	37.36	15.57	0.55 +/- 0.35	21.05	6.09	-24.99	6.34
5.5.21	VM-2	15.8 +/- 2.1	78 +/- 3.0	-2.2	10.7	39.07	24.49	0.35 +/- 0.07	21.05	5.73	-24.30	5.31
13.5.21	VM-1	21.2 +/- 1.0	94 +/- 3.3	-2.1	9.5	37.36	22.76	1.14 +/- 0.53	24	7.57	-24.64	4.49
13.5.21	VM-5	11.0 +/- 1.7	52 +/- 5.2	-2	ND	ND	ND	0.77 +/- 0.31	24	10.99	-17.13	4.41
21.5.21	VM-1	21.2 +/- 1.4	78 +/- 0.9	-2	7.9	35.64	19.85	2.18 +/- 0.90	24	5.83	-24.61	5.06
21.5.21	VM-5	5.3 +/- 1.6	42 +/- 0.7	-2	ND	ND	ND	1.52 +/- 0.93	24	13.80	-15.90	4.65
24.5.21	AG-1	21.7 +/- 0.5	90 +/- 2.5	-2.5	5	44.16	10.10	0.25 +/- 0.10	24	11.15	-27.05	6.27
24.5.21	IB-1	23.5 +/- 3.0	84 +/- 2.3	-1.9	9.2	33.92	24.31	4.04 +/- 1.18	24	6.02	-26.74	3.48
24.5.21	IB-2	26.5 +/- 2.5	107 +/- 1.3	-1.9	6.6	33.92	17.44	0.50 +/- 0.22	24	5.54	-24.98	6.29
25.5.21	VM-1	15.9 +/- 1.0	70 +/- 2.3	-2	7.9	35.64	19.85	2.39 +/- 0.74	24	7.13	-23.09	5.24
25.5.21	VM-2	22.1 +/- 0.7	75 +/- 2.1	-2	7.4	35.64	18.59	3.14 +/- 1.56	24	6.48	-24.20	5.42
25.5.21	VM-3	14.2 +/- 1.6	72 +/- 1.7	-2	9.5	35.64	23.87	3.59 +/- 0.71	24	8.54	-21.84	3.96

ND represents measurement not taken.

and LLT sites was from *Nitzschia* spp. (11%), *C. closterium* (21%) *N. transitas* (27%), *F. cylindrus* (31%), *N. septentrionalis* (35%), *F. oecania* (39%), *Entomoneis* spp. (43%), *P. taeniata* (47%) and *Gymnodinium* spp. <10µm (50%). In May, however, the HLT and LLT assemblages were similar, indicating that community composition was similar irrespective of light climate, sampling location or sampling date (2D Stress = 0.16, Fig. 4b). In May, the community composition of both HLT and LLT sites (ANOSIM R = 0.00, p > 0.05; Fig. 3) were dominated by *Nitzschia* spp., specifically, *N. frigida* (Fig. 3).

At an individual species level, we found significant relationships between the relative abundance and light transmissivity for five taxa (Fig. 5). For the most predominant species, *N. frigida*, the percentage contribution to the community decreased as light transmissivity

increased ( $F_{1,28} = 6.30$ ,  $p < 0.05$ ;  $R^2 = 0.18$ ). In contrast, for the other four taxa, *Gymnodinium* spp. ( $F_{1,26} = 13.77$ ,  $p < 0.05$ ;  $R^2 = 0.35$ ), colony-forming *Navicula* spp. ( $F_{1,23} = 11.36$ ,  $p < 0.05$ ;  $R^2 = 0.33$ ), Dinophyceae ( $F_{1,27} = 6.58$ ,  $p < 0.05$ ;  $R^2 = 0.20$ ) and *Thalassiosira* spp. ( $F_{1,24} = 14.05$ ,  $p < 0.05$ ;  $R^2 = 0.37$ ), their percentage contribution to the community increased as under-ice light transmissivity increased. No trend between under ice light and contribution to the community was found for the other taxonomic groups (Table S6).

During April and May, we detected patterns in species occurrences. While there was a consistently negative correlation between *Nitzschia* spp. and all other taxa (Fig. 6a), we did detect strong positive correlations between the presence of *Thalassiosira* spp., *Raphidophyceae* spp. and *Pyramimonas* spp., high co-occurrence of *Pleurosigma* spp. and

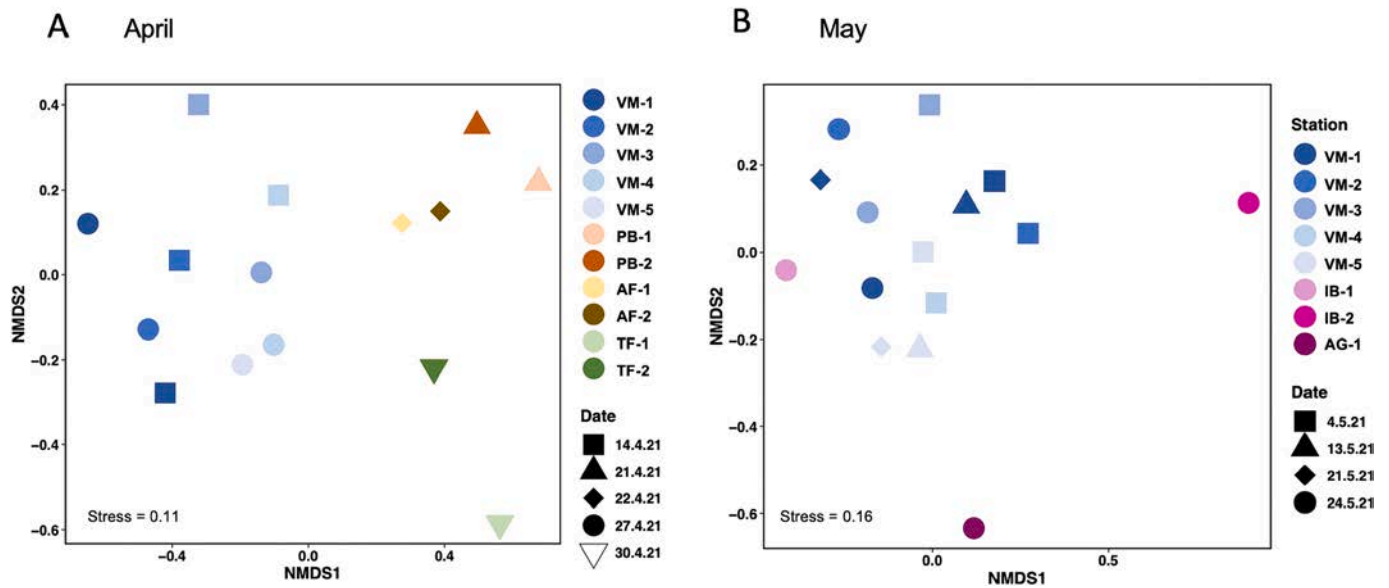


Fig. 4. Non-metric multidimensional scaling (nMDS) of microalgal communities for (A) April and (B) May, based on resemblance using Bray-Curtis similarity. Sample sites are shown by colour and dates by shapes. The 2D stress is shown in the lower left.

*Haslea* spp., as well as high co-occurrence of *Fragilariopsis* spp. with solitary *Navicula* spp. (Fig. 6a). Environmental conditions explained 58.7% (on two canonical axes) of the variability in community composition ( $F_{15} = 3.37$ ,  $p < 0.05$ , Fig. 6b). Abundance of *N. frigida* and *Thalassiosira* spp. was most strongly associated with chl *a* concentration, whilst the prevalence of *Entomoneis* spp., *C. closterium*, *Navicula* spp. (solitary and colony forming), *Gymnodinium* spp. and *Fragilariopsis* spp. was explained by percent incoming PAR more than any other variable (Fig. 6b). Brine salinity was the most explanatory variable for the presence of *Pleurosigma* spp., while the contribution from Dinophyceae appeared to be linked to  $\delta^{15}\text{N}$  (Fig. 6b).

### 3.6. Relationships between light transmissivity and community diversity

Accounting for all sampling events across time and space (both April and May), sea ice algal species diversity increased with increasing percent incoming PAR ( $F_{1,28} = 4.6$ ,  $p < 0.05$ ;  $R^2 = 0.14$ ; Fig. 7a). However, we detected a decline in diversity from April to May. Using the five-time repeated transect from the outermost (VM-5) to the innermost (VM-1) part of Van Mijenfjorden (Fig. 1), we found that diversity at the outer site (VM-5) declined significantly through time ( $F_{1,2} = 29.17$ ,  $p < 0.05$ ;  $R^2 = 0.94$ ; Fig. 7b) as did the inner site (VM-1), with a sharp dip on the 27<sup>th</sup> April ( $F_{1,3} = 28.03$ ,  $p < 0.05$ ;  $R^2 = 0.90$ ; Fig. 7b). Interestingly, this temporal decline in diversity was independent of light transmissivity and the changes that resulted in lower diversity differed between sites. As time progressed, the community at the VM-5 site had an increase in the relative abundance of *N. frigida* and *C. closterium* concurrent with a decrease in *Gymnodinium* spp., *Haslea* spp., *Fragilariopsis* spp. and *Navicula* spp. In contrast, the community at VM-1 saw an increase in *N. frigida* and *C. closterium*, with a decline in *Gymnodinium* spp. and *Pleurosigma* spp. as the season progressed. Whilst light transmissivity was not linked to the diversity index within sites, light transmissivity likely influenced the differences in community composition between the two sites (ANOSIM  $R = 0.28$ ,  $p < 0.05$ ), as the sampling sites within Van Mijenfjorden differed in modelled percent incoming PAR during the sampling period (ANOVA:  $F_{4,14} = 3.63$ ,  $p < 0.05$ ), with the greatest difference observed between VM-1 and VM-5 sites (Tukey's HSD:  $p < 0.05$ , 95% CI = [-0.04 – 3.53]). No relationship was found between cell density and percent incoming PAR ( $F_{1,28} = 4.27$ ,  $p > 0.05$ ;  $R^2 = 0.13$ ).

## 4. Discussion

In this study, we investigated bottom ice microalgal community composition in land-fast sea ice at both temporal and spatial scales. We evaluated under-ice light using a light transmittance model based on the physical parameters of ice thickness and snow depth. Validating against our *in situ* measurements, we found that modelled results were in good agreement with measured values and were thereby used to avoid the variability inherent in obtaining light data *in situ* that is complicated by time of day or variable weather conditions. Whilst it is difficult to directly compare under-ice light measurements with those measured in previous studies, as the light transmissivity is determined by snow depth and ice thickness which vary widely, the under-ice light values presented in this study ( $0 - 193$ ,  $\bar{X} = 35 \mu\text{mol photons m}^{-2}\text{s}^{-1}$ ) were primarily within the expected spring range in high latitudes for the observed sea ice and snow conditions (Campbell et al., 2016; Leu et al., 2010). The few unusually high values ( $> 100 \mu\text{mol photons m}^{-2}\text{s}^{-1}$ ) recorded were taken at sites with snow depth  $< 5$  cm and ice thickness  $< 50$  cm.

Under-ice light transmittance, as a function of ice thickness and snow depth, was related with the sea ice microalgal community composition. We found under-ice light transmittance to have a stronger association with community composition than other environmental variables, including temperature, ice salinity, brine volume and under-ice water nutrient concentration. Whilst initial community composition may play a role in determining the composition throughout the season, it was not able to be quantitatively evaluated as not all sampling sites were revisited throughout the season. The association between under-ice light and community composition was particularly evident during the early-mid growth season. In April, the communities exposed to higher under-ice light conditions were typically more diverse, with higher relative abundance of common ice-associated taxa such as *Navicula* spp., *C. closterium* and *Fragilariopsis* spp. This may reflect that increased light transmitted to the bottom ice, until a threshold, drives an increased growth rate in many bottom ice taxa (Hegseth, 1992). Similar patterns of enhanced diversity with increased under-ice light transmittance have been observed previously in both the Arctic Ocean (Hop et al., 2020) and the Barents Sea (Hegseth & von Quillfeldt, 2022).

One of the most prevalent species throughout our study was *N. frigida*, a species endemic to sea ice communities. This species has been found to form vast blooms throughout the Arctic (Hegseth & von

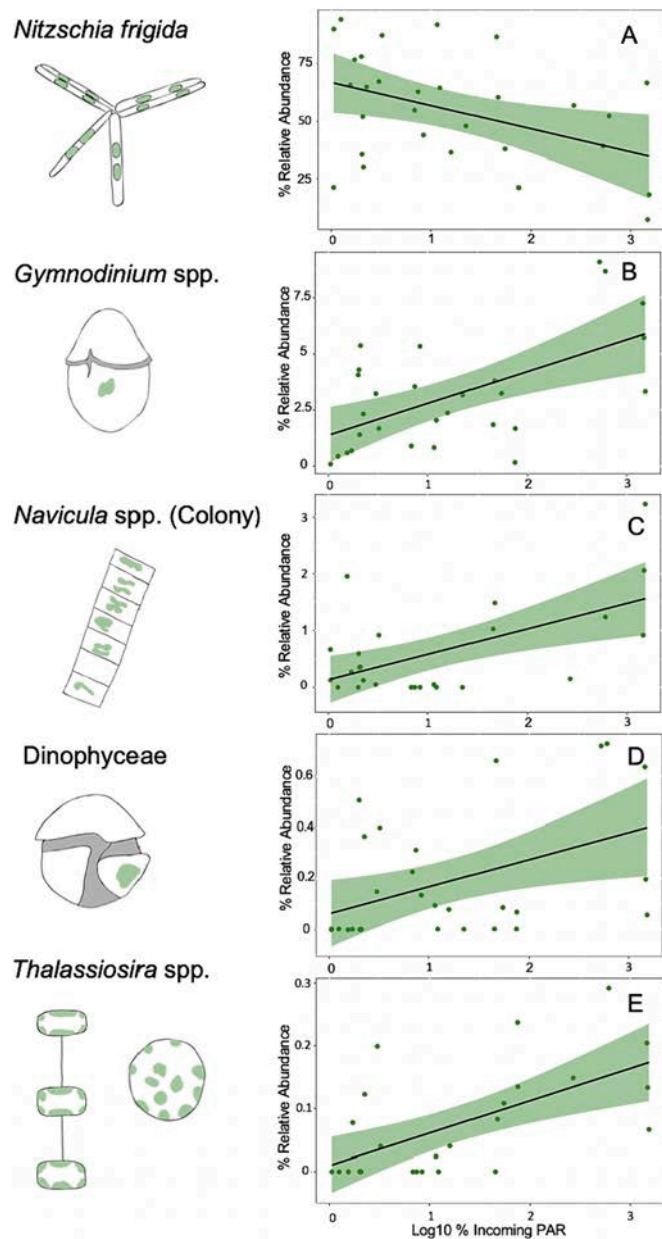


**Fig. 5.** Significant relationships for species-specific relative contribution to community composition vs. Log<sub>10</sub> percent (%) incoming PAR during April and May, (A) *Nitzschia frigida*, (B) *Gymnodinium* spp., (C) Colony forming *Navicula* spp., (D) Dinophyceae and (E) *Thalassiosira* spp.. Data are fitted using linear regression with 95% confidence intervals (shading).

Quillfeldt, 2022; Hop et al., 2020). The relative abundance of *N. frigida* was negatively correlated with light and strongly associated with increased chl *a* concentration. These relationships were reflected in the onset of *N. frigida* blooms observed as the season progressed, coinciding with a reduction in under-ice light transmissivity, due to unusually high snow fall in the late spring (Norwegian Meteorological Institute, 2023). By early May, *N. frigida* dominated the communities at all sites, resulting in reduced overall diversity. This dominance by *N. frigida* during May could explain why no relationship was observed between under-ice light and diversity in May, and possibly indicates that light has a less distinct effect on the diversity of more established ice algal communities. When a higher proportion of incoming light was transmitted under the ice, a higher abundance of Dinophyceae overall was found (Fig. 5), yet a contrasting temporal effect was also detected, with a relative increase in abundance during seasonal progression despite lower light transmission.

This suggests that it was the lower nitrate concentrations later in the season, evidenced by the elevated  $\delta^{15}\text{N}$ , that favoured the Dinophyceae, potentially having a greater influence on their proliferation than light. This increase in Dinophyceae dominance with seasonal progression is consistent with the patterns suggested by other studies (Alou-Font et al., 2013; Hegseth & von Quillfeldt, 2022; Rozanska et al., 2009) and such seasonal successions in taxa are seen across a range of systems (e.g. McMinn & Hodgson, 1993; Winder & Varpe, 2020).

Concomitant with influencing the community composition, light transmissivity was positively correlated with  $\delta^{13}\text{C}$  enrichment and increased C:N, mirroring previous work (Gosselin et al., 1990; Lee et al., 2008a), and demonstrating how light directly affects the biochemical composition of ice algae. The  $\delta^{13}\text{C}$  values and C:N ratios within sea ice have been documented to range from -27 to -11‰ (Leu et al., 2020; Pineault et al., 2013), and 3 to 24 mols (Niemi & Michel, 2015), respectively, and our results are in line with these findings. Interestingly, we found no correlation between  $\delta^{13}\text{C}$  content and protist abundance or chl *a*, unlike the positive correlations observed previously (Gradinger, 2009; Pineault et al., 2013). In dense sea ice assemblages which are highly productive and space limited, we expected to find enriched  $\delta^{13}\text{C}$  values due to preferential assimilation of  $^{12}\text{C}$  and minimal replenishment to the inorganic carbon pool (Pineault et al., 2013), so the lack of relationships between  $\delta^{13}\text{C}$  with either protist abundance or chl *a* within this study, could potentially be explained by the relatively low biomass accumulated at the sites. Whilst the chl *a* concentrations are within the expected range for Arctic land-fast ice, they are on the lower end and do not represent a dense bloom scenario (Campbell et al., 2016; Leu et al., 2020; Runge, 2021). In addition, the relationship between stoichiometric C:N ratios and under-ice light only, coupled with the fact that C:N ratios were typically at the Redfield Ratio of 6.6 or below, validates the greater influence of light than nutrient limitation at most sites (Campbell et al., 2016; Gosselin et al., 1990). On the other hand,  $\delta^{15}\text{N}$  levels decreased with increasing protist abundance and were inversely related to the abundance of all taxa, particularly *N. frigida*. This relationship was not observed previously (Pineault et al., 2013). The observed decline in  $\delta^{15}\text{N}$  levels could suggest an increase in nutrient recycling, relative abundance of autotrophs or dissolved inorganic nitrogen reduction (Pineault et al., 2013) with higher algal density, thus the  $\delta^{15}\text{N}$  levels were not necessarily linked to under-ice light.

Based on the water column nutrient concentrations, the sites sampled were not nutrient limited, which differs from previous observations from late in the bottom ice algal season (Leu et al., 2020). This may be due to relatively low biomass accumulation at all sites, leaving a reservoir of unused nutrients. However, absolute values of nutrients within the sea ice algal boundary layer were not obtained and therefore, we cannot say with certainty that the microalgal cells were not experiencing some level of nutrient stress. That said, the assemblages in Tempelfjorden in late April and VM-5 (the outermost site in VM) in mid-late May were experiencing enriched  $\delta^{13}\text{C}$  values between -14 and -17‰ and C:N ratios of >10, similar to those observed at high under-ice light sites in Van Mijenfjorden previously (Leu et al., 2020). Whilst it is possible that these sites were experiencing the onset of nutrient depletion within the ice, the under-water  $\text{NO}_3^- + \text{NO}_2^-$  concentrations were still replete at all sites with values >1.5  $\mu\text{M}$ . Rather than depletion of nitrate, it is possible that high light conditions could have resulted in a skewed uptake of C through the accumulation of C-rich storage compounds (Søreide et al., 2006), which can have significant consequences for transfer of energy through the marine food web (Hessen et al., 2008).

The unique community composition found at the TF-1 site (closest to the ice-edge) was unexpected and possibly a result of the site experiencing melting of the ice at the ice-ocean interface. It was characterised by high under-ice light (>100  $\mu\text{mol photons m}^{-2}\text{s}^{-1}$ ), low brine salinity, low chl *a* concentrations and seawater temperatures of -1.6 °C. These conditions may explain why the dominant species was *Entomoneis* spp, a large cryobenthic diatom which has been shown to perform well in low salinity melt conditions (Ryan et al., 2004). It is important to note that



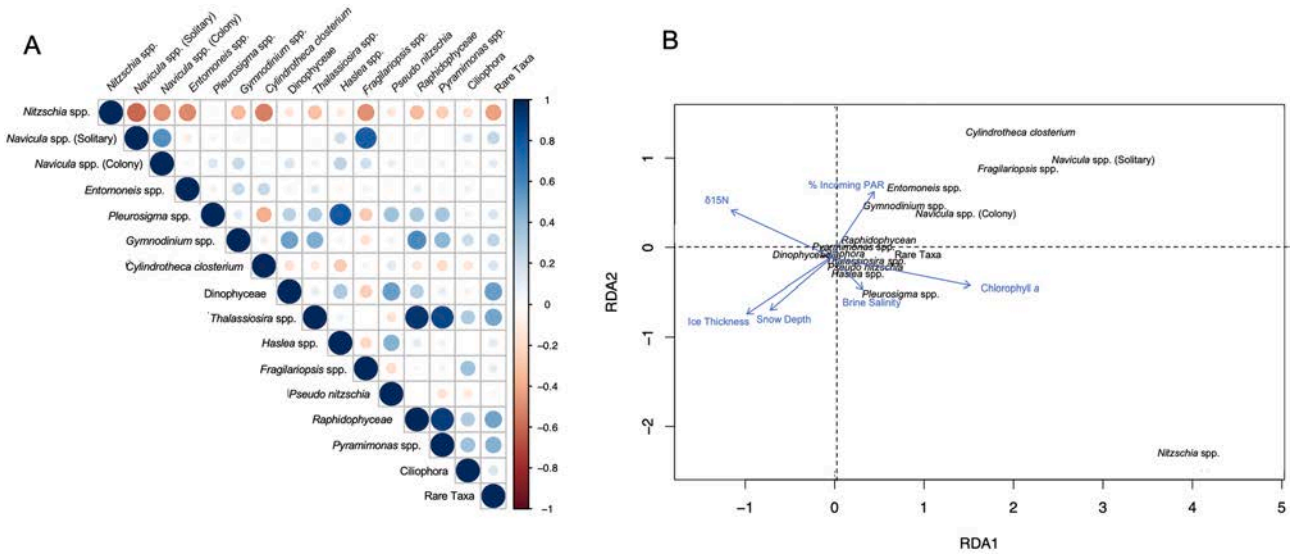


Fig. 6. (A) Correlation matrix of the relative abundance of main taxonomic groups found throughout April and May 2021, in land-fast ice, Svalbard, Norway. The strength of the positive (blue) and negative (red) correlations is displayed according to dot size. (B) Redundancy analysis (RDA) biplot of the relative abundance of taxonomic groups with environmental variables. Only significant vectors are shown.

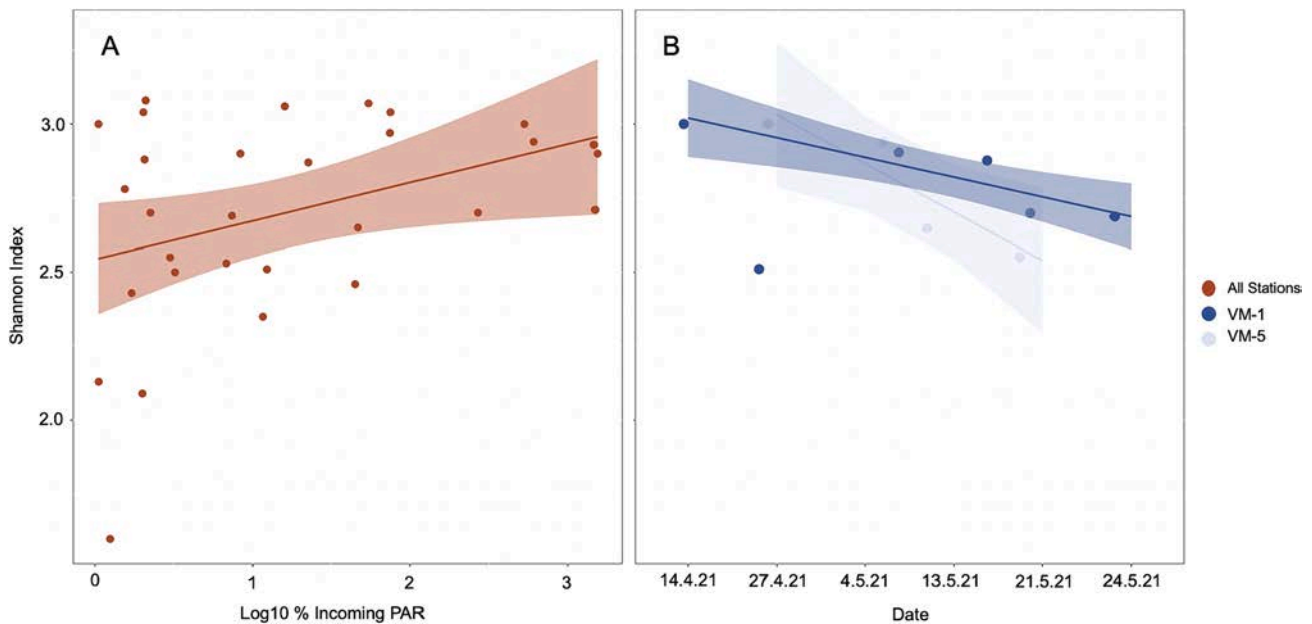


Fig. 7. Spatial and temporal microalgal diversity dynamics (A) in relation to Log10 percent (%) incoming PAR for all data and (B) as a function of time for the outermost (VM-5) (light blue) and innermost (VM-1) (dark blue) sites within Van Mijenfjorden. Data are fitted using linear regression with 95% confidence intervals (shading). The outlier on 27<sup>th</sup> April has been excluded from the regression within the VM-1 site data.

when considering all sampling sites, *Entomoneis* spp. was not correlated to brine salinity, however another large solitary diatom, *Pleurosigma* spp., was positively correlated with brine salinity, thus brine salinity is unlikely to be the only driver of relatively high abundance of *Entomoneis* spp. at TF-1. A unique community composition was also observed in the assemblage at TF-2, with high relative abundance of *C. closterium*, however it did not appear to be melting out as the site had higher brine salinity and lower under ice water temperatures of  $-1.8^{\circ}C$ . Thus, based on the RDA it is likely that this assemblage is explained primarily by high light transmissivity (22% incoming PAR).

Previous studies have shown that the composition of the ice algal community can affect sympagic-pelagic-benthic coupling, as the melt community may seed the pelagic ecosystem, shaping the ensuing

phytoplankton blooms (Jin et al., 2016; Michel et al., 1993; Pineault et al., 2013). An ice community dominated by colonial taxa forming aggregates has been shown to shift the dominance of the pelagic community from diatom to flagellate dominated, as the ice-associated aggregates of diatoms sink rapidly to the ocean floor (Tedesco et al., 2012). In addition, in the early season when grazing pressure in the pelagic zone is minimal, ice algae sinking to the ocean floor is an important food source for the benthos (McMahon et al., 2006) which may persist year round (Koch et al., 2023). Combined, these processes influence which taxa and nutrients are available to be transferred through trophic levels via pelagic and benthic pathways. The low  $\delta^{13}C$  values observed in the water column indicate that the ice-associated algae had not yet made a quantitatively significant contribution to the pelagic community, likely

due to timing and the temperature of the ice, as most communities had not reached the end of season melt (i.e. under water ice temperatures remained at  $< -1.8^{\circ}\text{C}$ , with some exceptions) and generally low light levels reaching the water column (i.e. 19 of 30 sites experienced  $< 20$   $\mu\text{mol photons m}^{-2}\text{s}^{-1}$ ).

The strong links between the availability of ice algae and reproduction in some zooplankton species reinforces the importance of ice algae to the extent of secondary production and nutrition supplied to the marine food web, with estimates of the carbon contribution derived from sea ice algae to some zooplankton species being as high as 60% (Runge & Ingram, 1988; Søreide et al., 2013; Søreide et al., 2006). For example, reproduction in *Calanus glacialis* has been shown to begin under the sea ice, prior to the pelagic blooms, with availability of ice algae for grazing bringing forward oogenesis and oocyte maturation (Durbin & Casas, 2014). Ice algae availability can also boost fecundity, as the population reach higher numbers when the first feeding naupliar stage aligns with the subsequent pelagic phytoplankton bloom (Ringuette et al., 2002; Søreide et al., 2010) and it has been proposed that a longer ice-covered season could result in a longer spawning season and larger cohort for *C. glacialis* (Durbin & Casas, 2014). Copepods have also been observed to preferentially consume ice algae over pelagic phytoplankton during the reproductive period (Durbin & Casas, 2014). This is likely due to a preference for cells containing higher lipid content, such as has often been measured in sea ice algae at the end of the spring season (Lee et al., 2008b; Smith et al., 1993).

The rapidly declining expanse and duration of land-fast ice in the Arctic means that communities reliant on this icy habitat are experiencing an ecosystem in flux, where snow and ice thickness are likely to vary across space and time. The implications of this instability will be highly variable light transmissivity, which in turn alters ice algal community composition, and thus likely the sea ice and pelagic primary and secondary production, as well as benthic productivity (Currie et al., 2021). Under a future scenario of warmer water and air temperatures, Arctic sea ice and snow depth are projected to be thinner (Kacimi & Kwok, 2022; Renner et al., 2014; Webster et al., 2014), thereby permitting greater light transmittance through the ice. Whilst our findings are constrained to correlative relationships, if our data are indicative of broader Arctic bottom ice communities, then these data suggest that a higher light under-ice environment could reshape the bottom ice algal communities towards higher diversity, with a greater contribution of dinoflagellates. Any shift away from diatoms and towards dinoflagellates would have trophic and biogeochemical implications, influencing both the transfer of energy through the food web and oceanic mineral cycling. For example, copepods and especially *Calanus* spp., the dominant zooplankton in Arctic waters, have a strong reliance on carbon derived from a diatom-based diet (Søreide et al., 2008). A reduced relative contribution of diatoms and a higher relative abundance of dinoflagellates would affect the fatty acid content available to higher trophic levels, as diatoms are high in C16 PUFA, essential fatty acids (20:5n-3) and omega-7 fatty acids (16:1n-7), whilst dinoflagellates are high in C18 and C22 PUFA (Dalsgaard et al., 2003). In addition, a shift to a dinoflagellate dominated community would alter ocean biogeochemistry, as diatoms have a unique siliceous cell structure that acts as ballast, making them effective at exporting carbon to ocean depths and key players in biogenic silicon cycling (Baines et al., 2010). That said, the high, late-season snowfall observed during this study meant that light transmissivity declined as time progressed, highlighting how the stochasticity of snow fall adds a layer of complexity to the seasonality of light (which generally increases with the onset of Arctic summer). As lower light transmissivity correlated with a less diverse ice algal community, depending on the dominating taxa, this too would influence carbon transfer through the food web. A community dominated by colonial species such as *N. frigida*, or larger solitary species such as *Pleurosigma* spp. or *Entomoneis* spp., affects grazing efficiency in smaller copepod species, whereas smaller algal taxa reduce grazing efficiency in larger copepod species (Levinson et al., 2000). Such a shift

has been observed in the Antarctic krill *Euphasia superba*, which showed only 50% grazing efficiency for phytoplankton  $< 20 \mu\text{m}$  (Boyd et al., 1984). Given the potential for higher precipitation (snowfall) to occur in the Arctic in the short-medium term (Liu et al., 2012; van Pelt et al., 2016), which would invariably reduce light transmittance to under ice communities (Perovich, 2007), we may see ice algal communities that are less diverse. Should the increased precipitation come as rain however, which is increasing in parts of the Arctic (Hansen et al., 2014), the snow cover would be reduced and the light transmittance would increase, potentially resulting in a more diverse ice algae community, as described above. Such conditions would also likely limit ice algae community establishment and biomass due to bottom ablation (Juhl & Krembs, 2010). While continuing and rapid environmental change is an established component of global warming, due to the many complexities of interactions and feedback mechanisms, the direction of the change is less decided.

This seasonal study has offered a unique insight into algal community composition in Arctic land-fast sea ice across broad temporal and spatial scales and examined the relationship between the community structure and environmental variables with a particular focus on the under-ice light environment. We showed that the bottom ice community composition was strongly correlated with under-ice light transmissivity, with algal assemblages generally exhibiting greater species diversity when experiencing more light early in the productive season. These findings are important, because shifts in ice algal community composition can have both trophic effects through changes to size and food quality, and biogeochemical implications. Furthermore, these data intimate that the tight coupling between ice algae abundance and zooplankton success would be affected by alterations to sea ice thickness and snow cover, with the precise direction of change being interwoven with the extent and direction of environmental change. Through revealing the importance of light availability on shaping Arctic land-fast ice algal communities, we have provided baseline data that can help inform predictive models to better constrain the ecological impacts of environmental change to polar marine food webs, which depend on these ice-based organisms.

#### CRediT authorship contribution statement

**Rebecca J. Duncan:** Conceptualization, Methodology, Formal analysis, Investigation, Data curation, Writing – original draft, Visualization, Funding acquisition. **Janne E. Søreide:** Conceptualization, Data curation, Funding acquisition, Methodology, Resources, Supervision, Writing – review & editing. **Oystein Varpe:** Conceptualization, Methodology, Supervision, Writing – review & editing. **Józef Wiktor:** Supervision, Validation, Writing – review & editing. **Vanessa Pitusi:** Data curation, Investigation, Writing – review & editing. **Elaine Runge:** Investigation, Writing – review & editing. **Katherina Petrou:** Conceptualization, Methodology, Supervision, Writing – review & editing.

#### Declaration of competing interest

The authors declare that they have no known competing financial interests or personal relationships that could have appeared to influence the work reported in this paper.

#### Data availability

Data will be made available on request.

#### Acknowledgements

Duncan RJ is supported by an Australian Government Research Training Program Scholarship, an AINSE Ltd. Postgraduate Research Award (PGRA) and an Arctic Field Grant (310664) provided by the Research Council of Norway (RCN). Runge E was also supported with an

Arctic Field Grant (310692). Further, funding was provided through the 2017-2018 Belmont Forum and BiodivERsA joint call for research proposals, under the BiodivScen ERA-Net COFUND programme, and with the funding organisations RCN (296836) and National Science Centre Poland (UMO-2015/17/B/NZ8/02473)

## Appendix A. Supplementary data

Supplementary data to this article can be found online at <https://doi.org/10.1016/j.pocean.2024.103248>.

## References

- Allaart, L., Müller, J., Schomacker, A., Rydningen, T.A., Håkansson, L., Kjellman, S.E., Mollenhauer, G., Forwick, M., 2020. Late Quaternary glacier and sea-ice history of northern Wijdefjorden, Svalbard. *Boreas* 49 (3), 417–437.
- Alou-Font, E., Mundy, C.-J., Roy, S., Gosselin, M., Agustí, S., 2013. Snow cover affects ice algal pigment composition in the coastal Arctic Ocean during spring. *Mar. Ecol. Prog. Ser.* 474, 89–104.
- Archer, S.D., Leakey, R.J., Burkill, P.H., Sleight, M.A., Appleby, C.J., 1996. Microbial ecology of sea ice at a coastal Antarctic site: community composition, biomass and temporal change. *Mar. Ecol. Prog. Ser.* 135, 179–195.
- Arrigo, K.R., 2014. Sea ice ecosystems. *Ann. Rev. Mar. Sci.* 6, 439–467.
- Baines, S.B., Twining, B.S., Brzezinski, M.A., Nelson, D.M., Fisher, N.S., 2010. Causes and biogeochemical implications of regional differences in silicification of marine diatoms. *Global Biogeochem. Cycles* 24 (4), GB4031.
- Barrie, A., Davies, J., Park, A., Workman, C., 1989. Continuous-flow stable isotope analysis for biologists. *Spectroscopy* 4 (7), 42–52.
- Berggreen, U., Hansen, B., Kiørboe, T., 1988. Food size spectra, ingestion and growth of the copepod *Acartia tonsa* during development: Implications for determination of copepod production. *Mar. Biol.* 99 (3), 341–352.
- Boetius, A., Albrecht, S., Bakker, K., Bienhold, C., Felden, J., Fernández-Méndez, M., Hendricks, S., Katlein, C., Lalonde, C., Krumpen, T., 2013. Export of algal biomass from the melting Arctic sea ice. *Science* 339 (6126), 1430–1432.
- Boyd, C.M., Heyraud, M., Boyd, C.N., 1984. Feeding of the Antarctic krill *Euphausia superba*. *J. Crustac. Biol.* 4 (5), 123–141.
- Campbell, K., Mundy, C., Landy, J., Delaforge, A., Michel, C., Rysgaard, S., 2016. Community dynamics of bottom-ice algae in Dease Strait of the Canadian Arctic. *Prog. Oceanogr.* 149, 27–39.
- Campbell, K., Mundy, C., Belzile, C., Delaforge, A., Rysgaard, S., 2018. Seasonal dynamics of algal and bacterial communities in Arctic sea ice under variable snow cover. *Polar Biol.* 41 (1), 41–58.
- Campbell, K., Mundy, C., Juhl, A.R., Dalman, L.A., Michel, C., Galley, R.J., Else, B.E., Geilfus, N.X., Rysgaard, S., 2019. Melt procedure affects the photosynthetic response of sea ice algae. *Front. Earth Sci.* 7, 21.
- Comeau, A.M., Philippe, B., Thaler, M., Gosselin, M., Poulin, M., Lovejoy, C., 2013. Protists in Arctic drift and land-fast sea ice. *J. Phycol.* 49 (2), 229–240.
- Connan-McGinty, S., Banas, N.S., Berge, J., Cottier, F., Grant, S., Johnsen, G., Kopec, T. P., Porter, M., McKee, D., 2022. Midnight sun to Polar Night: A model of seasonal light in the Barents Sea. *J. Adv. Model. Earth Syst.* 14 (10), e2022MS003198.
- Cota, G., Legendre, L., Gosselin, M., Ingram, R., 1991. Ecology of bottom ice algae: I. Environmental controls and variability. *J. Mar. Syst.* 2 (3–4), 257–277.
- Cox, G.F., Weeks, W.F., 1983. Equations for determining the gas and brine volumes in sea-ice samples. *J. Glaciol.* 29 (102), 306–316.
- Currie, A.A., Marshall, A.J., Lohrer, A.M., Cummings, V.J., Seabrook, S., Cary, S.C., 2021. Sea ice dynamics drive benthic microbial communities in McMurdo Sound, Antarctica. *Frontiers in Microbiology* 12, 745915.
- Dalsgaard, J., John, M.S., Kattner, G., Müller-Navarra, D., Hagen, W., 2003. Fatty acid trophic markers in the pelagic marine environment. *Adv. Mar. Biol.* 46, 226–340.
- Duncan, R.J., Nielsen, D., Søreide, J.E., Varpe, Ø., Tobin, M.J., Pitusi, V., Heraud, P., Petrou, K., 2024. Biomolecular profiles of Arctic Sea-ice diatoms highlight the role of under-ice light in cellular energy allocation. *ISME Commun.* 4 (1), 1–15.
- Duncan, R.J., Nielsen, D.A., Sheehan, C.E., Deppeler, S., Hancock, A.M., Schulz, K.G., Davidson, A.T., Petrou, K., 2022. Ocean acidification alters the nutritional value of Antarctic diatoms. *New Phytol.* 233 (4), 1813–1827.
- Durbin, E.G., Casas, M.C., 2014. Early reproduction by *Calanus glacialis* in the Northern Bering Sea: the role of ice algae as revealed by molecular analysis. *J. Plankton Res.* 36 (2), 523–541.
- Edler, L., Elbrächter, M., 2010. The Utermöhl method for quantitative phytoplankton analysis. In: Karlson, B. (Ed.), *Microscopic and Molecular Methods for Quantitative Phytoplankton Analysis*. United Nations Educational, Scientific and Cultural Organization (UNESCO), Paris, pp. 13–20.
- Fernández-Méndez, M., Katlein, C., Rabe, B., Nicolaus, M., Peeken, I., Bakker, K., Flores, H., Boetius, A., 2015. Photosynthetic production in the central Arctic Ocean during the record sea-ice minimum in 2012. *Biogeosciences* 12 (11), 3525–3549.
- Forwick, M., Vorren, T.O., Hald, M., Korsun, S., Roh, Y., Vogt, C., Yoo, K.-C., 2010. Spatial and temporal influence of glaciers and rivers on the sedimentary environment in Sassenfjorden and Tempelfjorden, Spitsbergen. *Geol. Soc. Lond. Spec. Publ.* 344 (1), 163–193.
- Gosselin, M., Legendre, L., Theriault, J.C., Demers, S., 1990. Light and nutrient limitation of sea-ice microalgae (Hudson Bay, Canadian Arctic). *J. Phycol.* 26 (2), 220–232.
- Gosselin, M., Levasseur, M., Wheeler, P.A., Horner, R.A., Booth, B.C., 1997. New measurements of phytoplankton and ice algal production in the Arctic Ocean. *Deep Sea Res. Part II* 44 (8), 1623–1644.
- Gradinger, R., 2009. Sea-ice algae: Major contributors to primary production and algal biomass in the Chukchi and Beaufort Seas during May/June 2002. *Deep Sea Res. Part II* 56 (17), 1201–1212.
- Haarpaintner, J., Haugan, P.M., Gascard, J.-C., 2001. Interannual variability of the Storfjorden (Svalbard) ice cover and ice production observed by ERS-2 SAR. *Ann. Glaciol.* 33, 430–436.
- Hansen, B.B., Isaksen, K., Benestad, R.E., Kohler, J., Pedersen, Å.Ø., Loe, L.E., Coulson, S. J., Larsen, J.O., Varpe, Ø., 2014. Warmer and wetter winters: characteristics and implications of an extreme weather event in the High Arctic. *Environ. Res. Lett.* 9 (11), 114021.
- Hegseth, E.N., 1992. Sub-ice algal assemblages of the Barents Sea: species composition, chemical composition, and growth rates. *Polar Biol.* 12, 485–496.
- Hegseth, E.N., von Quillfeldt, C., 2022. The Sub-Ice Algal Communities of the Barents Sea Pack Ice: Temporal and Spatial Distribution of Biomass and Species. *Journal of Marine Science and Engineering* 10 (2), 164.
- Hessen, D.O., Leu, E., Færøvig, P.J., Petersen, S.F., 2008. Light and spectral properties as determinants of C: N: P-ratios in phytoplankton. *Deep Sea Res. Part II* 55 (20–21), 2169–2175.
- Hitchcock, G.L., 1982. A comparative study of the size-dependent organic composition of marine diatoms and dinoflagellates. *J. Plankton Res.* 4 (2), 363–377.
- Holm-Hansen, O., Riemann, B., 1978. Chlorophyll a determination: improvements in methodology. *Oikos* 30, 438–447.
- Hop, H., Vihtakari, M., Bluhm, B.A., Assmy, P., Poulin, M., Gradinger, R., Peeken, I., von Quillfeldt, C., Olsen, L.M., Zhitina, L., 2020. Changes in sea-ice protist diversity with declining sea ice in the Arctic Ocean from the 1980s to 2010s. *Front. Mar. Sci.* 7, 243.
- Horner, R. (Ed.), 1985. *Sea Ice Biota*, 1st edition ed. CRC Press, Boca Raton, USA.
- Høyland, K.V., 2009. Ice thickness, growth and salinity in Van Mijenfjorden, Svalbard, Norway. *Polar Research* 28 (3), 339–352.
- Institute, N.M., 2023. *Svalbard LH Meteorological Station Snow Depth*. Retrieved 24.9.23 from Norwegian Meteorological Institute. <https://www.yr.no/en/statistics/graph/5-99840/Norway/Svalbard/Svalbard/Svalbard%20LH?q=2021>.
- Ji, R., Jin, M., Varpe, Ø., 2013. Sea ice phenology and timing of primary production pulses in the Arctic Ocean. *Glob. Chang. Biol.* 19 (3), 734–741.
- Jin, M., Popova, E.E., Zhang, J., Ji, R., Pendleton, D., Varpe, Ø., Yool, A., Lee, Y.J., 2016. Ecosystem model intercomparison of under-ice and total primary production in the Arctic Ocean. *J. Geophys. Res.* Oceans 121 (1), 934–948.
- Juhl, A.R., Krembs, C., 2010. Effects of snow removal and algal photoacclimation on growth and export of ice algae. *Polar Biol.* 33, 1057–1065.
- Kacimi, S., Kwok, R., 2022. Arctic Snow Depth, Ice Thickness, and Volume From ICESat-2 and CryoSat-2: 2018–2021. *Geophys. Res. Lett.* 49 (5), e2021GL097448.
- Koch, C.W., Brown, T.A., Amiraux, R., Ruiz-Gonzalez, C., MacCorquodale, M., Yundaguarin, G.A., Kohlback, D., Loseto, L.L., Rosenberg, B., Hussey, N.E., 2023. Year-round utilization of sea ice-associated carbon in Arctic ecosystems. *Nat. Commun.* 14 (1), 1964.
- Kunisch, E., Graeve, M., Gradinger, R., Haug, T., Kovacs, K.M., Lydersen, C., Varpe, Ø., Bluhm, B., 2021. Ice-algal carbon supports harp and ringed seal diets in the European Arctic: evidence from fatty acid and stable isotope markers. *Mar. Ecol. Prog. Ser.* 675, 181–197.
- Kvernvik, A.C., Hoppe, C.J.M., Greenacre, M., Verbiest, S., Wiktor, J.M., Gabrielsen, T. M., Reigstad, M., Leu, E., 2021. Arctic sea ice algae differ markedly from phytoplankton in their ecophysiological characteristics. *Mar. Ecol. Prog. Ser.* 666, 31–55.
- Lee, S.H., Whitedge, T.E., Kang, S.-H., 2008a. Carbon uptake rates of sea ice algae and phytoplankton under different light intensities in a landfast sea ice zone, Barrow, Alaska. *Arctic* 61 (3), 281–291.
- Lee, S.H., Whitedge, T.E., Kang, S.-H., 2008b. Spring time production of bottom ice algae in the landfast sea ice zone at Barrow, Alaska. *J. Exp. Mar. Biol. Ecol.* 367 (2), 204–212.
- Leu, E., Wiktor, J., Søreide, J., Berge, J., Falk-Petersen, S., 2010. Increased irradiance reduces food quality of sea ice algae. *Mar. Ecol. Prog. Ser.* 411, 49–60.
- Leu, E., Søreide, J., Hessen, D., Falk-Petersen, S., Berge, J., 2011. Consequences of changing sea-ice cover for primary and secondary producers in the European Arctic shelf seas: timing, quantity, and quality. *Prog. Oceanogr.* 90 (1–4), 18–32.
- Leu, E., Brown, T.A., Graeve, M., Wiktor, J., Hoppe, C.J., Chierici, M., Fransson, A., Verbiest, S., Kvernvik, A.C., Greenacre, M.J., 2020. Spatial and temporal variability of ice algal trophic markers—with recommendations about their application. *Journal of Marine Science and Engineering* 8 (9), 676.
- Levinsen, H., Turner, J.T., Nielsen, T.G., Hansen, B.W., 2000. On the trophic coupling between protists and copepods in arctic marine ecosystems. *Mar. Ecol. Prog. Ser.* 204, 65–77.
- Li, Z., Zhao, J., Su, J., Li, C., Cheng, B., Hui, F., Yang, Q., Shi, L., 2019. Spatial and temporal variations in the extent and thickness of arctic landfast ice. *Remote Sens.* 12 (1), 64.
- Liu, J., Curry, J.A., Wang, H., Song, M., Horton, R.M., 2012. Impact of declining Arctic sea ice on winter snowfall. *PNAS* 109 (11), 4074–4079.
- McMahon, K.W., Ambrose Jr, W.G., Johnson, B.J., Sun, M.-Y., Lopez, G.R., Clough, L.M., Carroll, M.L., 2006. Benthic community response to ice algae and phytoplankton in Ny Ålesund, Svalbard. *Mar. Ecol. Prog. Ser.* 310, 1–14.
- McMinn, A., Hodgson, D., 1993. Summer phytoplankton succession in Ellis Fjord, eastern Antarctica. *J. Plankton Res.* 15 (8), 925–938.

- Michel, C., Legendre, L., Therriault, J.-C., Demers, S., Vandeveld, T., 1993. Springtime coupling between ice algal and phytoplankton assemblages in southeastern Hudson Bay. *Canadian Arctic. Polar Biology* 13 (7), 441–449.
- Michel, C., Legendre, L., Ingram, R., Gosselin, M., Levasseur, M., 1996. Carbon budget of sea-ice algae in spring: Evidence of a significant transfer to zooplankton grazers. *J. Geophys. Res. Oceans* 101 (C8), 18345–18360.
- Niemi, A., Michel, C., 2015. Temporal and spatial variability in sea-ice carbon: nitrogen ratios on Canadian arctic shelf: temporal and spatial variability in sea-ice carbon: Nitrogen ratios. *Elementa* 3, 1–12.
- Oksanen, J., Blanchet, F.G., Kindt, R., Legendre, P., Minchin, P.R., O'hara, R., Simpson, G.L., Solymos, P., Stevens, M.H.H., Wagner, H., 2013. Package 'vegan'. Community ecology package, version 2 (9), 1–295.
- Palmisano, A.C., SooHoo, J.B., Sullivan, C.W., 1985. Photosynthesis-irradiance relationships in sea ice microalgae from McMurdo sound, Antarctica. *J. Phycol.* 21 (3), 341–346.
- Parsons, T.R., 2013. A manual of chemical & biological methods for seawater analysis. Elsevier, New York, USA.
- Perovich, D.K., 1996. The optical properties of sea ice. *U. S. Cold Reg. Res. and Eng. Lab. Monogr.* 96–1.
- Perovich, D.K., 2007. Light reflection and transmission by a temperate snow cover. *J. Glaciol.* 53 (181), 201–210.
- Petrou, K., Ralph, P., 2011. Photosynthesis and net primary productivity in three Antarctic diatoms: possible significance for their distribution in the Antarctic marine ecosystem. *Mar. Ecol. Prog. Ser.* 437, 27–40.
- Pfister, G., McKenzie, R., Liley, J., Thomas, A., Forgan, B., Long, C.N., 2003. Cloud coverage based on all-sky imaging and its impact on surface solar irradiance. *J. Appl. Meteorol. Climatol.* 42 (10), 1421–1434.
- Pineault, S., Tremblay, J.E., Gosselin, M., Thomas, H., Shadwick, E., 2013. The isotopic signature of particulate organic C and N in bottom ice: Key influencing factors and applications for tracing the fate of ice-algae in the Arctic Ocean. *J. Geophys. Res. Oceans* 118 (1), 287–300.
- Quetin, L., Ross, R., 1985. Feeding by Antarctic Krill, *Euphausia superba*: does size matter?. In: *Antarctic Nutrient Cycles And Food Webs*. Springer: Berlin/Heidelberg, Germany, pp. 372–377.
- Ratkova, T.N., Wassmann, P., 2005. Sea ice algae in the White and Barents seas: composition and origin. *Polar Res.* 24 (1–2), 95–110.
- Renner, A.H., Gerland, S., Haas, C., Spreen, G., Beckers, J.F., Hansen, E., Nicolaus, M., Goodwin, H., 2014. Evidence of Arctic sea ice thinning from direct observations. *Geophys. Res. Lett.* 41 (14), 5029–5036.
- Riebesell, U., Schloss, I., Smetacek, V., 1991. Aggregation of algae released from melting sea ice: implications for seeding and sedimentation. *Polar Biol.* 11, 239–248.
- Ringuette, M., Fortier, L., Fortier, M., Runge, J.A., Bélanger, S., Larouche, P., Weslawski, J.-M., Kwasiński, S., 2002. Advanced recruitment and accelerated population development in Arctic calanoid copepods of the North Water. *Deep Sea Res. Part II* 49 (22–23), 5081–5099.
- Rozanska, M., Gosselin, M., Poulin, M., Wiktor, J., Michel, C., 2009. Influence of environmental factors on the development of bottom ice protist communities during the winter-spring transition. *Mar. Ecol. Prog. Ser.* 386, 43–59.
- Runge, J.A., Ingram, R.G., 1988. Underice grazing by planktonic, calanoid copepods in relation to a bloom of ice microalgae in southeastern Hudson Bay. *Limnol. Oceanogr.* 33 (2), 280–286.
- Runge, J., Ingram, R.G., 1991. Under-ice feeding and diel migration by the planktonic copepods *Calanus glacialis* and *Pseudocalanus minutus* in relation to the ice algal production cycle in southeastern Hudson Bay, Canada. *Mar. Biol.* 108, 217–225.
- Runge, E. (2021). *Timing and magnitude of sea ice algal blooms in Svalbard archipelago: synthesis of chlorophyll a and driving physical environmental variables from 2007 to 2021* [Master Thesis, University of Copenhagen].
- Ryan, K., Ralph, P., McMinn, A., 2004. Acclimation of Antarctic bottom-ice algal communities to lowered salinities during melting. *Polar Biol.* 27 (11), 679–686.
- Ryan, K., Tay, M., Martin, A., McMinn, A., Davy, S., 2011. Chlorophyll fluorescence imaging analysis of the responses of Antarctic bottom-ice algae to light and salinity during melting. *J. Exp. Mar. Biol. Ecol.* 399 (2), 156–161.
- Sackett, O., Petrou, K., Reedy, B., De Grazia, A., Hill, R., Doblin, M., Beardall, J., Ralph, P., Heraud, P., 2013. Phenotypic plasticity of southern ocean diatoms: key to success in the sea ice habitat? *PLoS One* 8 (11), e81185.
- Shapiro, S.S., Wilk, M.B., 1965. An analysis of variance test for normality (complete samples). *Biometrika* 52 (3/4), 591–611.
- Smith, R., Anning, J., Pierre Clement, G., 1988. Abundance and production of ice algae in Resolute Passage, Canadian Arctic. *Mar. Ecol. Prog. Ser.* 48, 251–263.
- Smith, R.E., Cavaletto, J.F., Eadie, B., Gardner, W.S., 1993. Growth and lipid composition of high Arctic ice algae during the spring bloom at Resolute, Northwest Territories, Canada. *Mar. Ecol. Prog. Ser.* 97 (1), 19–29.
- Somerfield, P.J., Clarke, K.R., Gorley, R.N., 2021. Analysis of similarities (ANOSIM) for 2-way layouts using a generalised ANOSIM statistic, with comparative notes on Permutational Multivariate Analysis of Variance (PERMANOVA). *Austral Ecol.* 46 (6), 911–926.
- Søreide, J.E., Hop, H., Carroll, M.L., Falk-Petersen, S., Hegseth, E.N., 2006. Seasonal food web structures and sympagic-pelagic coupling in the European Arctic revealed by stable isotopes and a two-source food web model. *Prog. Oceanogr.* 71 (1), 59–87.
- Søreide, J.E., Falk-Petersen, S., Hegseth, E.N., Hop, H., Carroll, M.L., Hobson, K.A., Blachowiak-Samolyk, K., 2008. Seasonal feeding strategies of *Calanus* in the high-Arctic Svalbard region. *Deep Sea Res. Part II* 55 (20–21), 2225–2244.
- Søreide, J.E., Leu, E.V., Berge, J., Graeve, M., Falk-Petersen, S., 2010. Timing of blooms, algal food quality and *Calanus glacialis* reproduction and growth in a changing Arctic. *Glob. Chang. Biol.* 16 (11), 3154–3163.
- Søreide, J.E., Carroll, M.L., Hop, H., Ambrose Jr, W.G., Hegseth, E.N., Falk-Petersen, S., 2013. Sympagic-pelagic-benthic coupling in Arctic and Atlantic waters around Svalbard revealed by stable isotopic and fatty acid tracers. *Mar. Biol. Res.* 9 (9), 831–850.
- Søreide, J.E., Dmoch, K., Blachowiak-Samolyk, K., Trudnowska, E., Daase, M., 2022. Seasonal mesozooplankton patterns and timing of life history events in high-arctic fjord environments. *Front. Mar. Sci.* 9, 1–19.
- Tedesco, L., Vichi, M., Thomas, D.N., 2012. Process studies on the ecological coupling between sea ice algae and phytoplankton. *Ecol. Model.* 226, 120–138.
- Tomas, C.R., 1997. Identifying marine phytoplankton. Academic Press: San Diego, USA.
- Urbański, J.A., Litwicka, D., 2022. The decline of Svalbard land-fast sea ice extent as a result of climate change. *Oceanologia* 64 (3), 535–545.
- van Pelt, W.J., Kohler, J., Liston, G., Hagen, J.O., Luks, B., Reijmer, C., Pohjola, V.A., 2016. Multidecadal climate and seasonal snow conditions in Svalbard. *J. Geophys. Res. Earth Surf.* 121 (11), 2100–2117.
- Varpe, Ø., Daase, M., Kristiansen, T., 2015. A fish-eye view on the new Arctic lightscape. *ICES J. Mar. Sci.* 72 (9), 2532–2538.
- Vonnahme, T., 2021. *Microbial diversity and ecology in the coastal Arctic seasonal ice zone*. [Doctoral Dissertation, University in Tromsø].
- Webster, M.A., Rigor, I.G., Nghiem, S.V., Kurtz, N.T., Farrell, S.L., Perovich, D.K., Sturm, M., 2014. Interdecadal changes in snow depth on Arctic sea ice. *J. Geophys. Res. Oceans* 119 (8), 5395–5406.
- Wickham, H., Chang, W., Wickham, M.H., 2016. Package 'ggplot2'. *Create elegant data visualisations using the grammar of graphics*. Version 2 (1), 1–189.
- Wickham, H., Averick, M., Bryan, J., Chang, W., McGowan, L.D.A., François, R., Grolemund, G., Hayes, A., Henry, L., Hester, J., 2019. Welcome to the Tidyverse. *Journal of Open Source Software* 4 (43), 1686.
- Wiktor, J., Okolodkov, J., Vinogradova, K., 1995. *Atlas of the Marine Flora of Southern Spitsbergen*. Polish Academy of Sciences Institute, Gdansk, Poland.
- Winder, M., Varpe, Ø., 2020. Interactions in plankton food webs: seasonal succession and phenology of Baltic Sea zooplankton. In: *Zooplankton Ecology*. CRC Press Taylor & Francis Group, Boca Raton, USA, pp. 162–191.
- Yu, Y., Stern, H., Fowler, C., Fetterer, F., Maslanik, J., 2014. Interannual variability of Arctic landfast ice between 1976 and 2007. *J. Clim.* 27 (1), 227–243.

# Biomolecular profiles of Arctic sea-ice diatoms highlight the role of under-ice light in cellular energy allocation

Rebecca J. Duncan<sup>1,2,\*</sup>, Daniel Nielsen<sup>1</sup>, Janne E. Søreide<sup>2</sup>, Øystein Varpe<sup>3,4</sup>, Mark J. Tobin<sup>5</sup>, Vanessa Pitusi<sup>2,6</sup>, Philip Heraud<sup>7</sup>, Katherina Petrou<sup>1</sup>

<sup>1</sup>School of Life Sciences, University of Technology Sydney, Sydney, New South Wales, 2007, Australia

<sup>2</sup>Department of Arctic Biology, The University Centre in Svalbard, Longyearbyen, 9170, Norway

<sup>3</sup>Department of Biological Sciences, University of Bergen, Bergen, 5020, Norway

<sup>4</sup>Norwegian Institute for Nature Research, Bergen, 5006, Norway

<sup>5</sup>Australian Synchrotron—ANSTO, Clayton, Victoria, 3168, Australia

<sup>6</sup>Department of Arctic and Marine Biology, University in Tromsø (UiT), Tromsø, 9010, Norway

<sup>7</sup>Centre for Biospectroscopy, School of Chemistry, Monash University, Clayton, Victoria, 3800, Australia

\*Corresponding author: Rebecca J. Duncan, University Technology Sydney, School of Life Sciences, Building 7, 67 Thomas St, Ultimo, New South Wales, 2007, Australia. Email: rebecca.duncan@uts.edu.au

## Abstract

Arctic sea-ice diatoms fuel polar marine food webs as they emerge from winter darkness into spring. Through their photosynthetic activity they manufacture the nutrients and energy that underpin secondary production. Sea-ice diatom abundance and biomolecular composition vary in space and time. With climate change causing short-term extremes and long-term shifts in environmental conditions, understanding how and in what way diatoms adjust biomolecular stores with environmental perturbation is important to gain insight into future ecosystem energy production and nutrient transfer. Using synchrotron-based Fourier transform infrared microspectroscopy, we examined the biomolecular composition of five dominant sea-ice diatom taxa from landfast ice communities covering a range of under-ice light conditions during spring, in Svalbard, Norway. In all five taxa, we saw a doubling of lipid and fatty acid content when light transmitted to the ice–water interface was >5% but <15% (85%–95% attenuation through snow and ice). We determined a threshold around 15% light transmittance after which biomolecular synthesis plateaued, likely because of photoinhibitory effects, except for *Navicula* spp., which continued to accumulate lipids. Increasing under-ice light availability led to increased energy allocation towards carbohydrates, but this was secondary to lipid synthesis, whereas protein content remained stable. It is predicted that under-ice light availability will change in the Arctic, increasing because of sea-ice thinning and potentially decreasing with higher snowfall. Our findings show that the nutritional content of sea-ice diatoms is taxon-specific and linked to these changes, highlighting potential implications for future energy and nutrient supply for the polar marine food web.

**Keywords:** sea-ice microalgae, Svalbard, single cell, lipid, fatty acid, under-ice light, inter-species variability

## Introduction

The ecosystem within and directly below Arctic sea ice is highly seasonal, with light playing a critical role in its structure and functioning, through its influence on the productivity of the under-ice photosynthetic primary producers. The formation of landfast ice typically occurs in winter when darkness persists for 24 h. During this time, the early microbial community of sea-ice microalgae are captured within the brine pockets of the sea ice [1]. As the light returns to high latitudes in the early spring, dormant and vegetative sea-ice microalgae become active and begin to photosynthesise [2]. Early spring is characterized by sufficient inorganic nutrients supplied from the water below, but low light levels, which limit microalgal biomass and primary production [1, 3]. As spring progresses, light becomes abundant, resulting in peak productivity where ice algae can bloom, forming a key source of energy and nutrients for zooplankton and benthic reproductive cycles [4–6]. At our study sites at 78°N, the transition from

perpetual darkness to constant daylight (the midnight sun) is rapid and occurs inside 42 days [7]. During this period, light reaching the sea-ice algae changes from being limiting to potentially harmful, if snow cover is absent [1, 8]. As summer approaches, despite abundant light, the lower nutrient concentrations [9, 10], increasing water temperatures and rapid brine drainage [11, 12], start to limit sea-ice algal productivity and, ultimately the higher summer temperature causes the ice to melt completely, releasing the microbial community living within the brine channels into the pelagic and benthic zones below [6].

The amount of light reaching the ice–water interface is dependent on snow depth and sea-ice thickness, which can be highly variable in space and time. As global temperatures rise with climate change, it is expected that snow and ice dynamics will change [13–15], and consequently the seasonal progression of the under-ice community will change as well. Whilst it is well-established that Arctic sea ice extent is declining [16–19] and

Received 6 December 2023. Revised: 13 December 2023. Accepted: 14 December 2023

© The Author(s) 2024. Published by Oxford University Press on behalf of the International Society for Microbial Ecology.

This is an Open Access article distributed under the terms of the Creative Commons Attribution License (<https://creativecommons.org/licenses/by/4.0/>), which permits unrestricted reuse, distribution, and reproduction in any medium, provided the original work is properly cited.

becoming thinner [20–22], which alone would drive higher under-ice light levels, it is possible that the Arctic may experience increased precipitation in the form of higher snowfall in the short to medium term, because of increased storms and more open water [14, 23]. The influence of snow depth on light attenuation is far greater than sea ice alone. Snow-free ice can transmit up to 80% of incoming photosynthetically active radiation (PAR) [24, 25], whereas a 10 cm layer of fresh snow can effectively block light, reducing visible light transmission to <5% of incoming PAR [26]. As such, if the sea ice covered areas of the Arctic were to experience higher snowfall with global warming, despite thinner ice, under-ice light levels could be significantly reduced, modifying the growth conditions for the microalgae below.

Environmental conditions affect the allocation of photosynthetically derived carbon within polar ice algae, determining their biomolecular (i.e. lipid, carbohydrate, fatty acids, and protein) composition ([27], and references within). In turn, the biomolecular composition of ice algae determines the energy and nutrients available to the polar marine food web [28]. In actively growing ice algae, lipid may constitute up to 20% of dry weight and 60% of particulate organic matter composition [29, 30]. Lipids are the most energy-rich biomolecule with a caloric value of approximately twice that of carbohydrate and protein [31, 32] and transfer much of the energy between levels of the food web. Lipid content available at the primary production level is important for development, growth rate [33] and the amount of secondary production [34]. Because of the synthesis of fatty acids (FAs), in particular polyunsaturated fatty acids (PUFA), being tightly coupled to photosynthesis, eukaryotic algae are the main source of FAs to the marine food web [35, 36]. In sea-ice associated ecosystems, ice algae have been shown to be responsible for up to 50% of the FAs present in higher trophic levels, including fish, seals, and seabirds [37, 38]. In particular, FAs, including saturated (SAFA), monounsaturated (MUFA) fatty acids, and PUFAs, impact zooplankton fecundity and larval development [39, 40], as they are critical for membrane development, growth, and reproduction [35]. Their importance is evident from the high efficiency with which they are transferred through the trophic levels, with PUFAs shown to be transferred twice as efficiently from primary to secondary trophic levels compared with bulk carbon [41, 42]. Carbohydrates are also important biomolecules in terms of energy transfer [32], and play an important role in contributing to the cellular carbon pool [43]. Particularly under nutrient-depleted conditions, carbohydrates are a reserve product that can be drawn upon for lipid synthesis [44, 45]. Proteins are important for providing cellular nitrogen reserves and are the primary source of amino acids (AA) [46], which are vital for organism growth and survival, as regulators of metabolic pathways and as the structural elements of enzymes [47]. For heterotrophic organisms, non-essential AAs can be synthesized *de novo*; however, essential AAs must be provided by diet of which microalgae are the primary source in marine ecosystems [35]. Whilst polar ice algae typically have a relatively reduced photosynthate allocation to protein compared with other biomolecules [28, 48], they have a high transfer efficiency through food webs [49].

In the highly seasonal environment of the Arctic, in which productivity is severely restricted for much of the year, the provision of biomolecular energy from sea-ice algae is important for the transfer of energy through the polar marine ecosystem [50]. The value of sea-ice algae as food is linked also to the time in which they bloom. They are the primary source of carbon in the early spring [51–53] before pelagic phytoplankton proliferate [54], and

some Arctic zooplankton have evolved to temporally align their reproductive cycle with this early food availability.

Studies on natural sea-ice algal communities have investigated nutrient content (e.g. lipid and protein content) at the community scale ([27], and references within), with only two studies looking at the effects of light on the biomolecular composition of Arctic diatoms at a taxon-specific level [55, 56]. Our study investigates the influence of the under-ice light conditions on the allocation of biomolecules, including lipids, proteins, and carbohydrates, in five Arctic ice-associated pennate diatoms: *Nitzschia frigida* (colonial), *Pleurosigma* spp. (solitary), *Navicula* spp. (solitary), *Haslea* spp. (solitary), and *Entomoneis* spp. (solitary), taken from natural communities within the landfast sea ice in Svalbard, Norway. Using synchrotron-based Fourier transform infrared (s-FTIR) microspectroscopy (Fig. 1) to analyse individual cells, we uncover taxon-specific patterns in biomolecular production and allocation, providing insight into how sea-ice algae nutritional content may change with climate-driven shifts in community composition.

## Materials and methods

### Study area

This study was conducted within Tempelfjorden and Van Mijenfjorden in Svalbard, Norway (Fig. 2; Table S1) on 30 April and 4–5 May 2021, respectively. Within Van Mijenfjorden, five sites were sampled once along a transect from the inner to the outer fjord (VM-1–5), capturing a gradient of ice thickness and snow depth. A site from Tempelfjorden (TF-2) was sampled once and included because of its thinner sea ice and snow depth, providing data from an environment of higher light transmissivity to the ice–water interface. Both fjords are located on the west coast of Svalbard and are influenced by glacial run-off [57]. Additionally, both fjords are comprised of an outer basin up to 120-m deep and inner basin up to 70-m deep (Van Mijenfjorden) and 60-m deep (Tempelfjorden). However, unlike Tempelfjorden, Van Mijenfjorden is a partially enclosed fjord meaning it has longer and more predictable sea ice cover [57]. Detailed analysis of the under-ice protist community composition at all sites is available in Duncan et al. [58].

### Sample collection

At each sampling site, six ice cores were extracted ~0.5–1-m apart, using a Kovacs core barrel (9 cm diameter; Kovacs Enterprise, Oregon, USA). The bottom 3 cm (at the ice–water interface) of each core was retained, as this is where the microbial community was concentrated [59–61]. Cores were then pooled into triplicates, as cores 1–2, 3–4, and 5–6, and 100 ml of filtered sea water (GF/F, nominal pore size 0.7  $\mu$ m) was added for every centimetre of core to minimize osmotic stress [62, 63] after which the samples were allowed to melt in darkness for 24 h at 4°C. To concentrate the cells, 100 ml from each of the three samples was centrifuged at 1000 rpm (Universal 320, Hettich, Germany) for 4 min and the supernatant removed. The remaining sample was then transferred to 2 ml Eppendorf tubes and centrifuged at 1000 rpm (Mikro 185, Hettich) for 2 min before the supernatant was removed, and the sample was fixed by addition of formalin (5% v/v) in FSW for later analysis.

### Environmental parameters

#### Physical parameters

Three snow depth measurements were taken to the nearest 0.5 cm using a standard ruler, to determine the average snow depth per core. Ice thickness was measured using a Kovacs ice thickness

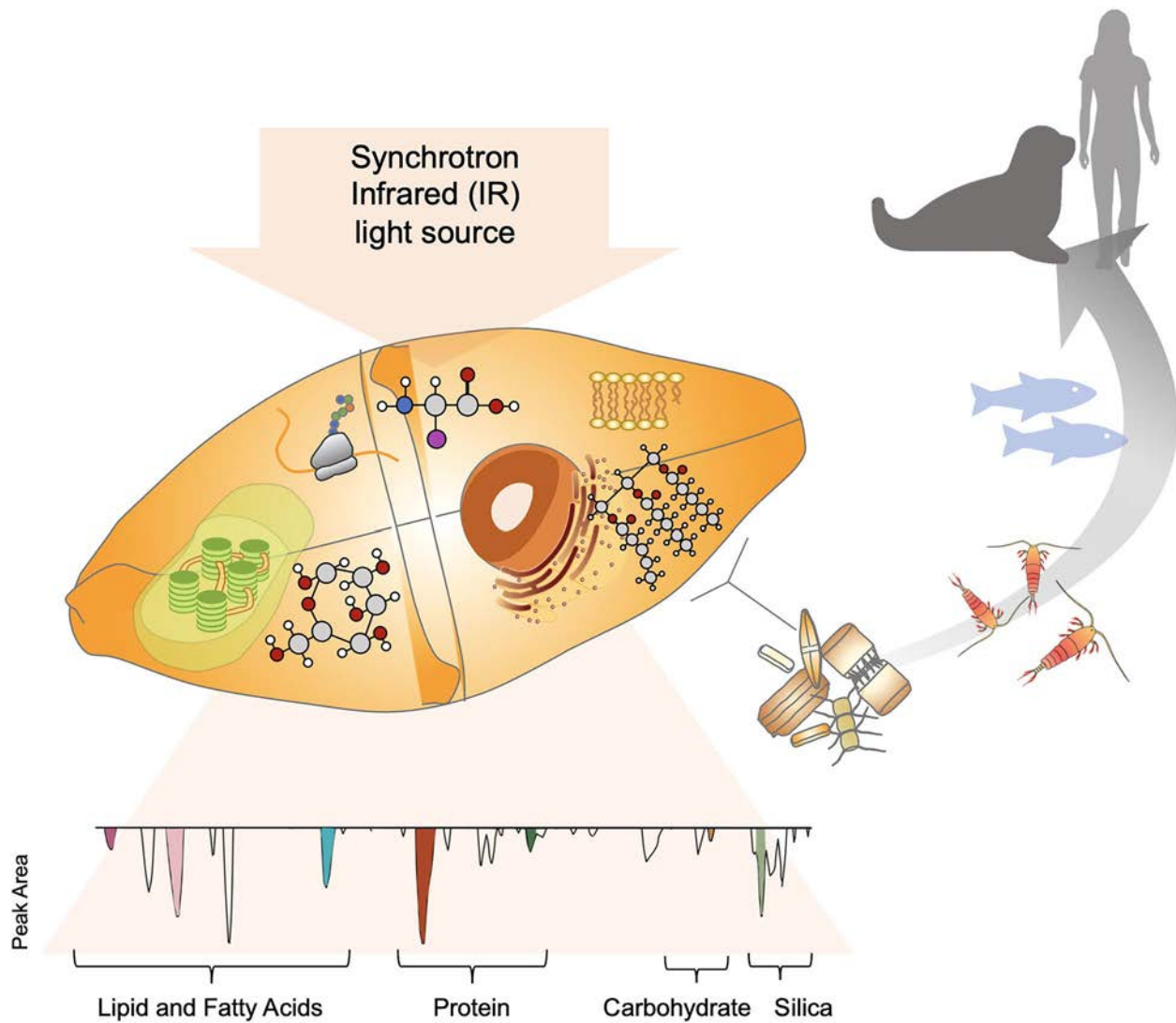


**Figure 1.** Conceptual model of the synchrotron IR light source measuring and the biomolecules within an individual cell, and the corresponding wavelengths on the IR spectrum (second derivative transformed) (bottom), in which the shaded sections represent the peak area of the biomolecules studied; a simplified overview of the transfer of these biomolecules up the polar marine food chain is displayed (right).

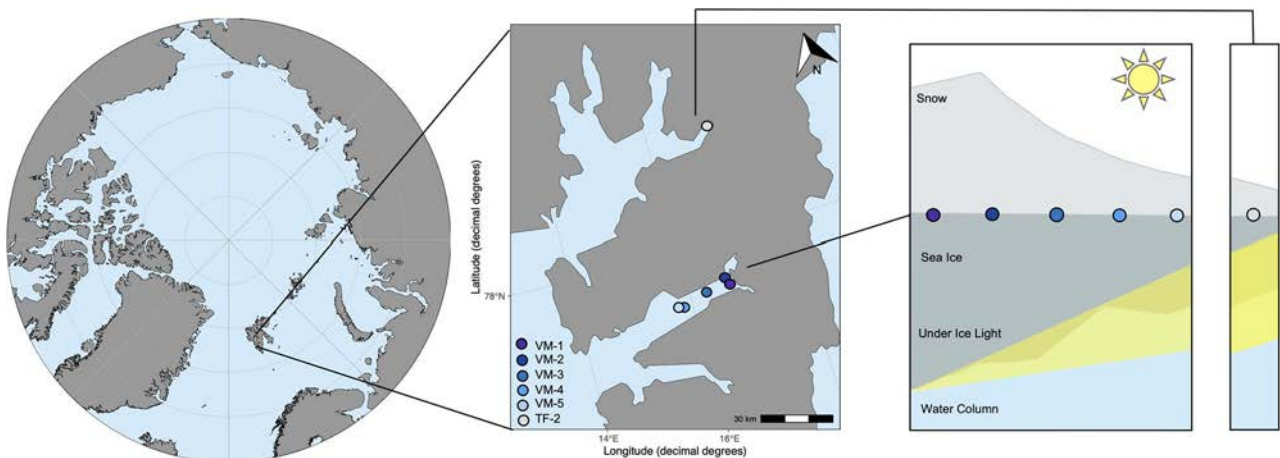


**Figure 2.** Location of Svalbard, Norway, within the Arctic (left), sampling locations visited between April and May 2021 in Svalbard (middle), overview of the snow depth, sea ice thickness, and under-ice light at each of the sampling stations (right).

gauge. Water temperature was measured just below the ice-water interface using a CTD probe (STD/CTD SD204, SAIV A/S; Bergen, Norway). At each sampling site, ~100 ml of the water

from directly below the ice surface was collected in acid washed bottles for nutrient analysis. The samples were frozen until analysis, when they were melted and 4 M  $\text{H}_2\text{SO}_4$  was added for

**Table 1.** IR band assignments for s-FTIR microspectroscopy used in this study.

Wave number (cm <sup>-1</sup> )	Band assignment	Reference
~3011	$\nu(\text{C-H})$ of cis C=CH- from unsaturated lipids	Vongsvivut et al. [108]
~2960	$\nu_{\text{as}}(\text{C-H})$ from methyl (-CH <sub>3</sub> ) groups of lipids and proteins	Vongsvivut et al. [108]
~2921	$\nu_{\text{as}}(\text{C-H})$ from methylene (-CH <sub>2</sub> ) from saturated lipids	Vongsvivut et al. [108]
~2852	$\nu_{\text{s}}(\text{C-H})$ from methylene (-CH <sub>2</sub> ) from saturated lipids	Vongsvivut et al. [108]
~1744	$\nu(\text{C=O})$ from ester carbonyl group from lipid triglycerides and fatty acids	Vongsvivut et al. [108]
~1549	Amide II mode from proteins; mainly $\delta(\text{N-H})$ of amides	Heraud et al. [109]
~1400	$\nu_{\text{s}}(\text{COO}^-)$ from carboxylated molecules	Sackett et al. [110]
~1377	$\delta_{\text{s}}(\text{CH}_3)$ and $\delta_{\text{s}}(\text{CH}_2)$ of lipids and proteins	Heraud et al. [111]
~1241	$\nu_{\text{as}}(\text{PO}_2^-)$ of the phosphodiester backbone of nucleic acids, phosphorylated proteins, and phosphorylated lipids	Whelan et al. [112] and Sackett et al. [110]
~1146	$\nu_{\text{s}}(\text{C-O})$ from carbohydrates	Heraud et al. [113]
~1080	$\nu_{\text{s}}(\text{Si-O})$ from silica	Beardall et al. [114] and Sackett et al. [115]

preservation in transport for analysis at Akvaplan-niva, Norway. The nitrate plus nitrite ( $\text{NO}_3^- + \text{NO}_2^-$ ) (NOx), phosphate ( $\text{PO}_4^{3-}$ ), silicic acid ( $\text{Si}(\text{OH})_4$ ), and ammonium ( $\text{NH}_4$ ) concentrations ( $\mu\text{M}$ ) were measured simultaneously on a San++ 5000 automated analyser (Skalar: Breda, the Netherlands), with separate analysis channels for the four nutrients. The detection limits were 0.02  $\mu\text{M}$  for NOx, 0.01  $\mu\text{M}$  for phosphate, 0.25  $\mu\text{M}$  for silicic acid, and 0.3  $\mu\text{M}$  for ammonium. Stable isotope analysis of the 0–3 cm section of sea ice was performed in an elemental analyser isotope ratio mass spectrometry system, as previously published [64].

### Light measurements and modelling

Incoming photosynthetically active radiation (PAR) was measured at each sampling site in Van Mijenfjorden using a LI-190 quantum air sensor placed on the sea ice surface and a LI-192 underwater quantum sensor placed on a weighted frame positioned through a 10-cm hole in the sea ice, with measurements collected using a LI-1500 Data Logger (LI-COR, Nebraska, USA). To avoid shadowing of the measurement area, all sensors faced south with operations performed north, and the area was undisturbed. However, at Tempelfjorden, the underwater quantum sensor failed. Therefore, to ensure light transmittance values were available from all sampled sites and determined using a consistent methodology, and to utilize our unique *in situ* surface light measurements, the under-ice light measurements were modelled. Light at the ice-water interface under the sea ice was estimated using *in situ* measured irradiance at the top of snow and ice, and then attenuation through snow and ice was determined using attenuation coefficients of 20  $\text{m}^{-1}$  for snow, 5  $\text{m}^{-1}$  for the top 10 cm of ice, and 1  $\text{m}^{-1}$  for ice below the top 10 cm [65, 66], using the following equation:

$$E_z = E_0 \cdot \exp(-K_d \cdot Z) \quad (1)$$

where ( $E_z$ ) is irradiance at sampling depth,  $E_0$  is the surface irradiance ( $\mu\text{mol photons m}^{-2} \text{ s}^{-1}$ ),  $K_d$  is the diffuse light attenuation coefficient ( $\text{m}^{-1}$ ), and  $Z$  is the sampling depth (m). Light values at the ice-water interface were converted to percent incoming PAR to account for the measured *in situ* irradiance above-ice being taken at various times of day and with a range of cloud coverage conditions, which have a substantial effect on light levels [67, 68]. Below we use light transmissivity as a descriptive term for percent incoming PAR and have divided the sites into those receiving < 5% incoming PAR as low light transmissivity (LLT) sites, and those

receiving > 5% incoming PAR as high light transmissivity (HLT) sites.

### Species-specific biomolecular composition by Fourier transform infrared

The biomolecular composition of five selected taxa (*N. frigida*, *Pleurosigma* spp., *Navicula* spp., *Haslea* spp., and *Entomoneis* spp.) (Table S2) was determined using synchrotron-based FTIR microspectroscopy on hydrated, formalin-fixed (5% v/v final concentration) cells. All cells were measured as single cells, i.e. not dividing or associated with a chain. The *Navicula* spp. group consisted primarily of *Navicula transitas*, *Navicula directa*, and *Navicula valida*. Samples were loaded (3  $\mu\text{l}$ ) directly into a micro-compression cell between two 13 mm diameter 0.5-mm thick  $\text{CaF}_2$  windows [69]. Using the Infrared (IR) Microspectroscopy Beamline at the Australian Synchrotron, Victoria, spectral data of individual cells (between 1 and 20 cells per taxon per site, Table S3) were collected in transmission mode. Each biomolecule absorbs a specific range of IR wavelengths, and a set of well-defined absorbance bands between 3050–2800  $\text{cm}^{-1}$ , and 1770–1100  $\text{cm}^{-1}$  have been determined (Table 1). Spectra were acquired over the measurement range 4000–800  $\text{cm}^{-1}$  with a Vertex 80v FTIR spectrometer (Bruker Optic, Ettlingen, Germany) in conjunction with an IR microscope (Hyperion 3000, Bruker) fitted with a narrow-band mercury cadmium telluride detector cooled with liquid nitrogen. The use of hydrated cells as opposed to desiccated samples has been shown to limit light scattering effects [70]. Co-added interferograms (sample  $n=32$ , background  $n=64$ ) were collected at a wavenumber resolution of 4  $\text{cm}^{-1}$ . To allow for measurements of individual cells, all measurements were made in transmission mode, using a measuring aperture diameter of 6.9  $\mu\text{m}$  (area = 37.4  $\mu\text{m}^2$ ) for the smaller taxa (*N. frigida*, *Navicula* spp., and *Haslea* spp.) and 12.5  $\mu\text{m}$  (area = 122.7  $\mu\text{m}^2$ ) for the larger taxa (*Pleurosigma* spp. and *Entomoneis* spp.). All cells were measured with multiple points across the cell surface to account for heterogeneity in the cell structure and distribution of biomolecules (Fig. 3). Spectral acquisition and instrument control were achieved using Opus 7.5 software (Bruker). Analyses were performed within 6 months of samples being collected and fixed. All samples were kept refrigerated between fixation and analysis.

### Data analyses

IR spectral data were analysed in R v4.2.2 [71]. Data were smoothed (4 pts either side) and second derivative (third-order



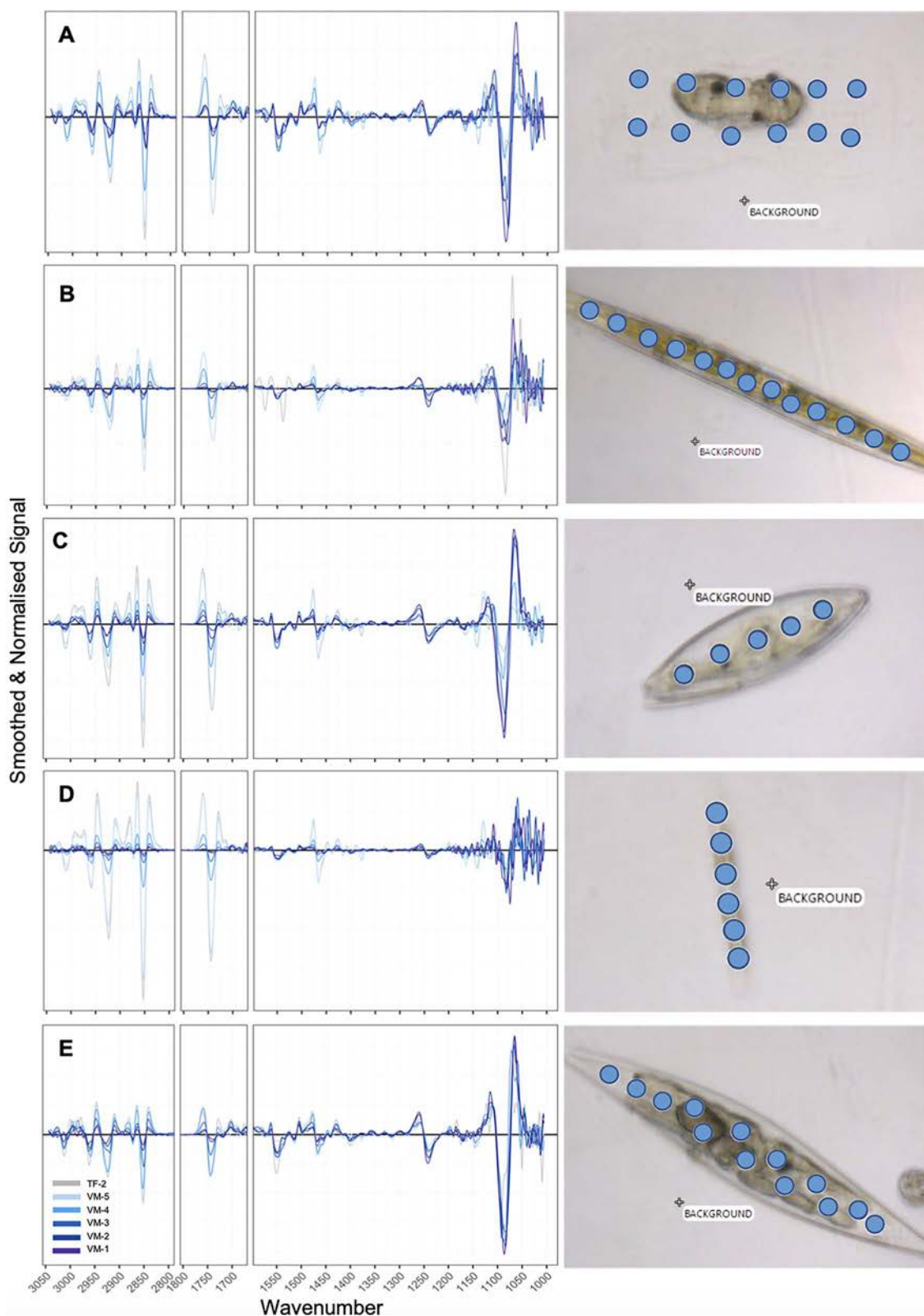


**Figure 3.** Smoothed and normalized spectra of each of the five taxa, (A) *Entomoneis* spp., (B) *Haslea* spp., (C) *Navicula* spp., (D) *N. Frigida*, (E) *Pleurosigma* spp., with each site denoted through a gradient; images of example cells of each taxa (right) with dots denoting the s-FTIR measurement points (where the aperture (actual measuring area) for each point was larger than the point indicated), demonstrating the entire cell contents were measured.

polynomial) transformed using the Savitzky–Golay algorithm from the `prospectr` package [72] and then normalized using Standard Normal Variate (mean centred and SD of 1) (Fig. 3). Biomolecular content for each measured cell was estimated

based on integrating the area under each assigned peak (Table 1), using the Beer–Lambert Law, which assumes a direct relationship between absorbance and analyte concentration to determine metabolite content [73].

Relationships between biomolecular content and environmental variables (% incoming PAR, nitrate and silicate concentration in the water at ice–water interface, bottom-ice temperature and salinity and water temperature at the ice–water interface) were investigated using Spearman's rank correlation coefficient (Table S4). As % incoming PAR was the most highly correlated with the biomolecular profile, relationships between biomolecular content and percent incoming PAR were estimated using principal component analyses (PCA) and with linear regressions applied to the mean peak area at each incoming % PAR level (i.e. each sampling site) ( $\pm$  95% confidence interval) for each taxon. Because of the difference in absorption properties of biomolecules, the integrated peak areas provide relative changes between samples, meaning any quantitative measure of change can only be applied within compounds. The Shapiro–Wilks [74] test for normality showed the data required  $\log_{10}$  transformation before analysis. The number of cells measured ranged from 1 to 20 per taxa, per site (Table S3). Because of the low abundance of *Haslea* spp. and *Pleurosigma* spp. at TF-2, however, no confidence interval was applied to the linear regressions beyond 15.2% incoming PAR. Relationships between lipid and protein content, lipid and carbohydrate content, and carbohydrate and protein content, with increasing light reaching the ice–water interface, were also investigated using linear regression. Fixed factor linear regression models, with under-ice light level (HLT vs LLT) as the factor, were used to determine that these regressions were improved when separated according to HLT sites (VM-4, VM-5, TF-2) and LLT sites (VM-1–3) sites. Statistical significance of the regressions was concluded based on the *F* statistic ( $P < .05$ ) and strength of fit estimated using  $R^2$ . The residuals of all regressions were verified for homoscedasticity. All analyses were performed using R Studio v. 2022.02.03 [71] and the add-on packages ggplot v. 3.3.6 [75], dplyr v. 1.0.8 [76], corrplot [77], and vegan v. 2.6–4 [78].

## Results

### Physical parameters

Within Van Mijenfjorden, snow depth and ice thickness decreased towards the fjord opening. The outermost site (VM-5) had ice thickness of  $52 \pm 3.5$  cm and a snow depth of  $4.8 \pm 3.5$  cm, allowing 15% incoming PAR at the ice–water interface, and the innermost site (VM-1) had ice thickness of  $92 \pm 3.2$  cm and snow depth of  $14.3 \pm 0.7$ , allowing 1.5% incoming PAR (for data on all sites, see Table 2). The Tempelfjorden site (TF-2) had the highest incoming PAR at 23%, with an ice thickness of  $38 \pm 1.1$  cm and snow depth of  $3.4 \pm 0.7$  cm. Based on the average incoming PAR of  $640 \mu\text{mol m}^{-2} \text{s}^{-1}$ , measured *in situ* at the snow surface of the sampling sites, this equates to a range of 8–148  $\mu\text{mol m}^{-2} \text{s}^{-1}$  transmitted through the snow and ice to the bottom ice community. In mid-April, all VM sites experienced < 3% incoming PAR; however, by late April, VM-4 and VM-5 experienced 23% and 14% incoming PAR, respectively. Seawater nutrient concentrations were relatively high, with nitrate concentrations ranging from 2.18  $\mu\text{M}$  (VM-4) to 1.92  $\mu\text{M}$  (TF-2) (Table 2) and silicate concentrations ranging from 2.81  $\mu\text{M}$  (VM-4 and 5) to 2.5  $\mu\text{M}$  (VM-1). Taken from the sea ice, stable isotope of carbon ( $\delta^{13}\text{C}_{\text{VPDB}}$  (‰)) was more enriched at HLT sites ( $t(2) = 4.02$ ,  $P < 0.05$ ), averaging  $-17.42 \pm 3.2$  at the HLT sites (TF-2, VM-4, VM-5) and  $-24.85 \pm 0.5$  at the LLT sites (VM-1–3). Ice temperature in the 0–3 cm section was between  $-2.1$  and  $-2.2^\circ\text{C}$  at all VM sites and  $-2.7$  at TF-2, whereas the under-ice water temperature ranged from at  $-1.61^\circ\text{C}$  (VM-4) to  $-1.86$  (VM-2). Bottom bulk ice salinity ranged from 10.7 (VM-2) to 3.7 (VM-4). Given that bottom ice temperature was consistently below

the seawater freezing point ( $-1.7^\circ\text{C}$ ), brine volume remained well within the reasonable range for communities to inhabit sea ice (>5%) [77] and all sites were nutrient replete (>1.9  $\mu\text{M}$ ), these environmental variables were unlikely significant drivers for any observed metabolomic changes. In contrast, under-ice light transmittance (through snow and ice), was the most variable environmental variable across sites, but also the one that correlated most strongly and consistently with biomolecular content (Table S5) and therefore the focus of this study. For more details and further physical parameters, see Table 2 and [58].

### Species-specific biomolecular composition

Across all five taxa, lipid (ester carbonyl) and carbohydrate content generally increased with increasing percent incoming PAR until 15% surface irradiance, after which, the content plateaued or declined in all taxa except for *Navicula* spp., which saw a continued increase up to 23% incoming PAR (Fig. 4; Table S5). The other photosynthetically derived biomolecules, including unsaturated FAs, SAFAs, saturated lipids, and lipids (CH-stretch II), followed the same increasing trend with percent incoming PAR until  $\sim$ 15% (Fig. 4; Table S5). We saw no clear trend associated with percent incoming PAR for the other functional biomolecules, i.e. protein (amide II) and phosphorylated molecules (Fig. 4; Table S5). Carboxylated molecules experienced a decline with increasing percent incoming PAR in all taxa except *Pleurosigma* spp. (Fig. 4).

The correlation matrix shows clear separation in the relationships between photosynthetically derived and structural biomolecules (Fig. 5A). We saw strong positive correlations (>0.75) amongst the lipid compounds (ester carbonyls, saturated lipids, SAFAs, and unsaturated FAs), and moderate positive correlations with carbohydrates (>0.50, Fig. 5A). Furthermore, these photosynthetically derived biomolecules were only weakly correlated with protein and phosphorylated molecule content (<0.3), and negatively correlated with carboxylated molecules (<−0.3). Structural biomolecules (protein, phosphorylated molecules, carboxylated molecules) were positively correlated with one another (>0.6, Fig. 5A).

Analysing all peak areas of all five taxa from all sites, we found clustering according to a light gradient (Fig. 5A), with PC1 explaining 61.9% of the variation in biomolecular content, correlating with the gradient in percent incoming PAR. The difference observed across PC1 was driven by lipid, saturated lipid, SAFA, unsaturated FA, lipid (CH-stretch II), and carbohydrate bands, corresponding with their measured increase with increasing transmitted irradiance (Fig. 4). The next main source of variation along the PC-2 was driven by the difference in protein (amide II), carboxylated molecules, and phosphorylated molecule content, explaining 28% of the variation (Fig. 5B). Separation of the data by taxa reveals that this variation is likely species derived, with *N. frigida* and *Haslea* spp., clustering separately to *Navicula* spp., *Pleurosigma* spp., and *Entomoneis* spp., particularly within the LLT sites (Fig. 5B).

To estimate the key changes to biomolecular content and carbon allocation in the cell, the relationships between lipid, protein, and carbohydrate were investigated for each taxon using linear models. Including low (<5% incoming PAR) and high (>5% incoming PAR) light as fixed factors improved the model outcome, resulting in two regressions for each comparison. A positive correlation between lipid and carbohydrate was observed at HLT conditions only ( $F_{1,182} = 92.95$ ,  $P < .05$ ;  $R^2 = 0.34$ , Fig 6A) and the same correlation was observed for each species individually (Table S5). No correlation between lipid and carbohydrate was observed at LLT sites when all species were considered together (Fig. 6A).

**Table 2.** Parameters measured associated with sea ice core extraction; snow depth ( $\pm$  SD,  $n=18$ ), ice thickness ( $\pm$  SD,  $n=6$ ), % incoming PAR, and under ice light ( $\mu\text{mol m}^{-2} \text{s}^{-1}$ ); measurements from within the bottom 3 cm of sea ice core: temperature ( $^{\circ}\text{C}$ ), bulk salinity (ppt), brine salinity (ppt), brine volume (% of ice volume), chlorophyll *a* concentration ( $\text{mg/m}^2$ ) ( $n=3$ ), particulate organic carbon to particulate organic nitrogen ratio (C:N); parameters measured in under-ice water at each sampling site: ammonium ( $\text{NH}_4$ ), silicate ( $\text{Si(OH)}_4$ ), nitrate ( $\text{NO}_3$ ), and phosphate ( $\text{PO}_4$ ) concentrations ( $\mu\text{M}$ ) and temperature ( $^{\circ}\text{C}$ ), where N.D. denotes not measured.

Sea ice												Under-ice water				
Date	Station	Snow depth (cm)	Ice thickness (cm)	% incoming PAR	Light ( $\mu\text{mol m}^{-2} \text{s}^{-1}$ )	Ice temperature ( $^{\circ}\text{C}$ )	Ice salinity (ppt)	Brine salinity (ppt)	Brine volume (%)	Chlorophyll ( $\text{mg/m}^2$ )	C:N	$\text{NH}_4$ ( $\mu\text{M}$ )	$\text{Si(OH)}_4$ ( $\mu\text{M}$ )	$\text{NO}_3$ ( $\mu\text{M}$ )	$\text{PO}_4$ ( $\mu\text{M}$ )	Temperature ( $^{\circ}\text{C}$ )
5.5.21	VM-1	14.3 $\pm$ 0.7	92 $\pm$ 3.2	1.5	12.52	-2.1	6.5	37.36	15.57	0.48 $\pm$ 0.3	6.09	<1	2.50	2.10	0.20	-1.71
5.5.21	VM-2	15.8 $\pm$ 2.1	78 $\pm$ 3.0	1.3	8.66	-2.2	10.7	39.07	24.49	0.29 $\pm$ 0.0	5.73	<1	2.60	2.08	0.20	-1.86
4.5.21	VM-3	10.0 $\pm$ 0.9	74 $\pm$ 2.6	4.2	17.14	-2.2	10.4	39.07	23.81	1.90 $\pm$ 0.2	6.02	<1	2.71	2.14	0.21	-1.81
4.5.21	VM-4	7.0 $\pm$ 3.2	50 $\pm$ 2.2	10.3	68.17	-2.1	3.7	37.36	8.86	0.63 $\pm$ 0.1	7.50	<1	2.81	2.18	0.23	-1.61
4.5.21	VM-5	4.8 $\pm$ 3.5	52 $\pm$ 3.5	15.2	99.29	-2.2	5.6	39.07	12.82	0.86 $\pm$ 0.2	6.92	<1	2.81	2.14	0.23	N.D.
30.4.21	TF-2	3.4 $\pm$ 0.7	38 $\pm$ 1.1	23.2	104.19	-2.7	9.2	47.53	17.25	2.82 $\pm$ 1.0	10.18	<1	2.71	1.92	0.20	-1.80

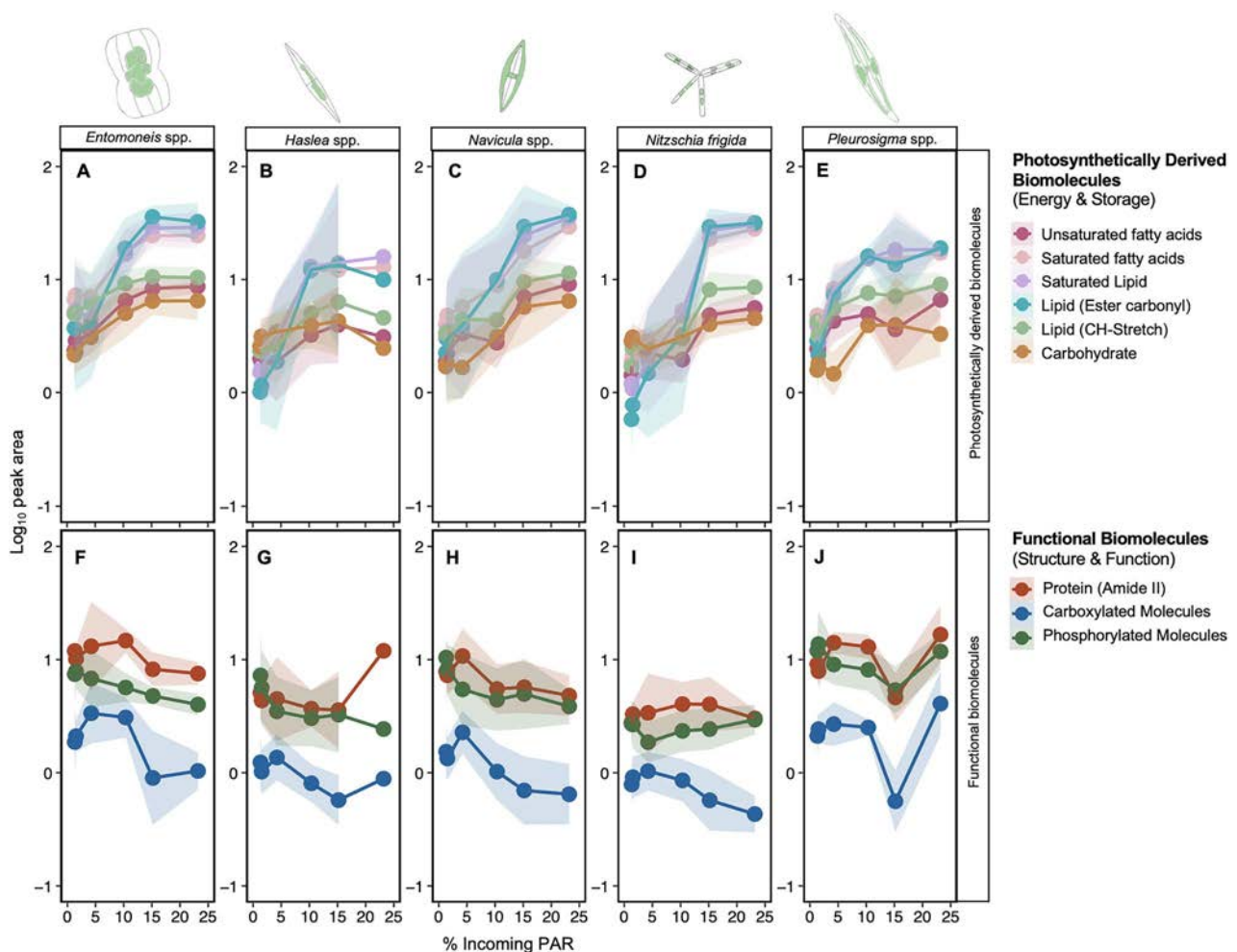


**Figure 4.** Mean cell-specific biomolecular content (based on normalized peak areas—see Table 1) for photosynthetically derived (energy-rich, storage) biomolecules (unsaturated fatty acids, saturated fatty acids, saturated lipids, lipids (ester carbonyl), lipids (CH-stretch II), and carbohydrates) (A) *Entomoneis* spp., (B) *Haslea* spp., (C) *Navicula* spp., (D) *N. Frigida*, (E) *Pleurosigma* spp., and functional (structural and cell function) biomolecules (protein (amide II), carboxylated molecules, phosphorylated molecules) (F) *Entomoneis* spp., (G) *Haslea* spp., (H) *Navicula* spp., (I) *N. Frigida*, (J) *Pleurosigma* spp. as a function of the proportion of light reaching the ice–water interface; shading indicates 95% confidence intervals, applied to log-transformed data.

We saw a positive correlation between lipid and protein in all species under LLT conditions ( $F_{1,98} = 271.8$ ,  $P < .05$ ;  $R^2 = .58$ , Fig 6B; Table S5). This was also observed at HLT when all species were considered together ( $F_{1,182} = 10.15$ ,  $P < .05$ ;  $R^2 = 0.06$ , Fig. 6B), driven

by the positive correlations in *Entomoneis* spp. and *Haslea* spp. only (Table S5). A strong parallel shift in increasing lipid content from LLT to HLT conditions was observed in all five taxa (Fig. S1). For carbohydrate, a weak negative correlation relationship with

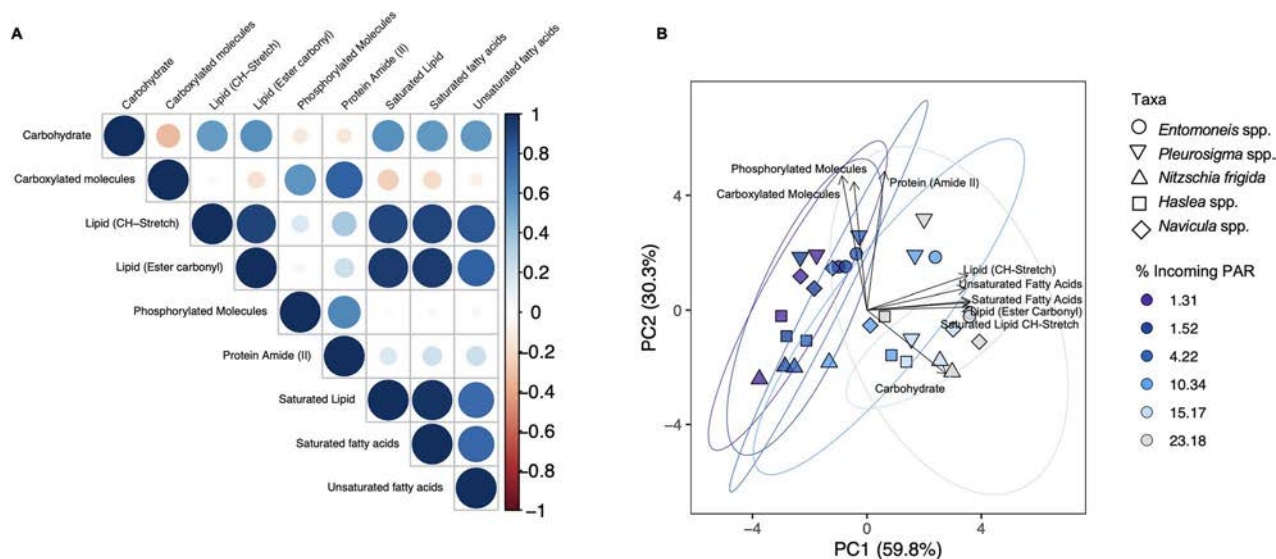


**Figure 5.** (A) Correlation plot based on Spearman's rank correlation coefficient for biomolecular content across all taxa and sampling sites, where gradient is used to represent the strength of correlation (and blue represents positive whilst red represents negative correlation); (B) PCA of biomolecular content at each under-ice light level for all taxa combined (*Entomoneis* spp., *Haslea* spp., *Navicula* spp., *N. Frigida*, and *Pleurosigma* spp.); direction and strength of individual biomolecules are displayed with ordination bi-plot overlay.

protein content was observed in the LLT sites when all species were considered together (Fig 6C), whereas a positive correlation was observed at HLT sites. Similar to lipids, *Entomoneis* spp. and *Haslea* spp. only exhibited increases in carbohydrate content under HLT, with minimal changes to protein content (Table S5).

Integration of the silica peaks (maxima at  $1080\text{ cm}^{-1}$ ) for each species and site revealed that silica concentration declined with declining percent incoming PAR in all species (Fig. 7A–E). For *Entomoneis* spp. ( $F_{1,66} = 44.94$ ,  $P < .05$ ;  $R^2 = 0.41$ ), *Haslea* spp., ( $F_{1,55} = 14.77$ ,  $P < .05$ ;  $R^2 = 0.22$ ), *Navicula* spp. ( $F_{1,104} = 107.6$ ,  $P < .05$ ;  $R^2 = 0.51$ ), and *Pleurosigma* spp. ( $F_{1,40} = 21.67$ ,  $P < .05$ ;  $R^2 = 0.35$ ), the decline in silica content was linear with declining percent incoming PAR, whereas for *N. frigida* ( $F_{2,106} = 26.2$ ,  $P < .05$ ;  $R^2 = 0.33$ ), the decline was observed until  $\sim 15\%$  incoming PAR, after which it plateaued, suggesting a minimum level of silicification had been reached.

## Discussion

Biomolecules supplied by sea-ice microalgae to the polar marine food web are important, particularly as the primary food supply early in the season, but also as a source of essential fatty acids for zooplankton reproduction. Microalgal biomolecular composition, however, is environmentally determined [27] and therefore even subtle shifts in the physio-chemical conditions of the surrounding environment can affect the nutritional content supplied to the marine food web. In this study, key environmental variables (temperature, nutrients, salinity, etc.) varied minimally across the sites and were generally within the expected range for spring [79], whereas snow and sea-ice thickness varied more and the resulting under-ice light transmittance strongly correlated with biomolecular changes.

Across all five taxa, we found that increasing under-ice light availability led to an increase in lipids, fatty acids, and carbohydrates, and that lipid accumulation was preferentially allocated over carbohydrates at higher irradiances. In most cases, the increases in lipids, fatty acids, and carbohydrates were observed until  $\sim 15\%$  incoming PAR, at which point saturation occurred. This observed threshold could be because of the highest

irradiances causing photoinhibition and thus limiting further biomolecular production [80–82], as the measured irradiances for VM-5 and TF-2 were outside the typical spring bloom range ( $>20\%$  incoming PAR or  $>100\ \mu\text{mol m}^{-2}\ \text{s}^{-1}$ ) [27]. Evidence of photoinhibition has been observed in sea-ice microalgae at similar light levels [82–84] and is generally a result of synthesis of photoprotective pigments, changes to chlorophyll content, and downregulation of photosystem II [84]. The greatest increase in lipid content with increasing under-ice light was observed in *N. frigida* until 15% incoming PAR, which aligns with previous observations that *N. frigida* accumulated higher lipid stores than *Attheya* spp. and pennate ribbon colonies [56]. The exception to the observed light threshold was *Navicula* spp., which continued to increase lipid and carbohydrate content beyond 15% incoming PAR, suggesting morphological or photophysiological differences in this taxon. One explanation for this difference could be that *Navicula* spp. often have large central regions with chloroplasts concentrated along the cell wall [85] and low intracellular chlorophyll under high light conditions as a photoadaptive strategy [86], minimizing photoinhibition and leaving substantial space for lipid accumulation in oil droplets within the cytoplasm [87]. In Antarctic sea-ice microalgal communities, *Navicula* spp. were found also to have a higher lipid content compared with other taxa [88, 89].

There are several plausible explanations for the conserved response of the relative increases in lipid, fatty acid, and carbohydrate with increasing light transmittance, these include: (i) increased growth rate (assuming a pre-bloom phase), (ii) increased requirement for carbon storage in preparation for dormancy (assuming a post-bloom phase), or (iii) the onset of nutrient limitation as a result of increasing algal biomass restricting nutrient influx within the ice. It is likely that the higher light communities (HLT) were experiencing higher growth rates relative to the LLT communities, because of the greater light availability driving more photosynthesis [90]. The samples from the HLT sites were also more enriched with  $^{13}\text{C}$ , a parameter often associated with higher growth rates in microalgal species [91], lending further support to the idea that the increased lipid and carbohydrates were a result of higher growth rates.

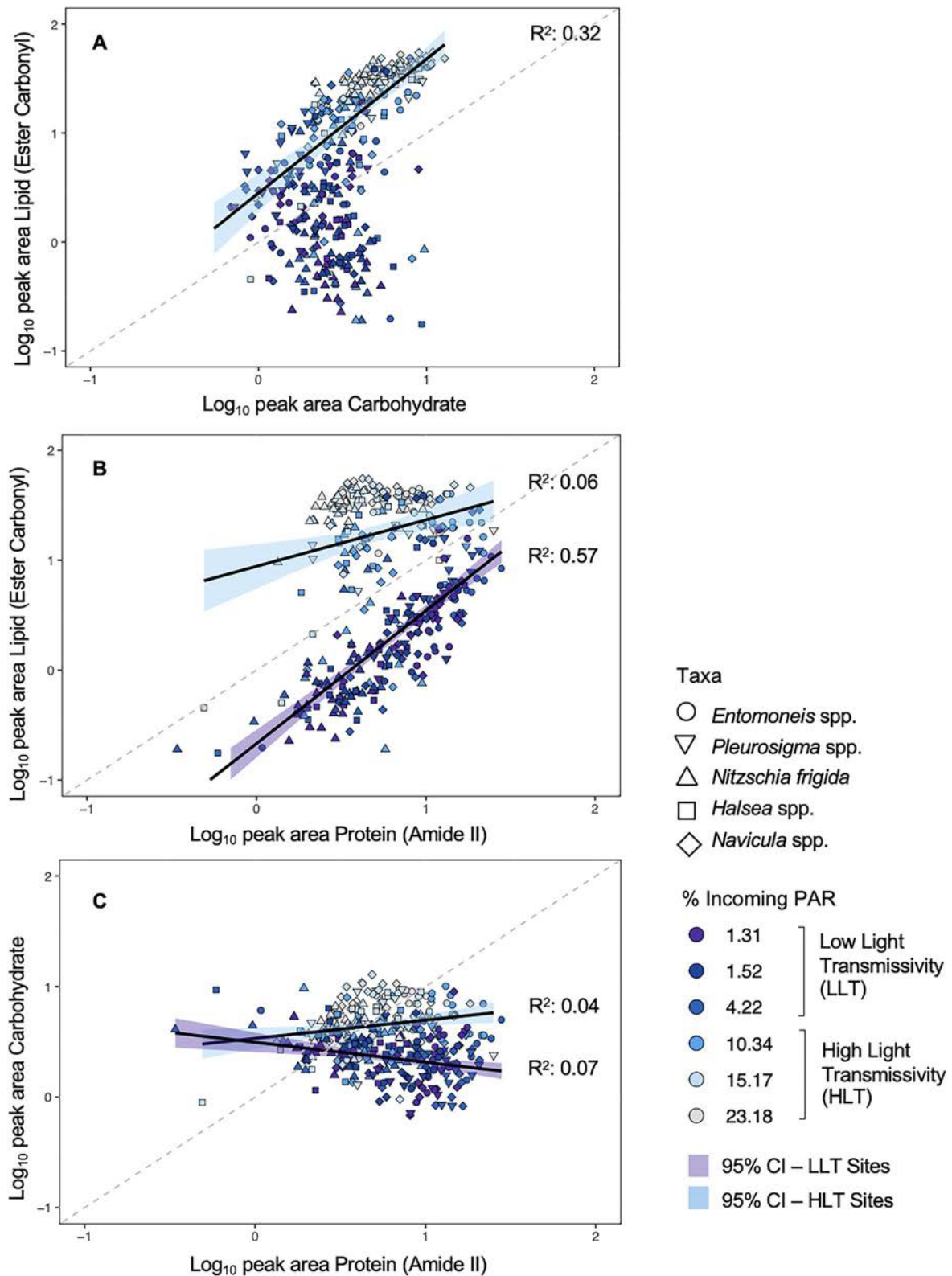


**Figure 6.** (A) Lipid (ester carbonyl) vs. carbohydrate content, (B) lipid (ester carbonyl) vs. protein (amide II) content, and (C) carbohydrate vs. protein content, based on normalized peak areas, for all taxa combined and. Data are divided into HLT sites (VM-4, VM-5, TF-2) and LLT sites (VM-1–3), with light levels indicated with a gradient fill and taxa are denoted by shape; the data are fitted with linear regressions, with 95% confidence intervals (shading), applied to log-transformed data; only statistically significant regressions are shown.

Whilst surrounding  $\text{CO}_2$  concentrations were not evaluated, they were unlikely to have influenced  $^{13}\text{C}$  enrichment, as the  $\text{CO}_2$  concentration in brine channels is typically determined by

temperature, which was consistent across our sites [92]. Under the assumption that the  $^{13}\text{C}$  is because of higher growth rates, the increase in lipid content may be attributed primarily to structural

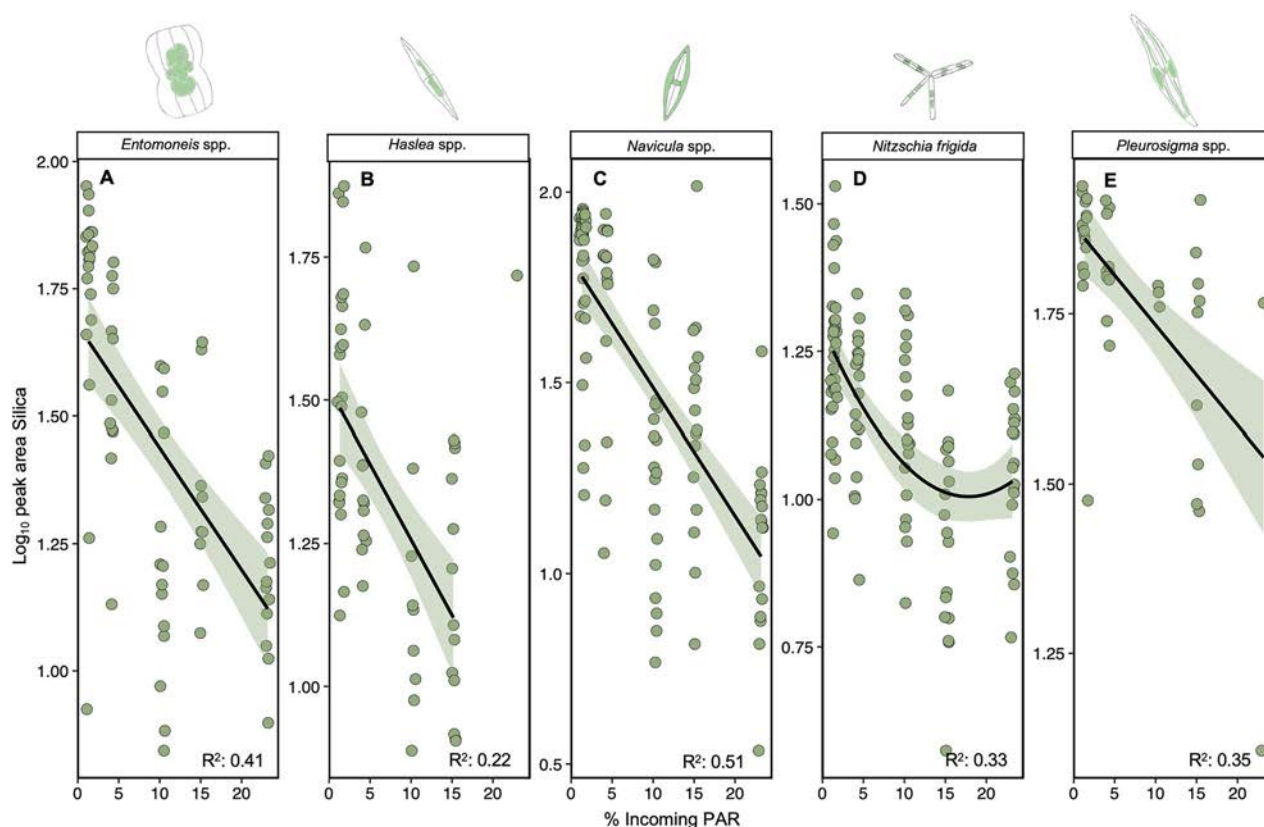


**Figure 7.** Silica content (based on normalized peak areas) with increasing percent photosynthetic active radiation (PAR) reaching the ice–water interface, per taxa; each data point represents one measured cell; the data are fitted with linear regressions, with 95% confidence intervals (shading), applied to log-transformed data; only statistically significant regressions are shown.

lipids, as microalgae tend to accumulate structural (polar), over storage (neutral), lipids alongside an increase in growth rate, and as a response to early season light intensification [30]. An increase in growth rate and structural lipid content may explain the concurrent increase observed in other biomolecules, including carboxylated molecules [93] and unsaturated FAs, as PUFAs are found primarily in structural lipids [94].

An additional explanation for the increased lipid content with higher light transmittance lies with the fact that many sea-ice algal species have a dormancy strategy for overwintering, in which the cells increase their carbon reserves whilst reducing cellular metabolic activity and pigment content [95, 96]. This well-described strategy means that the increase in lipid, fatty acid, and carbohydrate measured in the cells from HLT sites in this study may reflect a response to increased light at the end of the growth season, when energy storage becomes a priority [97]. This physiological response may also explain the higher allocation to protein content relative to lipid and carbohydrate observed at LLT sites, as cell growth and division may have had lower priority at the HLT sites. The end-of-season response of reduced growth and increased allocation to storage molecules such as lipid, carbohydrate (specifically triacylglycerides and the polysaccharide storage polymer, glucan), and MUFA content has been observed previously in ice algal communities in response to increasing irradiance and decreasing nutrients characteristic of a post-bloom phase [80, 94, 98, 99]. Whilst nutrients were not limiting in the water under the ice at any of the sampling sites in this study, nor did we detect any decline over time [58], nutrient limitation within the boundary layer of the under-ice community cannot be ruled out, especially as cell densities increased. That said, the relatively low biomass accumulation at all sites, supported by the

low chlorophyll *a* values [100, 101], in addition with the ice C:N ratios being close to Redfield (6.6) in all sites except VM-4 and TF-2, makes the onset of nutrient limitation within the ice community, and therefore the third possible explanation, less likely. It is possible, that instead of one specific driver underpinning the measured response, a blend or cascade of these processes was at play, as both SAFA and unsaturated FA increased and responses were often species-specific, as well as spatially and temporally diverse. Of note, we observed large lipid droplets within cells from HLT sites during microspectroscopic measurements (personal observation), indicating that lipid was being accumulated for storage in some cells. Such changes in biomolecular content have been observed in different organisms as an adaptation to seasonality in resource availability and life stage requirements [102]. Most importantly, however, whether driven by changes in energy allocation towards higher growth rates or increased energy storage in preparation for dormancy, the change in biomolecular content correlated with under-ice light environment, signifying the importance of light in determining food and essential nutrient availability to primary consumers.

The biomolecules more closely associated with functional cellular components were shown to vary with light transmissivity and across species, with some evidence of size-class grouping. Lipid (CH-stretch II) content increased with light in all taxa. Conversely, in all taxa, except *N. frigida*, we saw a decrease in phosphorylated molecules with increasing light. We saw a more nuanced response in protein across the five taxa, with four taxa showing no change in cellular protein content with light, whereas for one of the smallest taxa, *Navicula* spp., protein content was negatively correlated with under-ice light availability (up to 15% incoming PAR). The lack of protein changes in the larger taxa corresponds

with a previous study that showed protein content in sea-ice algae to remain stable, independent of light conditions [56]. In contrast to our findings, earlier work observed higher protein content under low light conditions [28, 103], but this was attributed to higher nutrients in the surrounding environment, rather than the low light conditions [104]. This finding may indicate a potential size-specific biomolecular response, in which smaller taxa have a reduced requirement to allocate energy into protein compared with larger taxa.

In addition, we found silica content declined with increasing light transmittance in all five taxa with the exception of an upturn in silica content at the highest light level in *N. frigida*. Similar trends in decline have been observed previously in light levels up to  $150 \mu\text{mol m}^{-2} \text{ s}^{-1}$  [105], whereas the opposite direction of change has been shown at particularly elevated light levels ( $300 \mu\text{mol m}^{-2} \text{ s}^{-1}$ ) [106], meaning that there may be different mechanisms at play with respect to changes in diatom silicification and making the insights from this natural community study an important addition. The decrease in silica content observed with higher light conditions in this study could be attributed to higher growth rates. Changes in silicification has the potential to affect zooplankton grazing efficiency, as zooplankton have been shown to preferentially graze on less silicified diatoms [107] and reduced silica content may also mean the diatoms are more buoyant and therefore able to remain in the photic zone for longer when released from the sea ice, suggestive of potential changes to carbon flux.

The relationships between both photosynthetically derived and functional biomolecules and under-ice light have implications on energy supplied to the marine food web. In considering the prediction that parts of the Arctic may experience higher snowfall in the short-medium term [14, 23], and therefore less light under the sea ice, our results indicate that such environmental conditions would be concomitant with a shorter productive season, lower growth rates, and biomass accumulation, as well as a lower lipid, carbohydrate, fatty acid, and lipid (CH-stretch II) content in Arctic sea-ice algae. This would have significant implications for secondary production and beyond, with a reduced supply of organic carbon. In addition, critical biomolecules that are produced de novo, such as SAFAs, would likely be reduced, limiting supply to higher trophic levels [94]. Such reductions would be expected to have ramifications on secondary production and zooplankton fecundity [5]. Counter to the forecast of higher snowfall, if the increased precipitation comes in the form of rain or equally, as the warming ocean and air temperatures reduce ice thickness, then the under-ice light climate would increase. According to our data, the Arctic sea-ice algal communities could be expected to reduce silica content whilst increasing their lipid, carbohydrate, and fatty acid stores, at least until a certain threshold of incoming irradiance, beyond which could lead to photoinhibition, limiting photosynthetic energy production, and thereby biomolecular synthesis [81]. Higher under-ice light is likely to result in a higher relative abundance of *Navicula* spp., at the expense of the typically more dominant *N. frigida* [58], meaning that we might see even greater stores of lipid and carbohydrate with increasing under-ice light (beyond the threshold of 15% incoming PAR). Whilst higher under-ice light conditions may result in a community which is more calorific and nutrient rich, thinner sea ice conditions, and warmer ocean temperatures would likely shorten the ice-covered duration and/or result in earlier release of the community from the brine channels and therefore could result in a mismatch of energy supply for zooplankton reproduction [5]. In the most extreme case, where warming prevents sea ice from forming, the lack of substrate for sea-ice algae communities to develop would

mean that this energy source would no longer be available to fuel polar marine food webs as they emerge from winter darkness.

Our study has revealed the importance of characterizing taxonomically resolved biochemical changes under varying environmental conditions. This is particularly pertinent for Arctic marine ecosystems where the effects of climate change are already occurring. Whilst uncertainty remains about the direction and magnitude of change to future under-ice light regimes, the results herein indicate that the nutritional content of key ice algae taxa will vary in response to shifts in under-ice light conditions which may result in a net loss of nutritional output. In combination with environmentally driven shifts in Arctic sea-ice microalgal community composition, season duration, and biomass accumulation, these changes will have implications for the quality and quantity of energy supplied to the polar marine food web.

## Acknowledgements

R.J.D. is supported by an Australian Government Research Training Program Scholarship and an Australian Institute of Nuclear Science and Engineering (AINSE Ltd.) Postgraduate Research Award (PGRA). This research was supported by an Australian Research Council grant DP210101360 awarded to K.P. Part of this work was funded by the Australian Synchrotron through merit-based beamtime awarded on the Infrared Microscopy (IRM) beamline at the Australian Synchrotron, part of the Australian Nuclear Science and Technology Organisation (ANSTO) (AS213/IRM/17447). Funding was also provided by the Research Council of Norway (RCN) through an Arctic Field Grant in 2020 (310664), the ACCESS Project (296836), and the 2017–18 Belmont Forum and BiodivERsA joint call for research proposals, under the BiodivScen ERA-Net COFUND programme (296836/E40). The authors would like to thank Stuart Thomson and Elaine Runge for their valuable assistance with the field sampling.

## Author contributions

Rebecca J. Duncan (Conceptualization, Methodology, Formal analysis, Investigation, Data Curation, Writing—original draft, Visualization, Funding acquisition), Daniel Nielsen (Methodology, Software, Investigation, Data Curation, Writing—review & editing), Janne E. Søreide (Conceptualization, Methodology, Resources, Writing—review & editing, Supervision, Funding acquisition), Øystein Varpe (Conceptualization, Methodology, Writing—review & editing, Supervision), Mark J. Tobin (Validation, Writing—review & editing, Supervision), Vanessa Pitusi (Investigation, Data Curation, Writing—review & editing), Philip Héraud (Validation, Data Curation, Writing—review & editing), and Katherina Petrou (Conceptualization, Methodology, Funding acquisition, Writing—review & editing, Supervision)

## Supplementary material

Supplementary material is available at *ISME Communications* online.

## Conflicts of interest

None declared.

## Funding

R.J.D. is supported by an Australian Government Research Training Program Scholarship and an Australian Institute of Nuclear

Science and Engineering (AINSE Ltd.) Postgraduate Research Award (PGRA). This research was supported by an Australian Research Council grant DP210101360 awarded to K.P. Part of this work was funded by the Australian Synchrotron through merit-based beamtime awarded on the Infrared Microscopy (IRM) beamline at the Australian Synchrotron, part of the Australian Nuclear Science and Technology Organisation (ANSTO) (AS213/IRM/17447). Funding was also provided by the Research Council of Norway (RCN) through an Arctic Field Grant in 2020 (310664), the ACCES Project (296836), and the 2017–18 Belmont Forum and BiodivERsA joint call for research proposals, under the BiodivScen ERA-Net COFUND programme (296836/E40).

## Data availability

All data and processing scripts are available in the open repository Figshare. DOI: [10.6084/m9.figshare.24629718](https://doi.org/10.6084/m9.figshare.24629718).

## References

- Leu E, Mundy C, Assmy P et al. Arctic spring awakening–steering principles behind the phenology of vernal ice algal blooms. *Prog Oceanogr* 2015;**139**:151–70. <https://doi.org/10.1016/j.pocean.2015.07.012>.
- Hancke K, Lund-Hansen LC, Lamare ML et al. Extreme low light requirement for algae growth underneath sea ice: a case study from station Nord, NE Greenland. *J Geophys Res Oceans* 2018;**123**:985–1000. <https://doi.org/10.1002/2017JC013263>.
- Cota G, Legendre L, Gosselin M et al. Ecology of bottom ice algae: I. Environmental controls and variability. *J Mar Syst* 1991;**2**:257–77. [https://doi.org/10.1016/0924-7963\(91\)90036-T](https://doi.org/10.1016/0924-7963(91)90036-T).
- Durbin EG, Casas MC. Early reproduction by *Calanus glacialis* in the northern Bering Sea: the role of ice algae as revealed by molecular analysis. *J Plankton Res* 2014;**36**:523–41. <https://doi.org/10.1093/plankt/fbt121>.
- Sørdeide JE, Leu EV, Berge J et al. Timing of blooms, algal food quality and *Calanus glacialis* reproduction and growth in a changing Arctic. *Glob Chang Biol* 2010;**16**:3154–63. <https://doi.org/10.1111/j.1365-2486.2010.02175.x>.
- Renaud PE, Riedel A, Michel C et al. Seasonal variation in benthic community oxygen demand: a response to an ice algal bloom in the Beaufort Sea, Canadian Arctic? *J Mar Syst* 2007;**67**:1–12. <https://doi.org/10.1016/j.jmarsys.2006.07.006>.
- Cohen J, Berge J, Moline M, Johnsen G, Zolich A. Light in the polar night. In: Berge J, Johnsen G, Cohen J (eds.), *POLAR NIGHT Marine Ecology - Life and Light at the Dead of Night*. Vol. 4. Cham, Switzerland: Springer, 2020, 37–67. [https://doi.org/10.1007/978-3-030-33208-2\\_3](https://doi.org/10.1007/978-3-030-33208-2_3).
- Mock T, Thomas DN. Recent advances in sea-ice microbiology. *Environ Microbiol* 2005;**7**:605–19. <https://doi.org/10.1111/j.1462-2920.2005.00781.x>.
- Cota G, Prinsenberg S, Bennett E et al. Nutrient fluxes during extended blooms of Arctic ice algae. *J Geophys Res Oceans*. 1987;**92**:1951–62. <https://doi.org/10.1029/JC092iC02p01951>.
- Cota GF, Anning JL, Harris LR et al. Impact of ice algae on inorganic nutrients in seawater and sea ice in Barrow Strait, NWT, Canada, during spring. *Can J Fish Aquat Sci* 1990;**47**:1402–15. <https://doi.org/10.1139/f90-159>.
- Campbell K, Mundy CJ, Barber DG et al. Remote estimates of ice algae biomass and their response to environmental conditions during spring melt. *Arctic* 2014;**67**:375–87. <https://doi.org/10.14430/arctic4409>.
- Mundy C, Barber D, Michel C. Variability of snow and ice thermal, physical and optical properties pertinent to sea ice algae biomass during spring. *J Mar Syst* 2005;**58**:107–20. <https://doi.org/10.1016/j.jmarsys.2005.07.003>.
- Callaghan TV, Johansson M, Brown RD et al. The changing face of Arctic snow cover: a synthesis of observed and projected changes. *Ambio* 2011;**40**:17–31. <https://doi.org/10.1007/s13280-011-0212-y>.
- van Pelt WJ, Kohler J, Liston G et al. Multidecadal climate and seasonal snow conditions in Svalbard. *J Geophys Res Earth Surf* 2016;**121**:2100–17. <https://doi.org/10.1002/2016JF003999>.
- Yu Y, Stern H, Fowler C et al. Interannual variability of Arctic landfast ice between 1976 and 2007. *J Clim* 2014;**27**:227–43. <https://doi.org/10.1175/JCLI-D-13-00178.1>.
- Comiso JC, Parkinson CL, Gersten R et al. Accelerated decline in the Arctic Sea ice cover. *Geophys Res Lett* 2008;**35**:L01703. <https://doi.org/10.1029/2007GL031972>.
- Parkinson CL. Global Sea ice coverage from satellite data: annual cycle and 35-yr trends. *J Clim* 2014;**27**:9377–82. <https://doi.org/10.1175/JCLI-D-14-00605.1>.
- Stroeve J, Holland MM, Meier W et al. Arctic Sea ice decline: faster than forecast. *Geophys Res Lett* 2007;**34**:L09501. <https://doi.org/10.1029/2007GL029703>.
- Meredith M, Sommerkorn M, Cassotta S et al. Chapter 3: Polar regions. In: Pörtner H-O, Roberts D C, Masson-Delmotte V et al. (eds.) *The ocean and cryosphere in a changing climate*. A Special Report of the Intergovernmental Panel on Climate Change. Monaco: Intergovernmental Panel on Climate Change 2019, 203–320.
- Itkin P, Spreen G, Cheng B et al. Thin ICE and storms: sea ICE deformation from buoy arrays deployed during N-ICE 2015. *J Geophys Res Oceans* 2017;**122**:4661–74. <https://doi.org/10.1002/2016JC012403>.
- Willmes S, Heinemann G. Sea-ice wintertime lead frequencies and regional characteristics in the Arctic, 2003–2015. *Remote Sens* 2015;**8**:4. <https://doi.org/10.3390/rs8010004>.
- Renner AH, Gerland S, Haas C et al. Evidence of Arctic Sea ice thinning from direct observations. *Geophys Res Lett* 2014;**41**:5029–36. <https://doi.org/10.1002/2014GL060369>.
- Liu J, Curry JA, Wang H et al. Impact of declining Arctic Sea ice on winter snowfall. *PNAS* 2012;**109**:4074–9. <https://doi.org/10.1073/pnas.1114910109>.
- Taskjelle T, Granskog MA, Pavlov AK et al. Effects of an Arctic under-ice bloom on solar radiant heating of the water column. *J Geophys Res Oceans*. 2017;**122**:126–38. <https://doi.org/10.1002/2016JC012187>.
- Hamre B, Winther JG, Gerland S et al. Modeled and measured optical transmittance of snow-covered first-year sea ice in Kongsfjorden. *Svalbard J Geophys Res Oceans* 2004;**109**:C10006. <https://doi.org/10.1029/2003JC001926>.
- Perovich DK. Light reflection and transmission by a temperate snow cover. *J Glaciol* 2007;**53**:201–10. <https://doi.org/10.3189/172756507782202919>.
- Duncan RJ, Petrou K. Biomolecular composition of sea ice microalgae and its influence on marine biogeochemical cycling and carbon transfer through polar marine food webs. *Geosciences* 2022;**12**:38. <https://doi.org/10.3390/geosciences12010038>.
- Smith RE, Clement P, Cota GF et al. Intracellular photosynthate allocation and the control of Arctic marine ice algal production. *J Phycol* 1987;**23**:124–32. <https://doi.org/10.1111/j.1529-8817.1987.tb04434.x>.
- Falk-Petersen S, Sargent J, Henderson J et al. Lipids and fatty acids in ice algae and phytoplankton from the marginal ice



- zone in the Barents Sea. *Polar Biol* 1998;**20**:41–7. <https://doi.org/10.1007/s003000050274>.
30. Smith RE, Clement P, Head E. Biosynthesis and photosynthate allocation patterns of arctic ice algae. *Limnol Oceanogr* 1989;**34**: 591–605. <https://doi.org/10.4319/lo.1989.34.3.0591>.
  31. Kim BK, Lee JH, Yun MS, Joo H, Song HJ, Yang EJ, Chung KH, Kang SH, Lee SH High lipid composition of particulate organic matter in the northern Chukchi Sea. *Deep Sea Research Part II: Topical Studies in Oceanography* 2015; **120**:72–81. <https://doi.org/10.1016/j.dsr2.2014.03.022>.
  32. Hagen W, Auel H. Seasonal adaptations and the role of lipids in oceanic zooplankton. *Zoology* 2001;**104**:313–26. <https://doi.org/10.1078/0944-2006-00037>.
  33. Hygum B, Rey C, Hansen BW et al. Importance of food quantity to structural growth rate and neutral lipid reserves accumulated in *Calanus finmarchicus*. *Mar Biol* 2000;**136**:1057–73. <https://doi.org/10.1007/s002270000292>.
  34. Peltomaa ET, Aalto SL, Vuorio KM et al. The importance of phytoplankton biomolecule availability for secondary production. *Front Ecol Evol* 2017;**5**:128. <https://doi.org/10.3389/fevo.2017.00128>.
  35. Ruess L, Müller-Navarra DC. Essential biomolecules in food webs. *Front Ecol Evol* 2019;**7**:269. <https://doi.org/10.3389/fevo.2019.00269>.
  36. Guschina IA, Harwood JL. Algal lipids and effect of the environment on their biochemistry. In: Kainz M, Brett M, Arts M. (eds) *Lipids in Aquatic Ecosystems*. New York, U.S.A: Springer, 2009, 1–24.
  37. Budge S, Wooller M, Springer A et al. Tracing carbon flow in an arctic marine food web using fatty acid-stable isotope analysis. *Oecologia* 2008;**157**:117–29. <https://doi.org/10.1007/s00442-008-1053-7>.
  38. Amiraux R, Mundy C, Pierrejean M et al. Tracing carbon flow and trophic structure of a coastal Arctic marine food web using highly branched isoprenoids and carbon, nitrogen and sulfur stable isotopes. *Ecol Indic* 2023;**147**:109938. <https://doi.org/10.1016/j.ecolind.2023.109938>.
  39. Jónasdóttir SH, Trung NH, Hansen F et al. Egg production and hatching success in the *Calanoid copepods Calanus helgolandicus* and *Calanus finmarchicus* in the North Sea from march to September 2001. *J Plankton Res* 2005;**27**:1239–59. <https://doi.org/10.1093/plankt/fbi091>.
  40. Jónasdóttir SH, Visser AW, Jespersen C. Assessing the role of food quality in the production and hatching of *Temora longicornis* eggs. *Mar Ecol Prog Ser* 2009;**382**:139–50. <https://doi.org/10.3354/meps07985>.
  41. Mayor DJ, Cook K, Thornton B et al. Absorption efficiencies and basal turnover of C, N and fatty acids in a marine *Calanoid copepod*. *Funct Ecol* 2011;**25**:509–18. <https://doi.org/10.1111/j.1365-2435.2010.01791.x>.
  42. Gladyshev MI, Sushchik NN, Anishchenko OV et al. Efficiency of transfer of essential polyunsaturated fatty acids versus organic carbon from producers to consumers in a eutrophic reservoir. *Oecologia* 2011;**165**:521–31. <https://doi.org/10.1007/s00442-010-1843-6>.
  43. Finkel Z, Follows M, Irwin A. Size-scaling of macromolecules and chemical energy content in the eukaryotic microalgae. *J Plankton Res* 2016;**38**:1151–62. <https://doi.org/10.1093/plankt/fbw057>.
  44. Ahn SH, Whitledge TE, Stockwell DA et al. The biochemical composition of phytoplankton in the Laptev and east Siberian seas during the summer of 2013. *Polar Biol* 2019;**42**:133–48. <https://doi.org/10.1007/s00300-018-2408-0>.
  45. Hu Q. In: Richmond A. (ed.), *Environmental Effects on Cell Composition in: Handbook of Microalgal Culture: Biotechnology and Applied Phycology*. Oxford, U.K.: Blackwell Science Ltd, 2004, 114–122.
  46. Finkel ZV, Follows MJ, Liefer JD et al. Phylogenetic diversity in the macromolecular composition of microalgae. *PLoS One* 2016;**11**:e0155977. <https://doi.org/10.1371/journal.pone.0155977>.
  47. Wu G. Functional amino acids in growth, reproduction, and health. *Adv Nutr* 2010;**1**:31–7. <https://doi.org/10.3945/an.110.1008>.
  48. Palmisano AC, Sullivan CW. Pathways of photosynthetic carbon assimilation in sea-ice microalgae from McMurdo sound. *Antarctica Limnol Oceanogr* 1985;**30**:674–8. <https://doi.org/10.4319/lo.1985.30.3.0674>.
  49. Bhavya P, Kim BK, Jo N et al. A review on the macromolecular compositions of phytoplankton and the implications for aquatic biogeochemistry. *Ocean Sci* 2019;**54**:1–14. <https://doi.org/10.1007/s12601-018-0061-8>.
  50. Campbell K, Matero I, Bellas C et al. Monitoring a changing Arctic: recent advancements in the study of sea ice microbial communities. *Ambio* 2022;**51**:318–32. <https://doi.org/10.1007/s13280-021-01658-z>.
  51. Michel C, Legendre L, Ingram R et al. Carbon budget of sea-ice algae in spring: evidence of a significant transfer to zooplankton grazers. *J Geophys Res Oceans* 1996;**101**:18345–60. <https://doi.org/10.1029/96JC00045>.
  52. Selz V, Laney S, Arnsten AE et al. Ice algal communities in the Chukchi and Beaufort seas in spring and early summer: composition, distribution, and coupling with phytoplankton assemblages. *Limnol Oceanogr* 2018;**63**:1109–33. <https://doi.org/10.1002/lno.10757>.
  53. Tourangeau S, Runge J. Reproduction of *Calanus glacialis* under ice in spring in southeastern Hudson Bay. *Canada Mar Biol* 1991;**108**:227–33. <https://doi.org/10.1007/BF01344337>.
  54. Ji R, Jin M, Varpe Ø. Sea ice phenology and timing of primary production pulses in the Arctic Ocean. *Glob Chang Biol* 2013;**19**: 734–41. <https://doi.org/10.1111/gcb.12074>.
  55. Findlay C, Morrison J, Mundy C et al. Thermal source Fourier transform infrared microtomography applied to Arctic Sea ice diatoms. *Analyst* 2017;**142**:660–9. <https://doi.org/10.1039/C6AN02056A>.
  56. Pogorzelec NM, Mundy C, Findlay CR et al. FTIR imaging analysis of cell content in sea-ice diatom taxa during a spring bloom in the lower northwest passage of the Canadian Arctic. *Mar Ecol Prog Ser* 2017;**569**:77–88. <https://doi.org/10.3354/meps12088>.
  57. Høyland KV. Ice thickness, growth and salinity in van Mijenfjorden, Svalbard, Norway. *Polar Res* 2009;**28**:339–52. <https://doi.org/10.1111/j.1751-8369.2009.00133.x>.
  58. Duncan RJ, Søreide JE, Varpe Ø et al. Sea-ice community composition data analysed in: ‘Spatio-temporal dynamics in microalgal communities in Arctic land-fast sea ice’. *Figshare* 2023. Dataset. <https://doi.org/10.6084/m9.figshare.24802947>.
  59. Smith R, Anning J, Pierre CG. Abundance and production of ice algae in resolute passage. *Canadian Arctic Mar Ecol Prog Ser* 1988;**48**:251–63. <https://doi.org/10.3354/meps048251>.
  60. Lee SH, Whitledge TE, Kang S-H. *Carbon Uptake Rates of Sea Ice Algae and Phytoplankton under Different Light Intensities in a Landfast Sea Ice Zone*. Barrow, Alaska: Arctic, 2008, 281–91.
  61. Kvernvik AC, Hoppe CJM, Greenacre M et al. Arctic Sea ice algae differ markedly from phytoplankton in their ecophysiological characteristics. *Mar Ecol Prog Ser* 2021;**666**:31–55. <https://doi.org/10.3354/meps13675>.

62. Garrison DL, Buck KR. Organism losses during ice melting: a serious bias in sea ice community studies. *Polar Biol* 1986;**6**: 237–9. <https://doi.org/10.1007/BF00443401>.
63. Campbell K, Mundy C, Juhl AR et al. Melt procedure affects the photosynthetic response of sea ice algae. *Front Earth Sci* 2019;**7**:21. <https://doi.org/10.3389/feart.2019.00021>.
64. Barrie A, Davies J, Park A et al. Continuous-flow stable isotope analysis for biologists. *Spectroscopy* 1989;**4**:42–52.
65. Perovich DK. *The Optical Properties of Sea Ice*. Hanover, New Hampshire: CRREL Monograph, 1996, 96–1.
66. Varpe Ø, Daase M, Kristiansen T. A fish-eye view on the new Arctic lightscape. *ICES J Mar Sci* 2015;**72**:2532–8. <https://doi.org/10.1093/icesjms/fsv129>.
67. Connan-McGinty S, Banas NS, Berge J et al. Midnight sun to polar night: a model of seasonal light in the Barents Sea. *J Adv Model Earth Syst* 2022;**14**:e2022MS003198. <https://doi.org/10.1029/2022MS003198>.
68. Matuszko D. Influence of the extent and genera of cloud cover on solar radiation intensity. *Int J Climatol* 2012;**32**:2403–14. <https://doi.org/10.1002/joc.2432>.
69. Tobin MJ, Puskar L, Barber RL et al. FTIR spectroscopy of single live cells in aqueous media by synchrotron IR microscopy using microfabricated sample holders. *Vib Spectrosc* 2010;**53**: 34–8. <https://doi.org/10.1016/j.vibspec.2010.02.005>.
70. Bamberg KR, Wood BR, McNaughton D. Resonant Mie scattering (RMieS) correction applied to FTIR images of biological tissue samples. *Analyst* 2012;**137**:126–32. <https://doi.org/10.1039/C1AN15628D>.
71. Team R. *RStudio: Integrated Development for R*. 2022.02.3. Boston, MA: RStudio, PBC, 2022.
72. Stevens A, Ramirez-Lopez L. *An Introduction to the Prospectr Package*. R package version 0.2, 2014.
73. Wagner H, Liu Z, Langner U et al. The use of FTIR spectroscopy to assess quantitative changes in the biochemical composition of microalgae. *J Biophotonics* 2010;**3**:557–66. <https://doi.org/10.1002/jbio.201000019>.
74. Shapiro SS, Wilk MB. An analysis of variance test for normality (complete samples). *Biometrika* 1965;**52**:591–611. <https://doi.org/10.1093/biomet/52.3-4.591>.
75. Wickham H, Chang W, Wickham MH. Package ‘ggplot2’. Create elegant data visualisations using the grammar of graphics, version 3.3.6. New York, NY, U.S.A: Springer-Verlag, 2016.
76. Wickham H, François R, Henry L et al. Package ‘dplyr’. A grammar of data manipulation, version 1.0.8, 2023.
77. Wei T, Simko V, Levy M et al. Package ‘corrplot’. Visualization of a Correlation Matrix, version 0.92, 2021.
78. Oksanen J, Blanchet FG, Kindt R et al. Package ‘vegan’. Community ecology package, version 2.6-4, 2018.
79. Arrigo KR. Sea ice ecosystems. *Annu Rev Mar Sci* 2014;**6**:439–67. <https://doi.org/10.1146/annurev-marine-010213-135103>.
80. Gleitz M, Kirst G. Photosynthesis-irradiance relationships and carbon metabolism of different ice algal assemblages collected from Weddell Sea pack ice during austral spring (EPOS 1). *Polar Biol* 1991;**11**:385–92. <https://doi.org/10.1007/BF00239691>.
81. Cade-Menun BJ, Paytan A. Nutrient temperature and light stress alter phosphorus and carbon forms in culture-grown algae. *Mar Chem* 2010;**121**:27–36. <https://doi.org/10.1016/j.marchem.2010.03.002>.
82. Lund-Hansen LC, Hawes I, Hancke K et al. Effects of increased irradiance on biomass, photobiology, nutritional quality, and pigment composition of Arctic Sea ice algae. *Mar Ecol Prog Ser* 2020;**648**:95–110. <https://doi.org/10.3354/meps13411>.
83. Leu E, Graeve M, Wulff A. A (too) bright future? Arctic diatoms under radiation stress. *Polar Biol* 2016;**39**:1711–24. <https://doi.org/10.1007/s00300-016-2003-1>.
84. Petrou K, Hill R, Brown CM et al. Rapid photoprotection in sea-ice diatoms from the East Antarctic pack ice. *Limnol Oceanogr* 2010;**55**:1400–7. <https://doi.org/10.4319/lo.2010.55.3.1400>.
85. Poulin M, Cardinal A. Sea ice diatoms from Manitounuk sound, southeastern Hudson Bay (Quebec, Canada): II. *Naviculaceae*, genus *Navicula*. *Canad J Bot* 1982;**60**:2825–45. <https://doi.org/10.1139/b82-343>.
86. Robinson DH, Kolber Z, Sullivan CW. Photophysiology and photoacclimation in surface sea ice algae from McMurdo sound, Antarctica. *Mar Ecol Prog Ser* 1997;**147**:243–56. <https://doi.org/10.3354/meps147243>.
87. Maeda Y, Nojima D, Yoshino T et al. Structure and properties of oil bodies in diatoms. *Philos Trans R Soc Lond Ser B Biol Sci* 2017;**372**:20160408. <https://doi.org/10.1098/rstb.2016.0408>.
88. Priscu JC, Priscu LR, Palmisano AC et al. Estimation of neutral lipid levels in Antarctic Sea ice microalgae by Nile red fluorescence. *Antarct Sci* 1990;**2**:149–55. <https://doi.org/10.1017/S0954102090000190>.
89. Whitaker TM, Richardson MG. Morphology and chemical composition of a natural population of an ice-associated Antarctic diatom *Navicula glaciei*. *J Phycol* 1980;**16**:250–7. <https://doi.org/10.1111/j.1529-8817.1980.tb03027.x>.
90. Welch HE, Bergmann MA. Seasonal development of ice algae and its prediction from environmental factors near resolute, NWT, Canada. *Can J Fish Aquat Sci* 1989;**46**:1793–804. <https://doi.org/10.1139/f89-227>.
91. Fry B, Wainright SC. Diatom sources of 13 C-rich carbon in marine food webs. *Mar Ecol Prog Ser* 1991;**76**:149–57. <https://doi.org/10.3354/meps076149>.
92. McMinn A. Reviews and syntheses: ice acidification, the effects of ocean acidification on sea ice microbial communities. *Biogeosciences* 2017;**14**:3927–35. <https://doi.org/10.5194/bg-14-3927-2017>.
93. Gong Y, Miao X. Short chain fatty acid biosynthesis in microalgae *Synechococcus* sp. PCC 7942. *Marine drugs* 2019;**17**:255. <https://doi.org/10.3390/md17050255>.
94. Leu E, Wiktor J, Søreide J et al. Increased irradiance reduces food quality of sea ice algae. *Mar Ecol Prog Ser* 2010;**411**:49–60. <https://doi.org/10.3354/meps08647>.
95. Palmisano AC, Sullivan CW. Physiology of sea ice diatoms. I. Response of three polar diatoms to a simulated summer-winter transition. *J Phycol* 1982;**18**:489–98. <https://doi.org/10.1111/j.1529-8817.1982.tb03215.x>.
96. Niemi A, Michel C, Hille K et al. Protist assemblages in winter sea ice: setting the stage for the spring ice algal bloom. *Polar Biol* 2011;**34**:1803–17. <https://doi.org/10.1007/s00300-011-1059-1>.
97. Wagner H, Jakob T, Fanesi A et al. Towards an understanding of the molecular regulation of carbon allocation in diatoms: the interaction of energy and carbon allocation. *Philos Trans R Soc Lond Ser B Biol Sci* 2017;**372**:20160410. <https://doi.org/10.1098/rstb.2016.0410>.
98. Smith RE, Cavaletto JF, Eadie B et al. Growth and lipid composition of high Arctic ice algae during the spring bloom at resolute, northwest territories, Canada. *Mar Ecol Prog Ser* 1993;**97**:19–29. <https://doi.org/10.3354/meps097019>.
99. Smith R, Gosselin M, Taguchi S. The influence of major inorganic nutrients on the growth and physiology of high arctic ice algae. *J Mar Syst* 1997;**11**:63–70. [https://doi.org/10.1016/S0924-7963\(96\)00028-0](https://doi.org/10.1016/S0924-7963(96)00028-0).
100. Campbell K, Mundy C, Landy J et al. Community dynamics of bottom-ice algae in Dease Strait of the Canadian

- Arctic. *Prog Oceanogr* 2016;**149**:27–39. <https://doi.org/10.1016/j.pocean.2016.10.005>.
101. Leu E, Brown TA, Graeve M et al. Spatial and temporal variability of ice algal trophic markers—with recommendations about their application. *J Mar Sci Eng* 2020;**8**:676. <https://doi.org/10.3390/jmse8090676>.
  102. Varpe Ø. Life history adaptations to seasonality. *Integr Comp Biol* 2017;**57**:943–60. <https://doi.org/10.1093/icb/icx123>.
  103. Falkowski PG, LaRoche J. Acclimation to spectral irradiance in algae. *J Phycol* 1991;**27**:8–14. <https://doi.org/10.1111/j.0022-3646.1991.00008.x>.
  104. Mock T, Kroon BM. Photosynthetic energy conversion under extreme conditions—I: important role of lipids as structural modulators and energy sink under N-limited growth in Antarctic Sea ice diatoms. *Phytochemistry* 2002;**61**:41–51. [https://doi.org/10.1016/S0031-9422\(02\)00216-9](https://doi.org/10.1016/S0031-9422(02)00216-9).
  105. Taylor N. Silica incorporation in the diatom *Coscinodiscus granii* as affected by light intensity. *Br Phycol J* 1985;**20**:365–74. <https://doi.org/10.1080/00071618500650371>.
  106. Su Y, Lundholm N, Ellegaard M. The effect of different light regimes on diatom frustule silicon concentration. *Algal Res* 2018;**29**:36–40. <https://doi.org/10.1016/j.algal.2017.11.014>.
  107. Liu H, Chen M, Zhu F et al. Effect of diatom silica content on copepod grazing, growth and reproduction. *Front Mar Sci* 2016;**3**:89. <https://doi.org/10.3389/fmars.2016.00089>.
  108. Vongsivut J, Heraud P, Gupta A et al. FTIR microspectroscopy for rapid screening and monitoring of polyunsaturated fatty acid production in commercially valuable marine yeasts and protists. *Analyst* 2013;**138**:6016–31. <https://doi.org/10.1039/c3an00485f>.
  109. Heraud P, Wood BR, Beardall J et al. Probing the influence of the environment on microalgae using infrared and Raman spectroscopy. In: Kneipp K., Aroca R., Kneipp H. et al. (eds.), *New approaches in Biomedical Spectroscopy*. Washington DC, USA: American Chemical Society, 2007.
  110. Sackett O, Armand L, Beardall J et al. Taxon-specific responses of Southern Ocean diatoms to Fe enrichment revealed by synchrotron radiation FTIR microspectroscopy. *Biogeosciences* 2014;**11**:5795–808. <https://doi.org/10.5194/bg-11-5795-2014>.
  111. Heraud P, Wood BR, Tobin MJ et al. Mapping of nutrient induced biochemical changes in living algal cells using synchrotron infrared microspectroscopy. *FEMS Microbiol Lett* 2005;**249**:219–25. <https://doi.org/10.1016/j.femsle.2005.06.021>.
  112. Whelan D, Bambery K, Heraud P et al. Monitoring the reversible B to A-like transition of DNA in eukaryotic cells using Fourier transform infrared spectroscopy. *Nucleic Acids Res* 2011;**39**:5439–48. <https://doi.org/10.1093/nar/gkr175>.
  113. Heraud P, Stojkovic S, Beardall J et al. Inter-colonial variability in macromolecular composition in P-starved and P-replete *Scenedesmus* populations revealed by infrared microspectroscopy. *J Phycol* 2008;**44**:1335–9. <https://doi.org/10.1111/j.1529-8817.2008.00564.x>.
  114. Beardall J, Berman T, Heraud P et al. Approaches for determining phytoplankton nutrient limitation. 2001;**63**:44–69. <https://doi.org/10.1007/PL00001342>.
  115. Sackett O, Petrou K, Reedy B et al. Snapshot prediction of carbon productivity, carbon and protein content in a Southern Ocean diatom using FTIR spectroscopy. *ISME J* 2016;**10**:416–26. <https://doi.org/10.1038/ismej.2015.123>.



OPEN

## Seasonal environmental transitions and metabolic plasticity in a sea-ice alga from an individual cell perspective

Rebecca J. Duncan<sup>1,2</sup>✉, Janne E. Søreide<sup>2</sup>, Daniel A. Nielsen<sup>1</sup>, Øystein Varpe<sup>3,4</sup>, Józef Wiktor<sup>5</sup>, Mark J. Tobin<sup>7</sup>, Vanessa Pitusi<sup>2,6</sup> & Katherina Petrou<sup>1</sup>

Sea-ice microalgae are a key source of energy and nutrient supply to polar marine food webs, particularly during spring, prior to open-water phytoplankton blooms. The nutritional quality of microalgae as a food source depends on their biomolecular (lipid:protein:carbohydrate) composition. In this study, we used synchrotron-based Fourier transform infra-red microspectroscopy (s-FTIR) to measure the biomolecular content of a dominant sea-ice taxa, *Nitzschia frigida*, from natural land-fast ice communities throughout the Arctic spring season. Repeated sampling over six weeks from an inner (relatively stable) and an outer (relatively dynamic) fjord site revealed high intra-specific variability in biomolecular content, elucidating the plasticity of *N. frigida* to adjust to the dynamic sea ice and water conditions. Environmental triggers indicating the end of productivity in the ice and onset of ice melt, including nitrogen limitation and increased water temperature, drove an increase in lipid and fatty acids stores, and a decline in protein and carbohydrate content. In the context of climate change and the predicted Atlantification of the Arctic, dynamic mixing and abrupt warmer water advection could truncate these important end-of-season environmental shifts, causing the algae to be released from the ice prior to adequate lipid storage, influencing carbon transfer through the polar marine system.

**Keywords** Microalgae, Svalbard, *Nitzschia frigida*, Biogeochemical cycling, Sea ice, Arctic

The last half century has seen ocean temperatures rise and circulation patterns shift, resulting in a rapid decline in Arctic sea ice extent, thickness and area<sup>1–3</sup>. The increasing temperatures and advection of warmer, more saline Atlantic waters (AW) into the Arctic means that sea ice has become more prone to summer melting<sup>4</sup>, which has resulted in a decline in multi-year sea ice (MYI; sea ice which has survived multiple summers)<sup>5</sup>. Since 1999, the extent of MYI has diminished by ~50%<sup>2,6</sup>, and now covers less than a third of the Arctic Ocean (AO)<sup>7</sup>, meaning that first year ice (FYI; sea ice which completely melts each summer), which is thinner and more sensitive to changes in the physical environment, now dominates the Arctic<sup>2,3,8</sup>. Warmer surface water temperatures impede Arctic sea ice formation delaying freezing while also causing earlier melting<sup>3</sup>. This contracted period of FYI, with shortened timeframes between ice formation (late winter), substantial daylight returning to the Arctic (early spring) and melting of the ice from below (late spring/summer)<sup>9</sup>, results in a reduced window of productivity for sea ice associated ecosystems. These warming-associated changes in Arctic sea ice conditions have implications for the seasonal productivity and ecology of the polar marine ecosystem<sup>10,11</sup>.

Sea ice forms an important habitat for microalgae, which represent the primary source of energy for the marine ecosystem in the early spring, in the absence of other sources of primary production and prior to the late-spring/summer open-water phytoplankton blooms<sup>9,12</sup>. Through prolonging polar marine biological production<sup>13,14</sup> and this provision of food during the early phases of seasonal zooplankton reproduction, sea ice microalgae are an important factor in the quality and quantity of secondary production<sup>15–17</sup>. The nutritional quality of microalgae as a food source is dependent on which species are present and their individual elemental

<sup>1</sup>School of Life Sciences, University of Technology Sydney, Building 7, 67 Thomas St, Ultimo, NSW 2007, Australia. <sup>2</sup>Department of Arctic Biology, The University Centre in Svalbard, Longyearbyen, Norway. <sup>3</sup>Department of Biological Sciences, University of Bergen, Bergen, Norway. <sup>4</sup>Norwegian Institute for Nature Research, Bergen, Norway. <sup>5</sup>Institute of Oceanology, Polish Academy of Sciences, Sopot, Poland. <sup>6</sup>Department of Arctic and Marine Biology, University in Tromsø, Tromsø, Norway. <sup>7</sup>ANSTO-Australian Synchrotron, Clayton, VIC, Australia. ✉email: rebecca.duncan@uts.edu.au

stoichiometry, which reflects their biomolecular (lipid:protein:carbohydrate) composition<sup>18</sup>. Cell stoichiometry, and thus biomolecular composition, is sensitive to changes in environment, such as light<sup>19</sup>, temperature<sup>20,21</sup> and nutrient availability<sup>22,23</sup>, with shifts in each parameter affecting biomolecular stores in different ways. In sea ice microalgae, increasing irradiance transmitted through the ice can increase lipid production<sup>19</sup>, nutrient limitation has been shown to decrease protein and increase fatty acid (FA) content<sup>22,24</sup>, whilst increasing ocean temperatures have been observed to increase protein content and decrease FA content<sup>20,21,25</sup>. As such, shifts in the biomolecular composition of sea ice microalgae as a result of changing sea ice-surface ocean conditions, invariably influences Arctic food webs, local biogeochemistry and plays a vital role in determining the productivity of polar marine ecosystems (26 and references therein).

In natural systems, microalgal communities form complex functional networks, making it challenging to obtain knowledge on species' phenomes and metabolomes in a dynamic and multivariate environment. Species and communities adapt to changing environmental conditions either through phenotypic plasticity or genetically<sup>27</sup>. Seasonally, it is phenotypic adjustments to changes in environment that dominate, but the capacity for such plasticity varies across and within species. Therefore, to gain a systematic understanding of metabolic plasticity and uncover the phenome (set of traits modifiable for enhanced growth and survival) in natural biological systems, we need single-celled multiparameter measurements that can probe the changes occurring in individual cells in response to environmental shifts.

Here we use synchrotron-based Fourier transform infra-red microspectroscopy to measure the biomolecular content of *Nitzschia frigida* from natural sea ice habitat over the Arctic spring. *N. frigida* is one of the most prolific and ubiquitous Arctic sea ice diatoms, typically dominating first year sea ice assemblages<sup>9,28–30</sup>. It is a colony-forming pennate diatom which can often be observed as single cells early in the spring, increasingly creating arborescent colonies as spring progresses. In contrast to taxa such as *Chaetoceros* spp., *Thalassiosira* spp. and dinoflagellates that create resting spores to survive the long winter darkness<sup>31,32</sup>, *N. frigida* are thought to survive the winter in the epibenthic region, primarily through storing energy and reducing metabolic rate<sup>31,33</sup>. This energy storage strategy means that in addition to contributing substantially to spring primary production in the ice, following their release during ice melt, they strongly contribute to carbon flux as they are either consumed during descent<sup>34</sup> or exported to the benthos<sup>35,36</sup>. In this study, we investigated changes in the biomolecular content of *N. frigida* throughout the spring sea ice season until ice-melt (March–May), tracing the seasonal progression of nutritional content to document potential shifts in energy allocation that may link to survival during polar darkness.

## Materials & methods

### Study area

This study was conducted within Van Mijenfjorden in Svalbard, Norway (Fig. 1A) throughout April–May 2022. Two sites, one at the inner fjord (inner site; 77.80194 N, 15.76916 E) and one at the outer fjord (outer site; 77.84918 N, 16.7078 E), were sampled regularly (6–7.4.22; Week 1 (W1), 20–21.4.22; Week 3 (W3), 29–30.4.22; Week 4 (W4) and 12–13.5.22; Week 6 (W6)) to investigate seasonal changes in the biomolecular content of *N. frigida*, under different environmental conditions. Van Mijenfjorden is a partially enclosed fjord, with an inner basin approximately 70 m deep and an outer basin up to 120 m deep, located on the west coast of Spitsbergen, Svalbard, Norway<sup>37</sup>. The fjord experiences advection of warm, saline Atlantic water transported to the area by the West Spitsbergen Current (WSC), however this is substantially abated by the presence of the island Akseløya at the fjord mouth which allows for sea ice formation in winter. For further information on the conditions in Van Mijenfjorden see<sup>19,30</sup>. Sea-ice had been formed in the fjord since January, with closed drift-ice observed at the inner site from the 17.1.22 and from 24.1.22 at the outer site<sup>38</sup>.

### Sample collection

For each sampling event, six ice cores were extracted approximately 0.5 m apart, with a Kovacs core barrel (9 cm diameter; Kovacs Enterprise, Oregon, USA). The bottom 3 cm (at the ice-water interface) was retained, due to the microbial community being concentrated in this section of the ice<sup>39,40</sup>. The six ice cores were then pooled into triplicates, as cores 1–2, 3–4 and 5–6, and 100 mL of filtered sea water (FSW) (Glass Fibre Filter (GF/F), nominal pore size 0.7 µm) per centimetre of core was added to minimise osmotic stress<sup>41,42</sup>. The samples were then allowed to melt in darkness for 24 h at 4 °C. Cells were concentrated before biomolecular analysis; 100 mL from each of the three pooled samples was centrifuged at 1000 rpm (Universal 320, Hettich, Germany) for 4 min and the supernatant removed. The aliquot was then transferred to 2 mL Eppendorf tubes and centrifuged at 1000 rpm (Mikro 185, Hettich) for a further 2 min. The supernatant was again removed and the sample fixed by addition of formaldehyde (5% v/v) for later analysis. Additional cores were extracted for ice temperature (measured in situ), for bulk ice salinity (sectioned into 0–3 cm for bottom-ice and then 10 cm sections) and bulk ice nutrients (without the addition of FSW).

### Biological variables

#### *Chlorophyll a content*

Once the ice samples were completely melted, triplicate subsamples (150–400 mL) and a sample of under-ice water (500–1250 mL) were filtered (GF/F, 0.7 µm, Whatman, England) until visible colouration was observed on the filter. The filters were stored frozen (–80 °C) until extraction and the extractions were performed within three months of collection. The analyses were performed according to<sup>43</sup>. Briefly, filters were extracted in 10 mL methanol and kept refrigerated at 4 °C for 24 h prior to extraction, after which Chl *a* content was measured with a calibrated Trilogy fluorometer (Turner, California, USA), before and after acidifying the extracts with 5% HCl<sup>44</sup>.

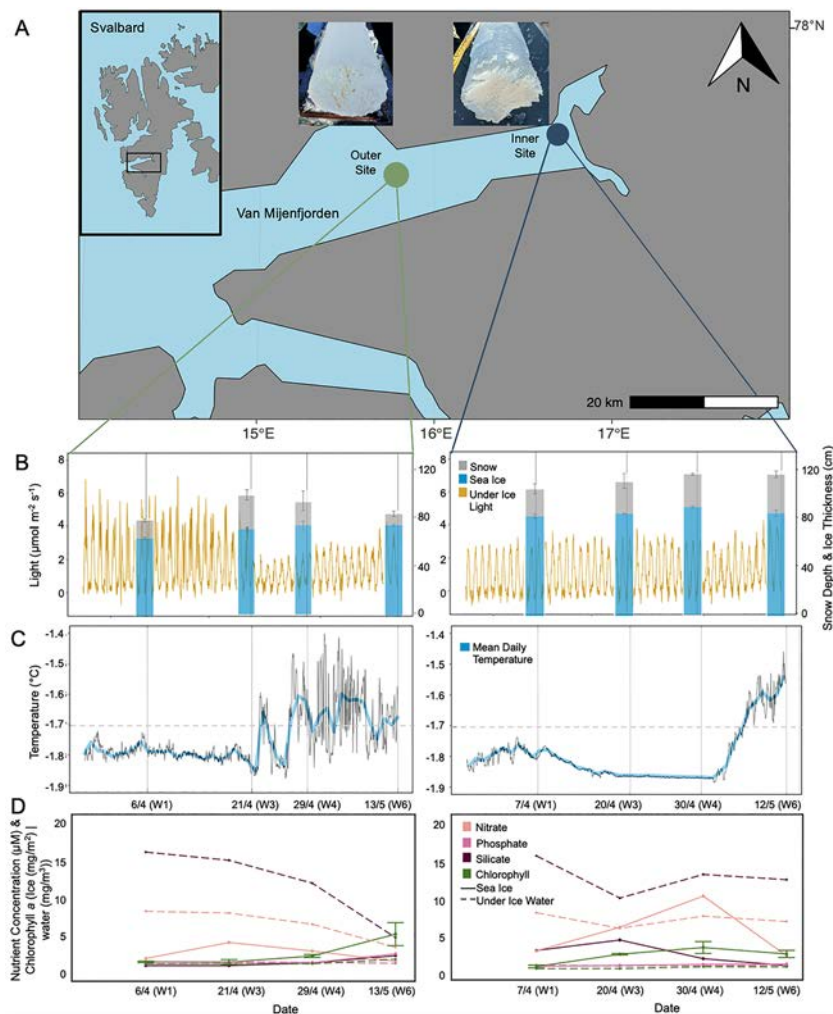


**Figure 1.** Location of sampling sites (A) visited between April–May 2022; inner site—blue dot and outer site—green dot, in Van Mijenfjorden, within Svalbard, Norway (inset box). Photographs of bottom ice cores collected from the inner and outer site on the 12.5.22 and 13.5.22 respectively, demonstrate more heterogeneity and lumping of biomass at the outer site. (B) Snow depth (cm)  $\pm$  SD (grey bars), sea ice thickness (cm)  $\pm$  SD (blue bars) and photosynthetically active radiation (PAR) ( $\mu\text{mol photons m}^{-2} \text{s}^{-1}$ ), measured by the light sensor deployed under the ice throughout the season (yellow line). (C) Under water temperature (black line) as measured by the temperature sensor deployed alongside the light sensor, solid line indicates average temperature (blue). (D) Nutrients and chlorophyll *a* concentration are displayed (bottom panel), including nitrate (light pink), phosphate (medium pink), silicate (dark pink) and chlorophyll *a* concentration (green) in the sea ice (solid line) and under-ice water (dashed line), on all sampling dates at the outer site (left) and inner site (right).

#### Community composition

From each sampling event, subsamples (100 mL) of the melted triplicate cores were collected into a brown bottle and preserved with glutaraldehyde (2% final conc.). Species composition was determined through the use of light microscopy; between 3 and 6 mL (depending on cell density) of the well-mixed subsamples were poured into an Utermöhl chamber with sedimentation cylinder (KC Denmark, Silkeborg, Denmark)<sup>45</sup> and the cells were allowed to settle for up to 24 h<sup>46</sup>. Cells were counted at 400 $\times$  magnification and identified to lowest possible taxonomic level. A whole chamber counting approach was employed to ensure rare taxa were captured. These analyses were conducted under a Nikon TS100 microscope within six months of sample collection.

#### Fatty acid composition

Samples from six pooled cores from each site on their final sampling date (inner site: 12.5.22 and outer site: 13.5.22) were filtered onto pre-combusted GF/F filters, until coloration was visible (300 mL from the outer site and 470 mL from the inner site). The filters were placed in glass vials with Teflon-lined caps and 8 mL of Methanol:dichloromethane was added and the vials were stored at  $-80^{\circ}\text{C}$  until analysis. Total lipid was extracted according to Folch et al. 1957, at Akvaplan Niva AS, Norway.

## Environmental variables

### Physical variables

Snow depth was measured three times in the close vicinity of the ice core extraction using a standard ruler, prior to core extraction. Ice thickness was measured at every core hole, after the core extraction, using a Kovacs ice thickness gauge. The ice temperature was measured in situ. Following complete melting of separate 10 cm sections, salinity of each section was measured (Thermo Scientific Orion Versa Star Pro). Based on these measurements, brine salinity and volume fractions were calculated according to Ref.<sup>47</sup>. A subsample of each pooled, melted ice cores was filtered onto pre-combusted GF/F filters until coloration was visible, for particulate organic carbon and particulate organic nitrogen (POC:PON) analysis. With each sampling event, a 0–3 cm section of an ice core was melted without the addition of FSW and then transferred to an acid washed bottle for bulk ice nutrient analysis. Also at each sampling event, approximately 100 mL of the water from directly below the ice-bottom surface was collected using a 5 L Niskin bottle (Hydro-Bios, Germany) and transferred to acid washed bottles for nutrient analysis. The nitrate plus nitrite ( $\text{NO}_3^- + \text{NO}_2^-$ ) ( $\text{NO}_x$ ), phosphate ( $\text{PO}_4^{3-}$ ) and silicic acid ( $\text{Si}(\text{OH})_4$ ) concentrations ( $\mu\text{M}$ ) for ice and surface water were measured simultaneously on a QuAAtro 39 nutrient analyzer (SEAL Analytical, United Kingdom), with separate analysis channels for the three nutrients. The detection limits were 0.01  $\mu\text{M}$  for  $\text{NO}_x$ , 0.02  $\mu\text{M}$  for phosphate and 0.02  $\mu\text{M}$  for silicic acid. POC:PON analysis and stable isotope analysis on the bottom-ice and surface water was performed at the UC Davis Stable Isotope Facility in an EA-IRMS system, according to Ref.<sup>48</sup>. The detection limits were 100  $\mu\text{g C}$  for  $\delta^{13}\text{C}$  and 20  $\mu\text{g N}$  for  $\delta^{15}\text{N}$ .

### Light measurements

At each sampling site, incoming photosynthetically active radiation (PAR) was measured using a LI-192 spherical underwater quantum sensor placed on a weighted frame moored ~1 m below the ice (from 26.3.22 until 13.5.22) recording PAR (400–700 nm) every minute (RBRsolo<sup>3</sup> PAR; RBR Global, Canada). Further, a temperature sensor (RBRsolo<sup>3</sup> T, accuracy of  $\pm 0.002$  °C) with every 0.5 min logger intervals was placed at the same depth. Albedo was calculated on each sampling date as snow reflected PAR, as proportion (%) of reflected PAR and incoming PAR to the snow surface, using a LI-190 quantum air sensor placed on the snow/sea ice surface to measure incoming PAR, and held level 1 m above the snow surface, facing the snow, to measure snow reflected PAR.

### Species-specific biomolecular content by synchrotron-FTIR

The biomolecular composition of *N. frigida* was determined using synchrotron based FTIR microspectroscopy on formalin-fixed (5% v/v final concentration) cells. To ensure true replication, all cells measured were single cells and not dividing or associated with another cell. Samples were loaded directly into a micro-compression cell between two 13 mm diameter 0.5 mm thick BaF<sub>2</sub> windows and spectral data of individual cells ( $\bar{x}$  = 26 cells per site, Table S1) obtained on the Infrared (IR) Microspectroscopy Beamline at the Australian Synchrotron, Melbourne. Each biomolecule absorbs a specific range of IR wavelengths, and a set of well-defined absorbance bands between 3050 and 2800  $\text{cm}^{-1}$ , and 1770–1100  $\text{cm}^{-1}$  have been determined (Table 1). Spectra were acquired over the measurement range 4000–800  $\text{cm}^{-1}$  with a Vertex 80v FTIR spectrometer (Bruker Optic, Ettlingen, Germany) in conjunction with an IR microscope (Hyperion 3000, Bruker) fitted with a narrow-band mercury cadmium telluride detector cooled with liquid nitrogen. To limit the light scattering effects, the measurements were performed on hydrated cells<sup>49</sup>. Co-added interferograms (sample n = 32, background n = 64) were collected at a wavenumber resolution of 4  $\text{cm}^{-1}$ . All measurements were made in transmission mode, using a measuring aperture diameter of 6.9  $\mu\text{m}$  (area = 37.4  $\mu\text{m}^2$ ). Cell compression was consistent ensuring the path length was uniform to account for any variation in cell size. To account for heterogeneity in the cell structure and distribution of biomolecules, all cells were measured with multiple points across the cell surface. Opus 8.0 software (Bruker) was used for both spectral acquisition and instrument control. Analyses were performed in July 2022 (within 6 months of samples being collected and fixed). All samples were kept refrigerated between fixation and analysis.

Wave number ( $\text{cm}^{-1}$ )	Band assignment	References
~ 3011	$\nu(\text{CH})$ —from unsaturated fatty acids	88
~ 2852	$\nu_s(\text{C-H})$ from methylene ( $-\text{CH}_2$ ) from saturated lipids (CH-Stretch IV)	
~ 2921	$\nu_{as}(\text{C-H})$ from methylene ( $-\text{CH}_2$ ) from saturated fatty acids	
~ 1744	$\nu(\text{C=O})$ ester carbonyl group from lipid triglycerides and fatty acids	
~ 1549	Protein (Amide II mode); mainly $\delta(\text{N-H})$ of amides	89
~ 1400	$\nu_s(\text{COO}^-)$ from carboxylated molecules	90
~ 1241	$\nu_{as}(\text{PO}_2^-)$ of the phosphodiester backbone of nucleic acids, phosphorylated proteins and lipids	90,91
~ 1191–1146	$\nu_s(\text{C-O})$ from carbohydrates	92
~ 1080	$\nu_s(\text{Si-O})$ from silica	93,94

**Table 1.** Infrared (IR) band assignments for s-FTIR microspectroscopy used in this study.

### Data analyses

Biomolecular content for each measured cell was determined by integrating the area under each assigned peak (Table 1), applying the Beer–Lambert Law assuming a direct relationship between absorbance and analyte concentration<sup>50</sup>. Data were smoothed (4 pts either side) and second derivative (3rd order polynomial) transformed using the Savitzky–Golay algorithm from the *prospectr* package<sup>51</sup>. Data were then normalised using Standard Normal Variate (SNV).

The community composition of all samples per site was contrasted by analysis of similarities (ANOSIM, Clarke & Warwick 1994), to determine if community composition was different between the inner and outer sites. Relationships between biomolecular content and sampling date and site were estimated using principal component analyses (PCA) and key biomolecular content per date was visualised using violin plots. To investigate which environmental variables account for a significant difference in the biomolecular content, redundancy analysis (RDA) was performed constrained to environmental variables ( $n=6$ ) with Monte Carlo permutations (999), following model optimisation, and only significant vectors displayed. Further redundancy analyses were performed, constrained to the stable isotopes ( $n=4$ ), to determine the effect on the differences in biomolecular composition. Regressions were tested for overall model significance of RDA analyses using the  $F$  statistic ( $P < 0.05$ ) and strength of fit using  $R^2$ . The residuals of all regressions were verified for homoscedasticity. The correlations between stable isotope of carbon ( $\delta^{13}\text{C}_{\text{VPDB}}$  (‰)) and lipid (ester carbonyl) and protein (amide II) content were visualised using boxplots. The Shapiro–Wilks<sup>52</sup> test for normality showed that the biomolecular content required  $\log_{10}$  transformation before analysis. All analyses were performed using RStudio v. 2023.09.463<sup>53</sup> and the add-on packages ‘*vegan*’ v.2.6-4<sup>54</sup>, ‘*ggplot2*’ v.3.3.6<sup>55</sup>, ‘*dplyr*’ v.1.3.0<sup>56</sup>, ‘*ggbreak*’ v.0.1.2<sup>57</sup>.

## Results

### Physical and chemical environment

Under ice light at the outer site oscillated between 0 and 7  $\mu\text{mol}/\text{s}/\text{m}^2$  until 21 April (W3), when it abruptly declined by ~50% (range: 0 and ~3  $\mu\text{mol}/\text{s}/\text{m}^2$ ), a shift coincident with a doubling of snow depth from  $15 \pm 0.7$  cm (W1) to  $27 \pm 2$  cm (W2) (Fig. 1B). Albedo was highest (94%) on W3, increasing from 76% during early April (W1) (Table 2) due to changes in snow properties. For the inner site, under ice light remained constantly low ( $0\text{--}3 \mu\text{mol}/\text{s}/\text{m}^2$ ) for the entire sampling period, consistent with minimal changes in snow ( $\bar{x} = 27 \pm 2$  cm) and ice depth (Fig. 1B, Table 2). We measured abrupt increases in water temperature over the sampling period at both sites (Fig. 1C). However, for the outer site, under ice temperature reached expected sea ice melting point ( $> -1.7$  °C) in W3, followed by oscillations between freezing and thawing temperatures, whereas warming occurred after W4 at the inner site, with a steady increase to  $-1.5$  °C (Fig. 1C). Sea ice thickness gradually increased with time at the outer site, ranging from  $64 \pm 1$  cm (W1) to  $74 \pm 1$  cm (W6), and increased from  $83 \pm 2$  cm (W1) to  $90 \pm 1$  cm (W4) at the inner site, before declining to  $85 \pm 3$  cm (W6). The bulk salinity in the bottom of the ice was similar between the two sites, ranging from 12.33 to 7.34 ( $\bar{x} = 10.1$ ) at the outer site and 13.14–8.9 ( $\bar{x} = 11.2$ ) at the inner site, with both sites experiencing the fresher conditions during W6 (Table 2). Brine volume did not vary between the two sites, ranging from 24 to 14% ( $\bar{x} = 20\%$ ) at the outer site and 28–19% ( $\bar{x} = 24\%$ ) at the inner site, with both sites experiencing the lowest brine volume during W6 (Table 2).

Ice  $\text{NO}_x$  concentrations peaked (3.2  $\mu\text{M}$ ) in W3 at the outer site, before declining to potentially limiting levels (0.6  $\mu\text{M}$ ) by W6. In contrast,  $\text{NO}_x$  concentrations were higher at the inner site (averaging  $5.0 \pm 3.7 \mu\text{M}$  throughout the study), with a peak concentration of 9.9  $\mu\text{M}$  in W4 (Fig. 1D). For the outer site,  $\text{Si}(\text{OH})_4$  concentration in the ice was not detected until W5 when it was low (0.4  $\mu\text{M}$ ), while  $\text{PO}_4^{3-}$  increased to 1.6  $\mu\text{M}$  in W6 (Table 2). Unlike the outer site, ice  $\text{Si}(\text{OH})_4$  concentrations were consistently detectable at the inner site, with the concentration ranging from 0.5 to 3.9  $\mu\text{M}$  (Fig. 1D). *Chl a* concentrations within the bottom ice gradually increased with time at both sites, peaking at W6 for the outer site and W4 for the inner site (Fig. 1D; Table 2). There was a visible change in the *chl a* biomass within the bottom-ice following the melting period at the outer site (Fig. 1D), in which the biomass was heterogenous and forming visible lumps. Pelagic *chl a* concentrations remained low throughout, increasing to 0.9 and 0.3  $\text{mg}/\text{mg}^3$  by W6 at both the outer and inner site, respectively (Table 3; Fig. 1). Seawater  $\text{NO}_x$  and  $\text{Si}(\text{OH})_4$  concentrations decreased with time at the outer site, but remained replete ( $\text{NO}_x$ : 2.5–7.5 and  $\text{Si}(\text{OH})_4$ : 0.9–3.8  $\mu\text{M}$ , respectively).  $\text{PO}_4^{3-}$  concentration remained constant (0.3–0.5  $\mu\text{M}$ ) and replete. For the inner site, concentrations of  $\text{NO}_x$  and  $\text{Si}(\text{OH})_4$  and  $\text{PO}_4^{3-}$  in the seawater remained relatively constant and replete ( $\text{NO}_x$ : 6.4–7.6  $\mu\text{M}$ ,  $\text{Si}(\text{OH})_4$ : 9.6–15.4  $\mu\text{M}$  and  $\text{PO}_4^{3-}$ : 0.4–0.5  $\mu\text{M}$ ) throughout the study (Fig. 1D). Molar ratios of C:N did not differ between sites (Table 2). However, there was a greater range in C:N (2.62–11.51) at the outer site than the inner site (2.75–5.40). Molar ratios of N:Si taken from the ice ranged between 0.44 and 5.29 at the outer site and 0.98 and 7.17 at the inner site, whilst the molar ratio of Si:P ranged between 0.85 and 0.95 at the outer site and from 0.70 to 8.36 at the inner site (Table 2). Bottom-ice POC and *Chl a* were found to be positively correlated at the outer site only ( $F_{1,2} = 51.72$ ,  $p < 0.05$ ,  $R^2 = 0.96$ ) and POC:*Chl a* did not exhibit a relationship with time at either site.

### Protist community composition

*Nitzschia frigida* was the most abundant taxa at all sites and all time points, making up between 31% of the community at the inner site during W4 and 56% at the outer site during W6 (Fig. 2), with an increase in abundance towards the end of the season. Sea ice community composition was similar across the two sites and all time points (ANOSIM  $R = 0.03$ ,  $p > 0.05$ ), although some apparent decline in the proportion of *Navicula* spp. and *Pleurosigma*/*Gyrosigma* spp. in conjunction with an increase in the proportion of dinoflagellates, including *Gymnodinium* spp. is evident at the outer site by W6 (Fig. 2).



Date	Station	Snow depth (cm)	Albedo (%)	Ice thickness (cm)	Ice temperature (°C)	Ice salinity (ppt)	Brine salinity (ppt)	Brine volume (%)	Chlorophyll <i>a</i> (mg/m <sup>3</sup> )	C:N	$\delta^{13}\text{C}_{\text{VPDB}}$ (‰)	$\delta^{15}\text{N}_{\text{VPDB}}$ (‰)	Si(OH) <sub>4</sub> (μM)	NO <sub>3</sub> <sup>-</sup> + NO <sub>2</sub> (μM)	PO <sub>4</sub> (μM)	Average water temperature (°C)
6.4.22 Week 1	Outer	15±0.7	76	64±1	-2.3	10.80	40.78	24	0.52±1	6.14	-25.01	3.81	N.D.	0.98	0.24	0.24
7.4.22 Week 1	Inner	22±2	95	83±2	-2.1	9.74	37.36	23	0.31±1.9	4.95	-31.31	2.04	15.61	7.46	0.51	-1.79
20.4.22 Week 3	Inner	27±4	77	85±0.5	-2.6	13.14	45.85	26	2.00±0.1	3.99	-28.91	2.56	15.37	7.62	0.51	-1.79
21.4.22 Week 3	Outer	27±2	94	70±1	-2.7	12.33	47.53	23	0.49±0.3	3.16	-26.5	2.18	9.62	5.52	0.40	-1.87
29.4.22 Week 4	Outer	19±5	90	73±3	-2.5	9.78	44.15	19	1.32±0.2	2.57	-26.86	4.69	14.48	7.22	0.53	-1.85
30.4.22 Week 4	Inner	28±0.5	93	90±1	-2.3	13.00	40.78	28	2.91±0.8	5.67	-24.83	4.03	11.33	5.70	0.45	-1.65
12.5.22 Week 6	Inner	32±1.5	78	85±3	-2.3	8.90	40.78	19	2.03±0.5	4.85	-26.08	3.49	12.84	7.17	0.41	-1.87
13.5.22 Week 6	Outer	9±1	88	74±1	-2.6	7.34	45.85	14	4.33±1.6	11.51	-16.29	4.24	12.13	6.44	0.47	-1.50
									0.88	6.33	-25.17	4.6	3.86	2.52	0.31	-1.67

**Table 2.** Parameters measured associated with sea ice core extraction (white) and under-ice water (blue); snow depth (±SD, n = 18), albedo (%), ice thickness (±SD, n = 6), temperature (°C), bulk ice salinity (ppt), brine salinity (ppt), brine volume (% of ice volume), chlorophyll *a* concentration (Ice mg/m<sup>2</sup>, n = 3 and Water mg/m<sup>3</sup>), particulate organic carbon (POC) to particulate organic nitrogen (PON) ratio (C:N), stable isotope of carbon  $\delta^{13}\text{C}_{\text{VPDB}}$  (‰), stable isotope of nitrogen  $\delta^{15}\text{N}_{\text{VPDB}}$  (‰), silicic acid (Si(OH)<sub>4</sub>), nitrate + nitrite (NO<sub>3</sub>), phosphate (PO<sub>4</sub>) concentrations (μM) and average water temperature at the ice-water interface(°C).

	Outer site	Inner site
	% FA	% FA
14:0	7.5	5.5
15:0	0.3	0.4
16:0	20	19
16:1 n-9	2.7	8.5
16:1 n-7	49	22
16:1 n-5	0.6	1.5
17:0 Phytanic	0.1	0.4
17:0	0.1	0.5
16:2 n-7	0.9	1.9
16:3 n-4	0.5	1.9
18:0	1.4	6.2
16:4 n-1	1.4	3.1
18:1 n-9	1	1.5
18:1 n-7	0.3	0.7
18:2 n-6	0.6	0.6
18:3 n-6	1.9	1
18:3 n-3	0.3	0.4
20:0	0.2	0.4
18:4 n-3	1.4	2.1
20:4 n-6	0.8	3.4
20:3 n-3	0.2	0.3
22:0	0.1	0.4
20:4 n-3	0.2	0.3
22:1 n-9	0.4	3.3
20:5 n-3	6.9	10
22:6 n-3	0.9	2.1
SUM FA of DM	52	25
SUM SAFA	30 (16)	35 (8.6)
SUM MUFA	54 (28)	38 (9.4)
SUM PUFA	16 (8.4)	28 (6.8)
SUM omega-3 FA	10 (5.2)	16 (3.9)
SUM omega-6 FA	3.3 (1.7)	5 (1.3)
SUM omega-9 FA	4.1 (2.1)	13 (3.3)
SUM EPA + DHA	7.8 (4.1)	13 (3.1)

**Table 3.** Fatty acid (FA) composition of the entire sea ice algae community at the inner and outer site of Van Mijenfjorden, Svalbard on the 12th May and 13th May 2022, respectively, as % total FA displayed (with SUM % total lipid dry matter (DM) displayed in brackets), for 6 ice cores pooled. FAs accounting for <0.1% of total in both sites are not displayed. FA: Fatty acids, PUFA: polyunsaturated fatty acids, MUFA: monounsaturated fatty acids, SAFA: saturated fatty acids, EPA: eicosapentaenoic acid and DHA: docosahexaenoic acid.

### Biomolecular composition

Spectral analyses revealed strong trends and differences in key biomolecular peaks across time for both sites (Fig. 3A,B). Principle component analysis on the nine selected biomolecular peaks of *N. frigida* from the outer site showed separation with time of sampling along PC1, explaining 68.2% of the variation (Fig. 3C). The temporal trend was primarily driven by relative increases in lipids and FAs at the last sampling time point (W6). For the inner site, PC1 explained 42.9% of the variation, with evidence of a temporal effect driven by increases in lipid and saturated FAs (Fig. 3D).

Integrated peak areas for selected biomolecules revealed high cell-specific variability in *N. frigida* from both sites (Fig. 4A–D). We detected a significant shift in biomolecular composition of *N. frigida* at the end time point for the outer site (Fig. 4A–D), where differences observed were driven by an increase in allocation to storage biomolecules i.e. lipid (ester carbonyl) ( $F_{1,93} = 148.6$ ,  $p < 0.05$ ,  $R^2 = 0.62$ ; Fig. 4B), saturated fatty acids (SFA) and unsaturated fatty acids (USFA) (Table S2). These increases were concomitant with a decrease in protein (Amide II) ( $F_{1,94} = 60.16$ ,  $p < 0.05$ ,  $R^2 = 0.39$ ; Fig. 4C), carbohydrates ( $F_{1,93} = 26.54$ ,  $p < 0.05$ ,  $R^2 = 0.22$ ; Fig. 4A), phosphodiester and carboxylated molecules (Table S2). In contrast, *N. frigida* cells from the inner site, showed a significant shift in biomolecular profiles from early April (W1) and the final time point (Fig. 4E–H), primarily driven by a relative increase in protein (Amide II) ( $F_{1,100} = 44.19$ ,  $p < 0.05$ ,  $R^2 = 0.31$ ; Fig. 4G) and decrease in carbohydrate content ( $F_{1,100} = 44.19$ ,  $p < 0.05$ ,  $R^2 = 0.31$ ; Fig. 4E). A significant increase in lipids (ester carbonyl)

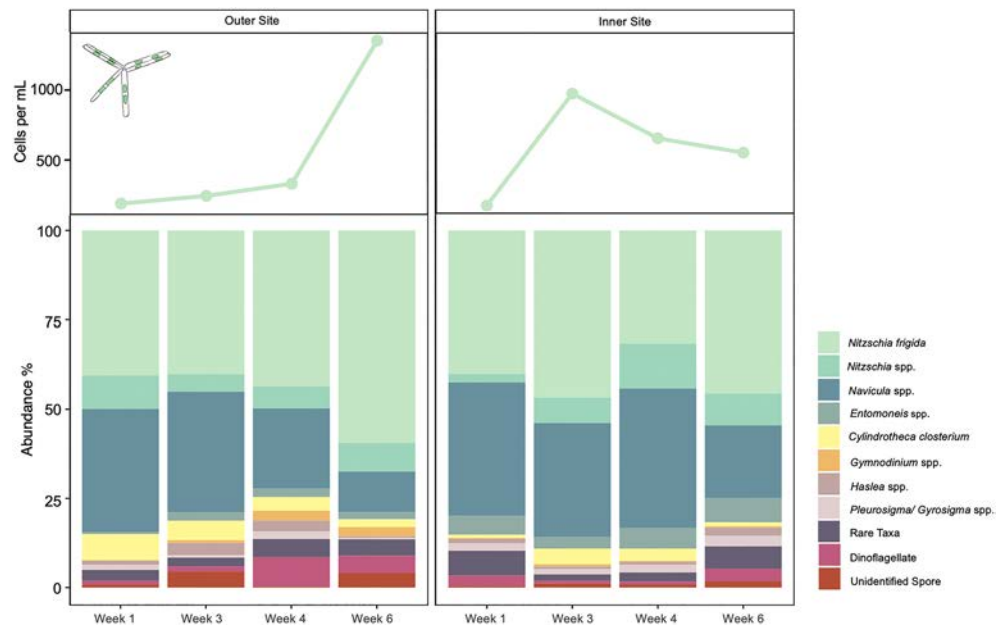


**Figure 2.** Bottom ice microalgal community composition from outer site (left) and inner site (right) sampled during April–May 2022, in Van Mijenfjorden, Svalbard, Norway. Raw counts of *Nitzschia frigida* cells per mL are displayed in the top panels, and the relative abundance (%) of taxonomic groups are shown in the lower panels. *Nitzschia* spp. includes all *Nitzschia* species identified with the exception of *Nitzschia frigida*. Rare Taxa includes: *Hantzchia* spp., *Diploneis littoralis*, *Stenoneis inconspicua*, *Pinnularia quadratarea*, *Plagiotropis* spp. *Manguinea rigida*, *Tropidoneis* spp.

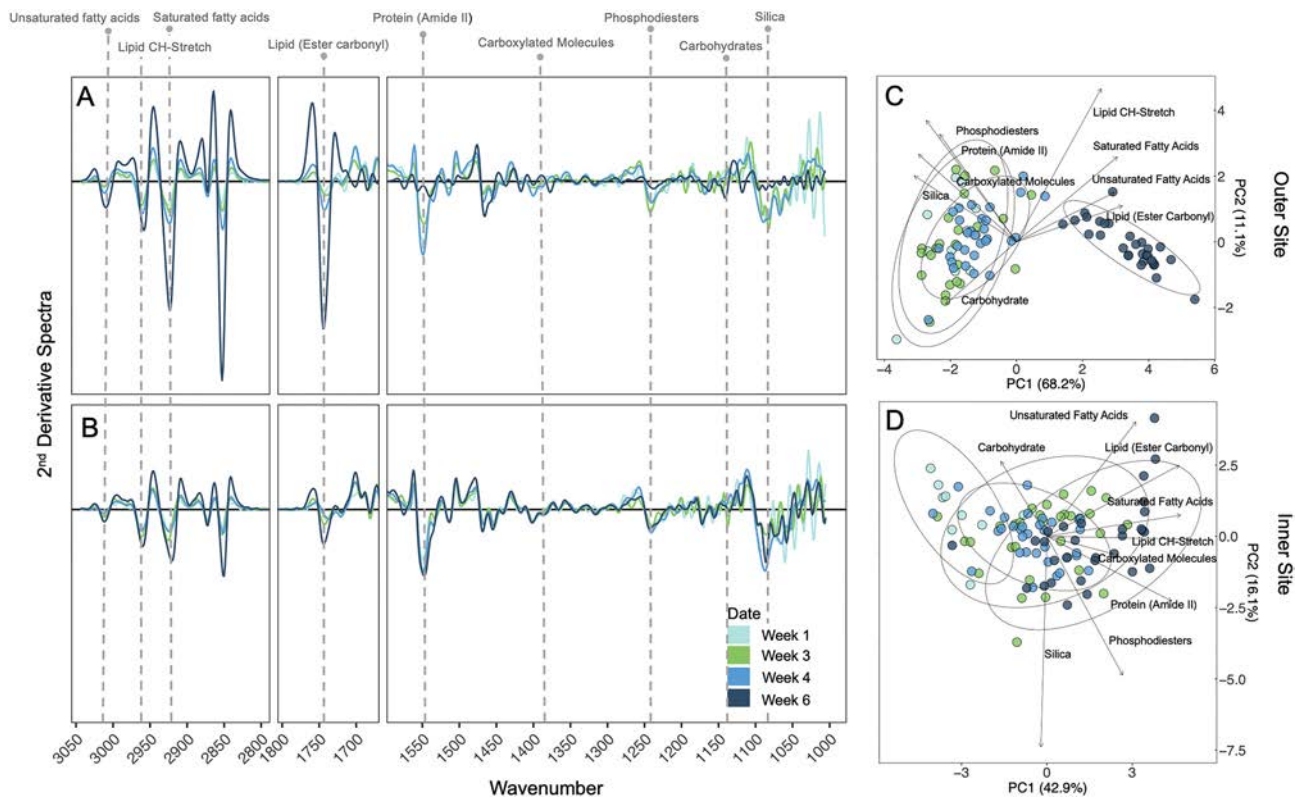


**Figure 3.** Smoothed and normalised 2nd derivative spectra for *Nitzschia frigida* at the (A) outer and (B) inner site with each sampling week denoted by colour gradient. Dashed vertical lines indicate respective wavenumber for peaks of interest. Principal component analysis (PCA) of biomolecular content at the (C) outer and (D) inner site with sampling week denoted by colour, in which each dot represents the measurements of one cell. Direction and strength of individual biomolecules are displayed with ordination bi-plot overlay.

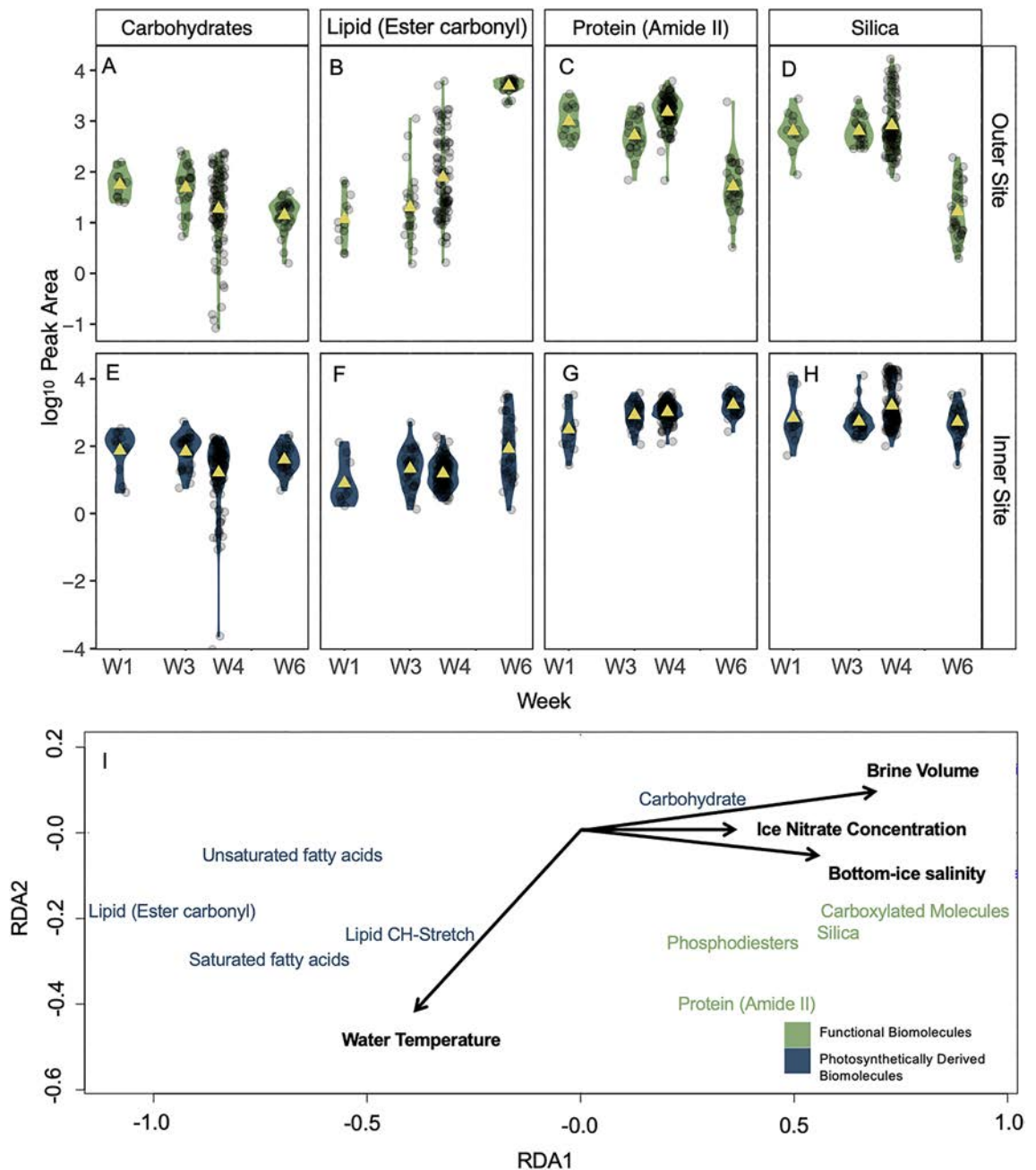


**Figure 4.** Biomolecular content based on normalised peak areas of specific biomolecules, for *Nitzschia frigida* per sampling week for the outer (A–D) and inner site (E–H); specifically (A, E) Carbohydrate (B, F) Lipid (Ester carbonyl), (C, G) Protein (Amide II) and (D, H) Silica content. Data are presented as violin plots where coloured shading indicates SE and a yellow triangle represents the mean, individual cells are shown by transparent dots. Site location is represented with colour; outer site (green; top panels) and inner site (blue; bottom panels). Redundancy analysis (RDA) biplot (I) of the mean biomolecular content (divided into functional biomolecules (cell structure and function) and photosynthetically derived biomolecules (energy and storage), denoted by colour) from each sampling site and date with environmental variables displayed with ordination bi-plot overlay. Only significant vectors are shown and RDA model is significant ( $p < 0.05$ ).

( $F_{1,99} = 26.99$ ,  $p < 0.05$ ,  $R^2 = 0.21$ ; Fig. 4F) and SFAs were also observed (Table S2). In addition to interrogating the biomolecules in the cell, we also looked for any changes in the silica peak at  $1150 \text{ cm}^{-1}$ . Unexpectedly, we saw a significant decline in biogenic silica in cells from the outer site by W6 (Fig. 4D), corresponding with the other significant changes in biomolecular components. No change in silica content was detected for *N. frigida* cells from the inner site (Fig. 4H).

Redundancy analysis revealed that the environmental parameters of brine volume, bottom-ice salinity and ice nitrate concentration combined explained 77% of the variability in biomolecular content across the two sites,

while seawater temperature explained 11% of the variability ( $F_6 = 2.92$ ,  $p < 0.05$ , Fig. 4E). Photosynthetically derived biomolecules (e.g. lipids and FAs) were negatively correlated with brine volume, bottom-ice salinity and ice nitrate, yet showed a positive relationship with these environmental parameters for the functional biomolecules (e.g. protein, phosphodiester and silica content) and carbohydrate content. Water temperature (i.e. freezing or melting the bottom of the sea ice) was shown to have the greatest positive effect on lipid (CH-stretch) content and an inverse relationship with carbohydrate content (Fig. 4E). Previous studies have found increasing light to drive increases in lipid and FA allocation in sea ice algae<sup>19,58,59</sup> but the typical increase light transmitted to the bottom-ice toward the end of the productive season was not observed in this study, excluding light as a significant driver in determining biomolecular changes.

### Fatty acid composition

Total fatty acid (FA) content of the outer site community was double (54% total lipid of dry matter) that of the inner site community (25% total lipid of dry matter) (Fig. 5A). The predominant FA at both sites was 16:1 n-7, followed by 16:0, 20:5 n-3 and 14:0 (Table 2), together accounting for 83.5% and 56.5% of FA content at the outer and inner sites, respectively. As a proportion of total FA content, both sites had a similar relative proportion of SAFA content (30% FA: inner site, 35% FA: outer site). However, the inner site had a relatively higher proportion of PUFA content (28% FA: inner site, 16% FA: outer site) and a lower proportion of MUFA content (38% FA: inner site, 54% FA: outer site) compared with the outer site (Fig. 5A). In addition, the proportion of omega-3 FA EPA + DHA (polyunsaturated eicosapentaenoic acid and docosahexaenoic acid) was almost double at the inner site (13% FA) compared to the outer site (7.8% FA). Comparing SAFA and USFA content from the total community analysis with the FTIR samples from the final time point, we see that in both *N. frigida* and the total community, the total FA content was substantially higher at the outer site (Fig. 5B). There was a strong

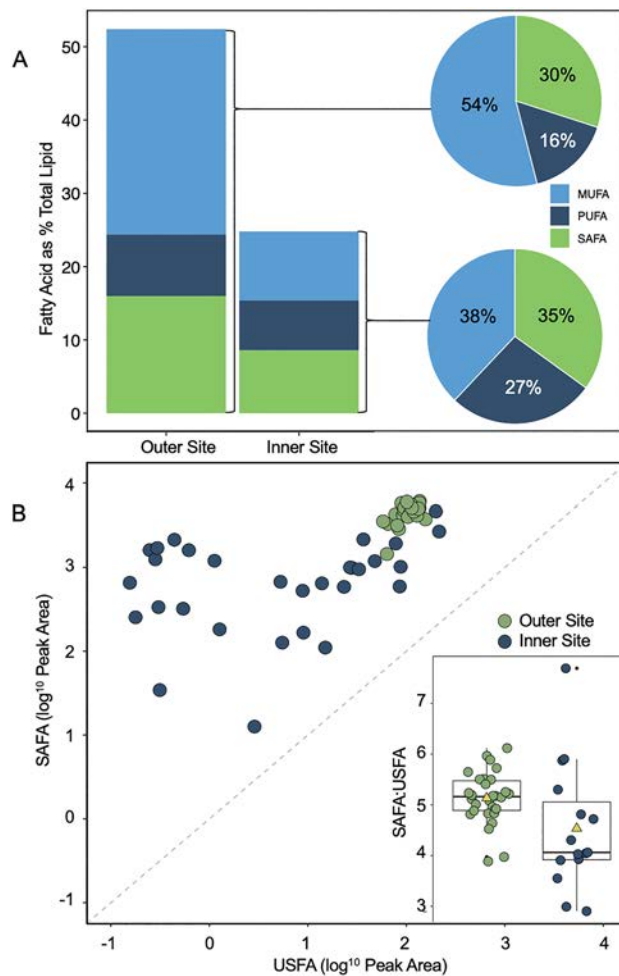


**Figure 5.** Fatty acid (FA) content as % total lipid content of the whole bottom ice community at the outer and inner site (A), during week 6. The different FA types, monounsaturated fatty acid (MUFA), polyunsaturated fatty acid (PUFA) and saturated fatty acid (SAFA) per site, are denoted by colour. Site-specific FA content as a proportion of total FA are presented in pie charts (right). Cell-specific SAFA vs. unsaturated fatty acid (USFA) content of *Nitzschia frigida*, as determined by s-FTIR (B), with site denoted by colour. The ratio of SAFA:USFA content per cell is displayed (inset), as a boxplot with yellow triangles representing the mean.

relationship between SAFA and USFA content at the outer site ( $F_{1,28} = 16.35$ ,  $p < 0.05$ ,  $R^2 = 0.37$ ) but not at the inner site ( $F_{1,28} = 2.4$ ,  $p > 0.05$ ,  $R^2 = 0.08$ ), where more variability was observed (Fig. 5B).

### $\delta^{13}\text{C}$ and $\delta^{15}\text{N}$ stable isotopes

Neither ice nor seawater  $\delta^{15}\text{N}_{\text{Air}}$  (‰) differed between sites, and showed no distinct pattern nor relationship to chl *a* concentrations (Fig. 6A,B). Conversely, under-ice seawater at both sites, and ice at the outer site, showed increased carbon-enrichment over time, with  $\delta^{13}\text{C}_{\text{VPDB}}$  (‰) ranging from  $-31.31$  to  $-25.17$  ‰ in the water and  $-25.01$  to  $-16.29$  ‰ in the ice at the outer site (Fig. 6A,B). Unlike the  $\delta^{15}\text{N}$  values, the  $\delta^{13}\text{C}$  values from the ice mirrored the patterns observed in the ice chl *a* concentration (Fig. 6A,B). There was no significant difference in carbon enrichment between the sites for the ice or under-ice water (Fig. 6A,B). Carbon enrichment was positively associated with storage biomolecular content (i.e. lipid and FAs), and inversely related to protein, carbohydrate, silica, carboxylated molecule and phosphodiester content (Fig. 6C). These relationships were driven by changes at the outer site only, where peak carbon enrichment was associated with the highest lipid content and lowest protein content (Fig. 6D).

### Discussion

Our study followed the seasonal progression in biomolecular composition of the key sea ice diatom, *N. frigida*. By sampling from two locations at four separate time points spanning five weeks during spring, we were able to capture spatial and temporal dynamics in environmental conditions from an inner (more stable) and an outer

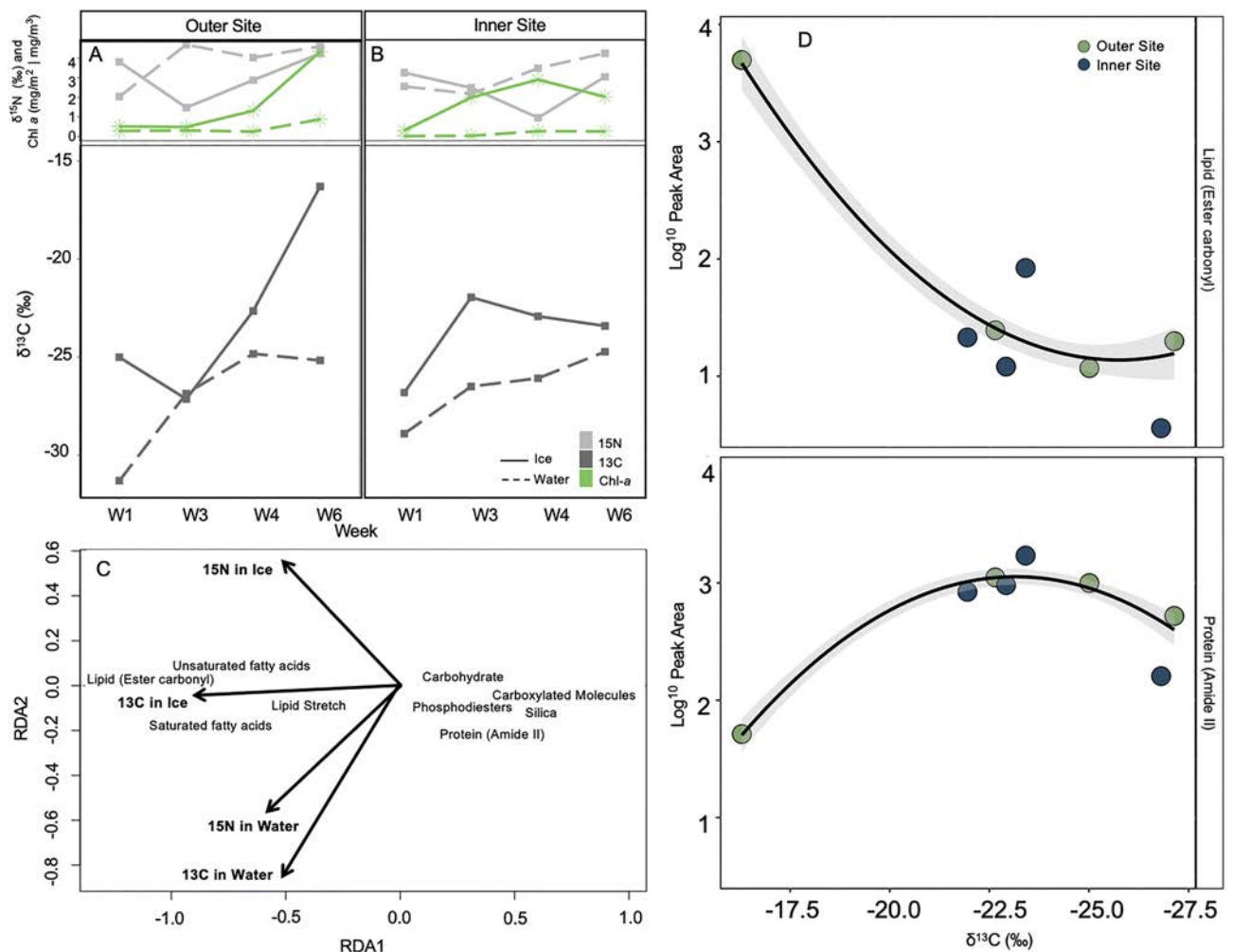


**Figure 6.**  $\delta^{15}\text{N}$  (light grey square),  $\delta^{13}\text{C}$  (dark grey square) and chlorophyll *a* content (green star) from the bottom-ice (solid line) and water directly below ice (stippled line) at the (A) outer site and (B) inner site, across all sampling weeks. Redundancy analysis (RDA) biplot (C) of the mean biomolecular content of *N. frigida* cells from each sampling site and time point with  $\delta^{13}\text{C}$  and  $\delta^{15}\text{N}$  stable isotope values from the sea ice and water below displayed with ordination bi-plot overlay, only significant vectors are shown and RDA model is significant ( $p < 0.05$ ). (D) Content of lipid (ester carbonyl; top panel) and protein (amide II) (bottom panel) vs.  $\delta^{13}\text{C}$  values, at the outer site (green) and inner site (blue). The data (both locations combined) are fitted with linear regressions, with 95% confidence intervals (grey shading).

(more dynamic) fjord site and look at them in relation to plasticity in biomolecular properties. Furthermore, by analysing individual cells we revealed high plasticity and individual variability in *N. frigida* cell content, with major changes becoming evident with the onset of seasonal melt. Close examination of the biomolecular profiles in relation to environmental variables, revealed that nitrogen limitation, in conjunction with warming sea temperatures and decreased brine volume, corresponded with increased lipid and FAs stores, and a decline in protein and carbohydrate. These shifts in metabolic energy allocation may be representative of the preparation for over wintering in *N. frigida* cells, as the Arctic summer advances.

Increasing ocean temperature is a key environmental trigger for initiating the seasonal transition from spring into Arctic summer. There was a two-week difference in the timing of warming between our two sites, making evident the influence ice melt can have on *N. frigida* populations. Throughout the study, the community was dominated by diatoms (predominantly *N. frigida*). Our microscopy findings were supported by the FA composition analyses, which showed 20:5 n3, C16 PUFAs and 16:1 n7—the diatom-marker FAs<sup>60</sup> as the primary constituents. From the onset of under-ice melt, we measured an increase in *N. frigida* numbers, as well as an increase in the proportion of dinoflagellates at the outer site, mirroring trends previously observed with seasonal progression<sup>30,61–63</sup>. Further, at the outer site with slightly younger ice, the under-ice melt resulted in a decrease in the proportion of *Navicula* spp. and increase in unidentified spores during mid-April (W3). The early warming at the outer site (starting W3), was followed by a series of temperature oscillations between freezing and thawing until mid-May (W6), causing physical changes to the bottom of the sea ice (i.e. removal of skeletal layer) and a reduction in brine volume (i.e. space for community colonisation). Interestingly, despite the loss of skeletal layer and reduction in brine volume from W4 onwards, the chl-*a* content within the ice increased at the outer site, forming a patchy distribution of biomass, still dominated by *N. frigida*. This ability for *N. frigida* to grow as large aggregates, likely provides a competitive advantage to *N. frigida* as it forms dendroid colonies, allowing it to remain on the bottom-ice, even in the absence of a skeletal-ice layer and expansive brine channel network. In addition, *N. frigida*, along with many other pennate diatoms, can produce exopolysaccharides (EPSs), creating a viscous biofilm and increasing cell adhesion to the bottom-ice<sup>64</sup>. These adaptations explain the sympagic biomass increase despite less advantageous sea ice conditions. The predominance of such aggregates has implications for secondary production and carbon export<sup>65</sup> with zooplankton unable to graze on larger food packages as effectively<sup>66</sup> and the aggregates falling to the sea floor more quickly<sup>67</sup>, enhancing carbon deposition.

Our single-celled approach revealed high intra-specific variability in biomolecular content, suggesting that *N. frigida* possess many plastic traits able to adjust to the dynamic spring sea ice and water conditions, providing a plausible evolutionary explanation for its ecological success in the sea ice and dominance throughout the entire productive season (Figs. 3, 4). We also detected considerable reduced variability in expressed lipid content at the last time point for the outer site, which could be indicative of strong environmental forcing causing cellular stress, whereby cells reach their phenotypic limit, in this case maximum production and storage of lipids. These changes coincided with significant decrease in protein and silica, supporting the idea of possible stress-induced changes in metabolic homeostasis. This type of latent stress response is often typical of variations in temperature<sup>21</sup>, such as the observed warming, reduced nitrogen availability<sup>23</sup>, and/or salinity<sup>68</sup>.

Alongside warming, nitrogen depletion, following its consumption by primary production, often signals the end of the productive ice-algae season<sup>62,69</sup>, and typically occurs with the beginning of the ice-breakup. As such, microalgal cells respond to nitrogen limitation by increasing lipid stores in preparation for dormancy<sup>22,59</sup>. Therefore, the rapid and significant increase in lipid accumulation by *N. frigida*, could be indicative of reduction in nitrogen availability<sup>70</sup>. The Redfield ratio for sea ice algae (amended to include the silicate requirement for diatoms) is generally accepted to be 106C:16N:15Si:1P<sup>44</sup>. Based on these requirements, in our study, nitrogen at the outer site could only have become limiting in mid-May, coinciding with the strongest biomolecular changes. The relatively constant and replete nitrogen levels within the other samples was likely due to exchange with seawater below the ice<sup>13</sup>, and/or remineralisation and nitrification<sup>71,72</sup> within the ice. Nitrate replenishment is indicated by low  $\delta^{15}\text{N}$  values and the relatively low chl *a* content and biomass, supported by the generally low C:N values (indicating low carbon), observed at the other sampling points throughout the season. Another indication of possible temperature and nitrogen stress was the observed decline in cellular energy allocation to protein and reduced carbohydrate content, as such shifts have been previously observed in nitrogen limited sea ice algal communities<sup>22,23,59</sup>. The biomolecular shifts in energy allocation toward lipid storage, suggest that under warmer, nitrogen limiting conditions, further growth is not prioritised.

While the inner site showed little variation over our seasonal sampling, the outer site community was found to have approximately double the total FA content than the inner site, with proportionally higher MUFA content on the final sampling date. This is consistent with increases in neutral lipids under nitrate limitation, and as primarily storage lipids, this demonstrates a response to stress and preparation for dormancy<sup>73,74</sup>. In addition, the outer site had substantially higher 16:1 n7 content, an indicator of the cell entering a storage and survival phase. The community from the inner site on the final sampling date was indicative of a community in exponential growth with proportionally more PUFAs (and specifically higher proportions of 20:5 n-3 and 16:4 n-1)<sup>75</sup>, and which is consistent with nitrate limited cells taken post-bloom<sup>60,75,76</sup>. The availability of PUFA content has been shown to determine zooplankton production and growth<sup>16,77,78</sup>. The omega-3 FAs (PUFAs) EPA and DHA are essential for growth and reproduction in all marine organisms and are key indicators of how nutrient rich a food source is, yet are produced exclusively by marine algae<sup>79</sup>. Furthermore, the increase in lipid observed in *N. frigida*, corresponding with an increase in total carbon enrichment ( $\delta^{13}\text{C}$ ) within the ice<sup>40</sup>, indicates that the biomolecular response of *N. frigida* could be representative of many taxa in the sea ice algae community. Taken together, the species-specific spectroscopy and community FA composition and carbon enrichment results from the outer site elucidate how end of season nitrate limitation alters the nutritional quality of food available to higher trophic levels.

In response to seasonal warming, another environmental change signalling the end of the ice season is a decrease in brine volume and associated freshening of the bottom-ice. While this process can occur during ice growth, drainage is often triggered by either warming at the ice surface (air temperature), or melting at the ice-water interface (water temperature)<sup>80</sup>. The hypersaline brine drains out to the ocean below and fresh meltwater from the ice percolates through the brine network, replacing the brine<sup>81</sup> and lowering interstitial salinity. In this study, we measured a decrease in brine volume and freshening of ice at the outer site on the last sampling time point, coinciding with detected changes in biomolecular profiles. Whilst the bulk ice salinity was within expected ranges for the end of the ice season (e.g.<sup>62,68,82</sup>) and brine volume remained above the 5% threshold necessary for colonisation<sup>83</sup>, the changes appeared to be sufficient to create environmental stress for the *N. frigida* cells. The move toward hypoosmotic conditions, which have been found to significantly lower photosynthetic efficiency in pennate ice diatoms<sup>68</sup>, could have induced strong increases in lipid storage and decreases in carbohydrate production as a means to prioritise energy storage over growth and development, in readiness for a period of dormancy<sup>22,74</sup>. Such adaptations to seasonality are commonly observed in many animals<sup>84</sup>, but are to a lesser degree documented for phytoplankton. Zooming in on individual properties of microalgae cells, as done in this study, adds much power when aiming to identify the extent of such adaptations in diatoms and other single cell organisms in the ocean. At the same time, the decrease in carbohydrate content and increase in lipid could be attributed also to the enduring higher average water temperatures ( $-1.65^{\circ}\text{C}$ , a temperature expected to melt sea ice from below) from the end of April. Similar biomolecular changes have been observed previously, albeit over a greater temperature change, e.g. between  $-1.8$  and  $+3^{\circ}\text{C}$ <sup>21</sup>. This is the first time such changes have been reported at the boundary temperature between melting and freezing. Given the above, it is likely that the combination of a decrease in brine volume, freshening of the bottom-ice and warmer under-ice water temperature contributed to creating a multi-stressor environment, and when combined with nitrogen limitation, directed metabolism and photosynthate allocation toward increased energy storage rather than continued growth and development.

Unlike nitrate, silicate was limiting at both sites throughout the season, with N:Si higher than Redfield (1.07) and Si:P lower than Redfield (15) at both sites<sup>85</sup>. As silicate is necessary for building and maintenance of diatom frustules<sup>86</sup>, under limitation, biogenic silica formation and therefore diatom growth, is constrained<sup>87</sup>. Our data showed a strong decline of biogenic silica in *N. frigida* at the final time point, which may be explained by the additional stress on the cells experiencing end of season conditions, compromising their growth and frustule formation.

The results from this study demonstrate how environmental conditions that lead to the sea ice algae community being ‘released’ from the ice, are important in terms of the cell’s viability for surviving ice free conditions, for carbon export, and for energy supply to the marine food web. With the onset of warming, the biggest environmental changes to influence *N. frigida* physiology, morphology and metabolism, were reduced brine volume and the onset of nitrogen limitation. The sea ice algal community, and *N. frigida* in particular, showed high phenotypic diversity and plasticity throughout the sea ice season, and appeared to ‘tolerate’ the dynamic freeze/thaw cycles, continuing to grow, independently or perhaps because of the variable conditions. Variability in the phenome of *N. frigida* was reduced as the season progressed towards ice-free conditions. We saw large changes in biomolecular composition, specifically an increase in lipid and FA storage, at the expense of protein and carbohydrate stores, associated with the onset of nitrogen limitation, marking the end of the sea ice algal growth season. As lipid stores and reduced metabolic rate are thought to be the key to the ability of *N. frigida* to survive summer and the six months of darkness that follow, these findings highlight the importance of this seasonal metabolic cascade for Arctic food web dynamics and carbon export. Our study revealed a significant decline in cell-specific silica content as the community approached the end of the cascade. This reduction in cell-specific silica content, has the potential to alter *N. frigida* sinking rates and grazability, thereby influencing carbon transfer. Conversely, these changes may be countered by the increased aggregation by *N. frigida*, which would likely result in a net increase in population sinking rate and provide additional protection from potential grazers. In the context of climate change, the predicted Atlantification of the Arctic would bring warmer water advection earlier in the season and/or create a more abrupt transition to the melting phase. This transition earlier in the season could obviate these important end-of-season environmental shifts, causing the algae to be released from the ice prior to significant biomass accumulation and sufficient lipid build-up and storage, with the onset of nitrogen limitation. Reduced biomass would likely alter food web dynamics, changing the quality and quantity of the food source at a critical time of development and seasonal growth, while diminished lipid stores upon meltout could result in fewer cells surviving dormancy. As lipids are the most energy dense of all biomolecules, taken together, such changes at the primary production level could result in less carbon transfer through the polar marine ecosystem.

## Data availability

All data are available in the open repository Figshare. <https://doi.org/10.6084/m9.figshare.25222808>.

Received: 22 February 2024; Accepted: 18 June 2024

Published online: 01 July 2024

## References

1. Yu, Y., Stern, H., Fowler, C., Fetterer, F. & Maslanik, J. Interannual variability of Arctic landfast ice between 1976 and 2007. *J. Clim.* **27**(1), 227–243 (2014).
2. Kwok, R. Arctic sea ice thickness, volume, and multiyear ice coverage: Losses and coupled variability (1958–2018). *Environ. Res. Lett.* **13**(10), 105005 (2018).
3. Stroeve, J. & Notz, D. Changing state of Arctic sea ice across all seasons. *Environ. Res. Lett.* **13**(10), 103001 (2018).



4. Årthun, M., Eldevik, T. & Smedsrud, L. H. The role of Atlantic heat transport in future Arctic winter sea ice loss. *J. Clim.* **32**(11), 3327–3341 (2019).
5. D. Perovich *et al.* Arctic Report Card: Sea Ice. NOAA. <https://www.arctic.noaa.gov/Report-Card> (2023).
6. Comiso, J. C. Large decadal decline of the Arctic multiyear ice cover. *J. Clim.* **25**(4), 1176–1193 (2012).
7. Maslanik, J., Stroeve, J., Fowler, C. & Emery, W. Distribution and trends in Arctic sea ice age through spring 2011. *Geophys. Res. Lett.* **38**(13) (2011).
8. Kacimi, S. & Kwok, R. Arctic snow depth, ice thickness, and volume from ICESat-2 and CryoSat-2: 2018–2021. *Geophys. Res. Lett.* **49**(5) (2022).
9. Leu, E. *et al.* Arctic spring awakening—Steering principles behind the phenology of vernal ice algal blooms. *Prog. Oceanogr.* **139**, 151–170 (2015).
10. Post, E. *et al.* Ecological consequences of sea-ice decline. *Science* **341**(6145), 519–524 (2013).
11. Varpe, Ø., Daase, M. & Kristiansen, T. A fish-eye view on the new Arctic lightscape. *ICES J. Mar. Sci.* **72**(9), 2532–2538 (2015).
12. Mundy, C. J. *et al.* Role of environmental factors on phytoplankton bloom initiation under landfast sea ice in Resolute Passage, Canada. *Mar. Ecol. Prog. Ser.* **497**, 39–49 (2014).
13. Cota, G., Legendre, L., Gosselin, M. & Ingram, R. Ecology of bottom ice algae: I. Environmental controls and variability. *J. Mar. Syst.* **2**(3–4), 257–277 (1991).
14. Ji, R., Jin, M. & Varpe, Ø. Sea ice phenology and timing of primary production pulses in the Arctic Ocean. *Glob. Chang. Biol.* **19**(3), 734–741 (2013).
15. Durbin, E. G. & Casas, M. C. Early reproduction by *Calanus glacialis* in the Northern Bering Sea: The role of ice algae as revealed by molecular analysis. *J. Plankton Res.* **36**(2), 523–541 (2014).
16. Søreide, J. E., Leu, E. V., Berge, J., Graeve, M. & Falk-Petersen, S. Timing of blooms, algal food quality and *Calanus glacialis* reproduction and growth in a changing Arctic. *Glob. Chang. Biol.* **16**(11), 3154–3163 (2010).
17. Kohlbach, D. *et al.* The importance of ice algae-produced carbon in the central Arctic Ocean ecosystem: Food web relationships revealed by lipid and stable isotope analyses. *Limnol. Oceanogr.* **61**(6), 2027–2044 (2016).
18. Finkel, M., Follows, J., Liefer, C., Brown, I. B. & Irwin, A. Phylogenetic diversity in the macromolecular composition of microalgae. *PLoS One.* **11**(5), e0155977 (2016).
19. Duncan, R. J. *et al.* Biomolecular profiles of Arctic sea-ice diatoms highlight the role of under-ice light in cellular energy allocation. *ISME Commun.* **4**(1) 1–15 (2024).
20. Teoh, M.-L., Chu, W.-L., Marchant, H. & Phang, S.-M. Influence of culture temperature on the growth, biochemical composition and fatty acid profiles of six Antarctic microalgae. *J. Appl. Phycol.* **16**, 421–430 (2004).
21. Torstensson, A., Jiménez, C., Nilsson, A. K. & Wulff, A. Elevated temperature and decreased salinity both affect the biochemical composition of the Antarctic sea-ice diatom *Nitzschia lecontei*, but not increased pCO<sub>2</sub>. *Polar Biol.* **42**, 2149–2164 (2019).
22. Mock, T. & Kroon, B. M. Photosynthetic energy conversion under extreme conditions—I: Important role of lipids as structural modulators and energy sink under N-limited growth in Antarctic sea ice diatoms. *Phytochemistry* **61**(1), 41–51 (2002).
23. Pogorzelec, N. M. *et al.* FTIR autecological analysis of bottom-ice diatom taxa across a tidal strait in the Canadian Arctic. *Elem. Sci. Anth.* **10**(1), 00094 (2022).
24. Mock, T. & Gradinger, R. Changes in photosynthetic carbon allocation in algal assemblages of Arctic sea ice with decreasing nutrient concentrations and irradiance. *Mar. Ecol. Prog. Ser.* **202**, 1–11 (2000).
25. An, M. *et al.* Temperature regulates fatty acid desaturases at a transcriptional level and modulates the fatty acid profile in the Antarctic microalga *Chlamydomonas* sp. ICE-L. *Bioresource Technol.* **134**, 151–157 (2013).
26. Duncan, R. J. & Petrou, K. Biomolecular composition of sea ice microalgae and its influence on marine biogeochemical cycling and carbon transfer through polar marine food webs. *Geosciences* **12**(1), 38 (2022).
27. Merilä, J. & Hendry, A. P. Climate change, adaptation, and phenotypic plasticity: The problem and the evidence. *Evolut. Appl.* **7**(1), 1–14 (2014).
28. Gosselin, M., Levasseur, M., Wheeler, P. A., Horner, R. A. & Booth, B. C. New measurements of phytoplankton and ice algal production in the Arctic Ocean. *Deep Sea Res. Part II Topical Stud. Oceanogr.* **44**(8), 1623–1644 (1997).
29. Syvertsen, E. E. Ice algae in the Barents Sea: Types of assemblages, origin, fate and role in the ice-edge phytoplankton bloom. *Polar Res.* **10**(1), 277–288 (1991).
30. Duncan, R. J. *et al.* Spatio-temporal dynamics in microalgal communities in Arctic land-fast sea ice. *Prog. Oceanogr.* **224**, 103248 (2024).
31. Palmisano, A. C. & Sullivan, C. W. Physiology of sea ice diatoms. II. Dark survival of three polar diatoms. *Can. J. Microbiol.* **29**(1), 157–160 (1983).
32. Hargraves, P. Diatom resting spores: Significance and strategies. *Survival Strategies Algae*. 49–68 (Cambridge University Press, 1983).
33. Qing, Z., Gradinger, R. & Qingsong, Z. Competition within the marine microalgae over the polar dark period in the Greenland Sea of high Arctic. *Acta Oceanol. Sinica* **2**, 233–242 (2003).
34. Tremblay, C., Runge, J. A. & Legendre, L. Grazing and sedimentation of ice algae during and immediately after a bloom at the ice-water interface. *Mar. Ecol. Prog. Ser.* **56**(3), 291–300 (1989).
35. McMahon, K. W. *et al.* Benthic community response to ice algae and phytoplankton in Ny Ålesund, Svalbard. *Mar. Ecol. Prog. Ser.* **310**, 1–14 (2006).
36. Aumack, C. & Juhl, A. Light and nutrient effects on the settling characteristics of the sea ice diatom *Nitzschia frigida*. *Limnol. Oceanogr.* **60**(3), 765–776 (2015).
37. Høyland, K. V. Ice thickness, growth and salinity in Van Mijenfjorden, Svalbard, Norway. *Polar Res.* **28**(3), 339–352 (2009).
38. Norwegian Ice Service. Ice Service Charts. *Norwegian Meteorological Institute*. <https://cryo.met.no/en/latest-ice-charts> (2023).
39. Smith, R., Anning, J. & Pierre Clement, G. Abundance and production of ice algae in Resolute Passage, Canadian Arctic. *Mar. Ecol. Prog. Ser.* **48**, 251–263 (1988).
40. Lee, S. H., Whittle, T. E. & Kang, S.-H. Carbon uptake rates of sea ice algae and phytoplankton under different light intensities in a landfast sea ice zone, Barrow, Alaska. *Arctic.* **61**(3), 281–291 (2008).
41. Garrison, D. L. & Buck, K. R. Organism losses during ice melting: A serious bias in sea ice community studies. *Polar Biol.* **6**, 237–239 (1986).
42. Campbell, K. *et al.* Melt procedure affects the photosynthetic response of sea ice algae. *Front. Earth Sci.* **7**, 21 (2019).
43. Holm-Hansen, O. & Riemann, B. Chlorophyll a determination: Improvements in methodology. *Oikos.* **30**(3), 438–447 (1978).
44. Parsons, T. R. *A Manual of Chemical & Biological Methods for Seawater Analysis* (Elsevier, 2013).
45. Utermöhl, H. Zur vervollkommnung der quantitativen phytoplankton-methodik: Mit 1 Tabelle und 15 abbildungen im Text und auf 1 Tafel. *Internationale Vereinigung für theoretische und angewandte Limnologie: Mitteilungen* **9**(1), 1–38 (1958).
46. Edler, L. & Elbrächter, M. The Utermöhl method for quantitative phytoplankton analysis. *Microscopic Mol. Methods Quantitative Phytoplankton Anal.* **110**, 13–20 (2010).
47. Cox, G. F. & Weeks, W. F. Equations for determining the gas and brine volumes in sea-ice samples. *J. Glaciol.* **29**(102), 306–316 (1983).
48. Barrie, A., Davies, J., Park, A. & Workman, C. Continuous-flow stable isotope analysis for biologists. *Spectroscopy* **4**(7), 42–52 (1989).

49. Bamberg, K. R., Wood, B. R. & McNaughton, D. Resonant Mie scattering (RMieS) correction applied to FTIR images of biological tissue samples. *Analyst* **137**(1), 126–132 (2012).
50. Wagner, H., Liu, Z., Langner, U., Stehfest, K. & Wilhelm, C. The use of FTIR spectroscopy to assess quantitative changes in the biochemical composition of microalgae. *J. Biophoton.* **3**(8–9), 557–566 (2010).
51. Stevens, A. & Ramirez-Lopez, L. An introduction to the prospectr package. R package version 0.2.7. (2014).
52. Shapiro, S. S. & Wilk, M. B. An analysis of variance test for normality (complete samples). *Biometrika* **52**(3/4), 591–611 (1965).
53. *RStudio: Integrated Development for R.* (2022). Posit Software, PBC, Boston, MA, USA.
54. Oksanen, J. *et al.* Package 'vegan: Community Ecology Package'. R package version 2.6-4. <https://CRAN.R-project.org/package=vegan> (2022).
55. Wickham, H., Chang, W. & Wickham, M. H. Package 'ggplot2'. Create elegant data visualisations using the grammar of graphics (Springer-Verlag New York, 2016). <https://ggplot2.tidyverse.org>.
56. Wickham, H. *et al.* tidy: Tidy Messy Data. R package version 1.3.0. <https://CRAN.R-project.org/package=tidy> (2023).
57. Xu, S. *et al.* Use ggbreak to effectively utilize plotting space to deal with large datasets and outliers. *Front. Genet.* **12**, 2122 (2021).
58. Smith, R.E., Cavalletto, J. F., Eadie, B. & Gardner, W. S. Growth and lipid composition of high Arctic ice algae during the spring bloom at Resolute, Northwest Territories, Canada. *Mar. Ecol. Prog. Ser.* **97**(1), 19–29 (1993).
59. Smith, R. E. & Herman, A. W. In situ patterns of intracellular photosynthate allocation by sea ice algae in the Canadian High Arctic. *Polar Biol.* **12**(6), 545–551 (1992).
60. Leu, E., Wiktor, J., Soreide, J., Berge, J. & Falk-Petersen, S. Increased irradiance reduces food quality of sea ice algae. *Mar. Ecol. Prog. Ser.* **411**, 49–60 (2010).
61. Hegseth, E. N. & von Quillfeldt, C. The sub-ice algal communities of the Barents Sea Pack Ice: Temporal and spatial distribution of biomass and species. *J. Mar. Sci. Eng.* **10**(2), 164 (2022).
62. Rozanska, M., Gosselin, M., Poulin, M., Wiktor, J. & Michel, C. Influence of environmental factors on the development of bottom ice protist communities during the winter–spring transition. *Mar. Ecol. Prog. Ser.* **386**, 43–59 (2009).
63. Mundy, C. J. *et al.* Characteristics of two distinct high-light acclimated algal communities during advanced stages of sea ice melt. *Polar Biol.* **34**(12), 1869–1886. (2011).
64. Krembs, C., Eicken, H. & Deming, J. W. Exopolymer alteration of physical properties of sea ice and implications for ice habitability and biogeochemistry in a warmer Arctic. *Proc. Natl. Acad. Sci.* **108**(9), 3653–3658 (2011).
65. Fernández-Méndez, M. *et al.* Composition, buoyancy regulation and fate of ice algal aggregates in the Central Arctic Ocean. *PLoS One* **9**(9), e107452 (2014).
66. Koski, M., Boutorh, J. & de La Rocha, C. (2017) Feeding on dispersed vs. aggregated particles: The effect of zooplankton feeding behavior on vertical flux. *PLoS One.* **12**(5), e0177958.
67. Riebesell, U., Schloss, I. & Smetacek, V. Aggregation of algae released from melting sea ice: Implications for seeding and sedimentation. *Polar Biol.* **11**, 239–248 (1991).
68. Forgereau Z. L. *et al.* Photophysiological responses of bottom sea-ice algae to fjord dynamics and rapid freshening. *Front. Mar. Sci.* **10** (2023).
69. Demers, S., Legendre, L., Maestrini, S. Y., Rochet, M. & Grant Ingram, R. Nitrogen nutrition of sea-ice microalgae. *Polar Biol.* **9**, 377–383 (1989).
70. Pogorzelec, N. M. *et al.* FTIR imaging analysis of cell content in sea-ice diatom taxa during a spring bloom in the lower Northwest Passage of the Canadian Arctic. *Mar. Ecol. Prog. Ser.* **569**, 77–88 (2017).
71. Clark, S., Granger, J., Mastorakis, A., Aguilar-Islas, A. & Hastings, M. An investigation into the origin of nitrate in Arctic sea ice. *Glob. Biogeochem. Cycles* **34**(2), e2019GB006279 (2020).
72. Fripiat, F. *et al.* New insights into sea ice nitrogen biogeochemical dynamics from the nitrogen isotopes. *Glob. Biogeochem. Cycles* **28**(2), 115–130 (2014).
73. Zhang, Q., Gradinger, R. & Spindler, M. Dark survival of marine microalgae in the high Arctic (Greenland Sea). *Polarforschung* **65**(3), 111–116 (1998).
74. Johnsen, G., Leu, E. & Gradinger, R. Marine micro- and macroalgae in the polar night," *Polar night marine ecology: Life and light in the dead of night.* 67–112 (2020).
75. Leu, E. *et al.* Fatty acid dynamics during the spring bloom in a High Arctic fjord: Importance of abiotic factors versus community changes. *Can. J. Fisheries Aquat. Sci.* **63**(12), 2760–2779 (2006).
76. Schmidt, K. *et al.* Essential omega-3 fatty acids are depleted in sea ice and pelagic algae of the Central Arctic Ocean. *Glob. Chang Biol.* **30**(1), e17090 (2024).
77. Jónasdóttir, S. H., Visser, A. W. & Jespersen, C. Assessing the role of food quality in the production and hatching of *Temora longicornis* eggs. *Mar. Ecol. Prog. Ser.* **382**, 139–150 (2009).
78. Jónasdóttir, S. H., Trung, N. H., Hansen, F. & Gärtner, S. Egg production and hatching success in the calanoid copepods *Calanus helgolandicus* and *Calanus finmarchicus* in the North Sea from March to September 2001. *J. Plankton Res.* **27**(12), 1239–1259 (2005).
79. Ackman, R. G. *Marine Biogenic Lipids, Fats and Oils.* (CRC Press, 1989).
80. Griewank, P. J. & Notz, D. Insights into brine dynamics and sea ice desalination from a 1-D model study of gravity drainage. *J. Geophys. Res. Oceans* **118**(7), 3370–3386 (2013).
81. D. Notz & M. G. Worster. Desalination processes of sea ice revisited. *J. Geophys. Res. Oceans.* **114**(C5) (2009).
82. Leu, E. *et al.* Spatial and temporal variability of ice algal trophic markers—With recommendations about their application. *J. Mar. Sci. Eng.* **8**(9), 676 (2020).
83. Golden, K. M., Eicken, H., Heaton, A., Miner, J., Pringle, D. & Zhu, J. Thermal evolution of permeability and microstructure in sea ice. *Geophys. Res. Lett.* **34**(16) (2007).
84. Varpe, Ø. Life history adaptations to seasonality. *Integr. Comp. Biol.* **57**(5), 943–960 (2017).
85. Brzezinski, M. A. The Si:C:N ratio of marine diatoms: Interspecific variability and the effect of some environmental variables. *J. Phycol.* **21**(3), 347–357 (1985).
86. Martin-Jézéquel, V., Hildebrand, M. & Brzezinski, M. A. Silicon metabolism in diatoms: implications for growth. *J. Phycol.* **36**(5), 821–840 (2000).
87. Gosselin, M., Legendre, L., Theriault, J. C. & Demers, S. Light and nutrient limitation of sea-ice microalgae (Hudson Bay, Canadian Arctic). *J. Phycol.* **26**(2), 220–232 (1990).
88. Vongsvivut, J. *et al.* FTIR microspectroscopy for rapid screening and monitoring of polyunsaturated fatty acid production in commercially valuable marine yeasts and protists. *Analyst* **138**(20), 6016–6031 (2013).
89. Heraud, P., Wood, B. R., Beardall, J. & McNaughton, D. Probing the influence of the environment on microalgae using infrared and raman spectroscopy. *New Approaches Biomed. Spectrosc.* **963**, 85–106 (2007).
90. Sackett, O. *et al.* Taxon-specific responses of Southern Ocean diatoms to Fe enrichment revealed by synchrotron radiation FTIR microspectroscopy. *Biogeosciences* **11**(20), 5795–5808 (2014).
91. Whelan, D. R. *et al.* Monitoring the reversible B to A-like transition of DNA in eukaryotic cells using Fourier transform infrared spectroscopy. *Nucleic Acids Res.* **39**(13), 5439–5448 (2011).
92. Heraud, P., Stojkovic, S., Beardall, J., McNaughton, D. & Wood, B. R. Intercolonial variability in macromolecular composition in P-starved and P-replete *Scenedesmus* populations revealed by infrared microspectroscopy 1. *J. Phycol.* **44**(5), 1335–1339 (2008).
93. Beardall, J. *et al.* A comparison of methods for detection of phosphate limitation in microalgae. *Aquat. Sci.* **63**(1), 107–121 (2001).

94. Sackett, O. *et al.* Snapshot prediction of carbon productivity, carbon and protein content in a Southern Ocean diatom using FTIR spectroscopy. *ISME J* **10**(2), 416–426 (2016).

## Acknowledgements

Duncan RJ is supported by an Australian Government Research Training Program Scholarship and an AINSE Ltd. Postgraduate Research Award (PGRA). Funding was also provided through the 2017–2018 Belmont Forum and BiodivErsA joint call for research proposal, under the BiodivScen ERA-Net COFUND programme, and with the funding organisations Research Council of Norway (RCN; project nr. 296836) and National Science Centre Poland (NSC; project nr. UMO2015/17/B/NZ8/02473) awarded to Søreide JE. In addition, RCN allocated funding through an Arctic Field Grant to Duncan RJ (33156) and Pitusi V (350579). This research was supported by an Australian Research Council Grant DP210101360 awarded to Petrou K. Part of this work was funded by the Australian Synchrotron through merit-based beamtime awarded on the Infrared Microscopy (IRM) beamline at the Australian Synchrotron, part of ANSTO (AS222/IRM/18486) awarded to Petrou K. The authors would like to thank Stuart Thomson, Einar Bergland and Stina Skånhoff for their valuable assistance with the field sampling.

## Author contributions

Conceptualisation: RJD, KP, JES, OV; Methodology: RJD, KP, JES, DN, OV; Formal Analysis: RJD; Investigation: RJD, JES, DN, VP; Software: DN; Data Curation: RJD, DN; Resources: KP, JES; Validation: JW, MT; Visualisation: RJD; Writing Original Draft: RJD; Writing – Review & Editing: KP, JES, DN, OV, JW, MT, VP; Supervision: KP, JES, OV, JW; Funding Acquisition: RJD, JES, VP.

## Competing interests

The authors declare no competing interests.

## Additional information

**Supplementary Information** The online version contains supplementary material available at <https://doi.org/10.1038/s41598-024-65273-0>.

**Correspondence** and requests for materials should be addressed to R.J.D.

**Reprints and permissions information** is available at [www.nature.com/reprints](http://www.nature.com/reprints).

**Publisher's note** Springer Nature remains neutral with regard to jurisdictional claims in published maps and institutional affiliations.



**Open Access** This article is licensed under a Creative Commons Attribution 4.0 International License, which permits use, sharing, adaptation, distribution and reproduction in any medium or format, as long as you give appropriate credit to the original author(s) and the source, provide a link to the Creative Commons licence, and indicate if changes were made. The images or other third party material in this article are included in the article's Creative Commons licence, unless indicated otherwise in a credit line to the material. If material is not included in the article's Creative Commons licence and your intended use is not permitted by statutory regulation or exceeds the permitted use, you will need to obtain permission directly from the copyright holder. To view a copy of this licence, visit <http://creativecommons.org/licenses/by/4.0/>.

© The Author(s) 2024

# Ocean acidification alters the nutritional value of Antarctic diatoms

Rebecca J. Duncan<sup>1,2</sup> , Daniel A. Nielsen<sup>1</sup> , Cristin E. Sheehan<sup>1,3</sup>, Stacy Deppeler<sup>4,5</sup> , Alyce M. Hancock<sup>4,6,7</sup> , Kai G. Schulz<sup>8</sup> , Andrew T. Davidson<sup>7,9</sup> and Katherina Petrou<sup>1</sup> 

<sup>1</sup>School of Life Sciences, University of Technology Sydney, Sydney, NSW 2007, Australia; <sup>2</sup>Department of Arctic Biology, The University Centre in Svalbard, Longyearbyen 9171, Norway; <sup>3</sup>Climate Change Cluster, University of Technology Sydney, Sydney, NSW 2007, Australia; <sup>4</sup>Institute for Marine and Antarctic Studies, University of Tasmania, Hobart, Tas. 7001, Australia; <sup>5</sup>National Institute of Water and Atmospheric Research, Wellington 6021, New Zealand; <sup>6</sup>Antarctic Gateway Partnership, Battery Point, Tas. 7004, Australia; <sup>7</sup>Antarctic Climate and Ecosystems Cooperative Research Centre, Hobart, Tas. 7001, Australia; <sup>8</sup>Centre for Coastal Biogeochemistry, Southern Cross University, East Lismore, NSW 2480, Australia; <sup>9</sup>Australian Antarctic Division, Department of the Environment and Energy, Hobart, Tas. 7050, Australia

## Summary

Author for correspondence:  
Katherina Petrou  
Email: [katherina.petrou@uts.edu.au](mailto:katherina.petrou@uts.edu.au)

Received: 7 July 2021  
Accepted: 7 November 2021

New Phytologist (2021)  
doi: 10.1111/nph.17868

**Key words:** climate change, diatoms, FTIR microspectroscopy, macromolecules, microalgae, phytoplankton, Southern Ocean.

- Primary production in the Southern Ocean is dominated by diatom-rich phytoplankton assemblages, whose individual physiological characteristics and community composition are strongly shaped by the environment, yet knowledge on how diatoms allocate cellular energy in response to ocean acidification (OA) is limited. Understanding such changes in allocation is integral to determining the nutritional quality of diatoms and the subsequent impacts on the trophic transfer of energy and nutrients.
- Using synchrotron-based Fourier transform infrared microspectroscopy, we analysed the macromolecular content of selected individual diatom taxa from a natural Antarctic phytoplankton community exposed to a gradient of  $f\text{CO}_2$  levels (288–1263  $\mu\text{atm}$ ).
- Strong species-specific differences in macromolecular partitioning were observed under OA. Large taxa showed preferential energy allocation towards proteins, while smaller taxa increased both lipid and protein stores at high  $f\text{CO}_2$ .
- If these changes are representative of future Antarctic diatom physiology, we may expect a shift away from lipid-rich large diatoms towards a community dominated by smaller taxa, but with higher lipid and protein stores than their present-day contemporaries, a response that could have cascading effects on food web dynamics in the Antarctic marine ecosystem.

## Introduction

Ocean acidification (OA) is one of the most prodigious and ubiquitous threats to the structure and function of marine life (Ross *et al.*, 2011; Kroeker *et al.*, 2013; Hancock *et al.*, 2020). Since the beginning of the industrial era, the world's oceans have sequestered *c.* 30% of anthropogenic  $\text{CO}_2$  emissions (Sabine *et al.*, 2004; Denman *et al.*, 2007; Le Quéré *et al.*, 2018). As a result, the average ocean surface water pH has fallen from *c.* 8.21 to 8.10 (IPCC, 2014), equivalent to a 29% increase in hydrogen ion ( $\text{H}^+$ ) concentrations. If  $\text{CO}_2$  emissions continue unabated (RCP8.5), atmospheric  $\text{CO}_2$  concentrations are estimated to rise from the current *c.* 410 ppmv to > 1000 ppmv by 2100 (IPCC, 2014), with the average ocean pH expected to further decline by up to 0.4 pH units (IPCC, 2014). The cold waters of the Southern Ocean (SO) result in higher than average  $\text{CO}_2$  uptake in this region (Khaliwala *et al.*, 2009; Frölicher *et al.*, 2015) and the naturally low saturation state (McNeil & Matear, 2008) renders the Antarctic marine ecosystem and its biota immediately vulnerable to the effects of OA.

Phytoplankton provide the nutritional base that underpins the wealth of life in the oceans. Their growth and productivity have been shown to be positively (Wu *et al.*, 2010; Tew *et al.*, 2014; Baragi *et al.*, 2015; Chen *et al.*, 2015), negatively (Chen & Durbin, 1994; Hoppe *et al.*, 2015; Shi *et al.*, 2017) and neutrally (Beardall & Raven, 2004; Berge *et al.*, 2010) affected by increased  $\text{CO}_2$  concentrations. Similarly, no definitive taxonomic or size-related shifts in phytoplankton community composition in response to OA have been determined (Feng *et al.*, 2009, 2010; Nielsen *et al.*, 2010; Eggers *et al.*, 2014; Bach & Taucher, 2019). This variability in phytoplankton community response to  $\text{CO}_2$  has been suggested to result from differences in the concentrations tested, for which low  $\text{CO}_2$  enhancement promotes growth with increased passive transfer of  $\text{CO}_2$  for photosynthesis, while higher  $\text{CO}_2$  inhibits growth in some taxa, possibly due to high energy costs associated with greater dependence on  $\text{H}^+$  pumps (Deppeler *et al.*, 2018; Paul & Bach, 2020). Nevertheless, the range in  $\text{CO}_2$ -driven responses to productivity and community composition, highlights the presence of interspecific differences in tolerance. Therefore, uncovering the tolerance and

thresholds of individual species is essential for understanding species and community responses to the projected OA.

In pelagic food webs, the effects of small changes in nutrient availability at the primary production level can have broad, cascading effects on higher trophic organisms (Moline *et al.*, 2001). Lipids, which are the most energy-rich macromolecules, contain much of the energy that is transferred among trophic levels (Hagen & Auel, 2001). Adequate lipid supply has been shown to be critical to the survival and reproduction of zooplankton (Graeve *et al.*, 1994; Lee *et al.*, 2006), particularly for Antarctic krill (Hagen & Auel, 2001) that require large lipid reserves over winter when primary production is scarce. Proteins are also a key source of energy (Hagen & Auel, 2001), the predominant source of amino acids (Ruess & Müller-Navarra, 2019), and a cellular nitrogen reservoir (Finkel *et al.*, 2016) for higher trophic levels. Macromolecular stores of primary producers are the cornerstone of productive marine ecosystems and changes in the partitioning of critical macromolecules contained in phytoplankton, such as proteins and lipids, inevitably alters the supply of energy and essential compounds to higher trophic levels.

Diatoms dominate much of the primary production in the SO (Wright *et al.*, 2010; Wolf *et al.*, 2013; Eggers *et al.*, 2014), particularly in coastal areas and along sea ice margins (Kang & Fryxell, 1993; Wright *et al.*, 2010). Diatoms form dense, siliceous cell walls known as frustules by converting soluble silicic acid into biogenic silica (Martin-Jézéquel *et al.*, 2000). These frustules provide the cell with ballast (Tréguer *et al.*, 2018), and afford the cell some defence against grazers (Hamm *et al.*, 2003). Despite this protective armour, the relatively high growth rates and generally larger cell sizes make diatoms a favourite food source for krill and other large zooplankton, delivering both quality and quantity of proteins and lipids necessary for growth and reproduction (Cowles *et al.*, 1988; Litchman *et al.*, 2007; Bhavya *et al.*, 2018). Indeed, Antarctic krill and copepods have been shown to selectively feed on diatoms (Cowles *et al.*, 1988; Head & Harris, 1994; Turner *et al.*, 2001; Haberman *et al.*, 2003) with a strong preference for less silicified diatoms, which has been shown to benefit copepod growth rate, egg production and hatching (Liu *et al.*, 2016). Enrichment of seawater with CO<sub>2</sub> has been shown to stimulate carbon fixation in diatoms, thereby reducing the nutrient content relative to carbon (Urabe *et al.*, 2003; Bellerby *et al.*, 2008; Engel *et al.*, 2008) and therefore food quality for zooplankton, yet little information is known about the effects of OA on diatom macromolecular composition. In one study, acidification (750 µatm) resulted in a decline in total fatty acids (FAs) in the discoid centric diatom *Thalassiosira weissflogii* that translated to a 10-fold decline in FAs in the fed copepods, causing significant declines in copepod somatic growth and egg production (Rossoll *et al.*, 2012). Given the importance of the diatom–zooplankton link in the Antarctic pelagic food web, these results emphasise the importance for understanding how OA may influence the nutritional quality of key primary producers.

Understanding which species within the phytoplankton community are affected by environmental change requires a depth of study that broader community analyses do not provide. Single-cell analyses on natural mixed communities provides a unique

insight into the extent to which a member of the community is affected, delivering unprecedented detail on potential physiological and ecological implications. In a parallel study on the same phytoplankton community, we used single-cell analyses to investigate the effects of OA on the silicification rates of several Antarctic marine diatoms from within a natural mixed community (Petrou *et al.*, 2019). This study uncovered species-specific sensitivities to acidification and revealed a potential threat of OA to diatoms. In another study, single-cell analyses were used to differentiate diatoms from contrasting Antarctic marine habitats based on the taxonomic-specific macromolecular fingerprint (Sheehan *et al.*, 2020). However, to date, no study has looked at the macromolecular profiles of individual diatoms from a natural, phytoplankton assemblage in response to increasing CO<sub>2</sub> concentration. Knowledge of species-specific macromolecular partitioning under high CO<sub>2</sub> may help to elucidate potential changes to the nutritional quality of primary producers and in combination with information on lower trophic feeding links, may refine our understanding of the role of diatoms in secondary production.

Using synchrotron-based Fourier transform infrared (FTIR) microspectroscopy, we determined the macromolecular composition of selected Antarctic marine diatoms from amongst a natural community following a 18-d exposure to different *f*CO<sub>2</sub> levels, delivering a snapshot of carbon partitioning as a response to OA. In our experiment, large volume mesocosms were used, ensuring the inclusion of the entire microbial community – phytoplankton, bacteria, viruses – and the influence of these interactions (predation, competition) among and between these trophic levels, improving our ability to extrapolate to natural systems (Cottingham *et al.*, 2005; Kreyling *et al.*, 2018). Furthermore, by exposing the communities to a gradient of increasing *f*CO<sub>2</sub>, we enhanced the predictive strength of our data (Havenhand *et al.*, 2010). Through single-cell analyses, we showed differential effects of OA on the partitioning of macromolecules by individual diatom taxa, offering insight into potential implications of *f*CO<sub>2</sub>-induced changes to energy availability and transfer through the Antarctic marine food web.

## Materials and Methods

### Experimental design and mesocosm set-up

Mesocosm set-up and conditions were as described previously (Deppeler *et al.*, 2018; Hancock *et al.*, 2018; Petrou *et al.*, 2019; Supporting Information Table S1). Briefly, a near-shore, natural Antarctic microbial community was collected from an ice-free area among broken fast ice *c.* 1 km offshore from Davis Station, Antarctica (68°35'S, 77°58'E) on 19 November 2014. This community was incubated in 6 × 650 l polyurethane tanks (mesocosms) across a gradient of *f*CO<sub>2</sub> levels (343, 506, 634, 953, 1140 and 1641 µatm; denoted M1–M6). These *f*CO<sub>2</sub> levels corresponded to pH values ranging from 8.17 to 7.57 (Table S1). The seawater was initially gravity fed through a 200 µm Arkal filter to exclude metazooplankton. Unavoidably, this filtration may also have removed some of the larger chain-forming diatom taxa as well. Temperature was maintained at 0.0 ± 0.5°C and the mesocosms were stirred continuously by a central auger (15 rpm)

for gentle mixing and covered with an air-tight lid. Irradiance was initially kept low ( $0.8 \pm 0.2 \mu\text{mol photons m}^{-2} \text{s}^{-1}$ ), while cell physiology was left to acclimate to increasing  $f\text{CO}_2$  levels (over 5 d). When target  $f\text{CO}_2$  levels were reached in all six mesocosms, light was gradually increased (days 5–8) to  $89 \pm 16 \mu\text{mol photons m}^{-2} \text{s}^{-1}$  on a 19 h : 5 h, light : dark cycle, to mimic current natural conditions. To generate the gradient in carbonate chemistry, filtered seawater saturated with  $\text{CO}_2$  was added to five of the mesocosms. One mesocosm remained at ambient levels, with regular filtered seawater (unenriched with  $\text{CO}_2$ ), to control for the physical disturbance and dilution from the  $\text{CO}_2$ -enriched seawater additions to the other mesocosms. Daily measurements were taken to monitor pH and dissolved inorganic carbon (DIC). The former was measured using the indicator dye *m*-cresol purple on a GBC UV-vis 916 spectrophotometer in a 10 cm temperature-controlled ( $25^\circ\text{C}$ ) cuvette (Dickson *et al.*, 2007). DIC was measured on an Apollo SciTech AS-C3 by infrared absorption and calibrated against certified reference material batch CRM127 (Dickson, 2010). Practical alkalinity (PA) was calculated at  $25^\circ\text{C}$ , as per Deppeler *et al.* (2018). For details of  $f\text{CO}_2$  manipulations, analytical procedures and calculations see Deppeler *et al.* (2018). Samples for physiological and macromolecular measurements in this study were taken on day 18, at the end of the incubation period (Deppeler *et al.*, 2018).

### Macronutrient analyses

Samples for macronutrient concentration for this study were obtained from each mesocosm on day 18, filtered through 0.45- $\mu\text{m}$  cellulose ester filters (Millipore) and frozen at  $-20^\circ\text{C}$ . Concentrations of nitrate/nitrite ( $\text{NO}_x$ ), soluble reactive phosphorus (SRP) and molybdate reactive silica (Silica) were determined following analysis described previously (Davidson *et al.*, 2016). Operational detection limits for  $\text{NO}_x$ , SRP and Silica were 0.14, 0.10 and 1.66  $\mu\text{M}$ , respectively.

### Diatom community structure

Samples for community structure and abundance were collected from each mesocosm on days 1, 3, 5, 8, 10, 12, 14, 16 and 18. These were microscopically analysed within 2 yr of collection as described in Hancock *et al.* (2018). Briefly, between 2 and 10 ml of refrigerated Lugol's concentrated fixed samples were placed in an Utermöhl cylinder (Hydro-Bios, Altenholz, Germany) and cells allowed to settle overnight. A stratified counting procedure was used to capture both small and large cells, with all cells  $> 20 \mu\text{m}$  identified and quantified at  $\times 200$  magnification, while those  $< 20 \mu\text{m}$  were assessed at  $\times 400$  magnification. Size categories were established via visual inspection with assistance of a graticule in the ocular or the light microscope. To determine growth condition (active or stationary) closest to time of macromolecular profiling (day 18), cell counts from days 14 to 18 for each taxon from each mesocosm (Hancock *et al.*, 2018) were used to estimate specific growth rates on day 18 (for complete growth curves, see Hancock *et al.*, 2018). Due to limitations in species identification for some taxa during FTIR microspectroscopy

measurements, some species were grouped. Selected taxa for determination of macromolecular composition in this study included *Chaetoceros* spp. (predominantly comprised of chains of *C. castracanei*, but also *C. tortissimus* and *C. bulbosus*), *Fragilariopsis cylindrus*, *Proboscia truncata*, *Stellarima microtrias* and large discoid centric ( $> 20 \mu\text{m}$ ) diatoms (including *Thalassiosira ritscheri* and unidentified large discoid centric diatoms ( $> 20 \mu\text{m}$ ), predominantly from the genus *Thalassiosira*). These taxa were selected for analyses, as they were the most prevalent large ( $> 10\text{--}15 \mu\text{m}$ ) diatoms to be found in all six tanks (Hancock *et al.*, 2018; Table S3) and together, they represent up to 11% of the diatom dominated community (Table S3; Hancock *et al.*, 2018). While their numerical contribution may be relatively minor, being the largest cells within the community, their contribution to the community macromolecular pool is significant. Furthermore, in analysing multiple taxa, we can uncover potential response diversity of macromolecular partitioning in diatoms to OA.

### Cell volume and photophysiological status

Cell volume was determined for selected taxa from M1 and M6 via light microscopy. Cells were imaged on a calibrated microscope (Nikon Eclipse Ci-L, Tokyo, Japan) and length, width and height (24–77 cells per taxa) determined using IMAGEJ software (Schneider *et al.*, 2012). Biovolume was then calculated according to the cell morphology and corresponding equations described by Hillebrand *et al.* (1999). To establish photophysiological status of individual taxa, maximum quantum yield of Photosystem II ( $F_V/F_M$ ) was measured on individual cells as described in Petrou *et al.* (2019). Briefly, mesocosm samples were loaded into a flow cell (Bioptech, Butler, PA, USA) and chlorophyll *a* fluorescence measurements made on randomly selected diatom cells using a pulse amplitude modulated fluorometer (Imaging PAM IMAG-K4; Walz GmbH, Effeltrich, Germany) mounted on a compound microscope (Axiostar plus, Zeiss, Germany). Following 10 min dark-adaptation, minimum fluorescence was recorded and then a saturating pulse of light was applied (SP width = 0.8 s; SP intensity = 10; using the special SP-routine) to obtain maximum fluorescence. From these two parameters  $F_V/F_M$  was calculated. All measurements were taken at  $\times 200$  magnification, with blue excitation light (440 nm) and at  $0^\circ\text{C}$ .

### Species-specific macromolecular content by FTIR

The macromolecular composition of the selected diatom taxa sampled from all six mesocosms on day 18 was determined using synchrotron-based FTIR microspectroscopy on formalin-fixed (2% v/v final concentration) cells. Samples were fixed directly after being taken from the mesocosm, kept refrigerated and analysed within 9 months. Measurements were made on hydrated cells, a method shown to limit light-scattering effects (Bamberg *et al.*, 2012) and processed according to previous studies (Sackett *et al.*, 2013, 2014; Sheehan *et al.*, 2020). Briefly, fixed cells were loaded directly onto a microcompression cell with a 0.3 mm thick  $\text{CaF}_2$  window (Tobin *et al.*, 2010). Spectral data of individual cells (between 15 and 49 cells per taxon per mesocosm; Table S2) were collected in transmission mode, using the Infrared

Microspectroscopy Beamline at the Australian Synchrotron, Melbourne, in November 2015. Spectra (one per cell) were acquired over the measurement range 4000–800  $\text{cm}^{-1}$  with a Vertex 80v FTIR spectrometer (Bruker Optics, Ettlingen, Germany) in conjunction with an FT-IR microscope (Hyperion 2000; Bruker) fitted with a mercury cadmium telluride detector cooled with liquid nitrogen. To reduce water vapour interference, the microscope stage was contained within a box flushed with dehumidified air. Co-added interferograms ( $n=64$ ) were collected at a wavenumber resolution of 6  $\text{cm}^{-1}$  s. To allow for measurements of individual cells, all measurements were made in transmission mode, using a measuring area aperture size of  $5 \times 5 \mu\text{m}$ . Spectral acquisition and instrument control were achieved using OPUS 6.5 software (Bruker). All cells were identified and inspected visually to ensure consistency across spectral measurements. In cases in which the taxon was much larger than the aperture, three scans from different areas of the cell were taken and averaged, ensuring full coverage of cellular components.

Normalised spectra of biologically relevant regions revealed absorbance bands representative of key macromolecules, from which five previously verified band assignments were selected for comparison within taxon and treatment (Table 1). In this study, the amide II band (*c.* 1540  $\text{cm}^{-1}$ ) was used as an indicator of cellular protein content, as the other major protein band, amide I was masked by water absorption. Lipids were primarily determined using the integrated peak of the ester carbonyl from lipids (*c.* 1745  $\text{cm}^{-1}$ ) as described previously (Heraud *et al.*, 2005), but with associated changes to saturated FAs. Carbohydrates were not measured, as the silica from diatoms overlaps with these bands.

## Data analyses

Infrared spectral data were analysed using custom-made scripts in R (R Core Team, 2021). The regions of 3050–2800, 1770–1100  $\text{cm}^{-1}$ , which contain the major biological bands (Table 1), were selected for analysis. Spectral data were smoothed (4 pts either side) and second derivative (third order polynomial) transformed using the Savitzky–Golay algorithm from the PROSPECTR package in R (Stevens & Ramirez Lopez, 2013) and then normalised using the method of Single Normal Variate. Macromolecular content for individual taxon was estimated based on integrating the area under each assigned peak (Table 1), providing metabolite content according to the Beer–Lambert law, which assumes a direct relationship between absorbance and

relative analyte concentration (Wagner *et al.*, 2010). Regression analyses were used to explore the functional relationships between  $f\text{CO}_2$  and macromolecular content. Because of their superior interpolation potential, gradient designs are generally considered more useful for model parameterisation (Havenhand *et al.*, 2010). They are also deemed more effective at exposing response patterns to environmental perturbation than replicated designs (Cottingham *et al.*, 2005; Riebesell & Gattuso, 2015; Kreyling *et al.*, 2018). Integrated peak areas provide relative changes in macromolecular content between samples. Because of the differences in absorption properties of macromolecules, peak areas can only be used as relative measure within compounds. Therefore, peak areas were visualised using free axes to improve readability and discourage comparison between macromolecules. To determine significant relationships between macromolecular content and  $f\text{CO}_2$  level, a linear regression at each  $f\text{CO}_2$  level ( $\pm 95\%$  confidence interval) was applied to each taxon. In cases in which the data were poorly explained by a linear fit, a second order polynomial regression was applied. The Shapiro–Wilks (Shapiro & Wilk, 1965) test for normality showed that the data required  $\log_{10}$  transformation before analysis. Regressions were tested for overall model significance using the  $F$  statistic ( $P < 0.05$ ) and strength of fit using  $R^2$ . The residuals of all regressions were verified for homoscedasticity. All analyses were performed using RSTUDIO v.1.3.959 (R Core Team, 2021) and the add-on packages GGLOT2 v.2.2.1 (Wickham, 2009) and DPLYR v.1.0.0 (Wickham *et al.*, 2020).

## Results

### Chemistry, cell density and photophysiology

There was significant drawdown of macronutrients from phytoplankton growth in the mesocosms by day 18.  $\text{NO}_x$  concentration began to decline from day 10, but did not fall below the limits of detection in any tank until day 18 (Deppeler *et al.*, 2018). By day 18, SRP was lowest (0.10  $\mu\text{M}$ ) in M1 (control) and highest (0.19  $\mu\text{M}$ ) in M6 (highest  $f\text{CO}_2$  treatment), while silica concentrations ranged from 85  $\mu\text{M}$  (M3) to 99  $\mu\text{M}$  (M6). DIC concentrations ranged from 2179 to 2360  $\mu\text{mol kg}^{-1}$  (M1–M6, respectively), matching a gradient in total pH from 8.17 to 7.57, while PA remained relatively consistent across the pH gradient, dropping only 10  $\mu\text{mol kg}^{-1}$  (Table S1). Salinity and temperature were consistent across all mesocosms (Table S1).

**Table 1** Infrared band assignments for Fourier transform infrared microspectroscopy used in this study.

Wave number ( $\text{cm}^{-1}$ )	Frequency range ( $\text{cm}^{-1}$ )	Assignment	Compound label	Reference
<i>c.</i> 2920	2939–2912	$\nu_{\text{as}}(\text{C-H})$ from methylene ( $-\text{CH}_2$ )	Saturated fatty acids	Vongsvivut <i>et al.</i> (2012)
<i>c.</i> 1745	1745–1734	$\nu(\text{C=O})$ of ester functional groups, from membrane lipids and fatty acids	Ester carbonyl	Murdock & Wetzel (2009); Vongsvivut <i>et al.</i> (2012)
<i>c.</i> 1545	1556–1540	$\delta(\text{N-H})$ of amides associated with protein	Protein (amide II)	Giordano <i>et al.</i> (2001)
<i>c.</i> 1452	1457–1446	$\delta_{\text{as}}(\text{CH}_3)$ and $\delta_{\text{as}}(\text{CH}_2)$ of proteins	Free amino acid	Petrou <i>et al.</i> (2018)
<i>c.</i> 1375	1340–1407	$\Delta_{\text{s}}(\text{CH}_3)$ and $\delta_{\text{s}}(\text{CH}_2)$ of proteins, and $\nu_{\text{s}}(\text{C-O})$ of $\text{COO}^-$ groups (carboxylic group)	Carboxylates	Giordano <i>et al.</i> (2001)

For all species except *P. truncata*, cell abundance was lowest in the highest  $f\text{CO}_2$  treatment with a general decreasing trend with increasing  $f\text{CO}_2$  levels following a peak density at  $427 \mu\text{atm}$  (Table S3). *P. truncata* had the lowest cell abundance at  $547 \mu\text{atm}$  and peak density at  $957 \mu\text{atm}$ . It is important to note that the five diatom taxa selected for this study comprised  $< 11\%$  of the total community in all  $f\text{CO}_2$  treatments. Cell volume ranged from the  $847 \pm 370 \mu\text{m}^3$  for the smallest taxa, *Chaetoceros* spp., to  $252\,445 \pm 180\,405 \mu\text{m}^3$  for the largest taxa, discoid centric ( $> 20 \mu\text{m}$ ) diatoms (Table S4). Broad indicators of the physiological state of the phytoplankton communities in the mesocosms showed that each community was photosynthetically active on day 18, where  $F_V/F_M$  values ranged between 0.61 and 0.70 (Table S3). There was however no apparent  $f\text{CO}_2$  response.

### Cell-specific macromolecular partitioning

Spectral analyses revealed taxonomic differences in macromolecular content and diverse response patterns to acidification. Between 6% and 31% of the variance in macromolecular content

was found to be explained by the variation in  $f\text{CO}_2$  (Table S5). In *Chaetoceros* spp., all investigated macromolecules showed a u-shaped response to acidification, with an initial drop in macromolecular content at moderate  $f\text{CO}_2$  enrichment, followed by an increase towards maximum macromolecular content in cells grown at the highest  $f\text{CO}_2$  level (Fig. 1a–e; Table S5). This u-shaped pattern, although nonsignificant, was also observed in day 18 growth rates, in which the *Chaetoceros* spp. in M3 and M4 had already entered stationary phase or were in decline (Fig. 1f). A consistent response pattern across all macromolecules was also detected for the pennate diatom *F. cylindrus*, but was the inverse of that seen for *Chaetoceros* spp., with an initial increase in macromolecular content with increased  $f\text{CO}_2$  and generally stabilising above  $700 \mu\text{atm}$ , indicating a possible threshold in  $f\text{CO}_2$ -induced synthesis of macromolecules (Fig. 2a–e; Table S5). Growth rates for *F. cylindrus* on day 18 were highest in M2–M4 and lower relative to M1 in the highest  $f\text{CO}_2$  conditions (Fig. 2f). In *P. truncata*, a positive relationship to increasing  $f\text{CO}_2$  was found for amide II, free amino acids and carboxylates, with minimum protein content in cells from M1 and maximum

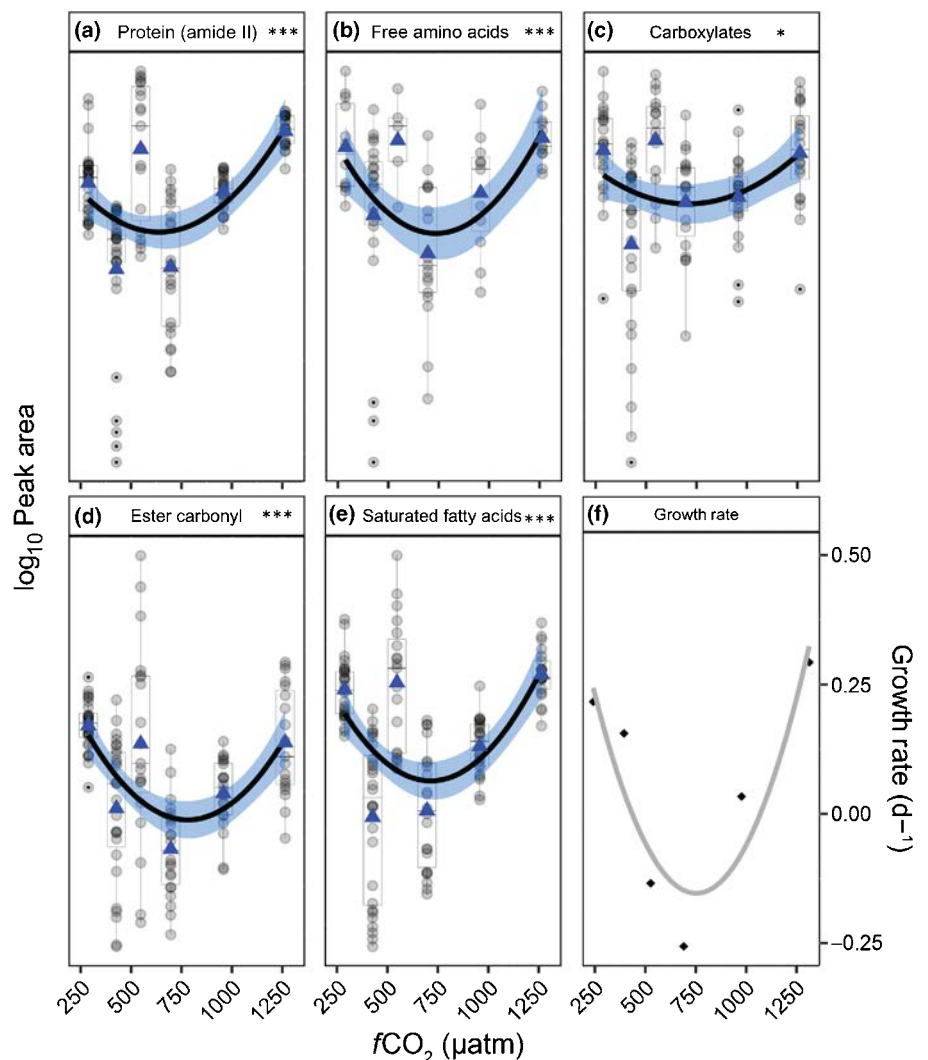


**Fig. 1** Cell-specific macromolecular content (based on normalised peak areas) and growth rates for *Chaetoceros* spp. (a–f) Relative content of selected macromolecules along an  $f\text{CO}_2$  gradient. Data are visualised using box plots with overlain grey dots showing the macromolecular content of individual cells from within  $f\text{CO}_2$  treatment mesocosm. Data are fitted with a second order polynomial regression, with 95% confidence intervals (dark blue shading), applied to log-transformed data (\*,  $P < 0.05$ ; \*\*\*,  $P < 0.0005$ ). The y-axis is free and units are arbitrary. Data means are displayed as blue triangles. (f) Growth rate ( $\text{d}^{-1}$ ) is displayed as diamonds, fitted with a second order polynomial regression (grey line).



protein content in cells from M6 (Fig. 3a–c; Table S5). By contrast, ester carbonyl and saturated FAs exhibited a bell-shaped response to  $f\text{CO}_2$ , with maximal lipid content at mid- $f\text{CO}_2$  (Fig. 3d,e; Table S5). We observed no significant effect of  $f\text{CO}_2$  on the growth rate of *P. truncata* (Fig. 3f).

The  $f\text{CO}_2$ -induced changes in macromolecules by the two discoid centric diatom groups, *S. microtrias* and the discoid centric group, differed greatly among compounds with strong similarities in responses of the two taxa (Figs 4, 5). For *S. microtrias*, protein from amide II exhibited a weak positive relationship ( $R^2 < 0.1$ ), while free amino acids showed a negative relationship and carboxylates a positive relationship with increasing  $f\text{CO}_2$  (Fig. 4a–c; Table S5). There was no response shown with saturated FAs, but a negative relationship was detected for ester carbonyl (Fig. 4d; Table S5). *S. microtrias* growth rates on day 18, showed the highest rate observed at the highest  $f\text{CO}_2$  level (Fig. 4f). For the large discoid centric diatoms, protein showed a weak, but significant u-shaped relationship (Fig. 5a). Similar to *S. microtrias*, a negative relationship was observed in free amino acid (Fig. 5b; Table S5), while carboxylates exhibited a positive response to increasing  $f\text{CO}_2$  (Fig. 5c; Table S5). Negative relationships were observed

with both ester carbonyl and saturated FAs (Fig. 5d,e; Table S5). These changes in macromolecular content occurred despite similar growth rates at all  $f\text{CO}_2$  concentrations (Fig. 5f).

### Lipid vs protein content

To explore overall shifts in macromolecular partitioning we used the protein to lipid ratio, providing a snapshot of the principle changes to carbon allocation by the cell (Heraud *et al.*, 2005). Lipids were positively correlated with protein in *Chaetoceros* spp. (Fig. 6a; Table S6), *F. cylindrus* (Fig. 6b; Table S6) and *P. truncata* (Fig. 6c; Table S6). Despite some grouping associated with an increase in protein with the highest  $f\text{CO}_2$  treatment, the lipid to protein ratio was largely unaffected by  $f\text{CO}_2$  in these taxa. We found no relationship between lipid and protein content for the two large discoid centric taxa, *S. microtrias* and discoid centrics (Fig. 6d,e; Table S6).

### Cell volume vs lipid and protein content

Under the lowest  $f\text{CO}_2$  (M1), there was a positive relationship between mean taxon-specific cell volume and protein (Fig. 7a;

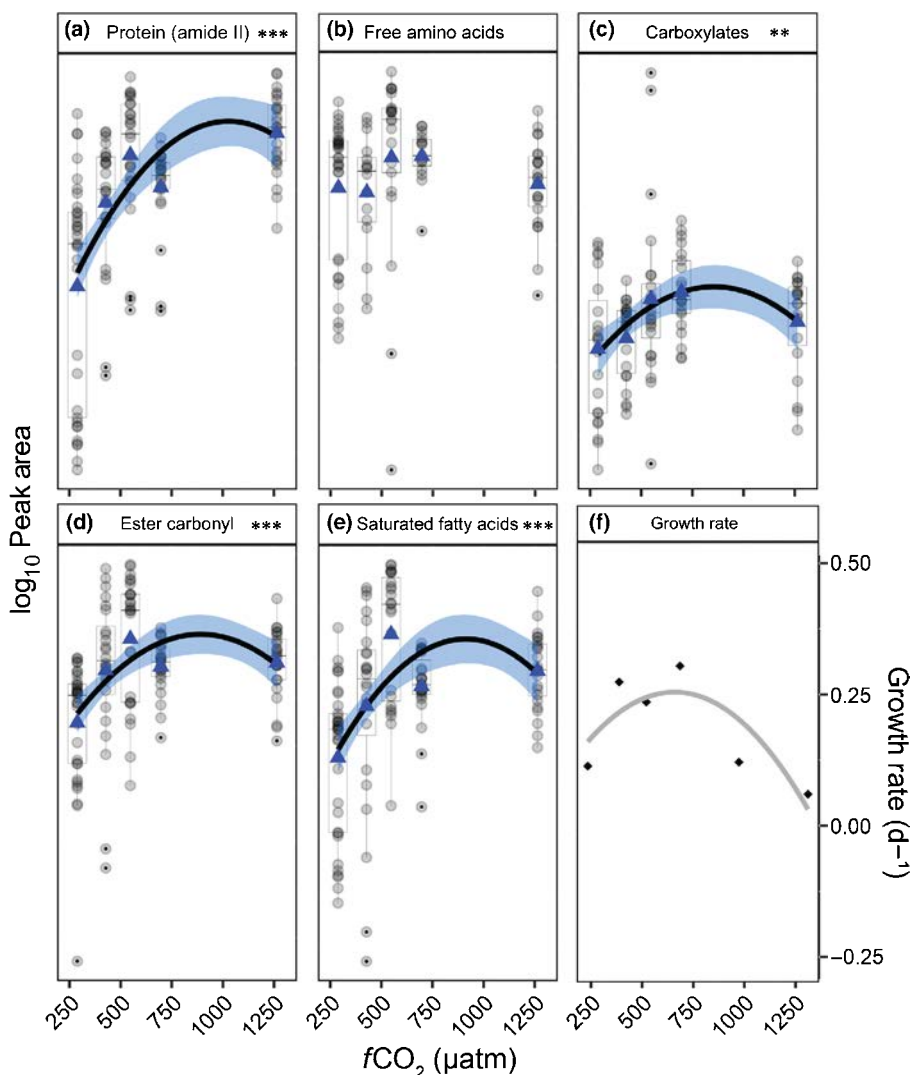


**Fig. 2** Cell-specific macromolecular content (based on normalised peak areas) and growth rates for *Fragilariopsis cylindrus*. (a–f) Relative content of selected macromolecules along an  $f\text{CO}_2$  gradient. Data are visualised using box plots with overlain grey dots showing the macromolecular content of individual cells from within  $f\text{CO}_2$  treatment mesocosm. Data are fitted with a second order polynomial regression, with 95% confidence intervals (dark blue shading), applied to log-transformed data (\*\*,  $P < 0.005$ ; \*\*\*,  $P < 0.0005$ ). The y-axis is free and units are arbitrary. Data means are displayed as blue triangles. (f) Growth rate ( $\text{d}^{-1}$ ) is displayed as diamonds, fitted with a second order polynomial regression (grey line).

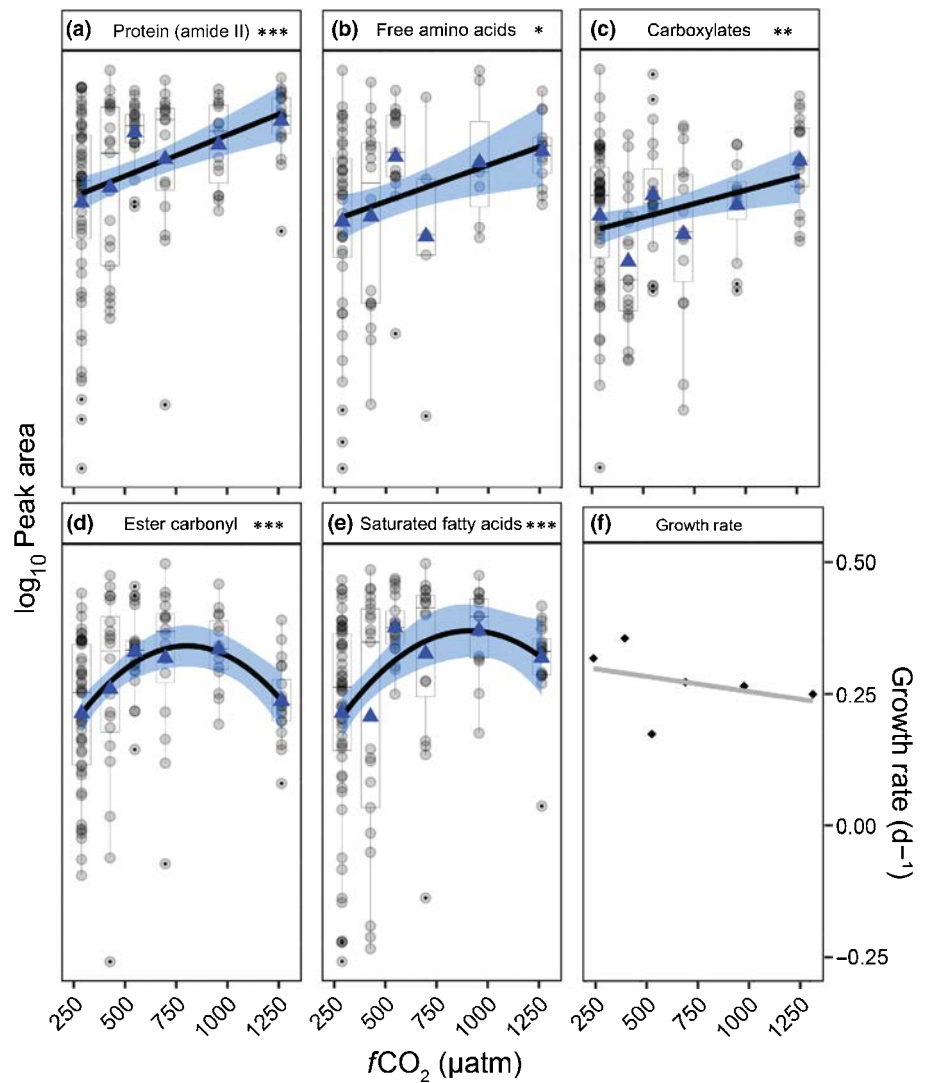


**Fig. 3** Cell-specific macromolecular content (based on normalised peak areas) and growth rates for *Proboscia truncata*. (a–f) Relative content of selected macromolecules along an  $f\text{CO}_2$  gradient. Data are visualised using box plots with overlain grey dots showing the macromolecular content of individual cells from within  $f\text{CO}_2$  treatment mesocosm. Data are fitted with a linear or a second order polynomial regression, with 95% confidence intervals (dark blue shading), applied to log-transformed data (\*,  $P < 0.05$ ; \*\*,  $P < 0.005$ ; \*\*\*,  $P < 0.0005$ ). The y-axis is free and units are arbitrary. Data means are displayed as blue triangles. (f) Growth rate ( $\text{d}^{-1}$ ) is displayed as diamonds, fitted with linear regression (grey line).

Tables S7, S8), however no relationship was observed for lipid (ester carbonyl) content (Fig. 7b; Tables S7, S8). We did, however, find positive relationships between the mean cell volume and protein content (Fig. 7c; Tables S7, S8) and a bell-shaped relationship between mean cell volume and lipid content in the highest  $f\text{CO}_2$  treatment (M6) (Fig. 7d; Tables S7, S8).

## Discussion

The diatom–zooplankton link of the food chain is the foundation of a productive marine ecosystem, whereby changes to food quality at the primary production level can have broad consequences for energy transfer through the food web (Arrigo, 2005; Rossoll *et al.*, 2012). The effects of anthropogenic environmental change are already manifesting in some physicochemical properties of the ocean, including declining pH and increasing sea surface temperatures (Gille, 2002; IPCC, 2014). These changes are expected to be accelerated in the SO (Larsen *et al.*, 2014; Deppeler & Davidson, 2017), in which ocean pH is projected to exceed levels used in M4 before the end of the century (McNeil & Matear,

2008). OA has been shown to influence the biochemical compositions of primary producers, and their subsequent nutrient transfer to higher trophic levels, potentially disrupting marine food webs (Jin *et al.*, 2020; Nagelkerken *et al.*, 2020). This study presents a snapshot of changes to macromolecular stores in Antarctic diatoms in response to short-term exposure to increases in  $f\text{CO}_2$ . We found that elevated  $f\text{CO}_2$  concentrations altered the way diatoms partition macromolecular content and that this partitioning differed among taxa, revealing some size-dependent relationships. Given the short duration of the study (18 d), it is unclear whether these results would be different under longer term exposure, however these data provide insight into the short-term response diversity within diatoms to acidification. Species-specific differences in resource partitioning between macromolecule storage, photosynthesis and growth, ultimately determine the quality and quantity of food available for higher trophic levels (Arrigo, 2005; Sackett *et al.*, 2016). It has been shown that acidifying ocean conditions can select for both small ( $< 20 \mu\text{m}$ ) (Brussaard *et al.*, 2013; Hoppe *et al.*, 2013, 2017; Davidson *et al.*, 2016; Hussherr *et al.*, 2017; Sugie *et al.*, 2020)

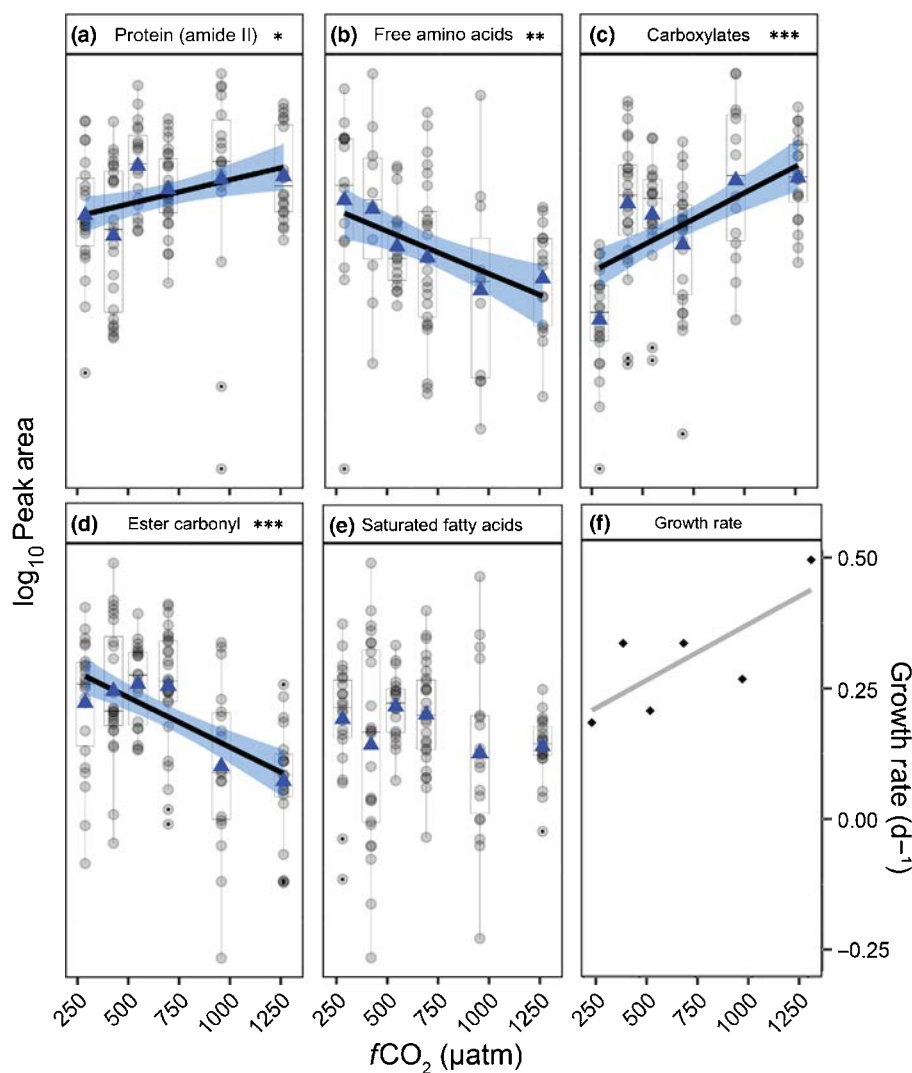


**Fig. 4** Cell-specific macromolecular content (based on normalised peak areas) and growth rates for *Stellarima microtrias*. (a–f) Relative content of selected macromolecules along an  $f\text{CO}_2$  gradient. Data are visualised using box plots with overlaid grey dots showing the macromolecular content of individual cells from within  $f\text{CO}_2$  treatment mesocosm. Data are fitted with linear regression, with 95% confidence intervals (dark blue shading), applied to log-transformed data (\*,  $P < 0.05$ ; \*\*,  $P < 0.005$ ; \*\*\*,  $P < 0.0005$ ). The y-axis is free and units are arbitrary. Data means are displayed as blue triangles. (f) Growth rate ( $\text{d}^{-1}$ ) is displayed as diamonds, fitted with linear regression (grey line).

and large ( $> 20 \mu\text{m}$ ) diatoms (Tortell *et al.*, 2008; Feng *et al.*, 2010; Eggers *et al.*, 2014; Bach & Taucher, 2019), depending on the starting community, duration of exposure and  $\text{CO}_2$  concentrations, and SO taxa appear to be more sensitive to these OA effects than equivalent Arctic taxa (Hoppe *et al.*, 2015). In light of the evidence that OA will select for particular phytoplankton taxa and/or size class (Hancock *et al.*, 2018; Sugie *et al.*, 2020), size-related changes to macromolecular stores could have significant implications for the trophic transfer of energy and nutrients through the marine food web.

In all five diatom groups, we saw an increase in protein content between M1 and M6. For *P. truncata* and *S. microtrias* the increase was linear, however for *F. cylindrus* the increase was linear only until M3, after which it plateaued. Both *Chaetoceros* spp. and the discoid centric group had highest protein content in M6, however they exhibited a u-shaped response to increasing  $f\text{CO}_2$ . The unexpected trend towards decline in growth rate despite increased protein content observed in *F. cylindrus*, may suggest increased energy use for protein synthesis and growth under higher  $f\text{CO}_2$ . This seems counterintuitive, as increasing  $\text{CO}_2$  has previously been shown to reduce gross metabolism in constantly

growing diatoms (Hennon *et al.*, 2015) because of the energy savings associated with downregulation of CCM activity (Hennon *et al.*, 2015, 2017), but this response may only hold true under low–moderate  $\text{CO}_2$  enrichment (Deppeler *et al.*, 2018). Carboxylates and amino acids are the major functional groups associated with cellular protein (Bromke, 2013). We saw similar responses for carboxylate content to increasing  $f\text{CO}_2$  in all taxa and consistent trends, within taxa, between free amino acids and proteins for *Chaetoceros* spp., and *P. truncata*, reflecting the role of amino acids in the synthesis of proteins and as precursors for metabolites with multiple functions in growth (Bromke, 2013). For the larger diatoms, *S. microtrias* and the discoid centric group, amino acids declined. Larger diatoms generally have substantial amino acid pools relative to protein content, in which amino acids can act as a nitrogen reservoir when availability is limiting (Admiraal *et al.*, 1986). Therefore, the decline of free amino acids with increasing  $f\text{CO}_2$  in the larger diatoms could suggest use of this nitrogen reservoir for protein generation (Dortch, 1982; Marañón *et al.*, 2013). Because protein content in primary producers is an important source of energy and amino acids for higher trophic levels, ecologically, its overall increase

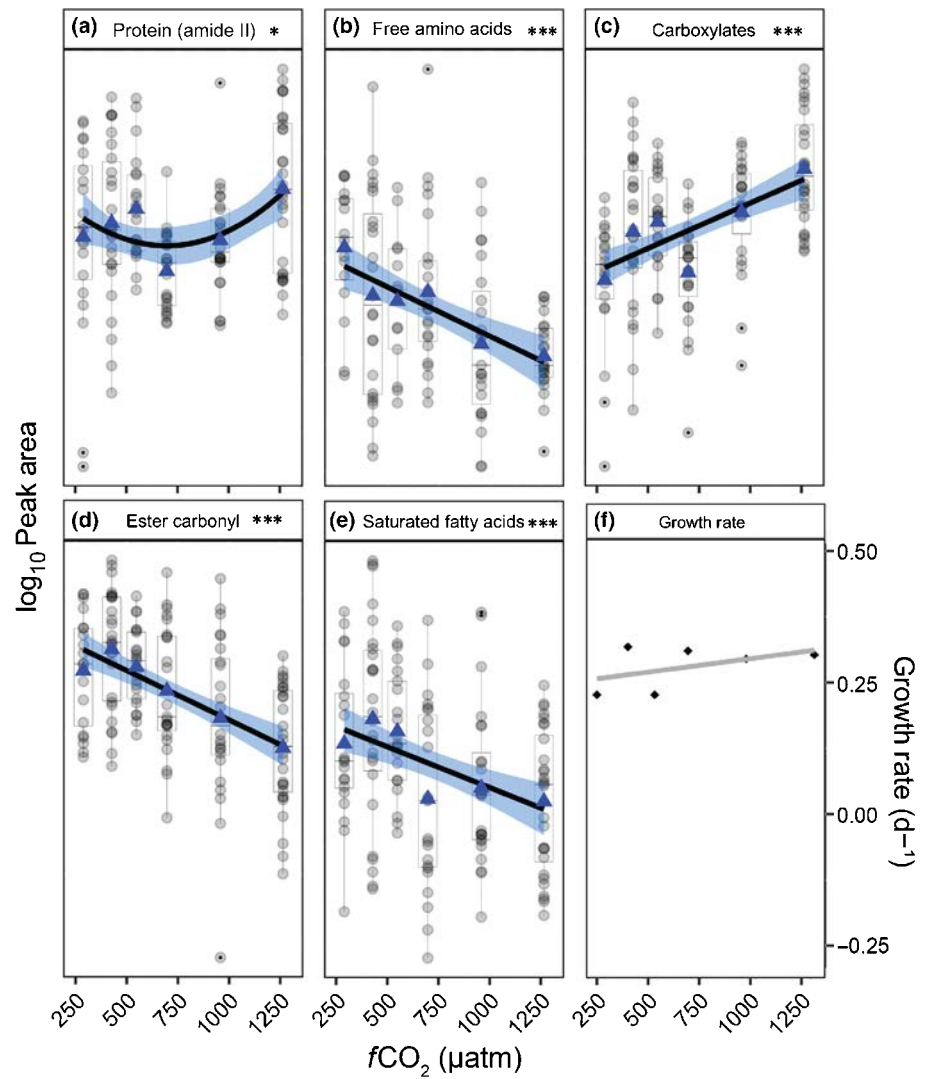


**Fig. 5** Cell-specific macromolecular content (based on normalised peak areas) and growth rates for discoid centric diatoms > 20  $\mu\text{M}$ . Relative content of selected macromolecules along an  $f\text{CO}_2$  gradient. Data are visualised using box plots with overlain grey dots showing the macromolecular content of individual cells from within  $f\text{CO}_2$  treatment mesocosm. Data are fitted with linear or second order polynomial regression, with 95% confidence intervals (dark blue shading), applied to log-transformed data (\*,  $P < 0.05$ ; \*\*\*,  $P < 0.0005$ ). The y-axis is free and units are arbitrary. Data means are displayed as blue triangles. (f) Growth rate ( $\text{d}^{-1}$ ) is displayed as diamonds, fitted with linear regression (grey line).

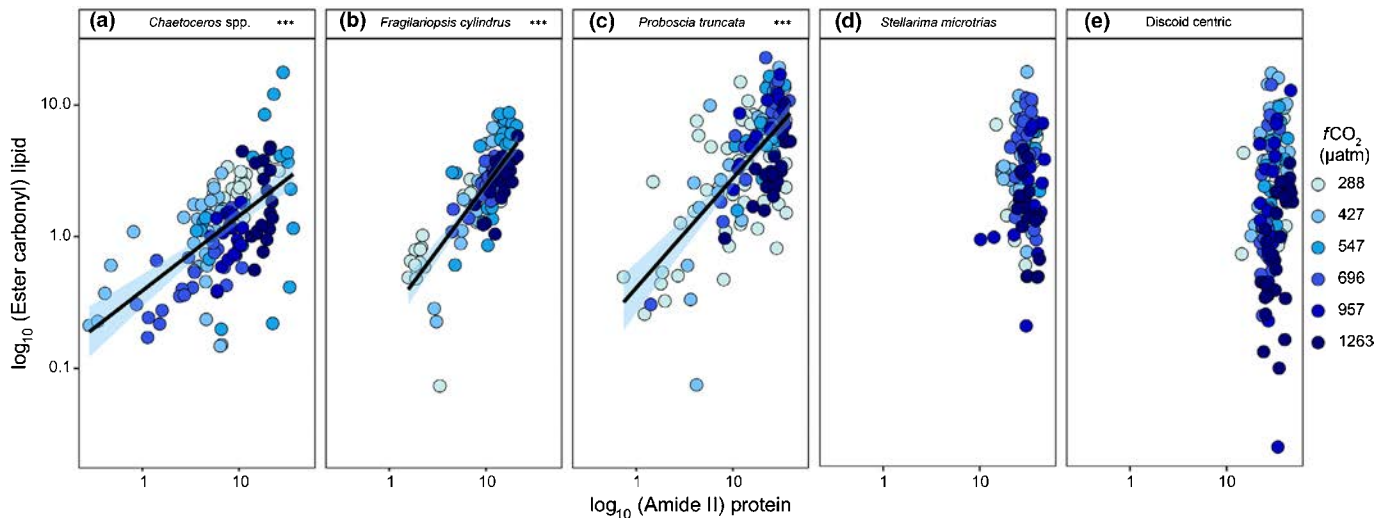


**Fig. 6** Lipid (ester carbonyl) to protein (amide II) ratios for (a) *Chaetoceros* spp., (b) *Fragilariopsis cylindrus*, (c) *Proboscia truncata*, (d) *Stellarima microtrias* and (e) discoid centric diatoms > 20  $\mu\text{M}$ . All data are  $\log_{10}$  transformed.  $f\text{CO}_2$  ( $\mu\text{atm}$ ) levels are represented by colour. Data are fitted with linear regression, with 95% confidence intervals (blue shading).

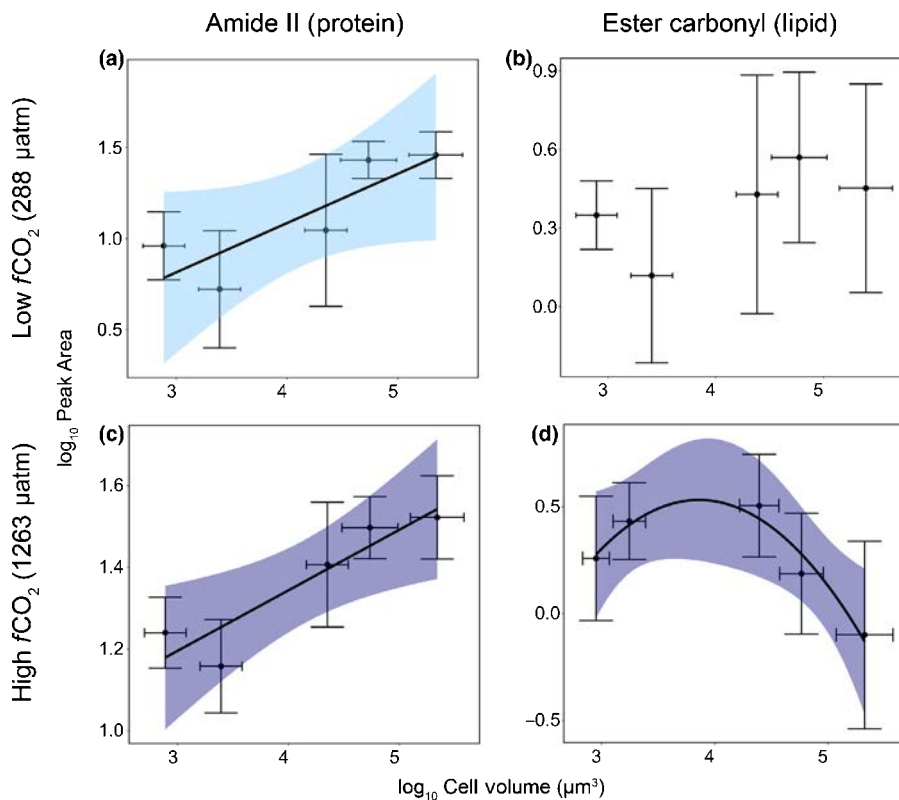


**Fig. 7** Cell volume ( $\mu\text{m}^3$ ) and protein (amide II) or lipid (ester carbonyl) content; (a, b) for diatoms in the low  $f\text{CO}_2$  treatment (288  $\mu\text{atm}$ ) and (c, d) high  $f\text{CO}_2$  treatment (1263  $\mu\text{atm}$ ). Data have been  $\log_{10}$  transformed and fitted with linear or a second order polynomial regression with 95% confidence intervals (shading). The data represent mean  $\pm$  SD ( $n > 19$ ), with all regressions applied to the mean.

between the lowest and highest  $f\text{CO}_2$  concentrations measured, suggests protein availability for secondary production may increase under OA.

The measured changes in lipids and FA content in response to  $f\text{CO}_2$  between taxa were more variable than those for protein. We found that increasing  $f\text{CO}_2$  resulted in decreased relative lipid content for the larger diatoms compared with a bell-shaped increase in lipid content for the smaller diatoms *F. cylindrus* and *P. truncata*. Because the effect for *Chaetoceros* spp. closely followed growth rate, it is likely that the response was related to growth phase and/or nutrient limitation rather than  $f\text{CO}_2$ , limiting the interpretation of  $f\text{CO}_2$  effects on macromolecular partitioning for *Chaetoceros* spp. particularly for M3 and M4 for which cells had reached stationary phase. These size-specific trends may be due to the larger diatoms in this study having a greater need to prioritise protein synthesis over lipid storage (although it is important to note that we did not differentiate between storage and structural lipid types in the analyses). In the two large discoid centric diatoms (*S. microtrias* and discoid centrics), the  $f\text{CO}_2$ -related decline in lipids was accompanied by an increase in relative protein content suggesting a shift in macromolecular energy partitioning with acidification. This loss in lipid content is congruent with a previous study that found that total FA content declined significantly in the discoid centric diatom *T. weissflogii* at high  $\text{CO}_2$  (Rossoll *et al.*, 2012). An increase in protein content at the expense of ester carbonyl, could be explained by the fact that ester carbonyl acts as a fixed carbon reservoir for protein biosynthesis in cells (Terry *et al.*, 1985; Stehfest *et al.*, 2005). Therefore, its degradation and decline could

be directly linked to increased protein production. Alternatively, changes to lipid content could be a strategy for regulating cell ballast. In a parallel study from the same mesocosm experiment, we measured significant declines in the silicification rates of these two taxa with acidification (Petrou *et al.*, 2019). We found that at the highest  $f\text{CO}_2$  (M6) treatment, silicification declined 59% and 39% in *S. microtrias* and discoid centrics, respectively (Petrou *et al.*, 2019). Extent of silicification contributes to diatom sinking rate (Miklasz & Denny, 2010), and therefore any reduction in silicification may increase diatom buoyancy. By decreasing cellular lipid content, the diatoms may counteract this loss in ballast, increasing their density and, therefore, decreasing buoyancy (Smayda, 1970), enabling the diatoms to regulate their depth within the water column.

In both *P. truncata* and *F. cylindrus*, an  $f\text{CO}_2$  threshold for increasing lipid content was observed, for which lipids increased until *c.* 950  $\mu\text{atm}$ , after which they declined. This initial increase in lipid reserves at moderate  $f\text{CO}_2$  enrichment, may reflect a boosted investment into energy stores, as the cells are relieved from potential carbon limitation (Halsey & Jones, 2015). However, as protein content continued to increase for both species beyond *c.* 950  $\mu\text{atm}$ , the threshold response of lipid content probably indicates that, once the CCMs are saturated, lipids are preferentially catabolised for energy to synthesise proteins and support growth (Stehfest *et al.*, 2005; Halsey & Jones, 2015). Alternatively, the shift could be due to higher energy requirements to support increased proton pumping at high  $f\text{CO}_2$  (Deppler *et al.*, 2018). This shift towards higher energy consumption indicates that  $\text{CO}_2$  concentrations  $> 1000 \mu\text{atm}$ , which are

predicted by 2100 (IPCC, 2014), could be a critical point of change for these species, a finding supported by our parallel mesocosm study (Deppeler *et al.*, 2018), which reported significant declines in carbon production by these taxa at  $f\text{CO}_2$  concentrations  $> 1140 \mu\text{atm}$ .

Our inability to detect any  $\text{NO}_x$  by day 18 alerted us to the possibility of nitrogen limitation in our mesocosms, which has the potential to confound any  $f\text{CO}_2$ -induced macromolecular responses. Indeed, in three of the mesocosms, the  $\text{NO}_x$  concentrations were strongly diminished by day 16; M1, M3 ( $1.5 \mu\text{M}$ ) and M4 ( $0.2 \mu\text{M}$ ) (Deppeler *et al.*, 2018), yet while these concentrations are low for SO waters, they are within the normal range of most oceanic waters and not generally considered limiting for microalgae (Voss *et al.*, 2013). Notwithstanding these low  $\text{NO}_x$  values, our data did not exhibit signs of limitation. Instead, the diatoms studied were still actively growing on day 18 (except *Chaetoceros* spp. from M3 and M4) and therefore unlikely have been nutrient limited, possibly supported by luxury uptake of nitrate at an earlier stage (Behrenfeld *et al.*, 2021). Furthermore, support for the unlikelihood that our data were affected by nutrient limitation is provided by the fact that removal of the data points for the mesocosms in which nitrate concentrations were low on day 16 (M1, M3 and M4) had little or no effect on the observed trends.

If our snapshot of macromolecular profiles in response to  $f\text{CO}_2$  enrichment is representative of the broader effect on phytoplankton nutritional quality in nature, selection for smaller diatoms (as was the case in our mesocosm community study, see Hancock *et al.*, 2018), with increased lipid and protein content per cell could translate to increased energy available for secondary production. Availability and transfer of lipids through the trophic web are particularly important, as lipids are the most energy-rich macromolecules, with an energy storage capacity of  $39.4 \text{ J mg}^{-1}$ , compared with  $23.6 \text{ J mg}^{-1}$  for proteins (Hagen & Auel, 2001). High lipid content in primary producers is essential to sustain growth, reproduction and ensure the survival of the aphotic Antarctic winter of higher trophic levels, from zooplankton to marine mammals and birds (Jones & Flynn, 2005; Klein Breteler *et al.*, 2005; Kattner *et al.*, 2007). Therefore, OA may result in higher secondary production. However, an increase in available lipid in small cells does not directly imply an increase in the calories transferred to higher trophic levels. Antarctic krill exhibit only 50% grazing efficiency for phytoplankton  $< 20 \mu\text{m}$  (Boyd & Heyraud, 1984; Quentin & Ross, 1985; Moline *et al.*, 2001), meaning a shift to a community dominated by small diatoms may have significant impacts on krill populations and the organisms that depend on them. Furthermore, krill and other large zooplankton have been demonstrated to have a grazing preference for larger cells (Meyer & El-Sayed, 1983; Quentin & Ross, 1985; Meyer *et al.*, 2003), which means that the decline in lipid measured in the larger diatoms in this study could directly affect large zooplankton populations. Indeed, copepod diets low in lipid content have been shown to cause significant declines in growth and fecundity (Shin *et al.*, 2003; Rossoll *et al.*, 2012). Considering the multiplicity of responses, the opposing effects of increased

available lipid content have to be weighed up with overall changes to trophic efficiency, which will probably be influenced by a shift in community composition, a decrease or change in average cell size (Hancock *et al.*, 2018) and reduced silicification (Petrou *et al.*, 2019), all of which affect grazing preference and efficiency. As such, an increase in energy available to secondary production under OA will not necessarily translate to increased energy transferred to higher trophic levels.

Taking a single-cell approach, we were able to differentiate diatom species responses to OA with increasing  $f\text{CO}_2$ . We saw clear species-specific trends in macromolecular stores despite high within-treatment variability. The variability observed between diatom populations may be attributed to differences in cell size and, therefore, differences in cellular nutrient requirement (Sarhou *et al.*, 2005), cell shape, which can also affect diffusion rates (Pahlow *et al.*, 1997; Mitchell *et al.*, 2013) or some other underlying physiological variant, such as photosynthesis and carbon acquisition strategies (Hennon *et al.*, 2017), however, none of these parameters were tested here. Instead, this species-specific variability reveals the adaptive potential of each taxon and, therefore, the potential resilience of that taxon to environmental change. Similarly, the broad within-species spread in macromolecular responses suggests large phenotypic plasticity in the taxa studied. Interestingly, we saw a general decrease in within-treatment variability with increasing  $f\text{CO}_2$ , suggesting a possible convergence of cell responses and, therefore, potential for reduced within-species plasticity. Ecologically, this could have implications for resilience to environmental change in future populations. Contrary to the commonly observed shift towards larger cells, the highest  $f\text{CO}_2$  levels of our community study selected for smaller diatoms (Hancock *et al.*, 2018). This loss of larger diatoms from the community could reduce the efficiency of energy transfer, as smaller cell sizes may be more difficult to graze on for some larger zooplankton. From a trophic energy perspective, reduced grazing efficiency or smaller krill populations due to a community dominated by smaller diatoms, despite a per cell increase in protein and lipid content, may in fact reduce the transfer efficiency of nutrients to higher predators (Fig. 8). This may be enhanced by concurrent sea surface temperature increases, which have been shown to contribute to polar phytoplankton communities being dominated by smaller cells (Mendes *et al.*, 2013, 2018; Coello-Camba *et al.*, 2014). Alternatively, when viewed in combination with reduced silicification in the taxonomic groups studied here, not only diatom sinking rates would be reduced, but also protection against grazing (Liu *et al.*, 2016), potentially increasing diatom predation in surface waters. Such a shift could counter some of the energy loss that might ensue with a trend towards a community dominated by smaller cells, while increasing recycling of carbon and silica via increased microbial loop activity. Deriving precise trophic projections based on the taxonomic variability in macromolecular responses described here is challenging due to the uncertainty around OA-driven changes to community composition and size structure. However, if our results hold true, they indicate that as the community becomes dominated by smaller, less silicified

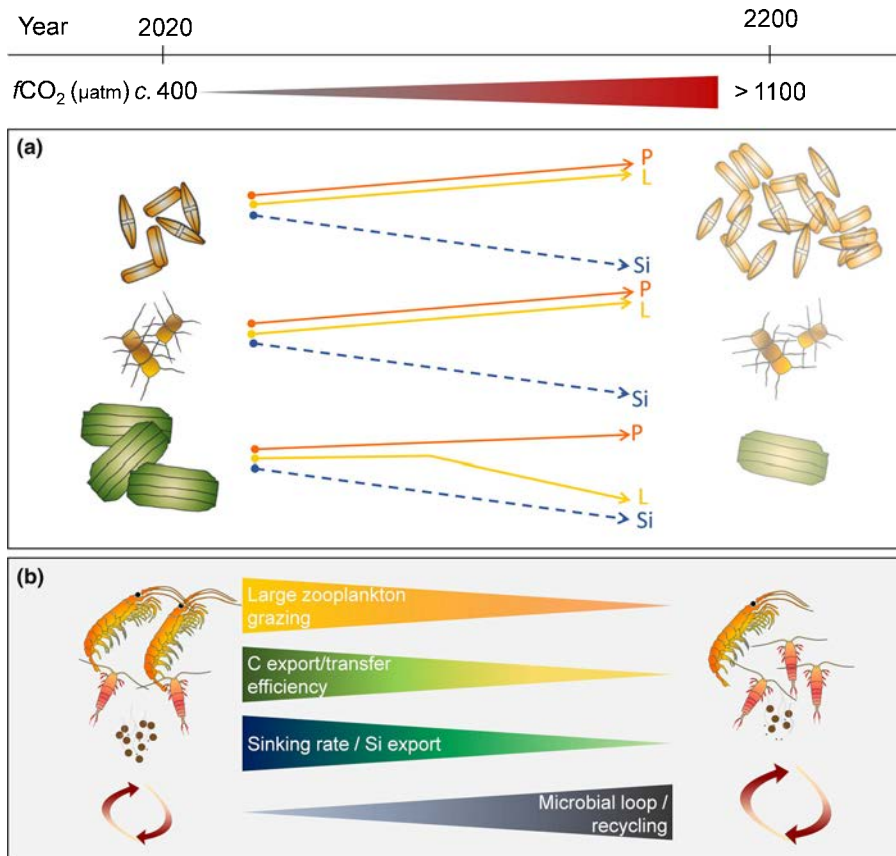


**Fig. 8** Summary of measured changes to diatoms under high  $f\text{CO}_2$  and expected ecological implications. (a) Projected increase in  $\text{CO}_2$  by the end of next century (2200) results in a shift in dominance towards smaller diatom species with increased lipid and protein content, but reduced silicification, while larger diatoms become scarce with lower lipid content and reduced silica content. (b) These changes alter food quality and availability for large zooplankton species such as krill and large copepods, affecting zooplankton growth and fecundity. A reduction in large diatoms and large zooplankton grazing would be likely to reduce carbon and silica export efficiency and alter energy transfer through to higher trophic organisms. Lowered silica production may alleviate some of this loss by increasing grazing on the abundant lipid and protein rich small diatoms by smaller zooplankton. Smaller cells and high grazing rates by smaller zooplankton would probably increase microbial loop activity and nutrient recycling in surface waters. Solid lines represent measured changes to relative protein (P) and lipid (L) content, while dashed lines represent the measured decline in silicification (Si) in the same diatoms from a parallel study (Petrou *et al.*, 2019).

taxa under OA, the increased protein and lipid may benefit some grazers, but may not be as effectively conveyed to higher trophic levels due to overall less efficient large zooplankton grazing (Fig. 8). Concurrently, the remaining large taxa would have less lipid, resulting in less energy available to large zooplankton, with biogeochemical consequences of reduced carbon export and increased nutrient remineralisation (Fig. 8). Therefore, while determining that the net effects of OA on trophic energy transfer is inherently complex, it is clear that OA drives changes in diatom macromolecular partitioning with the potential for significant implications on nutrient and energy supply to the Antarctic pelagic food web.

## Acknowledgements







We thank the Australian Synchrotron Principal Beamline Scientists Drs. Mark Tobin and Jitra-porn Vongsvivut for technical support in synchrotron IR microspectroscopy data acquisition. Part of this work was funded by the Australian Synchrotron through merit-based beamtime awarded on the Infrared Microscopy (IRM) beamline (AS153/IRM/10005) awarded to KP. Field support and sample collection was conducted as part of Australian Antarctic Science Project 4026 awarded to ATD. Samples were imported under permit no. IP13019928. RJD is supported by an Australian Government Research Training Program Scholarship and an AINSE Ltd. Postgraduate Research Award (PGRA), and research funding was provided by the

School of Life Sciences, University of Technology Sydney. The authors declare that they have no conflict of interest.

## Author contributions

RJD: formal analysis, data visualisation, writing original draft; DAN: data curation, formal analysis, writing review and editing; CES: investigation; SD: investigation, writing review and editing; AMH: investigation, writing review and editing; KGS: investigation, writing review and editing; ATD: conceptualisation, funding acquisition, investigation, writing review and editing; and KP: conceptualisation, methodology, investigation, data visualisation, supervision, funding acquisition, writing review and editing.

## ORCID

Stacy Deppeler  <https://orcid.org/0000-0003-2213-2656>  
 Rebecca J. Duncan  <https://orcid.org/0000-0003-2686-5654>  
 Alyce M. Hancock  <https://orcid.org/0000-0001-6049-5592>  
 Daniel A. Nielsen  <https://orcid.org/0000-0001-6678-5937>  
 Katherina Petrou  <https://orcid.org/0000-0002-2703-0694>  
 Kai G. Schulz  <https://orcid.org/0000-0002-8481-4639>

## Data availability

Data are available in Supporting Information and via the Australian Antarctic Division Data Centre (doi: 10.26179/ej5x-2h37).

## References

- Admiraal W, Peletier H, Laane RWPM. 1986. Nitrogen metabolism of marine planktonic diatoms; excretion, assimilation and cellular pools of free amino acids in seven species with different cell size. *Journal of Experimental Marine Biology and Ecology* 98: 241–263.
- Arrigo KR. 2005. Marine microorganisms and global nutrient cycles. *Nature* 437: 349–355.
- Bach TL, Taucher J. 2019. CO<sub>2</sub> effects on diatoms: a synthesis of more than a decade of ocean acidification experiments with natural communities. *Ocean Science* 15: 1159–1175.
- Bambery KR, Wood BR, McNaughton D. 2012. Resonant Mie scattering (RMieS) correction applied to FTIR images of biological tissue samples. *Analyst* 137: 126–132.
- Baragi LV, Khandeparker L, Anil AC. 2015. Influence of elevated temperature and pCO<sub>2</sub> on the marine periphytic diatom *Navicula distans* and its associated organisms in culture. *Hydrobiologia* 762: 127–142.
- Beardall J, Raven JA. 2004. The potential effects of global climate change on microalgal photosynthesis, growth and ecology. *Phycologia* 43: 26–40.
- Behrenfeld MJ, Halsey KH, Boss E, Karp-Boss L, Milligan AJ, Peers G. 2021. Thoughts on the evolution and ecological niche of diatoms. *Ecological Monographs* 91: e01457.
- Bellerby RGJ, Schulz KG, Riebesell U, Neill C, Nondal G, Heegaard E, Johannessen T, Brown KR. 2008. Marine ecosystem community carbon and nutrient uptake stoichiometry under varying ocean acidification during the PeECE III experiment. *Biogeosciences* 5: 1517–1527.
- Berge T, Daugbjerg N, Andersen BB, Hansen PJ. 2010. Effect of lowered pH on marine phytoplankton growth rates. *Marine Ecology Progress Series* 416: 79–91.
- Bhavya PS, Kim BK, Jo N, Kim K, Kang JJ, Lee JH, Lee D, Lee JH, Joo HT, Ahn SH *et al.* 2018. A review on the macromolecular compositions of phytoplankton and the implications for aquatic biogeochemistry. *Ocean Science Journal* 54: 1–14.
- Boyd CM, Heyraud M, Boyd CN. 1984. Feeding of the Antarctic Krill *Euphausia Superba*. *Journal of Crustacean Biology* 4: 123–141.
- Bromke MA. 2013. Amino acid biosynthesis pathways in diatoms. *Metabolites* 3: 294–311.
- Bruusaard CPD, Noordeloos AAM, Witte H, Collenteur MCJ, Schulz K, Ludwig A, Riebesell U. 2013. Arctic microbial community dynamics influenced by elevated CO<sub>2</sub> levels. *Biogeosciences* 10: 719–731.
- Chen CY, Durbin EG. 1994. Effects of pH on the growth and carbon uptake of marine phytoplankton. *Marine Ecology Progress Series* 109: 83–94.
- Chen G, Zhao L, Qi Y. 2015. Enhancing the productivity of microalgae cultivated in wastewater toward biofuel production: a critical review. *Applied Energy* 137: 282–291.
- Coello-Camba A, Agustí S, Holding J, Arrieta JM, Duarte CM. 2014. Interactive effect of temperature and CO<sub>2</sub> increase in Arctic phytoplankton. *Frontiers in Marine Science* 49: 1–10.
- Cottingham KL, Lennon JT, Brown BL. 2005. Knowing when to draw the line: designing more informative ecological experiments. *Frontiers in Ecology and the Environment* 3: 145–152.
- Cowles TJ, Olson RJ, Chisholm SW. 1988. Food selection by copepods: discrimination on the basis of food quality. *Marine Biology* 100: 41–49.
- Davidson AT, McKinlay J, Westwood K, Thomson PG, Van Den Enden R, De Salas M, Wright S, Johnson R, Berry K. 2016. Enhanced CO<sub>2</sub> concentrations change the structure of Antarctic marine microbial communities. *Marine Ecology Progress Series* 552: 93–113.
- Denman KL, Brasseur G, Chidthaisong A, Ciais P, Cox P, Dickinson R, Hauglustaine D, Heinze C, Holland E, Jacob D *et al.* 2007. Couplings between changes in the climate system and biogeochemistry. In: Solomon S *et al.*, eds. *Climate change 2007: the physical science basis. Contribution of Working Group I to the fourth assessment report of the Intergovernmental Panel on Climate Change*. Cambridge, UK and New York, NY, USA: Cambridge University Press, 499–563.
- Deppeler S, Petrou K, Schulz KG, Westwood K, Pearce I, McKinlay J, Davidson A. 2018. Ocean acidification of a coastal Antarctic marine microbial community reveals a critical threshold for CO<sub>2</sub> tolerance in phytoplankton productivity. *Biogeosciences* 15: 209–231.
- Deppeler SL, Davidson AT. 2017. Southern Ocean phytoplankton in a changing climate. *Frontiers in Marine Science* 4: 40.
- Dickson AG. 2010. Standards for Ocean measurements. *Oceanography* 23: 34–47.
- Dickson AG, Sabine CL, Christian JR. 2007. Guide to best practices for ocean CO<sub>2</sub> measurements. In: *PICES special publication 3, IOCCP report no. 8*. Sidney, BC, Canada: North Pacific Marine Science Organisation.
- Dortch Q. 1982. Effect of growth conditions on accumulation of internal nitrate, ammonium, amino acids, and protein in three marine diatoms. *Journal of Experimental Marine Biology and Ecology* 61: 243–264.
- Eggers SL, Lewandowska AM, Barcelos e Ramos J, Blanco-Ameijeiras S, Gallo F, Matthiessen B. 2014. Community composition has greater impact on the functioning of marine phytoplankton communities than ocean acidification. *Global Change Biology* 20: 713–723.
- Engel A, Schulz KG, Riebesell U, Bellerby R, Delille B, Schartau M. 2008. Effects of CO<sub>2</sub> on particle size distribution and phytoplankton abundance during a mesocosm bloom experiment (PeECE II). *Biogeosciences* 5: 509–521.
- Feng Y, Hare CE, Leblanc K, Rose JM, Zhang Y, DiTullio GR, Lee PA, Wilhelm SW, Rowe JM, Sun J *et al.* 2009. Effects of increased pCO<sub>2</sub> and temperature on the north atlantic spring bloom. I. The phytoplankton community and biogeochemical response. *Marine Ecology Progress Series* 388: 13–25.
- Feng Y, Hare CE, Rose JM, Handy SM, DiTullio GR, Lee PA, Smith WO, Peloquin J, Tozzi S, Sun J *et al.* 2010. Interactive effects of iron, irradiance and CO<sub>2</sub> on Ross Sea phytoplankton. *Deep-Sea Research Part I: Oceanographic Research Papers* 57: 368–383.
- Finkel ZV, Follows MJ, Liefer JD, Brown CM, Benner I, Irwin AJ. 2016. Phylogenetic diversity in the macromolecular composition of microalgae. *PLoS ONE* 11: e0155977.
- Frölicher TL, Sarmiento JL, Paynter DJ, Dunne JP, Krasting JP, Winton M. 2015. Dominance of the Southern Ocean in anthropogenic carbon and heat uptake in CMIP5 models. *Journal of Climate* 28: 862–886.
- Gille ST. 2002. Warming of the Southern Ocean since the 1950s. *Science* 295: 1275–1277.
- Giordano M, Kansiz M, Héraud P, Beardall J, Wood B, McNaughton D. 2001. Fourier transform infrared spectroscopy as a novel tool to investigate changes in intracellular macromolecular pools in the marine microalga *Chaetoceros muellerii* (Bacillariophyceae). *Journal of Phycology* 37: 271–279.
- Graeve M, Kattner G, Hagen W. 1994. Diet-induced changes in the fatty acid composition of Arctic herbivorous copepods: experimental evidence of trophic markers. *Journal of Experimental Marine Biology and Ecology* 182: 97–110.
- Haberman KL, Ross RM, Quetin LB. 2003. Diet of the Antarctic krill (*Euphausia superba* Dana): II. Selective grazing in mixed phytoplankton assemblages. *Journal of Experimental Marine Biology and Ecology* 283: 97–113.
- Hagen W, Auel H. 2001. Seasonal adaptations and the role of lipids in oceanic zooplankton. *Zoology* 104: 313–326.
- Halsey KH, Jones BM. 2015. Phytoplankton strategies for photosynthetic energy allocation. *Annual Review of Marine Science* 7: 265–297.
- Hamm CE, Merkel R, Springer O, Jurkojc P, Maiert C, Prechtelt K, Smetacek V. 2003. Architecture and material properties of diatom shells provide effective mechanical protection. *Nature* 421: 841–843.
- Hancock AM, Davidson AT, McKinlay J, McMinn A, Schulz KG, Van Den Enden RL. 2018. Ocean acidification changes the structure of an Antarctic coastal protistan community. *Biogeosciences* 15: 2393–2401.
- Hancock AM, King CK, Stark JS, McMinn A, Davidson AT. 2020. Effects of ocean acidification on Antarctic marine organisms: a meta-analysis. *Ecology and Evolution* 10: 4495–4514.
- Havenhand J, Dupont S, Quinn GP. 2010. Designing ocean acidification experiments to maximise inference. In: Riebesell U *et al.*, eds. *Guide to best practices for ocean acidification research and data reporting*. Luxembourg City, Luxembourg: Publications Office of the European Union, 67–79.
- Head EJH, Harris LR. 1994. Feeding selectivity by copepods grazing on natural mixtures of phytoplankton determined by HPLC analysis of pigments. *Marine Ecology Progress Series* 110: 75–83.
- Hennon GM, Ashworth J, Groussman RD, Berthiaume C, Morales RL, Baliga NS, Orellana MV, Armbrust EV. 2015. Diatom acclimation to elevated CO<sub>2</sub> via cAMP signalling and coordinated gene expression. *Nature Climate Change* 5: 761–765.



- Hennon GM, Limón MDH, Haley ST, Juhl AR, Dyhrman ST. 2017. Diverse CO<sub>2</sub>-induced responses in physiology and gene expression among eukaryotic phytoplankton. *Frontiers in Microbiology* 8: 2547.
- Heraud P, Wood BR, Tobin MJ, Beardall J, McNaughton D. 2005. Mapping of nutrient-induced biochemical changes in living algal cells using synchrotron infrared microspectroscopy. *FEMS Microbiology Letters* 249: 219–225.
- Hillebrand H, Dürselen CD, Kirschtel D, Pollinger U, Zohary T. 1999. Biovolume calculation for pelagic and benthic microalgae. *Journal of Phycology* 35: 403–424.
- Hoppe CJM, Hassler CS, Payne CD, Tortell PD, Rost BR, Trimbom S. 2013. Iron limitation modulates ocean acidification effects on Southern Ocean phytoplankton communities. *PLoS ONE* 8: e79890.
- Hoppe CJM, Holtz LM, Trimbom S, Rost B. 2015. Ocean acidification decreases the light-use efficiency in an Antarctic diatom under dynamic but not constant light. *New Phytologist* 207: 159–171.
- Hoppe CJM, Schuback N, Semeniuk DM, Maldonado MT, Rost B. 2017. Functional redundancy facilitates resilience of subarctic phytoplankton assemblages toward ocean acidification and high irradiance. *Frontiers in Marine Science* 4: 229.
- Husherr L, Lavesseur M, Lizotte M, Tremblay JÉ, Mol J, Thomas H, Gosselin M, Starr M, Miller LA, Jarníková T *et al.* 2017. Impact of ocean acidification on Arctic phytoplankton blooms and dimethyl sulfide concentration under simulated ice-free and under-ice conditions. *Biogeosciences* 14: 2407–2427.
- Intergovernmental Panel on Climate Change (IPCC). 2014. *Climate change 2014: impacts, adaptation and vulnerability: Part B: Regional aspects: Working Group II contribution to the fifth assessment report of the Intergovernmental Panel on Climate*. Cambridge, UK: Cambridge University Press.
- Jin P, Hutchins DA, Gao K. 2020. The impacts of ocean acidification on marine food quality and its potential food chain consequences. *Frontiers in Marine Science* 7: 543979.
- Jones RH, Flynn KJ. 2005. Nutritional status and diet composition affect the value of diatoms as copepod prey. *Science* 307: 1457–1459.
- Kang SH, Fryxell GA. 1993. Phytoplankton in the Weddell Sea, Antarctica: composition, abundance and distribution in water-column assemblages of the marginal ice-edge zone during austral autumn. *Marine Biology: International Journal on Life in Oceans and Coastal Waters* 116: 335–348.
- Kattner G, Hagen W, Lee RF, Campbell R, Deibel D, Falk-Petersen S, Graeve M, Hansen BW, Hirche HJ, Jónasdóttir SH *et al.* 2007. Perspectives on marine zooplankton lipids. *Canadian Journal of Fisheries and Aquatic Sciences* 64: 1628–1639.
- Khatiwalá S, Primeau F, Hall T. 2009. Reconstruction of the history of anthropogenic CO<sub>2</sub> concentrations in the ocean. *Nature* 462: 346–349.
- Klein Breteler WCM, Schogt N, Rampen S. 2005. Effect of diatom nutrient limitation on copepod development: role of essential lipids. *Marine Ecology Progress Series* 291: 125–133.
- Kreyling J, Schweiger AH, Bahn M, Ineson P, Migliavacca M, Morel-Journel T, Christiansen JR, Schtickzelle N, Larsen KS. 2018. To replicate, or not to replicate – that is the question: how to tackle nonlinear responses in ecological experiments. *Ecology Letters* 21: 1629–1638.
- Kroeker KJ, Kordas RL, Crim R, Hendriks IE, Ramajo L, Singh GS, Duarte CM, Gattuso JP. 2013. Impacts of ocean acidification on marine organisms: quantifying sensitivities and interaction with warming. *Global Change Biology* 19: 1884–1896.
- Larsen JN, Anisimov OA, Constable A, Hollowed AB, Maynard N, Prestrud P, Prowse TD, Stone JMR. 2014. Polar regions. In: Barros VR *et al.*, eds. *Climate change 2014: impacts, adaptation, and vulnerability. Part B: Regional aspects. Contribution of Working Group II to the fifth assessment report of the Intergovernmental Panel on Climate Change*. Cambridge, UK: Cambridge University Press, 1567–1612.
- Le Quééré C, Andrew RM, Friedlingstein P, Sitch S, Pongratz J, Manning AC, Korsbakken JI, Peters GP, Canadell JG, Jackson RB *et al.* 2018. Global carbon budget 2017. *Earth System Science Data* 10: 405–448.
- Lee R, Hagen W, Kattner G. 2006. Lipid storage in marine zooplankton. *Marine Ecology Progress Series* 307: 273–306.
- Litchman E, Klausmeier CA, Schofield OM, Falkowski PG. 2007. The role of functional traits and trade-offs in structuring phytoplankton communities: scaling from cellular to ecosystem level. *Ecology Letters* 10: 1170–1181.
- Liu H, Chen M, Zhu F, Harrison PJ. 2016. Effect of diatom silica content on copepod grazing, growth and reproduction. *Frontiers in Marine Science* 3: 89.
- Marañón E, Cermeño P, López-Sandoval DC, Rodríguez-Ramos T, Sobrino C, Huete-Ortega M, Blanco JM, Rodríguez J. 2013. Unimodal size scaling of phytoplankton growth and the size dependence of nutrient uptake and use. *Ecology Letters* 16: 371–379.
- Martin-Jézéquel V, Hillebrand M, Brzezinski MA. 2000. Silicon metabolism in diatoms: implications for growth. *Journal of Phycology* 36: 821–840.
- McNeil BI, Matear RJ. 2008. Southern Ocean acidification: a tipping point at 450-ppm atmospheric CO<sub>2</sub>. *Proceedings of the National Academy of Sciences, USA* 105: 18860–18864.
- Mendes CRB, Tavano VM, Dotto TS, Kerr R, de Souza MS, Garcia CAE, Secchi ER. 2018. New insights on the dominance of cryptophytes in Antarctic coastal waters: a case study in Gerlache Strait. *Deep-Sea Research Part II: Topical Studies in Oceanography* 149: 161–170.
- Mendes CRB, Tavano VM, Leal MC, de Souza MS, Brotas V, Garcia CAE. 2013. Shifts in the dominance between diatoms and cryptophytes during three late summers in the Bransfield Strait (Antarctic Peninsula). *Polar Biology* 36: 537–547.
- Meyer B, Atkinson A, Blume B, Bathmann UV. 2003. Feeding and energy budgets of larval Antarctic krill *Euphausia superba* in summer. *Marine Ecology Progress Series* 257: 167–177.
- Meyer MA, El-Sayed SZ. 1983. Grazing of *Euphausia superba* Dana on natural phytoplankton populations. *Polar Biology* 1: 193–197.
- Miklasz KA, Denny MW. 2010. Diatom sinking speeds: improved predictions and insight from a modified Stoke's law. *Limnology and Oceanography* 55: 2513–2525.
- Mitchell JG, Seuront L, Doubell MJ, Losic D, Voelcker NH, Seymour J, Lal R. 2013. The role of diatom nanostructures in biasing diffusion to improve uptake in a patchy nutrient environment. *PLoS ONE* 8: e59548.
- Moline MA, Claustre H, Frazer TK, Grzymkajski JOE, Schofield O, Verner M. 2001. Changes in phytoplankton assemblages along the Antarctic Peninsula and potential implications for the Antarctic food web. In: Davidson W *et al.*, eds. *Antarctic ecosystems: models for wider ecological understanding*. Christchurch, New Zealand: New Zealand Natural Sciences, 263–271.
- Murdock JN, Wetzel DL. 2009. FT-IR microspectroscopy enhances biological and ecological analysis of algae. *Applied Spectroscopy Reviews* 44: 335–361.
- Nagelkerken I, Goldenberg SU, Ferreira CM, Ullah H, Connell SD. 2020. Trophic pyramids reorganize when food web architecture fails to adjust to ocean change. *Science* 369: 829–832.
- Nielsen LT, Jakobsen HH, Hansen PJ. 2010. High resilience of two coastal plankton communities to twenty-first century seawater acidification: evidence from microcosm studies. *Marine Biology Research* 6: 542–555.
- Pahlow M, Riebesell U, Wolf-Gladrow A. 1997. Impact of cell shape and chain formation on nutrient acquisition by marine diatoms. *Limnology and Oceanography* 42: 1660–1672.
- Paul AJ, Bach LT. 2020. Universal response pattern of phytoplankton growth rates to increasing CO<sub>2</sub>. *New Phytologist* 228: 1710–1716.
- Petrou K, Baker KG, Nielsen DA, Hancock AM, Schulz KG, Davidson AT. 2019. Acidification diminishes diatom silica production in the Southern Ocean. *Nature Climate Change* 9: 781–786.
- Petrou K, Nielsen DA, Heraud P. 2018. Single-cell biomolecular analysis of coral algal symbionts reveals opposing metabolic responses to heat stress and expulsion. *Frontiers in Marine Science* 5: doi: 10.3389/fmars.2018.00110.
- Quentin LB, Ross RM. 1985. Feeding by Antarctic krill, *Euphausia superba*: does size matter? In: Siegfried WR, Condy PR, Laws RM, eds. *Antarctic nutrient cycles and food webs*. Berlin/Heidelberg, Germany: Springer, 372–377.
- R Core Team. 2021. *R: a language and environment for statistical computing*. Vienna, Austria: R Foundation for Statistical Computing.
- Riebesell U, Gattuso JP. 2015. Lessons learned from ocean acidification research. *Nature Climate Change* 5: 12–14.
- Ross PM, Parker L, O'Connor WA, Bailey EA. 2011. The impact of ocean acidification on reproduction, early development and settlement of marine organisms. *Water* 3: 1005–1030.
- Rossoll D, Bermúdez R, Hauss H, Schulz KG, Riebesell U, Sommer U, Winder M. 2012. Ocean acidification-induced food quality deterioration constrains trophic transfer. *PLoS ONE* 7: e34737.

- Ruess L, Müller-Navarra DC. 2019. Essential biomolecules in food webs. *Frontiers in Ecology and Evolution* 7: 269.
- Sabine CL, Feely RA, Gruber N, Key RM, Lee K, Bullister JL, Wanninkhof R, Wong CS, Wallace DWR, Tilbrook B *et al.* 2004. The oceanic sink for anthropogenic CO<sub>2</sub>. *Science* 305: 367–371.
- Sackett O, Armand L, Beardall J, Hill R, Doblin M, Connelly C, Howes J, Stuart B, Ralph P, Heraud P. 2014. Taxon-specific responses of Southern Ocean diatoms to Fe enrichment revealed by synchrotron radiation FTIR microspectroscopy. *Biogeosciences* 11: 5795–5808.
- Sackett O, Petrou K, Reedy B, De Grazia A, Hill R, Doblin M, Beardall J, Ralph P, Heraud P. 2013. Phenotypic plasticity of Southern Ocean diatoms: key to success in a sea ice habitat? *PLoS ONE* 8: e81185.
- Sackett O, Petrou K, Reedy B, Hill R, Doblin M, Beardall J, Ralph P, Heraud P. 2016. Snapshot prediction of carbon productivity, carbon and protein content in a Southern Ocean diatom using FTIR spectroscopy. *ISME Journal* 10: 416–426.
- Sarthou G, Timmermans KR, Blain S, Tréguer P. 2005. Growth physiology and fate of diatoms in the ocean: a review. *Journal of Sea Research* 53: 25–42.
- Schneider CA, Rasnada WS, Eliceiri KW. 2012. NIH image to IMAGEJ: 25 years of image analysis. *Nature Methods* 9: 671–679.
- Shapiro SS, Wilk MB. 1965. An analysis of variance test for normality (complete samples). *Biometrika* 52: 591–611.
- Sheehan C, Nielsen D, Petrou K. 2020. Macromolecular composition, productivity and dimethylsulfoniopropionate in Antarctic pelagic and sympagic microalgal communities. *Marine Ecology Progress Series* 640: 45–61.
- Shi Q, Xiahou W, Wu H. 2017. Photosynthetic responses of the marine diatom *Thalassiosira pseudonana* to CO<sub>2</sub>-induced seawater acidification. *Hydrobiologia* 788: 361–369.
- Shin K, Jang M-C, Jang P-K, Ju S-J, Lee T-K, Chang M. 2003. Influence of food quality on egg production and viability of the marine planktonic copepod *Acartia omorii*. *Progress in Oceanography* 57: 265–277.
- Smyda T. 1970. The suspension and sinking of phytoplankton in the sea. *Oceanography and Marine Biology: An Annual Review* 8: 353–414.
- Stehfest K, Toepel J, Wilhelm C. 2005. The application of micro-FTIR spectroscopy to analyze nutrient stress-related changes in biomass composition of phytoplankton algae. *Plant Physiology and Biochemistry* 43: 717–726.
- Stevens A, Ramirez-Lopez L. 2013. An introduction to the prospectr package. R package v.013. [WWW document] URL <https://CRAN.R-project.org/package=prospectr> [accessed 10 April 2020].
- Sugie K, Fujiwara A, Nishino S, Kameyama S, Harada N. 2020. Impacts of temperature, CO<sub>2</sub>, and salinity on phytoplankton community composition in the Western Arctic Ocean. *Frontiers in Marine Science* 6: 821.
- Terry KL, Hirata J, Laws EA. 1985. Light-, nitrogen-, and phosphorus-limited growth of *Phaeodactylum tricoratum* Bohlin strain TFX-1: chemical composition, carbon partitioning, and the diel periodicity of physiological processes. *Journal of Experimental Marine Biology and Ecology* 86: 85–100.
- Tew KS, Kao YC, Ko FC, Kuo J, Meng PJ, Liu PJ, Glover DC. 2014. Effects of elevated CO<sub>2</sub> and temperature on the growth, elemental composition, and cell size of two marine diatoms: potential implications of global climate change. *Hydrobiologia* 741: 79–87.
- Tobin MJ, Puskar L, Barber RL, Harvey EC, Heraud P, Wood BR, Bamberg KR, Dillon CT, Munro KL. 2010. FTIR spectroscopy of single live cells in aqueous media by synchrotron IR microscopy using microfabricated sample holders. *Vibrational Spectroscopy* 53: 34–38.
- Tortell PD, Payne CD, Li Y, Trimbom S, Rost B, Smith WO, Riesselman C, Dunbar RB, Sedwick P, DiTullio GR. 2008. CO<sub>2</sub> sensitivity of Southern Ocean phytoplankton. *Geophysical Research Letters* 35: L04605.
- Tréguer P, Bowler C, Moriceau B, Dutkiewicz S, Gehlen M, Aumont O, Bittner L, Dugdale R, Finkel Z, Iudicone D *et al.* 2018. Influence of diatom diversity on the ocean biological carbon pump. *Nature Geoscience* 11: 27–37.
- Turner JT, Ianora A, Miralto A, Laabir M, Esposito F. 2001. Decoupling of copepod grazing rates, fecundity and egg-hatching success on mixed and alternating diatom and dinoflagellate diets. *Marine Ecology Progress Series* 220: 187–199.
- Urabe J, Togari J, Elser JJ. 2003. Stoichiometric impacts of increased carbon dioxide on a planktonic herbivore. *Global Change Biology* 9: 818–825.
- Vongsvivut J, Heraud P, Zhang W, Kralovec JA, McNaughton D, Barrow CJ. 2012. Quantitative determination of fatty acid compositions in micro-encapsulated fish-oil supplements using Fourier transform infrared (FTIR) spectroscopy. *Food Chemistry* 135: 603–609.
- Voss M, Bange HW, Dippner JW, Middelburg JJ, Montoya JP, Ward B. 2013. The marine nitrogen cycle: recent discoveries, uncertainties and potential relevance of climate change. *Philosophical Transactions of the Royal Society of London. Series B: Biological Sciences* 368: 20130121.
- Wagner H, Liu Z, Langner U, Stehfest K, Wilhelm C. 2010. The use of FTIR spectroscopy to assess quantitative changes in the biochemical composition of microalgae. *Journal of Biophotonics* 3: 557–566.
- Wickham H. 2009. *GGPLOT2: elegant graphics for data analysis*. R package v.2.2.1. [WWW document] URL <https://ggplot2.tidyverse.org> [accessed 10 April 2020].
- Wickham H, François R, Henry L, Müller K. 2020. *DPLYR: a grammar of data manipulation*. R package v.1.0.0. <https://cran.r-project.org/package=dplyr> [accessed 10 April 2020].
- Wolf C, Frickenhaus S, Kiliyas ES, Peeken I, Metfies K. 2013. Regional variability in eukaryotic protist communities in the Amundsen Sea. *Antarctic Science* 25: 741–751.
- Wright SW, van den Enden RL, Pearce I, Davidson AT, Scott FJ, Westwood KJ. 2010. Phytoplankton community structure and stocks in the Southern Ocean (30–80°E) determined by CHEMTAX analysis of HPLC pigment signatures. *Deep-Sea Research Part II: Topical Studies in Oceanography* 57: 758–778.
- Wu Y, Gao K, Riebesell U. 2010. CO<sub>2</sub>-induced seawater acidification affects physiological performance of the marine diatom *Phaeodactylum tricoratum*. *Biogeosciences* 7: 2915–2923.

## Supporting Information

Additional Supporting Information may be found online in the Supporting Information section at the end of the article.

**Table S1** Summary of initial seawater (T0) conditions and mesocosm conditions on day 18.

**Table S2** Summary of number of cells, per taxa, per mesocosm, measured for species-specific macromolecular content using Fourier transform infrared microspectroscopy.

**Table S3** Cell density and community photosynthetic efficiency on day 18.

**Table S4** Mean cell volume ( $\mu\text{m}^3$ ) on day 18 for taxa from mesocosm 1 (M1) and mesocosm 6 (M6).

**Table S5** Statistical output of the species-specific regression models (Figs 1–5).

**Table S6** Statistical output of the lipid (ester carbonyl) to protein (amide II) ratio models (Fig. 6).

**Table S7** Data corresponding to cell volume ( $\mu\text{m}^3$ ) and protein (amide II) or lipid (ester carbonyl) content.

**Table S8** Statistical output of the cell volume ( $\mu\text{m}^3$ ) and protein (amide II) or lipid (ester carbonyl) content models (Fig. 7).

Please note: Wiley Blackwell are not responsible for the content or functionality of any Supporting Information supplied by the authors. Any queries (other than missing material) should be directed to the *New Phytologist* Central Office.